Amphiphilic Block Copolymers in Aqueous and Nonaqueous Emulsion Systems for Biomedical Applications

Dissertation

zur Erlangung des Grades

„Doktorin der Naturwissenschaften“

im Promotionsfach Chemie

am Fachbereich Chemie, Pharmazie, Geographie und Geowissenschaften

der Johannes Gutenberg-Universität

in Mainz

vorgelegt von

Nicole Beate Wutke

geboren in Augsburg

Mainz 2023

Die vorliegende Dissertation wurde in der Zeit von Dezember 2017 bis Juni 2021 am Max-Planck-Institut für Polymerforschung in Mainz unter der Betreuung von [redacted] und [redacted] durchgeführt.

Dekanin: [redacted]

1. Gutachterin: [redacted]

2. Gutachter: [redacted]

Tag der mündlichen Prüfung: 10.05.2023

Science doesn´t always go forwards. It´s a bit like doing a Rubik´s cube. You sometimes have to make more of a mess with a Rubik´s cube before you can get it to go right.

Jocelyn Bell Burnell

Table of Contents

Index of Abbreviations

Abbreviation	Meaning
^{13}C-NMR	carbon NMR spectroscopy
^{1}H-NMR	proton NMR spectroscopy
AIBN	azobisisobutyronitrile
b	*block*
BnBr	benzyl bromide
BnOH	benzyl alcohol
BSA	bovine serum albumin
cmc	critical micelle concentration
CyH	cyclohexane
δ	chemical shift
Đ	dispersity
d_H	hydrodynamic diameter
DCM	dichloromethane
DiPE	di*iso*propylether
DLS	dynamic light scattering
DMAEMA	2-(dimethylamino)ethyl methacrylate
DMAEMASB	2-(dimethylamino)ethyl-sulfobetaine methacrylate
DMAP	4-(dimethylamino)pyridine
DMF	dimethylformamide
DMSO	dimethylsulfoxide
DOSY NMR	diffusion-ordered NMR spectroscopy
DP	degree of polymerization
DSC	differential scanning calorimetry
EDC-HCl	1-ethyl-3-(3-dimethylaminopropyl)carbodiimide hydrochloride
eq	equivalents
Et_2O	diethylether
EtOAc	ethyl acetate
Fig.	figure
FT-IR	fourier transform infrared spectroscopy
GPC	gel permeation chromatography
HMBC	heteronuclear multiple bond correlation
HMDS	hexamethyldisilazane
HPLC	high performance liquid chromatography
HSA	human serum albumin
HSQC	heteronuclear single quantum coherence experiment
IMes	1,3-bis(2,4,6-trimethylphenyl)imidazole-2-ylidene
M_n	number average molar mass
M_w	weight average molar mass
ME	2-mercaptoethanol
MAPHOS	methacryloyloxyethylphosphoric acid
$MAPHOSMe_2$	2-dimethoxyphosphorylethylmethacrylate
MPC	2-methacryloyloxyethyl phosphorylcholine
MWCO	molecular weight cut off
NCA	*N*-carboxyanhydride
NEP	nonaqueous emulsion polymerization

NHC	*N*-heterocyclic carbene
NMR	nuclear magnetic resonance
NP	nanoparticle
p	packing parameter
PDI	perylene diimide
PDLS	poly(DL-serine)
PDLS(Bn)	poly(*O*-benzyl-DL-serine)
PEG	poly(ethylene glycol)
PDMAEMASB	poly(*N,N*-dimethylamino-2-ethlymethacrylatsulfobetaine)
PEO	poly(ethylene oxide)
PgMA	propargylmethacrylate
PDLS	poly(DL-serine)
PLS	poly(L-serine)
PLS(Bn)	poly(*O*-benzyl-L-serine)
PLS(Pyr)	poly(*O*-pyrenyl-L-serine)
PSer	poly serine
PI	poly(isoprene)
PLLA	poly(L -lactide)
PLMA	poly(laurylmethacrylat)
PMDETA	bis(2-dimethylaminoethyl)methylamin(*N,N,N',N'',N''*-Pentamethyldiethylen-triamin)
PMI	perylene monoimide
PMMA	poly(methyl methacrylate)
PMPC	poly(2-methacryloyloxyethylphosphorylcholin)
PTMAEMA	poly(*N,N,N*-trimethylamonium-2-ethylmethacrylat
ROP	ring opening polymerization
rt	room temperature
SB	sulfobetaine
SEM	scanning electron microscopy
SIMes	1,3-bis(2,4,6-trimethylphenyl)-4,5-dihydroimidazole-2-ylidene
TBAI	tetrabutylammonium iodide
TEA	triethylamine
TEM	transmission electron microscopy
Tf	transferrin
TFA	trifluoracetic acid
THF	tetrahydrofuran
TLC	thin-layer chromatography
TMAEMA	2-(trimethylamino)ethyl methacrylate
US	ultrasonication

1 General Introduction

Research in nanotechnology has gained growing attention in the past decades and with it the development and investigation of functional nanomaterials for various applications.[1] Nanomaterials are tiny materials with an overall size of 1-100 nm and they are coming in various shapes, resulting in unique physicochemical properties.[1] Nowadays, nanomaterials are used in almost all industries, ranging from cosmetics and paints, agriculture and food, textiles, electronics to biomedicine and drug delivery.[1] Especially its use in biomedicine has opened a whole new field of research; the development of functional drug carrier systems that are able to encapsulate and transport drug molecules to its target tissue.[2] In order to increase the number of applicable therapeutics and their efficacy and therefore increase the available therapeutic options to treat certain medical conditions, nanomaterials are of high interest in biomedicine.[2,3] Such carrier systems were proven to increase the drug´s efficacy by leading to longer retention times and slower or local release of a drug, which allows the use of lower doses and hence decreasing unwanted side effects.[1,4] Several types of drugs like proteins, antibodies, peptides and small molecules can be encapsulated by drug delivery systems.[3–5] This is a game-changing technology, as there are many potent drugs that have proven biological functions to treat several diseases and medical conditions.[4,6] But often, without any support material, these drugs cannot be used, because of lack of release control and targeting or fast clearance from the organism.[4,7] By encapsulating the drug into a versatile delivery system, we can gain control over the drug release. However, it is a huge challenge to develop a delivery system that meets all requirements to be applicable in biological environment and in treatment of a specific medical condition (Figure 1).

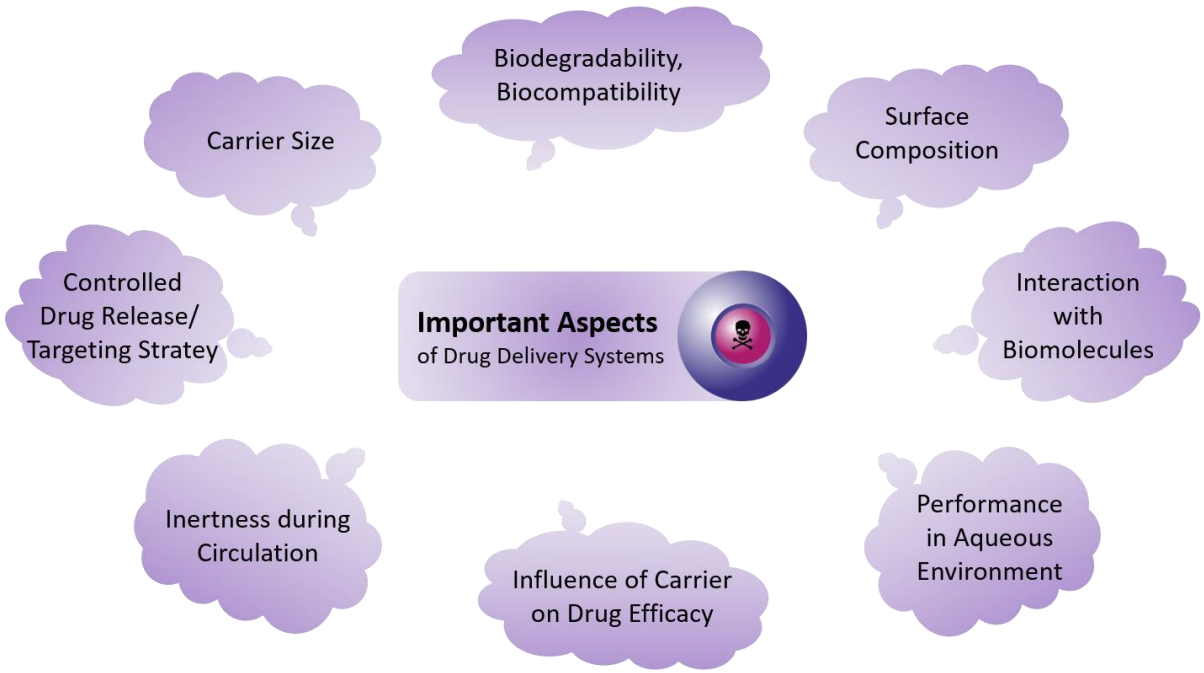

Figure 1: Key properties that have to be fulfilled in the development of a drug delivery system.

REQUIREMENTS FOR A FEASIBLE DRUG DELIVERY SYSTEM

There are key properties that have to be met in order to develop a feasible drug delivery system (Figure 1). The drug carrier system has to be biodegradable and fully biocompatible to ensure that the carrier material is not cytotoxic or biologically active itself to prevent undesired side effects.[8] The carrier needs to be fully inert during blood circulation in the organism and release the unmodified drug traceless to avoid changing the biological function of the molecule. The only acceptable influence of the drug delivery system on the drug is increasing efficacy and circulation time.[9,10] By finding a suitable targeting strategy, the drug release gets controllable and no off-target leakage is happening before the delivery system reaches the target tissue.[6] It is achieved by building in a trigger sequence into the carrier system that is activated by a specific mechanism in the target tissue.[6] This can be a material sensitive to certain pH, as the tumor microenvironment is known to be slightly more acidic than healthy tissue.[11] It can also be achieved by addressing a particular structure like a receptor or enzyme/protein that is overexpressed in the tumor tissue.[12,13] By incorporation of trigger sequences into the carrier surface that specifically react with these biomolecules, controlled local drug-release is enabled. [14,15] To reach and enter the target tissue, a certain carrier size is necessary, for example to pass the blood-brain-barrier or a cell membrane.[16] In cancer treatment, the size of the drug delivery system is strongly influencing its efficacy. While small molecule drugs can easily enter the tumor environment, they can diffuse out of the tissue again as fast, leading to low efficacy.[17,18] Nanosized drug delivery systems in contrast, are small enough to diffuse into the tumor environment, but once they entered the tumor tissue, they are kept inside by interstitial fluid pressure.[5,19] The result is the accumulation of the drug carriers in the tumor tissue, described by the enhanced permeability and retention (EPR) effect.[20] Such passive targeting can be achieved by the size of the carrier system to some extent.[5,21] In comparison to solution-based formulations, drug delivery by a nanocarrier can lead to increased accumulation of the drug in the tumor environment by up to 100-400% without diffusing back into the blood stream.[21] The last aspect is the surface composition of the carrier, which is crucial for its aggregation behaviour in aqueous solution and for interactions with biomolecules. In general, a polar surface is required to disperse the carrier in biological media.[20] The surface should be polar ionic to promote interactions with biomolecules like cells or proteins and polar non-ionic or zwitterionic to prevent these interactions, which can be both important depending on the corresponding application.[22] In conclusion, many requirements have to be addressed to obtain a feasible and applicable drug delivery system. This is a huge challenge many research groups try to overcome. Although there is a high number of potent concepts for drug delivery systems available, many of them suffer of major drawbacks preventing them to be widely used in biomedicine. The goal is to develop a controlled-release drug delivery system that is well-tolerated by the patients. Increasing the drug´s

efficacy allows the use of lower doses of the drug to reduce the severe side effects known from established cancer therapies.[21] This can be achieved by combining multiple effects like tailored targeting strategies and selective, local drug release together with passive targeting effects.

HISTORY OF NANOCARRIER SYSTEMS FOR DRUG DELIVERY

A brief look into scientific literature reveals numerous approaches of utilizing nanotechnology for drug delivery, with first attempts being performed in the 1950s, which underlines the potential of this technology for medical applications.[21] Commonly, nanoparticles have sizes between 1 and 100 nm and are significantly smaller than human cells (10-100 µm) and comparable to other biomolecules (10-100 nm), but larger than small-molecule drugs (Figure 2).[16] Consequently, drugs can be encapsulated in a nanocarrier, allowing their transport through blood vessels and into target tissue and cells, depending on the size and composition of the carrier particle and the way of administration. Nanocarriers consist of different materials and shapes, including organic and inorganic nanoparticles, liposomes, dendrimers or micellar aggregates.[21]

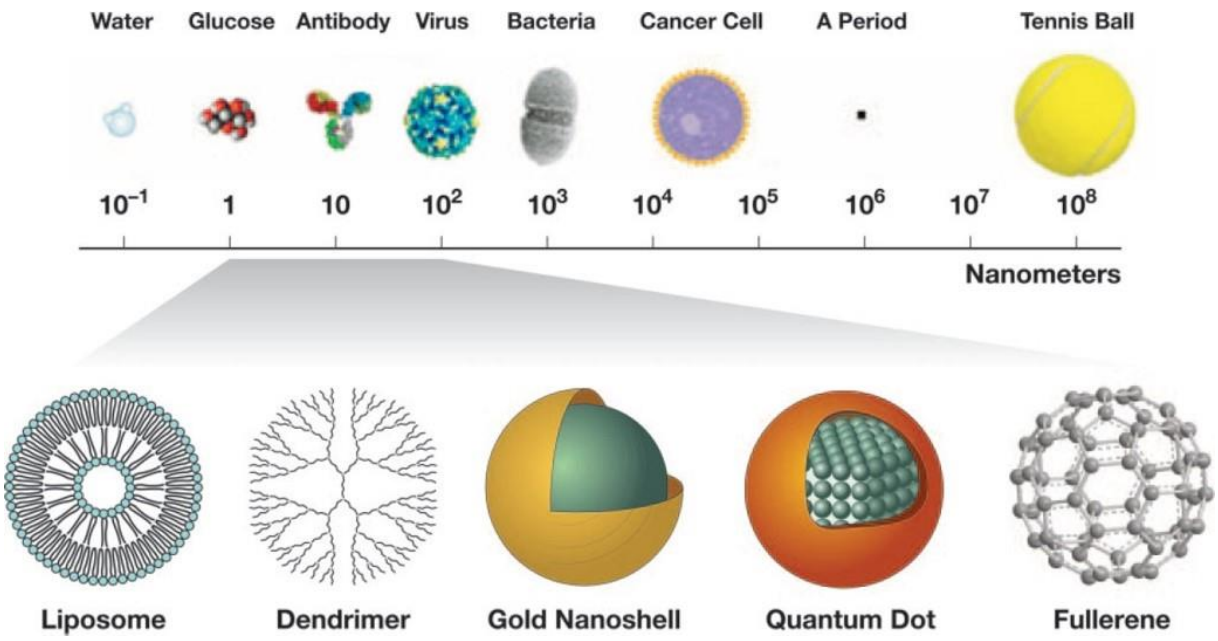

Figure 2: Relative size of nanoparticles compared with familiar items. (Reprinted with permission from [16]. Copyright 2005 John Wiley and Sons.)

The early attempts to create nanocarrier systems put special interest on the development of controlled-release mechanisms (Figure 3). It was of high importance that the drug is released at a slow and predetermined rate, resulting in higher efficacy of the active compound. This was achieved by utilizing physical principles like dissolution, diffusion, osmosis or ion-exchange mechanisms. The focus in the 1980s lied on self-regulation and long-term release systems and the idea of active targeting was born. These closed delivery systems should overcome challenges like drug leakage during circulation by insertion of internal triggers that allow selective drug release by interaction with their environment.

Overcoming the difficulties that came along with the idea of active targeting was not as successful until the early 2000s when nanotechnology made its way back into spotlight.[21] Even though lots of effort was put into the development of "real" active targeting delivery systems, it is an unsolved challenge to this day to program a nanocarrier that actively detects and moves towards its target.[23] In order to circumvent this limitation, potential selective targeting strategies were developed successfully within the last years.[21] They allow selective drug release by incorporating triggers into the particle surface that keep it inert during circulation and release the drug only at the desired target tissue by targeting specific receptors or antigens.[21] This was a huge step towards more effective drug delivery and increased efficacy of drugs at lower doses.[21] The result is the reduction of unwanted side effects that go along with most traditional cancer treatments that are administered systemically.[8,21] An example for selective targeting are nanocarriers that are surface-modified with folic acid, to target the folate receptor that is overexpressed in many tumor cells.[24,25] It is not present in healthy cells and therefore a potent target for selective targeting, already confirmed by *in vitro* and *in vivo* experiments.[24,25] In these studies, the nanoparticle-folic acid conjugates not only showed enhanced and selective targeting towards cells that contained the folate receptor[25], but also significant tumor suppression[24]. Consequently, this delivery system is currently evaluated in clinical trials.[24]

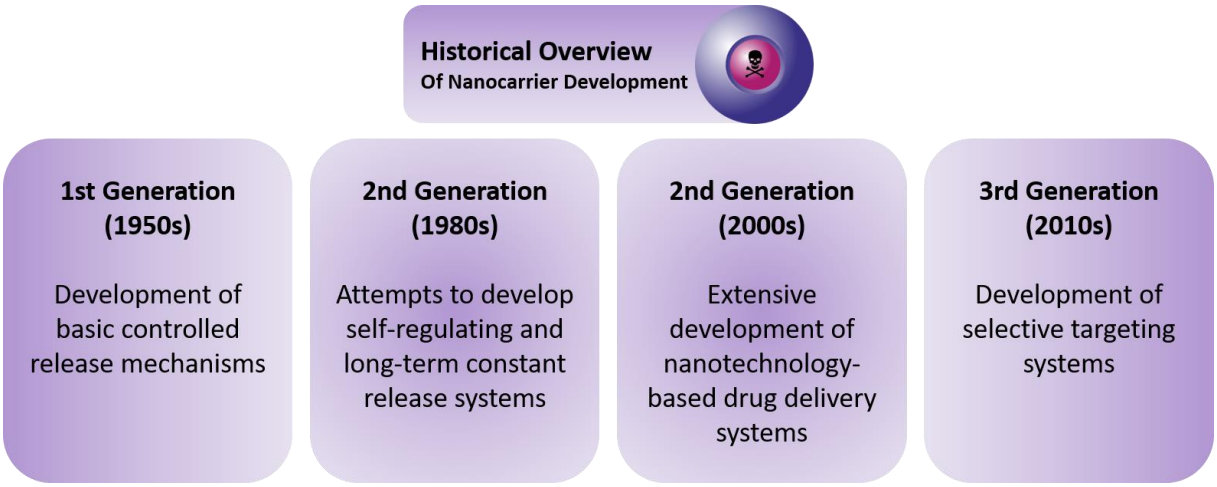

Figure 3: Historical overview of nanocarrier development over the past decades.[21]

NANOCARRIER SYSTEMS TODAY

Over the past two decades (2000s – 2010s) the main focus in the development of nanocarrier systems lied on selective targeting and eventually on smart nanocarrier systems that are distinguished by high sensitivity towards endogenous and exogenous stimuli, resulting in an improvement of controlled drug-release.[21] The insertion of stimuli-responsive polymers in the surface or shell of the nanocarrier leads to drug release by time, physical or chemical triggers, like temperature, magnetic fields, light, ionic strength, pH or enzymes. Suddenly, it was possible to create tailored delivery systems that were deliberately recognizing and interacting with biomolecules, opening a wide field of therapeutic applications by utilizing biomolecules like enzymes as specific triggers for the drug release.[1,3,21] If an enzyme-responsive sequence is incorporated into the carrier shell, it will be recognized by the corresponding enzyme and cleaved, resulting in degradation of the particle and drug release.[14] One example for this mechanism is the enzyme matrix metalloproteinase-2 (MMP-2) that is known to be overexpressed in many tumor cells, while healthy cells imply significantly lower concentrations of MMP-2.[26–28] This enzyme is able to cleave the peptide sequence PLGLAG, specifically, between glycine and leucine.[29] Building this enzyme sequence into a nanocarrier shell would results in cleavage of the peptide sequence and particle degradation upon incubation with MMP-2, enabling the release of an encapsulated drug (Scheme 1A).[15] Moreover, the study showed that the MMP-2 concentration in healthy cells that is typically lower than in cancerous cells, did not lead to any detectable cleavage of the peptide sequence. A scrambled sequence that consisted of the same amino acids in different order (LALGPG) did not show any cleavage as well, proving the selectivity of the trigger sequence (Scheme 1B).[15] These results were underlining the huge potential of the MMP-2 enzyme as a selective target for cancer treatment.

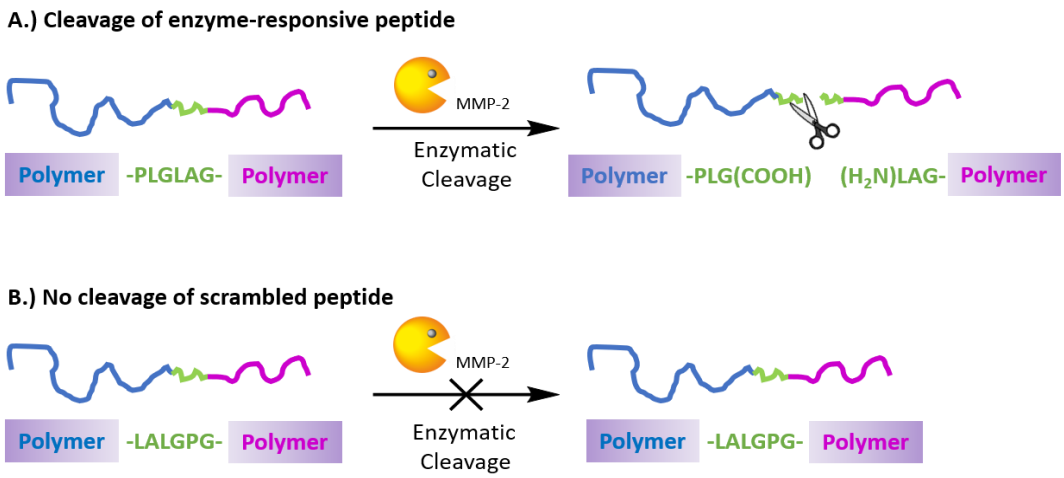

Scheme 1: Schematic representation of A.) The cleavage of a block copolymer at the enzyme-responsive sequence PLGLAG by MMP-2 and B.) no cleavage of the scrambled sequence LALGPG.

SURFACE COMPOSITION AS A KEY FACTOR FOR DRUG CARRIER SYSTEMS

The surface composition of drug carrier systems is an important factor for the performance under physiological conditions.[30] The particle surface has a direct influence on many other requirements for carrier systems that were described before (Figure 1). It is crucial for the aggregation behaviour and stability of the nanoparticle in aqueous environment.[31] Typically, all kinds of drug delivery systems need a polar surface to be homogeneously dispersible and remain stable in aqueous media without aggregation, premature degradation or clearance.[30] Biological media are not only consisting of water, but a variety of biomolecules (*e.g.,* proteins and cells) and electrolytes (*e.g.,* sodium chloride, phosphates) that can interact with the carrier system and affect its performance.[31] Depending on the chemical composition of the particle surface, different carrier systems show differing binding affinity to biomolecules. Polar functional groups can be divided into polar ionic and polar non-ionic structures. This is important, as their interaction with biomolecules, for example protein binding and the formation of a protein corona, is strongly depending on the presence and nature of charges.[22,32] Polar non-ionic groups, like polyethylene glycol (PEG), show very low interactions and hence, are used for surface modification to suppress interactions with the physiological environment.[7,18] In contrast, single-charged groups show very strong affinity to bind biomolecules and are prone to protein corona formation.[22] Zwitterionic surfaces have been reported to show a “repelling” effect towards proteins, resulting in anti-fouling properties.[32] Consequently, they have gained the attention of many research groups recently. Further research is required to gain a deeper understanding of the interactions between nanostructures and biomolecules to be able to predict their behaviour in physiological environment (Figure 4).

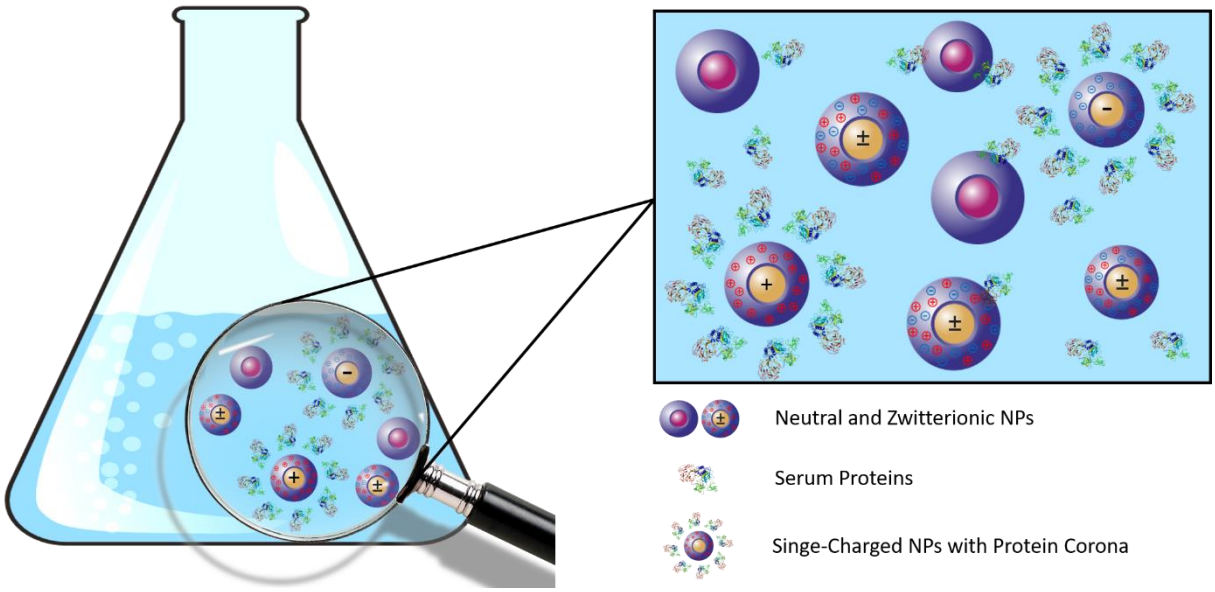

Figure 4: Nanoparticles showing a varying tendency for the interaction with biomolecules, like protein corona formation, depending on the particles´ surface composition.[33,34]

Another surface-related aspect is the implementation of a versatile selective targeting strategy into the carrier system by insertion of a stimuli-responsive trigger sequence into the particle shell. It is of importance to place the stimuli-responsive sequence in the shell or on the surface of the particle respectively, to be available for the trigger, whether it is an enzyme, a receptor or the pH of the surrounding tissue.[21] Therefore, it is mandatory to find a suitable synthesis strategy that allows tailoring of the carrier surface to the needs of the desired application.

SMART CORE SHELL NANOPARTICLES PREPARED BY NONAQUEOUS EMULSION POLYMERIZATION

Various types of carrier materials have been developed over the past decades.[21] One well-stablished strategy to fabricate organic core shell nanoparticles is nonaqueous emulsion polymerization. It allows carrying out organic syntheses under inert conditions in organic solvent. A wide range of polymerizations can be performed that require water- and oxygen-free conditions to produce polymeric nanoparticles.[35,36] Emulsion polymerizations can be conducted as suspension, mini emulsion or macro emulsion polymerization.[37] While suspension polymerization is carried out in a heterogeneous and emulsifier free system, mini and macro emulsion systems require an emulsifier that stabilizes the emulsion.[37–39] Two main physical effects determine the performance of the emulsion formation, coalescence and Ostwald ripening (Scheme 2).[40]

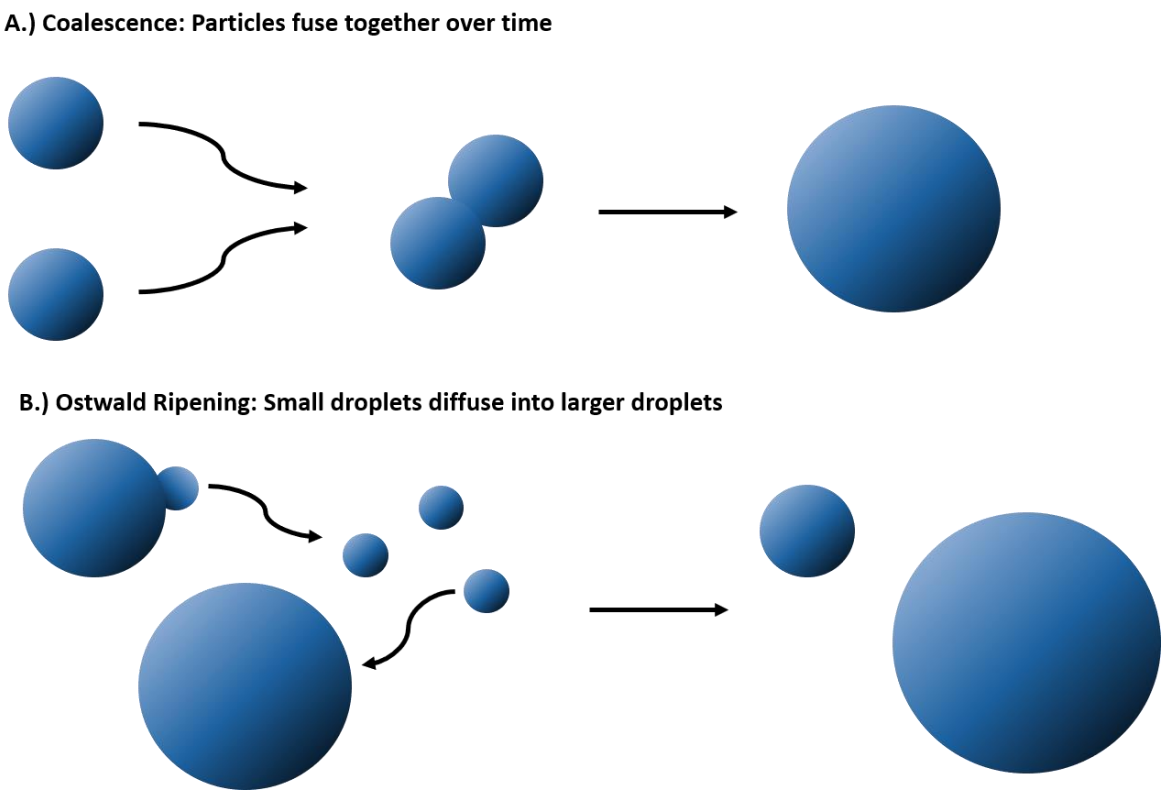

Scheme 2: Schematic representation of A.) Coalescence and B.) Ostwald Ripening.[40]

Coalescence is defined as the fusion of smaller droplets into larger ones over time (Scheme 2A). It can be inhibited by emulsifiers that lower the surface tension between the solvents to stabilize the emulsion.[38,39] Ostwald ripening describes the diffusion from smaller droplets into larger ones through the continuous phase (Scheme 2B). In contrast to coalescence, this process cannot be suppressed by surfactants. Instead, the process can be slowed down by adding a hydrophobe to an oil in water (O/W) emulsion or a lipophobe to a water in oil (W/O) emulsion.[40,41]

When an emulsion is formed, small droplets of one solvent (dispersed phase) are dispersed in another solvent (continuous phase). In emulsion polymerization, these small droplets are utilized as small reaction chambers, in which polymerizations are carried out, resulting in dispersed polymeric particles. In a classic O/W-emulsion, water is used as the continuous phase with a hydrophobic solvent dispersed in it.[36,37,39] Many organic reactions, including most polymerizations, are limited to the use of organic solvents, as they require water- and/or oxygen-free conditions. Water-based emulsion systems cannot be utilized for these kinds of reactions. To overcome this severe limitation, nonaqueous emulsion polymerization was developed where the emulsion system consists of organic solvents, exclusively. In the nonaqueous emulsion system, water-sensitive reagents like certain catalysts or monomers, are used successfully to produce polymer nanoparticles in one single step.[36,42,43] To form a nonaqueous emulsion, two organic solvents are required, a polar and nonpolar one, that are immiscible. One solvent is being used in excess as the continuous phase, while the other solvent is dispersed in it. To stabilize the emulsion, an amphiphilic polymer as emulsifier is added to reduce the interfacial tension between the two phases.[44] The first nonaqueous emulsions were consisting of either dimethylformamide (DMF) in *n*-hexane or acetonitrile (MeCN) in cyclohexane (CyH), while a wider range of solvent systems has been established over time.[36,42,43] To perform nonaqueous emulsion polymerization, the amphiphilic block copolymer is dissolved in the nonpolar solvent like cyclohexane (Scheme 3). By pointing the hydrophobic groups towards the solvent, micelles are formed. The monomer for the polymerization is dissolved in the dispersed phase, like acetonitrile, and added to the continuous phase, followed by ultrasonication to homogenize the mixture. A nonaqueous emulsion is formed. In the last step, all other components, like the initiator, catalyst or a drug are dissolved in the dispersed phase and added to the emulsion upon excessive stirring. The reagents are diffusing into the droplets where the polymerization takes place. To make sure that the polymer is formed exclusively inside the micellar reactors, at least one component (monomer, initiator, catalyst) must be soluble only in the dispersed phase. This compound should be added first.[45–48] The polymerization results in dispersed nanoparticles. The quality of the resulting particles is strongly depending on the quality of the emulsion in regards of micelle size and homogeneity. A homogeneous emulsion is likely to result in homogeneous particle dispersions.[37,46,49]

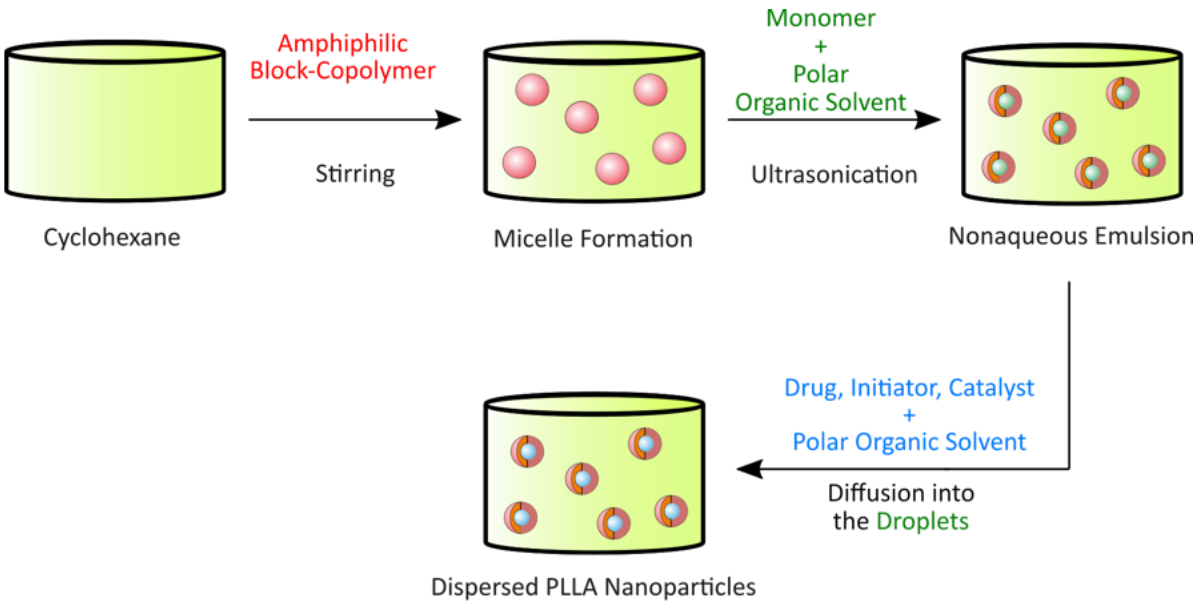

Scheme 3: Schematic step-by-step representation of the nonaqueous emulsion polymerization.[50]

Nonaqueous emulsion polymerization was barely used for drug delivery applications before and the emulsifiers typically consisted of classical polymers, like PI-*b*-PMMA.[47,51,52] These block copolymers are well-dispersible in nonpolar solvents, resulting in homogeneous particle dispersions with narrow size distributions.[51,52] Performing the particle synthesis in nonpolar emulsion is leading to a hydrophobic particle surface with the hydrophobic block of the emulsifier pointing towards the nonpolar, continuous phase. The resulting particles are not dispersible in aqueous solution and hence, not suitable for biomedical applications.[53] Nevertheless, nonaqueous emulsion polymerization provides easy and straight-forward access to a wide range of polymeric particles that are potential nanocarriers for drug delivery applications, if their surface composition could be altered. New approaches were needed to optimize the synthesis to obtain biocompatible nanoparticles with a polar surface. The synthesis of biocompatible poly(L-lactide) (PLLA) nanoparticles by nonaqueous emulsion polymerization was successfully performed by Robert Dorresteijn in our group.[15,49] Initially, he used a PI-*b*-PEO emulsifier that did not result in particles with a polar surface. In order to hydrophilize the particle surface, he used the PEG-based surfactant Lutensol to coat the particles with a polar polymer. The resulting particles with an additional layer of surfactant were well dispersible in water.[15,49] Adding another layer to the particles potentially hinders the drug release, as it would make a trigger sequence less approachable to the surrounding biological environment. The ultimate goal was to develop a biocompatible, amphiphilic block copolymer as emulsifier that provided a polar moiety on the particle surface. It required one consistent polar block that pointed towards the dispersed phase and one polarity-switchable, temporarily hydrophobic block that pointed towards the nonpolar, continuous phase. By removal of the hydrophobic groups after the particle synthesis, polar groups would be exposed at the particle surface, making the particles dispersible in aqueous solution. Such an

emulsifier, a PEG-*b*-PLG (Poly(L-glutamic acid)) derivative, was developed by Robert Dorresteijn. The glutamic acid side chain was modified with hydrophobic pyrene groups that were photocleavable by exposure to UV light. This technology allowed the fabrication of fully biocompatible PLLA core shell nanoparticles for drug delivery applications. Not only was it fully biocompatible and dispersible in water without an additional layer of surfactant, it had a built-in enzyme-responsive peptide sequence that is exclusively cleavable by the abovementioned enzyme MMP-2 (Scheme 4).[50,53]

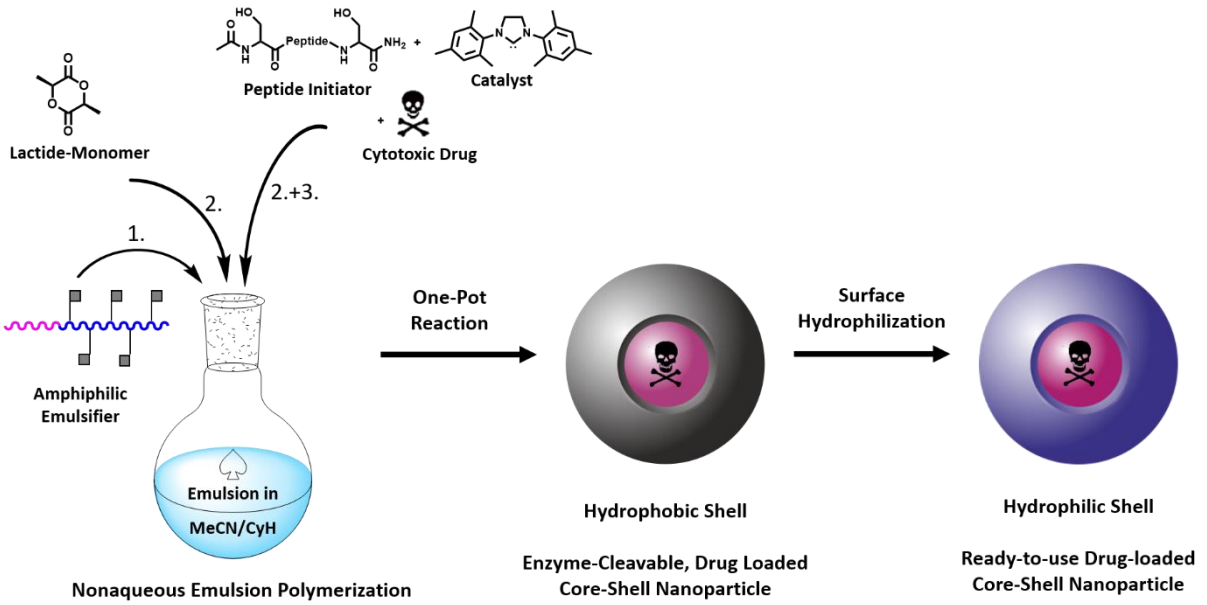

Scheme 4: One-pot approach to ready-to-use drug-loaded core-shell nanoparticles by nonaqueous emulsion polymerization.

The biodegradable emulsifier used for the particle formation was PEG-*b*-PLG with the poly(L-glutamic acid) block on the particle surface.[53] The particle surface consisted of single-charged, anionic molecules in aqueous solution and therefore, is prone to interactions with biomolecules like proteins, resulting in the formation of a protein corona.[54] Covering the particle surface with proteins can alter the aggregation behaviour and stability of the particles in physiological media.[31,55] It can lead to decreased drug release by hindering the enzyme MMP-2 to reach the trigger sequence at the particle surface to enable the particle cleavage.[56,57] In order to minimize protein interactions, a polar nonionic surface is desired. This should be achieved by exchanging the poly(amino acid) block in the emulsifier from poly(L-glutamic acid) to poly(L-serine) that has a nonionic hydroxy group in its side chain. The first results of the presented drug delivery system by Robert Dorresteijn were excellent in regards to selectivity of drug release and particle stability in biological media. In addition, it is a versatile one-pot approach for the synthesis of fully biocompatible, drug-loaded nanoparticles.[50] At the same time the studies led to the conclusion that some optimization of the surface composition is mandatory to prevent interaction with biomolecules in physiological media.

PREVENTION OF PROTEIN CORONA FORMATION BY ZWITTERIONIC SURFACES

Besides fully organic nanocarrier systems, polymer-coated inorganic nanoparticles (NP), like gold- or silver-based particles, are extensively investigated for drug delivery applications due to their unique physicochemical properties.[58] The surface composition of inorganic nanoparticles is crucial for their stability and performance in physiological environment.[59–61] The surface of a particle determines the binding affinity to biomolecules and interactions with electrolytes and can affect the performance of the system.[57,62] In order to prevent undesired aggregation and preliminary clearance of the particles, it is important to gain a deep understanding of these interactions to be able to tailor the nanocarrier to its application.[54,63] Biological media are consisting of a complex mixture of biomolecules that can interfere with the nanoparticles.[54,64] The particle stability and aggregation behaviour can be affected, for example by non-specific protein adsorption.[64] Protein adsorption leads to the formation of a dynamic protein layer around the particles, known as protein corona.[54] It is stabilized by protein-NP interactions that consist of protein-protein interactions and protein-NP binding affinities.[54,58,64] In a previous collaboration with the group of Wolfgang Parak, studies were performed on the interaction of gold nanoparticles with polymer-modified surfaces.[22,59,65] Methacrylic acid-based polymers were used for the stabilization of the particles. These amphiphilic polymers contained charged groups that were either positively or negatively charged. Both types of single-charged surfaces showed significant interaction with biomolecules and protein corona formation.[22] In contrast, zwitterionic surfaces are reported to show a repelling effect towards biomolecules and hence, prevent the formation of a protein corona.[22,55,64] Zwitterionic structures were evaluated as alternatives to nonionic surfaces that mainly have been studied in the past to suppress interactions with biomolecules.[32,64,66] A study on the potential of surface modification of gold nanoparticles with zwitterionic polymers is presented in this work (Chapter 6).

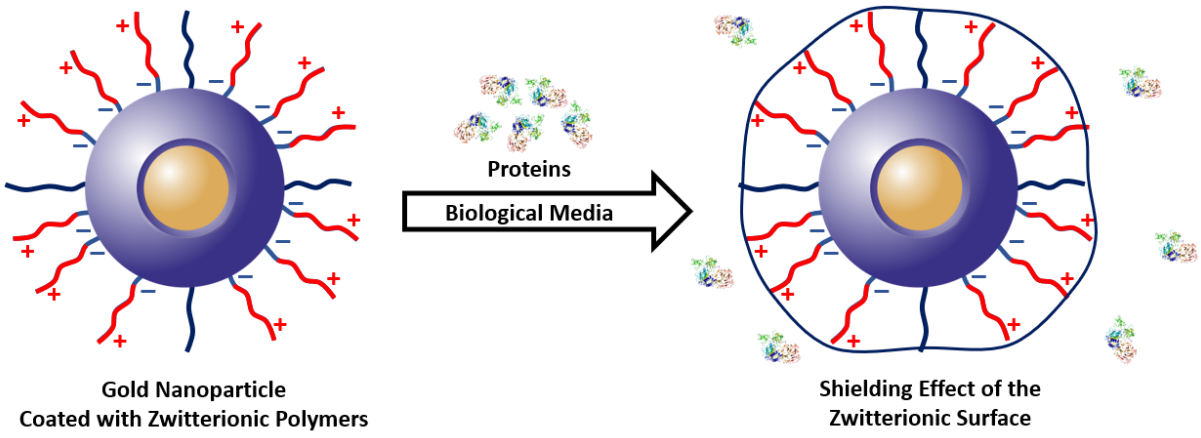

Scheme 5: Proposed shielding effect towards protein interactions of a zwitterionic nanoparticle surface in biological media.[22]

2 Motivation and Objectives

The scope of this thesis was the development of a nanocarrier system for drug delivery applications with emphasis on the investigation of the surface properties of such materials in respect of their behaviour in biological environment (Figure 5). Amongst other things, the surface composition of nanomaterials is crucial for their applicability in biological systems, as it determines factors like protein interaction, particle stability and retention time in the bloodstream.[6,9,54] The behaviour of nanomaterials in biological environment can differ dramatically, depending on their surface chemistry.[20,22] The development of a drug delivery system based on this knowledge and the study of its performance in biological environment was the main goal of this work.

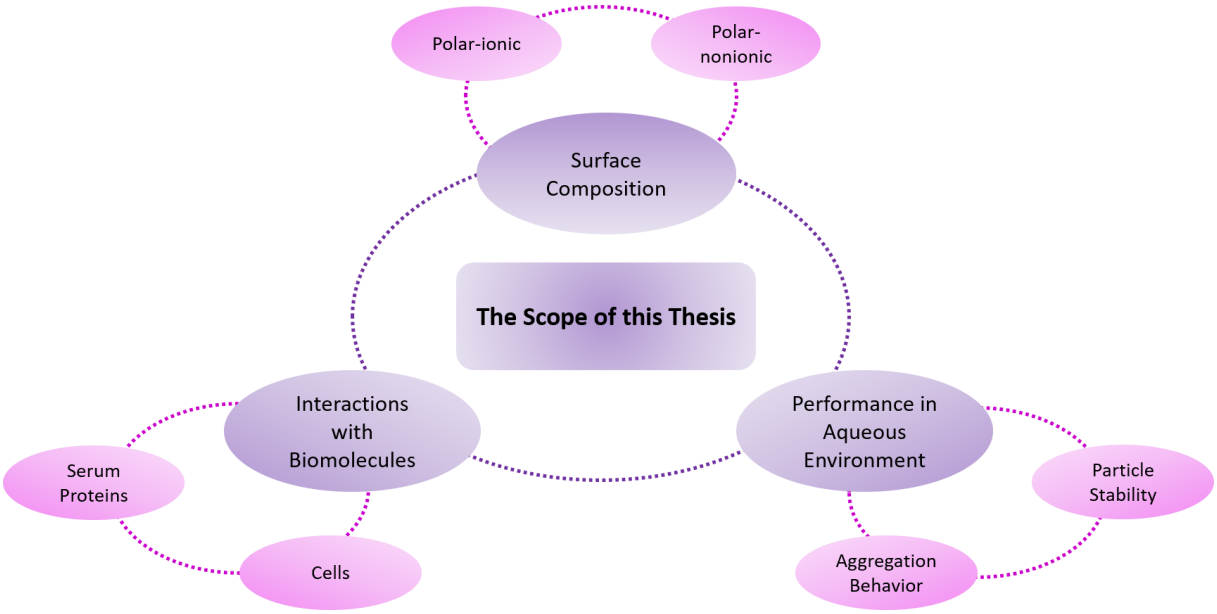

Figure 5: The main aspects addressed within this thesis are surface composition, interactions with biomolecules and performance in aqueous environment of surface-active nanoparticle systems.

In the main project, a nano drug carrier system for cancer therapy applications should be developed and optimized on the basis of the works of Robert Dorresteijn and Filiz Karagöz.[50,67] In order to obtain a feasible carrier system, five requirements were chosen to be addressed (Figure 6). The particles have to consist of fully biocompatible and biodegradable materials that show good cell viability to minimize side effects caused by the carrier system itself.[8] To transfer and disperse the carrier particles in aqueous media, they have to have a hydrophilic surface.[20] In addition, the particles need to show an appropriate retention time in the blood stream without interacting with biomolecules to prevent clearance from the system before reaching its target.[10,22] The ideal particle size to reach this was determined as around 100 nm in diameter.[16] Furthermore, inertness during blood circulation is mandatory and drug release has to take place only in the target tissue.[9] The particles should contain a built-in trigger in the particle shell in order to achieve controlled drug release.[6]

The synthesis of a stimuli-responsive nano drug carrier with a polar non-ionic surface should be conducted by nonaqueous emulsion polymerization. A specialty of this system should be the one pot synthesis approach, where all steps, from the particle synthesis and drug loading to the installation of the stimuli-responsive sequence, are performed in one single step. The ready-to-use particles should be investigated in respect of cell viability and drug release. Furthermore, the development of biocompatible amphiphilic block copolymers as emulsifiers for the nonaqueous emulsion polymerization was of special interest.

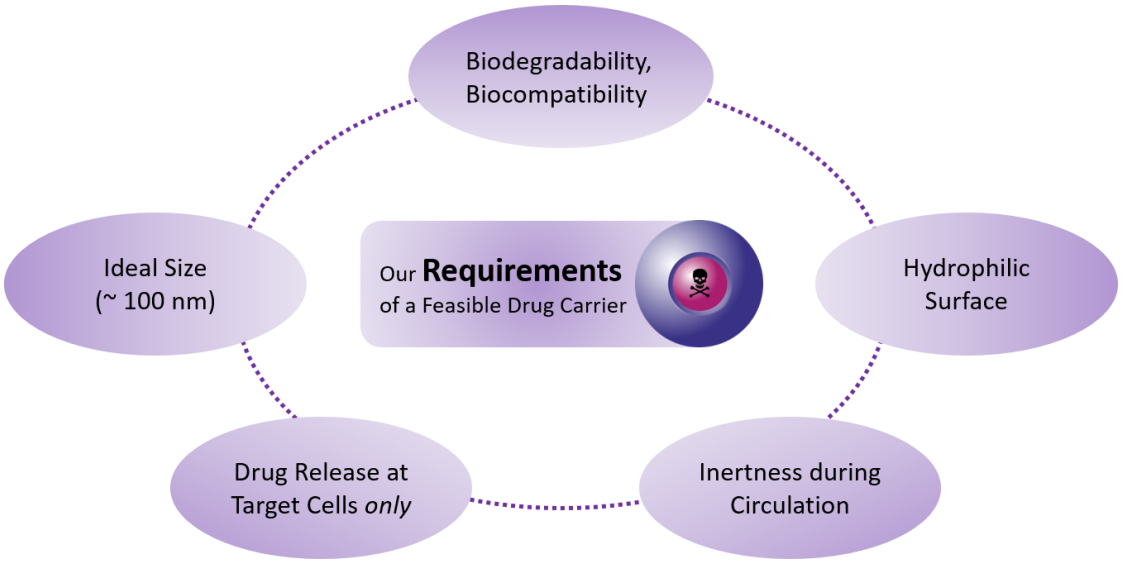

Figure 6: Requirements for the design of a feasible drug carrier system for cancer therapy.

In contrast, the scope of the second project was the investigation of the influence of charged surfaces on interactions with serum proteins.[64] Amphiphilic PMA-based copolymers with side chains containing different charges should be synthesized for the fabrication of polymer-coated gold nanoparticles. The influence of the differently charged particle surface on protein interactions as well as the particle stability in biological media was of special interest in this project (Figure 7).

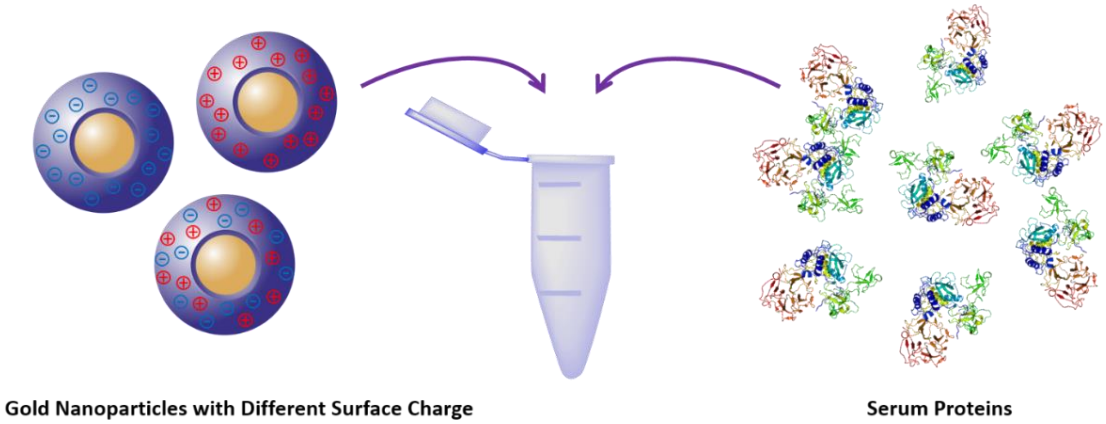

Figure 7: Investigation of the protein adsorption of nanoparticles with different surface charge.

3 Development of a stimuli-responsive nano drug carrier – Nanoparticle synthesis with biocompatible poly-O-benzyl-serine-based emulsifiers

3.1 Introduction

In this work, a stimuli-responsive nano carrier system was designed and fabricated by nonaqueous emulsion polymerization. This technique is very convenient to create ready-to-use, drug-loaded core-shell nanoparticles in a one-pot procedure.[67] By insertion of a stimuli-responsive sequence into the nanoparticle shell, a controlled release mechanism is ensured. When the nanoparticles are transferred into biological environment, they remain stable in healthy cells, while drug release is taking place specifically in the tumor tissue by enzyme-cleavage (Figure 8).[15]

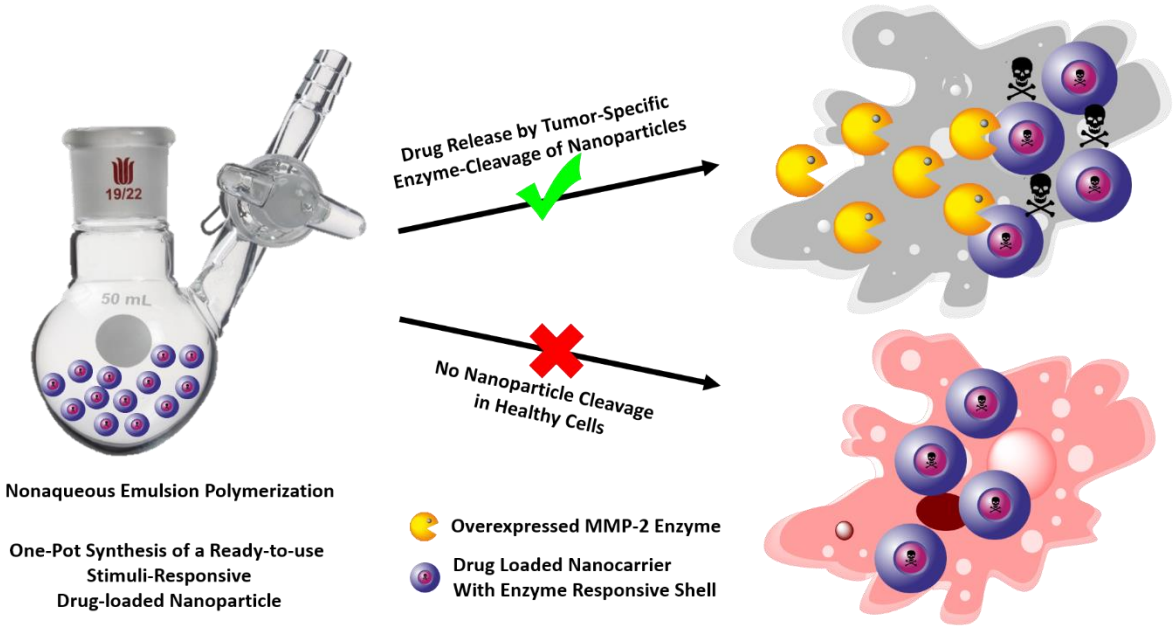

Figure 8: One-pot-synthesis of an enzyme-responsive drug carrier system for cancer therapy.

ENZYME-RESPONSIVE NANOPARTICLES FOR CONTROLLED DRUG RELEASE

The special feature of the system is the controlled-release mechanism. A built-in peptide sequence (PLGLAG) in the nanoparticle material is specifically cleavable by the enzyme matrix metalloproteinase-2 (MMP-2).[68] Matrix metalloproteinases are a family of enzymes that are associated with various physiological and pathological processes of tissue remodelling.[28] Amongst other things, the enzyme MMP-2 is known to be involved in tumor growth and metastasis.[28,68] By degradation of the extracellular matrix (ECM) the cancer cells are able to migrate out of the tumor and form metastases.[28] In pathological processes such es inflammation or tumor formation, overexpression and increased activity of MMPs was observed.[28] Therefore, addressing MMP-2 in cancer therapy is highly interesting to achieve targeted delivery.[68] We wanted to utilize the

overexpression of MMP-2 in tumor tissue by introducing the peptide sequence PLGLAG, that is known to be specifically cleavable by MMP-2, into the nanoparticle shell. While MMPs are present in healthy tissue as well, it was proven that the concentration is too low to achieve a measurable effect on MMP-triggered drug delivery systems and hence, can be considered as non-relevant.[15,50] Introducing the peptide sequence into the core-shell nanoparticle results in a drug carrier that is stable in healthy cells and releases the drug in tumor tissue specifically, where MMP-2 is present in significantly higher concentration.[28] When MMP-2 recognizes the PLGLAG-sequence in the particle-shell, it will cleave the peptides and eventually lead to particle degradation-induced drug-release. The locally released drug in the tumor will then kill the cancer cells (Figure 9).[69]

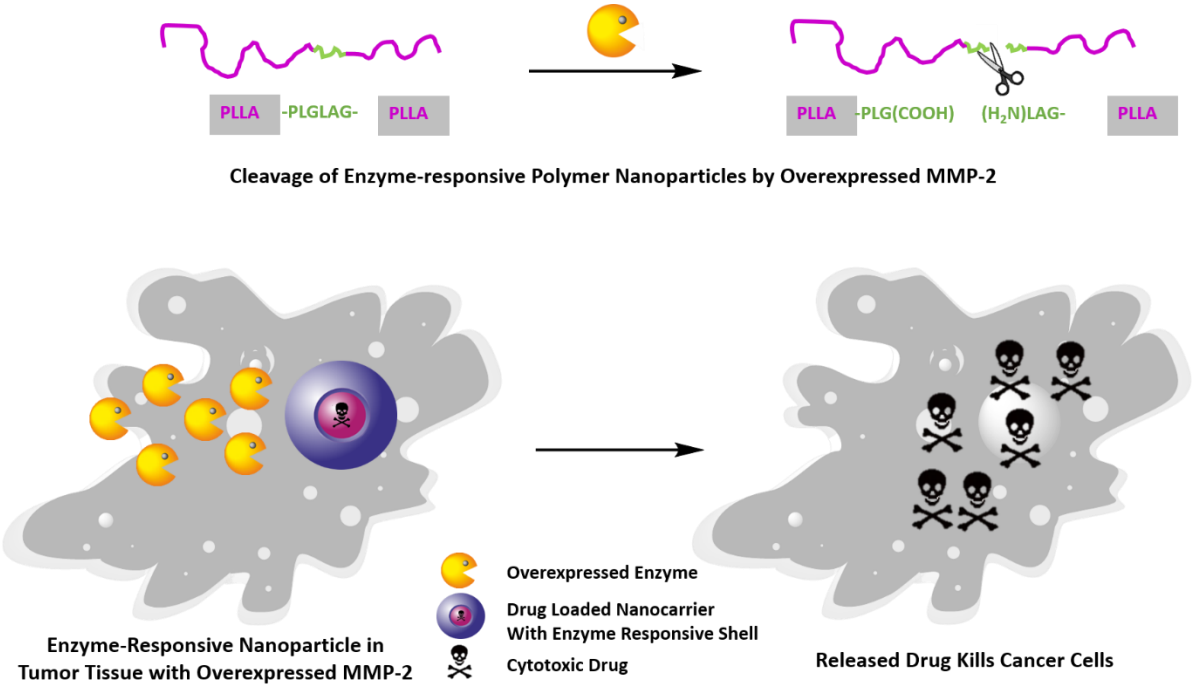

Figure 9: Drug release by enzyme-directed cleavage of the nanoparticles in the tumor tissue.

The specificity of MMP-2 towards the peptide sequence PLGLAG was verified in an experiment of Dorresteijn et al., where PLLA-*b*-peptide-*b*-PLLA triblock copolymers were synthesized, bearing either the enzyme-responsive PLGLAG or a scrambled sequence LALGPG.[15] The polymers were then incubated with MMP-2 and analyzed by MALDI-ToF MS before and after the treatment.[15] It was revealed that the PLLA-*b*-PLGLAG-*b*-PLLA was cleaved between the glycine and leucine during the incubation, as reported by Jiang et al.,[29] while the PLLA-*b*-LALGPG-*b*-PLLA did not show any mass difference before and after the incubation with the enzyme. This clearly proved the enzymatic cleavability of the triblock copolymers containing the PLGLAG sequence.[15]

CORE-SHELL NANOPARTICLES BY NONAQUEOUS EMULSION POLYMERIZATION

To produce drug-loaded, enzyme-responsive core shell nanoparticles, nonaqueous emulsion (NEP) polymerization was used. Nonaqueous emulsion polymerization is conducted in a mixture of two immiscible organic solvents, where the continuous phase is nonpolar, while the dispersed phase is polar. Therefore, it is a water-free, oil-in-oil (o/o) emulsion.[46] Addition of an emulsifier leads to the formation of reversed micelles, with the hydrophobic moiety pointing out to the continuous phase, stabilizing the droplets of polar solvent by reduction of the surface tension between the two phases.[37,46] The whole process of emulsion formation is highly complex and relies on many different parameters, like chemical composition of the emulsifier, the ratio of hydrophobic to hydrophilic moiety, temperature, solvents, surface tension, etc.[44,70] Classical block copolymers like polyisoprene-*b*-poly(methyl methacrylate) (PI-*b*-PMMA) are well established for emulsion polymerization applications and widely used in our group.[52,71] In contrast, introducing novel polymers as versatile emulsifiers for nonaqueous emulsion is a challenge itself and requires intense study and optimization.[53] When a suitable emulsifier was found, the fabrication of ready-to-use drug-loaded nanoparticles can be summarized in three basic steps (Scheme 6). First, the enzyme-responsive nanoparticles are synthesized and drug-loaded in a one-pot procedure by nonaqueous emulsion polymerization. Due to the hydrophobicity of the nanoparticle core, especially hydrophobic drugs, like 5-fluorouracil, can be encapsulated. The resulting nanoparticles have a hydrophobic surface that needs to be hydrophilized. Using photolabile hydrophobic groups on the surface allows easy removal of the groups under mild conditions by light exposure. The last step is the transfer of the now hydrophilic nanoparticles into the aqueous phase to obtain the dispersed particle solution that can be used for biomedical application without further processing.

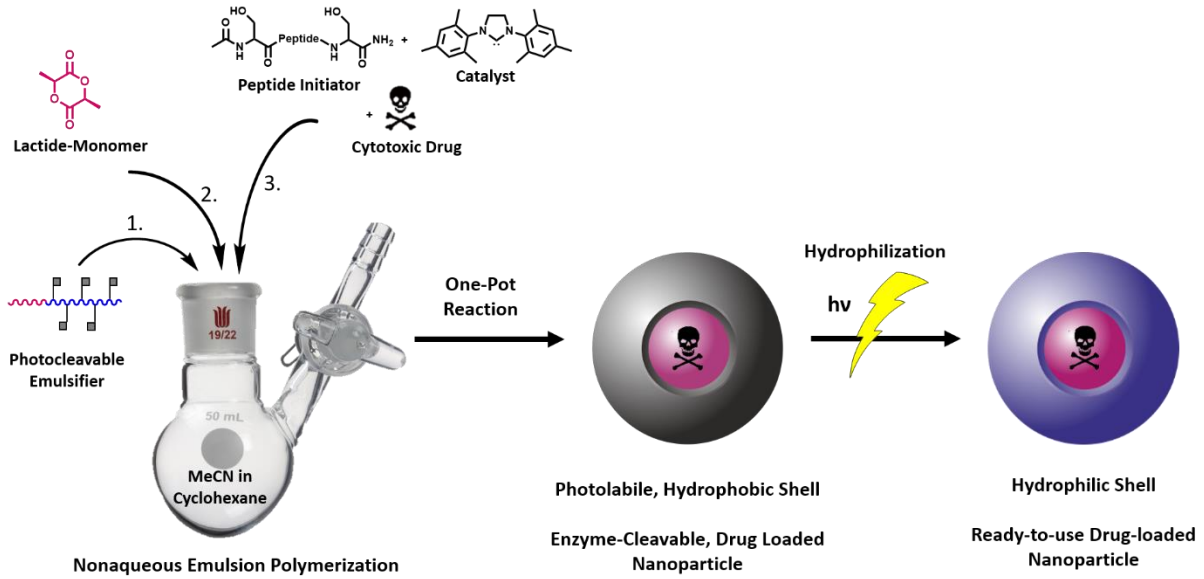

Scheme 6: Schematic overview of the one-pot synthesis of a stimuli-responsive nano carrier system for drug delivery.

The synthetic procedure of the nonaqueous emulsion polymerization consists of three steps (Scheme 7). First, the amphiphilic block copolymer is dispersed in the nonpolar solvent (e.g., cyclohexane) under stirring. The monomer, L-lactide in our case, is dissolved in a polar organic solvent that is immiscible with the nonpolar phase (e.g., MeCN) and added. Ultrasonication is supporting the formation of small droplets. Meanwhile, the drug, bifunctional peptide-based initiator (OH-peptide-OH) and catalyst (SIMes) is dissolved in the polar solvent and added. The polymerization is diffusion-controlled and taking place inside the micellar nanoreactors, resulting in dispersed PLLA nanoparticles. After the polymerization, the reaction mixture is dialysed against water to remove the organic solvents and reagents, followed by hydrophilization of the particles in order to disperse them in the aqueous phase.[50]

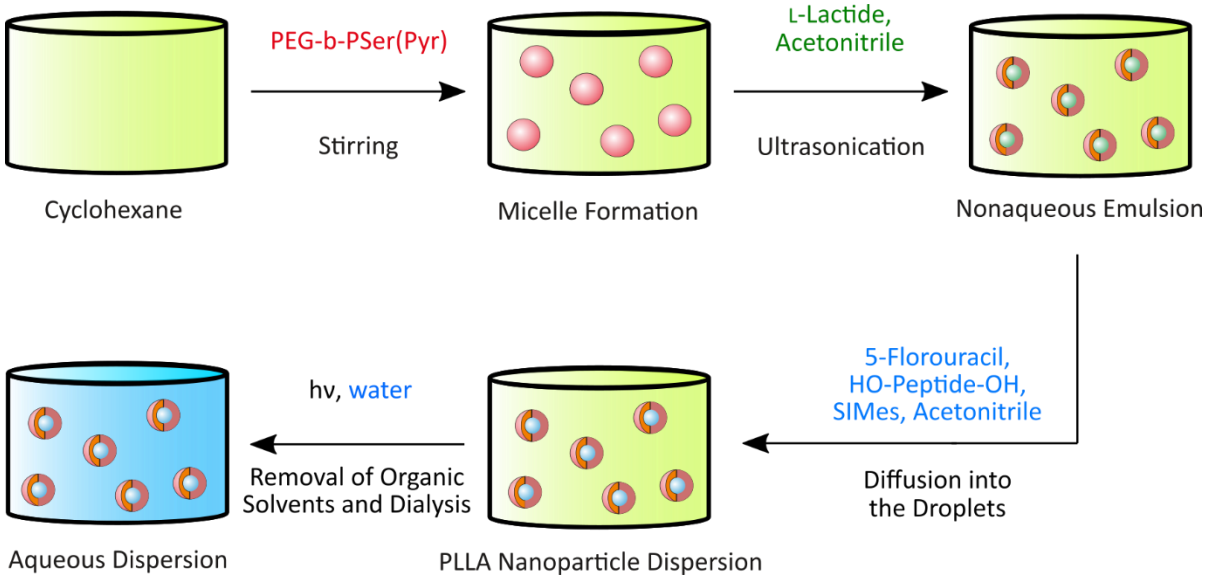

Scheme 7: Schematic step-by-step representation of the nonaqueous emulsion polymerization and particle transfer into aqueous solution.[50]

The enzyme-cleavable polylactide-*b*-PLGLAG-*b*-polylactide triblock copolymer is synthesized by ring opening polymerization (ROP) of L-lactide with the two terminal serine side chains of the peptide sequence (Scheme 8).[15] To avoid potentially cytotoxic metal catalysts in the system, the synthesis is catalysed by the organic NHC-catalyst SIMes, which can be easily removed by dialysis after the reaction. Carrying out the reaction in nonaqueous emulsion, stabilized by a macromolecular emulsifier, is leading to homogeneously dispersed core-shell nanoparticles.[53,67]

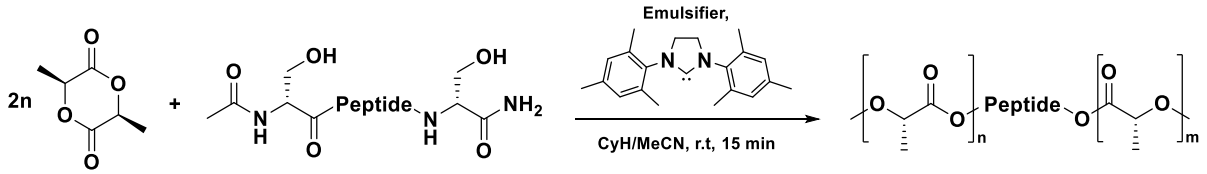

Scheme 8: Synthesis of the enzyme-cleavable triblock copolymer PLLA-b-peptide-PLLA by NHC-catalysed ROP, leading to PLLA nanoparticles stabilized by a macromolecular emulsifier.

After the synthesis, the ready-to-use drug-loaded and enzyme-cleavable core-shell nanoparticles are obtained. In comparison to other carrier systems like micellar structures, the composition of these particles is relatively complex (Figure 10). The particles are composed of a core that contains the encapsulated cytotoxic drug and the hydrophobic and enzyme-cleavable triblock copolymer PLLA-*b*-PLGLAG-*b*-PLLA that is entangled with the hydrophilic PEG block of the emulsifier.[50] The particle shell consists of the hydrophobic block of the emulsifier, in our case a side chain protected poly(amino acid). To promote the enzyme-triggered drug release, the emulsifier in the final system should contain the peptide sequence PLGLAG as well.

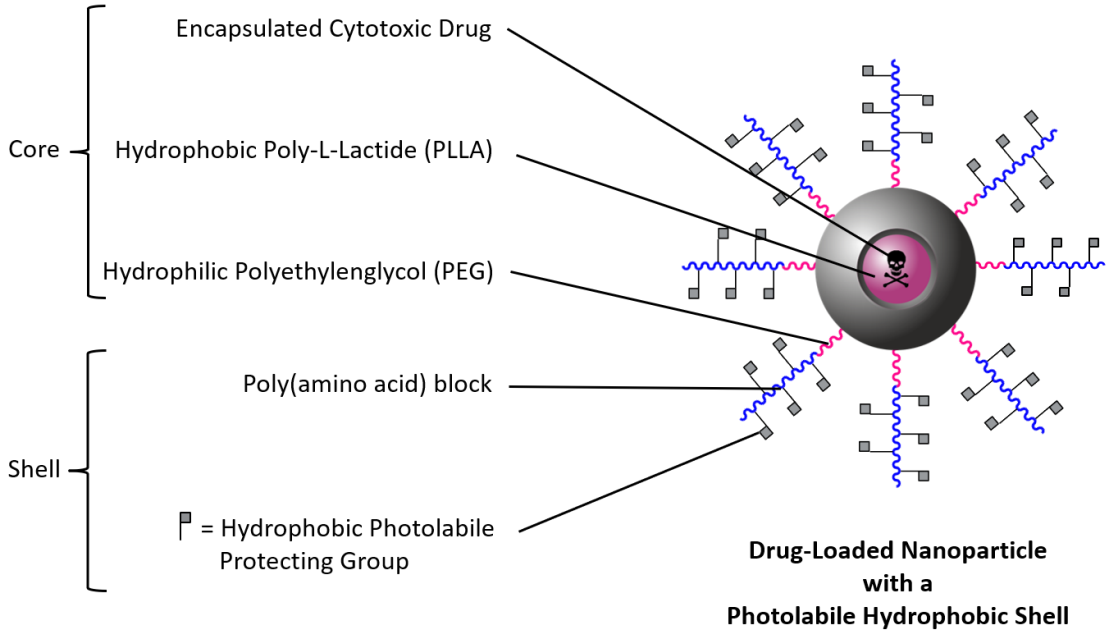

Figure 10: Overview of the composition of the core-shell nanoparticles after synthesis.

AMPHIPHILIC PEG-*b*-POLY(AMINO ACID) BLOCK COPOLYMERS AS BIODEGRADABLE EMULSIFIERS

Due to the hydrophobic surface of the resulting nanoparticles after the synthesis, a direct transfer into aqueous media is not possible. The particle surface needs to be hydrophilized before the introduction into biological environment. There are two options to obtain a hydrophilic particle surface post-synthetically. The first solution is coating the particles with an additional, hydrophilic layer. Typically, a non-ionic surfactant like the PEG-based Lutensol® (BASF) is applied to obtain stable aqueous particle dispersions.[49] This method is well-established, but it is hindering the drug-release mechanism, because the enzyme-responsive peptide sequence is coated with an additional polymeric layer and cannot be approached as easily by the enzyme MMP-2. To overcome this challenge, the second solution is applied by using block copolymers with switchable polarity as emulsifiers (Scheme 9).[53] In this case, the hydrophobic groups at the particle surface are cleaved after the synthesis to enable the

particle transfer into aqueous solution. Polar amino acids, with their functionalizable side chains and good biocompatibility, are the perfect building blocks to face this challenge.

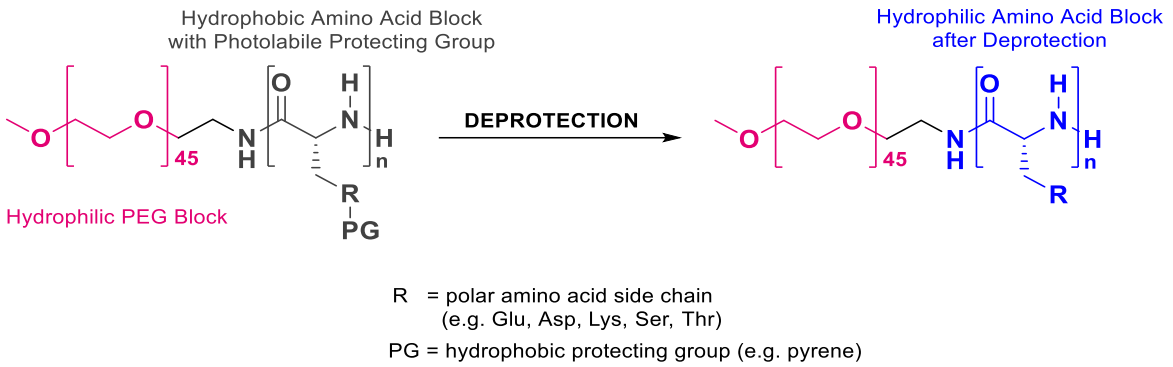

Scheme 9: Deprotection of amphiphilic PEG-b-Poly(amino acid) block copolymers consisting of a hydrophilic PEG block and a hydrophobic amino acid block with hydrophobic, photolabile protecting groups to obtain hydrophilic block copolymers.

Different poly(amino acids) were evaluated in our group regarding their performance as emulsifiers for NEP as well as their behaviour in biological environment. A clear benefit of amino acid-based emulsifiers is their biocompatibility, a mandatory feature for biomedical applications. Formerly, the focus lied on block copolymers containing glutamic acid or lysine. Pyrene-functionalized L-glutamic acid was polymerized and the resulting polymers were established as emulsifiers for nonaqueous emulsion polymerization and PLLA nanoparticles were successfully obtained with the PEG-*b*-PLG(Pyr) block copolymers.[53] After cleavage of the photosensitive pyrene protecting group, the particles were transferred into aqueous solution.[53] While glutamic acid-based polymers were working very well as emulsifiers for the nanoparticle formation, there are some disadvantages of an ionic particle surface in biological environment. The ionic side chain of glutamic acid is leading to particle aggregation in biological media due to low solubility, if the side chain is non-ionized.[72] In contrast, charged molecules are known to enhance protein corona formation in physiological environment, hindering the enzyme-triggered drug-release.[54,57]

SERINE AS A VERSATILE BUILDING BLOCK FOR BIODEGRADABLE BLOCK COPOLYMERS

In order to stay in the family of naturally occurring amino acids several ones with polar nonionic side chains are available, such as serine, threonine and tyrosine, all bearing a hydroxyl group. Conventional poly amino acids of these monomers are poorly reported in the literature despite their potential for drug delivery applications. Functionalization of the serine and threonine side chains is challenging due to low reactivity in standard reactions, like acylation. The activation of the hydroxy group often leads to elimination and formation of dehydroalanine.[73–75] Instead, these hydroxy-containing amino acids are commonly used as initiators for grafting in polymer chemistry.[76] Especially serine, the simplest

hydroxy-containing amino acid, is suitable as polar moiety for nanoparticle surfaces to allow the dispersion of the particles in biological media, as it does not interact as strongly with proteins compared to ionic materials.[54] The synthesis and characterization of various polymers of protected serine derivatives was reported decades ago, but barely developed for further use, although it is a potent building block for copolymer formation und post synthetic functionalization.[73,77,78] A major drawback of poly-L-serine that might explain the lack of interest besides the low reactivity of its side chain is the strong β-sheet formation of chains longer than seven L-serine units, resulting in poor solubility in organic and aqueous solution.[30,78] Yang et al. reported a significant increase of solubility and the degree of polymerization (DP) of poly serine by implementation of different ratios of D- and L-amino acid in order to disrupt the secondary structure of L-serine. Cell viability tests of the deprotected DL-serine polymers showed good results and support the idea of serine containing drug delivery systems.[72] This led to the conclusion that poly serine is a versatile polymer block for the development of biocompatible polymeric nanomaterials like particles or micelles and therefore, its aggregation properties should be studied extensively. Herein, detailed studies about the synthesis and aggregation behavior of L- and DL-serine polymers are presented in order to evaluate their potential as emulsifiers for nonaqueous emulsion polymerization to create nanoparticles with a polar nonionic surface.

3.2 Results and Discussion - Nanoparticle synthesis with *O*-benzyl-serine-based block copolymers as emulsifiers

3.2.1 Synthesis of *O*-benzyl-L-serine-based block copolymers

In this chapter, the synthesis and characterization of *O*-benzyl-serine based block copolymers were discussed. Furthermore, their applicability as emulsifiers in nonaqueous emulsion systems as well as their aggregation behavior in aqueous solution was investigated. *O*-benzyl-protected serine was used as a model system for serine derivatives with a hydrophobic side chain to evaluate its suitability for the fabrication of biodegradable and amphiphilic block copolymers. It is commercially available and the benzyl protecting group is stable against many chemical conditions, like a wide pH range.[79]

Before the polymerization of the poly(amino acid) block was performed, the *O*-benzyl-L-serine was transformed into an active species for ring opening polymerization (ROP), the *N*-carboxy-anhydride (NCA, **1**) derivative, by reaction of the amino acid with triphosgene. The monoterpene α-pinene was used as a scavenger for hydrochloric acid that is released during the reaction.[80] The successful conversion of the amino acid into the NCA **1** was confirmed by NMR spectroscopy (see Appendix, Figure 113 and Figure 114). The cyclic monomer was obtained in good yields of up to 86% and used for ring opening polymerization with either benzylamine or macromolecular mPEG-amine initiators and resulted in homo or block copolymers **2-4** (Scheme 10).[53]

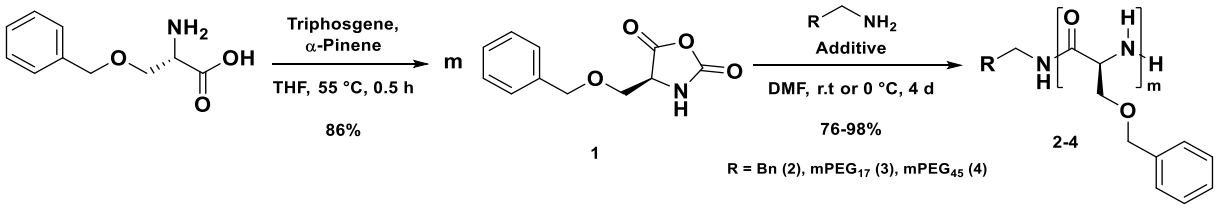

*Scheme 10: Synthesis of L-Ser(Bn)-NCA **1** and ring opening polymerization with benzylamine or mPEG macro initiators resulting in homo or block copolymers **2-4**.*

Amphiphilic emulsifiers for nonaqueous emulsion polymerization (NEP) need a hydrophobic block that is well dispersible in nonpolar organic solvents to form stable emulsions. Kevin Müller suggested a block ratio of 30:70 for classical emulsifiers, like PI-*b*-PMMA, for NEP, while Robert Dorresteijn proposed an ideal block ratio of 1:2 for pyrene-functionalized glutamic acid-based emulsifiers PEG-*b*-PLG(Pyr).[50,52] It was hypothesized that these block ratios are not equally ideal for poly-L-serine, as the chemical structure and polarities of these polymers are clearly different in the serine-based emulsifiers. Similar systems were not used for nonaqueous emulsions in the literature before, and therefore, polymers with various block ratios were synthesized to investigate the ideal block ratio for the PEG-*b*-PLS(Bn) system empirically. The ratio of the hydrophilic PEG and the hydrophobic poly-*O*-benzyl-L-serine (PLS(Bn)) block was varied in a range of 1:1 to 1:3 and the molecular weight ranged from 4-30 kDa (Table 2). In the first approach, the polymerization of the poly-*O*-benzyl-L-serine

block was conducted under standard conditions for ROP at room temperature in DMF. Urea was used as an additive to suppress the formation of secondary structures by inhibiting hydrogen bonding and hence increase the solubility of the polymer during the polymerization.[81,82] The initiator was $mPEG_{45}$-NH_2 (Mn = 2000 Da) for the first experiments to reach a high molecular weight, corresponding to Dorresteijn et al.[53]

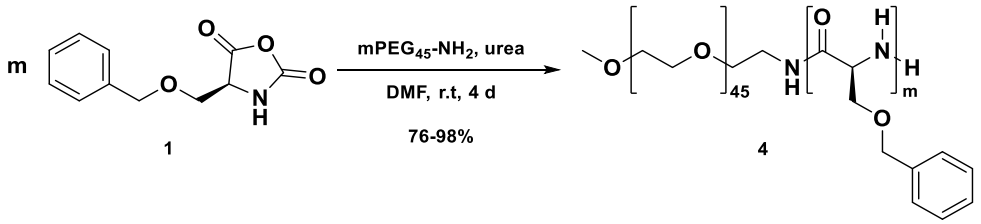

*Scheme 11: ROP of O-Benzylserine-NCA **1** with the $mPEG_{45}$-NH_2 macroinitiator resulted in the amphiphilic PEG-b-PLS(Bn) block copolymer **4**.*

Due to their amphiphilicity, the polymers showed very limited solubility in common solvents. Standard GPC or MALDI-TOF measurements to determine the molecular weight, degree of polymerization (DP) and polydispersity were not possible. The only suitable solvent for these polymers was dimethyl sulfoxide (DMSO). It was used as the deuterated solvent for NMR analysis (Figure 11). Proton was used to calculate the molecular weight and block ratio of the block copolymers and DOSY-NMR spectroscopy was utilized to confirm the covalent binding of the two polymer blocks (Figure 11, green line).

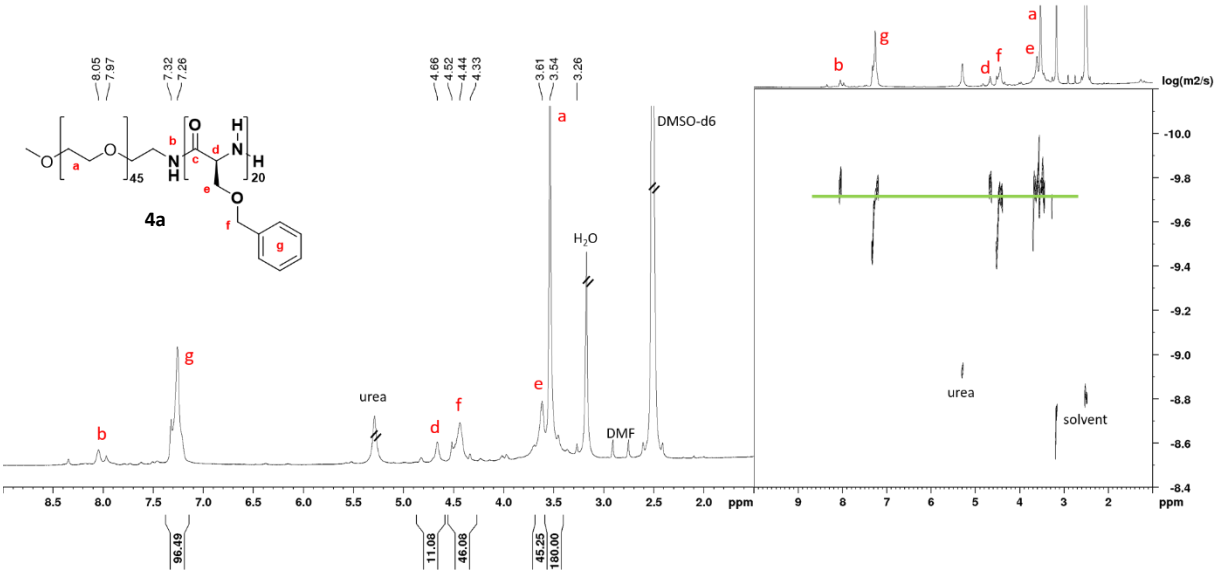

*Figure 11: ^{1}H-NMR and DOSY spectra (700 MHz, 333 K, DMSO-d_6) of the first block copolymer PEG_{45}-b-$PLS(Bn)_{20}$ (**4a**).*

The block ratio was calculated by the signal intensity ratio of the PEG-CH_2 peak at 3.54 ppm and the Benzyl-CH peak of *O*-benzyl-serine at 7.26 ppm. It resulted in a ratio of PEG to PLS(Bn) of 45:20 for the first polymerization, where the theoretical DP was 45 (Table 1, No. **4a**). Hence, the polymerization was not quantitative, which is indicated by a monomer conversion of 45% and a yield of 55%. In contrast, the monomer conversion reached 80% (DP_{exp} = 8), when a block ratio of 45:10 was desired (Table 1,

No. **4b**). Covalent attachment of the two polymer blocks was confirmed by DOSY-NMR. The proton signals of both blocks showed the same diffusion constant and therefore appear on the same level in the DOSY spectrum (Figure 11, green line). In order to optimize the polymerization and increase the DP of the *O*-benzyl-L-serine block to reach the desired block ratio of 1:2, several parameters of the polymerization were changed, apart from the solvent that was *N,N*-dimethylformamide in all experiments (Table 1).

INCREASE OF MONOMER FEED RATIO (DP_{theo}) AND MOLECULAR WEIGHT OF INITIATOR

In the next step, the monomer feed ratio DP_{theo} was increased to 105, which corresponds to a block ratio of 30:70. The approach resulted in a block ratio of 45:32, and therefore in a higher DP than in the first batch. At the same time the conversion was only 30% vs. 45% in the first batch (Table 1, No. **4c**). In the next approach a DP_{theo} of 135 was used and a DP_{exp} of 34 was obtained, indicating that a further increase of molar feed ratio did not result in an increase of the block length (Table 1, No. **4d**).

Table 1: Synthetic details of O-benzyl-L-serine homo and block copolymers, polymerized at room temperature.

No.	Sample	Initiator	DP_{theo} [a]	DP_{exp} [b]	Yield (%)	Mn [b] [Da]	Additive
4a	PEG_{45}-*b*-$PLS(Bn)_{20}$, ncs55	$mPEG_{45}$-NH_2	45	20	55	5500	urea
4b	PEG_{45}-*b*-$PLS(Bn)_{8}$, ncs56	$mPEG_{45}$-NH_2	10	8	80	3400	urea
4c	PEG_{45}-*b*-$PLS(Bn)_{32}$, ncs71	$mPEG_{45}$-NH_2	105	32	80	7600	urea
4d	PEG_{45}-*b*-$PLS(Bn)_{34}$, ncs72	$mPEG_{45}$-NH_2	135	34	78	8000	urea
3a	PEG_{17}-*b*-$PLS(Bn)_{41}$, ncs69	$mPEG_{17}$-NH_2	90	41	53	8000	urea
4e	PEG_{114}-*b*-$PLS(Bn)_{87}$, ncs73	$mPEG_{114}$-NH_2	266	87	79	20 000	urea
4f	PEG_{45}-*b*-$PLS(Bn)_{52}$, ncs97	$mPEG_{45}$-NH_2	150	52	79	11 200	GuHCl
4g	PEG_{45}-*b*-$PLS(Bn)_{57}$, ncs98	$mPEG_{45}$-NH_2	150	57	79	12 000	LiBr

[a] referring to molar feed ratio of monomer and initiator [mmol].
[b] [Mn]: total molecular weight of block copolymer, calculated by ^{1}H-NMR analysis.

In the next step, the molecular weight of the macroinitiator was varied and $mPEG_{17}$-NH_2 (Mn = 750 Da) was used for the polymerization that resulted in a DP_{exp} of 41 for the Poly(*O*-benzyl-L-serine) block (DP_{theo} = 90, conversion = 46%), meaning half of the monomer was consumed during the polymerization and a desirable block ratio of around 30:70 was obtained (Table 1, No. **3a**). The DP, block ratio and the monomer conversion were successfully increased by using a macroinitiator with

lower molecular weight. This can be explained by the lower amphiphilicity due to the lower hydrophilic moiety in the block copolymer. The molecular weight of the initiator was also varied to 5000 Da ($mPEG_{114}$-NH_2), where a DP_{exp} of 87 (DP_{theo} = 266) was obtained for the polypeptide block, corresponding to a conversion of 33% (Table 1, No. **4e**). The theoretical DP of 266 and the block ratio of 1:2 was not reached in this approach. It showed that in principle longer chains of the PLS(Bn) block are possible and correlate with the block length of the initiator. Again, this might be explained by the amphiphilicity of the polymer that led to a decreased solubility hindering further polymerization after reaching a certain block ratio. In conclusion, the block length of the initiator has a high impact on the polymerization of the NCA **1**. It was found to be beneficial to use shorter PEG chains to reach the desired block ratio of the two polymer blocks.

VARIATION OF THE CHAOTROPIC AGENT

According to standard reactions conditions for ROP of amino acid NCAs urea was typically used as a chaotropic agent to disrupt hydrogen bonding in the poly peptide chain and therefore increase its solubility.[81] To evaluate the role of these hydrogen bonding interactions within the poly(amino acid) block and its polymerization and solubility, the chaotropic agent was changed and the reaction was conducted in the presence of guanidine hydrochloride (GuHCl) and lithium bromide (LiBr) instead of urea. According to the Hofmeister series, the addition of salts to a (favorably aqueous) solution has an effect on the formation of hydrogen bonding and hydrophobic effects of a nonpolar molecule in solution.[81,82] Some salts (e.g., fluoride, ammonium ion) promote hydrogen bonding and therefore increase hydrophobic effects, leading to lower solubility of the nonpolar molecule. In contrast, chaotropic salts (e.g., guanidinium, bromide) decrease these effects, leading to the reduction of aggregation and therefor precipitation of the macromolecule from solution.[82] The above-mentioned salts urea, LiBr and GuHCl were evaluated in terms of their effectiveness in disrupting these hydrophobic effects in the ROP of *O*-benzyl-L-serine. The polymerizations were conducted at RT in the presence of either GuHCl or LiBr (Table 1, No. **4f**, **4g**), which resulted in a DP_{exp} of 52 for GuHCl (DP_{theo} = 150, conversion = 35%) and 57 for LiBr (DP_{theo} = 150, conversion = 38%). Even though the theoretical DP was not reached at all, the conversion was increased by 10% for the GuHCl approach and 13% for the LiBr approach in comparison to the previous approach with urea (Table 1, No. **4d**). The LiBr approach was the best result so far, and indicated that hydrogen bonding definitely plays a role in this reaction and can be decreased to some extent by chaotropic agents.

VARIATION OF THE POLYMERIZATION TEMPERATURE AND ATMOSPHERE

In the next step, the polymerization temperature was varied to determine the influence on the monomer conversion and block length of the resulting polymers. The macroinitiator $mPEG_{45}$-NH_2 (Mn = 2000 g/mol) and urea as the chaotropic agent was used. The polymerization temperature was increased from room temperature to 40, 50 and 60 °C. Only the latter could slightly increase the DP_{exp} to 41 (DP_{theo} = 150) at a monomer conversion of 27%. Raising the temperature to 60 °C provided a polymer with a block ratio of almost 1:1 (Table 2, No. **4h**), but it did not lead to major improvement. These results are matching with Vayaboury et al. that demonstrated the presence of a significant amount of dead polymer ends at elevated temperatures.[83] One approach was conducted not only under Argon atmosphere, but under subsequent Argon insertion into the reaction mixture to determine the influence of the in-situ produced carbon dioxide on the polymerization. There is evidence that high amounts of CO_2 in the reaction vessel actively hinders the ROP, as reported by Zou et al.[84] To promote the CO_2 removal, the reaction was conducted at 40 °C, resulting in a polymer with a DP_{exp} of 43 (DP_{theo} = 150, conversion: 29%), indicating that the subsequent removal of CO_2 does not explicitly improve the polymerization of O-benzyl-L-serine (Table 2, No. **4i**).

The next polymerizations were conducted at 0 °C, as suggested by Vayaboury et al., who describe that lowering the polymerization temperature is likely to increase the amount of living polymer ends and at the same time inhibiting possible side reactions, like cyclization or chain termination, without the need of additional reagents.[83,85] Thus, resulting in higher reactivity and eventually longer polypeptide blocks with narrow distribution. The reactions were conducted in the presence of LiBr as chaotropic agent and $mPEG_{45}$-NH_2, $mPEG_{17}$-NH_2 or benzyl amine as initiators. The first approach with $mPEG_{45}$-NH_2 resulted in a DP_{exp} of 54 for the polypeptide block (DP_{theo} = 105) with a monomer conversion of 51% (Table 2, No. **4j**). Therefore, the DP_{exp} is comparable to the approach with LiBr at room temperature, while the monomer conversion is higher. This indicates that it does not matter, if the molar feed ratio is 150 or 105 as both resulted in a DP_{exp} of around 55, which might be the limit of the block length of this building block in terms of solubility. This was different, when $mPEG_{17}$-NH_2 was used as hydrophilic moiety (Table 2, No. **3b**). The DP_{exp} of the polypeptide block was 47 at a DP_{theo} of 50, hence a monomer conversion of 94% was achieved. Again, this proves the higher effectiveness of LiBr as chaotropic agent, compared to urea in approach No. **3a**, where a DP_{exp} of 41 was obtained. In addition, using the shorter PEG_{17}-initiator led to the desired block ratio, in contrast to the PEG_{45}-initiator. The use of the monomer initiator benzyl amine resulted in a quantitative conversion and a homopolymer with a DP_{exp} of 50 was obtained (Table 2, No. **2b**). In summary, lowering the temperature did result in higher DPs, even though the difference for the PEG_{45} block copolymer was marginal. Changing the chaotropic agent to LiBr had a greater effect on the block ratio. For the

PEG_{45}-macroinitiator, the DP of the benzyl serine block was limited to around 55 in the described experiments, where the polymer solubility was decreased dramatically due to its amphiphilicity. This led to precipitation of the polymer during the reaction, hindering further polymerization.

Table 2: Synthetic details of O-benzyl-L-serine homo and block copolymers, polymerized at different temperatures.

No.	Sample	Initiator	DP_{theo} [a]	DP_{exp} [b]	Yield (%)	Mn [b] [Da]	T [c] [°C]	Additive
4h	PEG_{45}-*b*-$PLS(Bn)_{41}$, ncs76	$mPEG_{45}$-NH_2	150	41	82	9200	60	urea
4i	PEG_{45}-*b*-$PLS(Bn)_{43}$, ncs87	$mPEG_{45}$-NH_2	150	43	-	9600	40	urea, Ar-flow
4j	PEG_{45}-*b*-$PLS(Bn)_{54}$, ncs134	$mPEG_{45}$-NH_2	105	54	-	11 500	0	LiBr
3b	PEG_{17}-*b*-$PLS(Bn)_{47}$, ncs135	$mPEG_{17}$-NH_2	50	47	-	9000	0	LiBr
2b	Bn-*b*-$PLS(Bn)_{50}$, ncs136	Bn-NH_2	50	50	-	8900	0	LiBr

[a] referring to molar feed ratio of monomer and initiator [mmol]. [c] During polymerization.
[b] [Mn]: total molecular weight of block copolymer, calculated by ^{1}H-NMR analysis.

In summary, *O*-benzyl-L-serine produced amphiphilic block copolymers (**2-4**) with a hydrophilic PEG block of different block ratios and is therefore a potential material for the synthesis of biocompatible block copolymers. It turned out to be more challenging to polymerize L-serine derivatives compared to other protected polar amino acids like L-lysine or L-glutamic acid due to strong interactions within the polypeptide and the formation of β-sheet structures that affected the solubility of the polymer and further polymerization. The desired block ratio of 2:1 (PEG/PLS(Bn)) was not achieved with a $mPEG_{45}$-NH_2 macroinitiator (Mn = 2000 Da). The amphiphilicity of the polymer and the interactions in the polypeptide block limited the solubility of the polymer leading to precipitation and therefore hindering the further polymerization. Chaotropic agents like urea or lithium bromide were used to decrease hydrogen bonding within the polypeptide chain during the reaction. Replacing urea with LiBr instead of urea and decreasing the polymerization temperature to 0 °C, led to an increase of the DP_{exp} by up to 25%, compared to the use of urea at room temperature. Using a shorter PEG_{17}-NH_2 macroinitiator (Mn = 750 Da) resulted in full monomer conversion and a DP of 50 for the polypeptide, ressembling to the desired block ratio. The suitability of the block copolymers (**3-4**) for nonaqueous emulsion polymerization was evaluated in the next step, to ensure micelle formation in nonpolar solvents. Also, a solution had to be found to overcome the solubility problems of the PEG_{45}-*b*-PLS(Bn) block copolymers (**4**) during the polymerization, to produce high molecular weight polyserine block copolymers with the desired block ratio of 2:1.

3.2.2 Synthesis of *O*-benzyl-DL-serine-based block copolymers

Optimization of the polymerization with the above-mentioned parameters did not result in a major improvement of the poly(*O*-benzyl-L-serine) block length while using $mPEG_{45}$-NH_2 as macroinitiator. While other amino acids like L-glutamic acid or L-lysine are more likely to produce high molecular weight polymers that are well described in the literature, it seems to be more difficult to achieve the same results with serine derivatives.[72,86,87] Each amino acid has a tendency to form either α-helices or β-sheet structures or to disrupt them by the interaction of the amino acid side chains. While L-glutamic acid is commonly forming α-helices, L-serine is a strong β-sheet builder.[88,89] Using different chaotropic agents to disturb hydrogen bonding during the polymerization showed that the formation of secondary structures within the polypeptide chain interferes with further polymerization. Yang et al. showed that Poly-L-serine is challenging to polymerize due to strong β-sheet formation of the L-serine block.[72] One β-turn is constituted of 7 amino acid units and therefore polymerization of long blocks is hard to achieve as the block´s solubility decreases dramatically with each additional monomer unit.[78] While chaotropic agents are working very well for some amino acids yielding in high molecular weight polymers, the β-sheet formation and the resulting intramolecular interactions in the serine polymer chain might be too strong to be significantly influenced by addition of these salts. Amongst others, a common strategy to disrupt these structures and allow the synthesis of high molecular weight poly(amino acids) is building in so-called β-sheet breakers. While certain amino acids are able to suppress the β-sheet formation, the easiest way is using the racemic amino acid instead of the enantiomerically pure L-amino acid. By incorporating the D-amino acid into the polymer chain, the ordered β-sheet structure of L-serine is disrupted leading to random coil formation and the inhibition of hydrogen interactions that are responsible for the decreased solubility.[72,77] In this chapter, the synthesis of racemic poly-DL-serine block copolymers (**6-8**) by ROP is described. Along the lines of the L-serine derivative described above, commercially available *O*-benzyl-DL-serine was transformed into the *N*-carboxy anhydride **5** by triphosgene, followed by ROP of the NCA **5** with benzyl amine or a PEG-based macroinitiator to obtain amphiphilic block copolymers (**6-8**, Scheme 12). The structure and purity of the cyclic NCA **5** was confirmed by NMR spectroscopy (see Appendix; Figure 115, Figure 116).

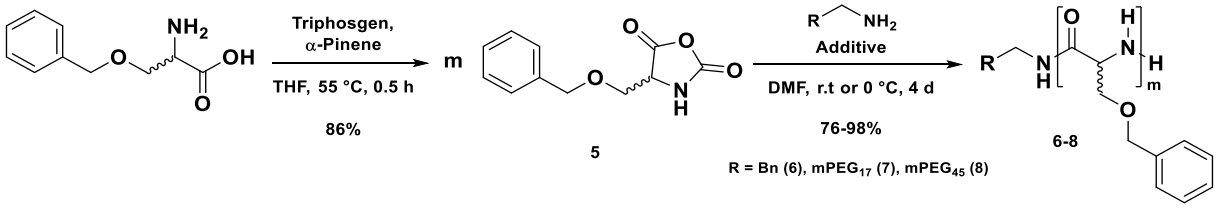

*Scheme 12: Synthesis of DL-Ser(Bn)-NCA **5** and ring opening polymerization with benzylamine or mPEG macro initiators, resulting in homo and block copolymers **6-8**.*

INFLUENCE OF THE CHAOTROPIC AGENT ON THE POLYMERIZATION DEGREE OF POLY BENZYL SERINE

The synthesis of the racemic block copolymers was conducted under various reaction conditions to evaluate, if there is an advantage of using the racemic amino acid compared to the enantiomerically pure L-amino acid (Table 3). First, the polymerization was performed at room temperature to compare the polymerization degree with the L-serine derivative at standard conditions. Urea was added to the reaction to inhibit the formation of secondary structures of the polypeptide chain and to increase the solubility of the polymer. Two experiments with $mPEG_{45}$-NH_2 as the macroinitiator resulted in DPs of the polypeptide block of 32 and 37 (DP_{theo} = 150), corresponding to a monomer conversion of 21% and 25% (Table 3, No. **8a-b**). Therefore, no improvement of the block length of poly(benzyl-DL-serine) was observed. Even the homo polymerization with benzylamine yielded in a DP of 37 at a DP_{theo} of 50, resembling to a monomer conversion of 74%, which is even lower than the best result achieved with L-serine (Table 3, No. **6a**). So far, there was no noteworthy improvement observed by using the racemic polymer instead of the L-serine derivative, when using urea at room temperature. In contrast, replacing urea with LiBr as the chaotropic agent had positive effects on the polymerization that was almost quantitative at room temperature (DP_{exp} = 49, DP_{theo} = 50, monomer conversion = 98%), when the shorter $mPEG_{17}$-NH_2 initiator was used (Table 3, No. **7a**).

*Table 3: Synthetic details of DL-Ser(Bn) homo and copolymers **6-8**.*

No.	Sample	Initiator	DP_{theo}[a]	DP_{exp}[b]	Yield (%)	Mn[b] [Da]	T[c] [°C]	Additive
8a	PEG_{45}-*b*-$PDLS(Bn)_{37}$, ncs100	$mPEG_{45}$-NH_2	150	37	63	7800	RT	urea
8b	PEG_{45}-*b*-$PDLS(Bn)_{32}$, ncs101	$mPEG_{45}$-NH_2	150	32	60	7600	RT	urea
6a	Bn-*b*-$PDLS(Bn)_{37}$, ncs102	Bn-NH_2	50	37	62	5800	RT	urea
7a	PEG_{17}-*b*-$PDLS(Bn)_{49}$, ncs105	$mPEG_{17}$-NH_2	50	49	55	9500	RT	LiBr
6b	Bn-*b*-$PDLS(Bn)_{50}$, ncs113	Bn-NH_2	50	50	quant.	9000	0	LiBr
7b	PEG_{17}-*b*-$PDLS(Bn)_{50}$, ncs112	$mPEG_{17}$-NH_2	50	50	quant.	9600	0	LiBr
8c	PEG_{45}-*b*-$PDLS(Bn)_{150}$, ncs111	$mPEG_{45}$-NH_2	150	150	quant.	28500	0	LiBr

[a] referring to molar feed ratio of monomer and initiator [mmol].
[b] [Mn]: total molecular weight of block copolymer, calculated by ^{1}H-NMR analysis.
[c] During polymerization.

DECREASE OF POLYMERIZATION TEMPERATURE

The next approaches were conducted with LiBr at 0 °C, as these conditions led to the best improvement in the L-serine polymerizations that were discussed before. Again, the initiators $mPEG_{45}$-NH_2 (Mn = 2000 g/mol), $mPEG_{17}$-NH_2 (Mn = 750 g/mol) and benzylamine were used to evaluate the role of the initiator in the reaction. The obtained polymers showed quantitative monomer conversions in all three attempts, which is a major improvement (Table 3, No. **6b, 7b, 8c**). The DP_{theo} of 50 for the polymerizations with benzylamine and $mPEG_{17}$-NH_2 (Table 3, No. **6b, 7b**) was achieved, as confirmed by calculations from the proton NMR. For the third polymerization (Table 3, No. **8c**) with $mPEG_{45}$-NH_2 the DP_{theo} of 150 was obtained, according to the proton NMR spectrum (Figure 12B). This is the highest DP that was obtained with $mPEG_{45}$-NH_2 in all attempts. This result indicated that using a racemic mixture of the serine NCA **5** combined with the right reaction conditions had the expected effect on the reaction and allows the fabrication of high molecular weight poly(*O*-benzyl-DL-serine) block copolymers (**6-8**).

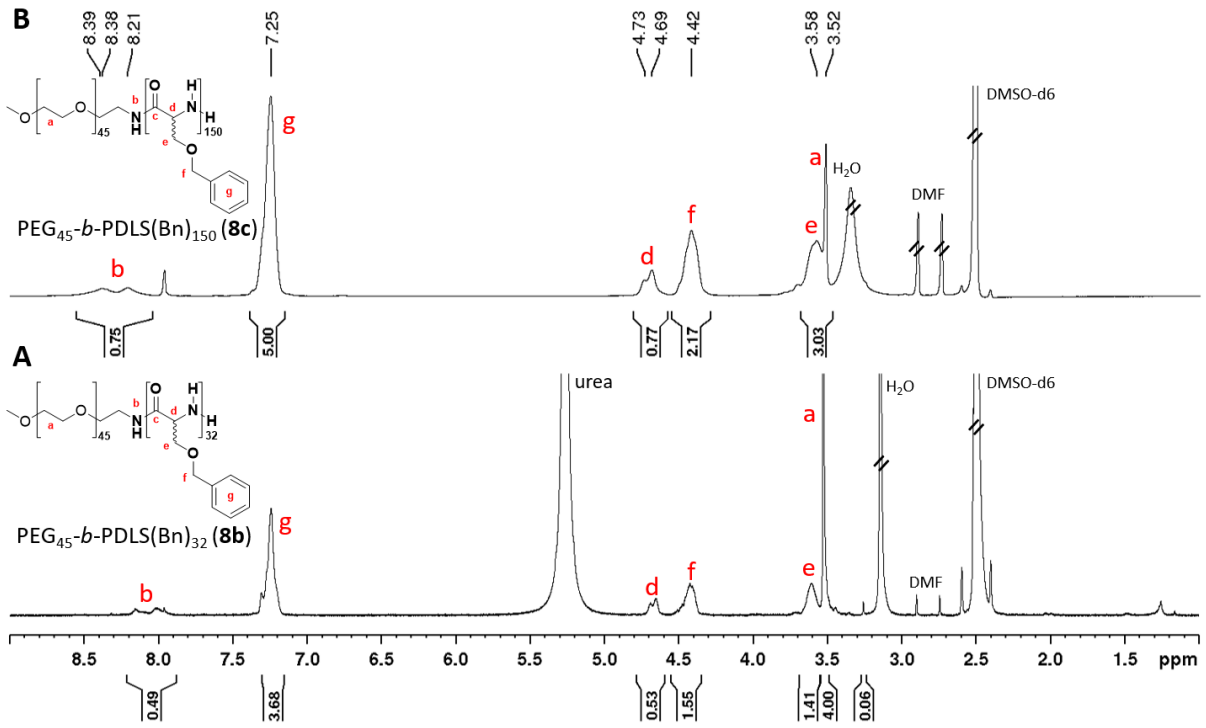

*Figure 12: ^{1}H-NMR spectra (700 MHz, 333 K, DMSO-d_6) of PEG_{45}-b-$PDLS(Bn)_{32}$ (A, **8b**) and PEG_{45}-b-$PDLS(Bn)_{150}$ (B, **8c**).*

The molecular weight and block ratio of the block copolymers was characterized by NMR spectroscopy as GPC analysis was not possible, due to amphiphilicity and limited solubility of the polymers in common solvents. The only suitable solvent for these polymers was dimethyl sulfoxide (DMSO). It was used as the deuterated solvent for NMR analysis (Figure 12). The block ratio was calculated from the signal intensity ratio of the PEG-CH_2 signal (a) at 3.52 ppm and the benzyl-CH signal of PDLS(Bn) (b) at

7.25 ppm in the proton NMR (Figure 12). The block ratios for the two PEG_{45}-*b*-PDLS(Bn) polymers were 45:32 for polymer **8b** (Figure 12A) and 45:150 for polymer **8c** (Figure 12B). The molecular weights were calculated by multiplication of the molecular weight of the monomer unit with the block length and addition of the PEG block and resulted in 7600 Da for PEG_{45}-*b*-$PDLS(Bn)_{32}$ (**8b**) and 28500 g/mol for PEG_{45}-*b*-$PDLS(Bn)_{150}$ (**8c**). By overlaying the spectra of both polymers, it is visible even without the integration that the signal intensity ratio of PEG_{45}-*b*-$PDLS(Bn)_{150}$ (**8c**) is significantly higher than PEG_{45}-*b*-$PDLS(Bn)_{32}$ (**8b**), when comparing the PEG-CH_2 signal with the serine signals. The covalent attachment of the hydrophilic PEG block and the hydrophobic PDLS(Bn) block of the block copolymers was confirmed by DOSY spectroscopy, where the signals of both blocks had the same diffusion constant and therefore belong to the same species. The DOSY spectra of the block copolymers PEG_{45}-*b*-$PDLS(Bn)_{32}$ (**8b**, Figure 13A, green line) and PEG_{45}-*b*-$PDLS(Bn)_{150}$ (**8c**, Figure 13B, green line) showed that all PEG and PDLS(Bn) signals had the same diffusion constant, visualized by the green line. This proved covalent attachment of the two blocks and therefore, the successful synthesis of block copolymers. In contrast, small molecules like the solvents between 2.50-3.33 ppm and urea at 5.28 ppm have different diffusion constants than the polymer species, but comparable values to each other as well.

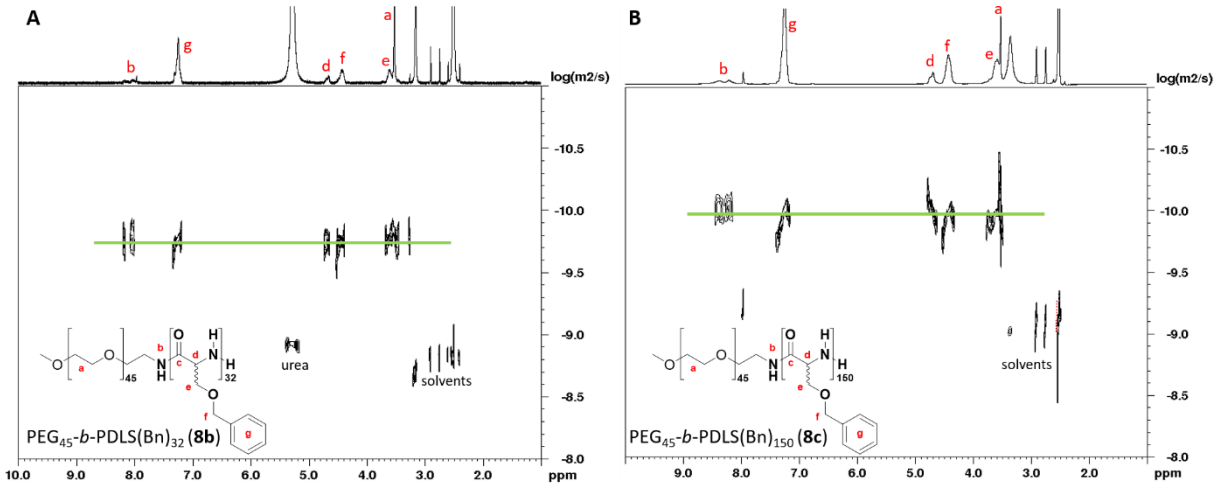

*Figure 13: DOSY-spectra (700 MHz, 333 K, DMSO-d_6) of PEG_{45}-b-$PDLS(Bn)_{32}$ (**8b**, A) and PEG_{45}-b-$PDLS(Bn)_{150}$ (**8c**, B).*

Not only the chemical composition of the synthesized polymers was investigated, but also the secondary structure of the poly-*O*-benzylserine block. In theory, L-serine is expected to form mainly β-sheets within the amino acid chain, while the incorporation of D-serine should lead to the (partial) disruption of the β-sheets and the formation of random coil structures.[72] Commonly, the secondary structure analysis is performed by circular dichroism (CD) spectroscopy, which was performed with the PEG-*b*-PSer(Bn) block copolymers as well. No chirality or secondary structures were detected for both, L- or DL-serine based polymers, during the measurement due to the absorption of the PEG block shielding the signal of the serine motif. PEG is known for steric shielding of proteins and peptides,

altering the results of the measurement.[90] Measuring the homopolymers instead would work in theory to confirm that the lack of signal was caused by the PEG block and not by the racemization of the L-serine block, but their solubility in aqueous solution was very limited. Therefore, FT-IR measurements of the polymers in solid state were performed to analyze the secondary structure of the serine block. The different secondary structures α-helix, β-sheet and random coil of proteins and peptides have IR bands at specific wavenumbers and hence, can be easily identified by the FT-IR spectra.[90–92] Figure 14 shows the FT-IR spectra of a selection of synthesized PEG-*b*-PSer(Bn) polymers.

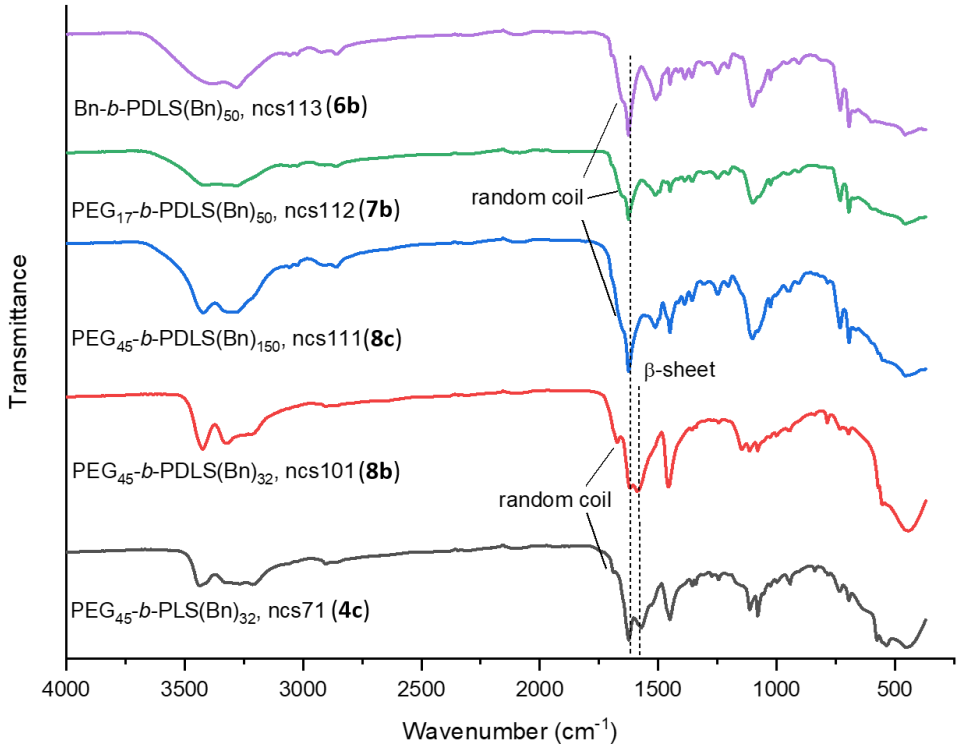

Figure 14: FT-IR spectra of L- and DL-serine polymers to compare the secondary structure depending on the polymerization temperature and polymer composition. Poly-L-serine shows pure ß-sheet conformation, indicated by the amide band I at 1618 and 1623 cm^{-1}, respectively, and the amide band II at 1586 and 1576 cm^{-1} (dotted line). The DL-polymers, synthesized at 0 °C, show both, ß-sheet and random coil formation, as expected.

The L-serine polymer PEG$_{45}$-*b*-PLS(Bn)$_{32}$ (**4c**, black) showed almost pure β-sheet structure as expected, indicated by the amide band I at 1618 and 1623 cm^{-1}, respectively, and the amide band II at 1586 and 1576 cm^{-1} (dotted line). The DL-serine equivalent PEG$_{45}$*b*-PDLS(Bn)$_{32}$ (**8b**, red) that was synthesized at room temperature, showed mostly β-sheet structure, but also random coil formation (amide band at 1656 cm^{-1}), as expected. This indicates that L-serine was polymerized preferentially in comparison to the D-amino acid. This preference was successfully challenged by polymerization of racemic *O*-benzyl-serine at 0 °C in the presence of LiBr, as the spectra of Bn-*b*-PDLS(Bn)$_{46}$ (**6b**, violet), PEG$_{17}$-*b*-PDLS(Bn)$_{50}$ (**7b**, green) and PEG$_{45}$-*b*-PDLS(Bn)$_{150}$ (**8c**, blue) showed. While β-sheets are still present (amide band at 1623 cm^{-1}), random coil structures were observed with significant intensity as well (amide band at 1656 cm^{-1}). Nevertheless, IR analysis clearly demonstrated that β-sheets are the

dominant secondary structure in the poly(*O*-benzyl-serine) chain. In conclusion, IR spectroscopy revealed the secondary structure of the polymers and demonstrated that the polymerization with racemic serine is successfully promoting the formation of random coil structures and minimizing the formation of rigid β-sheets when conducted under the right reaction conditions.

HYDROPHILIZATION OF THE BLOCK COPOLYMERS

In the next step, the cleavage of the benzyl protecting group in the polymer side chain was studied. The easy and reliant removal of the hydrophobic protecting group is an essential step of the nanoparticle synthesis to reveal the polar nature of the amino acid on the particle surface and allow the particle transfer into aqueous solution. Numerous conditions for the cleavage of benzyl protecting groups are reported in the literature, of which two of the main strategies were applied and tested.[79] First, cleavage by catalytic hydrogenation was performed in the presence of the common hydrogenation catalyst palladium on carbon (10 wt%) in a hydrogen atmosphere. The second attempt was done by acetic acid solution of hydrogen bromide in trifluoro acetic acid. The conversion of both experiments was monitored by NMR spectroscopy and revealed that no or only partial cleavage took place in both reactions after 1-2 days. A reason for the failed cleavage by hydrogenation might be the limited solubility of the amphiphilic starting material in various organic solvents, including common solvents for this reaction like methanol and tetrahydrofuran. This might have inhibited the quantitative reaction of the polymer with the catalyst. In contrast, the polymer was soluble in the HBr/TFA mixture, thus no quantitative cleavage was observed, even at high amounts of the reagents. Consequently, this protecting group is not fully compatible with our nanoparticle concept. Reliable cleavage of the protecting groups is required to hydrophilize the particle surface and make them dispersible in aqueous solution. In addition, mild reaction conditions of the cleavage are important to prevent particle degradation. Therefore, mild alternatives, like photolabile protecting groups, were evaluated subsequently, as reported by Dorresteijn et al.[53]

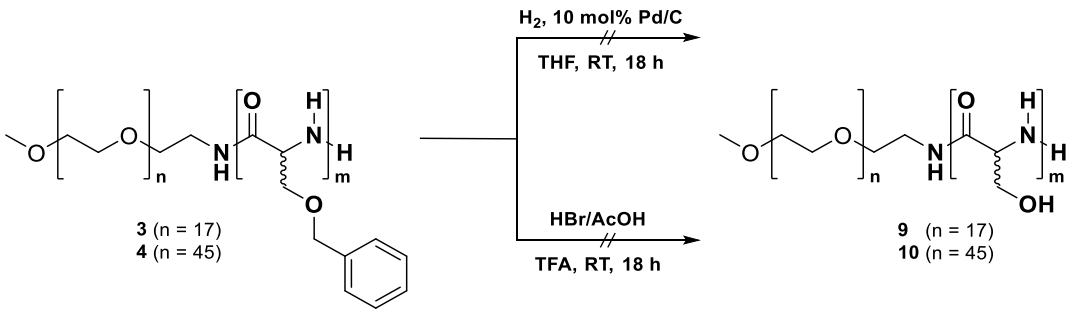

Scheme 13: Cleavage of benzyl protecting group by catalytic hydrogenolysis or under acidic conditions.

3.2.3 Nonaqueous emulsion polymerization with the *O*-benzyl-L-serine-based block copolymers

In the next step after the synthesis and characterization of the block copolymers, their performance as emulsifiers in nonaqueous solution was evaluated. Nonaqueous emulsion polymerization (NEP) is conducted in a mixture of two immiscible organic solvents, where the continuous phase is nonpolar, while the dispersed phase is polar. It is a water-free, oil-in-oil (o/o) emulsion. Addition of an emulsifier leads to the formation of reversed micelles, with the hydrophobic moiety pointing out to the continuous phase, stabilizing the droplets of polar solvent.[52] The whole process of emulsion formation is highly complex and relies on many different parameters, like chemical composition of the emulsifier, the ratio of hydrophobic to hydrophilic moiety, temperature, solvents, surface tension, etc.[36,70] Introducing novel polymers as versatile emulsifiers for nonaqueous emulsion is therefore a challenge itself and requires intense study and optimization. In our group, Robert Dorresteijn and Filiz Karagöz were able to use amphiphilic PEG-*b*-Polypeptide block copolymers as emulsifiers for NEP, using protected L-glutamic acid and L-lysine as hydrophobic blocks.[53] The following chapter is discussing the beforementioned PEG-*b*-PSer(Bn) polymers as potential emulsifiers for NEP. The amphiphilic polymers were synthesized for the use as emulsifiers in nonaqueous emulsion polymerization. Typically, the emulsifier was dissolved in the nonpolar organic solvent leading to a reversed micelle solution. The reagents, including the monomer L-Lactide, SIMes catalyst and an initiator, were dissolved in a polar organic solvent and added stepwise, resulting in poly-L-lactide core shell nanoparticles (**11**, Scheme 14).[53]

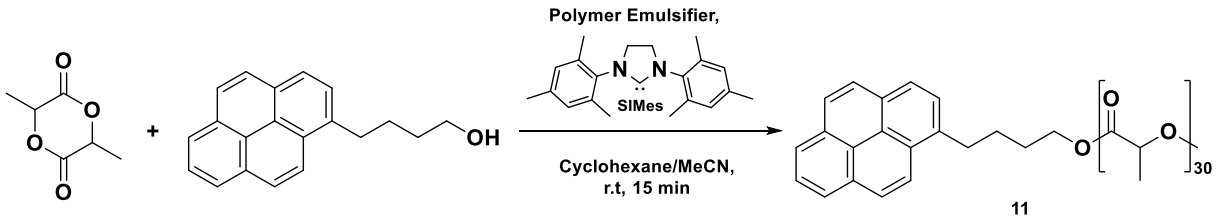

Scheme 14: Synthesis of PLLA nanoparticles with a pyrene butanol initiator and NHC catalyst SIMes by nonaqueous emulsion polymerization, stabilized by a polymer emulsifier.

PEG-*b*-poly-*O*-benzylserine polymers were not used as emulsifying agents before and little was known about their aggregation behaviour in either aqueous or nonaqueous solution. Therefore, a synthesis of the nanoparticles with an established emulsifier was performed first, in order to get a model system for comparison. The block copolymer polyisoprene-*b*-poly(methyl methacrylate) (PI-*b*-PMMA) is well established for emulsion polymerization applications.[52] It was synthesized by anionic polymerization by [redacted] and used for the following emulsion polymerization reaction.

SYNTHESIS OF A MODEL SYSTEM USING THE EMULSIFIER PI-*b*-PMMA FOR THE NEP OF PLLA

Introducing novel block copolymers as emulsifiers for nonaqueous emulsion polymerization can be challenging, if the polymers are not behaving like classical polymers. In order to get familiar with the NEP system, it was started with a model reaction using the block copolymer PI-*b*-PMMA, which is an established emulsifier for nonaqueous emulsions.[71] For the synthesis of the PI-*b*-PMMA-coated particles, the emulsifier was dissolved in cyclohexane under argon atmosphere and stirred overnight until fully dissolved. The L-lactide monomer was dissolved in acetonitrile and added to the emulsion, followed by 15 minutes of ultrasonication to enhance the diffusion of the monomer solution into the micelles. Then, the initiator 1-pyrenebutanol and the catalyst SIMes were dissolved in acetonitrile and added dropwise to the reaction mixture under vigorous stirring. 1-Pyrenebutanol was used as the initiator, because it is easy to identify in various characterization methods due to its remarkable aromatic system. The polymerization of the poly-L-lactide (PLLA) particles is limited by the diffusion of all reactants into the micellar core, and is therefore a diffusion-controlled reaction.[37,39] This mechanism is of importance, when evaluating the reaction time and monomer conversion. In comparison to a polymerization in solution, the reaction time can be higher in emulsion. The reaction was quenched by addition of a drop of acetic acid after 15 minutes. Size and morphology of the particles were analysed by DLS and SEM measurements (Figure 15). The DLS measurement resulted in a narrow size distribution and particle diameter of d_H = 100 (± 8.5) nm, as expected, and was confirmed by SEM measurements that showed homogeneously dispersed particles of spherical shape.

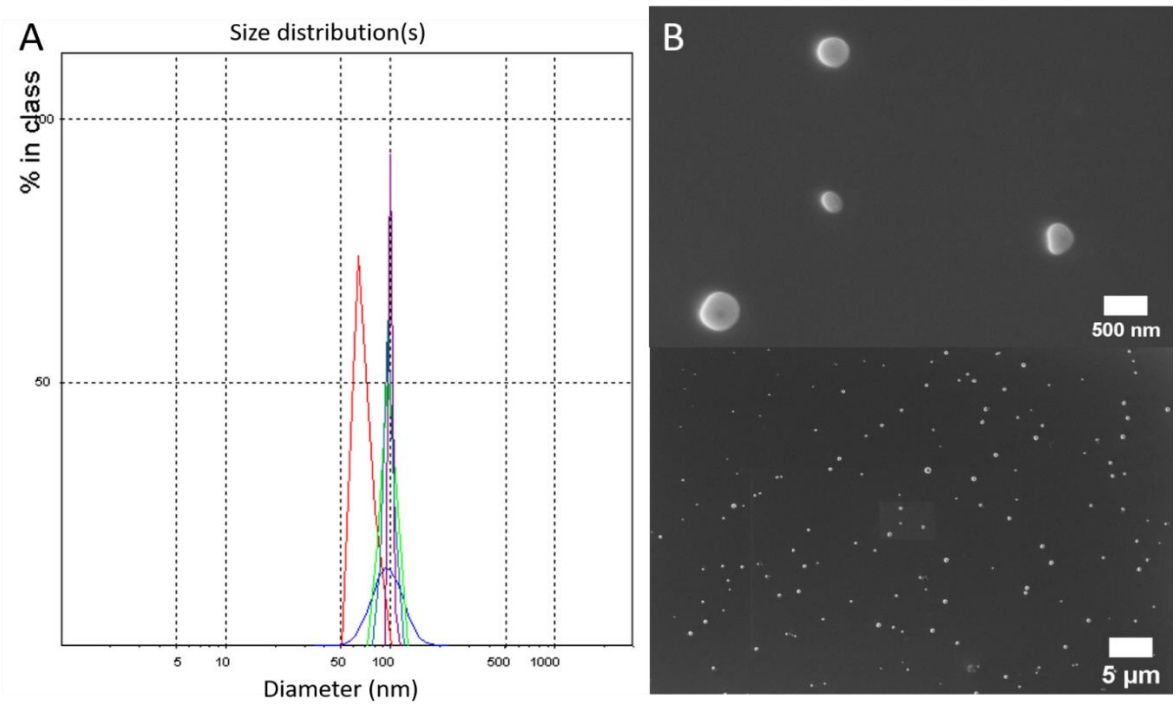

Figure 15: A) Size distribution of the PMMA-coated PLLA nanoparticles in cyclohexane, measured by DLS (d_H = 100 nm), and B) SEM images (d = 100 nm) of the PLLA particles after polymerization.

This synthetic protocol was resulting in homogeneously dispersed PLLA core shell nanoparticles with a desired diameter of 100 nm, when a well-dispersible emulsifier is used. In order to remove excess reagents and solvents, nanoparticles can be purified by different methods, of which some are more suitable for our system than others.[93] Typically, centrifugation is applied, which often results in irreversible agglomeration of soft particles, restraining proper redispersion. More gentle methods are sedimentation or dialysis of the particles to remove impurities. In either way, drying processes of the particles after the workup often lead to the formation of large aggregates.[93,94] In the case of the PMMA-coated PLLA nanoparticles, precipitation in methanol and drying was performed, followed by redispersion by stirring of the particles in cyclohexane for three days and occasional ultrasonication for 5 minutes. The particle diameter, determined by DLS, was d_H = 260 (± 210) nm and therefore doubled in size compared to the sample after the polymerization. While the particles were obtained with a narrow size distribution after the polymerization, they showed a broad size distribution after the redispersion including larger aggregates of around 1 µm (Figure 16A). The majority of particles were still in the 100 nm range, but some larger aggregates were present as well. SEM measurements confirmed the results of the DLS measurement, showing the presence of larger aggregates as well as properly dispersed particles after redispersion (Figure 16B). Overall, the redispersion of the dried particles was successful as most of the aggregates were redispersed by stirring and ultrasonication, which could be improved potentially by longer times of both, stirring and ultrasonication or alternatively, by more high-impact methods like high pressure homogenization.[95]

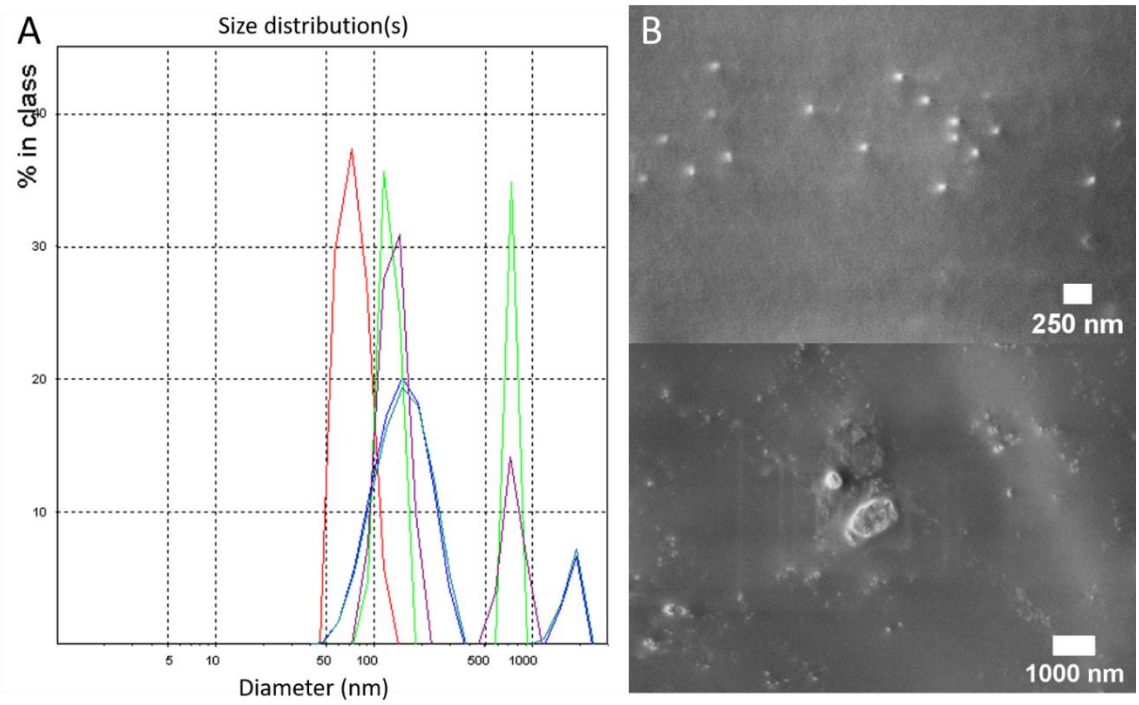

Figure 16: A) Size distribution of the PMMA-coated PLLA nanoparticles after redispersion in cyclohexane, measured by DLS, and B) SEM images of the PLLA particles after redispersion.

PEG-*b*-PLS(Bn)-STABILIZED NONAQUEOUS EMULSIONS

After introducing the model system with the PI-*b*-PMMA emulsifier for the fabrication of coated PLLA nanoparticles by nonaqueous emulsion polymerization, the PEG-*b*-PLS(Bn) block copolymers (**3**-**4**) were evaluated as potential emulsifiers for NEP. Polymers with various block ratios were tested to find the most suitable one to obtain monodispersed nanoparticles of proper size with diameters of around 100 nm. Therefore, the beforementioned experimental procedure was used (p. 33, Scheme 14), where the emulsifier was dissolved in the nonpolar solvent and stirred overnight, before the polymerization was conducted. During this study, not only polymers with varying block ratios were used, but also different emulsifier concentrations, reaction times and solvent systems were tested to obtain optimal results.

INITIAL NEP WITH A SERINE-BASED BLOCK COPOLYMER

In the first approach of NEP, PEG_{45}-*b*-$PLS(Bn)_{20}$ (**4a**) with a weight ratio of around 40:60 was tested. In The emulsifier was used at a concentration of 2.43 mg/mL in the MeCN/CyH solvent system. Even though the polymer was mostly, but not fully dissolved after 16 h of stirring and occasional ultrasonication, the emulsion polymerization was performed, followed by SEM measurements. The SEM images showed spherical particles with a diameter of around 1 µm, as well as some larger aggregates. The aggregates might have consisted of the excess, undissolved emulsifier or larger micelles that cannibalized smaller micelles, resulting in large structures (Figure 17).[94,96] Due to the present aggregates and large diameters of the particles, some optimization of the reaction was necessary, but this first result was a positive start for this study, as spherical particles were obtained.

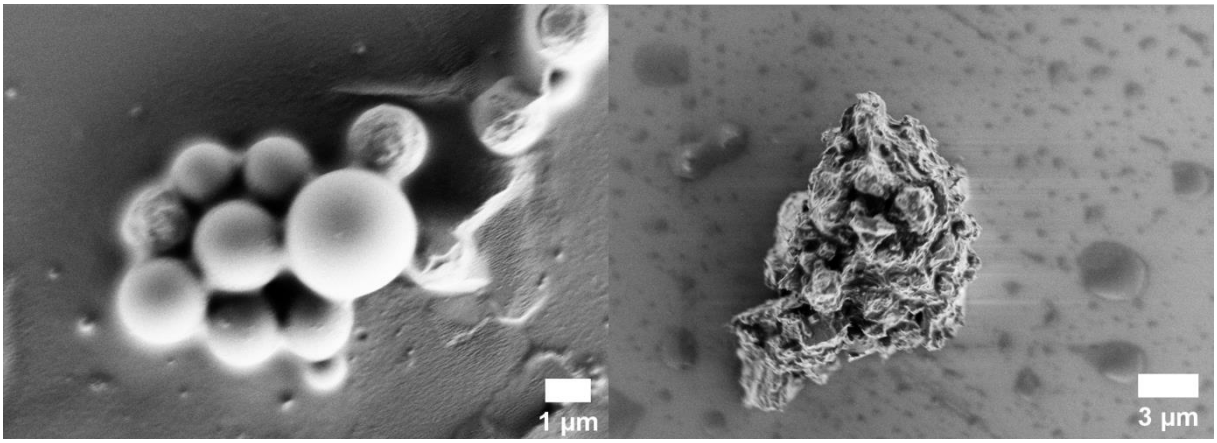

*Figure 17: SEM images of the PLLA nanoparticles after NEP with the emulsifier **4a**.*

In addition, DOSY-NMR spectroscopy was conducted to evaluate the diffusion constants of the emulsifier shell and the Pyrene-*b*-PLLA core. In theory, showing the same diffusion constant is not the ultimate confirmation of core shell nanoparticle existence. Nevertheless, it definitely proves successful block polymerization of L-lactide, whereas different diffusion constants are indicating the coexistence

of polymer and oligomer or monomer species in the solution. The DOSY spectrum showed that the signals of PEG-*b*-PLS(Bn) (**4a**), PLLA and the initiator pyrene show the same diffusion constant (green line), indicating that PLLA was polymerized successfully (Figure 18). In contrast, the monomer signals of the SIMes catalyst, the solvents were visible between 2.00-3.33 ppm below the green line.

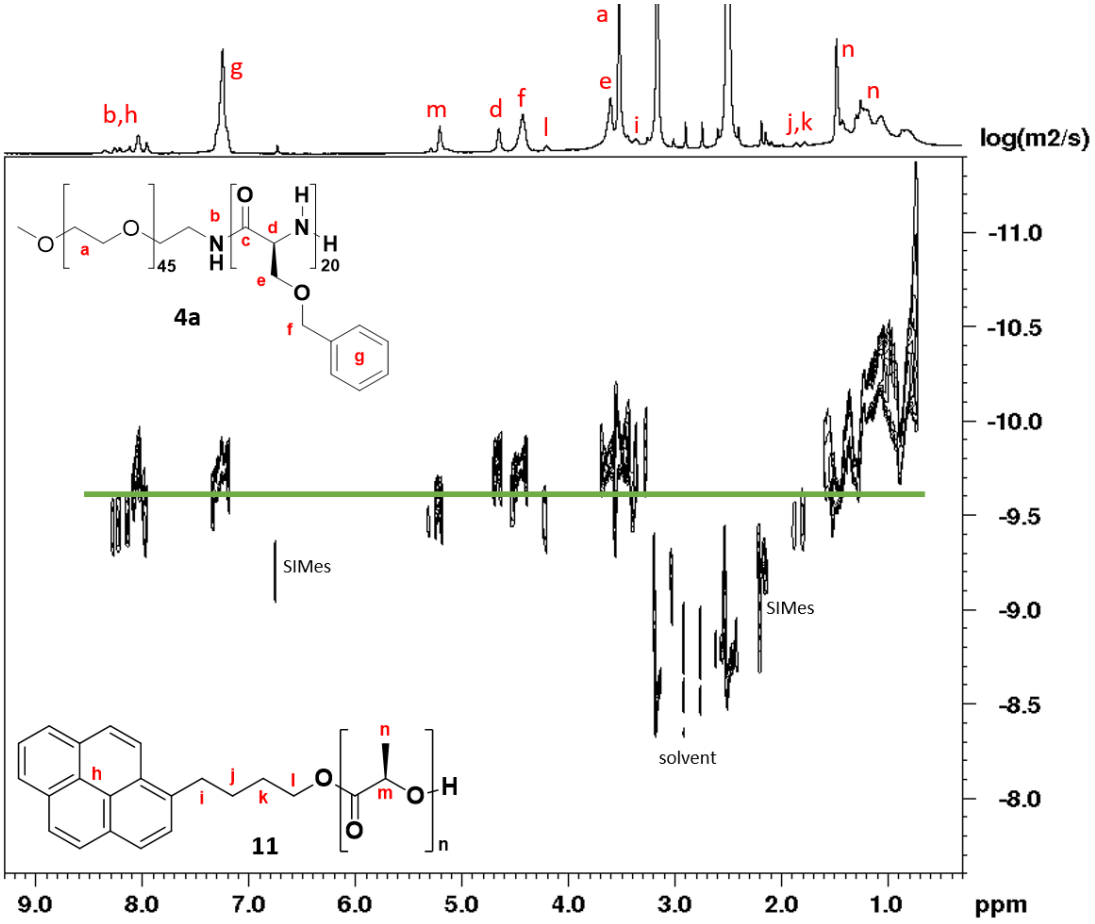

*Figure 18: DOSY-NMR spectrum (700 MHz, 298 K, DMSO-d_6) of the PLLA particles using the emulsifier PEG_{45}-b-$PLS(Bn)_{20}$ (**4a**).*

The polymerization degree of the PLLA was calculated by the signal intensity ratio of pyrene and lactide signals in the proton NMR. It has to be noted that when the nanoparticle core is properly coated and therefore solvent free, it is existing in solid phase and its signals can be barely or not visible at all, as it has low to no relaxation in solid state when measuring solution NMR.[97] Therefore, determination of the DP of PLLA by proton NMR is not quantitative, but can indicate successful polymerization. This was especially observed in the proton NMR of the PI-*b*-PMMA coated nanoparticles, where the PLLA core signals of the particles were barely visible, so that the success of the polymerization needed to be confirmed by further analysis. However, in the case of the PEG-*b*-PLS(Bn) coated particles the PLLA signals were visible (Figure 19, blue), as well as the signals of the emulsifier (red).

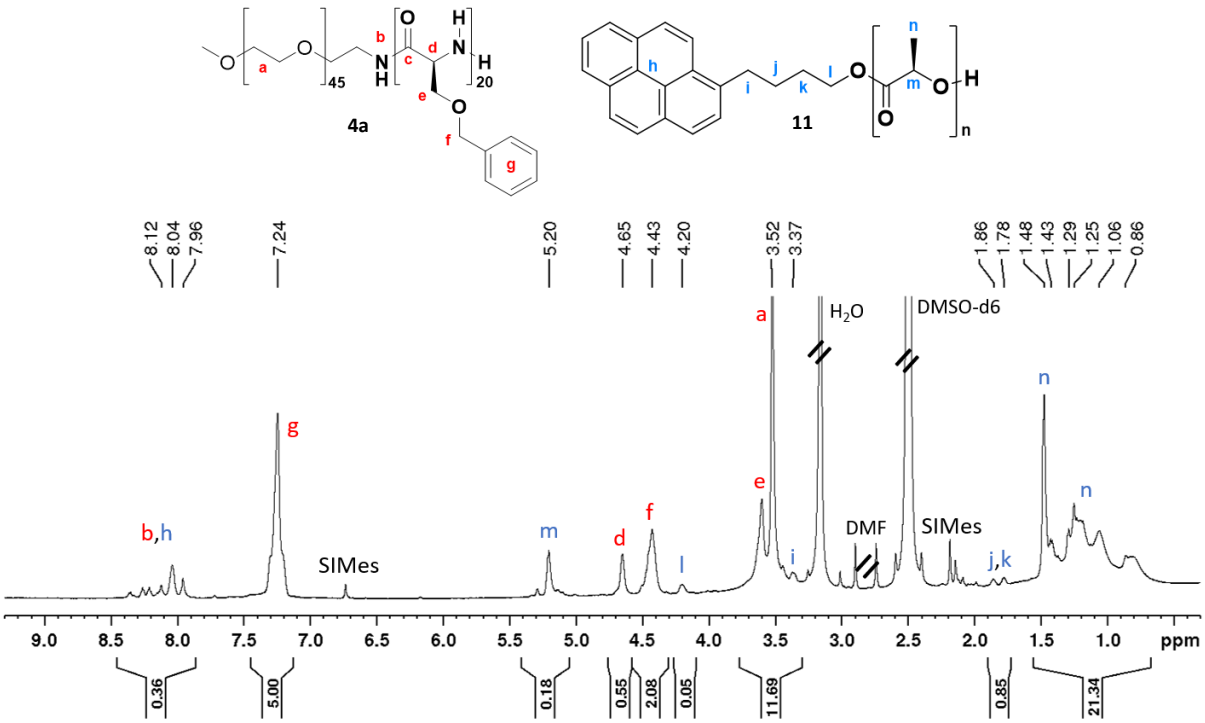

*Figure 19: 1H-NMR spectrum (700 MHz, 333 K, DMSO-d_6) of PEG_{45}-b-$PLS(Bn)_{20}$-coated (**4a**, red) PLLA (blue) nanoparticles.*

EMULSION FORMATION EXPERIMENTS

After the first emulsion polymerization, emulsion formation studies were conducted with PEG_{45}-*b*-$PLS(Bn)_{20}$ (**4a**, Table 4, No. **1-3**) to investigate the aggregation behaviour before further polymerization. The block copolymer with a weight ratio of around 40:60 was dissolved in either cyclohexane or acetonitrile, stirred and ultrasonicated, before DLS measurements were performed.

Table 4: DLS measurements after emulsion formation with PEG_{45}-b-$PLS(Bn)_{20}$ (ncs55) and PEG_{45}-b-$PLS(Bn)_8$ (ncs56).

No.	Emulsifier	Solvent	c [mg/mL]	d_H [µm]
1	PEG_{45}-*b*-$PLS(Bn)_{20}$, **4a**	CyH	2.43	> 10
2	PEG_{45}-*b*-$PLS(Bn)_{20}$, **4a**	CyH	1.22	-[1]
3	PEG_{45}-*b*-$PLS(Bn)_{20}$, **4a**	MeCN	2.43	2.65 ± 2.50
4	PEG_{45}-*b*-$PLS(Bn)_8$, **4b**	CyH	2.43	-[1]
5	PEG_{45}-*b*-$PLS(Bn)_8$, **4b**	MeCN	2.43	0.21 ± 0.01

[1] DLS measurement could not be performed due to aggregation and precipitation of the emulsifier.

First, the polymer was dissolved in cyclohexane at concentrations of 2.43 mg/mL and 1.22 mg/mL for direct comparison. The solution with higher polymer concentration resulted in large µm-sized aggregates that exceeded the measuring range of the DLS machine (> 10 µm). At c = 1.22 mg/mL, the emulsifier was not dispersible, and DLS measurements were not possible (Table 4, No. **2**). Hence, lowering the concentration did not result in optimization of the emulsion. In contrast, dissolving the

polymer in acetonitrile at c = 2.43 mg/mL resulted in slightly better dispersed emulsions with particle diameters of around 2 µm, according to the DLS measurement. This led to the conclusion that the block ratio of this polymer might not be suitable for emulsion polymerization in the MeCN/CyH solvent system, even though the block ratio was close to the proposed 1:2 ratio, reported by Dorresteijn et al. for similar systems.[15] The block copolymer PEG_{45}-*b*-$PLS(Bn)_8$ (**4b**) with a shorter hydrophobic block was tested as well (Table 4, No. 4). Its weight ratio of around 60:40 was inverted to PEG_{45}-*b*-$PLS(Bn)_{20}$ (**4a**). It was not expected to form stable emulsions in cyclohexane, as its hydrophobic block was too short and hence, not hydrophobic enough, to properly stabilize the emulsion. And indeed, the polymer did not dissolve in cyclohexane at all. In contrast, in polar acetonitrile it was fully dissolved and produced a monodispersed emulsion with particle diameters of 200 nm, correlating with the proposed the 1:2 ratio (Table 4, No. 5).[50] While the proposed weight ratio worked for the formation of a polar emulsion in acetonitrile with the polymer PEG_{45}-*b*-$PLS(Bn)_8$ (**4b**), PEG_{45}-*b*-$PLS(Bn)_{20}$ (**4a**) did not produce the same results in nonpolar solvents, despite its fitting weight ratio. At this point, a closer look was taken on the definition of the term “block ratio” of a polymer. While our group, amongst others, commonly used this term in regards of the polymerization degree of the two polymer blocks, the term is widely used in the literature as the molecular weight ratio of the blocks.[71,98] In classical polymers, like PMMA-*b*-PI, where both monomers have a comparable molecular weight, it does not make any significant difference, which definition for block ratio is used. In contrast, in the PEG-*b*-PSer(Bn) block copolymer the molecular weight of the PEG monomer is dramatically lower than of the serine monomers ($\Delta > 130$ g/mol). It makes a significant difference, if the molecular weight or DP ratio is taken into account, making it difficult to make reasonable comparisons with other block copolymers, when talking about the block ratio. This is clearly displayed in Table 5, where the DP ratio and weight ratio was almost inverted for most of the polymers. The second polymer showed very different values for the two ratios as well. A valid comparison with classical polymers is not reliable at all. In this work it will be differentiated between the DP and weight ratio. In order to optimize the stability of the emulsion, polymers with increased hydrophobic moieties were tested for emulsion formation in cyclohexane and emulsion polymerization. While the DP ratio of these polymers is between 50:50 and 60:40, the weight ratio of all these polymers is roughly meeting the desired value of 30:70, which was reported by Müller et al. for classical emulsifiers (Table 5).[52] All these polymers were tested to determine, if there was any difference in their ability to form stable emulsions in nonpolar solvents.

*Table 5: Overview of tested emulsifiers **4a-b** in comparison with **4d-n** with higher block lengths.*

No.	Polymer	DP_{PEG}	$DP_{PSer(Bn)}$	DP ratio	Weight ratio	Mn[a] [Da]
4a	PEG_{45}-*b*-$PLS(Bn)_{20}$	45	20	70:30	37:63	5500
4b	PEG_{45}-*b*-$PLS(Bn)_{8}$	45	8	85:15	58:42	3400
4c	PEG_{45}-*b*-$PLS(Bn)_{32}$	45	32	58:42	26:74	7600
4d	PEG_{45}-*b*-$PLS(Bn)_{34}$	45	34	57:43	25:75	8000
4m	PEG_{45}-*b*-$PLS(Bn)_{35}$	45	35	56:44	24:76	8200
4n	PEG_{45}-*b*-$PLS(Bn)_{38}$	45	38	54:46	23:77	8700
4h	PEG_{45}-*b*-$PLS(Bn)_{41}$	45	41	52:48	22:78	9200

[a] [Mn]: total molecular weight of block copolymer, calculated by ^{1}H-NMR analysis.

INFLUENCE OF A HIGHER HYDROPHOBIC MOIETY IN THE EMULSIFER ON THE NEP

While the polymer PEG_{45}-*b*-$PLS(Bn)_{32}$ (**4c**, weight ratio 26:74) did not show any solubility in cyclohexane and therefore no emulsion polymerization could be performed, the polymer PEG_{45}-*b*-$PLS(Bn)_{34}$ (**4d**), with almost identical weight ratio of 25:75, showed moderate solubility in cyclohexane and emulsion polymerization was performed. This very different behaviour of the two polymers was not expected, as they practically have the same block ratio, and are meeting the desired value of 30:70, at least in terms of weight ratio. A possible explanation might be a notable difference in the polydispersity, which could not be determined, as GPC measurements could not be performed and polydispersity is not measurable by NMR. In general, a broader polydispersity is considered more favourable for emulsion formation. The range of the block length of the polymer chains is broader and can arrange more easily into stable micelles by raising the free energy barriers of micelle formation and dissolution. This results in the formation of more uniform micelles, compared to monodisperse polymers.[99] Two experiments were conducted with the second emulsifier PEG_{45}-*b*-$PLS(Bn)_{34}$ (**4d**) at two different concentrations (c = 2.43 mg/mL and 1.22 mg/mL). At lower concentrations, the solubility of the emulsifier was increased, even though it was not fully dissolved in both samples. Nevertheless, an improvement in stability was observed compared to the first NEP approach, as both emulsions were stable for a short period of time without stirring. This was not the case for the emulsions with PEG_{45}-*b*-$PLS(Bn)_{20}$ (**4a**) that showed immediate sedimentation of the polymer as soon as stirring was stopped. Even though visually, the more diluted emulsion seemed to be better dispersed, the DLS showed the opposite case (Table 6, No. **2-3**).

*Table 6: DLS measurements after emulsion formation with PEG_{45}-b-$PLS(Bn)_{32}$ (**4c**) and PEG_{45}-b-$PLS(Bn)_{34}$ (**4d**).*

No.	Emulsifier	Solvent	c [mg/mL]	d_H [µm]
1	PEG_{45}-*b*-$PLS(Bn)_{32}$, **4c**	CyH	2.43	-[1]
2	PEG_{45}-*b*-$PLS(Bn)_{34}$, **4d**	CyH	2.43	1.85
3	PEG_{45}-*b*-$PLS(Bn)_{34}$, **4d**	CyH	1.22	-[1]

[1] DLS measurement could not be performed due to aggregation and precipitation of the emulsifier.

The higher concentrated emulsion of polymer **4d** showed a particle diameter of 1.85 µm, while the particle size of the more diluted sample could not be determined, due to precipitation of the polymer during the measurement. The polymerization was conducted with both emulsions under otherwise identical conditions. For the higher concentrated approach, particle size could not be measured by DLS after the reaction due to sedimentation of the particles during the measurement. The sample was then sedimented, washed with cyclohexane, precipitated in methanol and centrifuged. The isolated and dried particles were redispersed in cyclohexane and a particle size of 500 nm was measured by DLS. SEM images were recorded of the particle dispersion after the polymerization, where dispersed particles with a diameter of 100 nm were observed. Corresponding to previous samples, the particles looked like they were covered and agglomerated by excess emulsifier (Figure 20A), but nevertheless, dispersed particles of appropriate size were obtained. This "gluing" of the particles might explain the DLS results that did not match the SEM data. In contrast, the images of the redispersed sample showed very few particles, but large aggregates of µm-size instead (Figure 20B). Therefore, the redispersion was not successful and led to irreversible aggregation of the particles. An optimization of the workup process for the particle dispersion was then considered for following experiments.

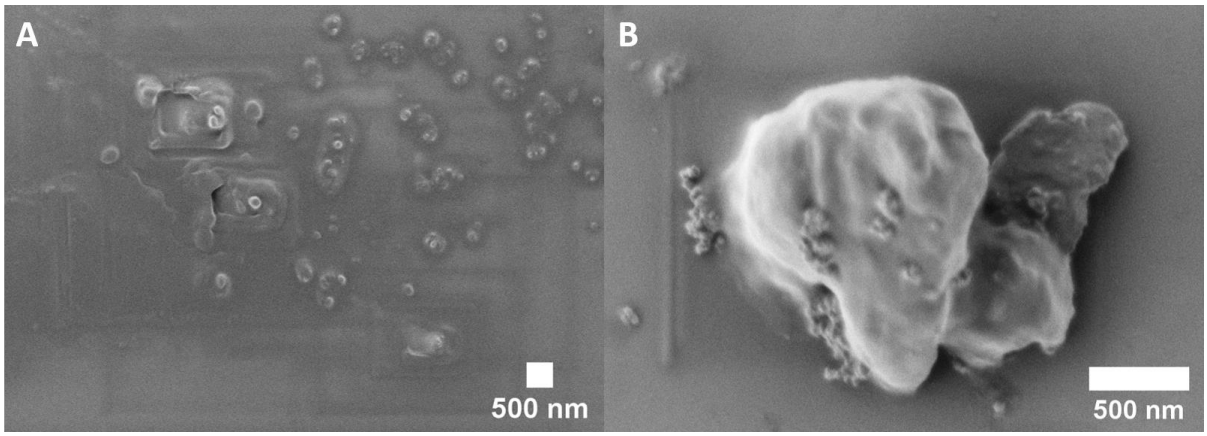

*Figure 20: SEM images of PEG_{45}-b-$PLS(Bn)_{32}$ (**4c**) coated nanoparticles A) after polymerization and B) after redispersion.*

The same workup procedure was used for the second approach with a lower emulsifier concentration. The particle size was determined by DLS after the polymerization and resulted in a hydrodynamic diameter of d_H = 218 ± 200 nm. The deviation in the DLS result indicated a broad size distribution, but the particle size was within the desired order of magnitude and did not show any particle aggregation.

For purification, the particles were washed with cyclohexane, precipitated in methanol and centrifuged before isolation. Redispersion of the particles was performed and resulted in particle diameters in the lower µm-range, indicating that the workup and redispersion process caused the particle aggregation. While the SEM images of the sample at higher concentration showed smaller particles than the DLS measurement, in this sample it was the other way round. SEM images showed only single particles with diameters of around 100 nm and few large aggregates after polymerization (Figure 21A). After the redispersion only few large aggregates were observed (Figure 21B). This led to the conclusion that the higher emulsifier concentration was resulting in higher yields of dispersed particles in comparison to lower emulsifier concentrations.

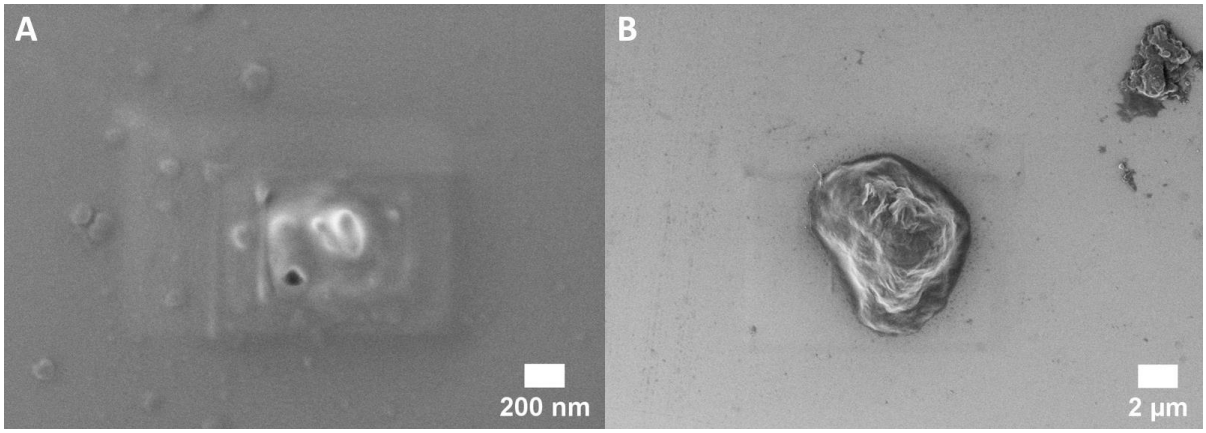

*Figure 21: SEM images of PEG_{45}-b-$PLS(Bn)_{32}$ (**4c**) coated PLLA nanoparticles A) after polymerization and B) after redispersion.*

In summary, the characterization of the dispersions indicated that the particle formation was more successful at higher emulsifier concentration, even though particle agglomeration was observed to some extent. A concentration between 2.43 mg/mL and 1.22 mg/mL or higher than 2.43 mg/mL should be tested in order to evaluate, if excess emulsifier is causing particle agglomeration at higher concentrations or if a concentration of 2.43 mg/mL is not high enough to form stable micelles.[94] Furthermore, the workup process, including the isolation and redispersion of the particles, was not ideal to preserve the particle morphology, as aggregation was observed after redispersion in cyclohexane. Besides that, the formation of nanoparticles with diameters of around 100 nm with the emulsifier PEG_{45}-*b*-$PLS(Bn)_{32}$ (**4c**) was successful, but optimization, in terms of emulsifier concentration and workup procedure, was necessary to improve the homogeneity of the particles.

In the next experiments, block copolymers with slightly higher hydrophobic ratios were used (Table 5, No. **4m, 4n, 4h**). PEG_{45}-*b*-$PLS(Bn)_{35}$ (**4n**, weight ratio 24:76) and PEG_{45}-*b*-$PLS(Bn)_{38}$ (**4m**, weight ratio 23:77), as well as PEG_{45}-*b*-$PLS(Bn)_{41}$ (**4h**, weight ratio 22:78) were tested. Emulsion polymerization was performed with all three emulsifiers and analysed by DLS to evaluate the resulting particle diameters (Table 7). An emulsifier concentration of 2.43 mg/mL was applied for PEG_{45}-*b*-$PLS(Bn)_{35}$ (**4n**)

and PEG_{45}-*b*-$PLS(Bn)_{38}$ (**4m**), while two different concentrations, 1.22 mg/mL and 2.70 mg/mL, were used for the NEP with PEG_{45}-*b*-$PLS(Bn)_{41}$ (**4h**).

*Table 7: DLS measurements after nonaqueous emulsion polymerization with the emulsifiers **4h**, **4m**, **4n** and after precipitation in methanol.*

No.	EP[2]	Emulsifier	Solvent	c [mg/mL]	d_H [µm]
1	15	PEG_{45}-*b*-$PLS(Bn)_{35}$, **4n**	MeCN/CyH MeOH	2.43	-[1] 1.50 ± 0.15
2	14	PEG_{45}-*b*-$PLS(Bn)_{38}$, **4m**	MeCN/CyH MeOH	2.43	-[1] 1.70 ± 0.15
3	17	PEG_{45}-*b*-$PLS(Bn)_{41}$, **4h**	MeCN/CyH MeOH	1.22	-[1] 7.00 ± 1.45
4	18	PEG_{45}-*b*-$PLS(Bn)_{41}$, **4h**	MeCN/CyH MeOH	2.70	1.00 ± 0.80 -[1]

[1] DLS measurement could not be performed due to aggregation and precipitation of the emulsifier.

[2] Numbering of experiment of the nonaqueous emulsion polymerization (ncsNW-epX).

DLS measurements were performed with the reaction mixture after the polymerization and after precipitation of the particles in methanol. During the first three reactions the particle dispersion collapsed and hence, no DLS measurements were possible after polymerization. The particles were washed twice with cyclohexane, sedimented and decanted, to remove excess emulsifier and starting materials. After precipitation in methanol, particle diameters of 1.70 ± 0.15 µm for EP15 and 1.50 ± 0.15 µm for EP14 were observed (Table 7, No. **1-2**). No improvement was achieved in regards to particle size by using these emulsifiers with a higher hydrophobic moiety, compared to the previous experiments. The DLS graphs showed multimodal size distribution with a significant number of larger aggregates in both cases, and hence, no homogeneous particle dispersions were obtained (Figure 22).

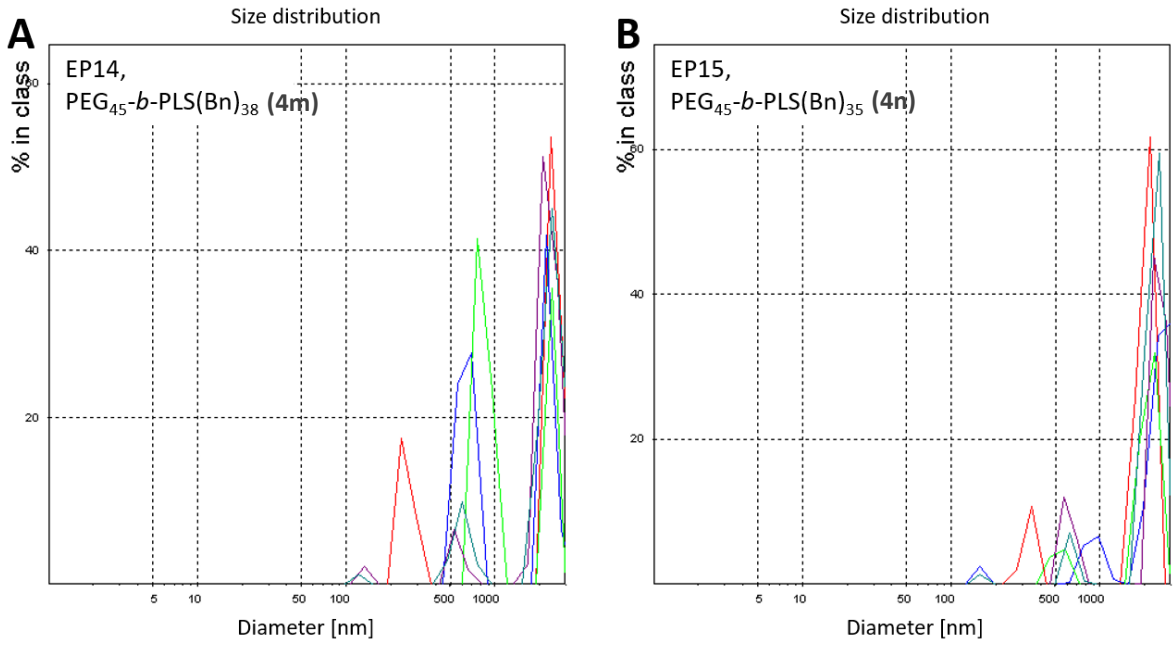

Figure 22: DLS measurements of A) EP14 and B) EP15 after precipitation in methanol.

The two polymerizations with emulsifier **4h** proved the observations that were made with **4d**, where the lower emulsifier concentration of 1.22 mg/mL did not lead to improvement of the particle size, but to higher aggregation tendency (Table 7, No. **3**). At a concentration of 1.22 mg/mL, a particle diameter of 7.00 ± 1.45 µm was observed by DLS and few particles of around 1 µm in diameter, so strong aggregation occurred during this approach (Figure 23A). The reaction at higher concentration (c = 2.70 mg/mL) resulted in a clearly smaller size distribution of 1.00 ± 0.80 µm (Table 7, No. **4**). The DLS graph showed less aggregates above 1 µm in diameter and most particles in the range of 500 nm (Figure 23B). In addition, the higher concentrated particle dispersion was the only dispersion of this set of experiments that was measurable by DLS after the polymerization, as it did not collapse immediately upon addition of the reagents.

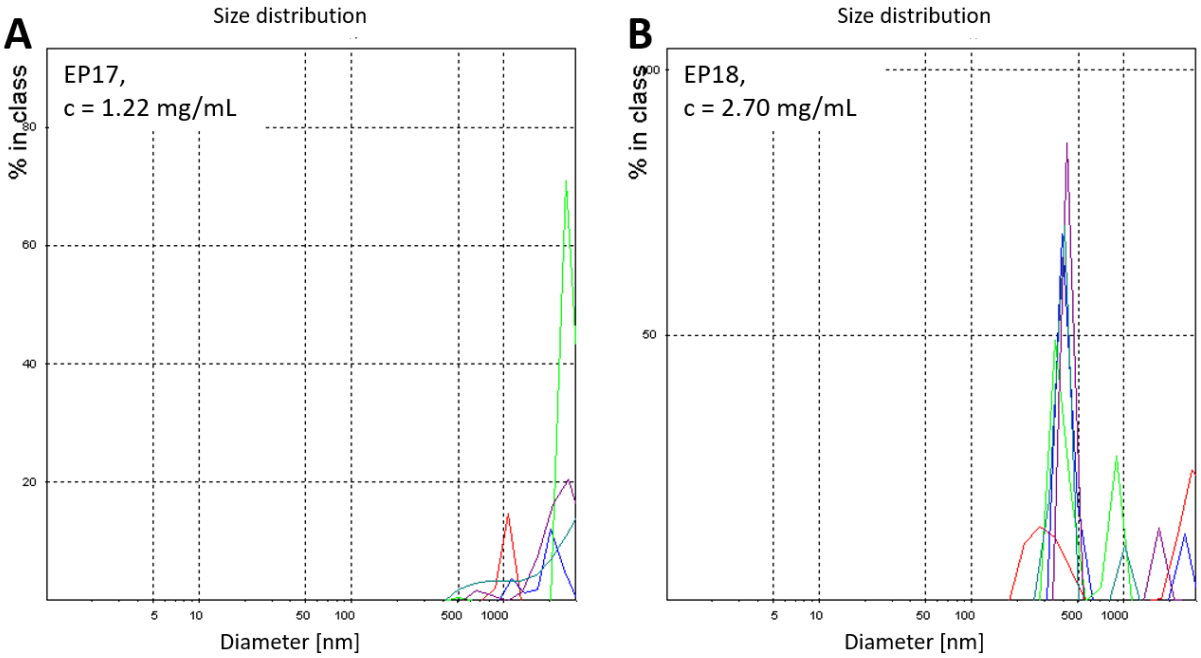

*Figure 23: DLS measurements of A) EP17 after precipitation in methanol and B) EP18 after polymerization with emulsifier **4h**.*

In conclusion, the emulsion polymerization, performed with the emulsifiers **4h** and **4m-n** did not lead to significant improvement in terms of particle size and size distribution of the resulting particle dispersions, as the DLS measurements revealed. Nevertheless, the DLS measurements of EP17 and EP18 proved once again that an emulsifier concentration of c = 1.22 mg/mL was not high enough to keep the emulsion stable during the polymerization. The higher emulsifier concentration led to smaller particles and reduced agglomeration of the resulting particles. Utilizing these polymers as emulsifiers in NEP did not result in the formation of stable and monodispersed emulsions.

INFLUENCE OF SHORTER HYDROPHILIC PEG_{17}-BLOCKS ON THE EMULSION FORMATION

The synthesis of emulsifiers with higher hydrophobic PLS(Bn) moieties was not successful with the PEG_{45}-block. Instead, a higher hydrophobic moiety was achieved by using a PEG macroinitiator with lower molecular weight of only 750 Da instead of 2000 Da. These polymers were used in the next step to evaluate the influence of the PEG block length on the emulsion formation. The polymer PEG_{17}-*b*-$PLS(Bn)_{41}$ (**3a**) has a weight ratio of 10:90, bearing a shorter PEG block and clearly higher hydrophobic moiety within the polymer than the previously discussed emulsifiers. Emulsion formation was studied by dissolving the polymer at a concentration of 2.43 mg/mL in cyclohexane and MeCN/CyH mixture (Table 8). In cyclohexane, large aggregates of µm-size were formed that precipitated during the DLS measurement. In the MeCN/CyH mixture, the polymer (**3a**) was mostly dissolved and resulted in a broad size distribution and a particle size of 5.65 ± 5.50 µm, which is a comparable, but slightly lower result than PEG_{45}-*b*-$PLS(Bn)_{20}$ (**4a**). The block ratio of 10:90 in this case, with a very dominant hydrophobic moiety, might be too high to stabilize the emulsion or the solubility of the PLS(Bn) block is low in cyclohexane.

*Table 8: DLS measurements after emulsion formation and NEP with PEG_{17}-b-$PLS(Bn)_{41}$ (**3a**).*

No.	EP[2]	Emulsifier	Solvent	c [mg/mL]	d_H [µm]
1	-	PEG_{17}-*b*-$PLS(Bn)_{41}$, **3a**	CyH	2.43	-[1]
2	-	PEG_{17}-*b*-$PLS(Bn)_{41}$, **3a**	MeCN/CyH	2.43	5.65 ± 5.50
3	32	PEG_{17}-*b*-$PLS(Bn)_{41}$, **3a**	MeCN/CyH	2.43	8.00
4	37	PEG_{17}-*b*-$PLS(Bn)_{41}$, **3a**	MeCN/CyH	1.62	0.65 ± 0.09

[1] DLS measurement could not be performed due to aggregation and precipitation of the emulsifier.
[2] Numbering of experiment of the nonaqueous emulsion polymerization (ncsNW-epX).

Although a stable and homogeneously dispersed emulsion was not obtained under these conditions, emulsion polymerization was conducted at c = 2.43 mg/mL in MeCN/CyH (EP32, Table 8, No.3) to fully compare this polymer to the previously used polymers. The solubility of the emulsifier PEG_{17}-*b*-$PLS(Bn)_{41}$ (**3a**) was slightly better than of PEG_{45}-*b*-$PLS(Bn)_{20}$ (**4a**) in the larger scale of the NEP. Nevertheless, DLS measurements after the polymerization showed a broad size distribution and the presence of large, µm-sized aggregates. To examine these results, SEM images were recorded of the diluted reaction mixture and after precipitation of the particles in methanol (Figure 24). After the polymerization, large aggregates of 1-2 µm were present as well as particles below 500 nm in diameter (Figure 24A, B), which confirmed the DLS results. After precipitation in methanol, the agglomerates were still visible (Figure 24C), but also spherical particles with diameters of around 100 nm were observed (Figure 24D). The morphology of the material was very heterogenous and the particles had a high tendency to form larger agglomerates. In comparison to the **4a**-coated particles, the particles produced with **3a** were smaller and in the desired range of 100 nm, but due to a high tendency to

agglomeration they were not homogeneously dispersed, as confirmed by DLS and SEM. Optimization of the reaction was necessary to increase homogeneity of the dispersion and reduce particle agglomeration. Nevertheless, this result was an improvement in terms of particle size and morphology, compared to the previous approaches.

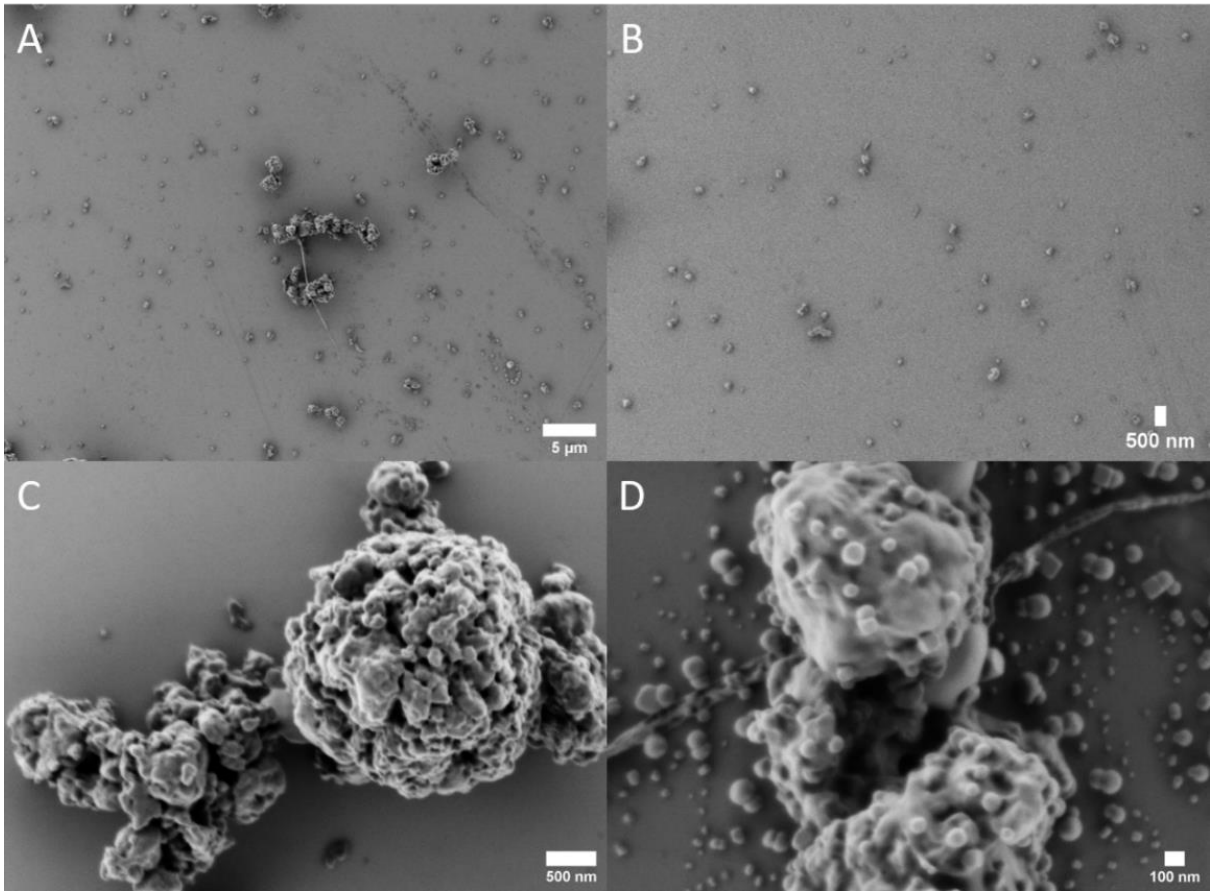

*Figure 24: SEM images of the PLLA nanoparticles, using emulsifier **3a**. A, B) dispersed in cyclohexane after the polymerization; C, D) after precipitation in methanol.*

The sample was then analysed by NMR spectroscopy. The DOSY-NMR spectrum was ambiguous, as it showed the same diffusion constant for the lactide methyl group signal (n) and the emulsifier signals (a-g), indicating that coated nanoparticles were obtained (Figure 25, green line), but one of the lactide signals was also in line with the pyrene butanol signal (l) and SIMes catalyst signal (Figure 25, grey line). This led to the conclusion that the reaction was not quantitative. Comparing the SIMes signals with the solvent signals, the diffusion constant differed and lied between the polymer and solvent signals. This indicated that the analysed material contained residual SIMes-*b*-PLLA oligomers, but not the pure starting materials. Nevertheless, these molecules were not fully removed as intended by washing and precipitation of the particles in methanol. Therefore, the purification of the nanoparticles should be done repeatedly to ensure the thorough removal of starting materials and by-products.

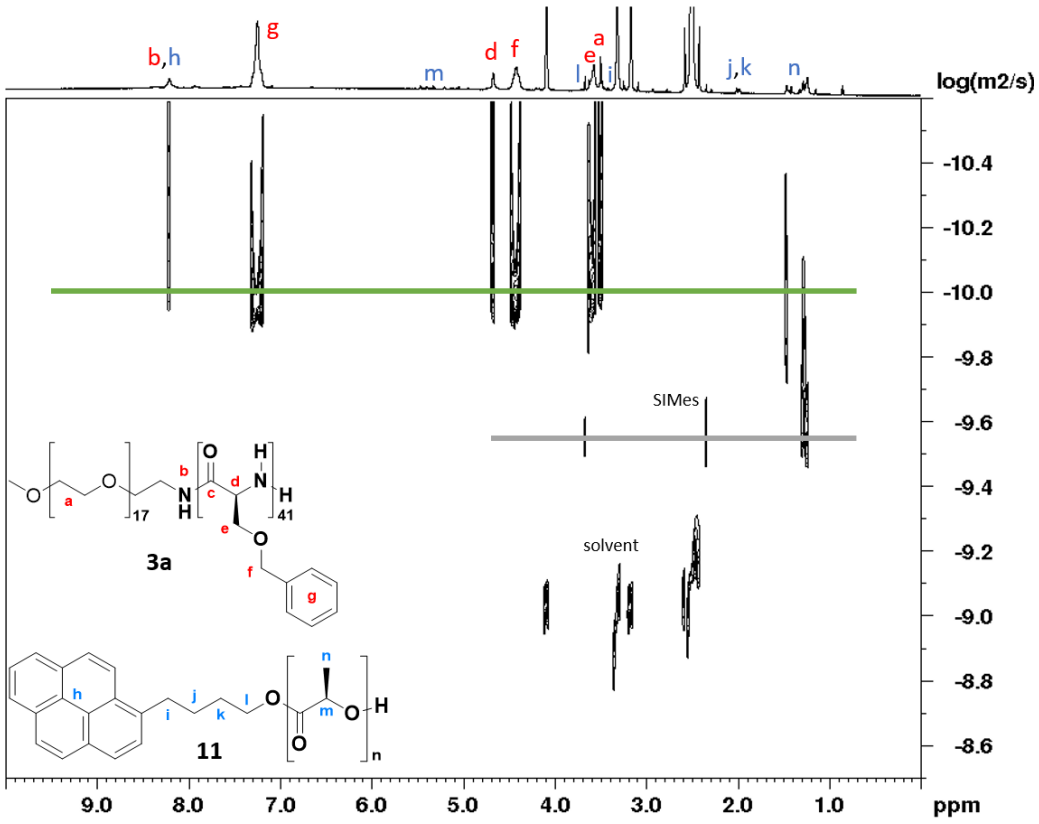

*Figure 25: DOSY NMR spectrum (700 MHz, 298 K, DMSO-d_6) of PEG_{17}-b-$PLS(Bn)_{41}$ (**3a**, red) coated PLLA (**11**, blue) nanoparticles (green line).*

Proton NMR analysis also showed that the signal intensities of the PLLA polymer were very small compared to previous experiments (Figure 26, h-m, blue signals), which led different conclusions. One possibility was that the monomer conversion was not quantitative within the reaction time of 15 minutes or due to collapsing of the emulsion upon addition of the reagents. Consequently, the signal intensities are low, because the PLLA did not reach its theoretical DP. Another possibility was that proper nanoparticle formation was achieved. The core shell structure has a shielding effect on the core signals of the particles.[97] Furthermore, the PLLA in the particle core was not fully dissolved in the NMR solvent and therefore showed low relaxation, resulting in poor signal intensities. This phenomenon is known in literature and was observed in the model system with PI-*b*-PMMA as well, where the core signals were barely visible in the proton NMR.[50] In addition, the α-CH of PLLA was supposed to appear as one singlet signal, while there were several signals observed. This indicated that the reaction conversion was very low in this approach and did not result in uniform PLLA polymers, but more likely in oligomers of different lengths that resulted in plenty singlets with slightly different shifts in the proton NMR. On top, the pyrene butanol signals were very weak and barely visible. While the DLS and SEM experiments gave a very positive impression of this approach, the NMR clearly showed that the monomer conversion was very low, probably due to early collapse of the reaction mixture upon addition of the reagents.

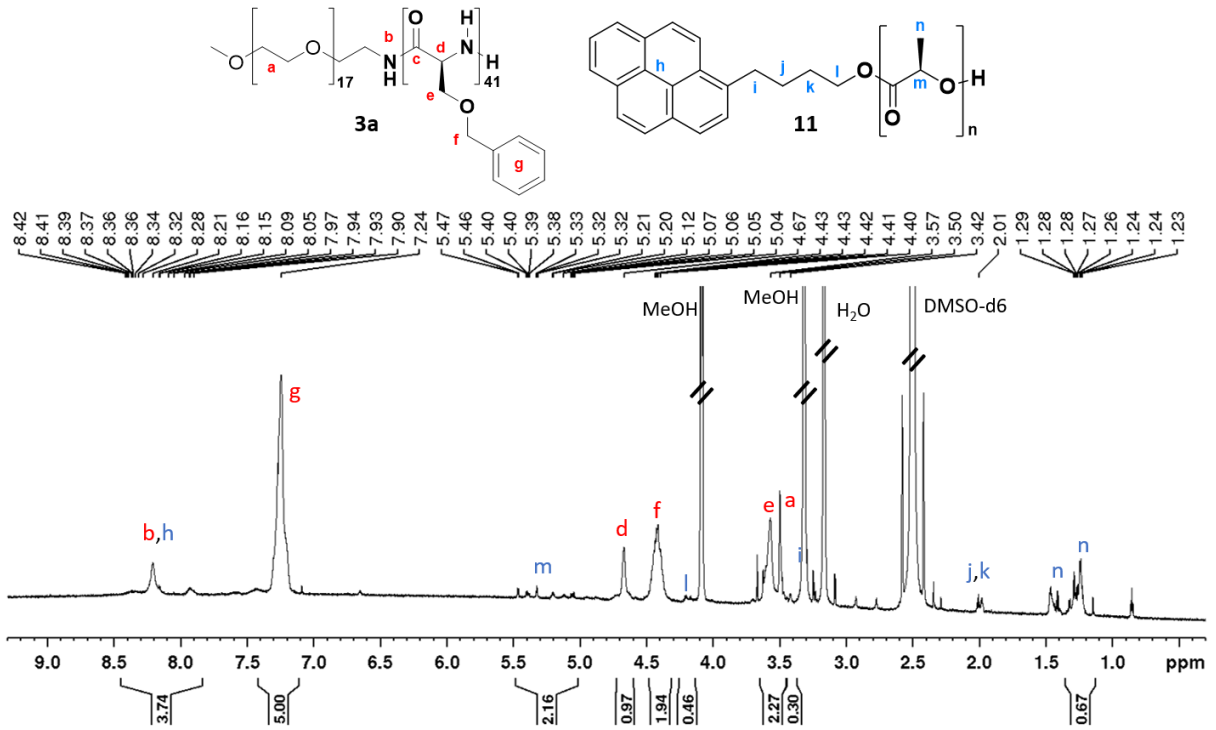

*Figure 26: ^{1}H-NMR spectrum (700 MHz, 298 K, DMSO-d_6) of PEG_{17}-b-$PLS(Bn)_{41}$ (**3a**, red) coated PLLA (**11**, blue) nanoparticles.*

After this first approach with PEG_{17}-*b*-$PLS(Bn)_{41}$ (**3a**), another approach with the same emulsifier was performed, using a slightly lower emulsifier concentration of 1.62 mg/mL (EP37, Table 8, No. 4). The concentration was decreased in order to evaluate, if the particle dispersion can be improved by tuning of the emulsifier concentration. It is known that high emulsifier concentrations can lead to increased particle agglomeration, caused by the excess polymer acting as glue between the nanoparticles.[94] After polymerization, a particle diameter of 650 ± 85 nm was obtained, which was not only significantly smaller, but also a narrow size distribution was achieved, compared to the first approach at higher emulsifier concentration. The SEM images showed dispersed particles and agglomerates below 1000 nm and very few larger aggregates, indicating that decreasing the emulsifier concentration to 1.62 mg/mL in fact led to an improvement of the resulting particles in terms of particle morphology and size distribution (Figure 27: SEM images of PLLA nanoparticles using PEG_{17}-b-$PLS(Bn)_{41}$ (**3a**) at c = 1.62 mg/mL, dispersed in cyclohexane.). The larger aggregates seemingly consisted of smaller particles that were clumped together.

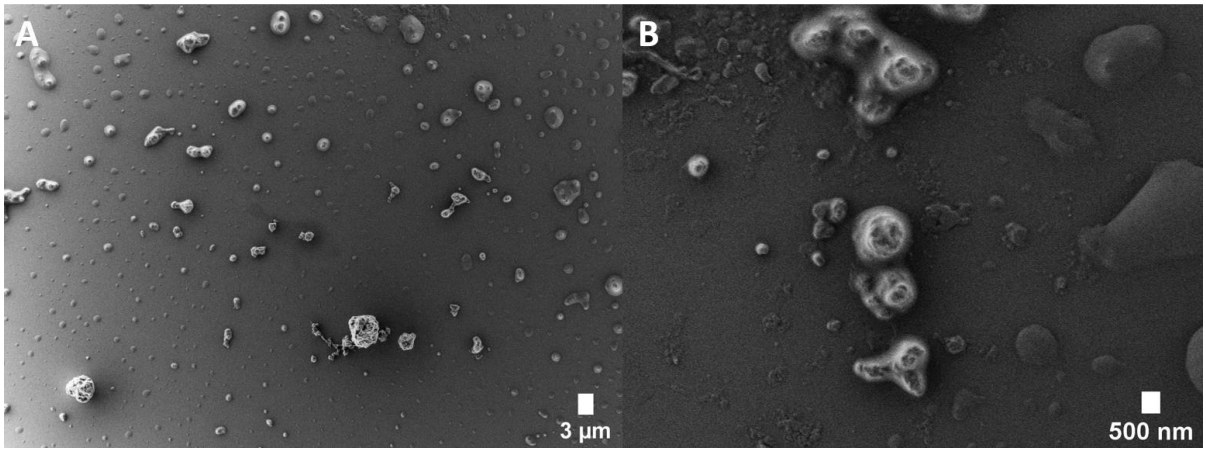

*Figure 27: SEM images of PLLA nanoparticles using PEG_{17}-b-$PLS(Bn)_{41}$ (**3a**) at c = 1.62 mg/mL, dispersed in cyclohexane.*

Proton NMR analysis of the sample showed that the polylactide signals (Figure 28, m-n) had the expected signal intensities and PLLA with a DP of around 35 was obtained. Besides that, some of the starting materials, SIMes and L-lactide, were visible in the spectrum as well. Consequently, and in contrast to the proton spectrum before, the spectrum below displayed that these core shell nanoparticles might be showing both, the core and shell signals, if PLLA was properly polymerized.

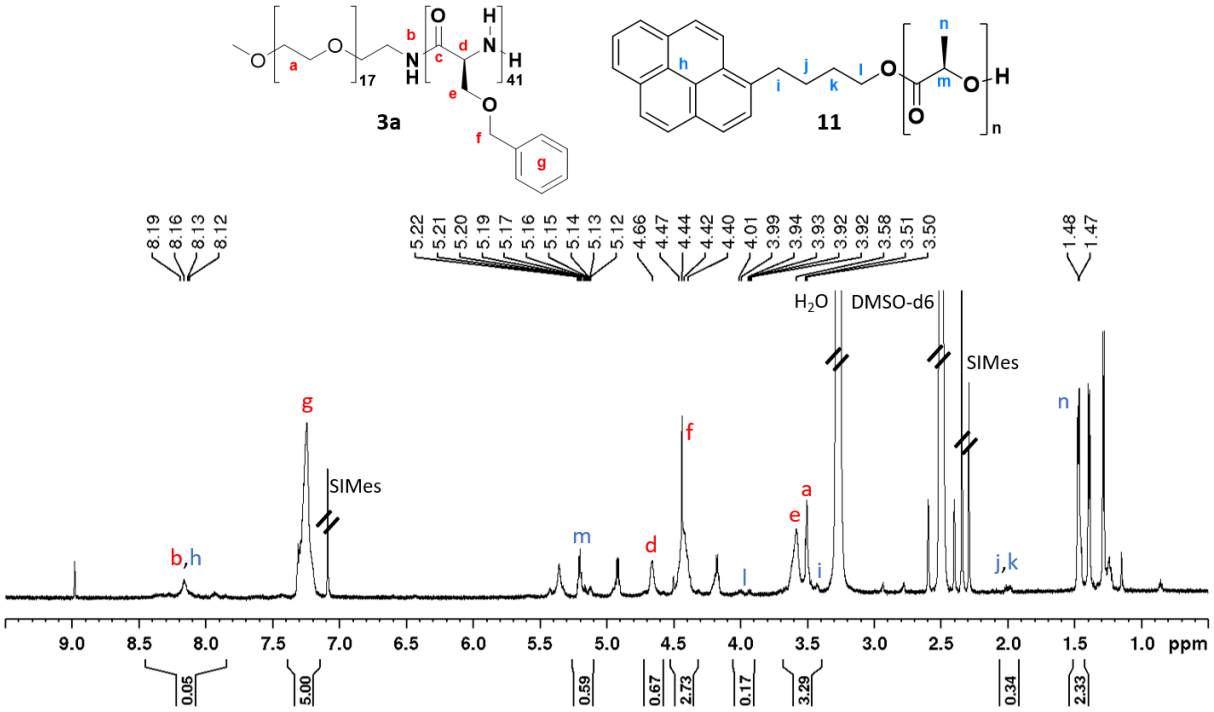

*Figure 28: ^{1}H-NMR spectrum (700 MHz, 298 K, DMSO-d_6) of PEG_{17}-b-$PLS(Bn)_{41}$ (**3a**, red) coated PLLA (**11**, blue) nanoparticles.*

When concluding the SEM and NMR results, the particle formation was successful and PLLA nanoparticles stabilized with the emulsifier PEG_{17}-*b*-$PLS(Bn)_{41}$ (**3a**) were obtained, which was also confirmed by DOSY spectroscopy, where PLLA and the emulsifier showed the same diffusion constant (Figure 29, green line). The reaction was improved to some extent by decreasing the emulsifier

concentration, which led to formation of dispersed particles and lower agglomeration. Though, there is room for improvement in terms of effective removal of starting materials, as these were not fully removed by repeated washing of the particles with cyclohexane (Figure 29, grey line).

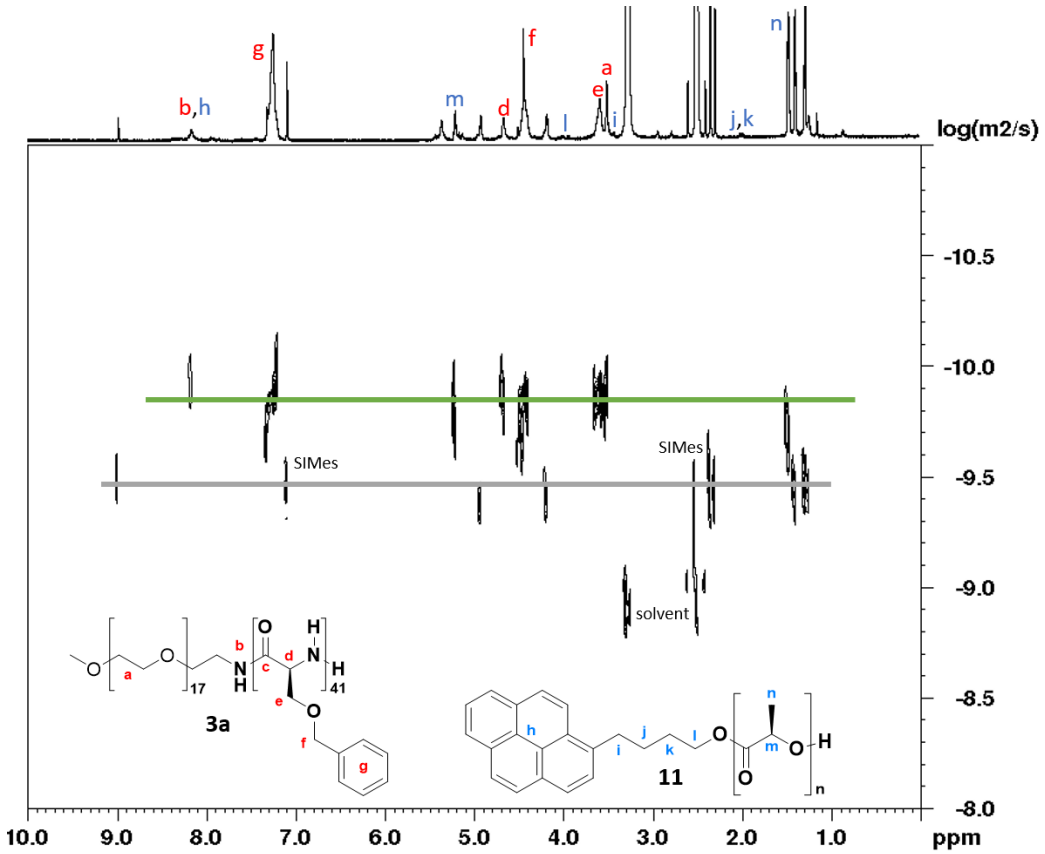

*Figure 29: DOSY NMR spectrum (700 MHz, 298 K, DMSO-d_6) of PEG_{17}-b-$PLS(Bn)_{41}$ (**3a**, red) coated PLLA (**11**, blue) nanoparticles (green line).*

In summary, the fabrication of PLLA nanoparticles, coated with a PEG-*b*-PLS(Bn) emulsifier, was conducted successfully and particles have been obtained. Depending on the block ratio and molecular weights of the polymers, the most promising emulsifiers were **4a, 4d** and **3a**, which all resulted in particle dispersions. Nevertheless, aggregation of these particles was a challenge that needs to be addressed by optimization of the reaction conditions and fine-tuning of the emulsifier block ratio. While tuning the emulsifier concentration was very effective to reduce particle agglomeration, reaction time or change of solvent system did not result in major improvement. In contrast to common literature and experience with other poly(amino acid) based block copolymers, usage of higher hydrophobic block ratios in the emulsifying polymers did not result in better dispersibility in nonpolar solvents.[53] Therefore, a different direction was taken to influence the aggregation behaviour of the *O*-benzyl-serine-based polymers by modifying the polypeptide secondary structure. L-serine has a strong tendency to form β-sheet structures, even at low DPs above 7. By incorporation of the D-enantiomer into the polymer backbone, the β-sheet formation is disrupted and a random coil

formation of the polypeptide chain is favoured, leading to better solubility and aggregation behaviour of the polymers by inhibition of the hydrogen bonding.[72] Utilizing the racemic block copolymers as emulsifiers is expected to improve the stability of the nonaqueous emulsions and the nanoparticle synthesis.

3.2.4 Nonaqueous emulsion polymerization with the *O*-benzyl-DL-serine-based block copolymers

The racemic block copolymers were synthesized in the same way as the L-serine analogues in order to achieve higher molecular weights and a longer hydrophobic block to promote homogeneous dispersion of these emulsifiers in nonpolar, organic solvents. It was expected that the racemic block was easier to polymerize quantitatively than the L-serine block. By incorporation of the D-serine into the polymer chain the β-sheet structure, that was believed to lead to polymer precipitation during the polymerization, was disrupted, resulting in random coil formation. However, no significant increase of the DP was achieved for most polymers, but a change in the aggregation behaviour of the polymer during the work-up procedure was observed. It was hypothesized that the secondary structure changed as expected, resulting in a different solubility behaviour of the polymer chains. In order to purify the block copolymers after the ring opening polymerization, they were precipitated in diethylether usually. While this worked very well for the L-serine-based polymers, the racemic emulsifiers did not precipitate in diethylether and instead formed an emulsion. While this was complicating the work-up, as the polymers needed to be centrifuged and not simply filtered, it was a potentially useful observation on their aggregation behaviour in nonpolar solvents, in comparison to the L-serine derivatives. Several block copolymers were synthesized using either PEG_{45} or PEG_{17} as the hydrophilic block and different block lengths of the hydrophobic PDLS(Bn) were produced. Some of these polymers had a weight ratio of around 30:70 (Table 9, No. **8a-b**), while others had a DP ratio of around 30:70 (Table 9, No. **7a, 8c**). It was evaluated, if these proposed ratios were applicable for the PSer(Bn)-based emulsifiers to form stable emulsions and whether the relevant parameter is the DP or weight ratio.

Table 9: Overview *of O*-benzyl-DL-*serine-based* emulsifiers.

No.	Polymer	DP_{PEG}	$DP_{PSer(Bn)}$	DP ratio	Weight ratio	Mn[a] [Da]
8a	PEG_{45}-*b*-$PDLS(Bn)_{37}$	45	37	55:45	23:77	8500
8b	PEG_{45}-*b*-$PDLS(Bn)_{32}$	45	32	58:42	26:74	7700
7a	PEG_{17}-*b*-$PDLS(Bn)_{49}$	17	49	26:74	8:92	9400
8c	PEG_{45}-*b*-$PDLS(Bn)_{150}$	45	150	23:77	7:93	28500

[a] [Mn]: total molecular weight of block copolymer, calculated by ^{1}H-NMR analysis.

INITIAL APPROACHES OF EMULSION FORMATION AND NEP WITH THE RACEMIC EMULSIFERS

Before the nanoparticle synthesis was performed with the racemic emulsifiers, emulsion formation in cyclohexane and diethylether was studied by DLS, as well as the stability of the emulsions upon addition of DMF or MeCN as the dispersed phase (Table 10). The two racemic block copolymers PEG_{45}-*b*-$PDLS(Bn)_{37}$ (**8a**, weight ratio: 23:77) and PEG_{45}-*b*-$PDLS(Bn)_{150}$ (**8c**, weight ratio: 7:93) were tested first. In cyclohexane the polymer **8a** did not dissolve at all, but formed large aggregates that precipitated immediately upon addition of the dispersed phase (Table 10, No. **1-2**). As a consequence, DLS measurements could not be performed. In diethylether, an emulsion was formed that was stable, even without stirring. Addition of the dispersed phase did not change the stability of the emulsion. Nevertheless, DLS measurements resulted in a broad size distribution for both samples, in DMF/Et_2O and MeCN/Et_2O, with average hydrodynamic diameters of 4-5 µm, consisting of particles with diameters of around 500 nm and larger aggregates (Table 10, No. **3-4**).

*Table 10: DLS measurements after emulsion formation with PEG_{45}-b-$PDLS(Bn)_{37}$ (**8a**) in different solvent systems.*

No.	EP[2]	Emulsifier	Solvent	c [mg/mL]	d_H [µm]
1	30-1	PEG_{45}-*b*-$PDLS(Bn)_{37}$, **8a**	MeCN/CyH	2.43	-[1]
2	30-2	PEG_{45}-*b*-$PDLS(Bn)_{37}$, **8a**	DMF/CyH	2.43	-[1]
3	30-3	PEG_{45}-*b*-$PDLS(Bn)_{37}$, **8a**	MeCN/Et_2O	2.43	5.40 ± 2.30
4	30-4	PEG_{45}-*b*-$PDLS(Bn)_{37}$, **8a**	DMF/Et_2O	2.43	4.15 ± 1.85

[1] DLS measurement could not be performed due to aggregation and precipitation of the emulsifier.
[2] Numbering of experiment of the nonaqueous emulsion polymerization (ncsNW-epX).

In conclusion, the polymer was not soluble in cyclohexane at all, but formed large aggregates that precipitated upon addition of the dispersed phase. In diethylether the polymer showed good solubility and formed semi-stable emulsions that sedimented over time without stirring. In parallel to the stability studies, emulsion polymerization was performed (p. 56, Table 11, No. **1**). In the first approach, the experimental procedure stayed unchanged for the racemic polymers, where the emulsifier **8a** was dissolved in cyclohexane (c = 2.43 mg/mL) and the reagents were added in acetonitrile. In contrast to the emulsion formation experiment, the polymer was mostly dissolved in the larger scale of the approach, after ultrasonication and stirring overnight, and polymerization was performed. The emulsion collapsed during the reaction and the particles precipitated, along the lines of the L-serine analogues. DLS measurements after the reaction resulted in a d_H of 12.8 ± 22.6 µm and revealed a broad size distribution, bearing nanometer-sized particles as well as large aggregates. Particles were washed repeatedly with cyclohexane and precipitated in methanol, resulting in a particle diameter of 13.2 ± 7.8 µm and a broad size distribution. Even though the particle size remained unchanged, the size distribution was narrower than before the purification, indicating that the work-up led to removal of large aggregates and starting materials. According to the SEM images, the reaction mixture consisted of particles and aggregates of various size (Figure 30A), showing many small particles with

diameters below 500 nm and larger µm-sized aggregates (Figure 30B), matching the DLS measurements. The images showed that precipitation in methanol led to dispersed particles with diameters of 100-200 nm that assembled into small piles (Figure 30D). Also, some raspberry-like agglomerates (d_H = 2 µm) of these small particles were observed (Figure 30C). In general, and as noted before, purification of nanoparticles can be challenging due to occurring aggregation.[93] However, in this case the precipitation led to the dissolution or removal of the large aggregates and potentially excess emulsifier, resulting in dispersed particles with diameters of around 100 nm, and well-defined, raspberry-like agglomerates with diameters of around 2 µm.

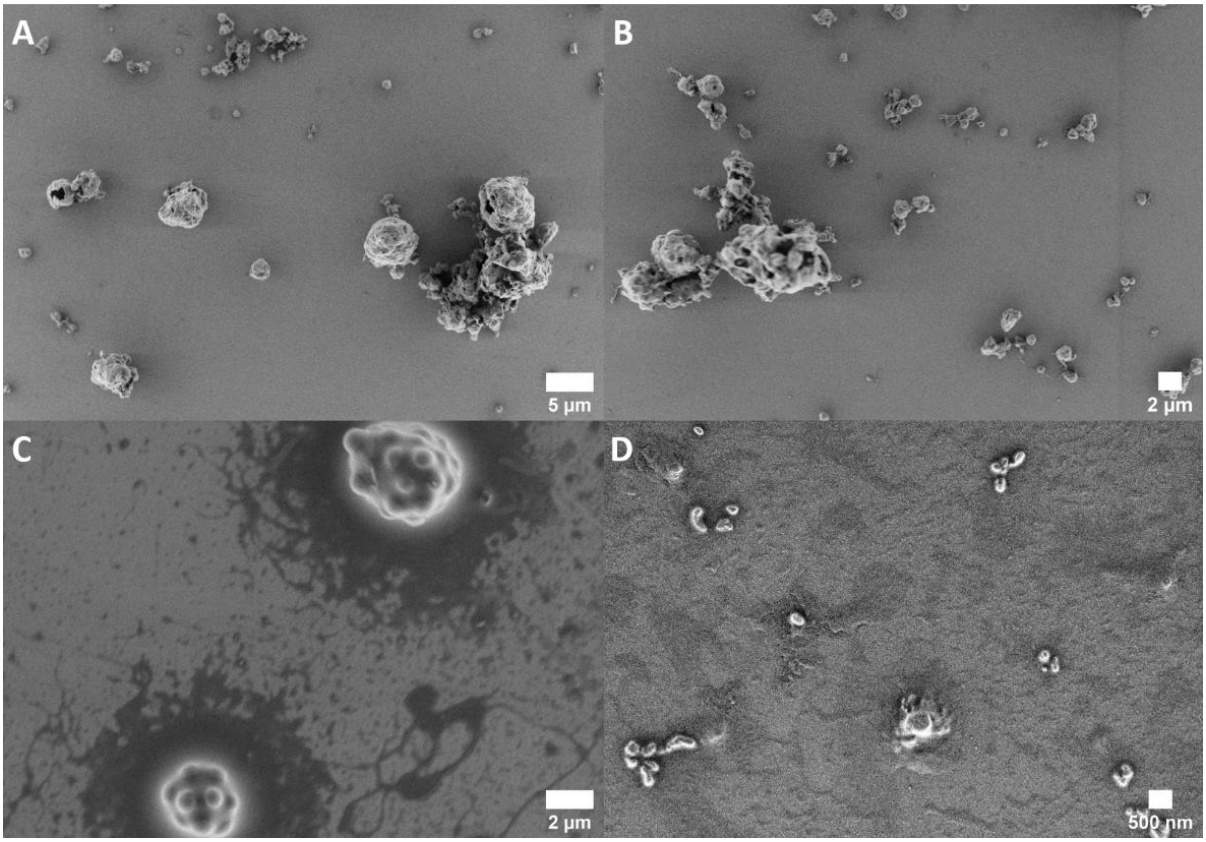

*Figure 30: SEM images of the PLLA nanoparticles using the racemic emulsifier PEG_{45}-b-$PDLS(Bn)_{37}$ (**8a**). A, B) Reaction mixture after polymerization and C, D) after precipitation in methanol.*

Proton- and DOSY-NMR spectroscopy was applied for structural analysis of the material. The proton spectrum showed the expected signals of both, emulsifier and 1-pyrenebutanol-initiated PLLA (Figure 31). The signal intensities of the PLLA (blue) were low compared to the emulsifier signals (red), which is expected for core shell particles, where the core signals are shielded by the particle shell and was observed as well in the spectrum of the model system with PI-*b*-PMMA and therefore might be an indicator for successful encapsulation of the PLLA by the emulsifier. In contrast, it can be an indicator for a low DP of PLLA and incomplete polymerization. The signal of the PEG block, which was incorporated into the particle core as well, showed lower intensity than in the original spectrum of the

block copolymer, which strongly supported the proposed core shell structure of the particles and resulting shielding effect of the particle core.

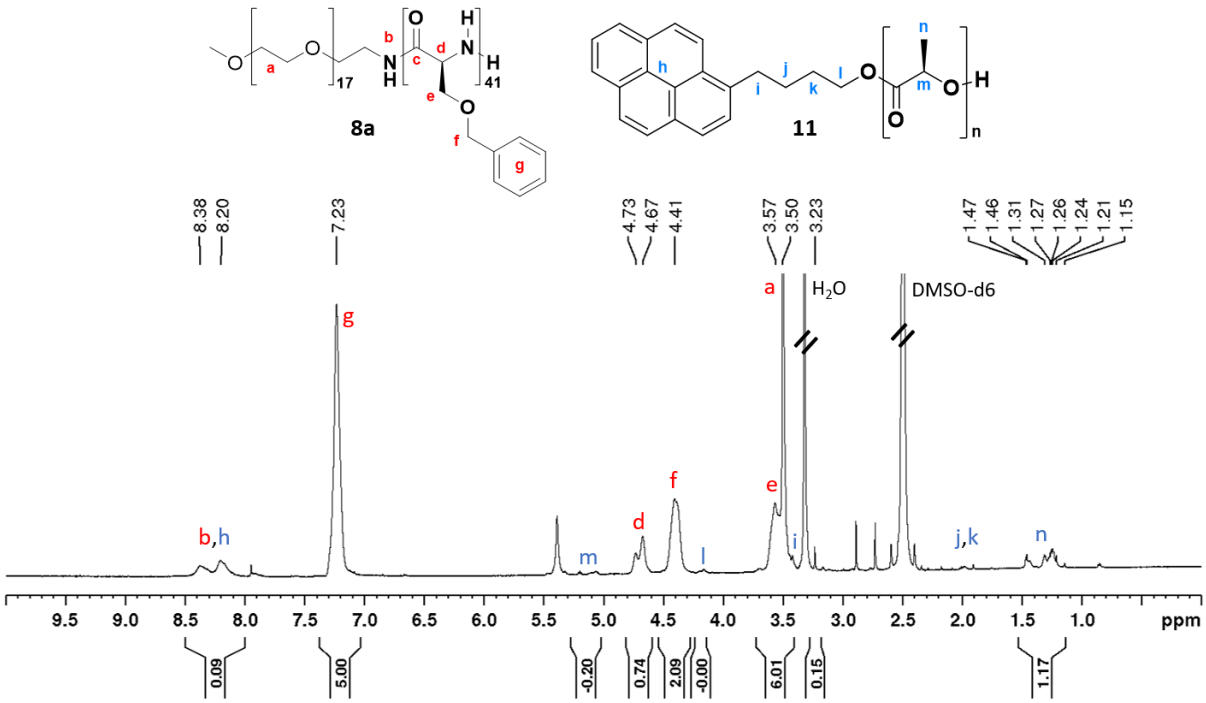

*Figure 31: ^{1}H-NMR spectrum (700 MHz, 298 K, DMSO-d_6) of PEG_{45}-b-$PLS(Bn)_{37}$ (**8a**, red) coated PLLA (**11**, blue) nanoparticles.*

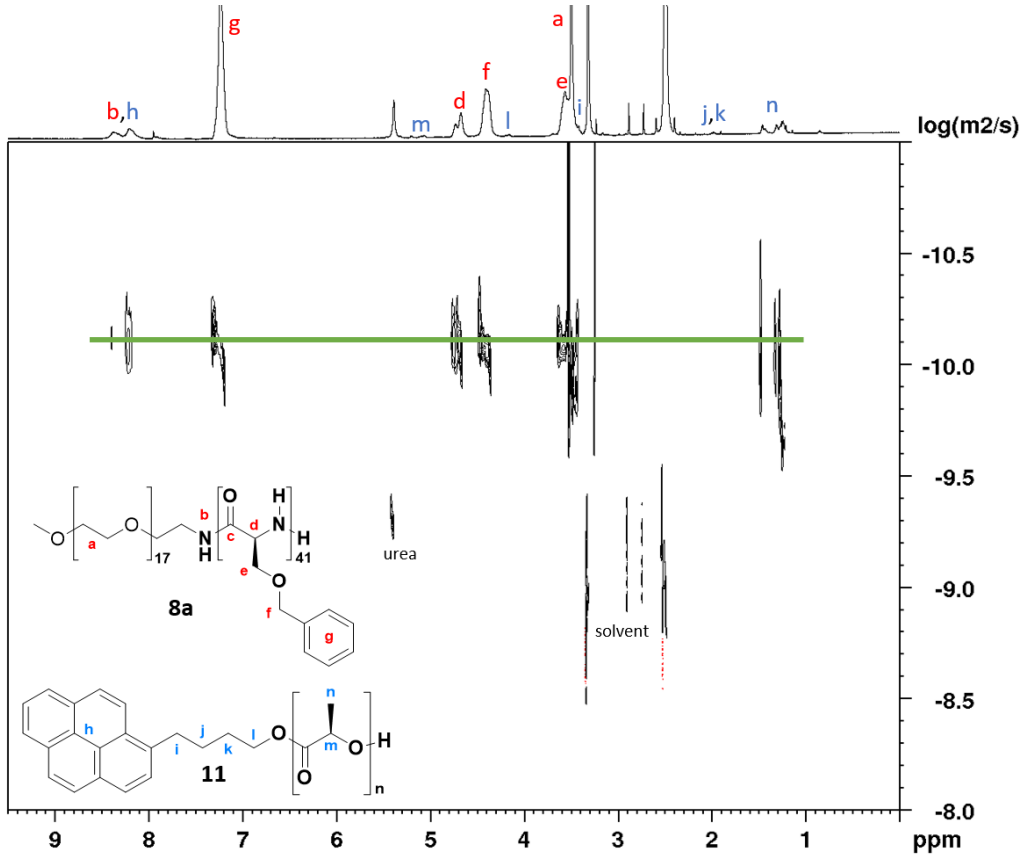

*Figure 32: DOSY NMR spectrum (700 MHz, 298 K, DMSO-d_6) of PEG_{45}-b-$PLS(Bn)_{37}$ (**8a**, red) coated PLLA (**11**, blue) nanoparticles (green line).*

The DOSY spectrum showed the same diffusion constant for both, PEG-*b*-PDLS(Bn) emulsifier (**8a**) and PLLA (Figure 32, green line). This was not a solid proof for particle existence by itself, but it indicated the successful polymerization of the lactide polymer by showing the same diffusion behaviour like the block copolymer species, while the remaining signals of the solvents showed different values. Nevertheless, this supported the theory that the encapsulation was successful, as PLLA polymer was obtained. In addition, no PLLA oligomers or starting materials were visible in the spectrum.

In summary, the emulsion polymerization with the racemic PEG-*b*-PDLS(Bn) emulsifier **8a** resulted in core shell nanoparticles of adequate size and shape, as confirmed by SEM and NMR spectroscopy. Nevertheless, there is room for improvement, as the particles were obtained with poor yield of around 10%. To determine, if the particles were lost during the workup or if the polymerization was not completed, the supernatant of the sedimentation was concentrated and the residue was analysed by DOSY-NMR and compared to the spectrum of the particles (Figure 33). The signals of the isolated particles (green line) displayed the same diffusion constant for PEG-*b*-PDLS(Bn) (a-g) and PLLA (h-n). In contrast, the spectrum of the residue (red) showed different diffusion constants for the signals of the emulsifier, the L-lactide and pyrene butanol, indicating that the supernatant contained a mixture of excess emulsifier and unreacted starting materials. The low yield of the reaction could be explained by the collapse of the emulsion during the reaction that prevented the starting materials from full reaction conversion, as the micellar microreactors were not in solution anymore.

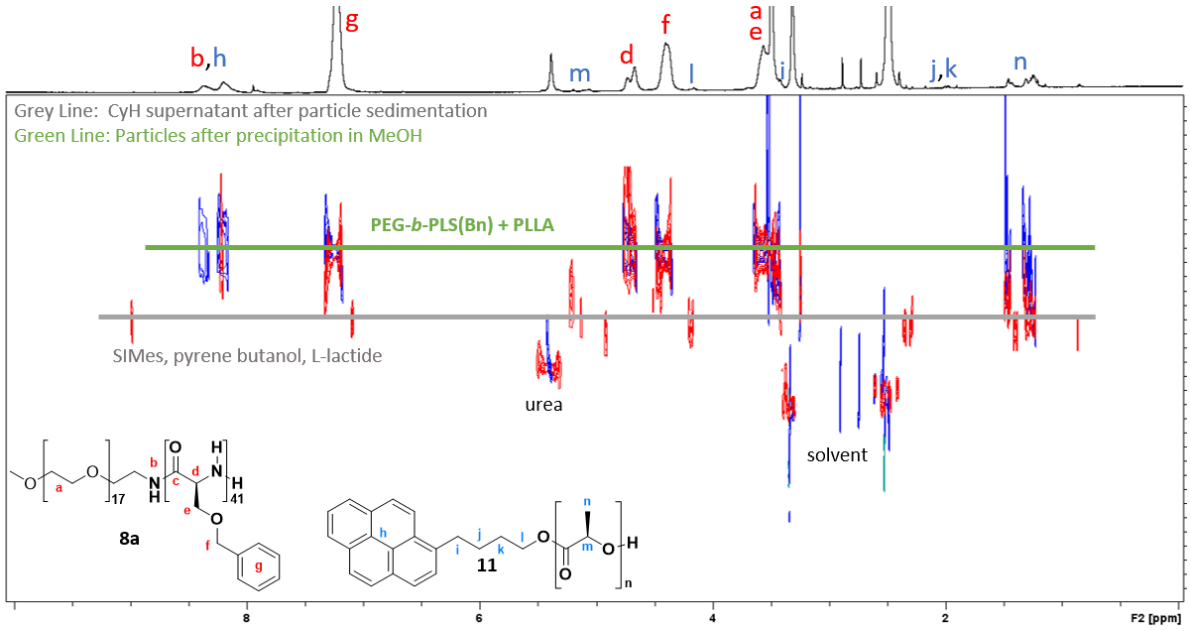

Figure 33: DOSY spectra overlay (700 MHz, 333 K, DMSO-d_6) of the coated PLLA nanoparticles after precipitation in methanol (green line) and the residue in the supernatant after sedimentation in cyclohexane (grey line).

The NMR analysis provided important information about the success of the reaction and the reason for the low yields. The fabrication of core shell nanoparticles of PLLA with the racemic emulsifier PEG_{45}-*b*-$PDLS(Bn)_{37}$ (**8a**) was indeed successful. The solubility and micelle formation in cyclohexane was slightly increased compared to the L-serine emulsifiers, but still not ideal to result in a stable emulsion that allowed the fabrication of coated PLLA nanoparticles in high yields. Optimization of the reaction was necessary by further tuning the solubility of the emulsifier in the continuous phase and therefore preventing the collapse of the emulsion during the polymerization. Nonetheless, spherical particles of desired size of around 100 nm were obtained. The polymerization was repeated at half scale and otherwise identical conditions to evaluate reproducibility and scalability (Table 11, No. **2**).

*Table 11: Summary of the NEPs with PEG_{45}-b-$PLS(Bn)_{37}$ (**8a**) at c = 2.43 mg/mL.*

No.	EP[1]	Emulsifier	Solvent	c [mg/mL]	t [min][2]	d_H [µm]
1	28	PEG_{45}-*b*-$PDLS(Bn)_{37}$, **8a**	MeCN/CyH MeOH	2.43	15	12.8 ± 22.6 13.2 ± 7.8
2	34	PEG_{45}-*b*-$PDLS(Bn)_{37}$, **8a**	MeCN/CyH	2.43	15	-[3]

[1] Numbering of experiment of the nonaqueous emulsion polymerization (ncsNW-epX). [2] reaction time
[3] DLS measurement could not be performed due to aggregation and precipitation of the emulsifier.

Large aggregates were present in the reaction mixture after the polymerization, according to DLS measurements. This was confirmed by the SEM images (Figure 34). In comparison to the approach before, the aggregates looked more homogeneous, consisting of few particles with diameters below 1000 nm, besides µm-sized agglomerates. After precipitation in methanol the SEM images showed few single aggregates of particles that were clumped together. In contrast to EP28, the particle morphology was not maintained after the precipitation of the particles in methanol.

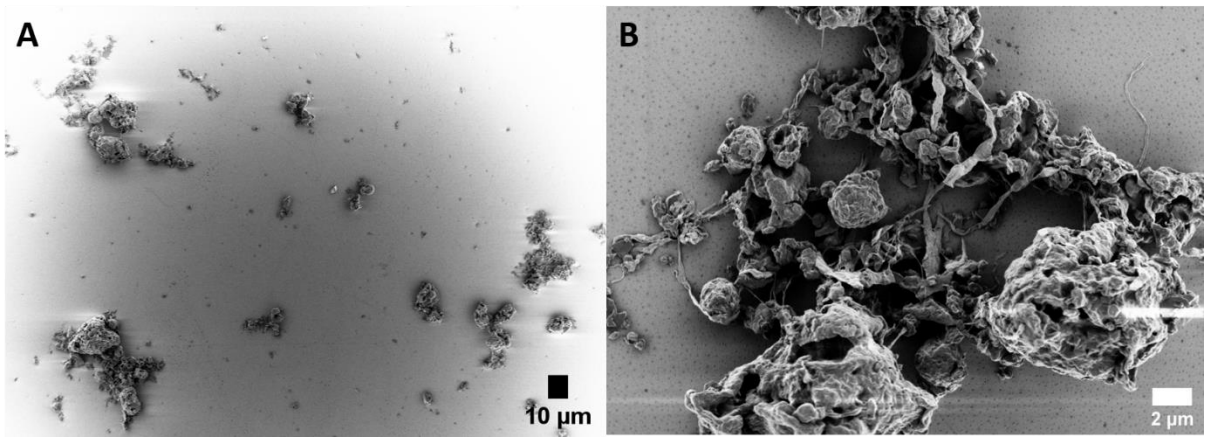

*Figure 34: SEM images of the PEG_{45}-b-$PDLS(Bn)_{37}$ (**8a**) coated PLLA nanoparticles (EP34), dispersed in cyclohexane.*

The DOSY spectrum showed the same diffusion constant for the PLLA and emulsifier signals (Figure 35, green line). This indicated that even though the emulsion collapsed during the reaction and the particles strongly aggregated, the polymerization of PLLA worked to some extent and the aggregates consisted of both, emulsifier and PLLA. The first two approaches also showed that using the proposed

concentration of 2.43 mg/mL is not ideal for the PEG-*b*-PDLS(Bn) emulsifier, especially at small scale, as it clearly increased the particle aggregation and did not result in homogeneously dispersed particle dispersions.

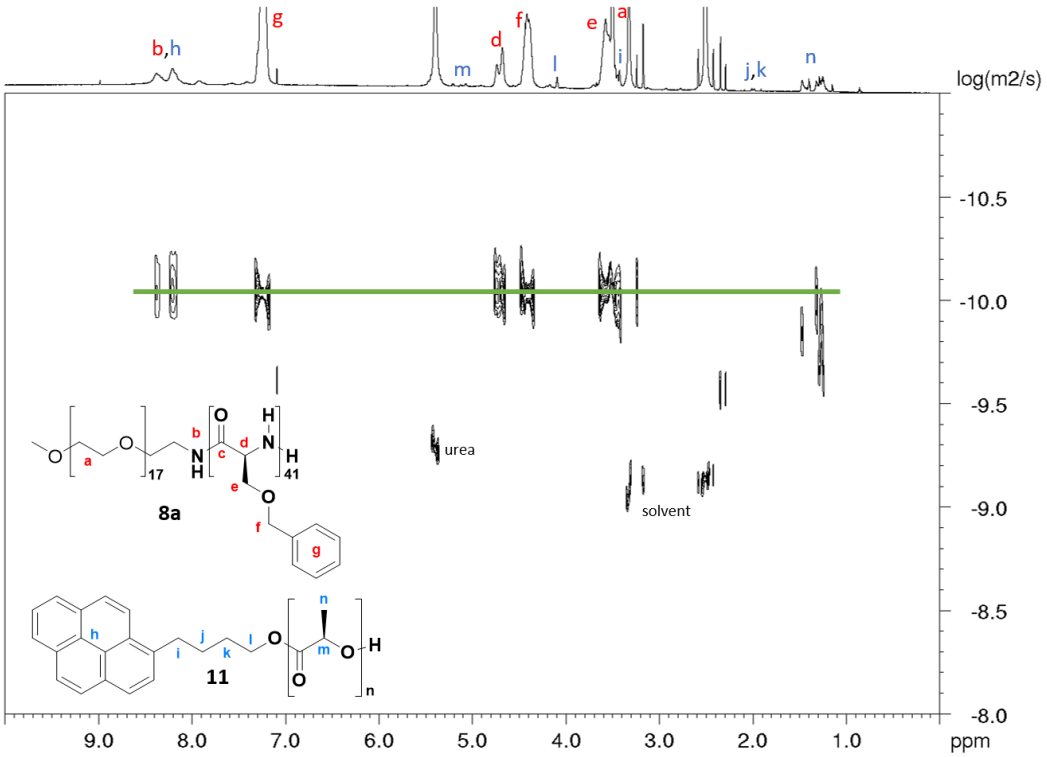

*Figure 35: DOSY NMR spectrum (700 MHz, 298 K, DMSO-d_6) of PEG_{45}-b-$PLS(Bn)_{37}$ (**8a**, red) coated PLLA (**11**, blue) nanoparticles (green line).*

INFLUENCE OF DECREASED EMUSLIFIER CONCENTRATION ON THE EMULSION STABILITY

The previous particle syntheses with the racemic emulsifiers resulted in nanoparticles, even though the result was beyond ideal in terms of yield and homogeneity of the particle dispersions. In order to evaluate the role of the emulsifier concentration on the aggregation behaviour of the particles, the concentration was decreased in the next approaches. The first polymerization of this series was conducted with the racemic emulsifier PEG_{45}-*b*-$PDLS(Bn)_{37}$ (**8a**) at a lower concentration of 1.22 mg/mL in MeCN/CyH (Table 12, No. **1**).

*Table 12: Summary of the NEPs with PEG_{45}-b-$PLS(Bn)_{37}$ (**8a**) at c = 1.22 mg/mL.*

No.	EP[2]	Emulsifier	Solvent	c [mg/mL]	t [min][1]	d_H [µm]
1	31	PEG_{45}-*b*-$PDLS(Bn)_{37}$, **8a**	MeCN/CyH	1.22	15	24.1 ± 11.3
2	35	PEG_{45}-*b*-$PDLS(Bn)_{37}$, **8a**	MeCN/CyH	1.22	15	5.34 ± 0.91

[1] reaction time [2] Numbering of experiment of the nonaqueous emulsion polymerization (ncsNW-epX).

While the emulsifier **8a** did mostly dissolve at this concentration, it precipitated immediately upon addition of the dispersed phase. The DLS measurement after the polymerization showed a broad size

distribution and large aggregates of around 24 µm. Therefore, this approach resulted in a heterogeneously dispersed mixture. The SEM images of the reaction mixture confirmed these results by showing lots of small particles below 50 nm that aggregated to small piles of 100-200 nm as well as large aggregates with diameters in the µm-range and worm-like structures (Figure 36 A, B). Compared to the previous experiments, the morphology of this approach was different, as it showed homogeneous and comparably well-defined particles, besides the large aggregates. The aggregates might have consisted of excess, unreacted emulsifier. The emulsion collapsed at an early stage during the polymerization. It was hypothesized that the particles might be "naked" PLLA particles that were not covered by the emulsifier. Consequently, this approach proved that a concentration of 1.22 mg/mL was too low for both, L- and DL-serine based emulsifiers.

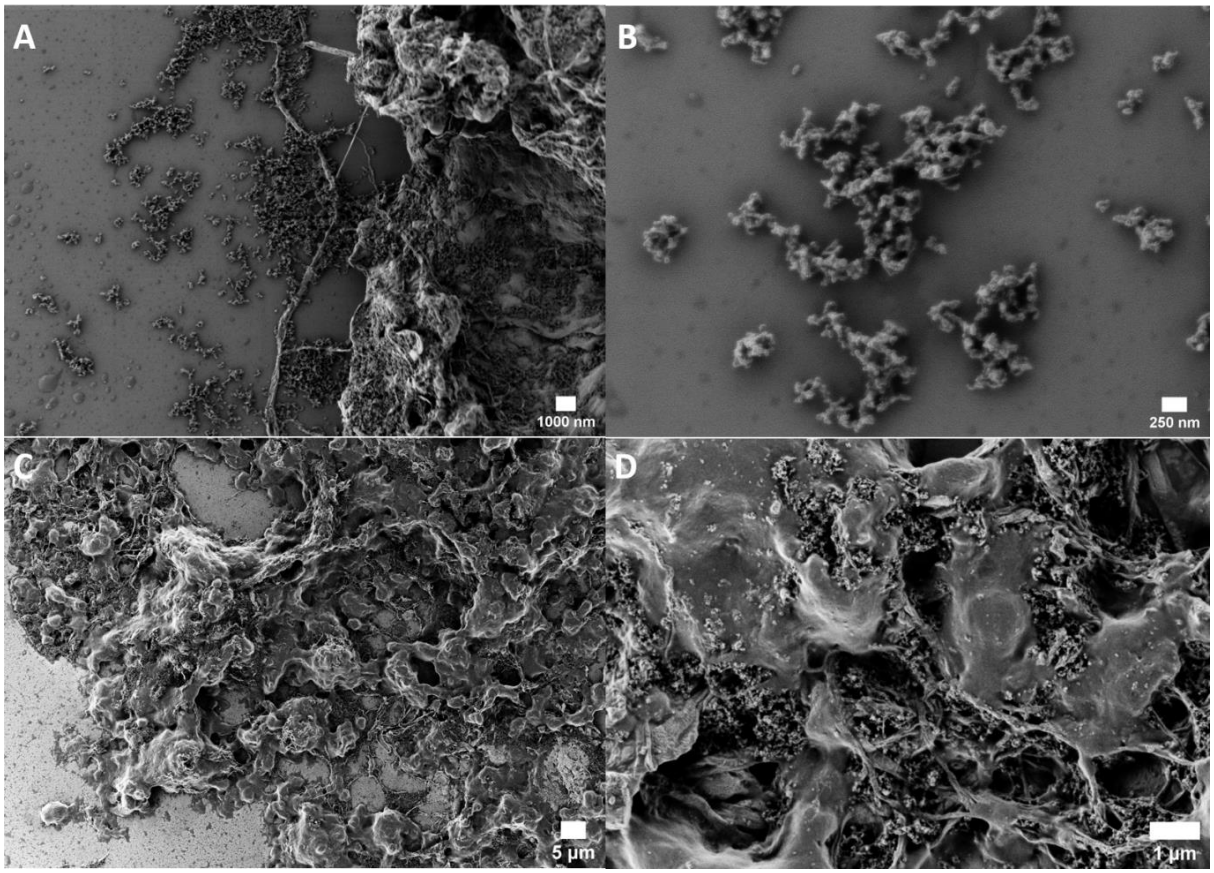

*Figure 36: SEM images of the PEG_{45}-b-$PDLS(Bn)_{37}$ (**8a**) coated PLLA nanoparticles (EP31), dispersed in cyclohexane.*

After precipitation of the particles in methanol, the SEM image showed a mixture of large particle aggregates with diameters of 1-5 µm and small particles (Figure 36 C, D). In comparison to the reaction mixture, the material looked less dispersed and clumped together. In some places the particles were covered by a consistent layer (Figure 36D). This could be explainedby smaller particles that clumped together by excess emulsifier, as reported by Dvorakova et al.[94] Alternatively, the excess emulsifier might have formed a thin layer on top of the particles during the evaporation process of the sample

preparation, as demonstrated by Nobutaka et al.[100] Overall, the decreased emulsifier concentration did not lead to an increase of the emulsion stability. Instead, it resulted in immediate collapse of the emulsion upon addition of the reagents, leading to the conclusion that an emulsifier concentration of 1.22 mg/mL was too low to form a stable emulsion. NMR analysis was used to prove, if naked PLLA nanoparticles or proper coating of the particles was obtained. The DOSY spectra of both approaches showed different diffusion constants for the emulsifier (Figure 37, red line) and PLLA signals (green line), confirming that the diffusion behaviour of PLLA and the emulsifier was different and consequently, the PLLA particles were not encapsulated by the emulsifier (Figure 37, red spectrum).

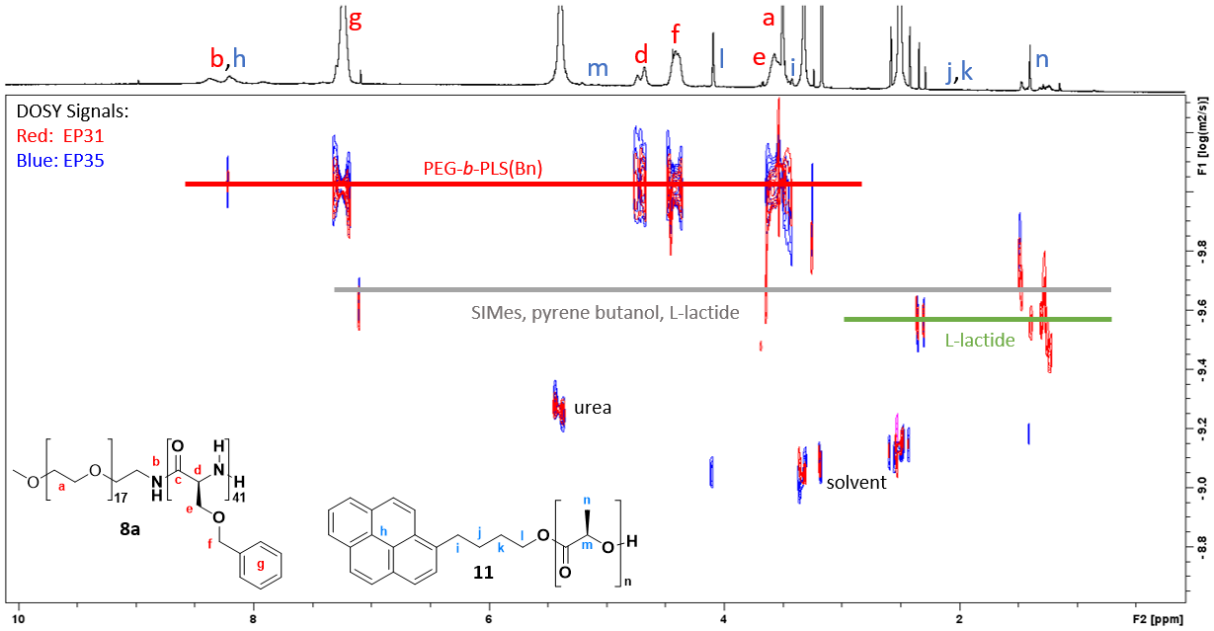

*Figure 37: Stacked DOSY spectra (700 MHz, 298 K, DMSO-d_6) of EP31 (red spectrum) and EP35 (blue spectrum), showing that the diffusion constant of the emulsifier (**8a**, red line) and PLLA (**11**, green line) are not identical in these two approaches.*

The amount of dispersed phase in an emulsion has direct effects on the emulsion stability and particle size in emulsion polymerization. Typically, reducing the dispersed solvent or increasing the concentration of the emulsifier leads to smaller particles until a plateau is reached by reducing the surface tension of the micelles.[94] In the next experiment not only the emulsifier concentration was halved (c = 1.22 mg/mL), but also the amount of the dispersed phase (Table 12, No. 2). There was no positive effect observed on the emulsion stability during the polymerization. Upon addition of the reagents, the emulsion collapsed. Nevertheless, the DLS measurement indicated smaller aggregates of 5.34 ± 0.91 µm, compared to the previous approach. The SEM images after the polymerization showed similar structures like the approach EP31. Very small particles (d > 50 nm) were formed that piled up together, resulting in a homogeneous morphology (Figure 38, A-B). Few coated particles with diameters of 100 nm were formed as well (Figure 38, C). In image D, the emulsifier is visible as a consistent thin layer on top of the particles (Figure 38, D). Decrease of emulsifier and dispersed phase

clearly led to smaller particles as expected. In comparison to EP31, smaller nanoparticles were produced. At the same time, SEM analysis cannot confirm, if these particles are coated or emulsifier-free. Along the lines of EP31, the DOSY spectrum showed different diffusion constants for PLLA (grey line) and the emulsifier (red line), and hence, coated PLLA nanoparticles could not be obtained (Figure 37, blue spectrum).

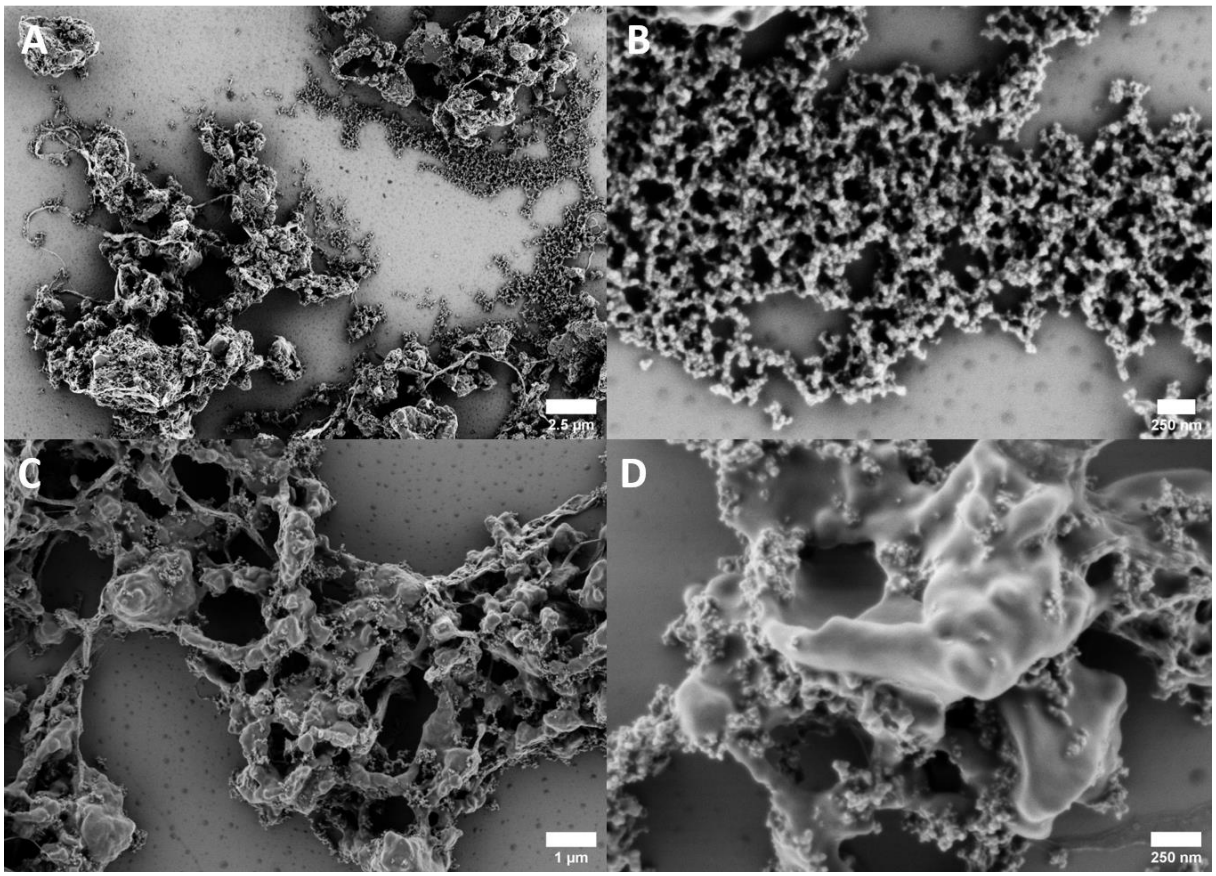

*Figure 38: SEM images of the PEG_{45}-b-$PDLS(Bn)_{37}$ (**8a**) coated PLLA nanoparticles (EP35), dispersed in cyclohexane.*

EFFECT OF DECREASED HYDROPHOBIC MOIETY IN THE EMULSIFIER ON THE NEP

In the next approaches, the emulsifier PEG_{45}-*b*-$PDLS(Bn)_{32}$ (**8b**) with a slightly shorter serine chain with a DP of 32 was used to study whether the slightly different block ratio makes a notable difference in the aggregation behavior. In addition, this polymer was synthesized at lower temperatures, which could have an effect on the polydispersity or enantiomer ratio of serine. In order to find the right concentration for this emulsifier, an emulsion formation study was performed first, where the polymer was dissolved in cyclohexane at different concentrations and the particle size was determined by DLS. The common literature describes a general decrease of particle size with increased emulsifier concentration[94]. With polymer **8b** the particle size distribution was decreased, and less aggregation was observed at higher dilution (Table 13). According to the emulsion formation study, the emulsifier performed better at lower concentration below 1 mg/mL in cyclohexane. In the following NEP, a

concentration of 1.62 mg/mL was used, after it was demonstrated that lower emulsifier concentrations were not leading to stable emulsions during the NEP. A concentration of c = 1.22 mg/mL was found to be too low to stabilize the dispersed phase during the reaction with the block copolymer PEG_{45}-*b*-$PDLS(Bn)_{37}$ (**8a**), resulting in the collapse of the emulsion upon addition of the reagents.

*Table 13: Summary of the emulsion formation experiments and NEP with PEG_{45}-b-$PLS(Bn)_{32}$ (**8b**) at c = 1.62 mg/mL.*

No.	EP[1]	Emulsifier	Solvent	c [mg/mL]	d_H [µm]
1	36-1-1	PEG_{45}-*b*-$PDLS(Bn)_{32}$, **8b**	CyH	2.43	0.05 – 10.5
2	36-1-2	PEG_{45}-*b*-$PDLS(Bn)_{32}$, **8b**	CyH	1.62	8.90 ± 4.10
3	36-1-3	PEG_{45}-*b*-$PDLS(Bn)_{32}$, **8b**	CyH	1.21	7.35 ± 2.70
4	36-1-4	PEG_{45}-*b*-$PDLS(Bn)_{32}$, **8b**	CyH	0.97	1.40 ± 1.15
5	38	PEG_{45}-*b*-$PDLS(Bn)_{32}$, **8b**	MeCN/CyH	1.62	0.40

[1] Numbering of experiment of the nonaqueous emulsion polymerization (ncsNW-epX).

The DLS measurement after the reaction showed a desirable size distribution of around 400 nm. It was confirmed by the SEM images, where particles in the range of 300 nm were visible, besides few larger aggregates in the µm-range (Figure 39, A). As the DLS measurement did not show any indication for particle aggregation, these aggregates might have formed by the solvent evaporation during the sample preparation on the silicon wafer. The SEM images showed particles with diameters below 500 nm that are clumped together by a thin layer of material, potentially consisting of excess emulsifier (Figure 39B).[94] Overall, this approach is a clear improvement, as dispersed nanoparticles were formed successfully, proving that a concentration of 1.62 mg/mL was significantly reducing aggregation, while the emulsifier was still able to stabilize the emulsion long enough to form nanoparticles. The aggregation of the particles needed to be prevented, to form a homogeneous particle dispersion to be used for further applications. Therefore, the reaction was further optimized in the following approaches.

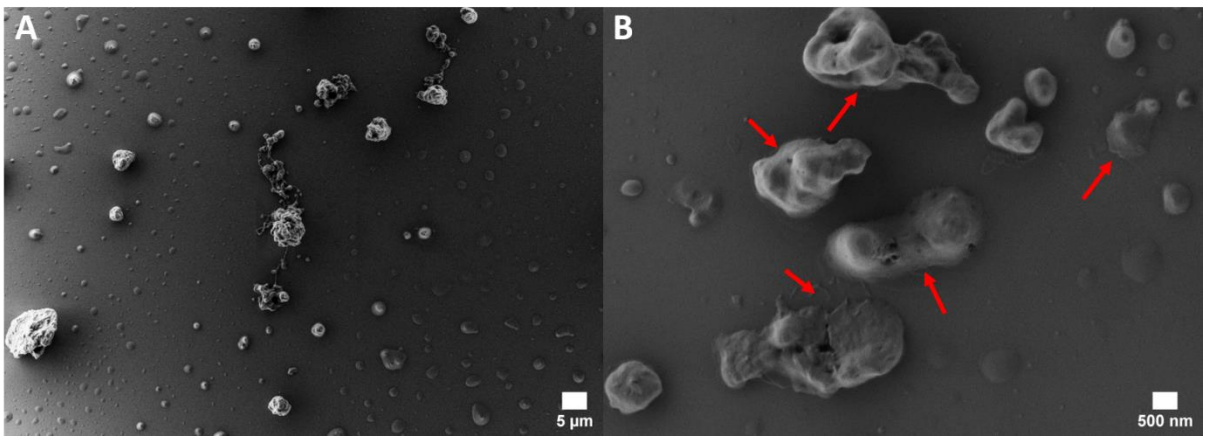

*Figure 39: SEM images of PEG_{45}-b-$PDLS(Bn)_{32}$ (**8b**) coated PLLA nanoparticles (EP38), dispersed in cyclohexane. B) Thin layers of excess material indicated by red arrows.*

The DOSY-NMR spectrum of these particles showed the PLLA (h-n) and emulsifier signals (a-g) having the same diffusion constant, which indicated particle formation and particularly successful polymerization of PLLA (Figure 40, green line). The signal intensities of PLLA in the proton NMR were lower than expected, which meant uncomplete polymerization, as observed in previous experiments, or successful encapsulation of the PLLA in the nanoparticle core. Most likely, it was a combination of both effects, as the starting materials pyrene butanol, L-lactide and the SIMes catalyst were visible in the DOSY spectrum as well (grey line).

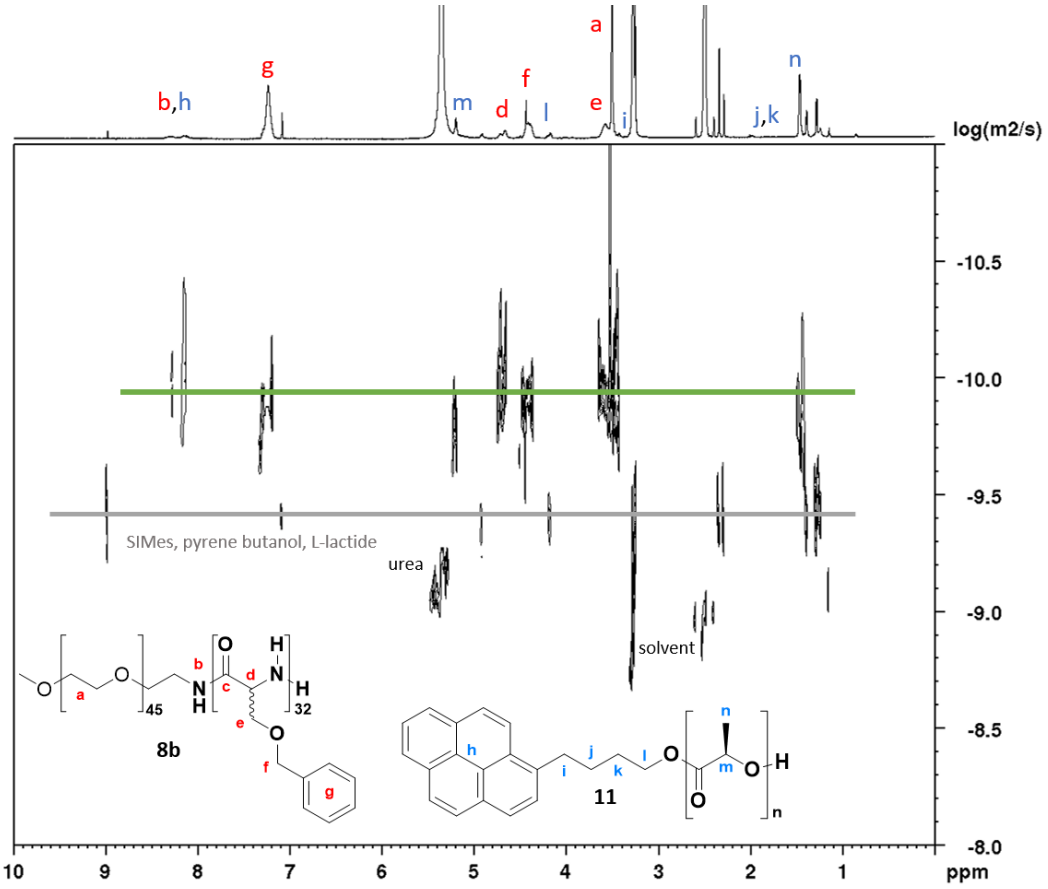

*Figure 40: DOSY NMR spectrum (700 MHz, 298 K, DMSO-d_6) of PEG_{45}-b-$PLS(Bn)_{32}$ (**8a**, red) coated PLLA (**11**, blue) nanoparticles (green line).*

In conclusion, the approach with PEG_{45}-*b*-$PDLS(Bn)_{32}$ (**8b**) at a concentration of 1.62 mg/mL led to the best results in terms of particle size and morphology so far. This concentration was in between the standard concentration of 2.43 mg/mL, where excess emulsifier promoted aggregation of the particles, clearly visible in the SEM images, and the halved concentration of 1.22 mg/mL that was too low to stabilize the dispersed phase properly and consequently, led to tiny, potentially uncoated PLLA particles below 50 nm. The reaction was not quantitative, as the starting materials in the DOSY spectrum indicated and therefore, there was still room for improvement in the fabrication of dispersed nanoparticles with these serine-based emulsifiers.

INFLUENCE OF A HIGHER HYDROPHOBIC BLOCK IN THE EMULSIFIER AND REACTION TIME ON THE NEP

To further screen the synthesized polymers for the ideal emulsifier, the following experiments were performed with another PEG_{45}-based polymer that contained a clearly higher hydrophobic moiety with a block ratio of 45:150 and a weight ratio of 7:93. This emulsifier, PEG_{45}-*b*-$PDLS(Bn)_{150}$ (**8c**), was used to determine, if a predominantly hydrophobic moiety was increasing the solubility of the polymer in the nonpolar solvent cyclohexane and forming homogeneous nonaqueous emulsions. The weight ratio of 7:93 was clearly beyond the proposed ratios of 40:60 to 30:70, while the DP ratio of 23:77 almost fit. To get a first impression of its aggregation behavior, an emulsion formation experiment was conducted by dissolving the polymer **8c** at different concentrations in cyclohexane. The size distribution of the resulting mixtures was determined by DLS measurements (Table 14, No. **1-4**) and revealed not only aggregation of the polymers and a resulting average particle size of 8-9 µm, but also stable values over a concentration range of 2.43-1.21 mg/mL (Table 14, No. **1-3**). The highest dilution of 0.97 mg/mL showed lower values of around 6 µm, but a broad size distribution. These results were differing from the experiment with PEG_{45}-*b*-$PDLS(Bn)_{32}$ (**8b**), where a gradual decrease in size was observed with higher dilution.

*Table 14: Summary of the emulsion formation experiments and NEP with PEG_{45}-b-$PLS(Bn)_{150}$ (**8c**).*

No.	EP[1]	Emulsifier	Solvent	c [mg/mL]	t [min][2]	d_H [µm]
1	36-3-1	PEG_{45}-*b*-$PDLS(Bn)_{150}$, **8c**	CyH	2.43	-	8.10 ± 4.00
2	36-3-2	PEG_{45}-*b*-$PDLS(Bn)_{150}$, **8c**	CyH	1.62	-	9.00 ± 3.20
3	36-3-3	PEG_{45}-*b*-$PDLS(Bn)_{150}$, **8c**	CyH	1.21	-	8.40 ± 4.40
4	36-3-4	PEG_{45}-*b*-$PDLS(Bn)_{150}$, **8c**	CyH	0.97	-	6.15 ± 15.1
5	40	PEG_{45}-*b*-$PDLS(Bn)_{150}$, **8c**	MeCN/CyH	2.43	15	~0.47
6	43	PEG_{45}-*b*-$PDLS(Bn)_{150}$, **8c**	MeCN/CyH	2.43	60	1.38 ± 0.59

[1] Numbering of experiment of the nonaqueous emulsion polymerization (ncsNW-epX). [2] reaction time

Based on the results of the emulsion formation experiments, emulsion polymerization with PEG_{45}-*b*-$PDLS(Bn)_{150}$ (**8c**) was performed in MeCN/CyH at a concentration of 2.43 mg/mL. In order to tackle the incomplete reaction conversion and poor yield of the previous reactions, two approaches were conducted to evaluate, if the reaction time had an impact on the reaction conversion: EP40 with the standard reaction time of 15 minutes and EP43 with a prolonged reaction time of 60 minutes (Table 14, No. **5-6**). The DLS measurement after 15 minutes of reaction time showed a particle diameter of around 470 nm. The SEM images showed spherical particles with a porous surface and an average diameter of 1-2 µm (Figure 41A-C). The sample showed few well-defined particles and no aggregation. Even though, the particle diameter was 10 x higher than desired, barely any aggregates were observed, which was a clear improvement. This indicated that the high hydrophobic moiety of the emulsifier

might have prevented particle aggregation. In the second experiment, the reaction time was prolonged to 1 hour to study the effect of the reaction time on the particle formation. The particle diameter, determined by DLS, was 1.38 µm, nearly 3 x higher than in the first reaction. The SEM images showed strong aggregation of the particles and no uniform morphology (Figure 41D-E). Aggregates with diameters of 1-5 µm were observed, besides few nanoparticles in the range of 200-300 nm that did not agglomerate (Figure 41E). By washing the material with cyclohexane, some excess material was removed, but the diameter of the material was still in the µm-range and the aggregates could not be separated, according to DLS and SEM analysis (Figure 41F). This led to the conclusion that the prolongation of the reaction time was resulting in irreversible aggregation of the produced particles.

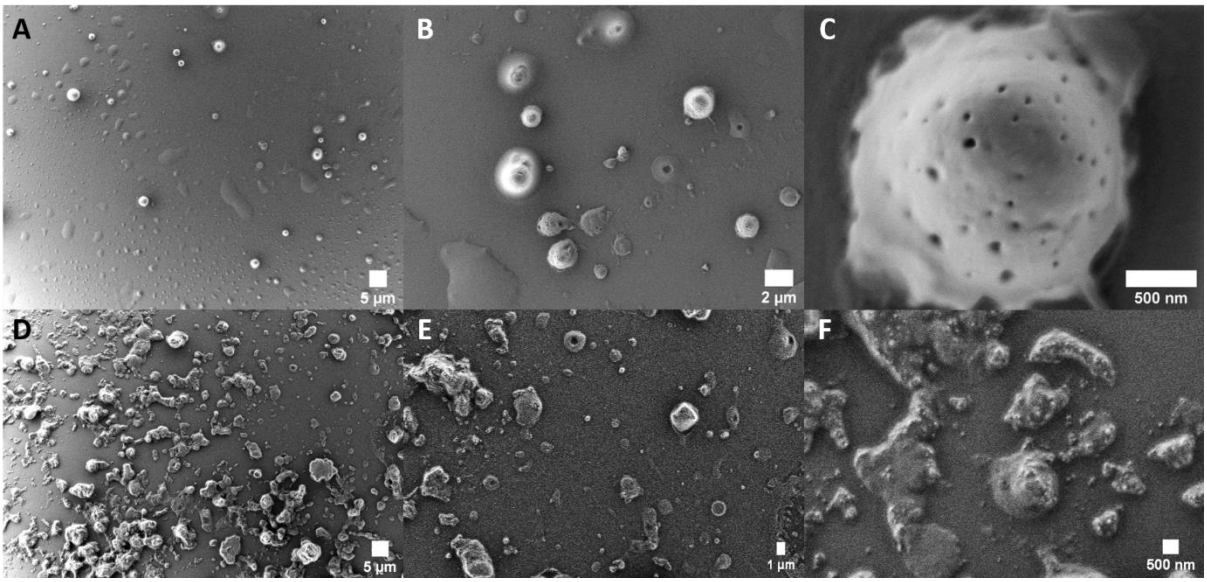

*Figure 41: SEM images of PEG_{45}-b-$PDLS(Bn)_{150}$ (**8c**) coated nanoparticles A-C) after 15 minutes reaction time and D-F) after 60 minutes reaction time; dispersed in cyclohexane.*

The DOSY-NMR analysis of these two samples both showed the same diffusion constant for the emulsifier and PLLA signals (Figure 42, green line). Significant amounts of unreacted starting materials were visible in the spectrum of the 15 minute-approach (red spectrum, grey line). These signals were not did not appear in the 60 minute-sample (blue spectrum). This led to the conclusion that the prolongation of the reaction time was resulting in higher monomer conversion, but at the same time to higher agglomeration of the particles. To optimize the outcome, the reaction time should be further studied to find out the “sweet spot” between maximum monomer conversion and minimal particle aggregation.

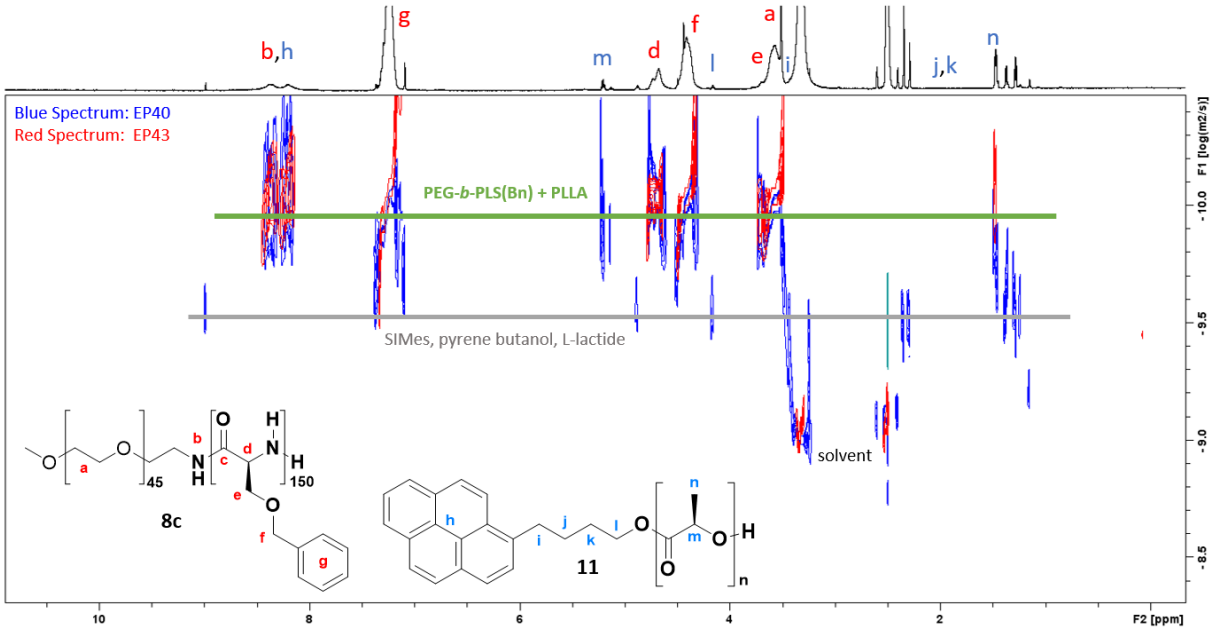

*Figure 42: DOSY spectra (700 MHz, 298 K, DMSO-d_6) of PEG_{45}-b-$PDLS(Bn)_{150}$ (**8c**) coated PLLA (**11**) nanoparticles after 15 minutes reaction time (blue spectrum) and after 60 minutes reaction time (red spectrum), showing that the diffusion constant of the emulsifier **8c** and PLLA **11** are identical in these two approaches (green line).*

In conclusion, most of the racemic emulsifiers containing a PEG_{45}-block, faced the problem of early collapse of the emulsion during the polymerization, resulting in incomplete conversion and low yields as well as agglomeration. Therefore, no major improvement compared to the L-serine polymers was achieved by using the racemic analogues. Nevertheless, some optimization was achieved in EP38, where spherical particles with diameters of 300 nm were formed by using an emulsifier concentration of c = 1.62 mg/mL and the racemic polymer PEG_{45}-*b*-$PDLS(Bn)_{32}$ (**8b**). With a clearly higher hydrophobic block, PEG_{45}-*b*-$PDLS(Bn)_{150}$ (**8c**) gave surprisingly good results in terms of particle morphology and aggregation behavior after 15 minutes of reaction time. Particles with a relatively narrow size distribution of 1 µm were obtained, which was a clear improvement to the approaches before, where broad size distributions were observed. Reaction prolongation to 60 minutes did result in strong and irreversible aggregation, but full reaction conversion. Therefore, the reaction time should be further optimized to find the perfect balance between maximum reaction conversion and low agglomeration.

INFLUENCE OF SHORTER PEG_{17}-*b*-PDLS(Bn) EMULSIFIERS ON THE EMULSION STABILITY

The polymerization degrees of the emulsifiers were optimized successfully for the PEG_{45}-derivatives by using the racemic serine monomer, and the desired block ratios and beyond were obtained. Yet the outcome in the emulsion polymerization did not meet the expectations, as aggregation and inhomogeneity of the particles were still unsolved issues. Therefore, another approach with shorter polymers was executed, using a PEG_{17}-derivative. The aim was to not only overcome the

polymerization limits of poly-*O*-benzylserine by needing shorter hydrophobic blocks to match the ideal block ratio, but also to achieve better solubility of the polymers by lower overall molecular weights. The previously described results with the L-serine analogues were positive, yet not ideal and hence, left some space for improvement. The racemic emulsifiers with the PEG_{17}-block were tested in nonaqueous emulsion to investigate if a lower molecular weight of the polymer was beneficial for the aggregation behavior and particle size. The particle formation with the PEG_{17}-*b*-$PLS(Bn)_{41}$ (**3a**) was successful in a previous approach, so the racemic analogue PEG_{17}-*b*-$PDLS(Bn)_{49}$ (**7a**) was tested next. Starting with an emulsion formation experiment at different concentrations in cyclohexane, the particle diameters remained stable at around 3-4 µm within a concentration range between 0.97-2.43 mg/mL (Table 15, No. **1-4**).

*Table 15: Summary of the emulsion formation experiments and NEP with PEG_{17}-b-$PLS(Bn)_{49}$ (**7a**).*

No.	EP[1]	Emulsifier	Solvent	c [mg/mL]	t [min][2]	d_H [µm]
1	36-2-1	PEG_{17}-*b*-$PDLS(Bn)_{49}$, **7a**	CyH	2.43	-	5 – 312
2	36-2-2	PEG_{17}-*b*-$PDLS(Bn)_{49}$, **7a**	CyH	1.62	-	3.50 ± 2.10
3	36-2-3	PEG_{17}-*b*-$PDLS(Bn)_{49}$, **7a**	CyH	1.21	-	2.85 ± 0.90
4	36-2-4	PEG_{17}-*b*-$PDLS(Bn)_{49}$, **7a**	CyH	0.97	-	4.00 ± 1.20
5	39	PEG_{17}-*b*-$PDLS(Bn)_{49}$, **7a**	MeCN/CyH	1.62	15	~0.22
6	42	PEG_{17}-*b*-$PDLS(Bn)_{49}$, **7a**	MeCN/CyH	1.62	60	1.75 ± 0.81
7	45	PEG_{17}-*b*-$PDLS(Bn)_{49}$, **7a**	DMSO/Et_2O	1.71	15	1.35 ± 0.16
			Et_2O[3]			0.99 ± 0.07

[1] Numbering of experiment of the nonaqueous emulsion polymerization (ncsNW-epX). [2] reaction time
[3] After one washing step with Et_2O

Based on the previous NEP´s, two emulsion polymerization experiments were conducted at a concentration of 1.62 mg/mL in MeCN/CyH with reaction times of 15 and 60 minutes (EP39 and EP42). The DLS measurements showed diameters of surprisingly accurate 220 nm after 15 minutes and a larger value of 1.75 µm after 60 minutes, following the trend of the previous experiments, where longer reaction times led to higher aggregation. The SEM images for the 60-minute approach showed that dispersed nanoparticles were not obtained, but large aggregates consisting of small particles that were clumped together (Figure 43D-F). In contrast, the SEM images of the 15-minute reaction showed well-defined spherical particles with diameters of 300-600 nm (Figure 43A-C). Overall, the sample looked very homogeneous, compared to previous approaches and very few aggregates of 1-2 µm were observed. This approach resulted in the best nanoparticles in terms of shape, size and morphology that were obtained with a serine-based emulsifier so far.

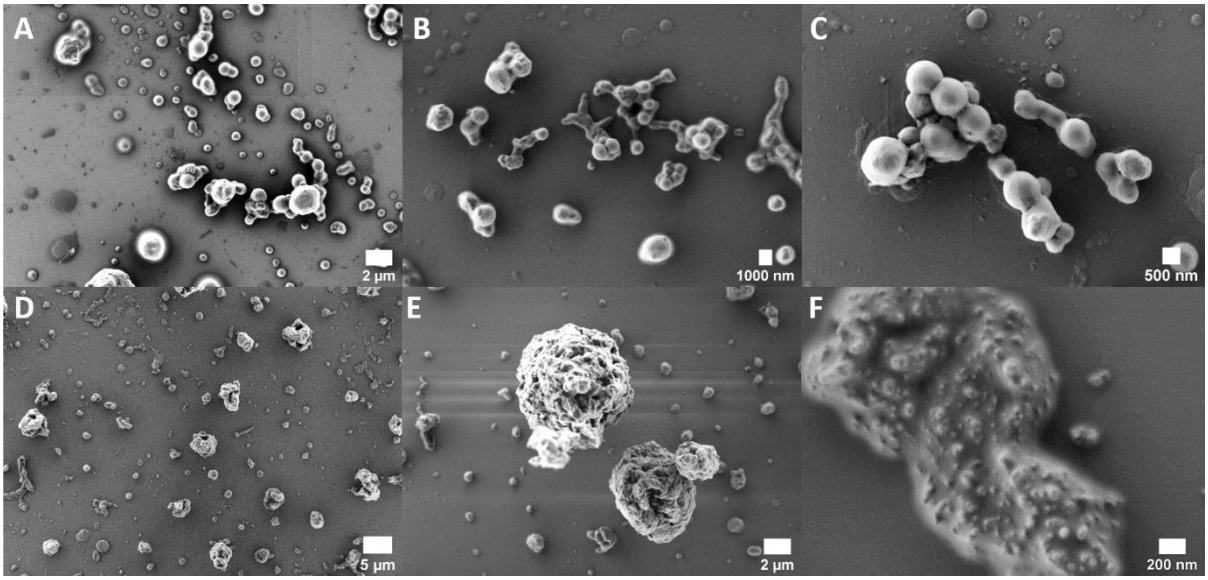

*Figure 43: SEM images of PEG_{17}-b-$PDLS(Bn)_{49}$ (**7a**) coated nanoparticles A-C) after 15 minutes reaction time and D-F) after 60 minutes reaction time; dispersed in cyclohexane.*

The DOSY spectra showed the same diffusion constant for PLLA (h-n) and emulsifier signals (a-g) for both approaches (Figure 44, green line). The PLLA signal intensity was very weak in the 60-minute approach (EP42, red spectrum), compared to the 15-minute reaction (EP39, blue spectrum), indicating lower chain length, resulting from low reaction conversion. Again, the 15 minute-approach (EP39) showed a significant amount of unreacted starting materials in the DOSY spectrum- These signals were not visible in the sample that was allowed to react for 60 minutes (EP42). This proved the hypothesis that the prolongation of the reaction time was resulting in higher monomer conversion, but at the same time in higher agglomeration of the particles.

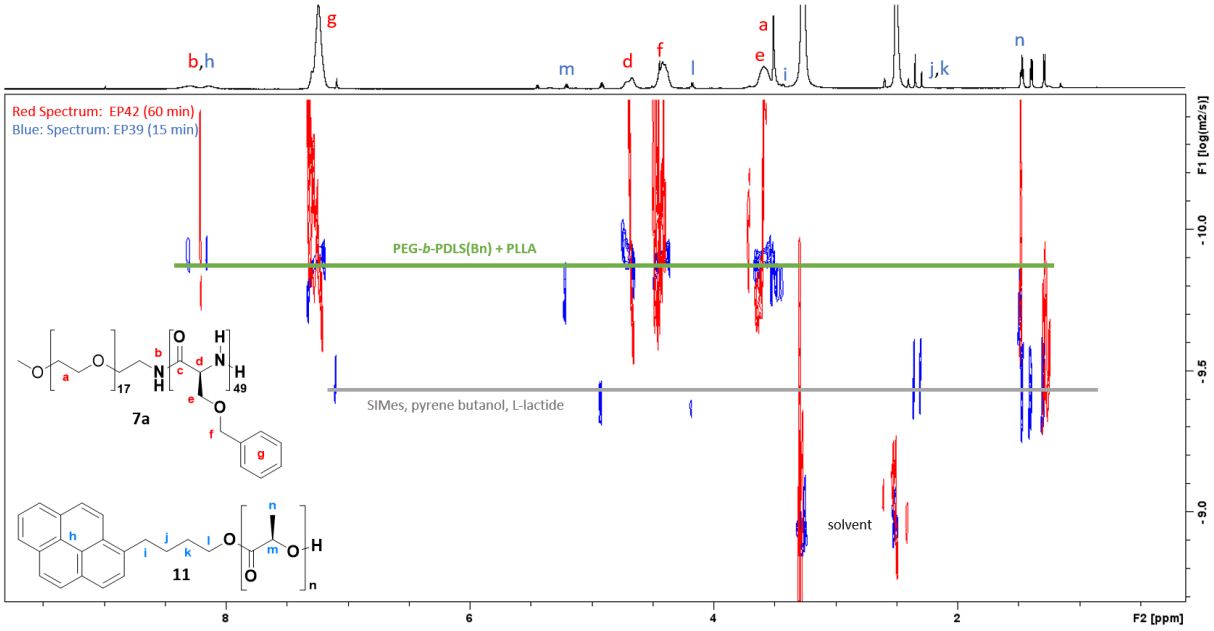

*Figure 44: DOSY spectra (700 MHz, 298 K, DMSO-d_6) of PEG_{17}-b-$PDLS(Bn)_{49}$ (**7a**) coated PLLA (**11**) nanoparticles (green line) after 15 minutes reaction time (blue spectrum) and after 60 minutes reaction time (red spectrum).*

INFLUENCE OF THE SOLVENT SYSTEM ON THE EMULSION POLYMERIZATION

During the synthesis of the racemic emulsifiers and especially their workup, the polymers behaved differently than the L-serine analogues. While the L-serine polymers precipitated, partially during the reaction in DMF, and in diethylether during the workup, the DL-serine polymers formed an emulsion. This led to the idea of changing the solvent system of the emulsion polymerization by using diethylether as the nonpolar phase, instead of cyclohexane, to obtain a stable emulsion and prevent it from collapsing during the polymerization. An experiment was performed with PEG_{17}-*b*-$PDLS(Bn)_{49}$ (**7a**) in DMSO/Et_2O as the solvent system at an emulsifier concentration of 1.71 mg/mL (Page 66, Table 15, No. **7**). DMSO was chosen as the dispersed phase, because it is the only polar, organic solvent that is immiscible with diethylether.[101] After 15 minutes of polymerization, the particle size, determined by DLS, was 1.35 µm, with a very narrow size distribution (Figure 45A). After sedimentation and washing of the particles with diethylether, the size distribution remained narrow, while the size slightly decreased to around 1 µm (Figure 45B). In comparison to EP39 with PEG_{17}-*b*-$PDLS(Bn)_{49}$ (**7a**) the particle diameter was higher, but the mixture was more homogenous in terms of particle size and showed no signs of aggregation.

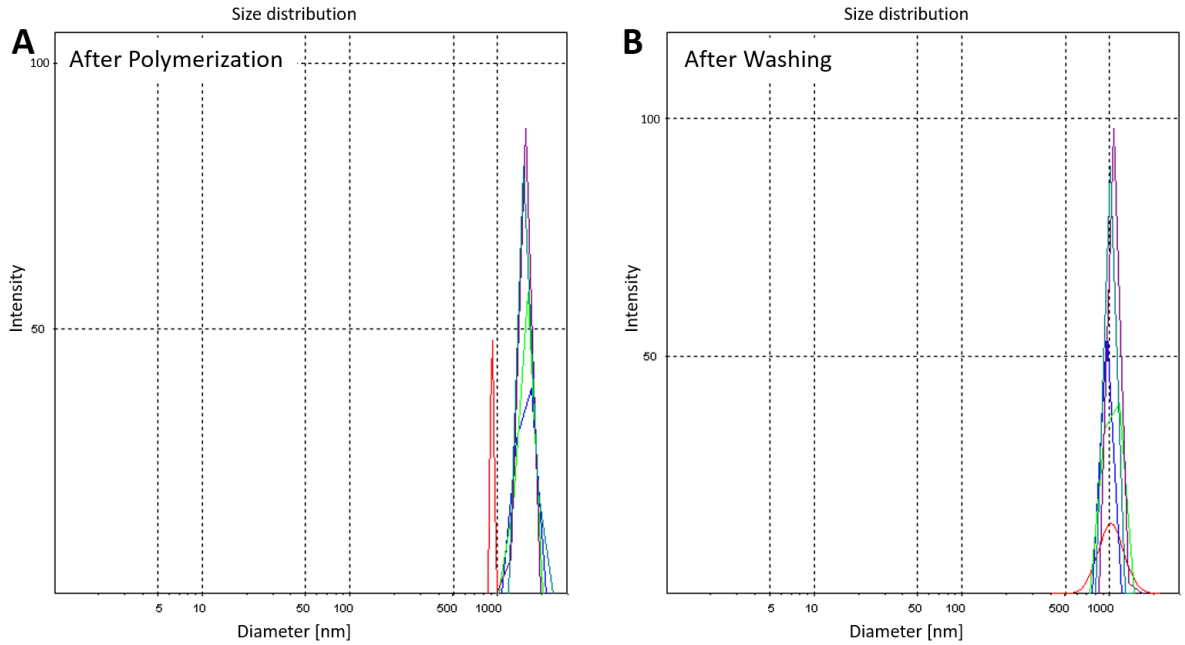

Figure 45: DLS measurements of EP45: A) After polymerization and B) after washing and sedimentation of the particles.

The SEM images of this approach were differing completely from what was indicated by the DLS measurements. No particle morphology was observed at all. Instead, the sample consisted of µm-sized aggregates (Figure 46A). A closer look into the aggregates revealed that they were built from smaller particles in the 100-200 nm range that were clumped together (Figure 46B). Nanoparticles were formed, but potentially aggregated during the sample preparation. When comparing the vapor

pressure of the former solvent system MeCN/CyH, both solvents evaporate simultaneously. In contrast, diethylether is highly volatile, therefore evaporating immediately at room temperature, while DMSO is barely evaporating at standard conditions, causing the nonpolar nanoparticles to agglomerate in the polar environment. This was also indicated by the heterogeneous distribution of the sample on the silicon wafer after sample preparation. A possible solution might be to wash the sample more extensively before the sample preparation to remove as much DMSO as possible to allow a more realistic insight into the particle morphology.

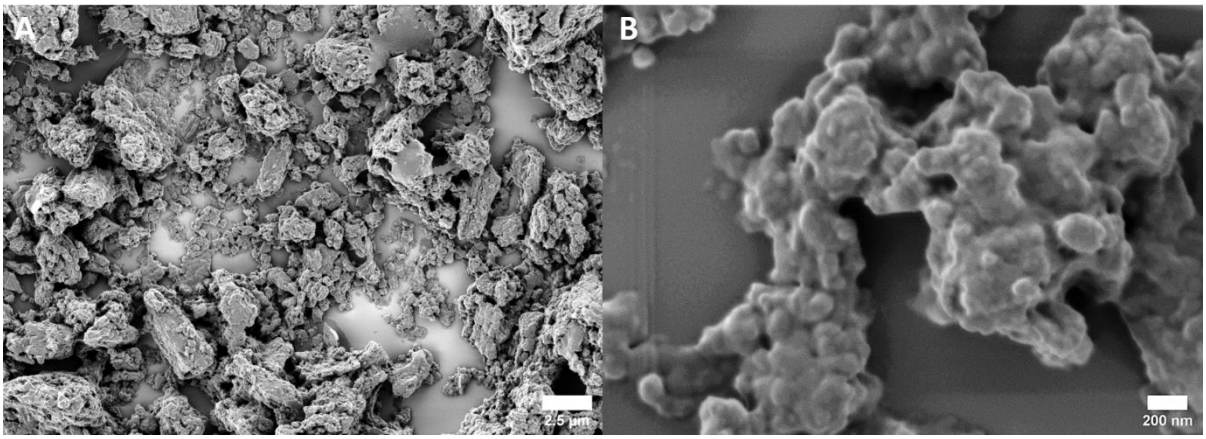

*Figure 46: SEM images of PEG_{17}-b-$PDLS(Bn)_{49}$ (**7a**) coated nanoparticles (EP45), dispersed in diethylether.*

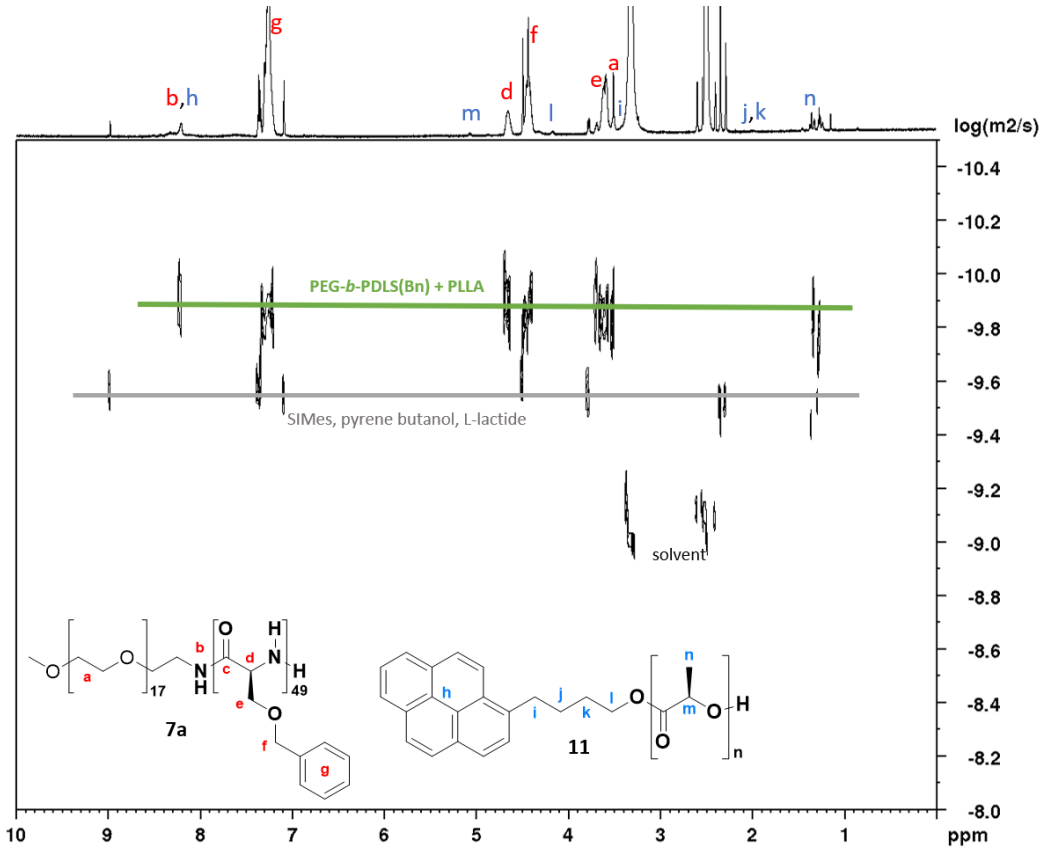

*Figure 47: DOSY-NMR spectrum (700 MHz, 298K, DMSO-d_6) of PEG_{17}-b-$PDLS(Bn)_{49}$ (**7a**) coated PLLA (**11**, blue) nanoparticles (green line).*

To find out more about the constitution of the material, NMR analysis was performed. The DOSY spectrum confirmed the polymerization of PLLA, showing the same diffusion constant for PLLA and emulsifier signals (Figure 47, green line), whereas the proton spectrum revealed that the signal intensities of PLLA were exceedingly low compared to previous experiments in the standard solvent system. In addition, the starting materials were present in significant amounts (grey line), proving that the reaction was not completed. As no other parameters were changed except of the solvents, one of them appeared to be problematic for the ROP of PLLA, causing the low monomer conversion. To further investigate, if the solvent system or one of the solvents inhibited the PLLA polymerization, solution polymerization of PLLA in different solvents was conducted. As the polymerization takes place in the dispersed phase in the emulsion polymerization, the polar solvents MeCN, DMF and DMSO were used and the polymers were analysed by GPC (Figure 48).

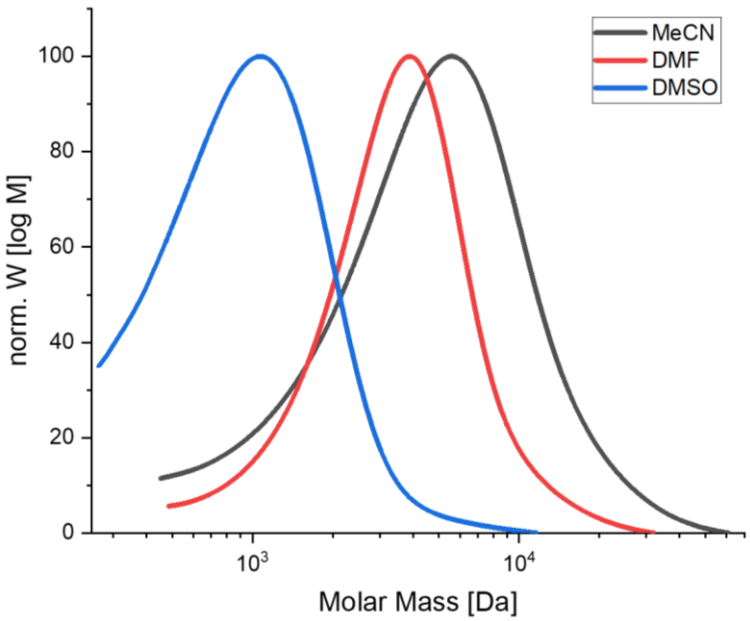

Figure 48: GPC graphs (measured in THF, against PS) of the PLLA polymers in MeCN (black), DMF (red) and DMSO (blue).

The GPC analysis confirmed the hypothesis that the polymerization in DMSO resulted in clearly lower molecular weight of 800 Da (Table 16, No. **1**), compared to 3000 Da in MeCN (No. **2**) and 2700 Da in DMF (No. **3**), as visualized in Figure 48. The polymerization in acetonitrile and DMF both led to comparably good results, being closer to the theoretical value of 5000 Da. While the polydispersity (Đ) of the PLLA was lower in DMF (1.58) than in MeCN (2.16), the molecular weight distribution of the polymer was higher in MeCN. The yield of the reactions followed the same trend. The polymerization in MeCN resulted in the highest yield of 73%, while the yield in DMF was only 35%. In DMSO PLLA was obtained with the lowest yield of only 10%.

Table 16: Comparison of the GPC data of the PLLA polymerization in solution, using different organic solvents.*

Approach	Solvent	Mw	Mn	Đ	Yield [%]
1	DMSO	1200	800	1.55	10
2	MeCN	6500	3000	2.16	73
3	DMF	4300	2700	1.58	35

*GPC was measured against PS, in THF at 30 °C.

As suspected, DMSO was inhibiting the polymerization of PLLA and was therefore not suitable as a solvent for the emulsion polymerization. Even though diethylether was a much better nonpolar solvent for the serine-based emulsifiers than cyclohexane, another solvent system is required, as DMSO is the only immiscible organic solvent for diethylether.[101] Ideally, the dispersed phase should be either DMF or MeCN, as both are proven solvents for nonaqueous emulsion polymerization. One nonpolar solvent that is immiscible with DMF and has similar properties as diethylether, is diisopropylether (DiPE). Therefore, the solvent system DMF/DiPE had huge potential for the NEP with serine-based emulsifiers. In a first solubility experiment, PEG_{45}-*b*-$PDLS_{49}$ (Bn) (**7a**) showed good solubility and aggregation behaviour in DMF/DiPE with micelle sizes of around 600 nm and a narrow size distribution. The detailed studies that were performed in this solvent system are discussed in chapter 4.3.

3.3 Summary and Outlook

The experiments discussed in this chapter showed that serine-based block copolymers are auspicious materials as emulsifiers for nonaqueous emulsion polymerization to fabricate core-shell nanoparticles. A drawback and the reason why serine-based polymers are not widely used yet is that their handling is not as easy as other amino acid-based copolymers, like L-lysine or L-glutamic acid base systems.[50,67] Responsible for this are the structural features, the strong β-sheet formation, and resulting aggregation behaviour of poly serines. Nevertheless, the amphiphilic PEG-*b*-Poly(O-benzyl-L-serine) block copolymers (**2-4**) were synthesized successfully with different block ratios. They were extensively studied as emulsifiers for nonaqueous emulsion polymerization to create biocompatible core-shell poly-L-lactide nanoparticles for therapeutic applications. Emulsion formation of the *O*-benzyl-L-serine-based polymers in the nonaqueous solvent cyclohexane was resulting in strong aggregation that hindered the formation of homogeneous nanoparticle dispersions. The following experiments were executed in order to optimize the reaction conditions that were adapted from the PEG-*b*-PLG(Pyr) system by Robert Dorresteijn,[50] and adapt them to our PEG-*b*-PLS(Bn) emulsion system (Figure 49).

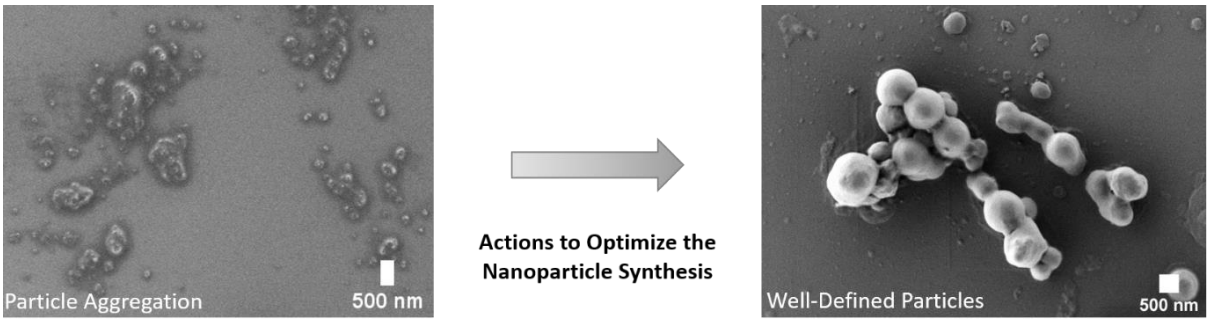

	The Problem	Starting Point	After Optimization
Done ✓	Strong particle aggregation in nonpolar cyclohexane was observed	PEG_{45}-b-PLS(Bn) with low hydrophobic moiety	Increase block length of hydrophobic PLS(Bn)
Done ✓	Excess emulsifier affected particle morphology	c = 2.43 mg/mL	c = 1.62 mg/mL
Done ✓	Desired emulsifier block ratios were not achieved	Enantiopure O-Bn-L-serine monomer	Using the racemic DL-serine analogue for ROP
Outlook	Emulsifiers did not fully dissolve in cyclohexane	MeCN/CyH solvent system	DMSO/Et2O, then DMF/DiPE
Outlook	Hydrophilization of emulsifier by Bn-deprotection failed	Bn protecting group as hydrophobic moiety	Photocleavable pyrene as hydrophobic moiety

Figure 49: Summary of the actions that were executed to adapt the nanoparticle synthesis by nonaqueous emulsion polymerization to the PEG-b-PSer(Bn) emulsifiers to obtain well-defined core-shell nanoparticles and outlook on the next steps to further optimize the particle synthesis with the serine-based emulsifiers.

By adjusting the block ratio of the polar and nonpolar blocks some improvement could be achieved and nanoparticles were formed successfully with the PEG-*b*-PLS(Bn) emulsifiers, even though a broad size distribution was obtained. Spherical particles with less aggregation were obtained by conducting the polymerization at a lower emulsifier concentration of 1.62 mg/mL instead of 2.43 mg/mL. To

suppress the agglomeration of the particles, another set of emulsifiers were synthesized by using the racemic *O*-benzyl-DL-serine, resulting in block copolymers with similar low block ratios of 45:35 of the PEG to PDLS(Bn) block. Decreasing the polymerization temperature to 0°C resulted in block copolymers with significantly higher DPs, like PEG_{45}-*b*-$PDLS(Bn)_{150}$ (**8c**). Using the emulsifier **8c** with a clearly higher hydrophobic moiety resulted in spherical nanoparticles with an average diameter of 470 nm that did not agglomerate, which was a huge improvement. The SEM images showed particles of 1 µm in diameter that might be caused by a swelling effect through solvent evaporation during the sample preparation. The best result in terms of size, shape and low aggregation was achieved by decreasing the polar block length to PEG_{17}. With PEG_{17}-*b*-$PDLS(Bn)_{49}$ (**7a**) spherical nanoparticles with a diameter of 210 nm, according to DLS, were obtained. The SEM images confirmed the successful synthesis of nanoparticles of appropriate size. This led to the conclusion that the serine-based polymers were suitable as emulsifiers for nonaqueous emulsion polymerization by not only adjusting the polymer composition but also the emulsifier concentration. However, another approach to optimize the reaction was the change of the solvent system as the emulsifiers showed higher solubility in the nonpolar solvent diethylether than in cyclohexane, demonstrated by emulsion formation experiments. The solvent system DMSO/diethylether was studied for emulsion polymerization of poly-L-lactide. It turned out that DMSO was hindering the quantitative polymerization of PLLA and hence, was not suitable for this reaction. A potential alternative system was identified with DMF/diisopropylether. An initial emulsion formation experiment resulted in good solubility and aggregation behaviour. It was studied in detail with another set of serine-based emulsifiers, discussed in the next chapter. The benzyl protected serine was used as a model system to evaluate the potential of serine polymers as emulsifiers for nonaqueous emulsion polymerization of PLLA core shell nanoparticles. The benzyl group is cleavable only under harsh conditions and the corresponding block copolymers showed strong aggregation tendencies in nonaqueous solution. As a consequence, it was not further studied after the described efforts and instead, an alternative protecting group strategy for serine was established. Nevertheless, the experiments with the PEG-*b*-PSer(Bn) block copolymers gave valuable insights into the aggregation behaviour of sidechain-protected polyserine in nonpolar emulsion systems. All following experiments were based on these initial findings, as serine-based polymers were never used before in nonaqueous emulsion polymerization. The next step was the introduction of an easily cleavable protecting group into the serine side chain, which is discussed in the following chapter.

3.4 Experimental Part

Synthesis of *O*-Benzyl-L-serine *N*-carboxy anhydride (L-Ser(Bn)-NCA, 1): *O*-Benzyl-L-serine (5.00 g, 25.6 mmol, 1.00 eq) was dissolved in dry THF (60 mL) under Argon atmosphere. α-pinene (8.10 mL, 51.2 mmol, 2.00 eq) was added as HCl scavenger and the reaction mixture was heated to 55°C. Meanwhile, triphosgene (5.02 g, 16.9 mmol, 0.66 eq) was dissolved in dry THF (20 mL) and added to the first solution. The mixture was stirred for 30 minutes until the solution turned clear. The RM was cooled to RT, while Argon was introduced into the mixture and then passed through a sodium hydroxide solution to remove excess phosgene. The solution was filtered over a plug of silica gel twice and the volume was reduced to 30%. The residual mixture was precipitated in cold *n*-hexane under vigorous stirring. After filtration of the precipitate, the product was recrystallized twice and dried under vacuum to obtain the L-Ser(Bn)-NCA (**1**) as colorless solid (4.07 g, 18.4 mmol, 83%). ^{1}H-NMR (300 MHz, DMSO-d_6, 300 K): δ = 9.11 (s, 1H, -NH), 7.43—7.23 (m, 5H, Ph-CH), 4.66 (t, 1H, α-CH), 4.53 (t, 2H, Ph-CH_2O), 3.69 (dd, 2H, β-CH_2) ppm. ^{13}C-NMR (75 MHz, DMSO-d_6, 300 K): δ = 170.0 (C=O), 152.2 (C=O), 137.6 (Ph-C), 128.3 (Ph-CH), 127.7 (Ph-CH), 127.4 (Ph-CH), 72.5 (Ph-CH_2), 67.7 (β -CH_2), 58.4 (α -CH) ppm.

***O*-Benzyl-DL-serine *N*-carboxy anhydride (DL-Ser(Bn)-NCA, 5)** was synthesized in the same way with a yield of 96%. ^{1}H-NMR (300 MHz, DMSO-d_6, 300 K): δ = 9.11 (s, 1H, -NH), 7.32 (m, 5H, Ph-CH), 4.66 (t, 1H, α-CH), 4.52 (t, 2H, Ph-CH_2O), 3.69 (dd, 2H, β-CH_2) ppm. ^{13}C-NMR (75 MHz, DMSO-d_6, 300 K): δ = 170.0 (C=O), 152.2 (C=O), 137.6 (Ph-C), 128.3 (Ph-CH), 127.7 (Ph-CH), 127.4 (Ph-CH), 72.5 (Ph-CH_2), 67.7 (β -CH_2), 58.4 (α -CH) ppm.

***O*-Benzyl-D-serine *N*-carboxy anhydride (D-Ser(Bn)-NCA, 12)** was synthesized in the same way with a yield of 88%. ^{1}H-NMR (300 MHz, DMSO-d_6, 300 K): δ = 9.11 (s, 1H, -NH), 7.41-7.23 (m, 5H, Ph-CH), 4.66 (t, 1H, α-CH), 4.53 (t, 2H, Ph-CH_2O), 3.69 (dd, 2H, β-CH_2) ppm. ^{13}C-NMR (75 MHz, DMSO-d_6, 300 K): δ = 170.3 (C=O), 152.2 (C=O), 137.6 (Ph-C), 128.4 (Ph-CH), 127.7 (Ph-CH), 127.4 (Ph-CH), 72.5 (Ph-CH_2), 67.7 (β -CH_2), 58.4 (α -CH) ppm.

Synthesis of Bn-PLS(Bn) homopolymer (2) and PEG-*b*-PLS(Bn) copolymer (3-4): L-Ser(Bn)-NCA (0.50 g, 2.26 mmol, 1 eq) was evacuated and flushed with Argon, then dissolved in 10 mL of dry DMF. The initiator Bn-NH_2 (5 µL, 45 µmol, 0.02 eq), mPEG_{17}-NH_2 (33.9 mg, 45 µmol, 0.02 eq) or mPEG_{45}-NH_2 (29.4 mg, 15 µmol, 0.0065 eq) and lithium bromide (0.127 g, 1.47 mmol, 0.65 eq) were dissolved in 5 mL of dry DMF and added to the first solution. The reaction mixture was stirred at 0 °C for 4 days. 3 mL of DMF was added to the RM and precipitated in cold diethyl ether under vigorous stirring. The precipitate was filtered and dried *in vacuo*. The polymer was obtained as colorless solid.

Bn-*b*-PLS(Bn) (**2**, 0.51 g) was obtained with 95% yield. ^{1}H-NMR (700 MHz, DMSO-d_6, 333 K): δ = 8.65-8.05 (m, NH), 7.48-7.31 (m, Ph-CH, Bn-NH_2), 7.25 (m, Ph-CH, Ser(OBn)), 4.68 (s, α-CH), 4.44 (m, Ph-CH_2, Ser(OBn)), 4.30 (m, Ph-CH_2 (Bn-NH_2)), 3.63 (m, β-CH_2) ppm. M_n = 8900 g/mol. DP = 50.

PEG_{17}-*b*-PLS(Bn) (**3**, 0.51 g) was obtained with 53% yield. ^{1}H-NMR (700 MHz, DMSO-d_6, 333 K): δ = 8.42-7.88 (m, NH), 7.25 (s, Ph-CH), 4.65 (s, α-CH), 4.43 (s, Ph-CH_2), 3.61 (s, β-CH_2), 3.52 (s, PEG-$\underline{CH_2}$), 3.40 (s, PEG-O$\underline{CH_3}$) ppm. M_n = 7800 g/mol. DP = 41.

PEG_{45}-*b*-PLS(Bn) (**4**, 0.40 g) was obtained with 80% yield. ^{1}H-NMR (700 MHz, DMSO-d_6, 333 K): δ = 8.35-7.82 (m, NH), 7.25 (s, Ph-CH), 4.65 (s, α-CH), 4.43 (s, Ph-CH_2), 3.61 (s, β-CH_2), 3.53 (s, PEG-$\underline{CH_2}$) ppm. M_n = 7600 g/mol. DP = 32.

Table 17: Synthetic details of O-benzyl-L-serine homo and diblock copolymers.

No.	***Sample***	***Initiator***	***DP_{theo}*** [a]	***DP_{exp}*** [b]	***Yield (%)***	***Mn*** [b] ***[Da]***	***T*** [c] ***[°C]***	***Additive***
4a	PEG_{45}-*b*-$PLS(Bn)_{20}$, ncs55	mPEG_{45}-NH_2	45	20	55	5500	RT	urea
4b	PEG_{45}-*b*-$PLS(Bn)_{8}$, ncs56	mPEG_{45}-NH_2	10	8	80	3400	RT	urea
4c	PEG_{45}-*b*-$PLS(Bn)_{32}$, ncs71	mPEG_{45}-NH_2	105	32	80	7600	RT	urea
4d	PEG_{45}-*b*-$PLS(Bn)_{34}$, ncs72	mPEG_{45}-NH_2	135	34	78	8000	RT	urea
3a	PEG_{17}-*b*-$PLS(Bn)_{41}$, ncs69	mPEG_{17}-NH_2	90	41	53	8000	RT	urea
4e	PEG_{114}-*b*-$PLS(Bn)_{87}$, ncs73	mPEG_{114}-NH_2	266	87	79	20 000	RT	urea
4f	PEG_{45}-*b*-$PLS(Bn)_{52}$, ncs97	mPEG_{45}-NH_2	150	52	79	11 200	RT	GuHCl
4g	PEG_{45}-*b*-$PLS(Bn)_{57}$, ncs98	mPEG_{45}-NH_2	150	57	79	12 000	RT	LiBr
4h	PEG_{45}-*b*-$PLS(Bn)_{41}$, ncs76	mPEG_{45}-NH_2	150	41	82	9200	60	urea
4n	PEG_{45}-*b*-$PLS(Bn)_{38}$, ncs74	mPEG_{45}-NH_2	120	38	82	8700	40	urea
4m	PEG_{45}-*b*-$PLS(Bn)_{35}$, ncs75	mPEG_{45}-NH_2	150	35	87	8200	40	urea
4i	PEG_{45}-*b*-$PLS(Bn)_{43}$, ncs87	mPEG_{45}-NH_2	150	43	- [d]	9600	40	urea, Ar-flow
4j	PEG_{45}-*b*-$PLS(Bn)_{54}$, ncs134	mPEG_{45}-NH_2	105	54	- [d]	11 500	0	LiBr
3b	PEG_{17}-*b*-$PLS(Bn)_{47}$, ncs135	mPEG_{17}-NH_2	50	47	- [d]	9000	0	LiBr
2b	Bn-*b*-$PLS(Bn)_{50}$, ncs136	Bn-NH_2	50	50	95	8900	0	LiBr

[a] referring to molar feed ratio of monomer and initiator [mmol].
[b] [Mn]: total molecular weight of block copolymer, calculated by ^{1}H-NMR analysis.
[c] During polymerization.
[d] Yield could not be determined, due to remaining additive in the obtained solid.

Bn-*b*-PDLS(Bn) (**6**, 0.51 g) was synthesized with 62% yield. ^{1}H-NMR (700 MHz, DMSO-d6, 333 K): δ = 8.22-7.92 (m, NH), 7.30 (m, Ph-CH, Bn-NH_2), 7.24 (m, Ph-CH, Ser(OBn)), 4.67 (d, α-CH), 4.40 (m, Ph-CH_2), 3.60 (m, β-CH_2) ppm*s*. M_n = 5800 g/mol. DP = 37.

PEG_{17}-*b*-PDLS(Bn) (**7**, 0.51 g) was synthesized with quantitative yield. ^{1}H-NMR (700 MHz, DMSO-d6, 298 K): δ = 8.55-8.03 (m, NH), 7.24 (s, Ph-CH), 4.72 (d, α-CH), 4.42 (m, Ph-CH_2), 3.58 (s, β-CH_2), 3.52 (s, PEG-$\underline{CH_2}$) ppm. M_n = 9600 g/mol. DP = 50.

PEG_{45}-*b*-PDLS(Bn) (**8**, 0.40 g) was synthesized with 60% yield. ^{1}H-NMR (700 MHz, DMSO-d6, 333 K): δ = 8.23-7.88 (m, NH), 7.25 (s, Ph-CH), 4.66 (d, α-CH), 4.41 (m, Ph-CH_2), 3.61 (s, β-CH_2), 3.54 (s, PEG-$\underline{CH_2}$) ppm. M_n = 7600 g/mol. DP = 32.

Table 18: Synthetic details of DL-Ser(Bn) homo and diblock copolymers.

No.	***Sample***	***Initiator***	***DP_{theo}[a]***	***DP_{exp}[b]***	***Yield (%)***	***Mn[b] [Da]***	***T[c] [°C]***	***Additive***
8a	PEG_{45}-*b*-$PDLS(Bn)_{37}$, ncs100	$mPEG_{45}$-NH_2	150	37	63	7800	RT	urea
8b	PEG_{45}-*b*-$PDLS(Bn)_{32}$, ncs101	$mPEG_{45}$-NH_2	150	32	60	7600	RT	urea
6a	Bn-*b*-$PDLS(Bn)_{37}$, ncs102	Bn-NH_2	50	37	62	5800	RT	urea
7a	PEG_{17}-*b*-$PDLS(Bn)_{49}$, ncs105	$mPEG_{17}$-NH_2	50	49	55	9500	RT	LiBr
6b	Bn-*b*-$PDLS(Bn)_{50}$, ncs113	Bn-NH_2	50	50	quant.	9000	0	LiBr
7b	PEG_{17}-*b*-$PDLS(Bn)_{50}$, ncs112	$mPEG_{17}$-NH_2	50	50	quant.	9600	0	LiBr
8c	PEG_{45}-*b*-$PDLS(Bn)_{150}$, ncs111	$mPEG_{45}$-NH_2	150	150	quant.	28500	0	LiBr

[a] referring to molar feed ratio of monomer and initiator [mmol].
[b] [Mn]: total molecular weight of block copolymer, calculated by ^{1}H-NMR analysis.
[c] During polymerization.

Nonaqueous Emulsion Polymerization (NEP) of PEG-*b*-PLS(Bn) coated PLLA Core Shell Nanoparticles*:* PLLA nanoparticles were synthesized as described in the literature.[49] PEG-*b*-PSer(Bn) copolymer (22.5 mg) in anhydrous cyclohexane (11.40 g, 9.25 mL) was ultrasonicated for 2 min. using a Bandelin Sonorex RK255H ultrasonic bath operating at 640 W, and stirred overnight at room temperature under inert atmosphere. L-Lactide (35.00 mg, 0.24 mmol, 1.00 eq) was dissolved in anhydrous acetonitrile (0.10 g, 0.125 mL). The emulsion was formed by dropwise addition of the monomer solution into the cyclohexane/PEG-*b*-PSer(Bn) dispersion and subsequent treatment with ultrasonication for 5 min. The catalyst SIMes (2.50 mg, 334 µmol, 0.034 eq) and the initiator 1-pyrenyl butanol (2.10 mg, 7.70 µmol, 0.032 eq) were dissolved in acetonitrile (0.10 g, 0.125 mL) and added dropwise to the emulsion under inert atmosphere. The emulsion was stirred for 15 min. at room temperature to result in PLLA nanoparticles. A sample was taken out of the final emulsion to analyze the particle size and morphology *via* DLS and SEM. The remaining emulsion was ultrasonicated for 1 min. and sedimented. After decantation of the supernatant, the particles were washed with cyclohexane. The washing step was repeated three times before the particles were precipitated in cold methanol. The solvent was removed and the resulting particles were dried *in vacuo*.

4 Development of a stimuli-responsive nano drug carrier – Nanoparticle synthesis with photolabile poly-*O*-pyrenyl-serine-based emulsifiers

4.1 Synthesis of a photocleavable serine-based building block for ROP

In this chapter, the synthesis of photocleavable serine-containing block copolymers as emulsifiers for NEP is discussed, following the concept of the previous chapter on serine-based materials. In order to utilize a block copolymer as an emulsifier, it needs an amphiphilic structure. In our case, we needed an amphiphilic block copolymer with a switchable hydrophobic block. The benzyl protecting group was not easily cleavable and therefore, another strategy was followed. Photolabile groups are usually hydrophobic and cleavable under mild conditions by UV-light exposure in the presence of water. Equipping our emulsifiers with a photolabile group allowed their convenient cleavage after the nanoparticle formation, resulting in a polarity switch of the particle surface from nonpolar to polar, as reported by Dorresteijn et al.[53] The now polar particles can be dispersed in aqueous phase and are ready to use, for example as drug carriers for biological applications. To achieve that, the serine side chain needed to be functionalized with a photocleavable protecting group, which turned out to be the first challenge in this project. While other amino acids, like glutamic acid, lysine or cysteine, have been functionalized with photoactive compounds before, little was found on the functionalization of the serine side chain in general, besides the classic phosphorylation reactions or protection with benzyl or tert-butyl groups.[53,102,103] A major problem of the functionalization of the serine side chain is the low reactivity of the hydroxy group. Primary aliphatic alcohols are low in reactivity in general.[74] Serine is a special case, as it has two more functional groups, an amine and carboxylic acid, which both are much more reactive than the hydroxy group, making it difficult to particularly address the hydroxy group without affecting the other functional groups.[74] An orthogonal protecting groups strategy for the two remaining functional groups was required to avoid side reactions on the one hand, and allow possibly harsh conditions to enable a reaction at the hydroxy group on the other hand, depending on the desired reaction type. Several possibilities to functionalize the serine side chain have been evaluated in terms of feasibility and stability during the whole synthesis route. Besides others, there are three common functional groups that can be created by reaction with a hydroxy group, which are ethers, carbonates and esters. Three possible synthesis paths were proposed for the functionalization of the serine side chain with a photolabile group (Scheme 15). The most favoured route was the ether synthesis, as ethers were the chemically most stable groups in this selection and therefore would easily tolerate the conditions of the following deprotection steps and NCA synthesis. The drawback of the ether synthesis was the harsh conditions needed to deprotonate the hydroxy group. The second route was the formation of a carbonate, which was a straight forward reaction, but the carbonate´s stability

was limited under harsh conditions, which eventually led to problems in the subsequent deprotection steps. The third way was the formation of an ester group, which had good stability towards moderate conditions, but could be saponified at high or low pH. It needed to be evaluated, if the ester was stable in the upcoming steps. In the end, the ester turned out to be the perfect combination of chemical stability and convenient synthesis to fabricate the desired polymeric material.

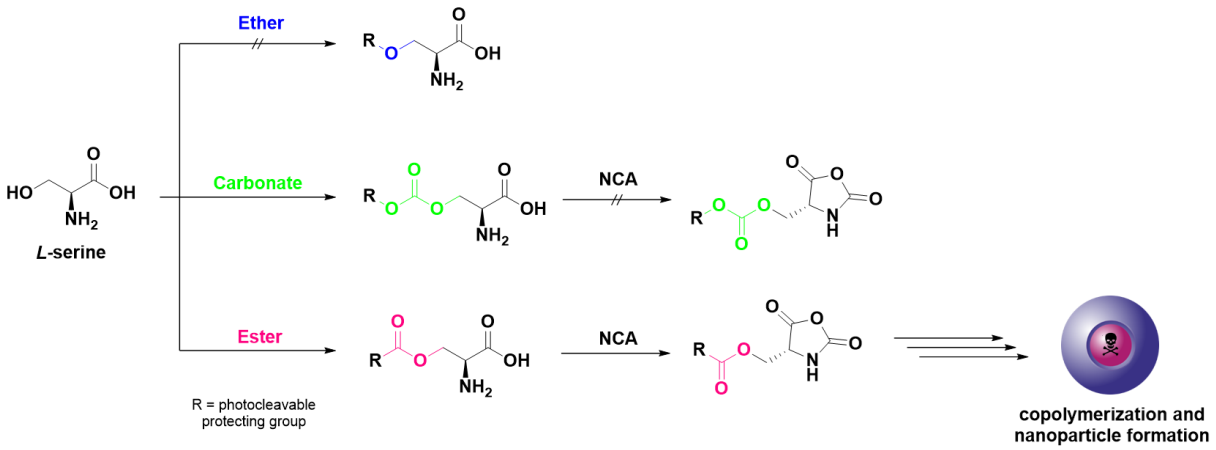

Scheme 15: Overview of the synthetic approach to obtain photocleavable serine-based building blocks to fabricate block copolymers for the formation of core shell nanoparticles.

Besides different functional groups, the photoactive protecting group was varied between three different groups (Figure 50). First, one of the most common photocleavable groups was applied, the *o*-nitro-benzyl group.[102] It has similar hydrophobicity like the previously used benzyl group and was therefore believed to lead to block copolymers with comparable aggregation behavior. On the other hand, it was questionable, if this group, the nitro-group in particular, would tolerate the harsh conditions of the ether synthesis. Therefore, another protecting group with similar features was chosen, the 2'-methyl acetophenone group, that did not have such a sensitive functionality.[104] The last group, the 1-acetyl pyrenyl group, was chosen to significantly increase the hydrophobicity in the serine side chain in order to evaluate its influence on the aggregation behavior of the corresponding block copolymers in nonaqueous solution. The pyrene group was deployed successfully by Dorresteijn et al. in the synthesis of photoactive L-glutamic acid-based block copolymers for nonaqueous emulsion polymerization in our group.[53]

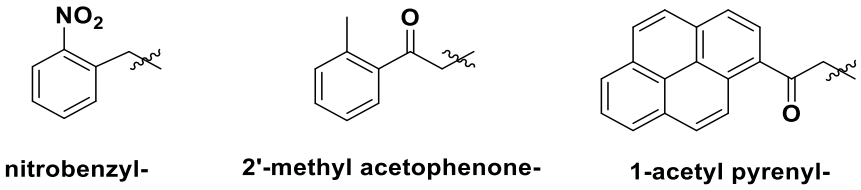

Figure 50: Photocleavable protecting groups to introduce into the serine side chain.

ETHER FORMATION

Ether formation is a well-established case of nucleophilic substitution, discovered by Alexander Williamson in the 19th century.[105] It is a two-step reaction, requiring the deprotection of an alcohol, followed by the reaction of the alkoxide with an organohalide resulting in chemically stable ethers.[79] Due to its high stability, the most favorable, yet challenging solution to create a photolabile serine derivative was the introduction of the photocleavable protecting group in the serine side chain by ether synthesis. The conversion rate and success of the ether formation is determined by the reactivity of the hydroxyl group, which is usually deprotonated by sodium or potassium or the corresponding hydride salts in the case of primary alcohols.[30] This requires the substrates to be chemically stable towards these harsh conditions, which is particularly challenging when using a serine derivative, where two more functional groups are present, an amine and a carboxylic acid, that show higher overall reactivity than the hydroxy group. Functionalization of the serine side chain is tricky. Not only the serine derivative needs to be stable towards the given conditions, but also the protecting group. As a consequence, literature addressing the side chain functionalization of serine was barely found, aside from a handful publications reporting other protecting groups than the common benzyl or *tert*-butyl groups.[30,106] Nevertheless, some approaches were published that were tested for reproducibility and applicability to obtain the desired molecule, which is discussed below.[30,106] In order to avoid side reactions and increase the amino acid´s solubility in organic solvents, an adequate protecting group strategy was needed. Not only did the protecting groups of the amine and carboxylic acid require to be stable against the conditions of the ether formation, they were also desired to be cleavable under the same conditions to spare an additional synthetic step. The synthetic route consisted of the protection of the N- and C-terminus of L-serine, followed by the introduction of the photolabile protecting group into the serine side chain by ether formation. Before the cyclization to the serine-NCA was conducted, the amine and carboxylic acid protecting groups were to be cleaved and eventually the ROP of the serine monomer would result in the photoactive serine-containing block copolymer (Scheme 16).

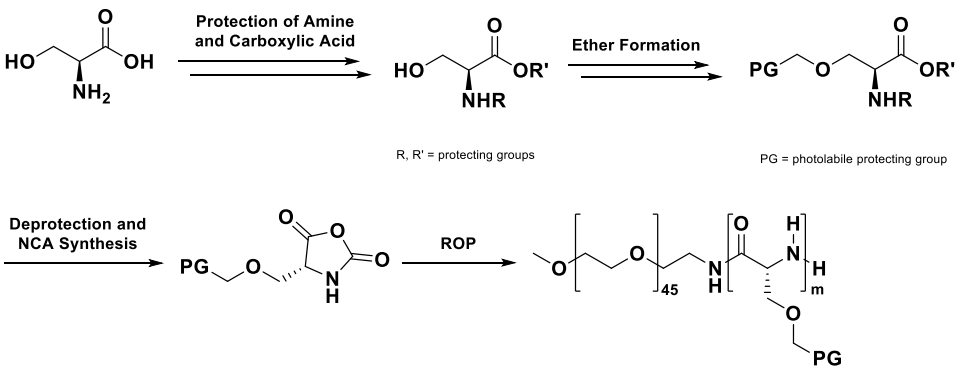

Scheme 16: Synthesis route of an amphiphilic block copolymer with a photoactive poly-L-serine ether block.

Using the strong base sodium hydride for the deprotonation of the hydroxy group in the serine side chain is the most frequently used method in literature for ether formation with benzyl bromide or methyl iodide and hence, the one that was focused on fist (Scheme 17).[30] Alternative reaction conditions and methods were tested as well. Besides using different photolabile substrates and various serine derivatives, alternative bases and solvents were evaluated.[106,107] Also, the ether formation with silver(I) oxide instead of sodium hydride was studied.[108] An alternative method to classic Williamson ether formation was the use of the trichloroacetimidate of the nitro-benzyl group in the presence of a Lewis acid, like boron trifluoride etherate or trifluoromethanesulfonic acid.[109,110]

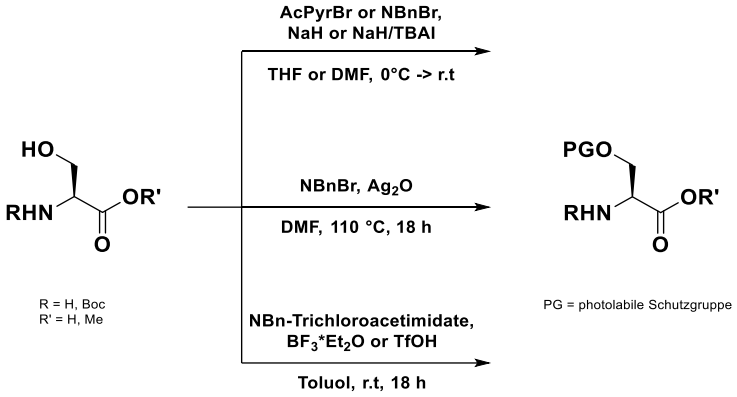

Scheme 17: Synthetic approaches for the ether formation with L-serine and a photocleavable protecting group.

It was believed that the ether formation was the most critical step of the abovementioned synthesis route and therefore, the protecting group strategy for the N- and C-terminus of the serine starting material was not fully optimized from the beginning, but decided by the commercial availability of protected serine derivatives to focus on the ether formation first. The first photoactive starting materials that were used in the following reactions were 1-(bromoacetyl)pyrene and 2-nitro-benzyl bromide, as these were successfully incorporated into the cysteine side chain in a previous project, resulting in the corresponding photocleavable thioethers.[111] The first reaction that was conducted was the ether formation of L-serine methyl ester and 1-(bromoacetyl)pyrene (Scheme 18). Therefore, the hydroxy group of the serine side chain was deprotonated with sodium hydride, followed by the addition of the bromide and stirring for two days (p. 89, Table 19, No. 1). After purification, the residue was analysed by proton NMR spectroscopy. The spectrum showed no evidence of the product **13**, as no amino acid signals were visible beside the aromatic protons. In a second approach, the solvent was changed from THF to DMF and the amount of sodium hydride was increased from one to three equivalents (p. 89, Table 19, No. 2). After 5 hours, TLC analysis showed the formation of a new spot at the baseline, while the bromide spot disappeared. But again, the product **13** could not be isolated, according to NMR analysis. The starting material 1-(bromoacetyl)pyrene was analysed as well, and was found to be partially degraded and therefore, it was not used anymore in the following reactions.

Instead, it was continued using 2-nitro-benzylbromide to evaluate if the reaction failed due to the degraded starting material, or if the reaction was not working in this setup generally.

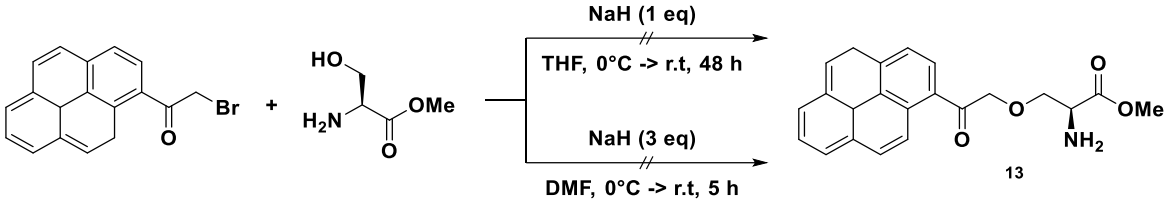

Scheme 18: Different reaction conditions of the ether formation of 1-(bromoacetyl)pyrene and L-serine methyl ester.

Three different conditions were evaluated for the ether formation of L-serine methyl ester and 2-nitro-benzyl bromide (Scheme 19). The first reaction was performed with 1 eq of sodium hydride in THF and resulted in a yield of 17% of *O*-nitro-benzyl serine methyl ester after two days of stirring (p. 89, Table 19, No. 3). In the second approach, the solvent was changed to DMF and the reaction time was decreased to 16 hours, after which the product H-Ser(NBn)-OMe (**14**) was obtained with a yield of 18% (Table 19, No. 4). The solvent change did not result in an increased reaction conversion, but in a reduction of reaction time to obtain the same poor yield as in THF. Nevertheless, these two reactions showed that it is possible to modify the serine side chain by ether formation, even though the yield of the reaction was quite low and needed to be optimized. Therefore, the third approach was conducted along the lines of the second reaction with the pyrene derivative, with 3 eq of sodium hydride in DMF (p. 89, Table 19, No. 5). This reaction did not result in any product formation at all. The increase of sodium hydride above 1 eq was not increasing the product conversion, but in contrast, had a negative impact on the reaction. One equivalent of base was sufficient for the ether formation, but the yield of up to 18% needed to be optimized, as the product was required in large scale for the polymer synthesis.

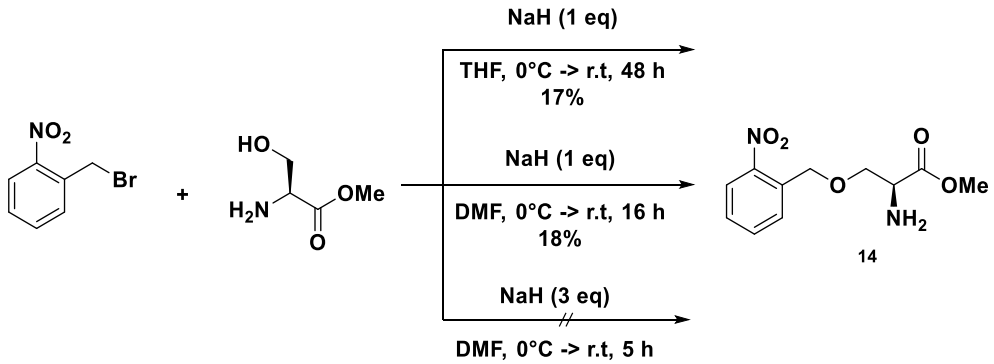

Scheme 19: Synthesis of O-nitro-benzyl-protected serine methyl ester by ether formation.

The ^{1}H-NMR spectrum showed that the product **14** was successfully isolated in the initial approach (Figure 51). The aromatic signals (i) with a signal intensity of four matched the expected intensity and pattern. The methylene group of the nitro-benzyl group (f) was observed at 4.12 ppm. The α- and β-signals (c, e) of serine were shifted slightly downfield, compared to L-serine methyl ester. And eventually, the proton signal of the hydroxyl group disappeared completely, indicating that the ether formation was successful. The ^{13}C-NMR spectrum underlined these results, where all expected signals were found in the expected region.

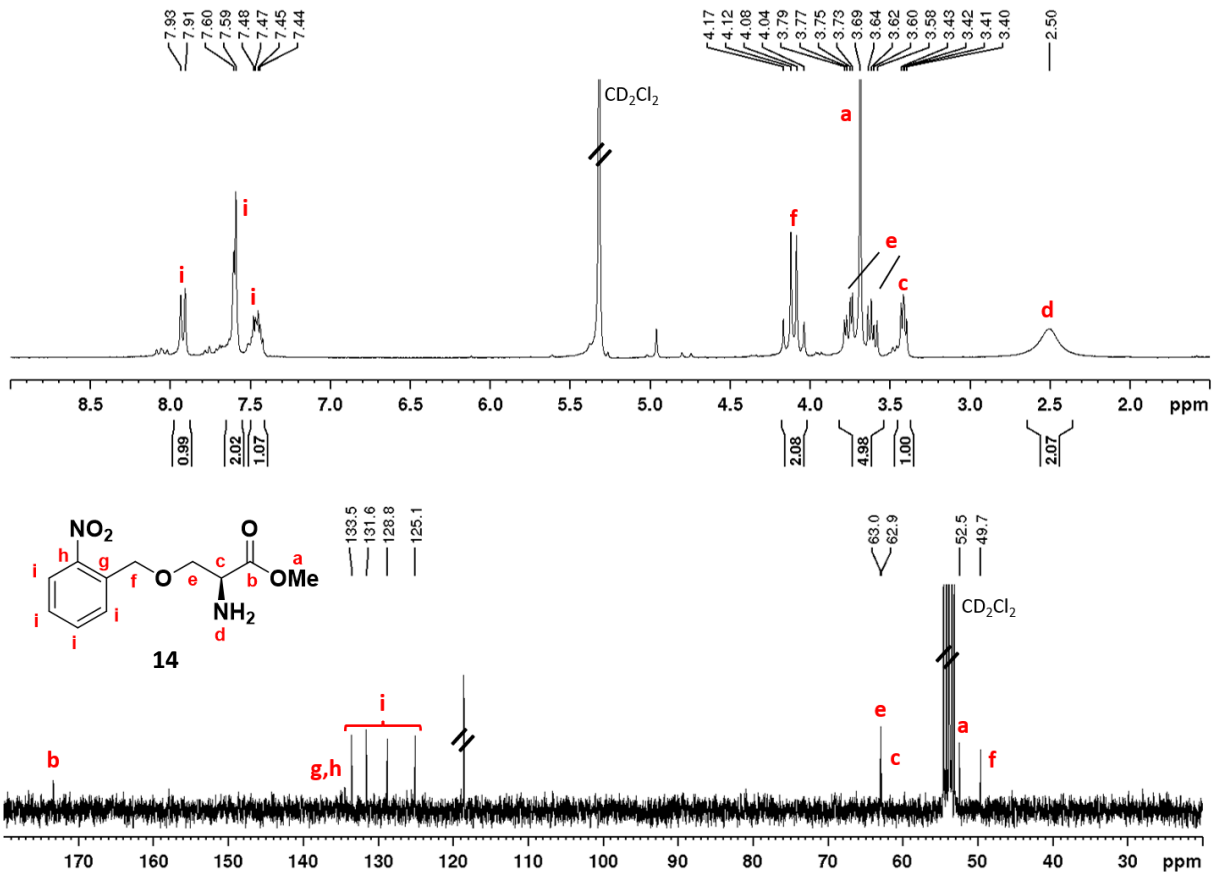

*Figure 51: ^{1}H- and ^{13}C-NMR spectra (CD_2Cl_2, 300 MHz, 298 K) of O-nitro-benzyl-protected serine methyl ester (**14**).*

The molecule was analysed by 2D-NMR spectroscopy to confirm the covalent attachment of the nitro-benzyl group to the serine side chain and to disprove that the 1D-NMR spectrum possibly showed a mixture of the two starting materials. The HMBC spectrum displayed two crucial signals proving the successful protection of the serine side chain (Figure 52). First, the α-proton of serine showed ^{4}J-coupling to the methylene group of the nitro-benzyl group (Figure 52, red dotted line) and second, the protons of beforementioned methylene group showed ^{3}J-coupling to the β-carbon of serine (green dotted line).

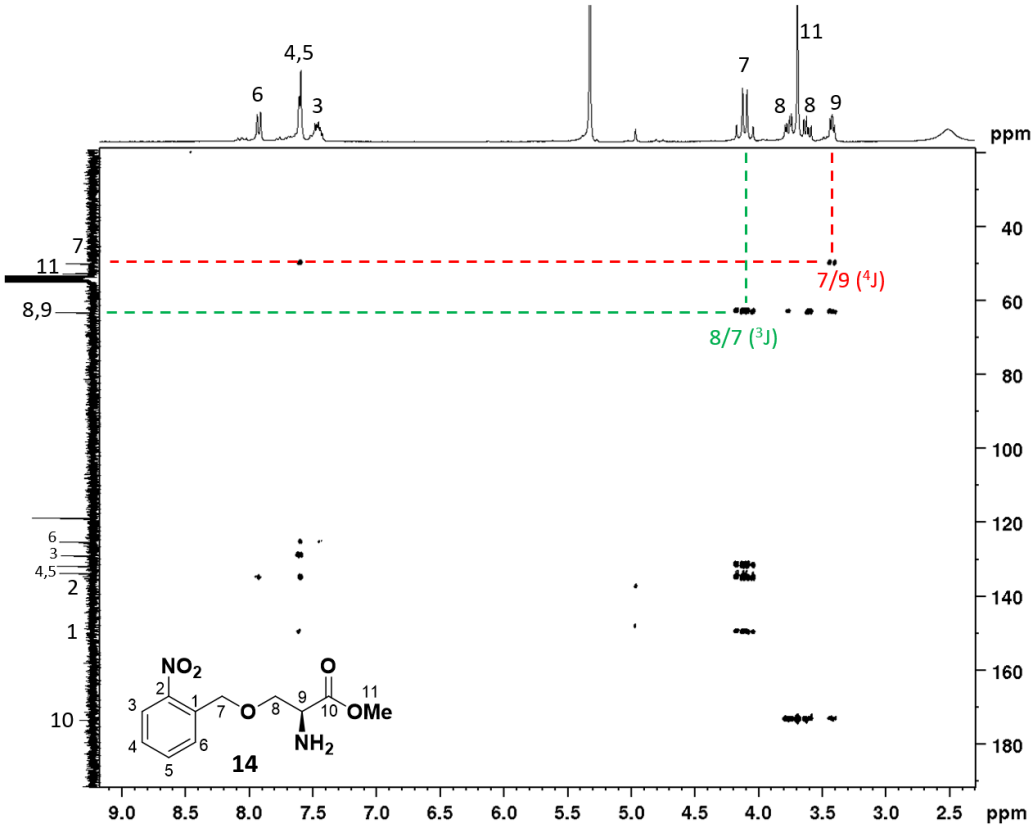

*Figure 52: HMBC spectrum (CD_2Cl_2, 300 MHz, 298 K) of O-nitro-benzyl-protected serine methyl ester (**14**).*

The last approach to protect the side chain of Boc-Ser-OH was conducted by using sodium hydride and a catalytic amount of tetra butyl ammonium iodide (TBAI; p. 89, Table 19, No. 6).[106] A compound was isolated successfully with a yield of 63%, but the NMR analysis revealed that the protection did not happen at the hydroxy group in the side chain (Scheme 20, **14-15**), but quantitatively formed an ester with the carboxylic acid instead (**16**).

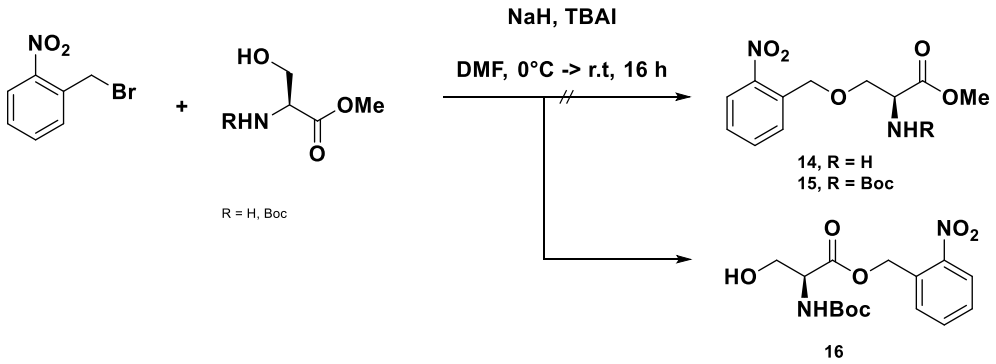

*Scheme 20: An approach to obtain O-nitro-benzyl-protected serine methyl ester by ether formation (**14,15**), using NaH and TBAI, led to the formation of the carboxylic acid ester instead (**16**).*

The comparison of the ^{1}H-NMR spectra of the obtained compound **16** and the *O*-nitro-benzyl-serine methylester (**14**) showed clearly that the spectra did not match and therefore, were not displaying the same molecule (Figure 53). The signal of the methylene group (f) did not only show a different pattern,

but was also shifted downfield from 3.98 to 5.49 ppm. The presence of the signal of the hydroxy proton (a) at 4.18 ppm was the ultimate confirmation that the reaction took place at the carboxylic acid instead of the hydroxyl group in the serine side chain.

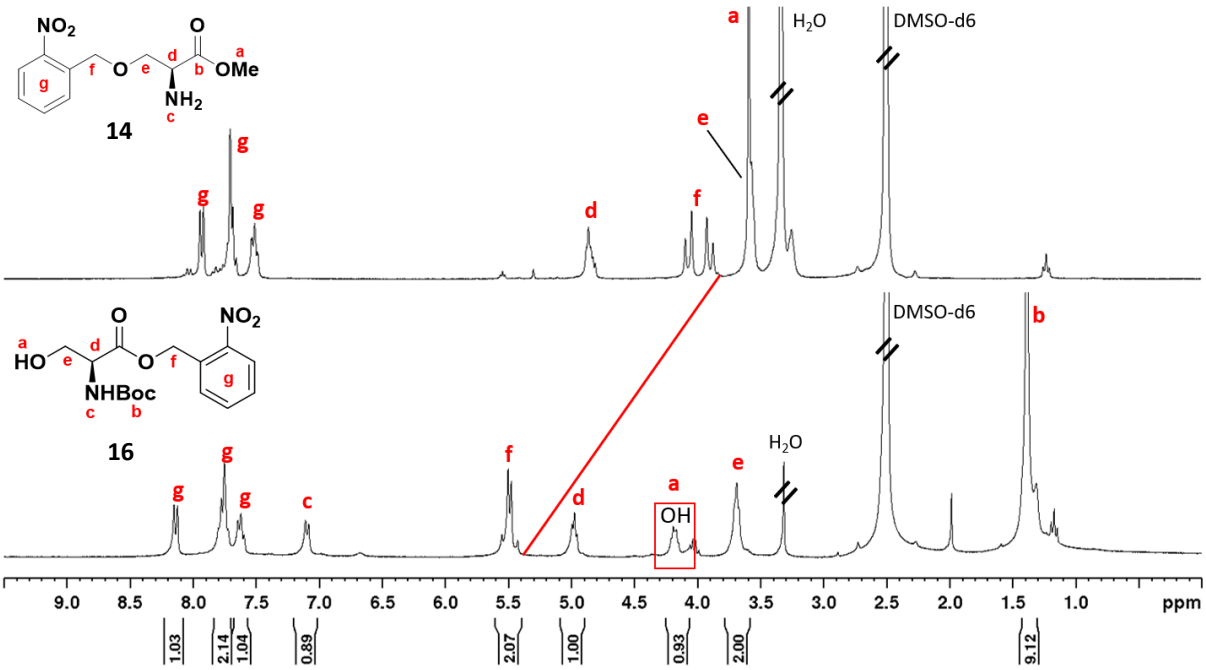

*Figure 53: ^{1}H-NMR spectra (DMSO-d_6, 300 MHz, 298 K) of O-nitro-benzyl-protected serine methyl ester (**14**) and Boc-Ser-nitro-benzyl ester (**16**).*

This led to a second approach using the described conditions, but with the methyl ester derivative Boc-Ser-OMe as the starting material to prevent the side reaction of 2-nitro-benzyl bromide with the carboxylic acid (p. 89, Table 19, No. 7). NMR analysis of the crude material revealed that no product was formed. Instead, it was indicated that the 2-nitro-benzyl bromide was partially degraded during the reaction, as a second set of signals was observed. In order to evaluate, if sodium hydride caused degradation of 2-nitro-benzyl bromide, an NMR experiment was conducted. Therefore, a proton NMR spectrum was measured of 2-nitro-benzyl bromide before and after addition of sodium hydride (Figure 54). While the 2-nitro-benzyl bromide spectrum showed the pure compound and all signals with the expected intensity, this changed when sodium hydride was added. The spectrum was measured 20 minutes after the addition of NaH, which was significantly shorter than the usual reaction time of the ether formation. Degradation of 2-nitro-benzyl bromide was observed. Not only were new signals visible in the aromatic region between 7.40-8.00 ppm and next to the methylene group between 4.50-5.30 ppm, the signal intensity of the methylene group (a) decreased from 2.00 to 1.68. This proved that the 2-nitro-benzyl bromide was showing a reaction with sodium hydride. It is reported that hydrides are able to reduce nitro-groups as well as displace halides from sp^3-carbons, which both could be the case here.[112,113] Usually, one equivalent of sodium hydride was used in the reactions and let

react with the serine derivative before addition of the bromide to avoid side reactions. Hypothesizing that the hydride would not deprotect the unreactive serine side chain quantitatively, this would prevent the ether formation in two ways. As the hydride would be available in the reaction mixture to some extent, it would react with the bromide and inhibit the reaction with the serine side chain. In addition, the serine side chain is not fully activated and therefore, no reaction can take place with the bromide. Based on these findings it was decided to not use the 2-nitro-benzyl bromide group anymore for the serine side chain protection. All approaches described below were conducted before this experiment.

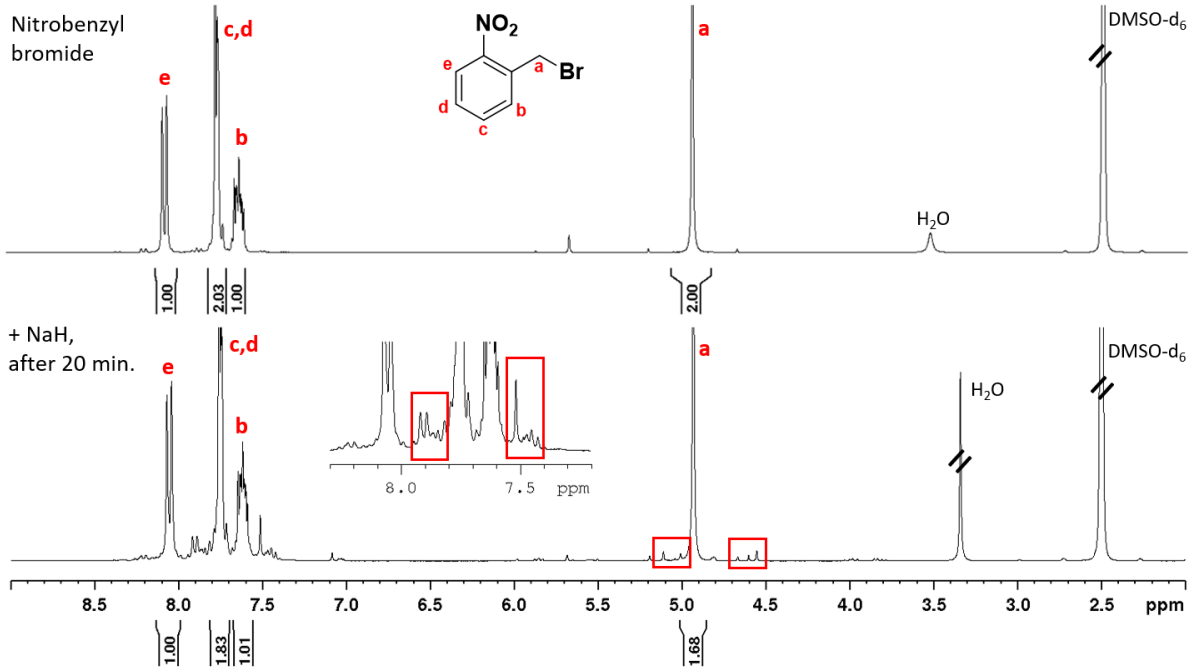

Figure 54: ^{1}H-NMR spectra (DMSO-d_6, 300 MHz, 298 K) before and after addition of sodium hydride.

The first approach to protect H-Ser-OMe with a 2-nitro-benzyl protecting group using sodium hydride in DMF led to product formation in low yields. To avoid side reaction of the unprotected carboxylic acid or amine of serine, the approach with sodium hydride and TBAI was repeated with the N- and C-protected derivative Boc-Ser-OMe (Scheme 21; Table 19, No. 8-9). NMR analysis of both experiments conducted in THF and DMF, did not show any product formation. Using the N- and C-protected serine derivative did not lead to any improvement. The reaction could not be reproduced with Boc-Ser-OMe as the starting material instead of Boc-Ser-OH.

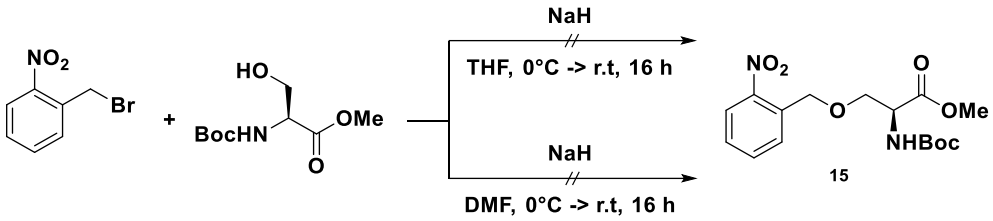

*Scheme 21: Synthesis of O-nitro-benzyl-protected Boc-serine methyl ester (**15**) by ether formation, using sodium hydride.*

The previously described approaches to optimize the reactions with 2-nitro-benzyl bromide were not successful, so another photolabile protecting group, *o*-methyl phenacylbromide, was tested.[104] Besides that, the reaction conditions were identical. Sodium hydride was used as the base to deprotonate the serine side chain and Boc-Ser-OMe was used as the starting material (Scheme 22; p. 89, Table 19, No. 10). After purification, a compound was isolated with a low yield of 6%.

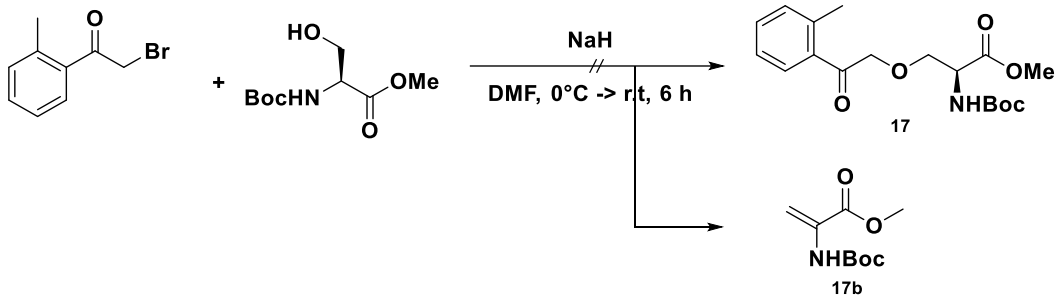

Scheme 22: o-Methyl phenacyl protection of Boc-serine methyl ester, using sodium hydride.

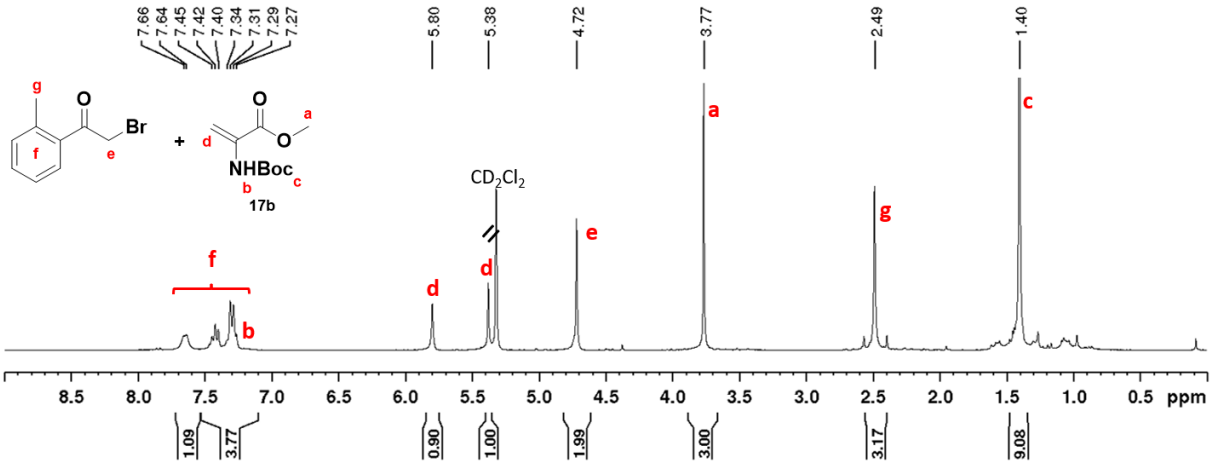

Figure 55: ^{1}H-NMR spectrum (CD_2Cl_2, 300 MHz, 298 K) of the isolated material after reaction of o-methyl phenacyl bromide and Boc-Ser-OMe.

The proton NMR spectrum gave the impression that the isolated material was a pure molecule at first, even though the signals did not match the desired molecule **17** (Figure 55). While the number of signals and their signal intensities were as expected, the α- and β-signals of the serine side chain were not displayed in the typical range of 3-5 ppm. Instead, two new singlet signals (d) appeared at 5.38 and 5.80 ppm, which is uncommon for side chain protons of amino acids. Instead, this is the specific region for alkene protons, leading to the assumption that a β-H-elimination took place in the serine side chain,

potentially resulting in dehydroalanine.[75] The signals of the *o*-methyl phenacyl group (e, f, g) in the proton spectrum were showing the expected signal intensity as well. In order to validate that the isolated material was a mixture of a *o*-methyl phenacyl species and the dehydroalanine derivative **17b**, 2D-NMR spectroscopy was performed (Figure 56). The HSQC spectrum showed that the two singlet signals at 5.38 and 5.80 ppm were bound to the same carbon atom (Figure 56A, red line), supporting the hypothesis that these were the two protons of an alkene. In terminal akenes, the protons are typically observed as two separate signals in proton NMR spectrum due to their cis and trans positions in the molecule.[114] The HMBC spectrum did not show any coupling signals between the two signals at 5.38 and 5.80 ppm and the carbon atom of the methylene group of the *o*-methyl phenacyl group (Figure 56B, red line). In addition, the protons of the methylene group did not show any coupling to the singlet signals as well (Figure 56B, green line). Therefore, the 2D spectra did not provide any evidence of a covalent connection between the *o*-methyl phenacyl species and the serine side chain, but indicated the formation of Boc-dehydroalanine methylester (**17b**). In conclusion, the reaction did not result in the desired product **17** and in addition, the isolated material was obtained in poor yield and therefore, this approach was not further studied.

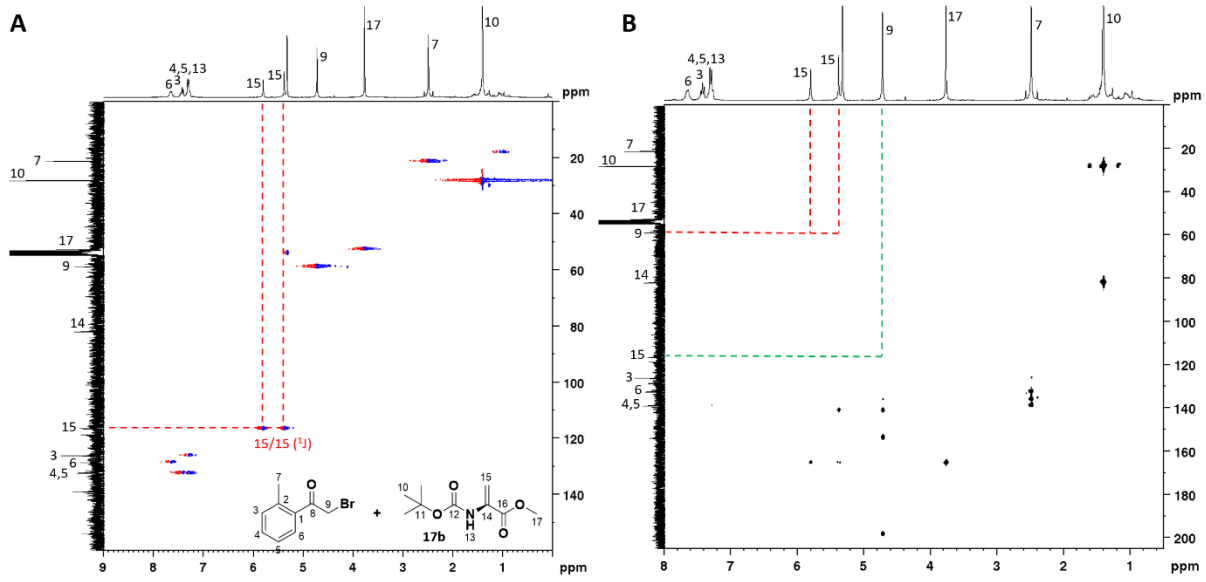

*Figure 56: HSCQ and HMBC spectra d(CD_2Cl_2, 300 MHz, 298 K) of the isolated material **17b** after reaction of o-methyl phenacyl bromide and Boc-Ser-OMe.*

In parallel, another variation of the ether synthesis with 2-nitro-benzyl bromide was tested, using silver(I) oxide, instead of sodium hydride to avoid degradation of the starting material (Scheme 23; Table 19, No. 11).[108] NMR analysis of the crude material did not show any product formation and therefore, this reaction was not further followed.

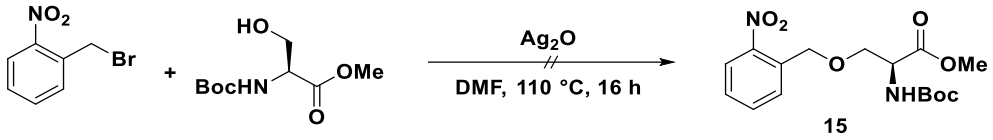

*Scheme 23: Synthesis of O-nitro-benzyl-protected Boc-serine methyl ester (**15**) by ether formation, using silver(I) oxide.*

The last method that was tested to protect the serine side chain with the photolabile 2-nitro-benzyl protecting group was by using the trichloroacetimidate derivative of the 2-nitro-benzyl group and a Lewis acid to allow ether formation (Scheme 24).[109,115] Two approaches were conducted using catalytic amounts of different Lewis acids, either boron trifluoride etherate or triflic acid (Table 19, No. 12-13). Both reactions did not lead to any product formation, but resulted in partial deprotection of the Boc group, according to NMR analysis. Consequently, this approach was not further studied.

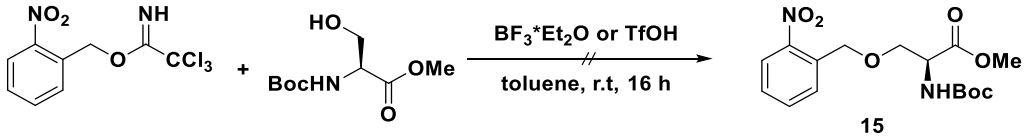

*Scheme 24: Synthesis of O-nitro-benzyl-protected Boc-serine methyl ester (**15**), using 2-nitro-benzyl trichloroacetimidate and a Lewis acid.*

Table 19: Summary of reaction conditions that were tested to introduce a photoactive group in the serine side chain by ether formation.

No.	Educt	Protecting Group	Reagents	Solvent	Temp.	Yield
1	H-Ser-OMe, ncs05	AcPyrBr	NaH	THF	0°C → r.t	✗
2	H-Ser-OMe, ncs07	AcPyrBr	NaH	DMF	0°C → r.t	✗
3	H-Ser-OMe, ncs06	NBnBr	NaH (1eq)	THF	0°C → r.t	17%
4	H-Ser-OMe, ncs08	NBnBr	NaH (1 eq)	DMF	0°C → r.t	18%
5	H-Ser-OMe, ncs13	NBnBr	NaH (3 eq)	DMF	0°C → r.t	✗
6	Boc-Ser-OH, ncs17	NBnBr	NaH, TBAI	DMF	-15°C → r.t	✗[1]
7	Boc-Ser-OMe, ncs35	NBnBr	NaH, TBAI	DMF	-15°C → r.t	✗
8	Boc-Ser-OMe, ncs24	NBnBr	NaH	DMF	0°C → r.t	✗
9	Boc-Ser-OMe, ncs34	NBnBr	NaH	THF	0°C → r.t	✗
10	Boc-Ser-OMe, ncs22	oMPBr	NaH	DMF	0°C → r.t	✗
11	Boc-Ser-OMe, ncs20,33	NBnBr	Ag_2O	DMF	110°C	✗
12	Boc-Ser-OMe, ncs28	NBn-Acetimidat	BF_3*Et_2O	Toluol	r.t	✗
13	Boc-Ser-OMe, ncs29	NBn-Acetimidat	TfOH	Toluol	r.t	✗

[1] Selective Protection of the carboxylic acid.

In conclusion, the synthesis of a photoactive serine derivative (**14**) as a building block for the ring opening polymerization was achieved by reaction of L-serine methyl ester and 2-nitro-benzyl bromide with sodium hydride in low yields of up to 18%. Numerous attempts to optimize the reaction and improve its yield were not successful and either led to the formation of by-products or to no product formation at all (Table 19). Due to the need of gram-scale amounts of the amino acid to produce various photoactive serine-containing block copolymers for nonaqueous emulsion polymerization, it was decided, based on economic and ecological reasons, to not further follow this ether formation route and instead, study alternative ways to functionalize the serine side chain with a photolabile protecting group.

GARNER ALDEHYDE ROUTE

An alternative synthetic route that leads to enantiomerically pure serine derivatives with a functionalized side chain was using the chiral building block 1,1-dimethylethyl 4-formyl-2,2-dimethyloxazolidine-3-carboxylate as an intermediate, better known as Garner´s aldehyde, reported first by Garner *et al*. in 1987 (Figure 57).[116] Nowadays it is widely used in multistep syntheses and one of the most cited chiral building blocks for enantiopure natural products, due to its broad application range.[117,118] Compared to a simple one-step protection reaction, it is relatively circuitous for a protecting group introduction, but it was believed to be a feasible approach to obtain the desired serine ether derivatives.

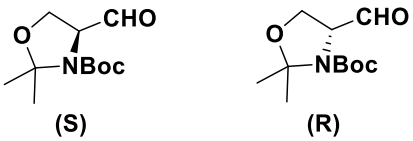

Figure 57: Structure of Garner´s aldehyde.

The synthetic route via the Garner´s aldehyde consisted of six steps, starting with the cyclization of Boc-Ser-OMe to obtain the dimethyloxazolidine (Scheme 25). In the original paper, the methyl ester was then reduced to the aldehyde.[116] Following the protocol of Garner and Park, it was reduced to the alcohol, followed by ether formation.[116] After ring opening, the *N,O*-acetal was obtained and the amine was re-protected with the Boc-group. The alcohol was oxidized to the carboxylic acid and the amine was deprotected, resulting in the side chain protected L-serine.[118]

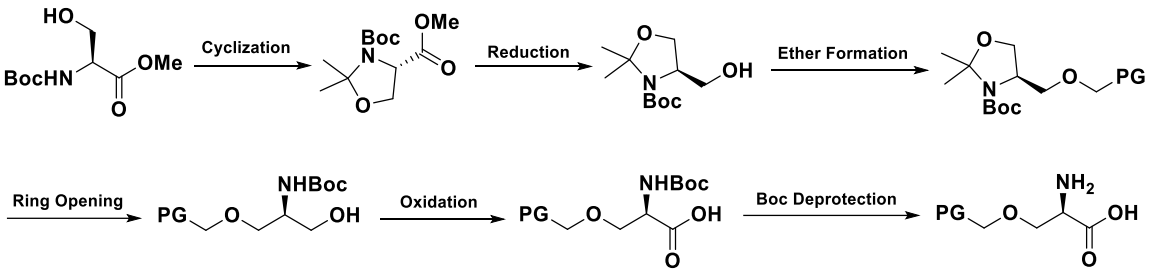

Scheme 25: Synthetic approach to a serine ether via the Garner´s a3aqqq7caldehyde route.

Before attempting to introduce a photolabile protecting group like the nitro-benzyl group, the synthesis route was conducted by incorporating a benzyl group to prove the concept of the Garner´s aldehyde route (Scheme 26). The cyclization was achieved by reaction of Boc-Ser-OMe with 2,2-dimethoxypropane and boron trifluoride etherate and the 2,2-dimethyloxazolidine (**18**) was obtained with 91% yield.[116] The alcohol (**19**) was obtained with a yield of 76% by reduction of the methyl ester with lithium aluminium hydride, followed by the ether synthesis with benzyl bromide and sodium hydride (**20**, 75% yield).[30,119] The next step contained the ring opening under acidic conditions, which

also resulted in the unwanted deprotection of the amine. The reprotection of the amine by treatment with Boc anhydride followed subsequently.[117,120] Eventually, the *N,O*-acetal (**21**) was obtained with 69% yield. To recreate the amino acid, the hydroxy group was oxidized by TPAP and NMO hydrate (**22**), followed by Boc-deprotection with trifluoracetic acid.[121] The *O*-benzyl protected serine (**23**) was successfully obtained with an overall yield of 47% over 6 steps.

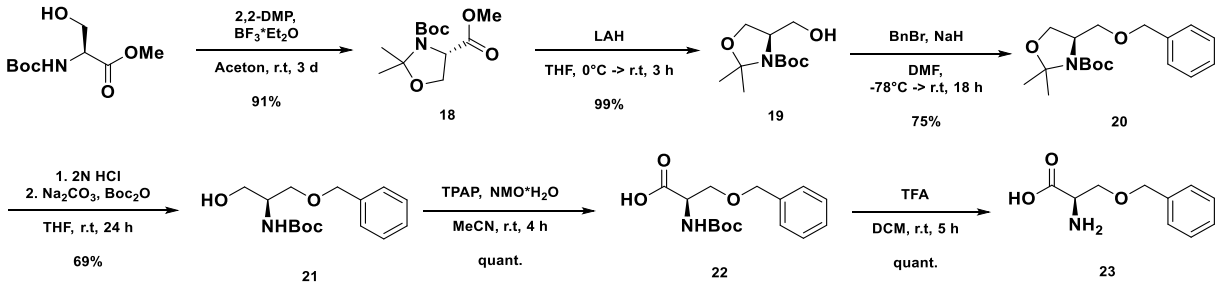

Scheme 26: Synthesis of the O-benzyl serine ether in six steps via the Garner´s Aldehyde route with an overall yield of 35%.

The synthesis of the hydroxy-containing dimethyloxazolidine (**19**) was successfully conducted in two steps and the product was isolated in good yields, as NMR analysis confirmed (Figure 58). The successful cyclization of the amino acid was indicated by the singlet signals of the two methyl groups (b) at 1.42 and 1.54 ppm that both showed the expected signal intensity of 3 each. After reduction of the methyl ester (**18**) to the alcohol (**19**), the singlet signal of the methoxy group (f) at 3.67 ppm disappeared and instead, two new signals were visible, the methylene group (e) at 3.88 ppm and the hydroxy proton (f) at 4.88 ppm, confirming that the desired molecule **19** was obtained.

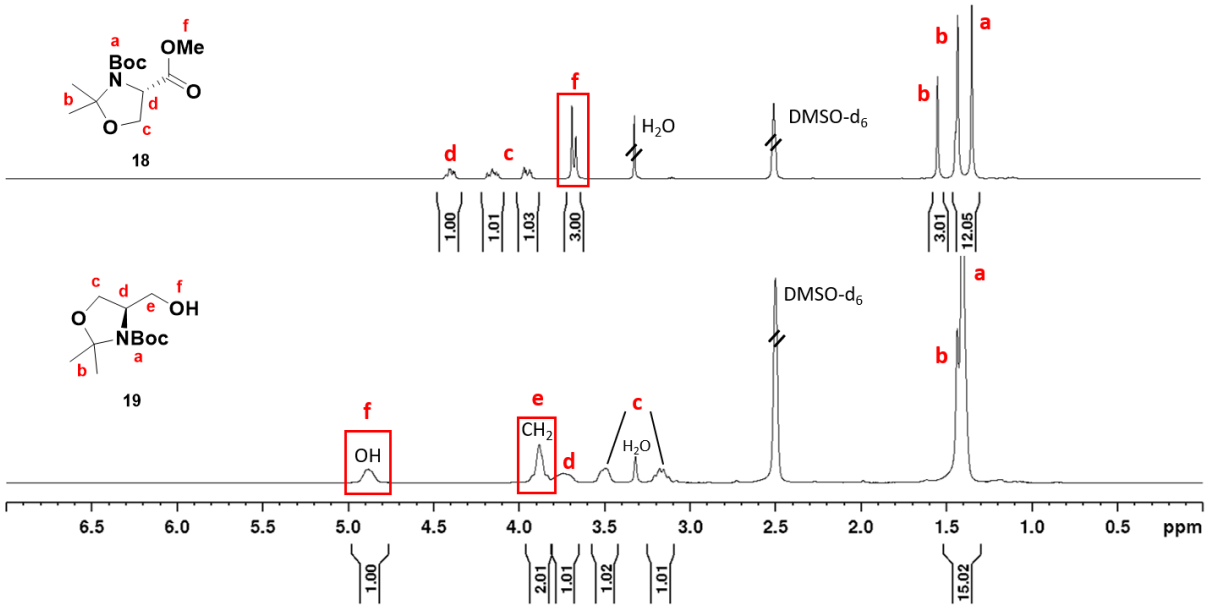

*Figure 58: ^{1}H-NMR spectra (DMSO-d_6 or CD_2Cl_2, 300 MHz, 298 K) of 2,2-dimethyloxazolidine-4-methylester (**18**) and 2,2-dimethyl-4-hydroxymethyl oxazolidine (**19**).*

The next step was the ether formation in the side chain of the Garner´s alcohol. Along the lines of the previously described efforts to obtain the desired ether-group in the serine side chain, four different conditions were tested to introduce the benzyl group, of which one led to the desired product **20** (Scheme 27).[79] All four reactions were analysed by TLC and proton NMR spectroscopy to monitor the reaction conversion. The first approach was conducted using benzyl alcohol and bismuth(III) bromide, according to Boyer et al.[122] According to the NMR analysis, the reaction did not result in any product formation as the hydroxy proton was visible with a signal intensity of 1. Instead, the deprotection of the Boc group was observed. Therefore, this reaction was discarded and not further followed. The second reaction was using benzyl bromide, sodium HMDS as the base and TBAI as the phase transfer catalyst.[123] The comparison of the TLC and proton NMR spectra with the starting material showed that the reaction resulted in the formation of the product, but at a low conversion below 15%. Therefore, this reaction was not further studied at first to find out, if the remaining conditions were leading to higher yields. The third reaction, a previously mentioned variation of the Williamson ether formation, was conducted using silver(I) oxide replacing the base.[124] The TLC analysis of the reaction showed the formation of many new spots, indicating that not only product was formed, but also a number of by-products. The product **20** was successfully isolated, but the yield was very low as expected. The NMR analysis indicated racemization of the product during the reaction, which was shown by signal splitting of the methyl and Boc signals, as well as the α-proton, which was a strong sign for the epimerization of the stereogenic centre. While this might be beneficial for the desired application, it might be problematic for others. Nevertheless, the low reaction conversion led to the disposal of this approach. The last approach was performed under classical Williamson ether formation conditions, using benzyl bromide and sodium hydride.[30] This reaction showed good conversion by TLC analysis and the product **20** could be isolated with a yield of 75%.

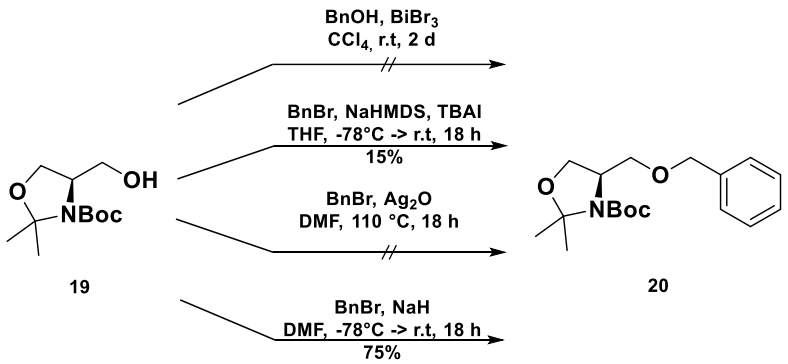

Scheme 27: Overview of the tested reaction conditions of the ether synthesis with benzyl bromide.

The comparison of the successfully obtained product and the starting material showed that the desired molecule, the benzyl protected dimethyloxazolidine (**20**) was obtained successfully (Figure 59). The α-proton (d) was shifted slightly downfield from 3.57 to 4.05 ppm and the signal of the benzylic

methylene group (f) at 4.55 ppm was observed with a signal intensity of 2, as expected. Eventually, the aromatic protons (g) with an intensity of 5 were observed as a multiplet between 7.21 and 7.45 ppm. This led to the conclusion that the product was successfully obtained by using the classic conditions of an ether formation reaction.

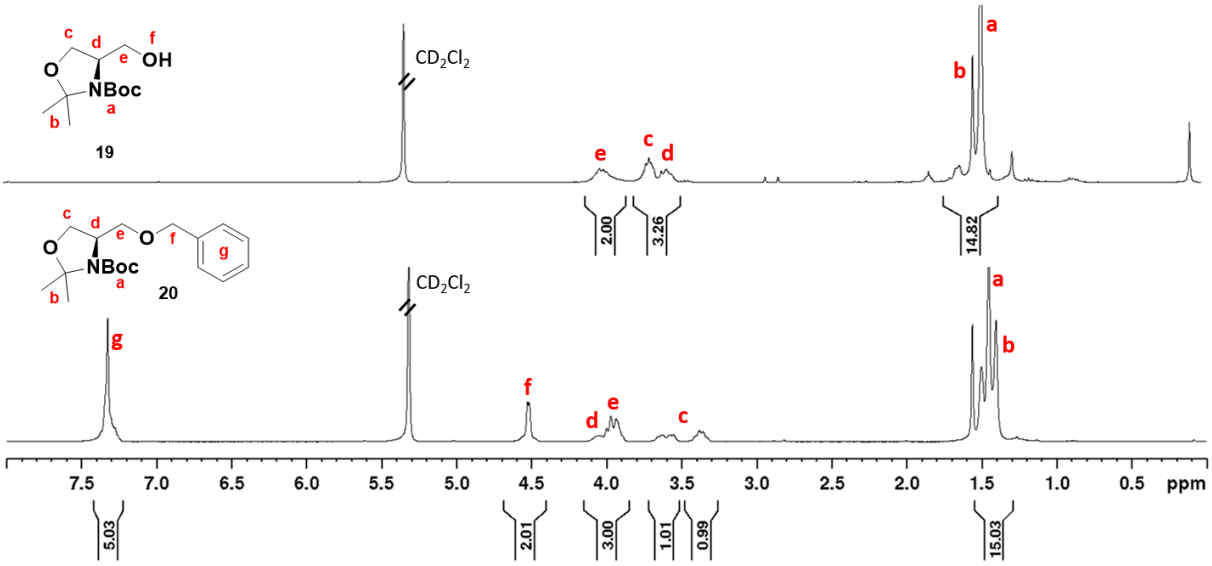

*Figure 59: ^{1}H-NMR spectra (CD_2Cl_2, 300 MHz, 298 K) of 2,2-dimethyl-4-hydroxymethyl oxazolidine (**19**) and the isolated ether (**20**) after reaction of the alcohol with benzyl bromide and sodium hydride.*

Before the synthesis was performed with the nitro-benzyl group, the next steps of the Garners´s aldehyde route were conducted with the benzyl-protected dimethyloxazolidine (**20**) to determine, if this route was successfully leading to the *O*-benzyl serine. Therefore, the benzyl-protected ether was used for the next step (Scheme 28), which included the ring opening in acidic conditions with hydrochloric acid, followed by treatment with Boc anhydride to reprotect the amine with a Boc group, as it was partially deprotected by the acidic conditions.[120] The *N,O*-acetal (**21**) was then oxidized to the carboxylic acid (**22**) by NMO hydrate and TPAP.[121] Eventually, the *N*-Boc-*O*-benzyl serine (**23**) was obtained with an overall yield of 35% over five steps.

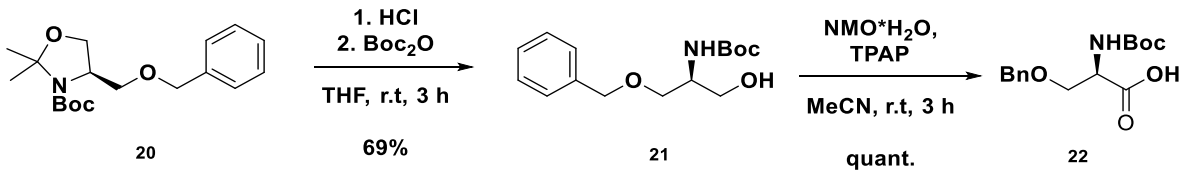

*Scheme 28: Ring opening and oxidation steps of the Garner´s aldehyde route to obtain N-Boc-O-benzyl serine (**22**).*

In order to obtain the photocleavable derivative of the dimethyloxazolidine, three approaches were conducted with nitro-benzyl bromide (Scheme 29). First, the reaction conditions of the successful etherification with benzyl bromide were applied using the photoactive nitro-benzyl bromide. During this first approach, sodium hydride was added to the reaction mixture at 0 °C, before the reaction was

allowed to warm to room temperature over 18 hours. NMR analysis did not show any product formation, indicated by the hydroxy proton with an unchanged signal intensity of 1. In the second approach, the reaction temperature was lowered to -78 °C to determine, if the reaction temperature has an impact on the reaction conversion. NMR analysis revealed that a second signal of the methylene group formed with low intensity, meaning that either the product was formed or nitro-benzyl bromide was partially degraded during the reaction. As the conversion was below 15%, this approach was not further studied and discarded. The third approach was performed with nitro-benzyl bromide and sodium HMDS. Here, a second set of nitro-benzyl bromide signals was observed in the aromatic region, but no second methylene group was observed, leading to the conclusion that these conditions, probably the strong base NaHMDS, led to degradation of the starting material and hence, was not suitable for this reaction.

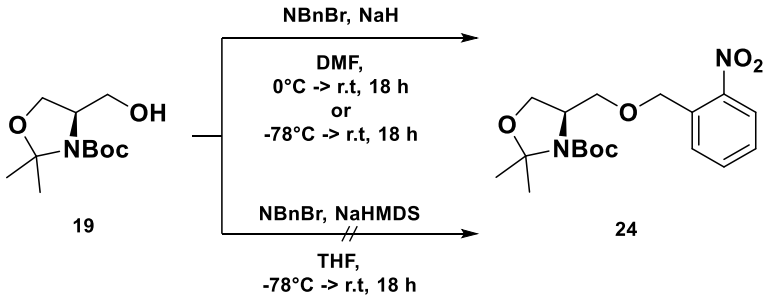

*Scheme 29: Ether (**24**) formation of Garner´s alcohol **19** with o-nitro-benzyl bromide, in respect to the reaction performed with benzyl bromide.*

In summary, despite the futile efforts to obtain the nitro-benzyl protected serine-derivatives, they could not be synthesized in high yields. This was indicating that the nitro-group is the limiting factor of the reaction. Considering the fact that the benzyl protection worked well under identical conditions using sodium hydride at low temperatures, there was no other reasonable explanation for the nitro-benzyl protection to not work out. This finding was contributing to the beforementioned NMR experiment of nitro-benzyl bromide and sodium hydride that showed that addition of sodium hydride to nitro-benzyl bromide led to the degradation of the material. Using benzyl bromide and sodium hydride was the only reaction condition that led to the desired product. The reaction was not reproducible with nitro-benzyl bromide, the desired protecting group. Paired with the relatively long synthesis route of six steps to conduct a protection reaction of a functional group led to the conclusion that this synthesis route was not feasible or efficient enough to fabricate the material in multigram scale that was needed for the following steps. Therefore, other synthetic strategies were tested to finally obtain serine derivatives with a photocleavable protecting group.

CARBONATE SYNTHESIS

The third approach to form a photoactive serine derivative was the insertion of the protecting group into the serine side chain as a carbonate group. Therefore, pyrene chloroformate (**25**) was synthesized by reaction of pyrene methanol with triphosgene and obtained with 79% yield (Scheme 30).[125] The carbonate group was formed by Boc-serine and pyrenyl chloroformate in the presence of pyridine.[126] The resulting carbonate **26** was obtained with a yield of 91%. Subsequently, the deprotection of the amine was conducted under acidic conditions, which did not only result in the cleavage of the Boc group, but also of the carbonate, according to the proton NMR analysis. This led to the conclusion that even though the formation of the carbonate was successful, this functional group was not suitable for the deprotection step at low pH. For the upcoming cyclization of the amino acid is also performed under acidic conditions. As a consequence, he carbonate group was not suitable for the desired application and this route was not further studied.

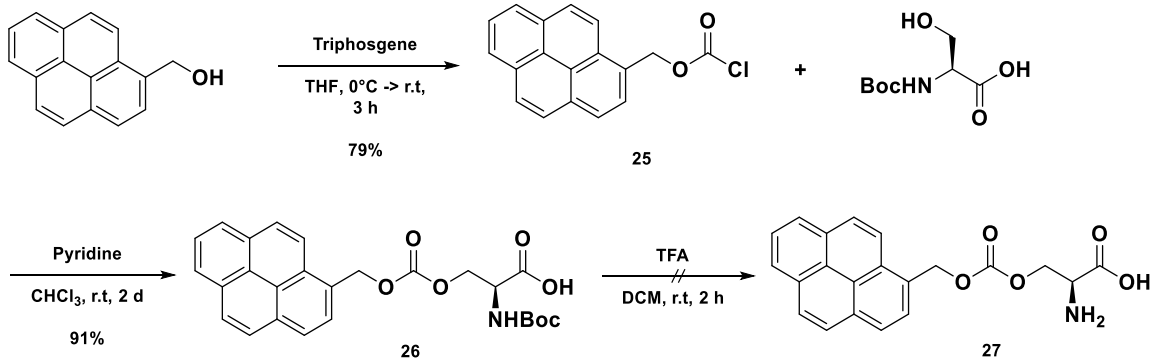

*Scheme 30: Introduction of a photoactive pyrene group into the serine side chain via carbonate (**26**) formation, followed by Boc deprotection (**27**).*

The molecules were characterized by NMR analysis (Figure 60). Pyren-1-ylmethyl chloroformate (**25**) showed all signals (a, b) with the expected intensity. The carbonate formation with Boc-Ser-OH caused the methylene group (b) to shift downfield from 5.34 to 6.70 ppm. All signals had the expected intensity and therefore, this synthesis of product **26** was considered successful. The last step, the Boc deprotection, turned out to not only result in the quantitative cleavage of the Boc group (f), indicated by the disappearing signal at 1.38 ppm, but also in partial cleavage of the carbonate group in the serine side chain. This was shown by the decrease of the signal intensity of the methylene signal (b) at 6.70 ppm from 2 to 1. Hence, this reaction led to the degradation of the material (**27**) due to the acidic conditions of the last deprotection step. As the next step, the NCA synthesis, is performed under acidic conditions as well, this functional group was not suitable for the fabrication of the NCA monomer. The reaction was not further optimized by using another protecting group strategy. Instead, the focus was shifted to other functional groups that show better stability under acidic conditions.

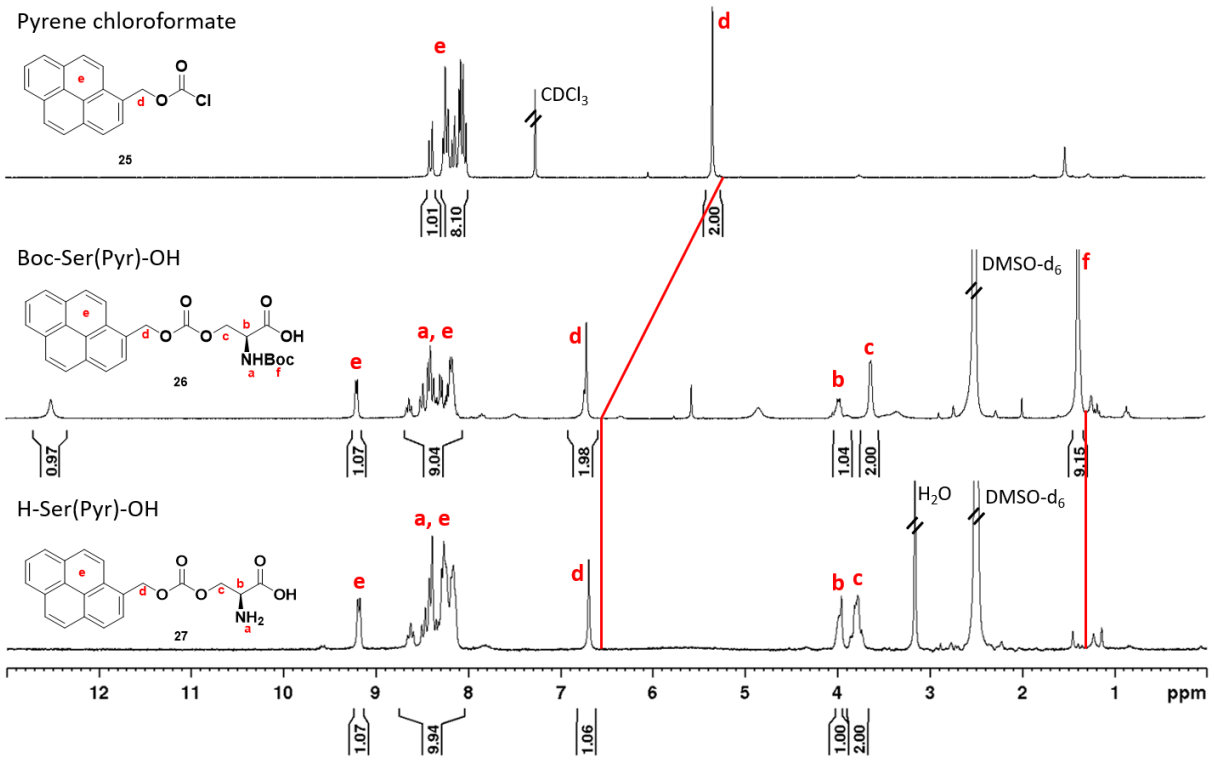

*Figure 60: ^{1}H-NMR spectra (DMSO-d_6 or $CDCl_3$, 300 MHz, 298 K) of pyrene chloroformate (**25**), Boc-Ser((pyren-1-ylmethyloxy)-carbonyl)-OH (**26**) and H-Ser((pyren-1-ylmethyloxy)carbonyl)-OH (**27**).*

ESTER SYNTHESIS

After testing three different synthetic routes to obtain photosensitive serine derivatives, which all had severe drawbacks, one last route remained undone, even though it appeared to be the most feasible route in retrospect. In this last approach, the photocleavable group was introduced into the serine side chain by classical coupling reaction that is widely used in peptide chemistry to introduce ester groups. Esters are known to be stable in neutral and slightly basic and acidic conditions, but in general they are not stable in media with very high or low pH. During the NCA synthesis hydrochloric acid is formed in significant amounts and therefore, the stability of the ester needed to be evaluated under these conditions. This route was considered an alternative, in case the ether synthesis was not working out, which turned out to be the case. The synthesis route from serine to a photosensitive block copolymer using the ester formation strategy was consisting of four steps (Scheme 31). First, a N- and C-protected serine derivative was used for the coupling reaction with a photosensitive molecule to form the ester group in the serine side chain. The protecting groups of the amine and carboxylic acid were cleaved in the following step to obtain the side chain protected serine, which was converted to the *N*-carboxy anhydride in the third step. This activated monomer was then polymerized by ring opening polymerization with the macroinitiator mPEG-NH_2 resulting in amphiphilic PEG-*b*-PSer(PG) block copolymers that can be hydrophilized by photocleavage.

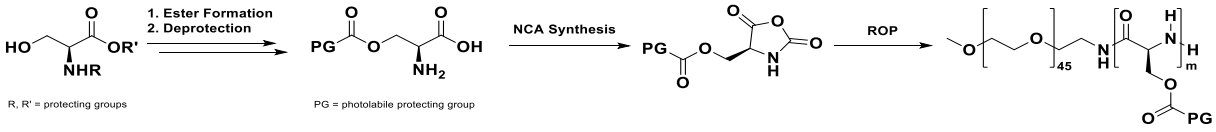

Scheme 31: Synthesis route of an amphiphilic block copolymer with a hydrophilic PEG block and a photoactive poly-L-serine ester block.

The protecting group that was chosen to be introduced into the serine side chain as an ester group was pyrene for two reasons. First, it was decided based on the fact that the nitro-benzyl group was not chemically stable against the conditions that were used in the previous approaches to form an ether group. To avoid the degradation of the starting material to happen again, the nitro-benzyl group was ruled out. Second, based on the performance of the benzyl-serine-based block copolymers that were hardly dispersible in nonpolar solvents, the hydrophobicity of the serine block was increased by the more hydrophobic pyrene. Using the highly hydrophobic pyrene that consists of four aromatic rings, instead of the benzyl group was believed to compensate the low polymerization degree of serine. The first approach to form an ester group in the serine side chain was not yet performed as a classical coupling reaction. Wu et al. reported the conversion of hydroxy-containing amino acids (serine, threonine, tyrosine) to an ester by reaction of the amino acid with acyl chlorides in plain TFA.[127] This reaction was tested before the coupling reaction, as no additional protection and deprotection steps

were required, according to the literature (Scheme 32). Therefore, 1-pyrenecarboxylic acid was reacted with oxalyl chloride to obtain pyrene-1-carbonyl chloride (**28**) in quantitative yield.[128] Along the lines of Wu et al., L-serine was reacted with pyrenyl-1-carbonyl chloride and the product (**29**) was obtained with a moderate yield of 46%. The next step, the NCA formation, was conducted under standard conditions with triphosgene in THF, but no product (**30**) could be obtained. Repeating the ester formation with racemic DL-serine did not lead to any reaction, according to TLC and NMR analysis.

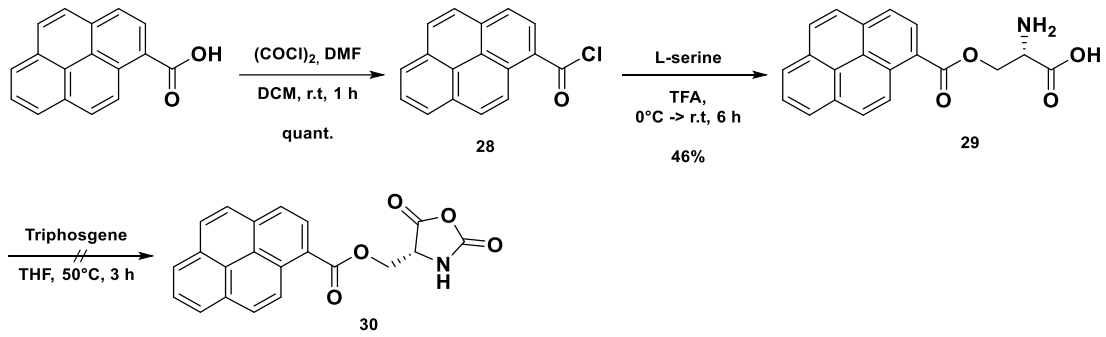

*Scheme 32: Chlorination of 1-pyrenecarboxylic acid (**28**), esterification of L-serine and pyrene-1-carbonyl chloride (**29**) and cyclization of O-pyrenyl-1-carbonyl)-L-serine to L-Ser(Pyr)-NCA (**30**).*

As the ester formation reaction was not resulting in high yields, was not reproducible for racemic DL-serine and the NCA could not be obtained with the L-serine derivative, it was decided to continue with the well-established coupling reaction instead of optimizing this reaction. The next approach to form an ester in the serine side chain was a variation of the Steglich esterification, using the coupling agent 1-Ethyl-3-(3-dimethylaminopropyl)carbodiimide hydrochloride (EDC-HCl) and *N,N*-dimethyl-aminopyridine (DMAP).[129,130] To avoid any side reactions, the N- and C-protected serine derivative Boc-L-Ser-OMe was reacted with 1-pyrenecarboxylic acid in a small-scaled test reaction and the product (31) was successfully obtained with a yield of 73% (Scheme 33).

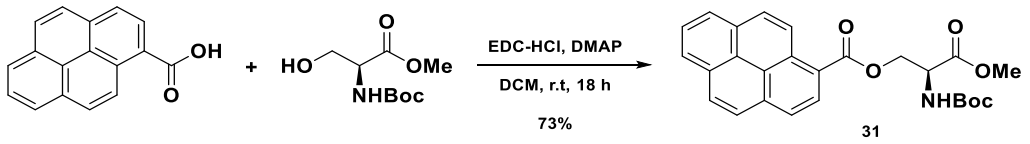

*Scheme 33: Coupling reaction of 1-pyrenecarboxylic acid and Boc-L-Ser-OMe to Boc-L-Ser(Pyr)-OMe (**31**).*

Proton NMR analysis confirmed that the reaction was successful and the desired material Boc-Ser(pyrene-1-carbnyl)-OMe (**31**) was obtained. All signals of serine and its Boc (f, 1.39 ppm) and methyl (d, 3.72 ppm) protecting groups, as well as the aromatic pyrene signals (a, 8.20-9.30 ppm) were observed with the expected signal intensity (Figure 61).

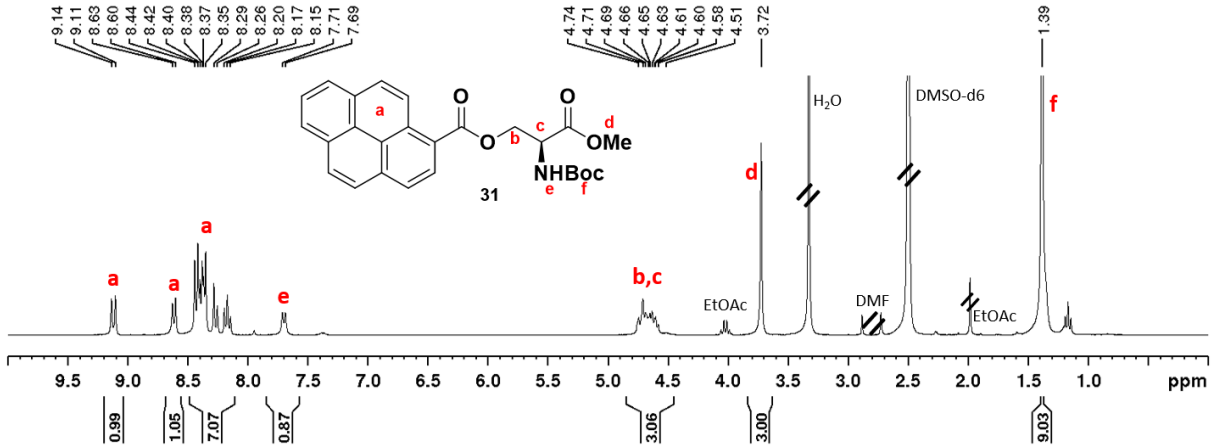

*Figure 61: ^{1}H-NMR spectrum (DMSO-d_6, 300 MHz, 298 K) of pyrene-protected Boc-Ser-OMe (**31**).*

The first approach to protect Boc-Ser-OMe with pyrene by coupling reaction was successful and the ester **31** was obtained with good yields, but the Boc and methyl protecting groups of the N- and C-terminus were hard to cleave without harming the ester group in the side chain due to the strong acidic and basic conditions needed. In addition, the deprotection of both groups required different conditions and would need two additional steps before the NCA synthesis could be conducted. Therefore, a protecting group strategy was required, where both groups were deprotected in one step without affecting the ester group in the side chain. The best solution was using benzylic protecting groups that showed excellent stability towards the reaction conditions of the coupling reaction and are cleavable under fairly mild conditions by catalytic hydrogenation. The pyrene protecting group was not affected by this reaction, as it did not have a benzylic methylene group that is mechanistically required for the deprotection by hydrogenation. The resulting synthetic route contained a one-pot reaction, in which the simultaneous deprotection of the N- and C-terminus was combined with the subsequent cyclization of the amino acid to the corresponding NCA monomer without the need of a purification step in between (Scheme 34, last step). Overall, the NCA monomer (**30**) was obtained in three steps. First, the carboxylic acid of commercially available Cbz-Ser-OH was protected with a benzyl protecting group, using benzyl bromide under basic conditions, resulting in Cbz-Ser-OBn (**32**) with a yield of 98%. The 1-pyrenyl serine ester (**33**) was formed by coupling reaction of Cbz-Ser-OBn and 1-pyrenecarboxylic acid with EDC-HCl and DMAP (69% yield). In a one-pot reaction, the Cbz and benzyl protecting groups were cleaved by catalytic hydrogenation in the presence of palladium on charcoal under hydrogen atmosphere, followed by addition of triphosgene to form the cyclic NCA monomer **30** with a yield of 96%. The N-carboxy anhydride of the *O*-pyrenyl serine ester (**30**) was obtained with an overall yield of 65% over three steps and in gram-scale.

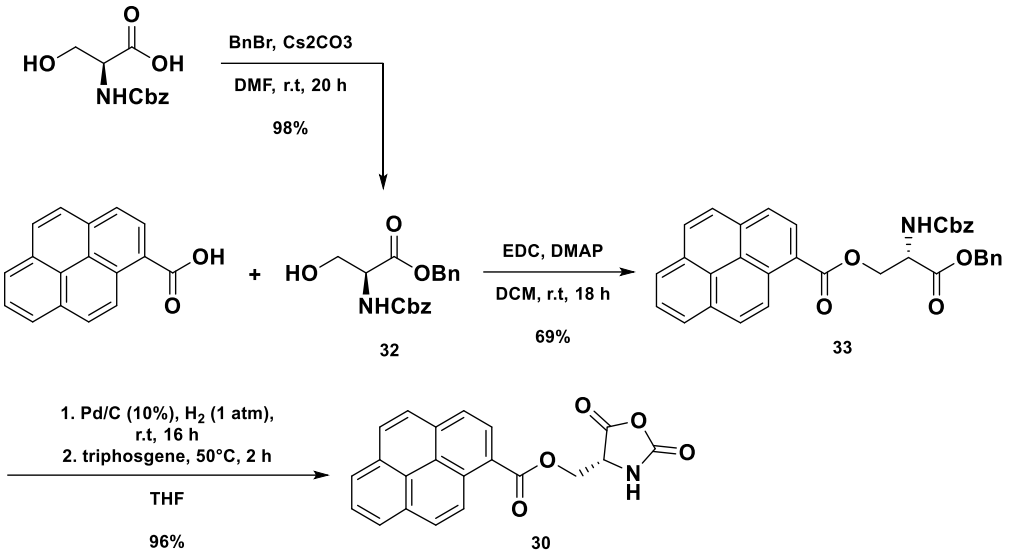

*Scheme 34: Coupling reaction of 1-pyrene carboxylic acid and Cbz-L-Ser-OBn (**32**), after benzyl-protection of the C-terminus of Cbz-L-ser-OH, followed by NCA synthesis to obtain L-Ser(Pyr)-NCA (**30**).*

Before the deprotection and cyclization steps were combined, both reactions were conducted as isolated steps to enable the characterization of the resulting molecules after each step and to monitor the deprotection of the amine and carboxylic acid by catalytic hydrogenation (Scheme 35).[131] The first approach of the deprotection step was conducted in methanol, which resulted in poor yield due to the limited solubility of the starting material in the solvent. The solvent was then changed to THF, resulting in quantitative deprotection after 16 hours, according to proton NMR analysis of the crude material. The NCA of 1-pyrenyl-L-serine ester (**30**) was then obtained successfully with a yield of 83% after reaction with triphosgene.[80]

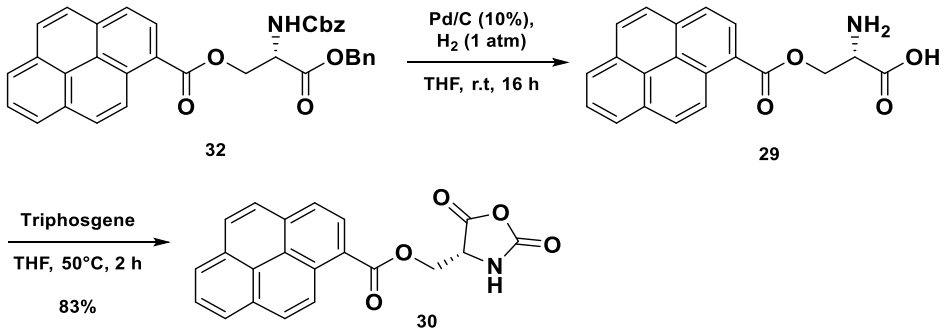

*Scheme 35: Deprotection of the N- and C-terminus by catalytic hydrogenation and cyclization of the 1-pyrenyl serine ester (**29**) to the corresponding NCA (**30**).*

The progress from obtaining Cbz-Ser-OBn (**32**) in the first step to the final product *O*-pyrenyl serine NCA (**30**) in the fourth step was monitored by proton NMR spectroscopy (Figure 62). After the benzyl protection of the carboxylic acid of serine in the first step, the intensity of the aromatic benzyl protons (a, h) at 7.24-7.42 ppm increased from 5 to 10, and a second singlet signal (b, g) appeared 5.14 ppm, showing that the incorporation of the benzyl group into the molecule was successful. After the

coupling reaction of Cbz-Ser-OBn and 1-pyrenecarboxylic acid, the signal of the hydroxy group of the serine side chain (e) at 4.98 ppm disappeared, while the other serine signals showed a downfield shift of 0.5-0.7 ppm each. The aromatic pyrene signals (e) appeared with an overall intensity of 9, as expected, in the region of 8.12-8.66 ppm as a multiplet and at 9.12 ppm as a doublet. The third step, the catalytic hydrogenation, resulted in the disappearance of the benzylic methylene signals (b, g) at 5.09 and 5.22 ppm and the aromatic proton signals (a, h) at 7.24-7.42 ppm. Eventually, the successful synthesis of the NCA **30** was confirmed by a downfield shift of the α-proton (c) from 4.62 to 5.05 ppm and the singlet signal at 9.45 ppm that is characteristic for the amide proton of N-carboxy anhydrides (f).

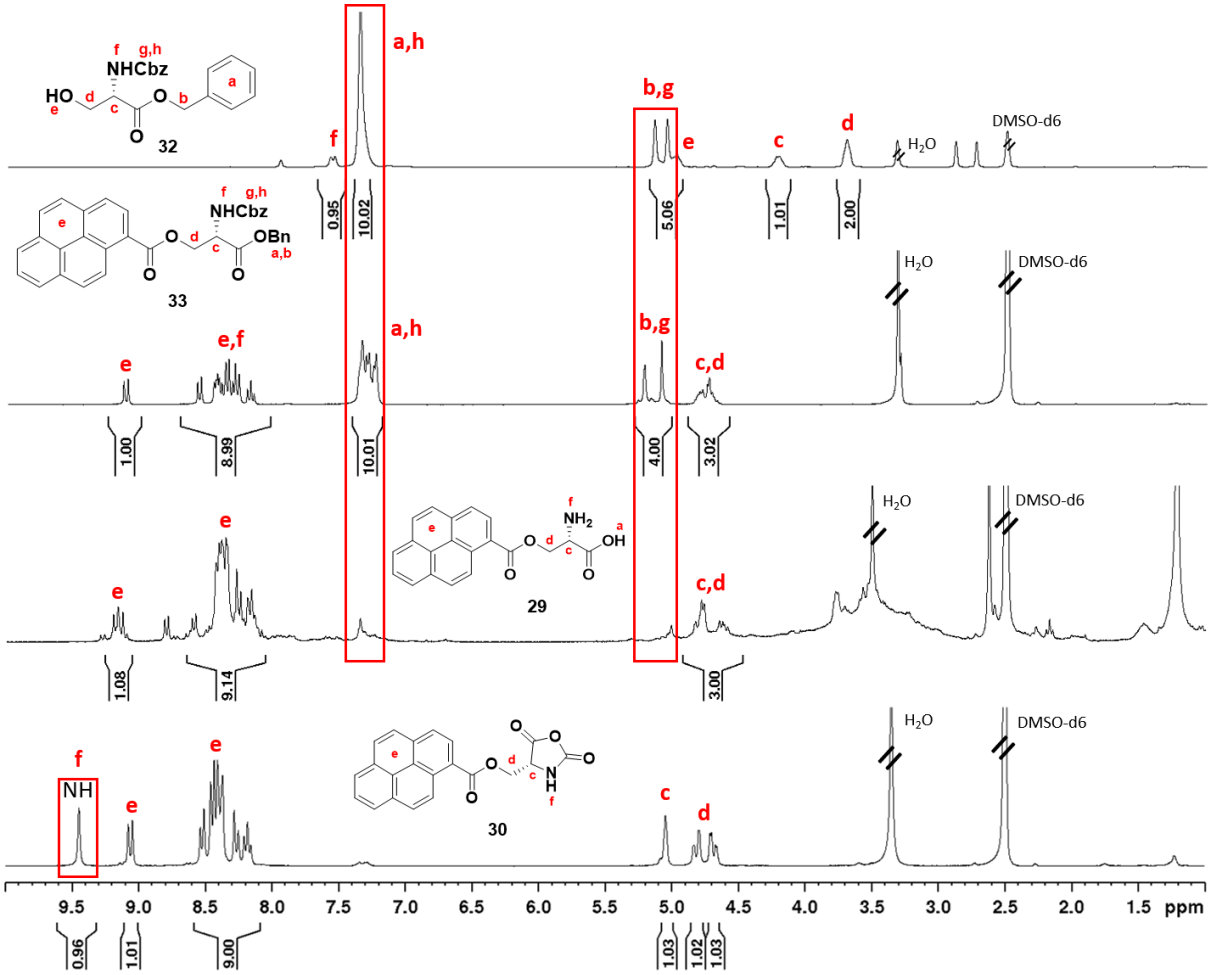

*Figure 62: ^{1}H-NMR spectra (DMSO-d_6, 300 MHz, 298 K) of Cbz-Ser-OBn (**32**), Cbz-Ser(pyrenyl-1-carbonyl)-OBn (**33**), O-(pyrenyl-1-carbonyl) serine (**29**) and O-(pyrenyl-1-carbonyl) serine-NCA (**30**).*

The deprotected amino acid (**29**) showed almost no solubility in THF and other solvents, making a proper workup difficult. As THF was used as a solvent for the NCA synthesis as well and charcoal is known to benefit the NCA reaction,[132] it was decided to combine the last two steps and add triphosgene to the reaction mixture without a workup in between (Scheme 36). This one-pot reaction

worked excellent and resulted in the formation of the *O*-pyrenyl serine NCA (**30**) with yields of up to 96%.

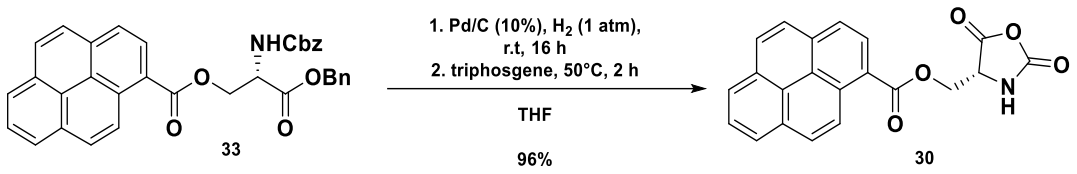

*Scheme 36: Deprotection and cyclization of the 1-pyrenyl serine ester (**33**) to the corresponding NCA building block **30**.*

The final O-pyrenyl serine NCA **30** after the one-pot reaction was analysed by proton and carbon NMR spectroscopy to confirm the molecule´s structure and purity (Figure 63). As described above, the shift of the α-proton (d) to 5.05 ppm and the characteristic singlet signal (e) at 9.45 ppm of the amide proton proved the success of the reaction. The carbon NMR spectrum showed all expected signals and especially the three carbonyl signals (b, f) at 152.1, 166.4 and 169.6 ppm of the NCA ring and the ester group were a significant proof that the desired molecule was obtained.

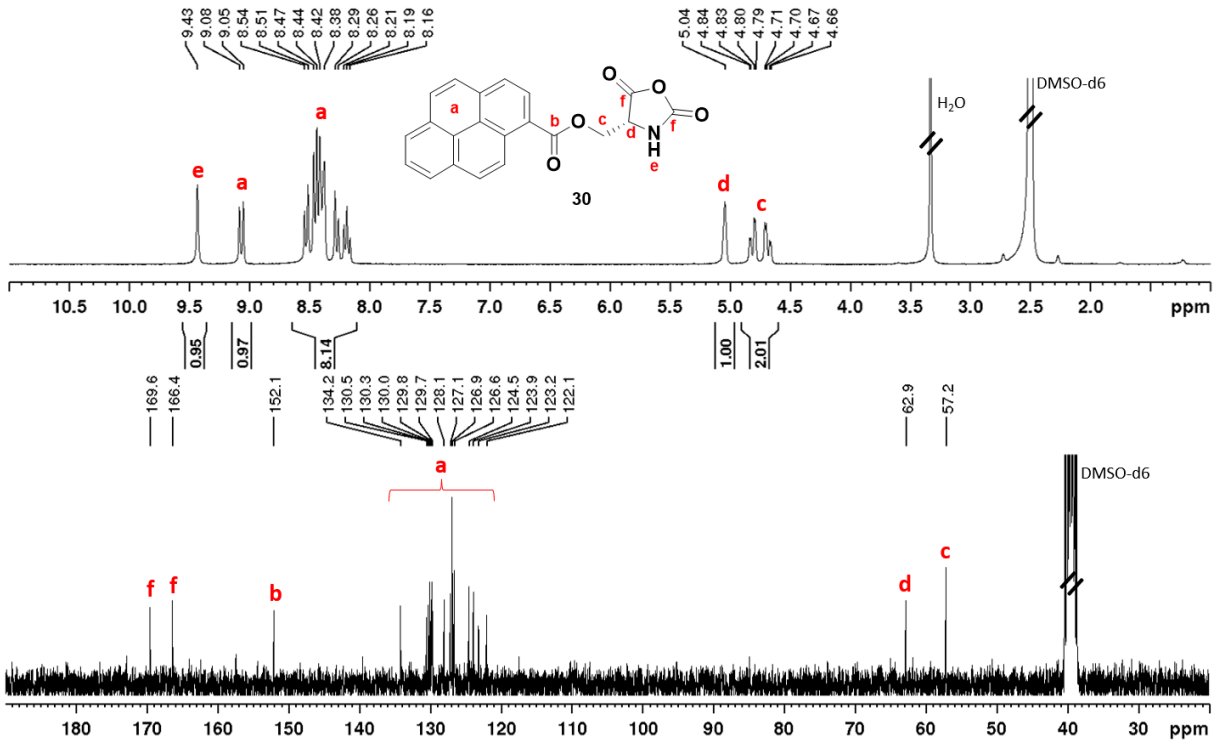

*Figure 63: ^{1}H- and ^{13}C-NMR spectra (DMSO-d_6, 300 MHz, 298 K) of O-(pyrenyl-1-carbonyl) serine NCA (**30**).*

In summary, the synthesis of a photocleavable serine derivative and its conversion to the activated monomer, the N-carboxy anhydride **30** was successful. While the first attempts to introduce the nitro-benzyl group into the serine side chain by forming an ether (**14**) were resulting in poor yields, the alternative route over the Garner´s aldehyde structure, was not leading to the desired nitro-benzyl protected serine derivative **24** at all. Test reactions that were performed to introduce a benzyl group

into the serine side chain were successful in both routes and led to the assumption that the nitro-group was the root cause of the problems. And indeed, NMR experiments with nitro-benzyl bromide and sodium hydride, the most commonly used base in this reaction, showed degradation of the material after only 20 minutes. Therefore, following attempts to introduce a photocleavable group were conducted with pyrene derivatives. The introduction of pyrene as a carbonate group was successful, but showed low stability towards low pH, making this functional group unsuitable for the following NCA synthesis that was carried out under acidic conditions. The last route, the formation of an ester group in the serine side chain by classical coupling reaction, finally worked well and led to the desired O-pyrenyl serine NCAs. This route was not only comparably short with three steps, but contained a one-pot reaction, where the deprotection and cyclization were carried out in one single step and resulted in excellent yields. In addition, this route was successfully carried out in multigram scale, which was an important aspect for the subsequent synthesis of different block copolymers. The synthesis was conducted successfully with the enantiomerically pure L-serine and D-serine as well as the racemic DL-serine in comparably high yields.

4.2 Synthesis of photocleavable PEG-*b*-PSer(Pyr) block copolymers

After successful synthesis of the *O*-(pyrene-1-carbonyl) serine NCA (**30**), the next step towards photosensitive amphiphilic block copolymers was the ring opening polymerization of the activated monomer. The reaction conditions were inspired by Dorresteijn et al., who successfully synthesized PEG-*b*-Poly[(1-pyrenylmethyl-) glutamate].[53] Polymerization of pyrene-functionalised L-glutamate resulted in block lengths of up to 90 units. It has to be noted that glutamic acid is an α-helix builder, while serine favours β-sheet formation, and therefore, glutamic acid is forming less sterically hindered and more flexible polymers that are more likely to aggregate into well-defined nanostructures in nonaqueous solution due to their linear, helical structure.[91] Nevertheless, it was believed that the pyrene group in the serine side chain could provide enough steric hindrance to inhibit β-sheet formation and promote random coil structures that are much more flexible and more likely to form nanostructures compared to benzyl serine. To investigate the aggregation behaviour of amphiphilic, pyrene-functionalised serine-containing polymers, block copolymers with different block ratios and molecular weights were synthesized and dispersed in nonaqueous solution. The results are summarized in this chapter. The first two ring opening polymerizations were conducted with either L- or DL-serine(pyrene-1-carbonyl) NCA (**30,34**) and $mPEG_{45}$-amine macro initiator, using urea as the β-sheet breaker (Scheme 10).[53,82] The reaction took place in DMF at room temperature and the polymers **35-37** were obtained with low yields of 18 and 29% (Table 20, **35a-b**). The third reaction was slightly modified, where lithium bromide was used instead of urea, and the reaction temperature was decreased to 0 °C, as these conditions resulted in higher DPs in previous experiments.[85] The polymer was obtained with a moderate yield of 45% (Table 20, **35c**).

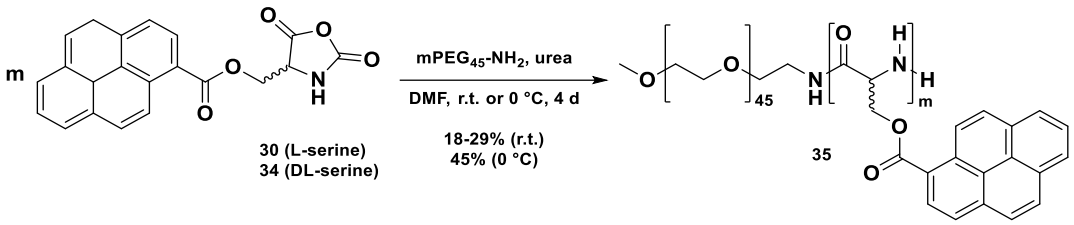

*Scheme 37: Ring opening polymerization of L- and DL-Ser(pyrenyl-1-carbonyl)-NCA (**30**) with $mPEG_{45}$-amine, resulting in the homo and block copolymers **35-37**.*

With lithium bromide at 0 °C a higher yield was achieved. At the same time, a higher DP (DP_{exp} = 10; DP_{theo} = 15) was obtained relatively, compared to the first two approaches. The theoretical DPs of the first two polymers (**35a-b**) were 90 and 10 and both were not achieved. Instead, the obtained DPs were 18 and 6. Polymerization at low temperatures and in the presence of lithium bromide as the β-sheet breaker led to higher monomer conversion. Compared to the beforementioned *O*-benzyl serine-based block copolymers (**2-4**, **6-8**), the resulting DPs of the pyrene-protected serine blocks were even lower. One reason might be the bulkiness of the pyrene group, making it difficult to align with the favoured

β-sheet formation. In addition, early precipitation of the polymers during the reaction was observed, meaning that the polymers did not stay in solution when reaching a certain block length due to its increasing amphiphilicity. As a consequence, the polymers were no longer available for further polymerization after precipitation. When comparing the L- and DL-serine based polymers, there was no significant difference observed.

*Table 20: Synthetic details of L- and DL-O-(pyrenyl-1-carbonyl) serine homo and copolymers **35-37**.*

No.	Polymer	Initiator	DP_{theo} [a]	DP_{exp} [b]	Yield [%]	Mn [b] [Da]	T [°C] [c]
35a	PEG_{45}-*b*-PLS(Pyr)$_{20}$, ncs175	mPEG_{45}-NH_2	90	20	18	7700	RT
35b	PEG_{45}-*b*-PDLS(Pyr)$_6$, ncs208	mPEG_{45}-NH_2	10	6	29	3900	RT
35c	PEG_{45}-*b*-PDLS(Pyr)$_{10}$, ncs209	mPEG_{45}-NH_2	15	10	45	5200	0
35d	PEG_{45}-*b*-PDLS(Pyr)$_{23}$, ncs198	mPEG_{45}-NH_2	90	23	38	9300	35
36	PEG_{17}-*b*-PDLS(Pyr)$_{22}$, ncs199	mPEG_{17}-NH_2	50	22	24	7700	35
37	Bn-*b*-PDLS(Pyr)$_{22}$, ncs200	Bn-NH_2	50	22	45	7000	35

[a] molar feed ratio of monomer and initiator [mmol]. [c] During polymerization.
[b] Mn of di-block copolymer, calculated by ^{1}H-NMR analysis.

All synthesized polymers **35-37** were analysed by proton and DOSY-NMR spectroscopy to prove covalent attachment of the polyserine block to the PEG block and to calculate the DP and molecular weight Mn. The proton and DOSY spectra of the di-block copolymer PEG_{45}-*b*-PLS(Pyr)$_{20}$ (**35a**) are shown below, representatively (Figure 64). In the proton NMR spectrum, all expected signals of both blocks were visible. The aromatic signals of the pyrene protecting group and the amide signals of the polymer back bone were in the region of 8.00-9.50 ppm. The α- and β-signals of the serine side chain were displayed in the region of 4.50-5.00 ppm. The characteristic PEG-CH_2 singlet signal was visible at 3.53 ppm. The DP was calculated by the signal intensity ratio of the PEG singlet and the α- and β-signals, which resulted in a ratio of 45:20 of the PEG to PLS(Pyr) block. The DOSY spectrum clearly showed that the diffusion constant of the PEG and PLS(Pyr) blocks was the same, indicated by the red line, proving that the two blocks were covalently bound and the polymerization was successful.

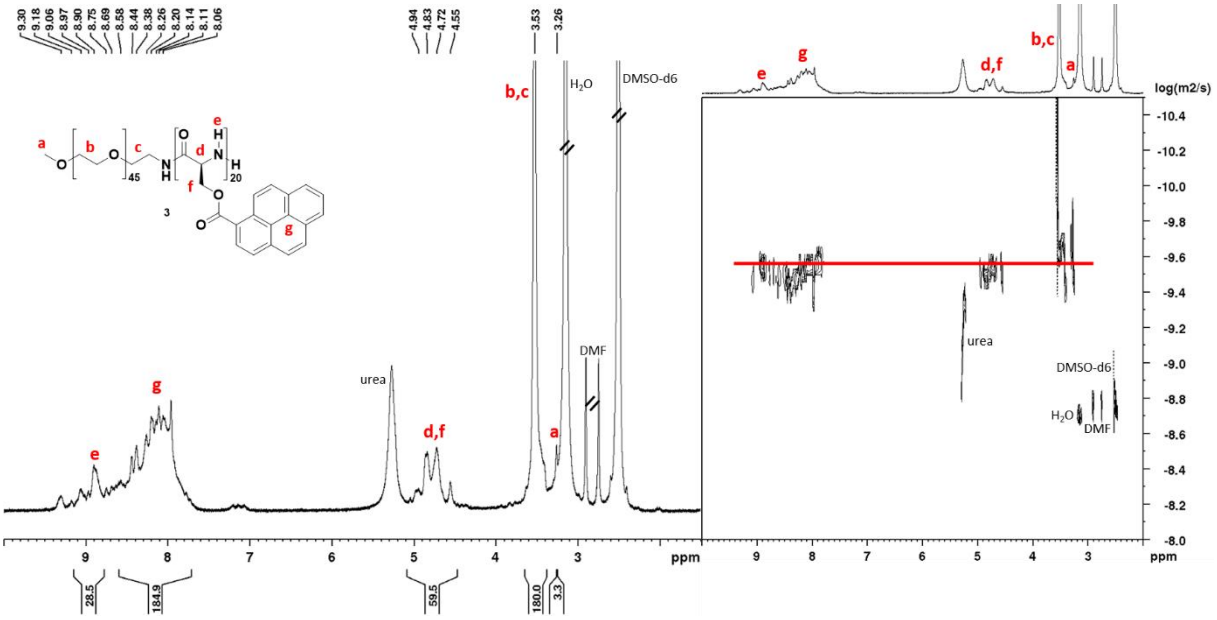

*Figure 64: ^{1}H- and DOSY-NMR spectra (DMSO-d_6, 700 MHz, 333 K) of the di-block copolymer PEG_{45}-b-$PLS(Pyr)_{20}$ (**35a**).*

Not only the chemical composition of the synthesized polymers was investigated, but also the secondary structure of the poly-*O*-(pyrene-1-carbonyl)serine block. In theory, L-serine was expected to form mainly β-sheets within the amino acid chain, while the incorporation of D-serine should lead to the disruption of the β-sheets and the formation of random coil structures.[72] Therefore, the block copolymers were analyzed in solid state by FT-IR measurements. The different secondary structures α-helix, β-sheet and random coil of proteins and peptides have IR bands at specific wavenumbers and can be easily identified by the FT-IR spectra.[91,92] The benzyl-protected block copolymers PEG-*b*-PSer(Bn) showed that the L-serine polymers favored the β-sheet formation, while the DL-serine polymers showed signals of both, β-sheet and random coil structures, as expected. Figure 65 displays the FT-IR spectra of a selection of synthesized PEG-*b*-PSer(Pyr) polymers, displaying that the situation was different for the PEG-*b*-PSer(Pyr) polymers. All L- and DL- serine based polymers, contained both, β-sheet and random coil structures. The β-sheet structure was indicated by the amide band I at 1632 cm^{-1} (dotted line), and the amide band II at 1593 and 1581 cm^{-1}. The presence of random coil formation was displayed by the amide band at 1663 cm^{-1}. While the intensities of both signals were similar for the PEG_{45}-polymers PEG_{45}-*b*-$PLS(Pyr)_{20}$ (**35a**) and PEG_{45}-*b*-$PDLS(Pyr)_{23}$ (**35d**), the shorter copolymer PEG_{17}-*b*-$PLS(Pyr)_{22}$ (**36**) showed predominantly β-sheet formation. The homopolymer Bn-*b*-$PDLS(Pyr)_{10}$ (**37**) resulted in the highest intensity ratio for random coil formation. It was hypothesized that the persistent formation of random coil structure was forced by the bulkiness of the pyrene group that sterically hindered the formation of ordered β-sheet structures.

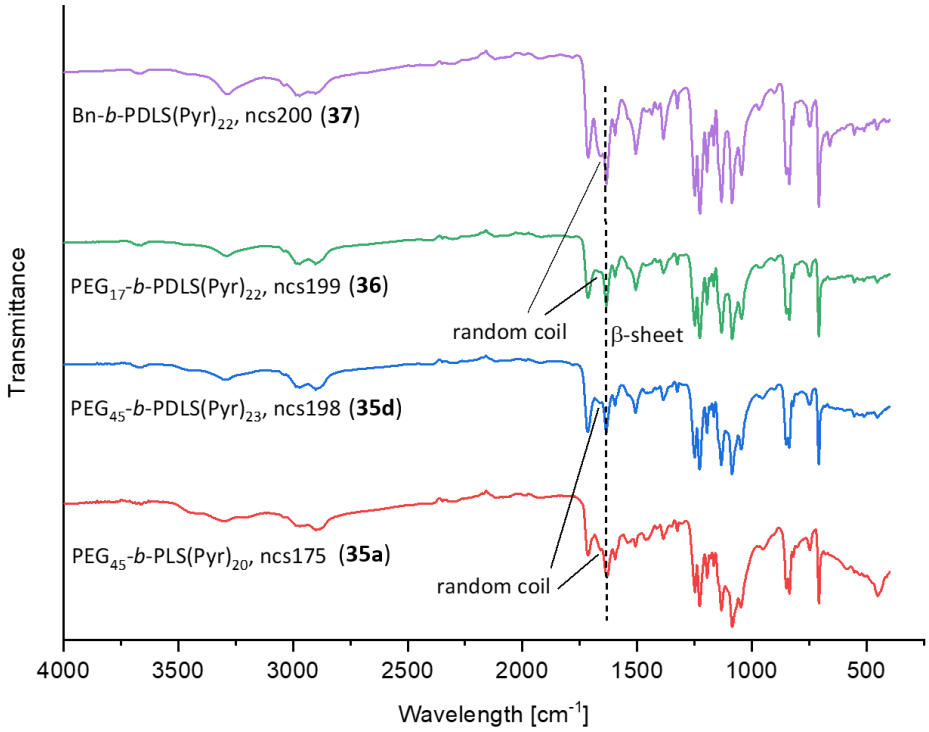

*Figure 65: FT-IR spectra of the L- and DL-serine di-block copolymers **35-37** to analyse the secondary structure of the polymers, depending on the polymerization temperature and polymer composition. All four polymers showed random coil and β-sheet conformation in different ratios. The β-sheet conformation was indicated by the amide band I at 1618 and 1623 cm^{-1}, respectively, and the amide band II at 1586 and 1576 cm^{-1} (dotted line).*

In the next approach, the reaction conditions were modified in order to increase the DP of the block copolymers (Scheme 38). First, the β-sheet breaker was changed to lithium bromide, which resulted in slightly higher DPs in previous experiments. The solvent was changed from DMF to a mixture of DCM/DMF (1:1) to increase the solubility of the polymers during polymerization. In addition, the reaction temperature was increased from room temperature to 35°C. The polymerization was conducted with three different initiators, $mPEG_{45}$-NH_2, $mPEG_{17}$-NH_2 and benzyl amine, to evaluate the dependence of the DP on the molecular weight of the initiator (Table 20, No. 4-6). The polymers **35-37** were obtained with low yields of 24-45% and slightly higher DPs of 22 and 23 respectively, compared to the first approaches. The nearly identical DP of the serine block of all three polymers indicated that the initiator did not have any impact, while modification of the solvent and temperature of the reaction led to slight improvement of the polymerization degree.

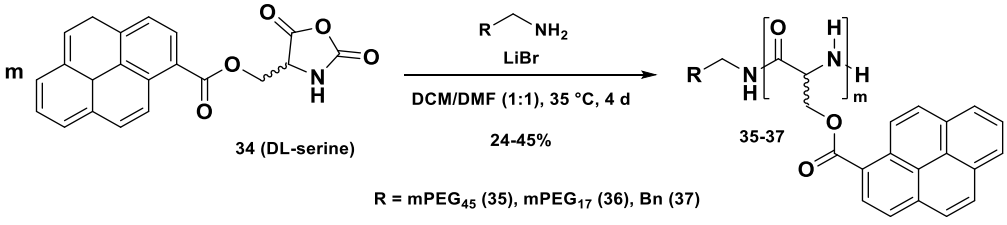

*Scheme 38: Ring opening polymerization of DL-Ser(pyrenyl-1-carbonyl)-NCA (**34**) with mPEG-amines or benzyl amine, resulting in homo or block copolymers **35-37**.*

In comparison to the previously discussed *O*-benzyl-serine based polymers (**2-4**, **6-8**), the polymerization of the *O*-(pyrene-1-carbonyl) serine NCA (**30**,**34**) led to early precipitation of the polymers during the reaction. Consequently, they resulted in even lower polymerization degrees due to the pyrene group, which was not only significantly more hydrophobic, but also bulkier and sterically more challenging than a benzyl group. The fact, that pyrene-functionalized glutamic acid was reported to be polymerizable with block lengths of up to 90 units, led to the conclusion that the bulkiness or hydrophobicity of the pyrene ring was not the problem *per se*.[53] Instead, this proved once more that the difficulties in achieving polymers with DPs of 50-100 was rooted in the serine itself. Taking into account that common literature on serine polymers describes homo and block copolymers with low DPs of maximum 10-20, regardless of the side chain protecting group, supported this hypothesis.[72] These findings were consistent with the results from the previous chapter on *O*-benzyl-serine based polymers. While the attempts to increase the block length of the *O*-benzyl-serine polymers were successful to some extent, the ideal block ratio of PEG and PLS(Bn) blocks for homogeneous dispersion in nonaqueous solution was not found for these block copolymers so far. Therefore, an alternative strategy was applied to increase the *O*-(pyrene-1-carbonyl) serine moiety in the block copolymers. By using homobifunctional diamino-PEG derivatives as macro initiators, symmetrical BAB-triblock copolymers were synthesized to increase the ratio of serine in the polymers and to study the influence of the modified block copolymers on the emulsion formation ability in nonaqueous solution. Triblock copolymers are known to be beneficial in the formation of micellar structures in solution, while di-block copolymers may prefer to aggregate to worm- or rod-like structures in some cases.[133,134] In addition, the packing parameters of triblock copolymers are higher compared to di-block copolymers, resulting in stable emulsions at relatively low DPs of the two hydrophobic blocks. [133,134] Two macroinitiators with the structure NH_2-PEG-NH_2 were used with molecular weights of 2000 and 3000 Da. Four ring opening polymerizations, two per initiator, were conducted with *O*-(pyrenyl-1-carbonyl)-DL-serine (**34**) in the presence of lithium bromide in DMF at room temperature (Scheme 39). The triblock copolymers **38-39** were obtained with moderate yields of 29-50% that were comparable to the yields of the di-block copolymers.

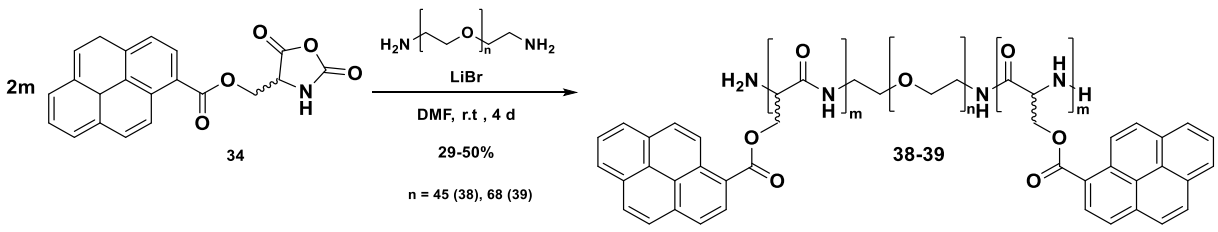

*Scheme 39: Ring opening polymerization of DL-Ser(pyrenyl-1-carbonyl)-NCA (**34**) with amino-PEG-amine, resulting in triblock copolymers (**38-39**).*

The theoretical DPs of the PDLS(Pyr) block were chosen in order to achieve an overall block ratio of 60:40 and 40:60 of the PEG and PDLS(Pyr) blocks to investigate, which ratios were feasible for the triblock copolymer synthesis. The first goal was a 40:60 ratio of hydrophilic to hydrophobic moiety, which was proposed as ideal for the formation of a homogeneous, nonaqueous emulsion.[50] When comparing the molar feed ratio and the obtained DP, the polymerizations with the shorter PEG_{45} block (**38a-b**, Mn = 2000 Da) resulted in higher DPs than the ones with the PEG_{68} block (**39a-b**, Mn = 3000 Da), as summarized in Table 21. The PEG_{45}-based triblock copolymers (**38a-b**) were obtained with DPs of 8/10 and 16/16, while the PEG_{68}-based polymers (**39a-b**) only achieved DPs of 8/14 and 6/22.

*Table 21: Synthetic details of O-(pyrenyl-1-carbonyl)-DL-serine triblock copolymers **38-39**.*

No.	Polymer	Initiator	DP_{theo}[a,b]	DP_{exp}[b,c]	Yield [%]	Mn[c] [Da]
38a	$PDLS(Pyr)_4$-*b*-PEG_{45}-*b*-$PDLS(Pyr)_4$, ncs204	NH_2-PEG_{45}-NH_2	10	8	50	4500
38b	$PDLS(Pyr)_8$-*b*-PEG_{45}-*b*-$PDLS(Pyr)_8$, ncs205	NH_2-PEG_{45}-NH_2	16	16	29	7000
39a	$PDLS(Pyr)_4$-*b*-PEG_{68}-*b*-$PDLS(Pyr)_4$, ncs206	NH_2-PEG_{68}-NH_2	14	8	48	5500
39b	$PDLS(Pyr)_3$-*b*-PEG_{68}-*b*-$PDLS(Pyr)_3$, ncs207	NH_2-PEG_{68}-NH_2	22	6	44	4900
38c	$PDLS(Pyr)_{17}$-*b*-PEG_{45}-*b*-$PDLS(Pyr)_{18}$, ncs210	NH_2-PEG_{45}-NH_2	40	35	52	13000

[a] molar feed ratio of monomer and initiator [mmol]. [c] Mn of triblock copolymer, calculated by ^{1}H-NMR analysis.
[b] DP * ½ = desired DP per serine block.

An interesting observation was made during the reaction workup of all four polymers. Usually, the di-block copolymers were precipitated in cold diethylether, a nonpolar solvent. This worked well for most of the di-block copolymers, while others resulted in emulsion formation. Once fully dried, these polymers were not well dispersible in nonpolar solvents and nonaqueous emulsion polymerization did not lead to homogeneously dispersed nanoparticles. However, the triblock copolymers did not precipitate in diethylether, but resulted in fine emulsions, which remained stable during centrifugation. Instead, they were precipitating in ethanol. This led to the conclusion that a polarity shift into the desired direction was possibly achieved to be utilized in nonaqueous emulsion polymerization. Another aspect was that these polymers, as proposed, were self-assembling to micellar structures more easily. A last experiment was conducted to generate a triblock copolymer with a higher molecular weight of 15 kDa and a block ratio of 20:45:20 (PDLS(Pyr)-*b*-PEG-*b*-PDLS(Pyr), **38c**). Therefore, a combination of the tested reaction conditions was used that led to the highest monomer conversion so far (Scheme 40). The reaction was conducted in the presence of lithium bromide and in a solvent mixture of DMF/DCM (3:1), while the reaction temperature was set to 0 °C. The polymer **38c** was obtained with the highest yield of 52% so far, and a block ratio of 17:45:18 (Table

21, No. 5). An overall ratio of hydrophilic PEG to hydrophobic PDLS(Pyr) of 45:35 was achieved and with it the goal of significantly increasing the serine ratio in the block copolymers.

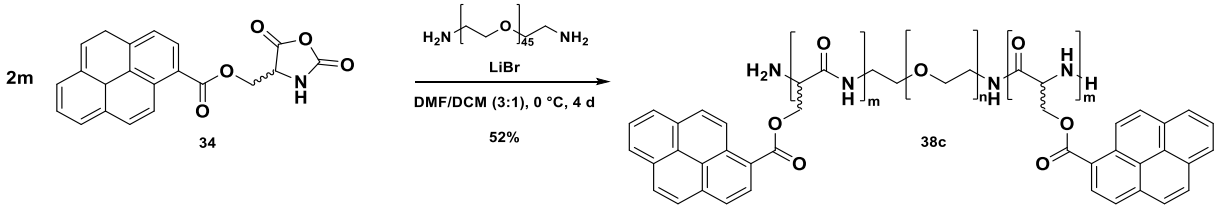

*Scheme 40: Ring opening polymerization of DL-Ser(pyrenyl-1-carbonyl)-NCA (**34**) with amino-PEG$_{45}$-amine, resulting in the triblock copolymer **38c**.*

In summary, a photocleavable pyrene-functionalized serine derivative (**33**) was synthesized successfully by classical coupling reaction and converted into the corresponding NCA (**30,34**). Amphiphilic di- and triblock copolymers with the structures PEG-*b*-PDLS(Pyr) (**35-36**) and PDLS(Pyr)-*b*-PEG-*b*-PDLS(Pyr) (**38-39**) were obtained *via* ring opening polymerization. Even though the theoretical DP could not be achieved in the ROP of these block copolymers, matching the previous observations with Bn-protected serine, the aggregation behavior of these polymers in nonaqueous solution was studied and nonaqueous emulsion polymerization was performed using the amphiphilic block copolymers as emulsifiers in order to obtain core shell PLLA nanoparticles.

4.3 Nonaqueous emulsion polymerization with the *O*-(pyrenyl-1-carbonyl)-serine-based block copolymers

EMULSION FORMATION

Before the nanoparticle fabrication by emulsion polymerization was performed, emulsion formation experiments with the *O*-(pyrene-1-carbonyl)-serine polymers were conducted to evaluate the right solvent system and emulsifier concentration. The quality of the emulsions was monitored by their size distributions, measured by DLS. These experiments were based on the results and observations described in the previous chapter about Bn-serine-based block copolymers. Supporting these findings, emulsion formation in diethylether was already observed during the workup of the block copolymers, while first attempts to disperse the polymers in cyclohexane resulted in visible aggregation of the material. It was decided to use diisopropylether as the nonpolar solvent for the emulsion formation of the three block copolymers PEG_{45}-*b*-$PLS(Pyr)_{20}$ (**35a**), PEG_{45}-*b*-$PDLS(Pyr)_{23}$ (**35d**) and PEG_{17}-*b*-$PDLS(Pyr)_{22}$ (**36**). The first two contained the longer PEG_{45}-block and a L- or DL-serine block, and the third polymer consisted of a shorter PEG_{17}-block and DL-serine (Table 22).

*Table 22: Composition of O-(pyrene-1-carbonyl)-serine-based di-block copolymers **35-36**.*

No.	Polymer	DP_{PEG}	$DP_{PSer(Pyr)}$	DP ratio	Weight ratio	Mn [Da]
1	PEG_{45}-*b*-$PLS(Pyr)_{20}$, **35a**	45	20	70:30	25:75	8300
2	PEG_{45}-*b*-$PDLS(Pyr)_{23}$, **35d**	45	23	65:35	20:80	9300
3	PEG_{17}-*b*-$PDLS(Pyr)_{22}$, **36**	17	22	44:56	10:90	7700

In order to improve the emulsion stability and compare the aggregation behaviour of serine-based block copolymers in nonaqueous solution, it was compared to similar systems in the literature.[135–139] The comparison of our own observations with the literature resulted in contrary trends in the aggregation behaviour. The results with Bn-serine-based systems already indicated that these polymers were behaving differently in solution compared to classical polymers. According to Dvorakova et al., an increase of emulsifier concentration resulted in decrease of particles size in a nonaqueous emulsion system with classical emulsifiers.[94] An emulsifier to dispersed phase ratio of 1:5 turned out to be the ideal ratio, resulting in spherical particles of around 100 nm without agglomeration in the literature.[94] In contrast, higher concentrations resulted in agglomerates, because the excess emulsifier "glued" the particles together. This is contrary to the findings of the serine polymers that showed better dispersion and less aggregation at lower emulsifier concentration with an improved emulsifier to dispersed phase ratio of 1:10. Similar systems, like the PEG-*b*-PGlu(Pyr) block copolymers that were reported by Robert Dorresteijn, were also following the trends of classical polymers in solution and were therefore not comparable to the PEG-*b*-PSer(Bn/Pyr) system.[53] One

reason for the clearly worse performance of the serine-based polymers was its secondary structure. While glutamic acid is an α-helix builder, resulting in linear helix strands with moderate solubility, serine naturally forms β-sheets that are held together by strong intramolecular hydrogen bond interactions leading to low solubility.[140,141] Another aspect that should be mentioned is the definition of the term "block ratio" of a polymer. While our group commonly used this term in regards of the polymerization degree of the two polymer blocks, the term is widely used in the literature as the molecular weight ratio of the blocks.[98] In classical polymers, like PMMA-*b*-PI, where both monomers have a comparable molecular weight, it does not make any significant difference, which definition for block ratio is used. In contrast, in the PEG-*b*-PSer(Bn) and even more in PEG-*b*-PSer(Pyr) the molecular weight of the PEG monomer is dramatically lower than of the serine monomers (Δ > 300 g/mol). It makes a huge difference, if the molecular weight or DP ratio is taken into account, making it difficult to make reasonable comparisons with other block copolymers, when talking about the block ratio. This is clearly displayed in Table 22, where the DP ratio (70:30) and weight ratio (25:75) is almost inverted for the first two polymers. The third polymer showed different values for the two ratios as well. A valid comparison with classical polymers was not reliable. For the emulsion formation of a block copolymer in a solvent, Robert Dorresteijn et al. reported a weight ratio of 0.34 wt% as the ideal value for the emulsifier PEG_{45}-*b*-$PLG(Pyr)_{90}$ in nonaqueous emulsion.[35] This weight ratio was chosen as the starting point for the emulsion formation with the PEG-*b*-PSer(Pyr) emulsifiers in diisopropylether. The first polymer PEG_{45}-*b*-$PLS(Pyr)_{20}$ (**35a**) resulted in a homogenous emulsion with a particle diameter of 440 nm at a concentration of 2.50 mg/mL (0.34 wt%, Table 23). Gradual dilution to 2.00 mg/mL (0.28 wt%) and 1.43 mg/mL (0.20 wt%) resulted in particle sizes of 500 and 460 nm and hence, did not lead to a remarkable change in particle diameter. After 12 hours of stirring, the particle diameter of the diluted emulsion decreased to 350 nm. In comparison to the PEG-*b*-PLS(Bn) polymers, not only the particle size was improved, but also the homogeneity and stability of the emulsion.

*Table 23: Concentration-dependent particle size measurements of nonaqueous emulsions with PEG_{45}-b-$PDLS(Pyr)_{20}$ (**35a**).*

No.	Solvent (DiPE[1])	c [mg/mL]	wt%[2]	Time[3] [h]	d_H [nm]
1	4.0 mL/2.90 g	2.50	0.34	2	440 ± 10
2	5.0 mL/3.63 g	2.00	0.28	1	500 ± 10
3	7.0 mL/5.08 g	1.43	0.20	1	460 ± 10
4	7.0 mL/5.08 g	1.43	0.20	16	350 ± 5

[1] Density: δ (DiPE) = 0,725 g/mL. [2] Weight ratio of polymer to solvent.
[3] Time of stirring between the dissolution of the emulsifier or further dilution and DLS measurement.

The second polymer PEG_{45}-*b*-PDLS(Pyr)$_{23}$ (**35d**) had a slightly higher hydrophobic moiety than the first and consisted of racemic serine, forming a homogenous emulsion. A particle diameter of 425 nm at a concentration of 2.50 mg/mL was determined by DLS (0.34 wt%, Table 24). No significant change of the particle size was achieved by dilution to an emulsifier concentration of 2.00 and 1.43 mg/mL. As expected, based on their comparable block length, both polymers showed similar aggregation behaviour.

*Table 24: Concentration-dependent particle size measurements of nonaqueous emulsions with PEG_{45}-b-PDLS(Pyr)$_{23}$ (**35d**).*

No.	Solvent (DiPE[1])	c [mg/mL]	wt%[2]	Time[3] [h]	d_H [nm]
1	4.0 mL/2.90 g	2.50	0.34	2	425 ± 20
2	5.0 mL/3.63 g	2.00	0.28	1	415 ± 5
3	7.0 mL/5.08 g	1.43	0.20	1	410 ± 10

[1] Density: δ (DiPE) = 0,725 g/mL. [2] Weight ratio of polymer to solvent.
[3] Time of stirring between the dissolution of the emulsifier or further dilution and DLS measurement.

The third polymer PEG_{17}-*b*-PDLS(Pyr)$_{22}$ (**36**) consisted of a shorter PEG block, compared to the previous polymers and resulted in smaller particle size of 353 nm at an emulsifier concentration of 2.50 mg/mL (0.34 wt%, Table 25). This showed that a higher hydrophobic moiety in the polymer led to smaller particle size, as expected. Dilution to 2.00 mg/mL resulted in an increase of particle size by 50 nm, allowing the conclusion that a weight ratio of 0.34%, as proposed, was a suitable value for the PEG-*b*-PSer(Pyr) system, while it was not optimal for the PEG-*b*-PSer(Bn) system. In addition, these experiments proved that the formation of an emulsion and its stability is significantly improved by using the more hydrophobic pyrene group in the serine side chain instead of the benzyl group.

*Table 25: Concentration-dependent particle size measurements of nonaqueous emulsions with PEG_{17}-b-PDLS(Pyr)$_{22}$ (**36**).*

No.	Solvent (DiPE[1])	c [mg/mL]	wt%[2]	Time[3] [h]	d_H [nm]
1	4.0 mL/2.90 g	2.50	0.34	2	335 ± 5
2	5.0 mL/3.63 g	2.00	0.28	1	385 ± 10

[1] Density: δ (DiPE) = 0,725 g/mL. [2] Weight ratio of polymer to solvent.
[3] Time of stirring between the dissolution of the emulsifier or further dilution and DLS measurement.

NONAQUEOUS EMULSION POLYMERIZATION

In the next step the polymers were utilized as emulsifiers for nonaqueous emulsion polymerization (NEP) of PLLA nanoparticles in order to evaluate, if the pyrene protecting group was contributing to the formation of homogeneous particle dispersions. The pyrene-functionalized block copolymers showed better solubility in ethers, like diethylether and diisopropylether (DiPE), than in cyclohexane (CyH). Nevertheless, the final nanoparticle synthesis was intended to be established in the MeCN/CyH solvent system. The first polymerizations were performed in the DMF/DiPE solvent system that was studied by the emulsion formation experiments. The first NEP approach was conducted with the emulsifier PEG_{45}-*b*-$PLS(Pyr)_{20}$ (**35a**). The polymer was stirred in diisopropylether (c = 2.43 mg/mL) overnight and resulted in a homogeneous emulsion. In contrast to the previous reactions with the Bn-functionalised block copolymers, the emulsion did not collapse upon addition of the reagents and polar solvent. After the polymerization, a DLS sample was taken, diluted with DiPE (1:5) and a size distribution of d_H = 2700 ± 250 nm was determined after ultrasonication (5 minutes). It showed that larger aggregates were present in the reaction mixture. To remove excess reagents and emulsifier that are known to promote particle agglomeration,[94] the particles were washed with DiPE extensively. The particle size distribution was significantly reduced to d_H = 1000 ± 180 nm by the washing step. To find out, if nanoparticles were formed during the reaction or large, inhomogeneous aggregates were obtained, the particle morphology from both samples was analysed by SEM (Figure 66). The reaction mixture (A, B) clearly consisted of spherical nanoparticles of around 100 nm in diameter that were piled up into larger agglomerates. After the washing step (C, D) the particles were arranged in larger aggregates. The nanoparticles were still visible as such and their morphology looked very uniform, but they seemed to be clumped together. This effect is called flocculation and happens, when the repulsion between particle surfaces in the emulsion is not strong enough, leading to clumping of the particles.[138,142] Flocs are formed that, depending on the density, either sediment or float upwards.[143] In this case, the particle surface consisted of aromatic groups that are known for pi stacking and interactions, also described as attractive, noncovalent interactions. Therefore, they are prone to agglomeration.[144,145] This flocculation has already been observed, when using the Bn-functionalized PEG-*b*-PSer(Bn) block copolymers, but it was not possible before to pinpoint particle sedimentation as the root cause, because particle aggregation was observed already before the washing. Nevertheless, spherical nanoparticles of desired size were obtained in this very first approach with the emulsifier PEG_{45}-*b*-$PLS(Pyr)_{20}$ (**35a**), which was a great outcome to build on.

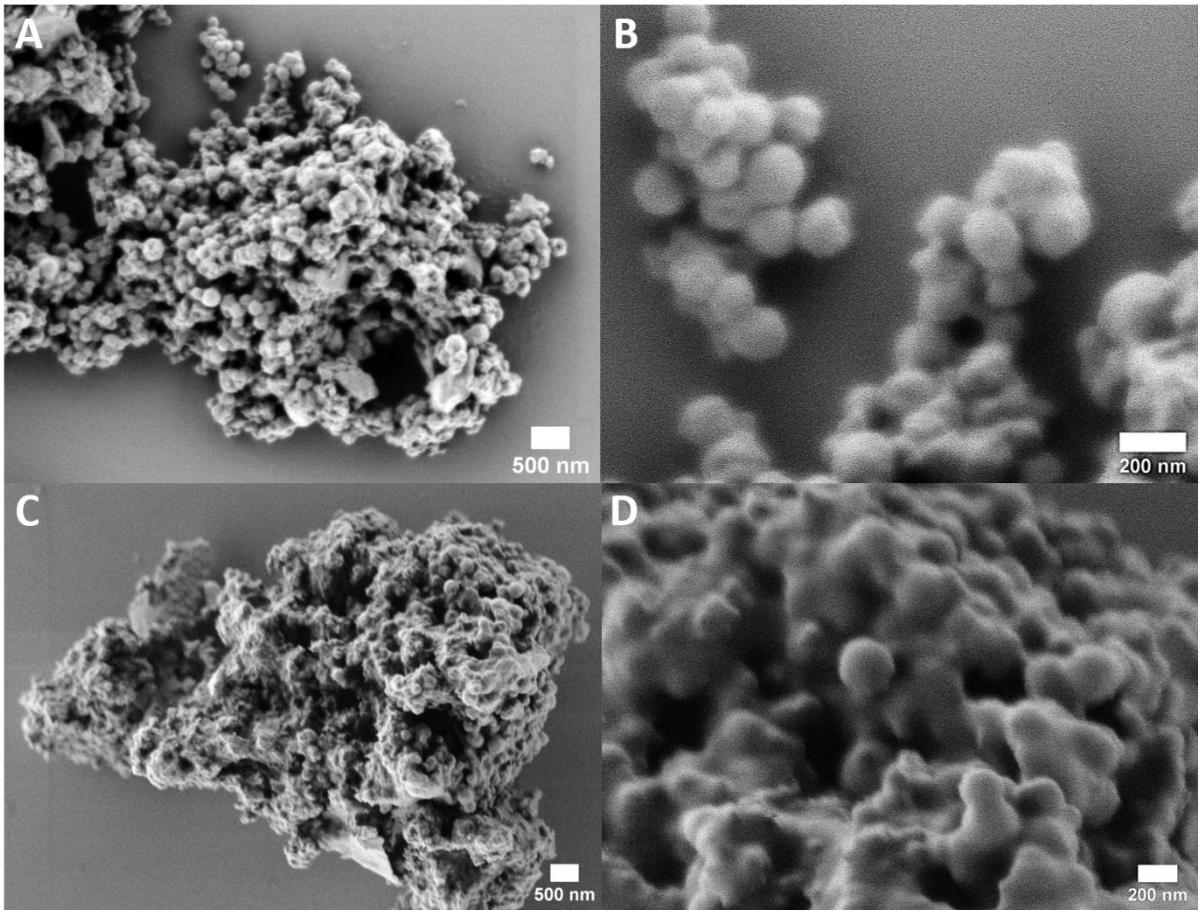

*Figure 66: SEM images of the PLLA nanoparticles using the emulsifier PEG_{45}-b-$PLS(Pyr)_{20}$ (**35a**). A, B) Diluted reaction mixture after polymerization and C, D) after one washing step.*

The second NEP approach was conducted with the emulsifier PEG_{45}-*b*-$PDLS(Pyr)_{23}$ (**35d**) that had a slightly higher hydrophobic block length and showed similar aggregation behaviour in the emulsion formation experiments. The main difference between the polymers was that the first one was consisting of an enantiomerically pure polypeptide block, while the second was containing a racemic block. Along the lines of the first approach, the emulsifier **35d** was forming a stable emulsion in DiPE (c = 2.43 mg/mL) and remained stable upon addition of the reagents. After the polymerization, the diluted DLS sample (1:5) resulted in a size distribution of d_H = 2100 ± 130 nm that was around 600 nm smaller the first approach. Sedimentation and washing of the particles resulted in smaller particles of d_H = 1200 ± 530 nm, according to DLS measurement, due to reduced aggregation tendency by removal of excess emulsifier.[94] The analysis of the particle morphology by SEM revealed significantly higher aggregation of the material in comparison to the first reaction that showed dispersed particles. Even though the reaction conditions were identical and the emulsifier was similar, the SEM images showed larger aggregates (Figure 67, A). These consisted of particles with diameters of 100-200 nm that were hardly visible, because of the material without specific morphology. The latter might potentially be excess emulsifier that was not used up for nanoparticle formation during the

reaction (Figure 67, B). This explained the diameters of 1-2 µm that resulted from the DLS measurements. The washing step resulted in smaller aggregates with a less dishevelled surface (Figure 67, C). In comparison to B, image D showed a smoother surface with more visible particles and again, flocculation of the spherical nanoparticles was observed. This approach with the emulsifier **35d** did result in nanoparticles with diameters of around 100 nm and hence, desired size, but they showed strong agglomeration and a less defined morphology compared to the first approach. As mentioned before, the only significant difference between both emulsifiers **35a** and **35d** was the use of L- vs. racemic serine, causing differences in the secondary structure of the polypeptide block. If racemic serine was indeed leading to stronger aggregation needed to be clarified by further investigation.

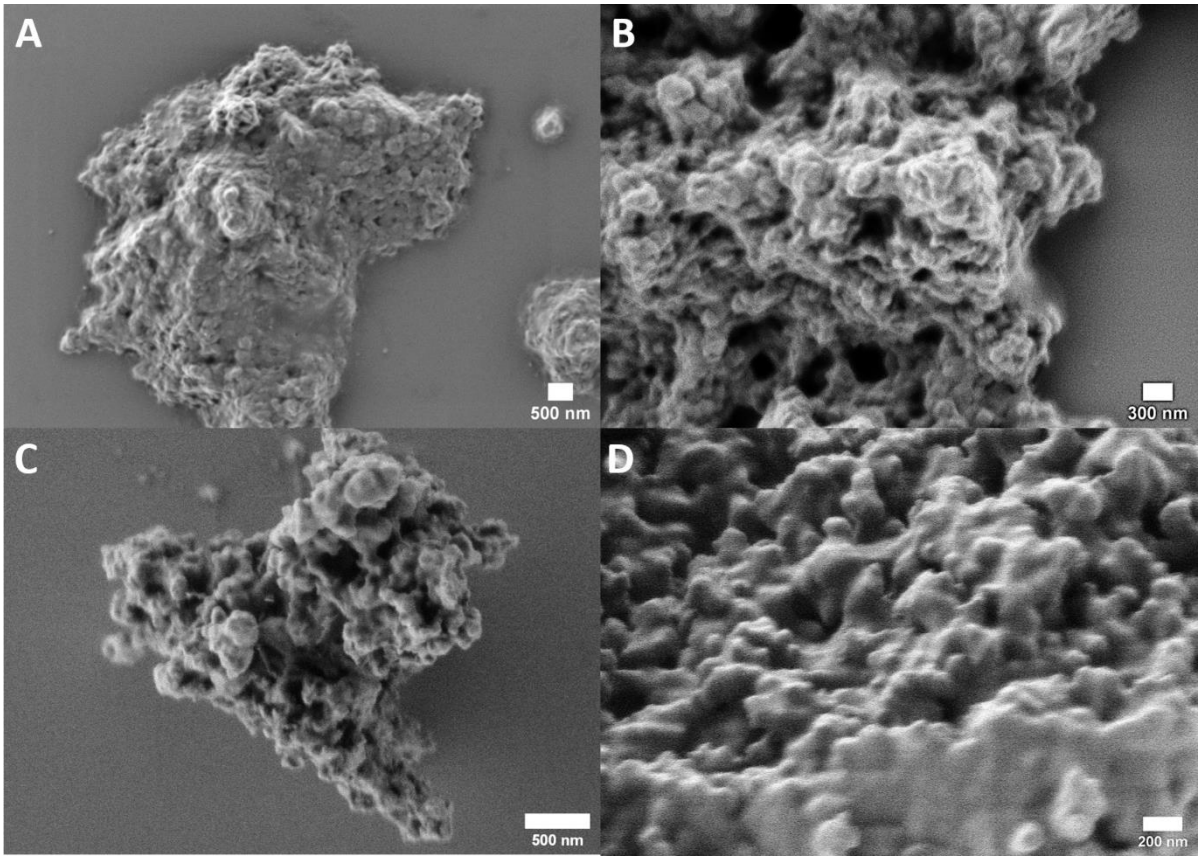

*Figure 67: SEM images of the PLLA nanoparticles using the emulsifier PEG_{45}-b-$PLS(Pyr)_{23}$ (**35d**). A, B) Diluted reaction mixture after polymerization and C, D) after one washing step.*

The third approach was conducted with the third polymer PEG_{17}-*b*-$PDLS(Pyr)_{22}$ (**36**) that consisted of racemic serine and a shorter PEG block. It was used in the same solvent system DMF/DiPE, but at a slightly higher concentration of c = 3.0 mg/mL. After stirring overnight, a stable emulsion was obtained and the polymerization was conducted, followed by DLS measurement. The approach resulted in a size distribution of d_H = 1200 ± 45 nm. The washing step resulted in significant reduction of the hydrodynamic diameter to d_H = 460 ± 20 nm. In order to verify that this approach led to smaller aggregates than the previous reactions, SEM samples were taken before and after the washing step

and analysed. Very noticeable was the first image that showed, besides fewer large aggregates, several circular assemblies of the particles on the wafer (Figure 68A, red arrows). It was caused by irregular evaporation of the solvents after sample application, as DiPE is a highly volatile solvent, while DMF is evaporating at a much slower rate at standard conditions causing the particles to assemble in the shape of the DMF droplets. Zooming into the assemblies showed that they consisted of piled up nanoparticles with diameters of 50-100 nm and remarkably homogeneous morphology (Figure 68B-D).

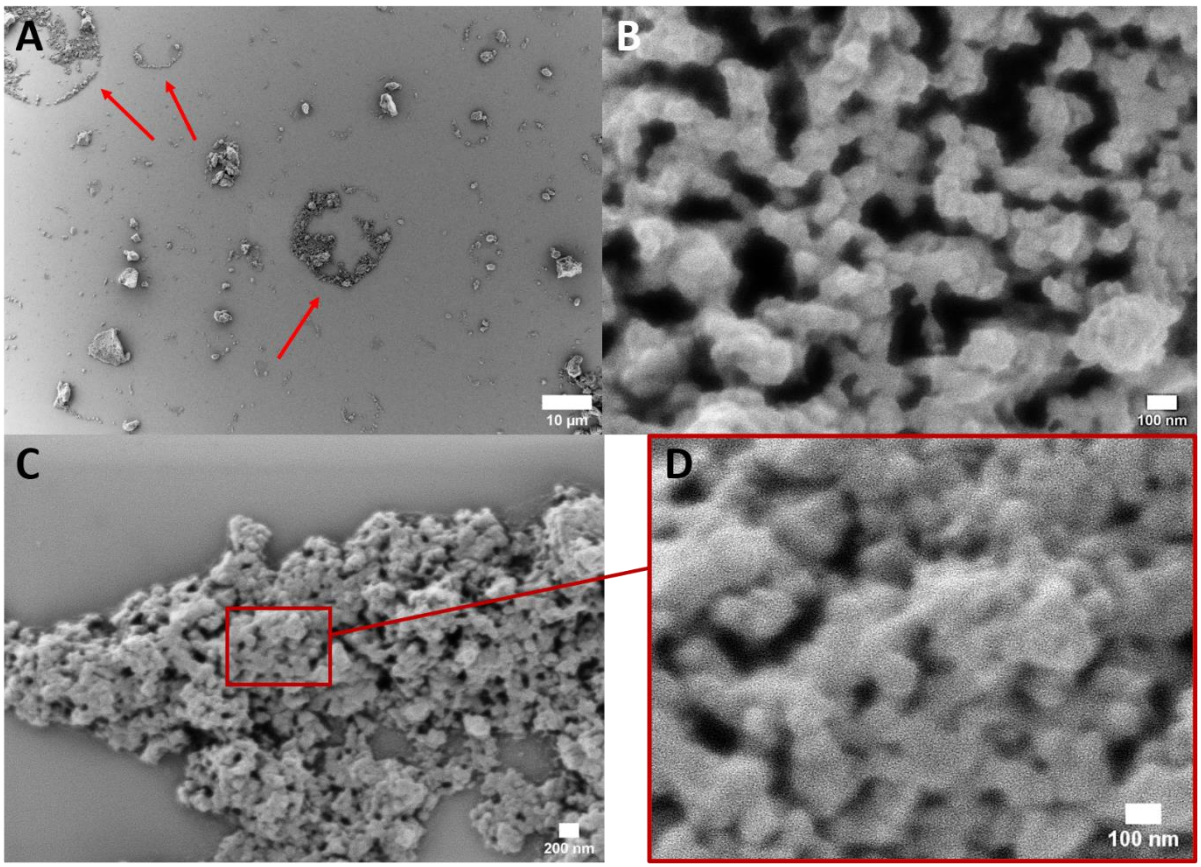

*Figure 68: SEM images of the diluted reaction mixture after polymerization of PLLA nanoparticles using the emulsifier PEG_{17} b-$PDLS(Pyr)_{22}$ (**36**). A) The assembly of particles in circles and B-D) nanoparticles within the circular assemblies.*

After the washing step, the morphology of the sample changed and was not mainly consisting of separated, piled up particles anymore. Few larger aggregates were observed that were covered with particles on their surface (Figure 69, A-B). Most of the particles were clumped together into small agglomerates with diameters of 200-500 nm (Figure 69, C-D). Interestingly, these were observed next to some plain, triangular structures that are believed to be either excess emulsifier that formed these symmetric structures or another impurity like remaining salts from the emulsifier synthesis. The structures were not observed before the washing step and are partially covering the aggregates (Figure 69, C), which led to the conclusion that a polymeric thin layer was formed by the excess emulsifier. Overall, this approach with emulsifier **36** led to surprisingly good results in terms of particle size and morphology compared to the previously discussed racemic polymer **35d**. Therefore, it could be ruled

out that the racemic composition of the polypeptide block is leading to higher agglomeration in general. More likely, this was an individual issue of that particular block copolymer. Overall, a gentle method for particle purification had to be established for our system to avoid morphology changes and flocculation during the workup of the reaction.

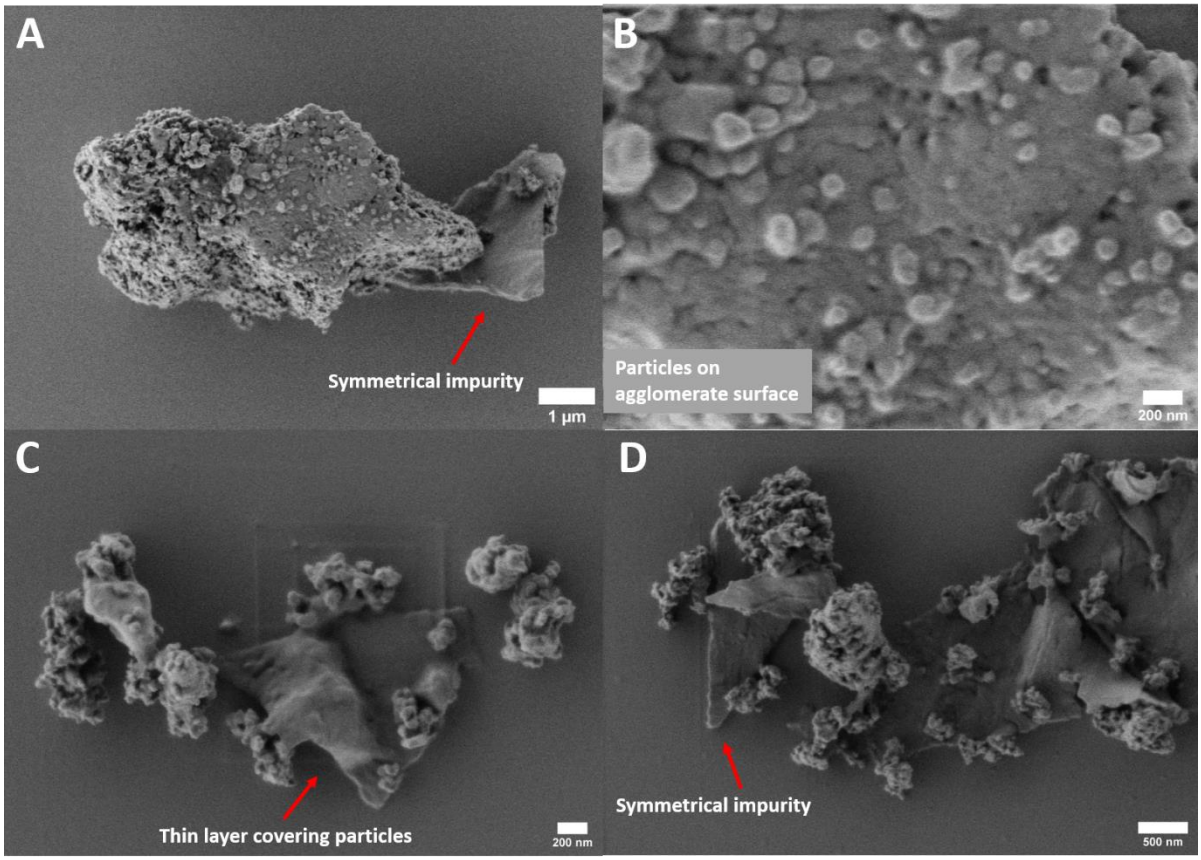

*Figure 69: SEM images of PLLA nanoparticles using the emulsifier PEG_{17}-b-$PLS(Pyr)_{22}$ (**36**) after one washing step.*

As mentioned before, the DMF/DiPE solvent system should be replaced by MeCN/CyH to avoid DMF as a solvent. DMF is not only affecting the SEM sample preparation by slow evaporation compared to diisopropylether, but it should be avoided in biological applications due to its cytotoxicity. While acetonitrile and cyclohexane are not acceptable in biological environment as well, they are easily removed by evaporation, while DMF is more persistent. For this purpose, the triblock copolymers with higher hydrophobic moiety were synthesized to study their dispersibility in cyclohexane. The first emulsion formation experiments showed that the triblock copolymers with relatively short PSer(Pyr) blocks with DPs of 3-8 per block were not redispersible in diisopropylether or cyclohexane, once they were fully dried *in vacuo*. The triblock copolymer $PDLS(Pyr)_{17}$-*b*-PEG_{45}-*b*-$PDLS(Pyr)_{18}$ (**38c**) were better dispersible and was therefore chosen for an NEP approach in the MeCN/CyH solvent system (c = 2.43 mg/mL). After the reaction, a DLS sample was taken and diluted with cyclohexane (1:1). The DLS measurement of the reaction mixture resulted in a particle size distribution

of d_H = 930 ± 40 nm. After washing of the particles, the particle size increased to d_H = 3500 ± 650 nm, indicating that once again, the washing step affected the particles negatively and resulted in strong aggregation. In order to study the morphology of the resulting particles, the sample was analysed by SEM before and after the washing step. Even though few nanoparticles were visible, overall, this approach did not result in dispersed particles, but in aggregates without any specific morphology and a broad size distribution (Figure 70A). In addition, the aggregates contained impurities of geometric shape, indicating that these were consisting of inorganic materials, like salts (Figure 70B-D, red arrows). Salts are known to influence particle assembly and lead to aggregation. They can either increase the stability of a particle dispersion or cause its collapse, depending on several factors like salt concentration.[146] In this case, it was likely residual lithium bromide from the emulsifier synthesis that remained in the material in significant amount.

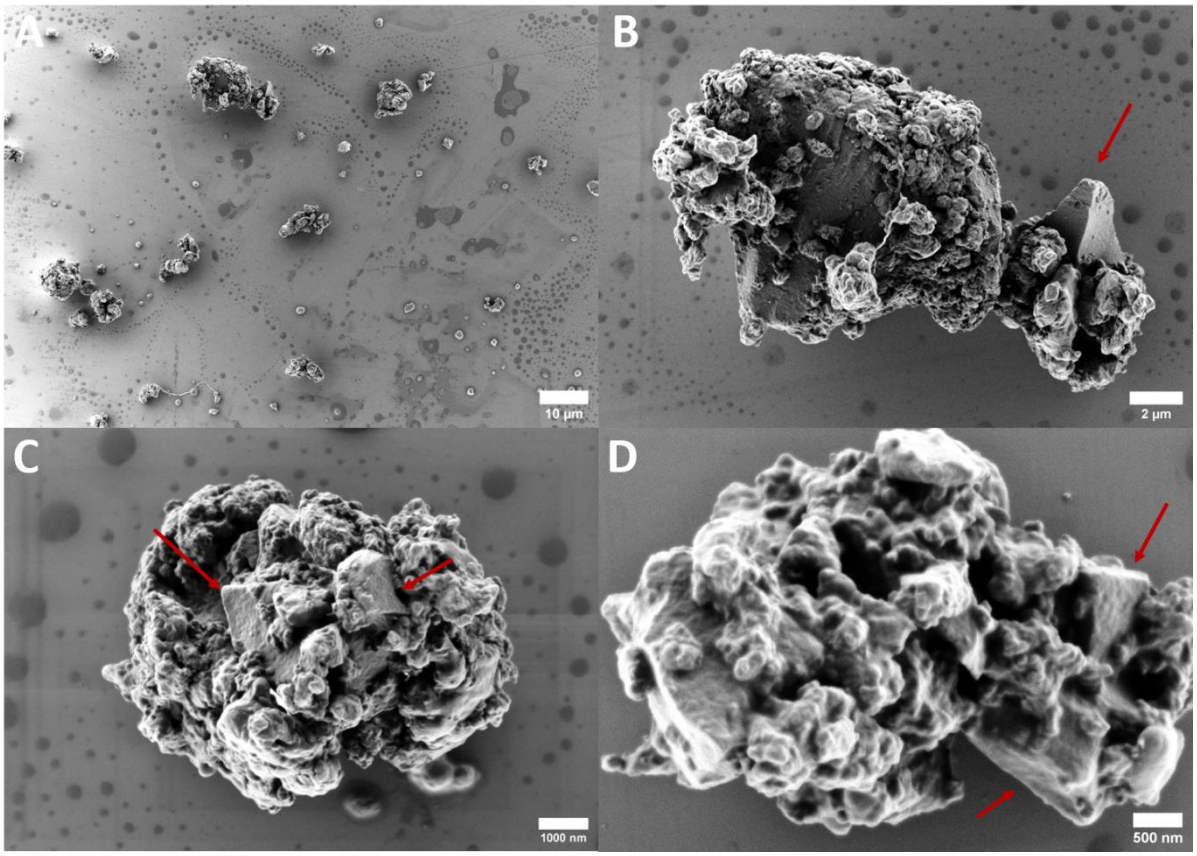

*Figure 70: SEM images of the diluted reaction mixture after polymerization of PLLA nanoparticles using the emulsifier PDLS(Pyr)$_{17}$-b-PEG$_{45}$-b-PDLS(Pyr)$_{18}$ (**38c**).*

The washing step did not result in any remarkable change in particle size or morphology (Figure 71). The impurity could not be removed and the particle aggregates are clustered around it (Figure 71B, red arrows).

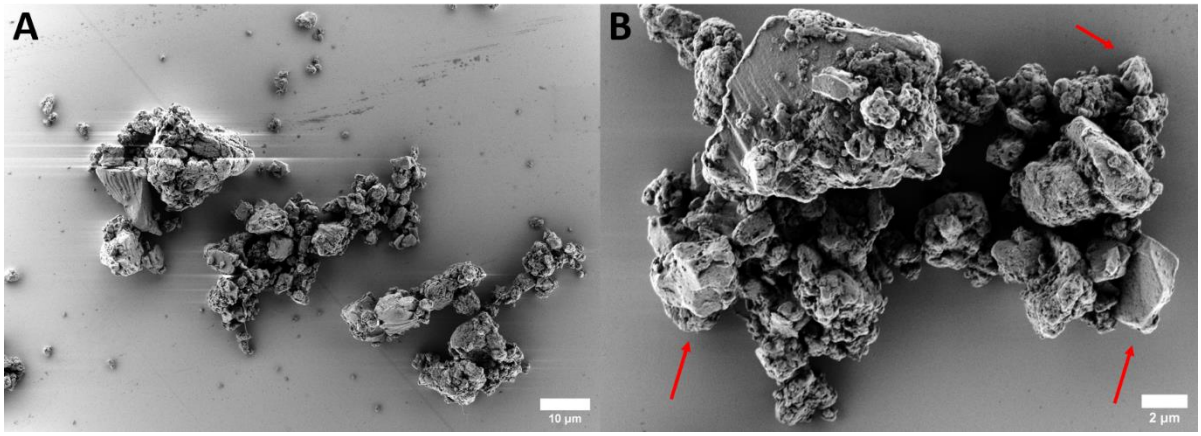

*Figure 71: SEM images of PLLA nanoparticles using the emulsifier PDLS(Pyr)$_{17}$-b-PEG$_{45}$-b-PDLS(Pyr)$_{18}$ (**38c**) after one washing step.*

Overall, the triblock copolymer **38c** was dispersible in cyclohexane and could potentially be used as an emulsifier in the MeCN/CyH solvent system. The first approach of emulsion polymerization was not leading to dispersed nanoparticles, but resulted in large aggregates. The reason for the strong agglomeration of the material was not the emulsifier itself, but impurities that remained in the emulsifier **38c** after its synthesis. Lithium bromide was present in significant amounts, causing the dispersion to aggregate. Therefore, this triblock copolymer has the potential to be used successfully in nonaqueous emulsion polymerization, but needed to be purified from all salt residues prior to further use. In summary, the pyrene functionalized di-block copolymers led to defined nanoparticles of desired size. Remarkable improvement was achieved in comparison to the benzyl-functionalized emulsifiers (Table 26Table 23: Concentration-dependent particle size measurements of nonaqueous emulsions with PEG$_{45}$-b-PDLS(Pyr)$_{20}$ (**35a**).). The purification of the nanoparticles needed to be optimized to avoid irreversible nanoparticle aggregation. This may be addressed by subsequent deprotection of the pyrene groups after the synthesis and particle transfer into aqueous solution, without an additional purification step in the nonpolar solvent.

*Table 26: Reaction parameters of the nonaqueous emulsion polymerizations performed with the O-(pyrene-1-carbonyl)-serine block copolymers (**35-38**).*

Sample	Emulsifier	Solvent system	Emulsifier [wt%]	d_h [nm]
Ep52	PEG$_{45}$-*b*-PLS(Pyr)$_{20}$, **35a**	DMF/DiPE	0.33	2700 ± 250
Washed				1000 ± 180
Ep53	PEG$_{45}$-*b*-PDLS(Pyr)$_{23}$, **35d**	DMF/DiPE	0.33	2100 ± 130
Washed				1200 ± 530
Ep54	PEG$_{17}$-*b*-PDLS(Pyr)$_{22}$, **36**	DMF/DiPE	0.40	1200 ± 40
Washed				450 ± 190
Ep59	PDLS(Pyr)$_{17}$-*b*-PEG$_{45}$-*b*-PDLS(Pyr)$_{18}$, **38c**	MeCN/CyH	0.33	930 ± 40
Washed				3500 ± 650

4.4 Summary and Outlook

The goal of this chapter was the synthesis of a photocleavable serine derivative to fabricate amphiphilic and photolabile block copolymers. These should have been utilized as emulsifiers for nonaqueous emulsion polymerization of core-shell nanoparticles. The first step of the synthesis route was the functionalization of the serine side chain with a photoactive protecting group. Three possible ways were defined: Creating an ether, carbonate or ester group. It was started with the most stable of the three, the ether group. Numerous attempts to obtain a photocleavable serine ether failed or resulted in low yields. Ultimately, it was decided to not follow this route anymore, as the polymerization step required large-scale synthesis of the amino acid building blocks. The second path successfully resulted in pyrene carbonate-functionalized serine. It was produced in gram-scale, but the protecting group was cleaved under acidic conditions. This functional group was not suitable for the following NCA synthesis that was carried out in acidic conditions. The last synthesis path included the formation of an ester in the serine side chain and indeed, the desired pyrene-functionalised serine ester (**33**) was obtained by standard coupling reaction in good yields and multigram-scale. It was then transformed into the NCA (**30,34**), which was used as the activated monomer in the following ROP to create PEG-*b*-PSer(Pyr) block copolymers. The polymerization was conducted using PEG amine macroinitiators that resulted in di-block copolymers (**35-37**). Along the lines of the benzyl analogues, the theoretical DP was not achieved and optimization of the reaction conditions did not result in significant improvement. As a consequence, the block length of the hydrophobic block was not as high as desired. A strategy to increase the hydrophobic moiety was the synthesis of ABA triblock copolymers, consisting of two, relatively short hydrophobic blocks. These polymerizations worked well and the corresponding polymers (**38-39**) were obtained with improved yields.

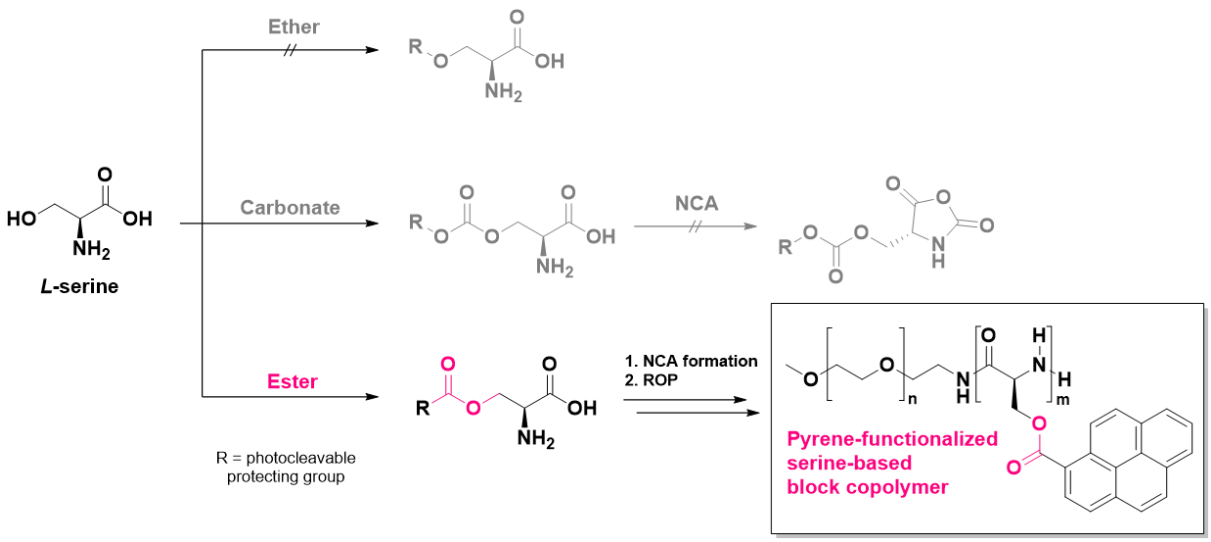

Figure 72: Possible synthesis paths for the pyrene functionalization of serine. Ether and carbonate formation were not successful, but eventually, the desired building block was obtained in large scale by ester formation, followed by block copolymer synthesis by ROP.

Emulsion formation experiments were carried out and the pyrene-containing di-block copolymers formed stable and homogeneous emulsions, as determined by DLS measurements. This was a massive improvement in comparison to the aggregation behaviour of the Bn-serine polymers that showed strong aggregation in nonpolar organic solvents. Nonaqueous emulsion polymerization was then performed with these di-block copolymers as emulsifiers in DMF/DiPE and the results were as good as expected. Spherical particles with diameter of around 50-100 nm and homogeneous morphology, as shown by SEM, were obtained. These were awesome results, even though there was still some space for improvement. The particle purification partially resulted in flocculation of the particles. The SEM images showed that the particles were clumped together after the sedimentation step. In order to establish the pyrene-functionalized emulsifiers in the MeCN/CyH solvent system, the triblock copolymers with higher hydrophobic moiety were synthesized to study their dispersibility in cyclohexane. Indeed, the polymer PDLS(Pyr)$_{17}$-*b*-PEG$_{45}$-*b*-PDLS(Pyr)$_{18}$ (**38c**) showed good dispersibility in cyclohexane. The first emulsion polymerization of the triblock copolymer in MeCN/CyH did result in large aggregates without any specific morphology. This was caused by significant amounts of lithium bromide that remained in the emulsifier despite purification after the synthesis. Therefore, no final conclusion could be drawn from that first approach of emulsion polymerization and further investigation will be required. Overall, the formation of dispersed nanoparticles with the PEG-*b*-PSer(Pyr) emulsifiers was successful.

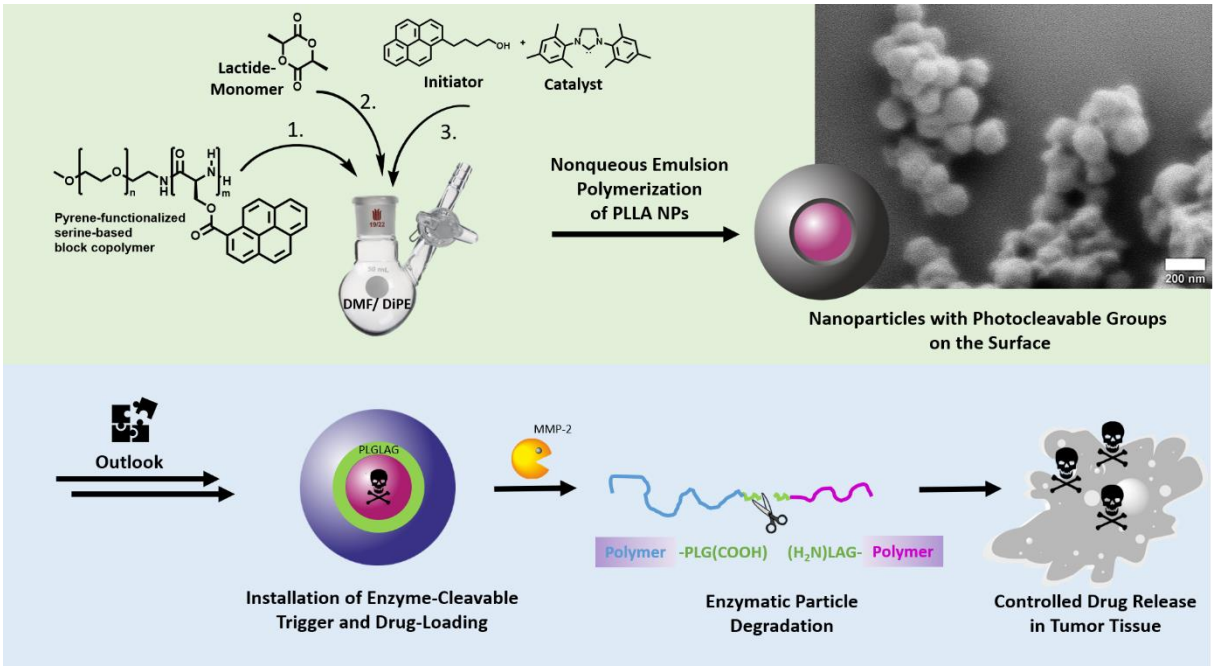

Figure 73: Synthesis of well-defined nanoparticles by using PEG-b-PLS(Pyr) block copolymer as emulsifier in nonaqueous emulsion polymerization of PLLA and outlook on the next steps, the installation of an enzyme-cleavable peptide sequence in the particle shell and the drug loading to allow controlled drug release in the tumor tissue.

Changing the solvent system and optimize the purification of the resulting particles without changing their morphology would be the next steps to finalize the fabrication of these nanoparticles and ensure its reproducibility. Combined with optimizing the purification of the particles, the transfer of the particles into the aqueous phase by photo-cleavage of the pyrene group would be the next step. Finally, the introduction of the enzyme-cleavable peptide sequence into the particle shell and the drug encapsulation should be included into the emulsion polymerization step to equip the particles with the cancer drug and the trigger sequence to allow drug release. Finally, the efficacy of the drug release should be investigated in first *in vitro* studies to test our system

.

4.5 Experimental Part

ETHER FORMATION

Synthesis of *O*-nitro-benzyl-L-serine methyl ester (14)

Method A: A solution of L-serine methyl ester hydrochloride (0.25 g, 1.61 mmol, 1.00 eq) in 3 mL THF was added dropwise to a solution of sodium hydride (dispersed in mineral oil, 0.35 g, 1.61 mmol, 1.00 eq) in 2 mL THF at 0°C under inert atmosphere and allowed to stir at 0 °C until the evolution of hydrogen gas ceased. Nitro-benzyl bromide (0.07 g, 1.77 mmol, 1.10 eq) was dissolved in 2 mL THF and added. The reaction mixture was allowed to react at 0 °C for 30 minutes, then stirred at room temperature for 48 h. The resulting solution was poured into ice water and the mixture was extracted with DCM. The organic layer was washed twice with cold H_2O, before it was concentrated and dried under vacuum. The product **14** was purified by column chromatography twice (DCM pure -> DCM/methanol, 10:1; DCM/methanol, 30:1, 5% triethyl amine) and obtained as a yellow resin (0.074 g, 0.29 mmol, 18%).

Method B: A solution of L-serine methyl ester hydrochloride (0.25 g, 1.61 mmol, 1.00 eq) in 3 mL DMF was added dropwise to a solution of sodium hydride (dispersed in mineral oil, 0.35 g, 1.61 mmol, 1.00 eq) in 2 mL DMF at 0°C under inert atmosphere and allowed to stir at 0 °C until the evolution of hydrogen gas ceased. Nitro-benzyl bromide (0.19 g, 4.82 mmol, 3.00 eq) was dissolved in 2 mL DMF and added. The reaction mixture was allowed to react at 0 °C for 30 minutes, then stirred at room temperature for 16 h. The resulting solution was poured into ice water and the mixture was extracted with DCM. The organic layer was washed twice with cold H_2O, before it was concentrated and redissolved in methanol, followed by precipitation in *n*-hexane. The product **14** was purified by column chromatography (DCM pure -> DCM/methanol, 20:1) and obtained as a brown resin (0.072 g, 0.28 mmol, 17%).

^{1}H-NMR (300 MHz, CD_2Cl_2, 300 K): δ = 7.92 (d, 1H, ^{3}J = 8.1 Hz, Ph-CH), 7.60 (m, 2H, Ph-CH), 7.46 (td, 1H, Ph-CH), 4.10 (q, 2H, Ph-CH_2O), 3.79-3.57 (dd, 2H, β-CH_2), 3.69 (s, 3H, OCH_3), (t, 1H, α-CH), 2.50 (s, 2H, NH_2) ppm. ^{13}C-NMR (75 MHz, DMSO-d6, 300 K): δ = 173.5 (C=O), 134.5 (Ph-C), 133.5 (Ph-CH), 131.5 (Ph-CH), 128.8 (Ph-CH), 125.1 (Ph-CH), 63.0 (β-CH_2), 62.9 (α-CH), 52.5 (CH_3), 49.7 (Ph-CH_2) ppm.

GARNER ALDEHYDE ROUTE

Synthesis of 3-(*tert*-butyl)-4-methyl-(*S*)-2,2-dimethyloxazolidine-3,4-dicarboxylate (18)

Boc-L-Serine methyl ester (5.00 g, 22.8 mmol, 1.00 eq) was dissolved in a mixture of acetone (65 mL) and 2,2-dimethoxypropane (25.0 mL, 205 mmol, 9.00 eq). Boron trifluoride diethyl etherate (0.03 mL, 2.28 mmol, 0.10 eq) was added. The solution was stirred at room temperature for 2 h. The reaction conversion was monitored by TLC. The reaction mixture was concentrated and the residue was dissolved in DCM. The organic layer was washed with a mixture of saturated, aqueous $NaHCO_3/H_2O$ (1:1) and brine, before it was dried with anhydrous Na_2SO_4, filtered and concentrated. The crude product **18** was purified by column chromatography (cyclohexane/ethyl acetate, 4:1) and the pure material was obtained as yellow oil (5.36 g, 20.7 mmol, 91%). ^{1}H-NMR (300 MHz, CD_2Cl_2, 300 K): δ = 4.39 (dd, 1H, α-CH), 4.05 (m, 2H, β-CH_2), 3.73 (s, 3H, OCH_3), 1.60 (s, 3H, CH_3), 1.46 (s, 3H, CH_3), 1.39 (s, 9H, Boc-CH_3) ppm. ^{13}C-NMR (75 MHz, CD_2Cl_2, 300 K): δ = 172.1 (C=O), 94.7 (C_q), 80.4 (Boc-C_q), 66.7 (α-CH), 59.7 (β -CH_2), 52.6 (OCH_3), 28.4 (Boc-CH_3), 25.1 (CH_3), 24.5 (CH_3) ppm. TLC: R_f = 0.52 (cyclohexane/ethyl acetate, 3:1).

Synthesis of (*R*)-*N*-Boc-4-(hydroxymethyl)-2,2-dimethyloxazolidine (19)

Lithium aluminium hydride (1 M in THF, 0.39 mL, 0.39 mmol, 1.00 eq) was added in portions to a stirred solution of 3-(*tert*-butyl)-4-methyl-(*S*)-2,2-dimethyloxazolidine-3,4-dicarboxylate (0.10 g, 0.39 mmol, 1.00 eq) in dry THF (3.5 mL) at –15 °C. The reaction mixture was stirred for 2 h and allowed to warm to room temperature. After completion of the reaction, the reaction mixture was cooled to –15 °C again and the excess amount of LAH was quenched by slow addition of ethyl acetate (10 mL) and water (5 mL). The white precipitate was removed by filtration through a bed of Celite and then washed with ethyl acetate (3 x 50 mL). The organic layers were combined and dried with anhydrous Na_2SO_4. The solution was concentrated under reduced pressure to obtain a pale-yellow oil, which upon purification by column chromatography on silica gel (cyclohexane/ethyl acetate, 10:1) furnished the alcohol **19** (88.0 mg, 0.381 mmol, 99%) as a colourless oil. ^{1}H-NMR (300 MHz, DMSO-d6, 300 K): δ = 4.89 (m, 1H, OH), 3.88 (t, 2H, Ph-CH_2O), 3.73 (t, 1H, α-CH), 3.50 (dd, 1H, β-CH_2), 3.15 (dd, 1H, β-CH_2), 1.43 (2s, 15H, Boc-CH_3, 2xCH_3) ppm. TLC: R_f = 0.14 (cyclohexane/ethyl acetate, 3:1).

Synthesis of (*R*)-*N*-Boc-4-((benzyloxy)methyl)-2,2-dimethyloxazolidine (20)

Sodium hydride (dispersed in mineral oil, 0.03 g, 0.65 mmol, 1.50 eq) was added to a solution of (*R*)-*N*-Boc-4-(hydroxymethyl)-2,2-dimethyloxazolidine (0.10 g, 0.43 mmol, 1.00 eq) in DMF (2.5 mL) at -78 °C and stirred for 20 minutes. Benzyl bromide (0.10 mL, 0.87 mmol, 2.00 eq) was then added at -78 °C. The reaction mixture was stirred for 18 h and allowed to warm to room temperature. The resulting solution was then poured into ice water. The mixture was extracted with ethyl acetate and the organic

layer was washed with cold water twice. The solution was dried with anhydrous Na_2SO_4, concentrated and dried under vacuum. The product **20** (0.10 g, 0.32 mmol, 75%) was obtained after purification by column chromatography (cyclohexane/ethyl acetate, 5:1). ^{1}H-NMR (300 MHz, CD_2Cl_2, 300 K): δ = 7.33 (m, 5H, Ph-CH), 4.52 (t, 2H, Ph-CH_2O), 4.03 (t, 1H, α-CH), 4.52 (), 3.97 (dd, 2H, α-CH-$\underline{CH_2}$O), 3.50 (dd, 2H, β-CH_2) ppm. TLC: R_f = 0.64 (cyclohexane/ethyl acetate, 3:1).

Synthesis of (*S*)-*tert*-butyl (1-(benzyloxy)-3-hydroxypropan-2-yl)carbamate (21)

To a solution of (*R*)-*N*-Boc-4-((benzyloxy)methyl)-2,2-dimethyloxazolidine (98.0 mg, 0.31 mmol, 1.00 eq) in THF (1.5 mL) was added 2 N hydrochloric acid (0.61 mL, 1.22 mmo, 4.00 eq) and stirred for 2 h at room temperature. After basification with sodium carbonate (162 mg, 0.92 mmol, 3.00 eq), di-*tert*-butyl dicarbonate (0.33 mL, 1.52 mmol, 5.00 eq) was added and the resulting mixture was stirred at room temperature for 24 h. The solvent was removed under reduced pressure. The residue was dissolved in DCM and the organic layer was washed twice with cold water and dried with anhydrous Na_2SO_4. The solution was concentrated and dried under vacuum. The product **21** (65 mg, 0.23 mmol, 75%) was obtained after purification by column chromatography (cyclohexane/ethyl acetate, 3:1 -> 1:2). ^{1}H-NMR (300 MHz, CD_2Cl_2, 300 K): δ = 7.34 (m, 5H, Ph-CH), 5.12 (s, 1H, OH), 4.51 (s, 2H, Ph-CH_2), 3.82-3.51 (m, 5H, α-CH, β-CH_2, CH_2O), 2.48 (s, 1H, NH), 1.42 (s, 9H, Boc-CH_3) ppm. TLC: R_f = 0.11 (cyclohexane/ethyl acetate, 3:1).

CARBONATE SYNTHESIS

Synthesis of pyren-1-ylmethyl chloroformate (25)

Triphosgene (1.69 g, 5.68 mmol, 0.66 eq) was dissolved in anhydrous THF (5 mL) under inert atmosphere and cooled down to 0 °C. 1-pyrene methanol (2.00 g, 8.61 mmol, 1.00 eq) was dissolved in 10 mL THF and added slowly to the first solution over a period of 10 minutes. The mixture was stirred at 0 °C for 1 h and then allowed to warm to room temperature. After 18 h of stirring the excess phosgene was removed by purging the solution with argon for 2 h (the phosgene was absorbed in a NaOH solution). The solution was concentrated to 30% of its volume and the residue was precipitated in cold *n*-hexane. The precipitate was filtered and washed with *n*-hexane. The product **25** (2.01 g, 6.83 mmol, 79%) was dried and obtained as off-white solid. ^{1}H-NMR (250 MHz, CD_2Cl_2, 300 K): δ = 8.39 (d, 1H, Ph-CH), 8.29-7.97 (m, 8H, Ph-CH), 5.34 (s, 2H, Ph- CH_2) ppm. ^{13}C-NMR (75 MHz, CD_2Cl_2, 300 K): δ = 172.3 (C=O), 134.0 (Ph-C_q), 132.2 (Ph-C_q), 130.9 (Ph-C_q), 130.5 (Ph-C_q), 129.3 (Ph-C_q), 128.6 (Ph-CH), 128.2 (Ph-CH), 127.8 (Ph-CH), 127.5 (Ph-CH), 126.4 (Ph-CH), 125.8 (Ph-CH), 125.3 (Ph-C_q), 124.9 (Ph-CH), 122.9 (Ph-CH), 44.9 (Ph-CH_2) ppm. TLC: R_f = 0.61 (cyclohexane/ethyl acetate, 5:1).

Synthesis of *N*-(*tert*-butoxycarbonyl)-*O*-((pyrene-1-methoxy)carbonyl)-L-serine (26)

A solution of pyren-1-ylmethyl chloroformate (0.25 g, 1.22 mmol, 1.00 eq) in 5 mL chloroform was added dropwise to a suspension of Boc-L-Ser-OH (0.36 g, 1.22 mmol, 1.00 eq) in chloroform (5 mL), under argon atmosphere, followed by addition of 1.0 mL pyridine (12.4 mmol, 10.2 eq). The solution was stirred for 30 minutes at room temperature until the solution turned homogenous. The reaction was monitored by TLC, until no pyren-1-ylmethyl chloroformate was observed. The solution was concentrated and pyridine was removed by coevaporation with *n*-heptane three times. The residue was dried under vacuum. The product **26** was obtained as yellow solid (0.51 g, 1.11 mmol, 91%) and used without further purification. ^{1}H-NMR (300 MHz, DMSO-d6, 300 K): δ = 12.50 (s, 1H, COOH), 9.19 (s, 1H, Ph-CH), 8.66-8.08 (m, 9H, Ph-CH, NH), 6.70 (s, 2H, Ph-CH_2O), 3.97 (q, 1H, α-CH), 3.63 (d, 2H, β-CH_2), 1.38 (s, 9H, Boc-CH_3) ppm.

ESTER SYNTHESIS

Synthesis of *N*-(benzyloxycarbonyl)-L-serine benzyl ester (32a)

Cbz-L-Ser-OH (2.00 g, 8.36 mmol, 1.00 eq) was dissolved in anhydrous DMF (20 mL). Cesium carbonate (1.63 g, 5.02 mmol, 0.60 eq) was added and the mixture was stirred at room temperature for 15 min. Benzyl bromide (1.04 mL, 8.78 mmol, 1.05 eq) was added dropwise. The stirring was maintained for 18 h. Then, the mixture was diluted with water and extracted with ethyl acetate three times. The organic layer was washed with water and brine and dried with anhydrous Na_2SO_4. After filtration the solution was concentrated and the residue was dried under vacuum. The crude product **32a** was obtained as colourless solid (2.80 g, 8.50 mmol, quant.) und used without further purification. ^{1}H-NMR (300 MHz, DMSO-d6, 300 K): δ = 7.57 (s, 1H, NH), 7.36 (m, 10H, Ph-CH), 5.14 (s, 2H, Ph-CH_2), 5.05 (s, 2H, Ph-CH_2), 4.98 (td, 1H, OH), 4.22 (dt, 1H, α-CH), 3.70 (t, 2H, β-CH_2) ppm. ^{13}C-NMR (75 MHz, DMSO-d6, 300 K): δ = 170.8 (C=O), 156.2 (C=O), 136.9 (Ph-C_q), 135.9 (Ph-C_q), 128.5 (Ph-CH), 128.4 (Ph-CH), 128.0 (Ph-CH), 127.9 (Ph-CH), 127.8 (Ph-CH), 127.6 (Ph-CH), 65.9 (Ph-CH_2), 65.6 (Ph-CH_2), 61.3 (β -CH_2), 56.8 (α -CH) ppm. TLC: R_f = 0.16 (cyclohexane/ethyl acetate, 3:1).

***N*-(benzyloxycarbonyl)-DL-serine benzyl ester** (**32b**, 13.6 g, 41.3 mmol) was obtained with a yield of 99%. ^{1}H-NMR (300 MHz, DMSO-d6, 300 K): δ = 7.59 (s, 1H, NH), 7.35 (m, 10H, Ph-CH), 5.15 (s, 2H, Ph-CH_2), 5.06 (s, 2H, Ph-CH_2), 5.01 (td, 1H, OH), 4.23 (dt, 1H, α-CH), 3.71 (t, 2H, β-CH_2) ppm. ^{13}C-NMR (75 MHz, DMSO-d6, 300 K): δ = 170.7 (C=O), 156.1 (C=O), 136.9 (Ph-C_q), 135.9 (Ph-C_q), 128.4 (Ph-CH), 128.3 (Ph-CH), 127.9 (Ph-CH), 127.8 (Ph-CH), 127.7 (Ph-CH), 127.6 (Ph-CH), 65.9 (Ph-CH_2), 65.6 (Ph-CH_2), 61.2 (β -CH_2), 56.9 (α -CH) ppm. TLC: R_f = 0.16 (cyclohexane/ethyl acetate, 3:1).

***N*-(benzyloxycarbonyl)-D-serine benzyl ester** (**32c**, 7.37 g, 22.2 mmol) was obtained with a yield of 95%. ^{1}H-NMR (300 MHz, DMSO-d6, 300 K): δ = 7.58 (s, 1H, NH), 7.35 (m, 10H, Ph-CH), 5.15 (s, 2H, Ph-CH_2), 5.05 (s, 2H, Ph-CH_2), 5.00 (td, 1H, OH), 4.22 (dt, 1H, α-CH), 3.70 (t, 2H, β-CH_2) ppm. ^{13}C-NMR (75 MHz, DMSO-d6, 300 K): δ = 170.7 (C=O), 156.1 (C=O), 136.9 (Ph-C_q), 136.0 (Ph-C_q), 128.4 (Ph-CH), 128.3 (Ph-CH), 127.9 (Ph-CH), 127.8 (Ph-CH), 127.7 (Ph-CH), 127.6 (Ph-CH), 65.9 (Ph-CH_2), 65.6 (Ph-CH_2), 61.2 (β -CH_2), 56.8 (α -CH) ppm. TLC: R_f = 0.16 (cyclohexane/ethyl acetate, 3:1).

Synthesis of *N*-(benzyloxycarbonyl)-*O*-(pyrene-1-carbonyl)-L-serine benzyl ester (33a)

1-Pyrenecarboxylic acid (0.44 g, 1.80 mmol, 0.99 eq), EDC*HCl (0.36 g, 1.88 mmol, 1.03 eq) and DMAP (3.35 mg, 0.27 mmol, 0.15 eq) were dissolved in DCM (11 mL) and stirred for 15 minutes. Cbz-L-serine-OBn (0.60 g, 1.82 mmol, 1.00 eq) was added and the solution was then stirred at room temperature for 22 h. Water was added to the reaction mixture and extracted with DCM. The organic layer was washed with water and brine, dried with anhydrous Na_2SO_4 and concentrated. The residue was dried under vacuum. The product **33a** (0.65 g, 1.17 mmol, 64%) was obtained as yellow solid after purification by column chromatography (cyclohexane/ethyl acetate, 6:1). ^{1}H-NMR (300 MHz, DMSO-d6, 300 K): δ = 9.12 (s, 1H, NH), 8.60-8.12 (m, 9H, Pyr-CH), 7.29 (m, 10H, Ph-CH), 5.22 (s, 2H, Ph-CH_2), 5.09 (s, 2H, Ph-CH_2), 4.80 (dt, 1H, α-CH), 4.74 (m, 2H, β-CH_2) ppm. ^{13}C-NMR (75 MHz, DMSO-d6, 300 K): δ = 169.7 (C=O), 166.7 (C=O), 156.2 (C=O), 136.8 (Ph-C_q), 135.8 (Ph-C_q), 134.0 (Pyr-C_q), 130.5-122.6 (28xC, Pyr-CH, Pyr-C_q), 66.6 (Ph-CH_2), 65.8 (Ph-CH_2), 64.0 (β -CH_2), 53.4 (α-CH) ppm. TLC: R_f = 0.40 (cyclohexane/ethyl acetate, 3:1). Chiral HPLC: (THF/n-Heptane, 24:76; 1 mL/min); t_R = 12.7 min.

***N*-(benzyloxycarbonyl)-*O*-(pyrene-1-carbonyl)-DL-serine benzyl ester** (**33b**, 10.5 g, 18.8 mmol) was obtained with a yield of 69%. ^{1}H-NMR (300 MHz, DMSO-d6, 300 K): δ = 9.12 (s, 1H, NH), 8.60-8.12 (m, 9H, Pyr-CH), 7.30 (m, 10H, Ph-CH), 5.23 (s, 2H, Ph-CH_2), 5.10 (s, 2H, Ph-CH_2), 4.81 (dt, 1H, α-CH), 4.75 (m, 2H, β-CH_2) ppm. ^{13}C-NMR (75 MHz, DMSO-d6, 300 K): δ = 169.6 (C=O), 166.6 (C=O), 156.2 (C=O), 136.8 (Ph-C_q), 135.7 (Ph-C_q), 134.0 (Pyr-C_q), 130.5-122.6 (28xC, Pyr-CH, Pyr-C_q), 66.5 (Ph-CH_2), 65.7 (Ph-CH_2), 64.0 (β -CH_2), 53.3 (α-CH) ppm. TLC: R_f = 0.40 (cyclohexane/ethyl acetate, 3:1). Chiral HPLC: (THF/n-Heptane, 24:76; 1 mL/min); t_R = 12.7 min, 13.7 min (Ratio: 50:50).

***N*-(benzyloxycarbonyl)-*O*-(pyrene-1-carbonyl)-D-serine benzyl ester** (**33c**, 3.51 g, 6.29 mmol) was obtained with a yield of 69%. %. ^{1}H-NMR (250 MHz, DMSO-d6, 300 K): δ = 9.12 (s, 1H, NH), 8.60-8.12 (m, 9H, Pyr-CH), 7.29 (m, 10H, Ph-CH), 5.23 (s, 2H, Ph-CH_2), 5.10 (s, 2H, Ph-CH_2), 4.80 (dt, 1H, α-CH), 4.75 (m, 2H, β-CH_2) ppm. ^{13}C-NMR (75 MHz, DMSO-d6, 300 K): δ = 169.6 (C=O), 166.6 (C=O), 156.2 (C=O), 136.8 (Ph-C_q), 135.7 (Ph-C_q), 134.0 (Pyr-C_q), 130.5-122.6 (28xC, Pyr-CH, Pyr-C_q), 66.5 (Ph-CH_2),

65.7 (Ph-CH_2), 64.0 (β -CH_2), 53.3 (α-CH) ppm. TLC: R_f = 0.40 (cyclohexane/ethyl acetate, 3:1). Chiral HPLC: (THF/n-Heptane, 24:76; 1 mL/min); t_R = 13.7 min.

Synthesis of *O*-(pyrene-1-carbonyl)-L-serine (29)

Cbz-L-Ser(Pyr)-OBn (1.00 g, 1.79 mmol, 1.00 eq) and 10% palladium on charcoal (65.0 mg, 0.61 mmol, 0.34 eq) was dissolved in 15 mL THF under inert atmosphere and stirred. Hydrogen gas was induced into the reaction mixture for 10 minutes to saturate the atmosphere. The solution was stirred for 18 h at ordinary pressure and temperature. The solvent was removed under reduced pressure and the crude product H-L-Ser(Pyr)-OH **29** was used without further purification. ^{1}H-NMR (300 MHz, DMSO-d6, 300 K): δ = 8.90-8.06 (m, 9H, Pyr-CH), 4.79 (m, 1H, α-CH), 4.61 (m, 2H, β-CH_2) ppm.

Synthesis of *O*-(pyrenyl-1-carbonyl)-L-serine-*N*-carboxy anhydride (30)

H-L-Ser(Pyr)-OH (0.60 g, 1.80 mmol, 1.00 eq) was dissolved in anhydrous THF (3.0 mL). Triphosgene (0.35 g, 1.19 mmol, 0.66 eq) was dissolved in 2.5 mL THF and added dropwise to the first solution. The suspension was heated to 50°C and stirred for 2 h until all solids were dissolved. The reaction mixture was cooled to room temperature and Argon was bubbled through the solution for 1 h to remove excess phosgene, which was introduced into a NaOH solution. The reaction mixture was filtered once over silica and twice over a bed of celite to remove the catalyst. The filtrate was concentrated to 30% and the residue was precipitated in cold *n*-hexane to provide L-Ser(Pyr)-NCA **30** (0.49 g, 1.48 mmol, 83%) as a light yellow solid. ^{1}H-NMR (300 MHz, DMSO-d6, 300 K): δ = 9.45 (s, 1H, NH), 9.07 (d, 1H, Pyr-CH), 8.55-8.13 (m, 8H, Pyr-CH), 5.05 (t, 1H, α-CH), 4.75 (dd, 2H, β-CH_2) ppm. ^{13}C-NMR (75 MHz, DMSO-d6, 300 K): δ = 169.6 (C=O), 166.4 (C=O), 152.1 (C=O), 131.2 (Ph-C_q), 130.5-122.1 (15xC, Pyr-CH, Pyr-C_q), 62.9 (β -CH_2), 57.2 (α-CH) ppm.

One-Pot-Synthesis of *O*-(pyrenyl-1-carbonyl)-L-serine-*N*-carboxy anhydride (30)

Cbz-L-Ser(Pyr)-OBn (1.00 g, 1.79 mmol, 1.00 eq) and 10% palladium on charcoal (65.0 mg, 0.61 mmol, 0.34 eq) was dissolved in 10 mL THF under inert atmosphere and stirred. Hydrogen gas was induced into the reaction mixture for 10 minutes to saturate the atmosphere. The solution was stirred for 18 h at ordinary pressure and temperature, before 5 mL THF were added to the grey and slurry solution. Triphosgene (0.35 g, 1.19 mmol, 0.66 eq) was dissolved in 2 mL THF and added dropwise to the reaction mixture. The suspension was heated to 50°C and stirred for 2 h until all solids were dissolved. The reaction mixture was cooled to room temperature and Argon was bubbled through the solution for

1 h to remove excess phosgene, which was introduced into a NaOH solution. The reaction mixture was filtered once over silica and twice over a bed of celite to remove the catalyst. The filtrate was concentrated to 30% and the residue was precipitated in cold *n*-hexane to provide Ser(Pyr) NCA (0.62 g, 1.71 mmol, 96%) as a light yellow solid. ^{1}H-NMR (300 MHz, DMSO-d6, 300 K): δ = 9.45 (s, 1H, NH), 9.07 (d, 1H, Pyr-CH), 8.55-8.13 (m, 8H, Pyr-CH), 5.05 (t, 1H, α-CH), 4.75 (dd, 2H, β-CH_2) ppm. ^{13}C-NMR (75 MHz, DMSO-d6, 300 K): δ = 169.6 (C=O), 166.4 (C=O), 152.1 (C=O), 131.2 (Ph-C_q), 130.5-122.1 (15xC, Pyr-CH, Pyr-C_q), 62.9 (β -CH_2), 57.2 (α-CH) ppm.

***O*-(pyrenyl-1-carbonyl)-DL-serine-*N*-carboxy anhydride** (**34**, 4.25 g, 11.8 mmol) was obtained with a yield of 94%. ^{1}H-NMR (300 MHz, DMSO-d6, 300 K): δ = 9.43 (s, 1H, NH), 9.07 (d, 1H, Pyr-CH), 8.56-8.15 (m, 8H, Pyr-CH), 5.04 (t, 1H, α-CH), 4.75 (dd, 2H, β-CH_2) ppm. ^{13}C-NMR (75 MHz, DMSO-d6, 300 K): δ = 169.6 (C=O), 166.4 (C=O), 152.1 (C=O), 131.2 (Ph-C_q), 130.5-122.1 (15xC, Pyr-CH, Pyr-C_q), 62.9 (β -CH_2), 57.2 (α-CH) ppm.

POLYMER SYNTHESIS

Synthesis of Bn-PLS(Pyr) homopolymer (37) and PEG-*b*-PLS(Pyr) copolymer (35-36)

L- or DL-Ser(Pyr)-NCA (0.50 g, 2.26 mmol, 1 eq) was evacuated and flushed with Argon, then dissolved in 10 mL of dry DMF. The initiator Bn-NH_2 (5 µL, 45 µmol, 0.02 eq), mPEG_{17}-NH_2 (33.9 mg, 45 µmol, 0.02 eq) or mPEG_{45}-NH_2 (29.4 mg, 15 µmol, 0.0065 eq) and lithium bromide (0.127 g, 1.47 mmol, 0.65 eq) were dissolved in 5 mL of dry DMF and added to the first solution. The reaction mixture was stirred at 0°C, room temperature or 35 °C for 4 days. 3 mL of DMF was added to the RM and precipitated in cold diethyl ether under vigorous stirring. The precipitate was filtered and dried *in vacuo*. The polymer was obtained as light-yellow solid.

Bn-*b*-PDLS(Pyr) (**37**, 0.36 g) was obtained with 45% yield. ^{1}H-NMR (700 MHz, DMSO-d6, 333 K): δ = 8.22-7.35 (m, NH, Pyr-CH), 7.10 (m, Ph-CH, Bn-NH_2), 5.40 (s, α-CH), 4.69 (m, β-CH_2) ppm. M_n = 7000 g/mol. DP = 22.

PEG_{17}-*b*-PDLS(Pyr) (**36**, 0.10 g) was obtained with a yield of 24%. ^{1}H-NMR (700 MHz, DMSO-d6, 333 K): δ = 9.14 (s, NH), 8.68-7.38 (m, Pyr-CH), 5.40 (s, α-CH), 4.67 (m, β-CH_2), 3.46 (s, PEG-$\underline{CH_2}$) ppm. M_n = 7700 g/mol. DP = 22.

PEG_{45}-*b*-PLS(Pyr) (**38**, 0.10 g) was obtained with a yield of 18%. ^{1}H-NMR (700 MHz, DMSO-d6, 333 K): δ = 9.36-8.78 (m, NH), 8.73-7.8 (m, Pyr-CH), 4.95-4.50 (m, α-CH, β-CH_2), 3.53 (s, PEG-$\underline{CH_2}$), 3.26 (s, PEG-O$\underline{CH_3}$) ppm. M_n = 7700 g/mol. DP = 20.

*Table 27: Synthetic details of L- and DL-O-(pyrenyl-1-carbonyl) serine homo and diblock copolymers **35-37**.*

No.	*Polymer*	*Initiator*	*DP_{theo}[a]*	*DP_{exp}[b]*	*Yield [%]*	*Mn^b [Da]*	*T [°C][c]*
35a	PEG_{45}-*b*-PLS(Pyr)$_{20}$, ncs175	$mPEG_{45}$-NH_2	90	20	18	7700	RT
35b	PEG_{45}-*b*-PDLS(Pyr)$_6$, ncs208	$mPEG_{45}$-NH_2	10	6	29	3900	RT
35c	PEG_{45}-*b*-PDLS(Pyr)$_{10}$, ncs209	$mPEG_{45}$-NH_2	15	10	45	5200	0
35d	PEG_{45}-*b*-PDLS(Pyr)$_{23}$, ncs198	$mPEG_{45}$-NH_2	90	23	38	9300	35
36	PEG_{17}-*b*-PDLS(Pyr)$_{22}$, ncs199	$mPEG_{17}$-NH_2	50	22	24	7700	35
37	Bn-*b*-PDLS(Pyr)$_{22}$, ncs200	Bn-NH_2	50	22	45	7000	35

[a] molar feed ratio of monomer and initiator [mmol]. [c] During polymerization.
[b] Mn of di-block copolymer, calculated by ^{1}H-NMR analysis.

Synthesis of PDLS(Pyr)-*b*-PEG-*b*-PDLS(Pyr) triblock copolymers (38-39)

DL-Ser(Pyr)-NCA (0.50 g, 2.26 mmol, 1 eq) was evacuated and flushed with Argon, then dissolved in 10 mL of dry DMF. The initiator Bn-NH_2 (5 µL, 45 µmol, 0.02 eq), $mPEG_{17}$-NH_2 (33.9 mg, 45 µmol, 0.02 eq) or $mPEG_{45}$-NH_2 (29.4 mg, 15 µmol, 0.0065 eq) and lithium bromide (0.127 g, 1.47 mmol, 0.65 eq) were dissolved in 5 mL of dry DMF and added to the first solution. The reaction mixture was stirred at 0°C, room temperature or 35 °C for 4 days. 3 mL of DMF was added to the RM and precipitated in cold diethyl ether under vigorous stirring. The precipitate was filtered and dried *in vacuo*. The polymer was obtained as light-yellow solid.

PDLS(Pyr)-*b*-PEG_{45}-*b*-PDLS(Pyr) (**38**, 0.12 g) was obtained with a yield of 29%. ^{1}H-NMR (700 MHz, DMSO-d6, 298 K): δ = 9.27-7.51 (m, NH, Pyr-CH), 5.42-4.94 (m, α-CH), 4.67 (m, β-CH_2), 3.48 (s, PEG-$\underline{CH_2}$) ppm. M_n = 7000 g/mol. DP = 16.

*Table 28: Synthetic details of O-(pyrenyl-1-carbonyl)-DL-serine triblock copolymers **38-39**.*

No.	*Polymer*	*Initiator*	*DP_{theo}[a,b]*	*DP_{exp}[b,c]*	*Yield [%]*	*Mn^c [Da]*
38a	PDLS(Pyr)$_4$-*b*-PEG_{45}-*b*-PDLS(Pyr)$_4$, ncs204	NH_2-PEG_{45}-NH_2	10	8	50	4500
38b	PDLS(Pyr)$_8$-*b*-PEG_{45}-*b*-PDLS(Pyr)$_8$, ncs205	NH_2-PEG_{45}-NH_2	16	16	29	7000
39a	PDLS(Pyr)$_4$-*b*-PEG_{68}-*b*-PDLS(Pyr)$_4$, ncs206	NH_2-PEG_{68}-NH_2	14	8	48	5500
39b	PDLS(Pyr)$_3$-*b*-PEG_{68}-*b*-PDLS(Pyr)$_3$, ncs207	NH_2-PEG_{68}-NH_2	22	6	44	4900
38c	PDLS(Pyr)$_{17}$-*b*-PEG_{45}-*b*-PDLS(Pyr)$_{18}$, ncs210	NH_2-PEG_{45}-NH_2	40	35	52	13000

[a] molar feed ratio of monomer and initiator [mmol]. [c] Mn of triblock copolymer, calculated by ^{1}H-NMR analysis.
[b] DP * ½ = desired DP per serine block.

Nonaqueous Emulsion Polymerization of PEG-*b*-PLS(Pyr) coated PLLA Core Shell Nanoparticles*:* PLLA nanoparticles were synthesized as described in the literature.[49] PEG-*b*-PSer(Pyr) copolymer (22.5 mg) in anhydrous cyclohexane (11.40 g, 9.25 mL) was ultrasonicated for 2 min. using a Bandelin Sonorex RK255H ultrasonic bath operating at 640 W, and stirred overnight at room temperature under inert atmosphere. L-Lactide (35.00 mg, 0.24 mmol, 1.00 eq) was dissolved in anhydrous acetonitrile (0.10 g, 0.125 mL). The emulsion was formed by dropwise addition of the monomer solution into the cyclohexane/PEG-*b*-PSer(Pyr) dispersion and subsequent treatment with ultrasonication for 5 min. The catalyst SIMes (2.50 mg, 334 µmol, 0.034 eq) and the initiator 1-pyrenyl butanol (2.10 mg, 7.70 µmol, 0.032 eq) were dissolved in acetonitrile (0.10 g, 0.125 mL) and added dropwise to the emulsion under inert atmosphere. The emulsion was stirred for 15 min. at room temperature to result in PLLA nanoparticles. A sample was taken out of the final emulsion to analyze the particle size and morphology *via* DLS and SEM. The remaining emulsion was ultrasonicated for 1 min. and sedimented. After decantation of the supernatant, the particles were washed with cyclohexane. The washing step was repeated three times before the particles were precipitated in cold methanol. The solvent was removed and the resulting particles were dried *in vacuo*.

5 Aggregation behavior of serine-based block copolymers in aqueous solution

5.1 Introduction

Amphiphilic block copolymers are widely used for the formation of micellar or vesicular structures in aqueous solution, leading to potent carrier systems that can encapsulate active components like dyes or drugs. Therefore, they are used for various applications like bio imaging and drug delivery.[139,147] Many therapeutically active molecules show poor solubility in aqueous solution due to their hydrophobic nature, hindering their efficient delivery to the target tissue.[148,149] To overcome this challenge, a carrier system is required that allows the encapsulation and transport of the drug to its target.[136] One alternative approach to the beforementioned nanoparticle-based carrier systems are micellar or vesicular aggregates, consisting of amphiphilic block copolymers. The amphiphilic structure of the block copolymers causes the self-assembly of the polymers in solution.[135,137,150] The polymers consist of a hydrophilic block that is oriented towards the aqueous medium, serving as the micellar corona, and a hydrophobic block that forms the micellar core, being able to stabilize the hydrophobic drug.[136,150] The main driver for the aggregation process is the prevention of energetically unfavorable hydrophobe-water interactions.[135,151] The size and shape of polymeric aggregates can be tailored by the chemical composition of the block polymers. The molecular weight, block ratio, secondary structure and solubility of the polymer in aqueous solution have an impact on the final aggregate.[135,150] The typical scale of polymeric aggregates is 10-500 nm, while diameters below 100 nm are favorable for biomedical applications to prevent early clearance by the mononuclear phagocyte system and allow passive targeting by the EPR effect.[137] Various shapes are known like spherical micelles, worm-like assemblies or polymersomes that are not only influenced by the polymer structure and block ratio, but also by the preparation method and concentration.[134,135] To allow the formation of such aggregates the polymer is dispersed in solution at a certain concentration, the critical micelle concentration (cmc).[152–154] Below this concentration the polymers exist as unimers in the solution, while at a polymer concentration equal or greater than the cmc micellar structures are formed.[148] Whether micellar spheres, rod-like assemblies or polymersomes will be formed from an amphiphilic block copolymer, is determined by the inherent molecular curvature and its influence on the packing ability of the copolymer chains.[134,135] The dimensions of a copolymer chain can lead to a dimensionless “packing parameter”, p, that helps to predict the final morphology of the aggregate after the self-assembly. A smaller packing parameter ($p \leq ⅓$) indicates a smaller volume of the hydrophobic block, but a higher curvature, indicating a spherical aggregation. A packing parameter of $⅓ \leq p \leq ½$ and a medium curvature suggest the formation of cylindrical or rod-like assemblies, while a

high packing parameter in the range of ½ ≤ *p* ≤ 1 and a low curvature implies the formation of polymersomes (Figure 74).[135]

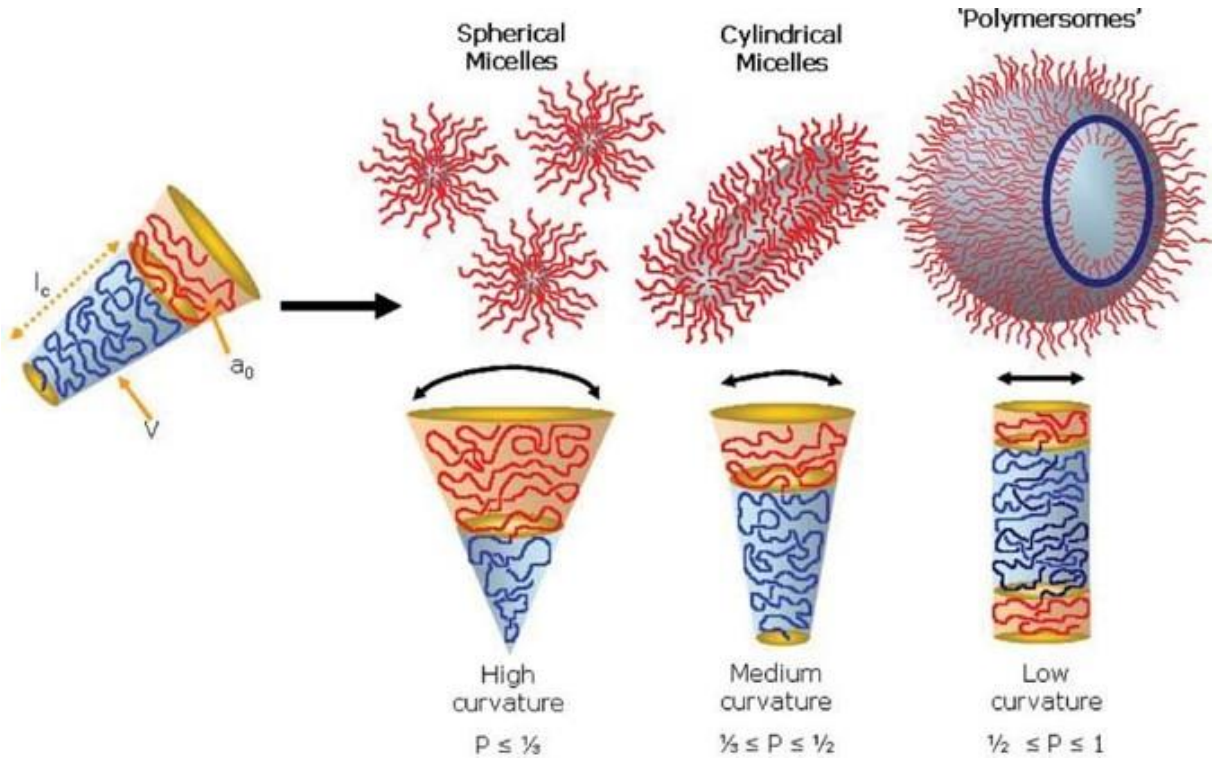

Figure 74: Shape of self-assembled polymeric aggregates from amphiphilic block copolymers in aqueous solution depending on the packing parameter (p), resulting from polymer block ratio and the inherent molecular curvature, respectively. Hydrophilic blocks (red) form the micellar corona, hydrophobic blocks (blue) form the micellar core.[135] *(Copyright by John Wiley and Sons, Ltd., printed with permission.)*

While the physical properties of the formation and behavior of such polymeric aggregates in solution are very complex and widely studied, the calculations of packing parameters of non-conventional polymers are not easy to perform and were not applied in this work. Instead, this chapter describes an experimental approach to investigate the aggregation behavior of the serine-based block copolymers PEG-*b*-PSer(Bn) in aqueous media and their performance as micellar or vesicular drug carrier systems, including the formation and drug encapsulation of the carrier, as well as cell viability and cell uptake studies.

5.2 Results and Discussion

The formation of reversed micelles in nonaqueous solution did not result in homogeneous and stable emulsions with the amphiphilic, serine-based PEG-*b*-PSer(Bn) block copolymers. As a consequence, the formation of dispersed core shell nanoparticles was difficult, mostly leading to particle agglomeration and poor yields. To evaluate the performance of these block copolymers in classical emulsions, the aggregation behavior of the serine-based block copolymers in aqueous solution was studied. The idea was to take advantage of the strong interactions of the benzyl serine block to form stable classical micellar structures in aqueous solution. In contrast to the nonaqueous solution, the hydrophilic polyethylenglycol, as the water-soluble polymer block, built the micellar shell in water, while the hydrophobic *O*-benzylserine block formed the core of the aggregates. In addition, it was evaluated, if the aggregation behavior differed for the L- and DL-serine polymers. Two polymer samples were used, one containing the L-serine block (PEG_{45}-*b*-$PLS(Bn)_{32}$, ncs71, **4c**) and one with the DL-serine block (PEG_{45}-*b*-$PDLS(Bn)_{32}$, ncs101, **8b**). Both polymers had similar block ratios of 45 to 32 to ensure comparability of the experiments. At this relatively high DP of the hydrophobic block, the formation of vesicular structures was expected that are known to be more stable and have better encapsulation efficiency than micelles.[135] In order to pre-evaluate the tendency of these polymers to form some kind of supramolecular structures in aqueous solution, an NMR experiment was conducted. Two samples of the racemic polymer PEG_{45}-*b*-$PDLS(Bn)_{32}$ (**8b**) were prepared in either DMSO-d_6 or D_2O and proton NMR spectra were measured (Figure 75). When thermodynamically stable micellar structures are formed, the core´s signals are typically barely or not visible at all, as the inner block is not dissolved in the solvent. Instead, it is present as a separate, solid microphase and therefore shows no relaxation during the NMR measurement.[133,150] The spectrum measured in DMSO-d_6 showed all expected signals of both, the PEG (signal f) and PDLS(Bn) (signals a-e) block (Figure 75, A), meaning there was no micelle formation observed. In contrast, in the spectrum measured in D_2O only the PEG signal at 3.68 ppm was clearly visible, while the signals of the poly peptide block were barely visible (Figure 75, B). The signal intensity of the aromatic CH protons (signal b) at 7.77 ppm decreased significantly, as well as the α- and β-protons of the serine side chain (signal c, d). This indicated that the polymer **8b** aggregated to some kind of supramolecular structures in aqueous solution, where the water-soluble PEG block was forming the micellar shell, while the core consisted of the insoluble hydrophobic PDLS(Bn) block, as expected.

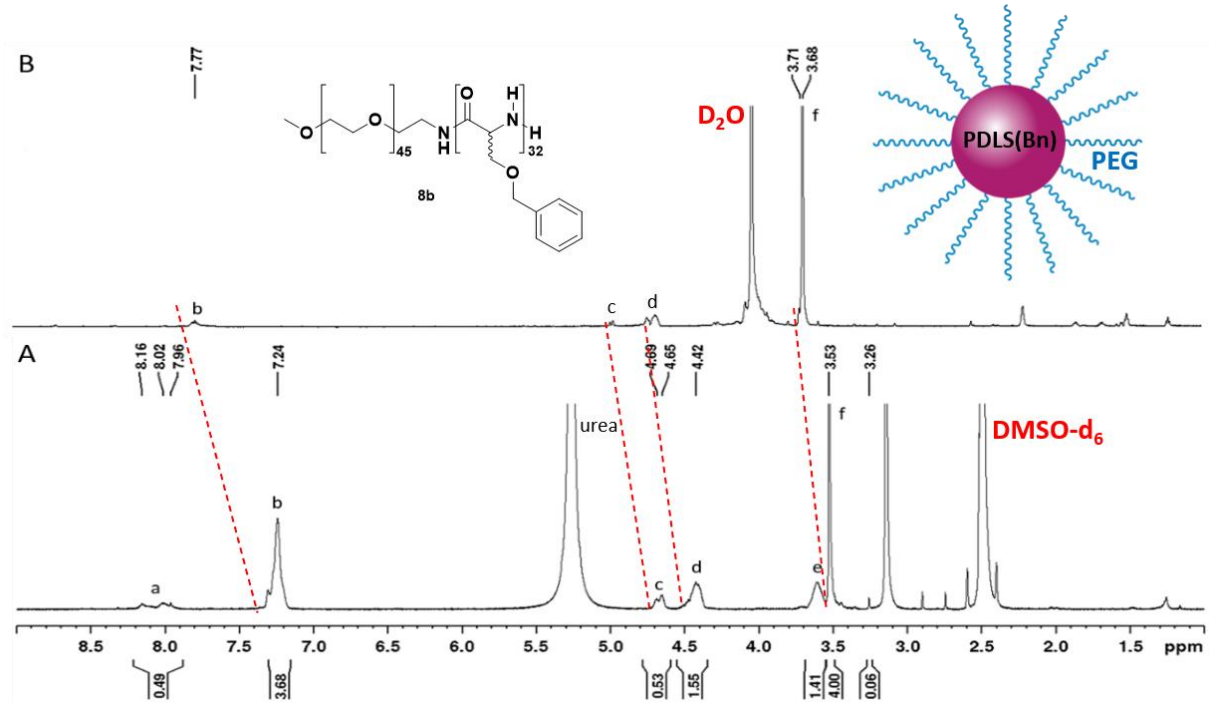

*Figure 75: [1]H-NMR spectra (333K, 700 MHz) of PEG_{45}-b-$PDLS(Bn)_{32}$ block copolymer (**8b**) in A) DMSO-d_6 and B) D_2O to prove the formation of supramolecular structures in aqueous solution.*

Various methods for the fabrication of well-dispersed aqueous micelles are reported in the literature.[137,152,155] Two of the most common methods are the thin film formation method (TFF) and the dialysis method, which were both employed to evaluate the most suitable method for the PEG-*b*-PSer(Bn) system. First, the micelles were prepared by TFF method. Dissolution of the polymer in a volatile solvent is required. Evaporation of the solvent leads to the formation of a thin polymer film in the flask and by dropwise addition of water and gentle stirring the micelles are formed.[155] Alternatively, the micelles were produced by dialysis method. The polymers (**4c**,**8b**) were dissolved in DMSO at concentrations of 1-3 mg/mL and dialyzed against MilliQ water overnight.[152]

Table 29: Hydrodynamic diameters of the aggregates after preparation by TFF or dialysis, measured by DLS.

No.	Polymer	Sample Name	Preparation	c [mg/mL]	d_H [nm]
1	PEG_{45}-*b*-**PLS**$(Bn)_{32}$ (**4c**)	ncs71_DMSO1	TFF w/ DMSO[1]	1.00	Aggregates[2]
2	PEG_{45}-*b*-**PDLS**$(Bn)_{32}$ (**8b**)	ncs101_DMSO1	TFF w/ DMSO[1]	1.00	Aggregates[2]
3	PEG_{45}-*b*-**PLS**$(Bn)_{32}$ (**4c**)	ncs71_DMSO_TF	TFF	1.00	460 ± 10
4	PEG_{45}-*b*-**PDLS**$(Bn)_{32}$ (**8b**)	Ncs101_DMSO_TF	TFF	1.00	500 ± 3
5	PEG_{45}-*b*-**PLS**$(Bn)_{32}$ (**4c**)	ncs71_DMSO2	Dialysis	1.00	240 ± 150
6	PEG_{45}-*b*-**PDLS**$(Bn)_{32}$ (**8b**)	ncs101_DMSO2	Dialysis	1.00	125 ± 60
7	PEG_{45}-*b*-**PLS**$(Bn)_{32}$ (**4c**)	ncs71_DMSO3	Dialysis	0.67	105 ± 2
8	PEG_{45}-*b*-**PDLS**$(Bn)_{32}$ (**8b**)	ncs101_DMSO3	Dialysis	0.67	120 ± 4
9	PEG_{45}-*b*-**PLS**$(Bn)_{32}$ (**4c**)	ncs71_DMSO4	Dialysis	3.00	560 ± 15
10	PEG_{45}-*b*-**PDLS**$(Bn)_{32}$ (**8b**)	ncs101_DMSO4	Dialysis	3.00	235 ± 5

[1] DMSO could not be fully evaporated, so dialysis was performed. [2] DLS measurement was performed after freeze drying and redispersion.

The size of the micelles was mainly determined as hydrodynamic diameter d_H via DLS after dialysis and ultrasonication (Table 29). The benzyl-serine-containing polymers were found to be insoluble in volatile solvents like dichloromethane or chloroform, but showed good solubility in high-boiling DMSO. First attempts (Table 29, No. 1-2) to evaporate DMSO under reduced pressure to apply the thin film formation method, did not result in remarkable evaporation after six hours, even at elevated temperatures. The solutions were then transferred into dialysis bags and dialyzed against MilliQ water overnight. After dialysis, these solutions where freeze dried and redispersed, according to recent literature protocols[137], but DLS measurements did not show any micelles in the nanometer range, but large aggregates instead. During the freeze-drying process, the micelles probably collapsed and did not rearrange by redispersion in water.[137] As a consequence, the following micelle solutions were used straight after dialysis for further investigations. A second attempt to form thin films by DMSO evaporation took 3 days under reduced pressure at room temperature (Table 29, No. 3-4). The polymer films were then redissolved in MilliQ water and stirred for 7 days. DLS measurements of the two samples showed average micelle diameters of 460 and 500 nm and a broad size distribution (Figure 76A). It was stated that this method was not suitable for these materials at all and the following approaches were conducted by dialysis method. The next approach was performed by dialysis and resulted in aggregates with favorable diameters of 240 nm and 125 nm (Table 29, No. 5-6). The diameter of the L-serine-based aggregates was clearly decreased from 240 to 105 nm by decreasing the polymer concentration from 1.0 mg/mL to 0.67 mg/mL (Table 29, No. 7). Using the DL-serine-based polymer did not change the size at higher dilution, resulting in a particle size of 120 nm at c = 0.67 mg/mL (Table 29, No. 8). In contrast to the prior samples, both samples at higher dilution showed narrow and monomodal size distributions (**4c**: Figure 76B; **8b**: Appendix, Figure 117B). While the literature reports a reciprocally proportional correlation of micelle size and polymer concentration, these materials proved once again to behave differently.[135,137,148] Approach No. 7 resulted in clearly smaller micelle size (>50%) by decreasing the polymer concentration by 30%. Another experiment was performed with a polymer concentration of 3.0 mg/mL to validate this trend and indeed, the diameter of the L-serine-based micelles was 560 nm, while the size of the DL-serine-based micelles increased to 235 nm (Table 29, No. 9-10). Furthermore, the DLS measurement revealed that these results were based on the presence of larger aggregates and a bimodal size distribution (Figure 76C), indicating that the micelles were agglomerating at high concentrations of the PLS(Bn) polymer **4c**. In addition, the PDLS(Bn) aggregates (**8b**) were shown to be less sensitive to concentration changes, as the particle size was almost identical at 1.0 mg/mL and 0.67 mg/mL and almost doubled at 3.0 mg/mL, while the L-serine aggregates were five times larger at 3.0 mg/mL compared to 0.67 mg/mL. These findings

matched with the observations in nonaqueous solution, where a lower polymer concentration was also found to result in smaller particles and reduced agglomeration.

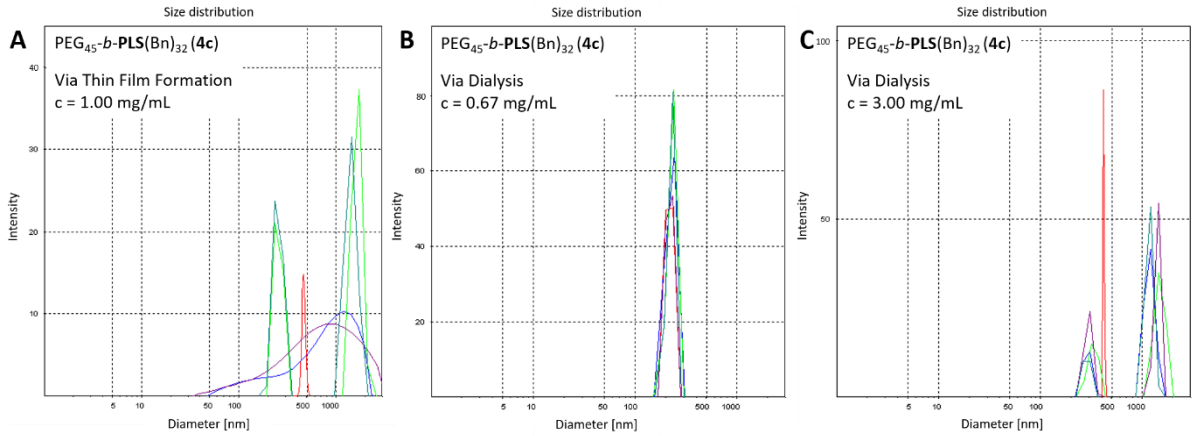

*Figure 76: Size distribution of aqueous micelles of L-serine polymers (**4c**) after preparation by TFF at c = 1.00 mg/mL vs. dialysis at c = 0.67 mg/mL and 3.00 mg/mL.*

The micelle solutions were stored at 4 °C and their stability over time was evaluated by DLS measurements after three weeks (Table 30). Both samples showed diameters of around 100 nm and therefore excellent stability within this time period. The diameter of the L-micelles slightly increased by 10 nm, while the DL-micelles adjusted to a size of 90 nm that was 25 nm less than before. Both samples were stable over time and did not show any signs of agglomeration after three weeks of storage at 4 °C.

Table 30: Hydrodynamic diameters of the aq. micelles, measured by DLS after dialysis and after 3 weeks of storage at 4 °C.

Polymer	**Sample Name**	**c [mg/mL]**	**d_H [nm] after dialysis**	**d_H [nm] after 3 weeks**
PEG_{45}-b-**PLS**$(Bn)_{32}$ (**4c**)	ncs71_DMSO3	0.67	105 (± 2)	115 (± 2)
PEG_{45}-b-**PDLS**$(Bn)_{32}$ (**8b**)	ncs101_DMSO3	0.67	120 (± 4)	90 (± 1)

In order to visualize the morphology and shape of the micelles, cryo-TEM measurements were performed (Figure 77) and confirmed the spherical shape of the assemblies. The images of the PLS(Bn)-based assemblies (**4c**) displayed uniform uni- or bilamellar structures with a diameter of around 100 nm (Figure 77, A-C). The DL-serine-polymer sample (**8b**) showed mostly unilamellar structures of around 80-100 nm in diameter, but also larger ones with diameters of 200-500 nm (Figure 77, D-E). According to the cryo-TEM images the L-micelles showed a narrower size distribution than the DL-micelles, while the DLS measurements showed similar monomodal size distributions. This could be caused by the sample preparation, as such structures are known to be sensitive to changes of the aggregation state, influencing the final size and shape of the aggregates.[136,151] The PLS(Bn) agglomerates were possibly more stable towards the sample preparation conditions than the DL-serine

analogues. Aside from that, the cryo-TEM images together with the size distribution, indicated that the polymers were not self-assembling into micellar structures, but more likely into polymersomes or vesicles, as expected from the block ratio of the block copolymers.[134,135]

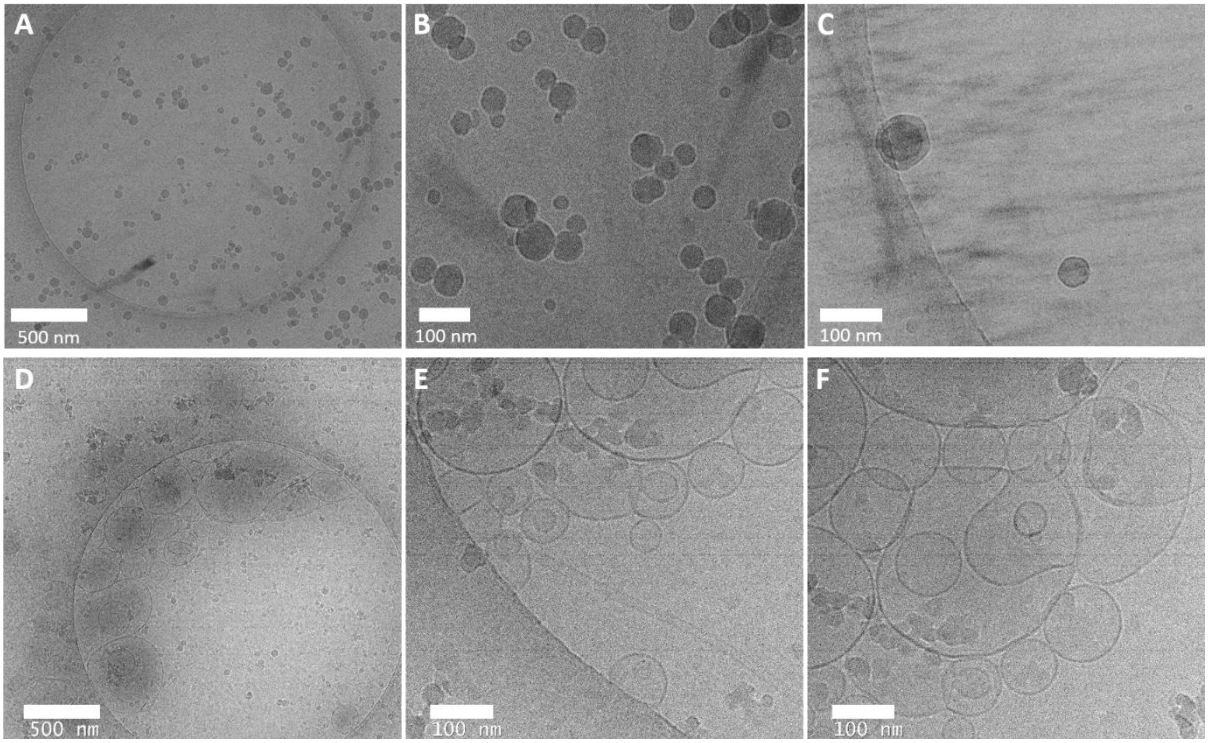

*Figure 77: Cryo-TEM images of the micelles of PEG_{45}-b-$PLS(Bn)_{32}$ (**4c**, A-C) and PEG_{45}-b-$PDLS(Bn)_{32}$ (**8b**, D-F).*

After it was confirmed that the serine-based block polymers self-assemble to vesicles, the aggregation and uptake behavior of both polymers was further studied and the critical micelle concentration (cmc) was determined. Therefore, fluorescence spectroscopy was performed using pyrene as the fluorescent probe. In theory, the fluorescence intensity of pyrene in aqueous solution changes when micelles or vesicles are formed, as it is diffusing into the hydrophobic core of the vesicles, causing the emission to increase.[156,157] At the same time, due to the local accumulation and close proximity of the pyrene molecules within the micellar core, excimer formation takes place that can be observed in the fluorescence spectrum by a broad emission peak at 475 nm, while the emission of the pyrene monomers occurs between 370-390 nm (Figure 78D).[158,159] The data was processed, according to common literature.[160] The intensity peaks I_1 at 372 nm and I_3 at 393 nm were extracted from the emission spectra and the quotient I_1/I_3 vs. polymer concentration $c_{polymer}$ was used for the determination of the cmc. The inflection point of the resulting graph is displaying the cmc. In the case of the PEG-*b*-PSer(Bn) polymers, the cmc could not be determined by this method. Usually, the intensity of pyrene increases with increasing polymer concentration due to the increasing interactions and decreasing distance of the pyrene molecules inside the micelles.[161] In the case of PEG-*b*-PLS(Bn) (**4c**), an inverse effect was observed in the emission spectra in terms of intensity

changes. Increasing the polymer concentration did result in a dramatic decrease of fluorescence intensity of the pyrene probe and no excimer formation at all, which led to the conclusion that Poly-*O*-Benzyl-Serine had a concentration-dependent fluorescence quenching effect on the fluorophore, as reported by Pandey et al. (Figure 78).[162] Both, L- and DL-polymer samples, caused the intensity to decrease with increasing polymer concentration (Figure 78A-B). To quantify the fluorescence quenching efficiency, I_1/I_0 was plotted against the polymer concentration, with I_0 being the initial intensity of pyrene in aqueous solution before the addition of the polymer. The resulting graphs showed that the L-serine polymers (**4c**) were up to 20% more efficient in quenching than the racemic polymers (**8b**) at a concentration of 1 mg/mL (Figure 78C). The strong intramolecular interactions of *O*-benzyl-L-serine and of its benzyl rings within the β-sheets might be the reason for this difference. Interactions like pi-pi stacking in the ordered β-sheets increase the electron density of the aromatic systems and with it the quenching efficacy, while random coil structures disturb the overlap of phenyl rings, leading to a less efficient quenching effect.[163]

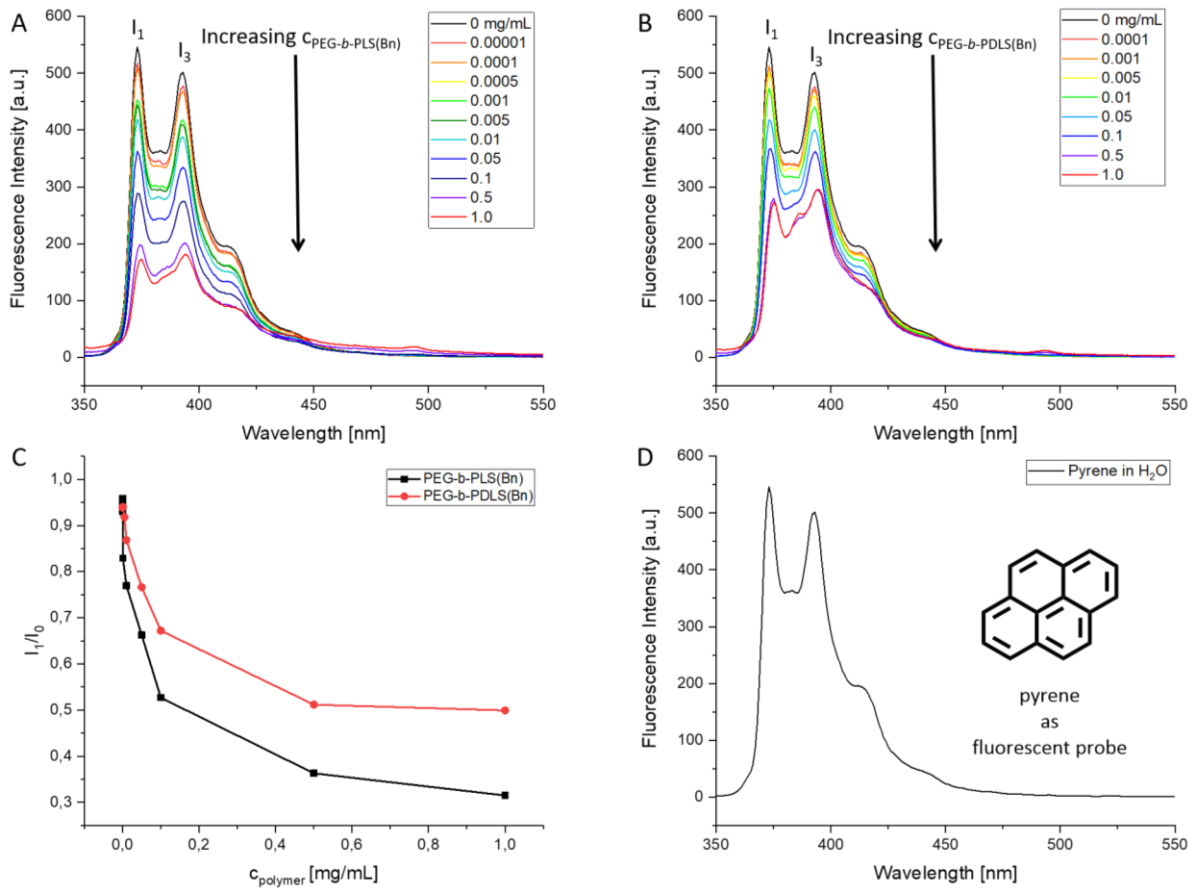

*Figure 78: Fluorescence spectra of a pyrene probe at various concentrations of A) PEG_{45}-b-$PLS(Bn)_{32}$ (**4c**) vesicles and B) PEG_{45}-b-$PLS(Bn)_{32}$ (**8b**) vesicles; C) quenching efficiency of both vesicle types in comparison and D) pyrene fluorescence in aqueous solution.*

To find out more about the quenching mechanisms and to evaluate benzyl serine as a possible fluorescence quencher and its applicability in biochemistry further studies are required. Detailed stationery and time-dependent observations of the quenching process can reveal information about the deactivation mechanisms of the fluorescent probe. This is used for different purposes in biochemistry already, *e.g.,* investigation of distances and orientational changes of different parts in biomolecules.[164]

Originally, the fluorescence measurements were intended to determine the cmc of both polymers and to gain better understanding of the aggregation behavior of the materials. In order to determine the cmc of the polymers without spectroscopic methods, tensiometry was performed. In tensiometry, the cmc is determined by measuring the surface tension of the solution in dependence of the polymer concentration. With increasing concentration, the surface tension decreases stepwise. When micellar structures are formed at a certain concentration, a sudden drop of surface tension is observed. This concentration is defined as the critical micelle concentration.[153,154] Both polymers PEG_{45}-*b*-$PLS(Bn)_{32}$ (**4c**) and PEG_{45}-*b*-$PDLS(Bn)_{32}$ (**8b**) were measured by tensiometry and showed comparable cmc values. A value of cmc = 240 mg/L was calculated for the L-polymer (**4c**) and cmc = 150 mg/L for the DL-polymer (**8b**, Figure 79), resulting in comparable stability of the aggregates. The random coil structure of the racemic polymer **8b** led to higher flexibility of the polymer chains and therefore facilitated the self-assembly in comparison to the more rigid β-sheet structures of the L-polymer **4c**.[165] To find out more about the influence of the polymer block ratio and the secondary structure of these materials on the self-assembly, polymers with different block ratios were used for the vesicle formation in aqueous solution and studied by DLS and tensiometry.

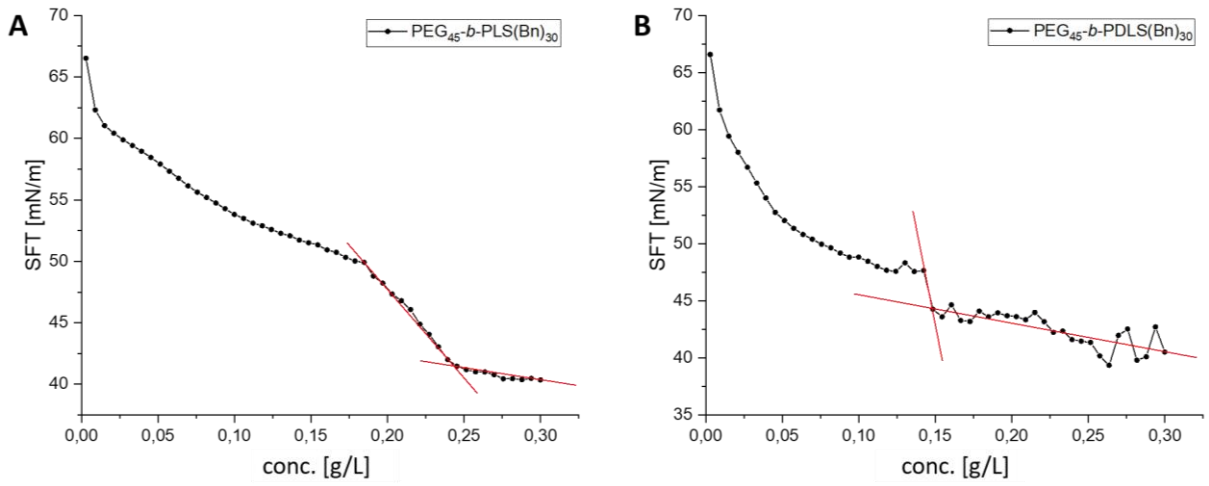

*Figure 79: Determination of the cmc in aqueous solution by tensiometry at room temperature: Graphs display the surface tension (SFT) vs. the polymer concentration [g/L] of A) the L-serine(Bn) polymer **4c** and B) the DL-serine(Bn) polymer **8b**.*

All samples were prepared in aqueous solution by dialysis method, as previously described. The polymer concentration after dialysis was adjusted to 0.5 mg/mL, which was the minimum concentration required for the tensiometry measurement. After the dialysis the samples were ultrasonicated for 3 minutes to homogenize the mixtures. While some of the samples were obtained as homogenous emulsions, others were rather heterogeneous and precipitated after a short period of time (Figure 80). The polymer PEG_{45}-*b*-$PLS(Bn)_{57}$ (**4g**) showed visible aggregation, even after stirring and ultrasonication, which was confirmed by DLS (Figure 80C). The tnsiometry measurement was not possible and no cmc could be determined for that sample. In contrast, the polymer with the lowest PLS(Bn) block, PEG_{45}-*b*-$PLS(Bn)_8$ (**4b**), was perfectly homogeneous and stable over time (Figure 80A). The other samples were all homogeneous but precipitated partially over time. By ultrasonication, these samples were successfully homogenized again.

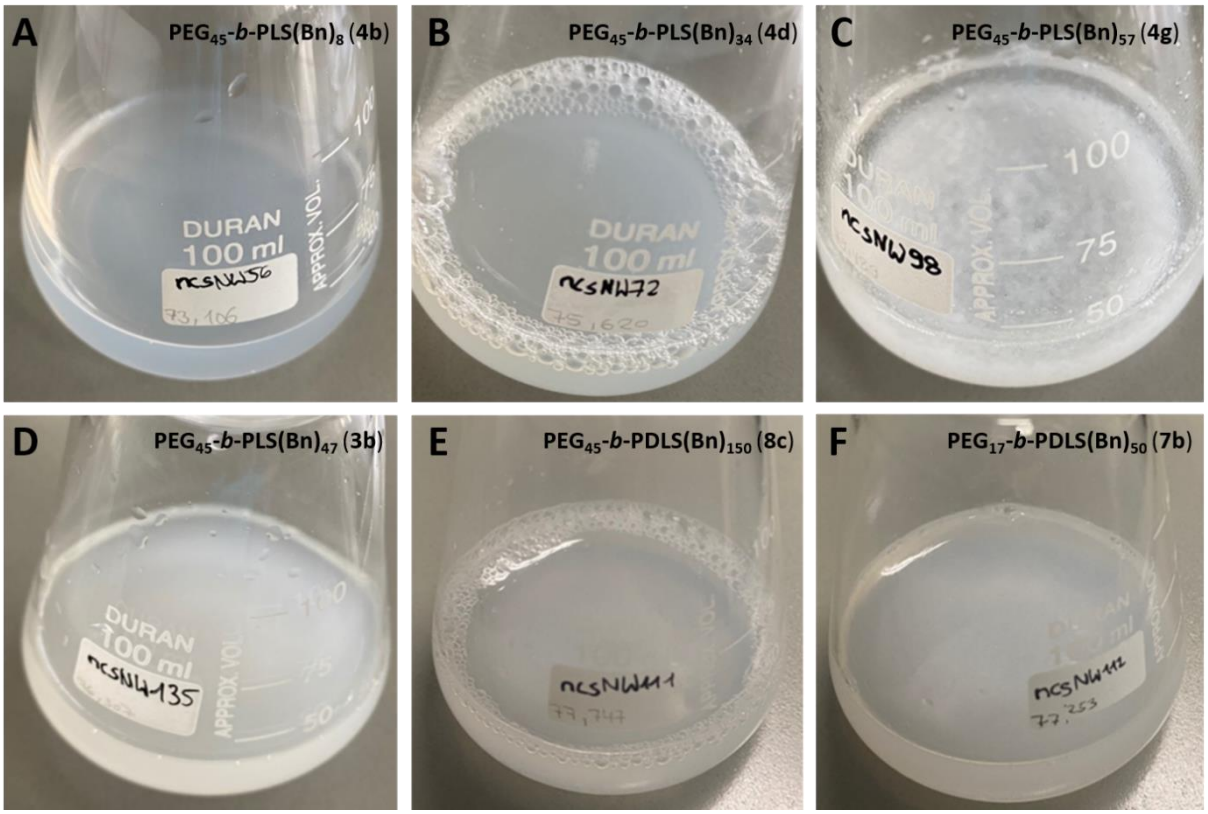

*Figure 80: The aqueous polymer solutions after dialysis, where some looked homogeneous (A, **4b**), while others showed strong aggregation and precipitation (C, **4g**).*

This series of measurements allowed several conclusions (Table 31). The L-serine polymers showed that the cmc increased almost linearly by using polymers with a higher hydrophobic block ratio. PEG_{45}-*b*-$PLS(Bn)_{34}$ (**4d**) showed that taking a polymer with a slightly longer peptide block (45:34) resulted in a slightly higher cmc of 0.260 g/L compared to 0.240 g/L of PEG_{45}-*b*-$PLS(Bn)_{32}$ (**4c**). The lowest cmc value of 0.115 g/L was obtained with the shortest PLS(Bn) block, PEG_{45}-*b*-$PLS(Bn)_8$ (**4b**), which was visibly the most homogenously dispersed sample. In contrast, the polymer with the highest

hydrophobic moiety, PEG_{45}-*b*-$PLS(Bn)_{57}$ (**4g**), did not result in a well-dispersed micelle solution, but in irreversible precipitation of the polymer and showed large aggregates by DLS. It was not included in the tensiometry measurement. PEG_{17}-*b*-$PLS(Bn)_{47}$ (**3b**), a PEG750-containing polymer with a relatively high hydrophobic ratio, resulted in a homogeneous mixture according to DLS, but was not stable over time. Due to the sedimentation of this sample during the measurement, the cmc could not be fully determined, but estimated from the graph at around 0.35 g/L. In conclusion, a molecular weight ratio of around 60:40 of the hydrophilic to hydrophobic block was shown to be ideal for the PEG-*b*-PLS(Bn) system. Compared to the L-serine polymers, the DL-serine analogues with comparable block ratios showed lower cmc values and no proportional trend between hydrophobic block ratio and cmc. Even high hydrophobic block ratios resulted in comparably low cmc values, which was ascribed to their differing secondary structure. PEG_{45}-*b*-$PDLS(Bn)_{180}$ (**8c**) and PEG_{17}-*b*-$PLS(Bn)_{50}$ (**7b**) with clearly higher hydrophobic moieties were tested next to PEG_{45}-*b*-$PDLS(Bn)_{32}$ and resulted in lower cmc values of 0.110 g/L, compared to 0.150 g/L. Nevertheless, all three values were lower than the cmc values of the L-serine polymers and in a narrow range between 0.10 and 0.15 g/L. The DLS measurement showed hydrodynamic diameters of around 1000 nm for both samples, which is ten times higher than for the first sample with PEG_{45}-*b*-$PDLS(Bn)_{32}$ (8**b**). This might be due to agglomeration of the sample or due to a different shape of the self-assembled aggregates, as DLS measurements are not reliable for non-spherical aggregates.[166] This was not further studied, as the following experiments were performed with the two polymers **4c** and **8b** that showed good overall performance, according to DLS and tensiometry results as well as visual inspection of the solutions.

Table 31: Hydrodynamic diameters and cmc values of the aqueous solutions of various O-benzyl-serine block copolymers with different block ratios.

Polymer	**c [mg/mL]**	**d_H [nm][1]**	**cmc [g/L][2]**
PEG_{45}-b-$PLS(Bn)_{32}$, **4c**	0.50	105 (± 2)	0.240
PEG_{45}-b-$PLS(Bn)_{8}$, **4b**	0.50	620 (± 30)	0.115
PEG_{45}-b-$PLS(Bn)_{34}$, **4d**	0.50	520 (± 25)	0.260
PEG_{45}-b-$PLS(Bn)_{57}$, **4g**	0.50	4220 (± 1480)	-
PEG_{17}-b-$PLS(Bn)_{47}$, **3b**	0.50	630 (± 5)	0.350
PEG_{45}-b-$PDLS(Bn)_{32}$, **8b**	0.50	120 (± 4)	0.150
PEG_{45}-b-$PDLS(Bn)_{150}$, **8c**	0.50	1220 (± 150)	0.110
PEG_{17}-b-$PDLS(Bn)_{50}$, **7b**	0.50	930 (± 75)	0.110

[1] determined by DLS measurement [2] determined by tensiometry

To visualize the results, the percentage of the serine block in the block copolymer was calculated from the DP and correlated with the cmc (Figure 81). For the L-serine polymers, the cmc increased almost

linearly with increasing hydrophobic poly-L-serine(Bn) block (black graph). The DL-serine polymers did not show a linear trend like the L-serine ones. They all resulted in similarly low cmc values below 0.15 g/L, even at high ratios of the DL-serine block (red graph). As mentioned before, this was explained by the random coil structure of the serine block, making it more flexible and less rigid, enabling the formation of a denser, more stable micellar core.

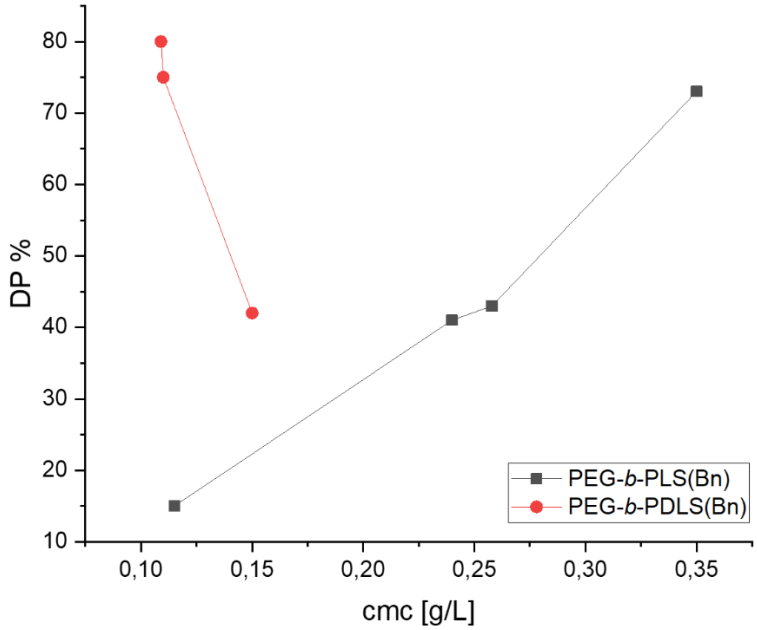

Figure 81: Correlation of the DP percentage of the O-benzyl-serine block in the polymer vs. the cmc.

It was demonstrated that both types of polymers, containing either the L-serine block or the DL-serine block, were self-assembling in aqueous solution. By producing several emulsions with polymers of different block ratios and analyzing them by DLS and tensiometry, a linear trend of cmc and hydrophobic benzyl serine block ratio was revealed for the L-serine polymers. The higher the DP of the L-serine in the polymer, the higher was the cmc. In contrast, the DL-serine polymers did not show such a clear trend. Instead, all the polymers showed significantly lower cmc values compared to the L-serine samples. This was explained by the different secondary structures of both materials. While the β-sheets of L-serine are more rigid and therefore harder to align to a compact inner core of the aggregate, the random coil chains of the DL-serine polymers are more flexible and form dense micellar cores more easily, even at higher block ratios. The best overall performance was shown by PEG_{45}-*b*-$PLS(Bn)_8$ (**4b**), which resulted in a homogeneous emulsion that was stable over time without any sedimentation. Confirming these observations, it had the lowest cmc value of 115 g/L amongst all tested L-serine polymers. The initial samples PEG_{45}-*b*-$PLS(Bn)_{32}$ (**4c**) and PEG_{45}-*b*-$PDLS(Bn)_{32}$ (**8b**) showed good overall performance as well. Not only did both show monodisperse aggregates with diameters of around 100 nm, they also resulted in stable emulsions with low cmc values. Cryo-TEM measurements approved the presence of polymersome structures in these samples, which was a good

precondition for biological applications due to their stability. Therefore, these two materials were chosen to be used in the following experiments, where the drug encapsulation was studied, as well as cytotoxicity and cell uptake.

CELL VIABILITY AND DRUG LOADING STUDIES

To study the drug loading efficiency of the PEG-*b*-PSer(Bn)-based polymersomes and their behavior in biological environment, a drug was encapsulated in the aggregates in the next step. The chemotherapeutic agent doxorubicin (DOX, Figure 82A) was selected for the encapsulation, as it is commonly used in literature as a model compound to test the cytotoxicity.[167–169] This is helpful to compare the performance of the polymersomes with other existing drug delivery systems. In addition, doxorubicin is a hydrophobic and aromatic molecule, which was believed to interact with the benzyl serine side chains to form stable drug-loaded aggregates. The formation and drug loading of the polymersomes was conducted in one step by dialysis method. Following Gu et al., a 1:2 weight ratio of DOX to polymer was used in a first attempt.[169] Both polymers, PEG_{45}-*b*-$PLS(Bn)_{32}$ (**4c**) and PEG_{45}-*b*-$PDLS(Bn)_{32}$ (**8b**), were used for the formation of drug-loaded polymersomes and analyzed by DLS to determine the hydrodynamic diameters. In both samples the d_H increased dramatically by the drug-encapsulation and resulted in 620 nm for the L-serine sample and 1830 nm for the DL-serine sample (Table 32, No. 1-2).

Table 32: Concentrations of the drug-loaded polymersomes and hydrodynamic diameters d_H, determined by DLS.

No.	Sample	Sample Name	Ratio (DOX:polymer)	c [mg/mL] after dialysis	d_H [nm]
1	PEG_{45}-*b*-$PLS(Bn)_{32}$ (**4c**)	ncs71_DMSO_DOX	1:2	0.80	620 (± 45)
2	PEG_{45}-*b*-$PDLS(Bn)_{32}$ (**8b**)	ncs101_DMSO_DOX	1:2	0.78	1830 (± 85)
3	PEG_{45}-*b*-$PLS(Bn)_{32}$ (**4c**)	ncs71_DOX2	1:10	1.19	250 (± 4)
4	PEG_{45}-*b*-$PDLS(Bn)_{32}$ (**8b**)	ncs101_DOX2	1:10	1.18	220 (± 10)

Swelling of the aggregates due to the drug loading is expected and reported in literature, but typically not exceeding a difference of 20 nm.[136] Also, more common weight ratios of drug and polymer were found to be in the range of 1:10 instead of 1:2, explaining the dramatic increase in diameter, caused by drug overloading of the vesicles. Nevertheless, successful encapsulation was confirmed by UV/VIS absorption measurements (Figure 82B). Compared to the free DOX solution, the absorption of the DOX-loaded vesicles was decreased, indicating the encapsulation of DOX.

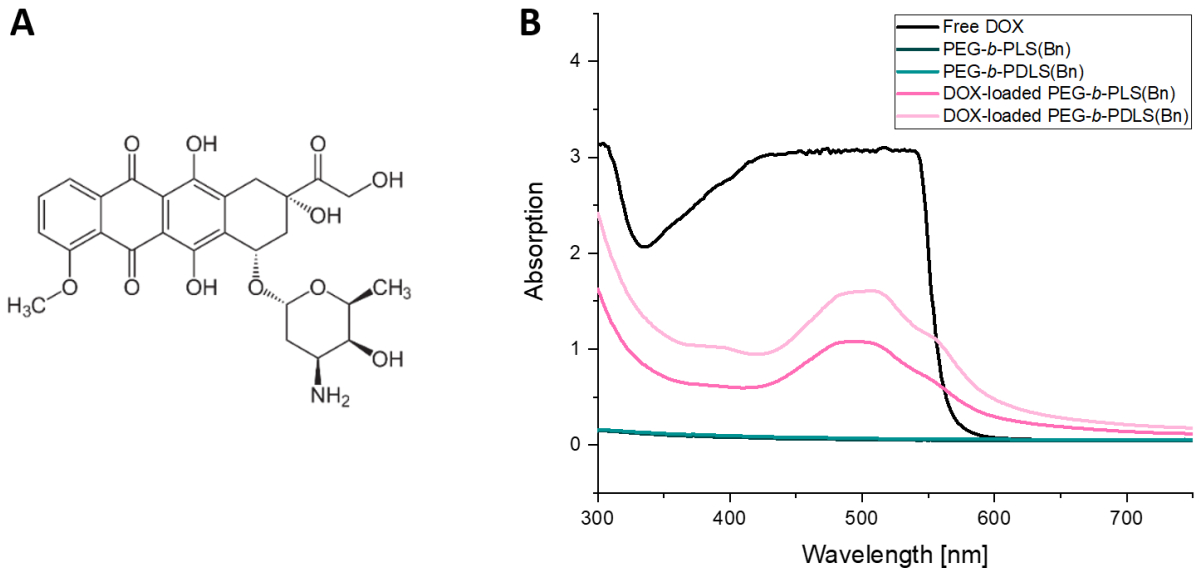

Figure 82: A) Molecular structure of doxorubicin (DOX) and B) UV/Vis absorption of free DOX (black) in comparison to DOX-loaded polymersomes (pink) and blank polymersomes (green).

In a second approach to form drug-loaded polymersomes, a 1:10 weight ratio of DOX and polymer was used in order to achieve smaller particle diameters of 100-200 nm. Indeed, the decrease of DOX led to smaller particle diameters of 250 nm for the L-serine sample and 220 nm for the DL-serine sample (Table 32, No. 3-4), according to DLS measurements. This led to the conclusion that the drug content has a huge impact on the vesicle size. Finally, with this approach DOX-loaded aggregates of adequate size were obtained. The drug loading was not only confirmed by UV/VIS, but could be followed visually during the process, as the color of the solutions changed (Figure 83). In DMSO, DOX hydrochloride appeared orange and changed to dark red after addition of triethylamine (Et_3N) to deprotonate the amine of the DOX salt. The color remained unchanged upon addition of the polymers. During the dialysis against water, the color of DOX changed to dark violet after water entered the dialysis membrane. With the formation of polymersomes and encapsulation of the DOX within the aggregates, the color of the solutions changed to shades of pink, indicating the successful encapsulation of DOX.

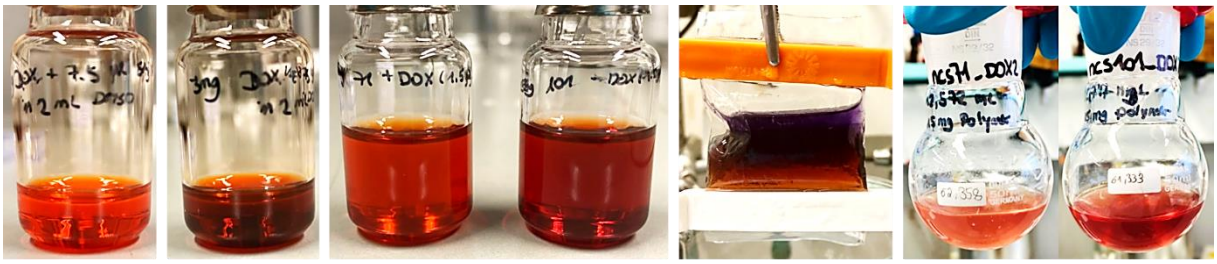

DOX-HCl in DMSO | *Free DOX in DMSO, after Et_3N addition* | *Free DOX and polymers in DMSO* | *Free DOX in water (violett)* | *DOX-encapsulated micelles in H_2O*

Figure 83: Colour change of doxorubicin in solution during the drug encapsulation process.

For the cell viability tests, fresh samples of drug loaded and especially plain vesicles of L- and DL-serine based polymers were prepared to eliminate the possibility of contamination of the samples with microbes like bacteria or fungi. Solutions with a higher polymer concentration of 1.5-2.0 mg/mL were required to test the cell viability at higher concentrations (Table 33). The DOX to polymer weight ratio was 1:10, as in the previous approach and the samples were prepared in the same way as before.

Table 33: Concentrations and hydrodynamic diameters of the unloaded and DOX-loaded samples for cell viability tests.

No.	Sample	c [mg/mL] for cell tests	c [mg/mL] for DLS	d_H [nm]
1	PEG_{45}-*b*-$PLS(Bn)_{32}$ (**4c**), ncs71_ DMSO6	2.00	2.00	2500 (± 105)
			1.00	250 (± 20)
2	PEG_{45}-*b*-$PLS(Bn)_{32}$ (**4c**), ncs71_DOX3	1.50	1.50	410 (± 70)
3	PEG_{45}-*b*-$PDLS(Bn)_{32}$ (**8b**), ncs101_ DMSO6	2.00	2.00	690 (± 10)
			1.00	180 (± 10)
4	PEG_{45}-*b*-$PDLS(Bn)_{32}$ (**8b**), ncs101_DOX3	1.50	1.50	490 (± 25)

The blank samples resulted in homogeneously dispersed solutions, even at increased concentrations of 2 mg/mL. DLS measurements of these concentrated samples resulted in hydrodynamic diameters of 2500 nm for the L-serine probe (**4c**) and 690 nm for the DL-serine probe (**8b**). It was hypothesized that due to the high polymer concentration the aggregates tend to agglomerate and therefore, a second measurement was performed with the samples after dilution to c = 1.0 mg/mL and indeed, the particle size decreased to 250 nm (**4c**) and 180 nm (**8b**), which were values within the expected range. The vesicles formed loose agglomerates at higher concentration that were dispersible by dilution and ultrasonication. In contrast, the DOX-loaded aggregates showed sedimentation at a concentration of 2 mg/mL and even though ultrasonication led to successful redispersion of the solutions, they were not stable for more than 10 minutes. Therefore, the solutions were diluted to 1.5 mg/mL and ultrasonicated again, which led to major improvement in the stability of the vesicles in solution. DLS measurements resulted in average diameters of 410 nm for the L-serine sample (**4c**) and 490 nm (**8b**) for the DL-serine based sample, which was believed to be an effect of the increased concentration of the samples as well. The blank aggregates of PEG_{45}-*b*-$PLS(Bn)_{32}$ (**4c**) and PEG_{45}-*b*-$PLS(Bn)_{32}$ (**8b**) resulted in colorless, slightly turbid solutions, while the DOX-loading of the vesicles led to a light pink color (Figure 84).

*Figure 84: Unloaded (colorless) and DOX-loaded (pink) polymersome solutions of PEG_{45}-b-$PLS(Bn)_{32}$ (**4c**, left) and PEG_{45}-b-$PDLS(Bn)_{32}$ (**8b**, right).*

In the next step, the cell viability was tested to find out more about the biocompatibility of the materials and their potential as drug delivery system. Polymersomes of the two polymers PEG_{45}-*b*-$PLS(Bn)_{32}$ (**4c**) and PEG_{45}-*b*-$PLS(Bn)_{32}$ (**8b**) were prepared in aqueous solution as blank and drug-loaded samples. The cell viability study was performed with all four samples on the A549 human lung adenocarcinoma cell line at five different polymer concentrations between 10-250 µg/mL (Figure 85). The data is presented as the percentage of living cells (Cell Viability (%)) and was compared to the control group that was not treated with anything (grey) and a DOX control that was treated with plain DOX (black).

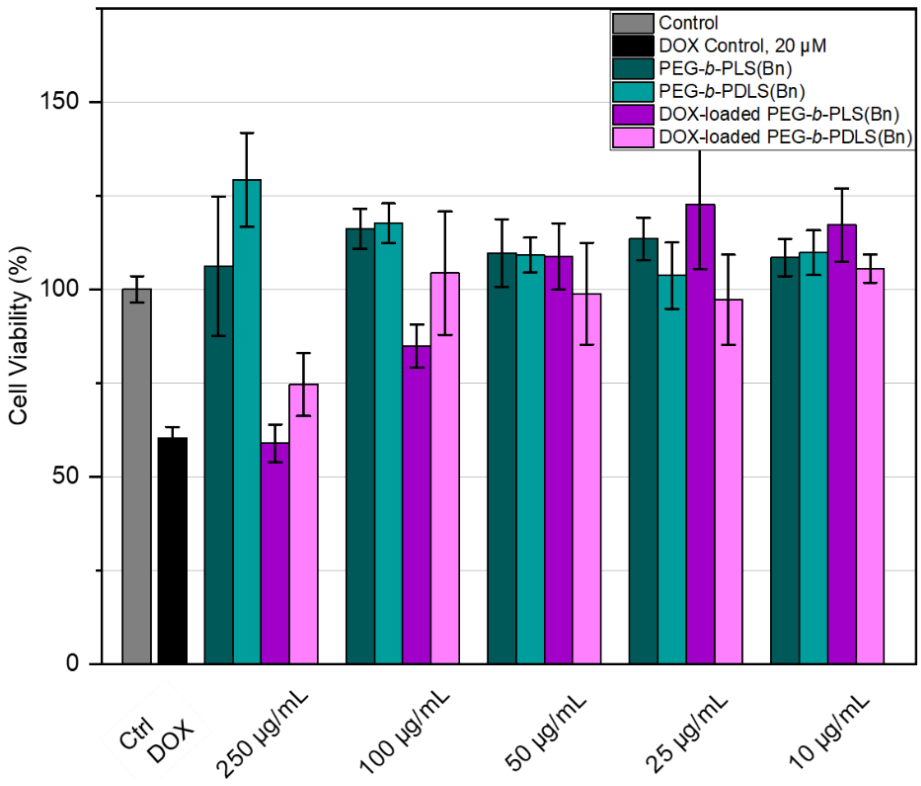

Figure 85: Cell viability tests of the unloaded and DOX-loaded micelles. The given concentrations are referring to the micelle concentrations. DOX was used at 10 wt% in respect to the polymersomes (performed by [redacted], A549 cells, 24 h of incubation, CellTiter-Glo® Luminescence Cell Viability Assay).

The blank vesicles showed good compatibility with the cells over the whole concentration range between 0.25 and 0.01 mg/mL of polymer, with no significant difference between the L- and DL-serine based materials. In all probes with the blank polymers, the cell viability is above 100% and hence, no cytotoxicity of the polymers was detected. This was a very good initial result, as 0.25 mg/mL, or 33 µM, could be considered a high concentration of polymer. For the DOX-encapsulated polymersomes, the outcome was different. Between 0.01 and 0.05 mg/mL, no effect was detected and the cell viability was around 100% in both, the L- and DL-serine samples. In contrast, the two higher concentrations 0.1 and 0.25 mg/mL did show an effect on the cell viability. It was assumed that below 0.1 mg/mL the concentration of DOX, which corresponded to 10wt% of polymer concentration, was simply too low to show any detectable effects on the cell viability. At a polymer concentration of 0.1 mg/mL, the L-serine samples (**4c**) showed a cell viability of 80%, while the DL-serine samples (**8b**) still showed 100% cell viability. At the highest concentration of 0.25 mg/mL, a cell viability of 60% for PEG_{45}-*b*-$PLS(Bn)_{32}$ (**4c**) and 75% for PEG_{45}-*b*-$PDLS(Bn)_{32}$ (**8b**) was observed. Therefore, a clear effect of the DOX-loaded vesicles was observed at the higher concentrations, where the L-serine aggregates were 15-20% more effective than the DL-analogues. In comparison to the DOX control that resulted in 60% cell viability at 20 µM of DOX, which correlated with the IC50 value of DOX on the A549 cells that is about 20-30 µM, the L-serine sample (**4c**) was just as effective, at a final DOX concentration of 0.043 µM, which was almost 500 times lower than the control. This led to the conclusion that the vesicles were clearly promoting the efficacy of DOX and that the cytotoxicity was definitely induced by the drug, as the blank samples at the same concentration did not show any negative effect on the cell viability. It was also hypothesized that the transport of DOX into the cell was improved by the encapsulation, leading to high cytotoxicity at much lower drug concentrations. In order to find out more about the transport mechanism of these materials, cell uptake experiments were conducted in the next step. The block copolymers needed to be marked with a fluorescent tag to be able to visualize them with a fluorescent microscope. Due to the slightly higher efficacy of the L-serine aggregates in the cytotoxicity assay, the cell uptake was performed with the L-serine polymers (**4c**). First, postsynthetic end group functionalization was conducted with PEG_{45}-*b*-$PLS(Bn)_{32}$ (**4c**) using pyrene as the fluorescent probe. Pyrene was chosen, because it does not interfere with the fluorescence of doxorubicin and can be viewed separately by fluorescence microscopy. To implement the fluorescent tag into the polymer, the terminal amine group of the polypeptide block was converted to an amide by coupling reaction with pyrene carboxylic acid. After the coupling reaction the polymer (**4c-pyr**) was purified and self-assembled by dialysis method in one step. Doxorubicin was added to one portion to encapsulate the drug. The blank and DOX-loaded fluorescence-labelled aggregates were diluted to 0.5 mg/mL for the cell uptake experiments and analyzed by DLS (Table 34).

*Table 34: Concentrations and hydrodynamic diameters of fluorescence-labelled polymersomes (**4c-pyr**) with and without encapsulated doxorubicin.*

Sample	c [mg/mL] after dialysis	c [mg/mL] for cell uptake	c [mg/mL] for DLS	d_H [nm]
Ncs214_ DMSO1	2.00	0.50	1.00	330
Ncs214_DOX1	2.00	0.50	1.00	460

Both samples resulted in homogeneous aqueous solutions of the polymer aggregates. As expected, the blank vesicles were colorless in solution, while the encapsulation of doxorubicin caused the pink coloration of the solution (Figure 86).

*Figure 86: Blank (left) and DOX-loaded (right) fluorescence-labelled polymersomes (**4c-pyr**) in aqueous solution.*

To confirm the successful incorporation of pyrene into the polymer and the encapsulation of doxorubicin, the fluorescence was measured of both samples at excitation wavelengths of 342 nm (A) and 480 nm (B) (Figure 87) in comparison to pyrene and doxorubicin in aqueous solution, respectively. The sample with the blank aggregates (Graph A, green) clearly showed the typical emission of pyrene monomers between 360-400 nm, as well as pyrene homo-excimer emission at 460 nm, while the DOX-loading indicated to cause the decrease of the pyrene monomer intensity (Graph A, pink). At an excitation wavelength of 480 nm, the fluorescence intensity of DOX was visible for the DOX-loaded aggregates (Graph B, pink), while the blank sample (Graph B, green) showed no fluorescence, as expected.

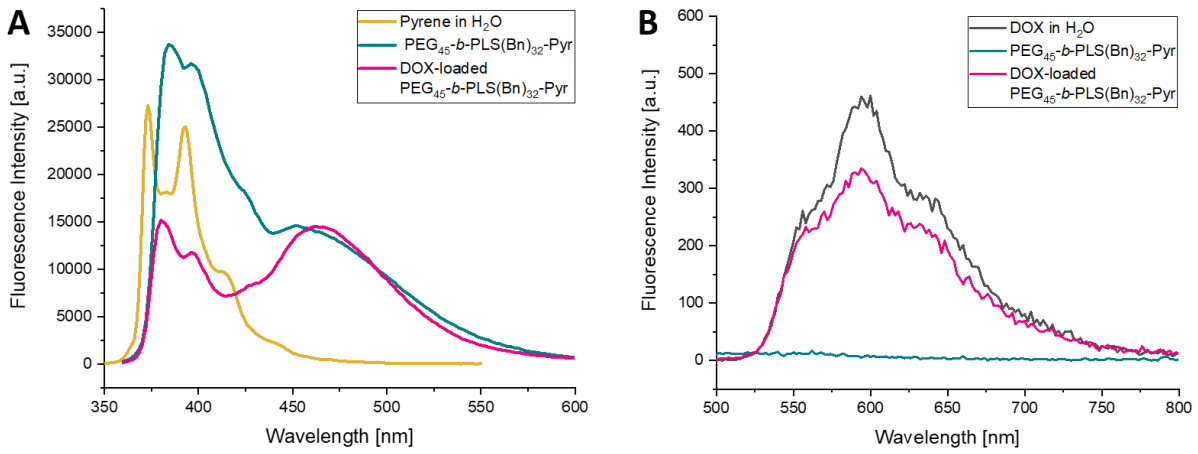

Figure 87: Fluorescence spectra of A) the blank and DOX-loaded pyrene-functionalized polymersomes in comparison to pyrene and B) in comparison to doxorubicin, in order to evaluate the successful end-functionalization of the pyrene and encapsulation of DOX.

The cell uptake experiment was conducted with the A549 human lung adenocarcinoma cell line with the fluorescence-labelled polymer PEG_{45}-*b*-$PLS(Bn)_{32}$-pyr (**4c-pyr**) that was self-assembled and drug-loaded with doxorubicin at a polymer concentration of 0.10 mg/mL (with 10wt% DOX) for 24 hours. The DOX control was used to visualize that pure DOX ws usually entering the cell and nuclei very fast and distributing over the whole cells. It was found that the blank vesicles tend to agglomerate in the cell medium, visible as bright blue dots in the fluorescence images below (Figure 88).

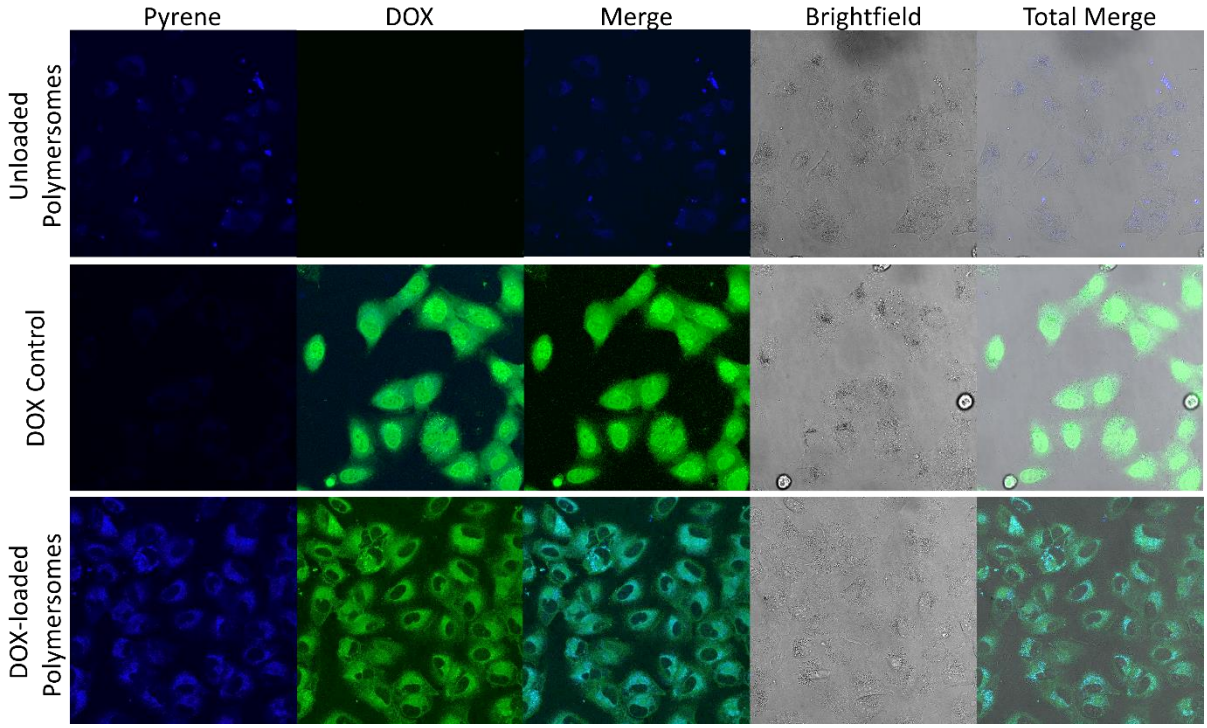

Figure 88: Cell uptake of blank and DOX-loaded aggregates with A549 cell line. Images were taken 24 h after incubation and at a polymer concentration of 0.10 mg/mL (performed by [redacted]).

The plain vesicles did not enter the cell nuclei at all, but were uptaken by the cells, if not agglomerated. In contrast, the drug-loaded aggregates showed lower agglomeration and were dispersed within the cells more homogeneously. The encapsulation of DOX in the polymersomes clearly changed the DOX distribution within the cells by preventing it to enter the cell nuclei after 24 hours of incubation, at which time the fluorescence images were recorded. This was indicating that the release of doxorubicin was very slow, compared to free DOX, or not happening at all within 24 hours. This was a good initial result, as it led to the conclusion that the vesicles were stable in the cell medium, if no trigger for the drug release was present. The drug-release may be addressed in a next step by incorporation of a trigger sequence into the polymer chain that is specifically cleaved by the conditions in the tumor environment to achieve controlled drug release. A potential system would be the beforementioned introduction of a peptide-sequence that is cleavable by the enzyme MMP-2, which is known to be overexpressed in certain tumor tissues.[26–28]

5.3 Summary and Outlook

Serine with its nonionic polar side chain is an interesting building block for the fabrication of polymeric materials as it is a naturally occurring molecule that is easily accessible, economical and functionalizable. The amphiphilic serine block copolymers that were discussed in this work, showed self-assembly in aqueous solution, opening a wide range of applications like biomedicine and drug delivery. The resulting vesicles showed good biocompatibility and stability in initial cell experiments (Figure 89, green part). Besides, interesting changes in aggregation behavior were observed, when the L-amino acid was replaced by the racemic mixture. In aqueous solution both, the L- and DL-serine based block copolymers showed good aggregation behavior and resulted in supramolecular structures. DL-serine based polymers showed lower cmc values that were independent of the block ratio. The L-serine analogues showed a linear correlation between hydrophobic block and increasing cmc values. The L-serine-based polymers showed slightly better performance in biological environment, as confirmed by cell viability tests. This indicated that following natural architectures was favorable. Nevertheless, the biocompatibility of both polymers, PEG-*b*-PLS(Bn) and PEG-*b*-PDLS(Bn), was confirmed, even at high polymer concentrations up to 250 µg/mL. Cell uptake experiments showed that the DOX-loaded vesicles were entering the cells. Compared to the free drug, the encapsulation of DOX into the PEG-*b*-PLS(Bn) assemblies resulted in very low to no DOX release within 24 hours of incubation, proving that the vesicles were stable during this time period. In addition, the encapsulation changed the distribution of DOX in the cells and prevented it to enter the cell nuclei. These results showed that this drug delivery system was able to enter the cells and remain stable for the given time period, if no trigger sequence for drug release was installed in the polymer.

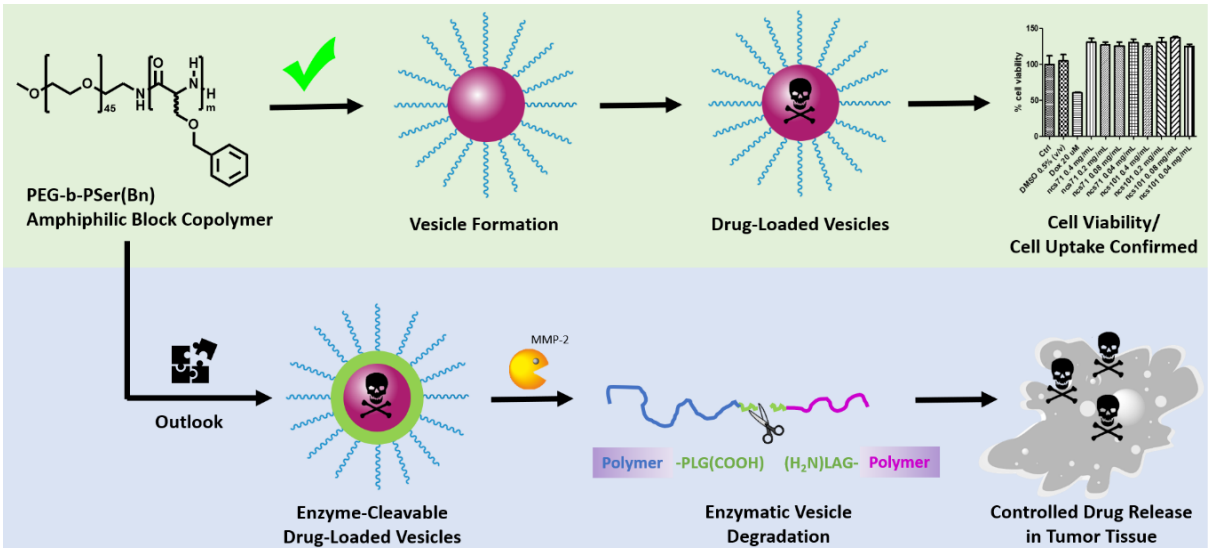

Figure 89: Formation of Drug-loaded vesicles with PEG-b-PSer(Bn) block copolymers was successful and cell viability and uptake experiments showed promising results for the next steps. Incorporation of an enzyme-cleavable sequence into the polymers is believed to result in controlled drug release by enzymatic vesicle degradation.

Overall, this was a promising result to build on, showing that this comparably simple drug delivery system was stable, if no trigger mechanism was incorporated into the polymer chain and bears the chance to build a potent carrier to safely deliver a drug into the tumor without drug leakage, followed by a controlled release of the drug at the target tissue. One possible approach for the introduction of a trigger-sequence is the use of an enzyme-cleavable peptide sequence that is built into the block copolymer. The peptide sequence PLGLAG is known to be specifically cleavable by the enzyme MMP-2 that is overexpressed in certain tumor tissue, while in healthy cells it is present in insignificant amounts.[26–28] If the drug delivery carrier is now equipped with this peptide sequence in the next step, it might be able to carry the drug safely into the tumor cell, where the MMP-2 will cleave the peptide and with it the polymer chain, resulting in collapse of the aggregates. The enzymatic degradation of the vesicle will then release the drug in the tumor tissue (Figure 89, blue part).

5.4 Experimental Part

MICELLE FORMATION

Micelle formation of PEG-*b*-PLS(Bn) and PEG-*b*-PDLS(Bn): Micelles were prepared by dialysis method. The block copolymer was dissolved in DMSO at a polymer concentration of c = 1-3 mg/mL with continuous stirring. The solution was dialyzed against MilliQ water for 24 h (MWCO = 1000 g/mol), while changing the water after 1, 2, 4 and 18 h. The resulting aqueous solution was transferred into a vial and ultrasonicated for 5 min. to form micelles of uniform size.

Formation of DOX-loaded micelles: 1.5 mg doxorubicin hydrochloride (1 eq) was dissolved in 1 mL DMSO and 3.5 µL triethylamine (10 eq) was added for neutralization of the molecule. 15 mg of polymer (weight ratio of DOX and polymer = 1:10) was dissolved in 4 mL DMSO and added to the first solution and transferred into a dialysis bag (MWCO = 1000 g/mol). The solution was dialyzed against MilliQ water for 24 h, while changing the water after 1, 2, 4 and 18 h. The resulting aqueous solution was transferred into a vial and ultrasonicated for 5 min. to form DOX-loaded micelles of uniform size.

Pyrene-functionalized micelles by end group functionalization of PEG-*b*-PLS(Bn) (4c-pyr): Pyrene carboxylic acid (1.6 mg, 63 µmol, 10 eq) was dissolved in 1 mL DMF. EDC x HCl (1.2 mg, 63 µmol, 10 eq) and DMAP (0.1 mg, 9 µmol, 1.5 eq) were added and stirred for 10 minutes at room temperature. PEG_{45}-*b*-$PLS(Bn)_{32}$ (5.0 mg) was dissolved in 1 mL DMSO and added to the first solution. The mixture was stirred for three days at room temperature. The mixture was transferred into a dialysis bag (MWCO = 1000 g/mol) and dialyzed against EtOH/MilliQ water for 6 h, changing the solvent 3x to remove excess reagents. Then, the resulting solution was divided into two portions, each with 2.5 mg polymer. One portion was diluted with 1 mL DMSO and dialyzed against MilliQ water to obtain plain micelles, while 1.3 mg Dox and 6 µL Et3N in 1 mL DMSO was added to the second, stirred for 10 minutes and dialyzed against MilliQ water overnight, too. The resulting aqueous solutions were transferred into vials and ultrasonicated for 5 min. to form plain and DOX-loaded micelles of uniform size.

CELL VIABILITY TESTS

Cell Culture: A549 Cells (German Collection of Microorganisms and Cell Cultures, Braunschweig) were cultured in high glucose DMEM supplemented with 10% FCS, 10% Penicillin/Streptomycin, 1% MEM non-essential amino acid at 37 °C/5% CO2. Passages of cells were made near confluency in a T-75 Flask following a standard trypsination protocol using Trypsin LE Express (ThermoFisher Scientific).

Cytotoxicity Assay: A549 cells (5000 cells/well) in a white 96-well (half-area) microplate and left to adhere overnight in an incubator at 37 °C/5% CO2. The cells were treated with the prescribed amount of polymers (0.05 – 0.2 mg/mL in DMEM) and were incubated for 24 h at 37 °C/5% CO2. The cell viability was subsequently tested using CellTiter-Glo® Luminescence Cell Viability Assay (Promega) according to manufacturer's protocol. Cells without treatment are referenced as blank and the data is represented as % cell viability. All measurements were performed in triplicates.

Cell Uptake: A549 cells are precultured in DMEM high glucose supplemented with 10% FBS and 1% penicillin/streptomycin. The cultures are passaged every 2-3 days at confluency and maintained between passages 3 - 20. The precultured cells were seeded at a density of 15.000 cells/well in an 8-well IBIDI confocal microscopy chamber and left to adhere overnight at 37 degrees Celsius, 5% CO2. The medium was aspirated and samples predissolved in DMEM were added into the wells. After incubation for 24 h, the cells were washed x3 with DMEM and imaged live using Leica SP5 confocal microscope with the following channels, pyrene (Ex. 400 nm, Em. 410 - 480 nm), Dox (Ex. 488 nm, Em. 500 - 650 nm).

6 Charged methacrylate-based terpolymers for the stabilization of gold nanoparticles in biological media

6.1 Introduction

Tailoring nanoparticles as drug delivery systems is of high interest due to the variety of possible applications. Consequently, there are numerous technologies and approaches.[2,3] Taking a deeper look at the chemical composition, nanoparticles can be divided into organic and inorganic nanoparticles. The previous chapters described organic nanoparticles for drug delivery applications, while this chapter is taking a deeper look on the advantages and challenges of inorganic nanoparticles in biomedical applications. Assuring the colloidal stability of nanoparticles in biological environment is a key factor to allow the delivery of the drug to the target tissue and avoid unwanted particle degradation.[57,64] Inorganic nanoparticles need to be stabilized in aqueous solution by organic monomers or polymers.[170] Biological media are consisting of a complex mixture of biomolecules that can interfere with the nanoparticles.[31] The particle stability and aggregation behaviour can be affected, for example by non-specific protein adsorption. Protein adsorption leads to the formation of a dynamic protein layer around the particles, known as protein corona. It is stabilized by protein-NP interactions that consist of protein-protein interactions and protein-NP binding affinities. [22,32]

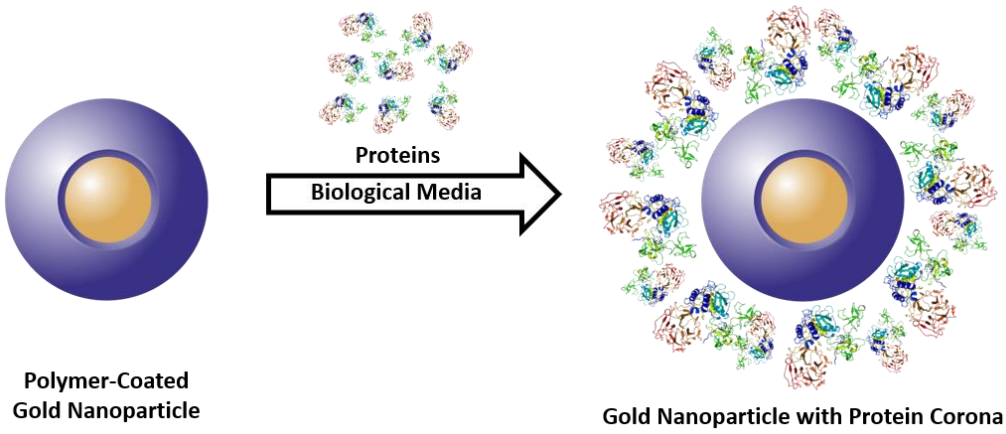

Scheme 41: Schematic representation of the protein corona formation around nanoparticles in biological environment.

Depending on the physicochemical properties and surface composition of the nanoparticles and nature of the proteins, the adsorption to the nanoparticle surface can affect the protein conformation.[171] This change can lead to altered properties of the NP-protein complex in comparison to the native protein and uncoated nanoparticle. It can impact the interaction of the NP-protein complex with the biological environment, influencing biological parameters like cell uptake, cytotoxicity and degradation of the nanoparticles.[65,172] Therefore, the surface interaction of nanoparticles with biomolecules needs to be understood to predict and adapt their behaviour in

physiological conditions. In order to prevent unwanted side effects, the interaction between particle surfaces and the biological medium should be minimized to suppress the formation of a protein corona. This can be achieved by modifying the nanoparticle surface with molecules that show low protein binding affinity.[22,32] Typically, non-ionic hydrophilic polymers are used for the nanoparticle coating.[7] The most prominent examples are polyethylene glycol derivatives (PEG) that are covalently attached to the particle surface.[173] This procedure is called PEGylation and was widely used over the last decades and became a standard procedure to prevent protein interactions.[90] The polymers have a shielding effect by formation of a hydration layer on the particle surface.[90,174] Nowadays, PEGylation is believed to be less effective than expected, as proteins are able to intrude into the PEG layer and influence the particle stability. [58,175]

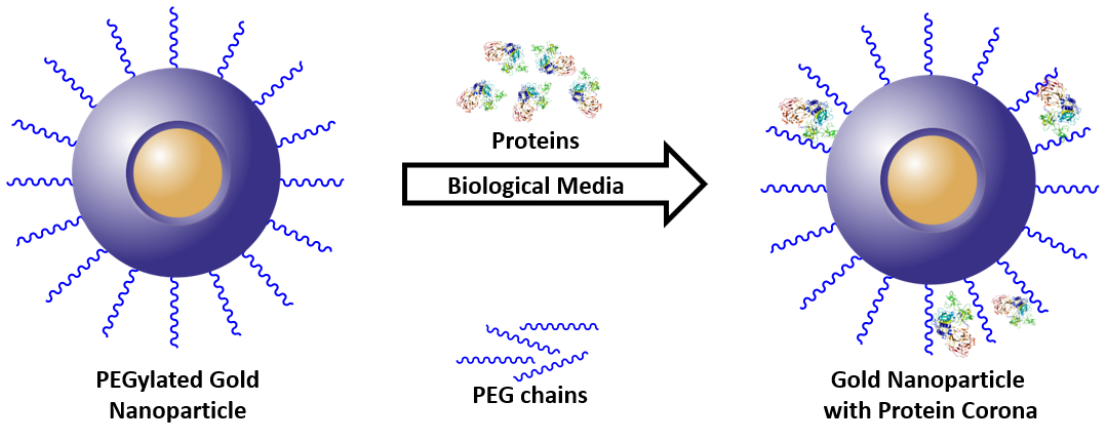

Scheme 42: Inhibition of protein corona formation in physiological media by PEGylation of nanoparticles.

Alternatives to hydrophilic non-ionic structures are zwitterionic materials that were shown to have anti-fouling properties against biomolecules like proteins, cells and bacteria.[176–178] Due to the two charged functional groups the water binding affinity is significantly increased in comparison to non-ionic polymers like PEG.[173] It was reported that zwitterionic nanoparticles showed longer blood-half life and lower accumulation in the liver and spleen due to their anti-fouling properties compared to their PEG-coated analogues.[179] While proteins can bind effectively to single-charged surfaces, they cannot adjust their quaternary structure to the charge distribution of zwitterionic surfaces, resulting in repulsion between the nanoparticles and proteins.[22,66,180] There are three possibilities to obtain a zwitterionic surface (Scheme 43). By coating the particles with a.) polymers consisting of zwitterionic monomers, b.) polymers containing the same molar ratio of positively negatively charged monomers or c.) by using a mix of positively and negatively charged polymers.[64] In this project, polymers with zwitterionic monomers to coat the nanoparticles were used (a.).

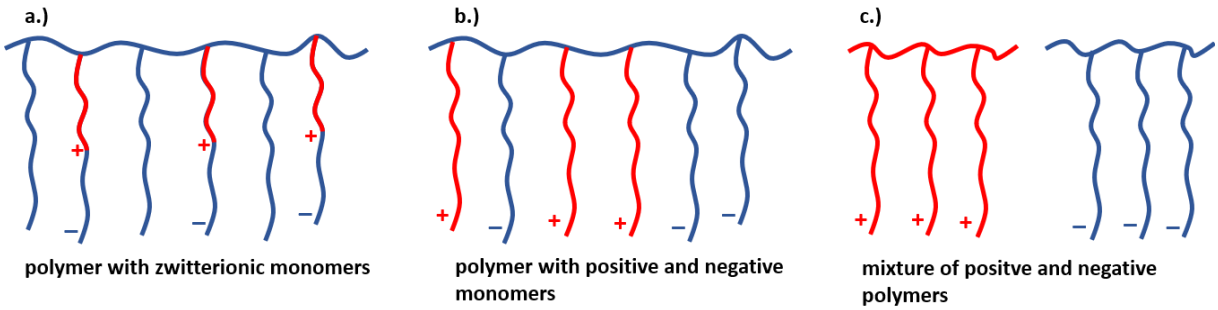

Scheme 43: Three different approaches of achieving a zwitterionic particle surface.

In contrast to zwitterionic surfaces that have a shielding effect towards biomolecules, single-charged materials show interactions with biomolecules like proteins. This is an unwanted side effect and not the only disadvantage of single-charged compared to zwitterionic surfaces.[66] A dispersion of nanoparticles coated with single-charged polymers in deionized water leads to significant increase of the hydrodynamic volume due to electrostatic repulsion of the charged functional groups in the polymer chain.[22,55] The interaction increases the distance between the charges, stabilizing the particles.[32,173] Addition of an electrolyte like sodium chloride weakens the repulsion and leads to aggregation, as the hydrodynamic volume is decreased by shrinking of the polymer chains.[173] In contrast, zwitterionic polymers interact with water molecules and promote the formation of a hydration layer around the particles in aqueous solution.[181] Addition of an electrolyte results in the expansion of the polymer chains, as the net attractive electrostatic interactions are shielded, resulting in increased polymer solubility and particle stabilization.[32,64] This effect was utilized in this project and the interaction of gold nanoparticles coated with zwitterionic polymers in comparison with positively and negatively charged polymers with physiological media was studied. The aim of this project was the fabrication of statistic methacrylic acid-based terpolymers containing charged side chains. These polymers were then used for the stabilization of inorganic gold nanoparticles in aqueous media. The structure of the polymers was inspired by previous works in our group in collaboration with the group of Prof. Dr. Wolfgang Parak. The terpolymers were consisting of three different methacrylate-based monomers (Figure 90).[22,55] The first monomer introduced the charged side chain into the polymer that was supposed to increase the nanoparticles solubility. The second monomer, lauryl methacrylate (LMA), was consisting of a long, nonpolar alkyl chain that contributed to the amphiphilicity of the polymer. The third monomer, propargyl methacrylate (PgMA), was used for the incorporation of an active compound, like a fluorescent dye, into the polymer to allow imaging of the particles in cell uptake experiments or alternatively, a biologically active compound like folic acid to incorporate a targeting unit into the nanoparticle.[182]

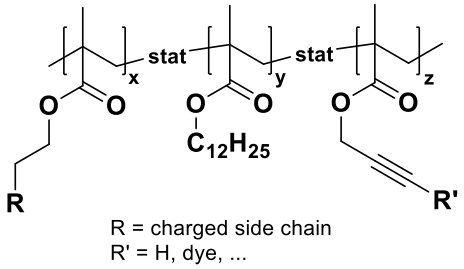

Figure 90: Chemical structure of the amphiphilic statistical terpolymers.

After synthesis, the polymers were used by our collaboration partners, the Parak group from university Hamburg, for the coating of inorganic gold nanoparticles (Scheme 44). The charged polymer side chains on the surface of the particles were supposed to increase their solubility in aqueous media. The influence of the charge density on the particle surface on the particle stability in biological environment was studied. A fluorescent dye was incorporated into the polymers to make the particles detectable in the cells. A set of experiments was performed to gain a deeper understanding of surface interactions of the nanoparticles with its environment.[22]

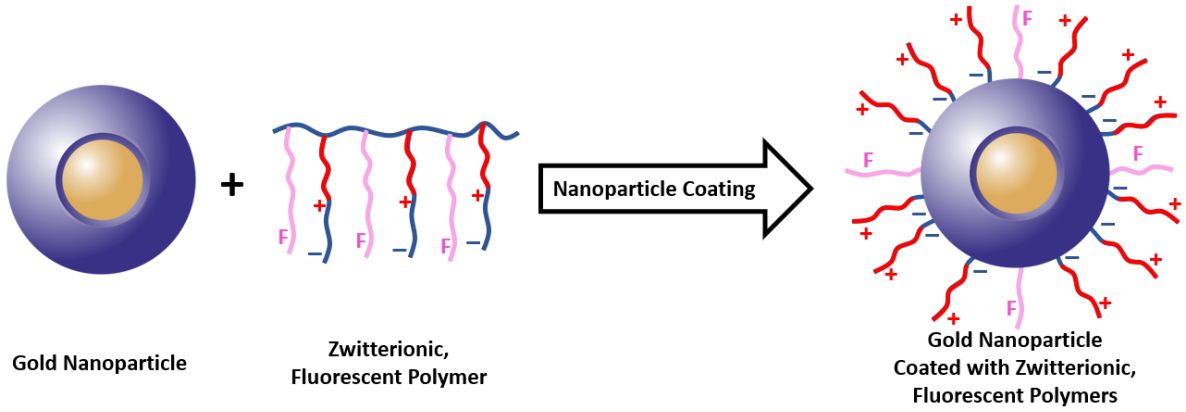

Scheme 44: Coating of inorganic gold nanoparticles with charged terpolymers.

Various polymers were synthesized by free radical polymerization, not only with different charges, but also with varying monomer ratios and molecular weight distribution.[22,55] The molecular weight distribution was controlled by the amount of radical initiator azobisisobutyronitrile (AIBN) and the chain transfer agent 2-mercaptoethanol (ME). The synthesized methacrylate-based polymers could be divided by their charge into four groups (Scheme 45). The polymers contained a positive, negative or zwitterionic charge. To create a positive charge the monomer 2-(trimethylamino)ethyl methacrylate (TMAEMA) was incorporated into the polymer. The negative charge was achieved by using the monomer methacryloyloxyethyl phosphoric acid (MAPHOS). Two different monomers were used to create zwitterionic polymers, 2-(dimethylamino)ethyl-sulfobetaine methacrylate (DMAEMASB) or 2-methacryloyloxyethyl phosphorylcholine (MPC). Not all of these monomers were used as the starting material in their charged form. Some were used as uncharged precursors, where the charge was

introduced by postsynthetic modification of the polymer. The positive charge of TMAEMA was obtained by methylation of 2-(dimethylamino)ethyl methacrylate (DMAEMA) with methyl iodide. The negative charge of MAPHOS was generated by saponification of the dimethyl phosphonate MAPHOSMe_2. The zwitterionic DMAEMASB was synthesized from DMAEMA and 1,3-propane sultone. The monomer MPC was used for the polymerization as received with its zwitterionic structure. The synthetic details are discussed in the following chapter.

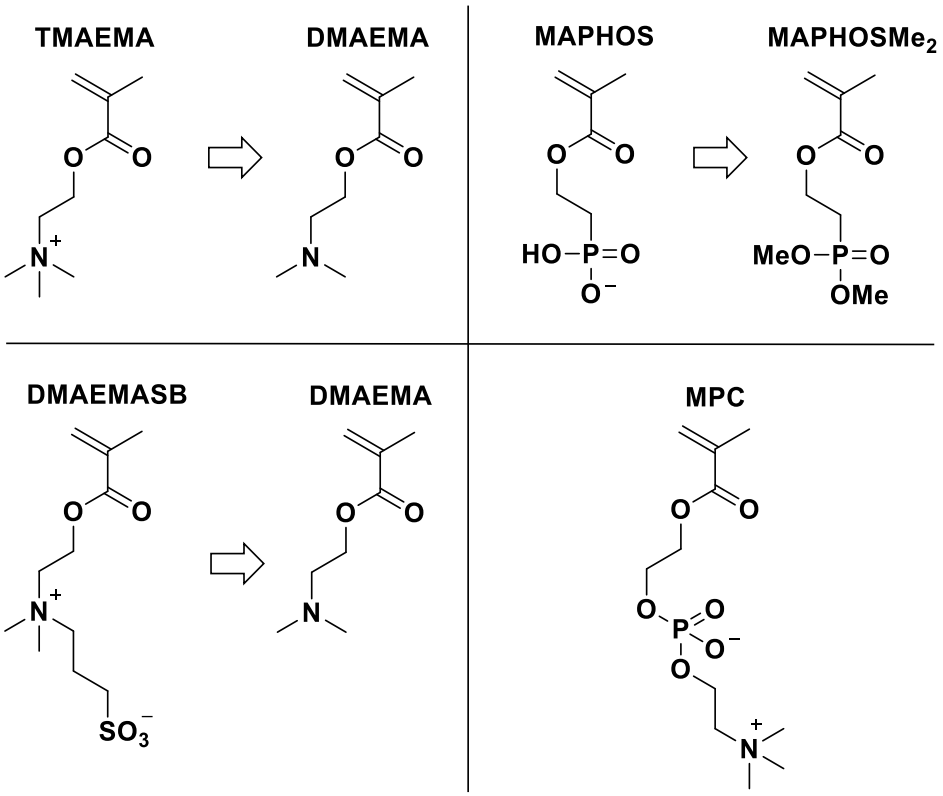

Scheme 45: Methacrylic acid-based monomers containing a positive, negative or zwitterionic charge.

6.2 Results and Discussion

The synthesis of charged amphiphilic copolymers *via* free radical polymerization and their use for the coating of Au NPs was performed in a collaboration with the research group of Prof. Dr. Wolfgang Parak (University Hamburg), resulting in polymer-coated charged Au-NPs with good colloidal stability in aqueous media. Previous projects from this collaboration already built a solid basis on the understanding of charged inorganic nanoparticles in biological environment.[22,59,170] The aim of this project was to gain a deeper understanding of the interactions between charged surfaces of nanoparticles with surrounding electrolytes and biomolecules that are present in physiological media. Special interest was lying on the antifouling properties of zwitterionic particles in such environment. The synthesis of the polymers was performed by our group and will be discussed below. A predefined set of polymers was synthesized, not only with different charges, but also with varying monomer ratios and molecular weight distribution in order to determine, whether the amphiphilicity and charge density of the polymers have an impact on the nanoparticle stability. This was challenging at the beginning, as reproduction of the reactions reported in literature was not successful.[22,55] The right molecular weights were not obtained, when following the reported experimental procedures.[22,59] There was no linear correlation observed between the amount of initiator or chain transfer agent and chain-growth and therefore, a 1:1 scale-up of the reaction was not possible. In addition, the original scale of the polymerizations was very small.[22] Consequently, the required amounts of reagents were difficult to keep constant. Inaccuracies in the initial weight of added reagents were leading to significant differences in the molecular weight distribution of the resulting polymers. The right reagent ratios needed to be determined empirically. Nevertheless, after scale-up of the reaction and the use of stock solutions for critical reagents, the inaccuracies were minimized and after some adjustments, the controllability of the molecular weight improved. Eventually, methacrylic acid-based polymers of defined molecular weight and block ratio were obtained and further functionalized by postsynthetic modification to introduce different charges into the polymer side chains, as described before in Scheme 45.

6.2.1 Negatively charged PMA-based terpolymers

SYNTHESIS OF PMA-BASED TERPOLYMERS BY RADICAL POLYMERIZATION

All fabricated polymers in this chapter were synthesized by free radical polymerization and consisted of three monomers. The first monomer determined the charge that was introduced post-synthetically and formed the polar moiety. It was exchanged, depending on the desired charge. The second monomer, LMA, was the nonpolar moiety of the polymer with its alkyl chain. The third block consisted of the alkyne-containing propargyl methacrylate that allowed postsynthetic modification with a dye or targeting unit by click reaction. Eventually, the negative charge was formed by saponification of the

phosphoric acid methyl ester in the MAPHOS side chain. The negatively charged terpolymers (**42,43**) were obtained with an overall yield of up to 52% over three steps (Scheme 46).

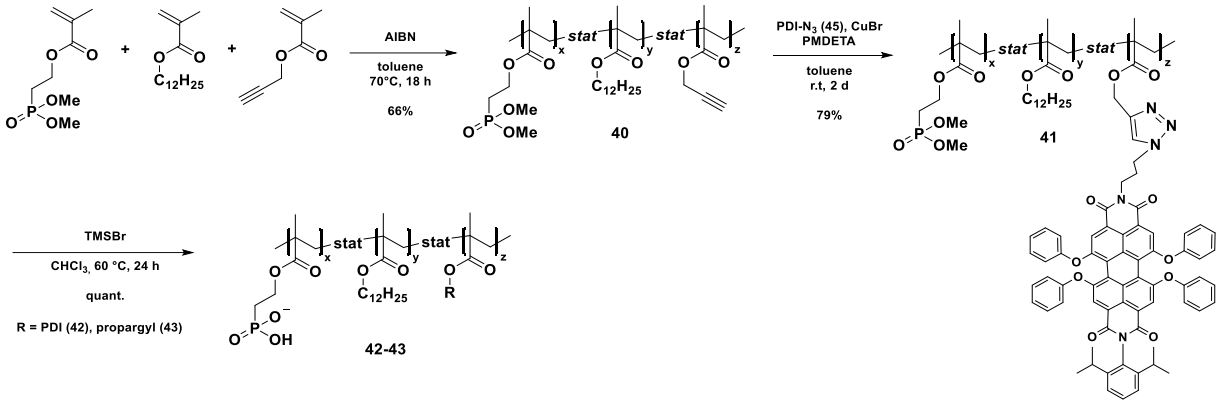

*Scheme 46: Synthesis overview of negatively charged (dye-labelled) terpolymers (**42,43**).*

The first PMA-based polymers that were synthesized were PMAPHOS(Me)$_2$-*stat*-PLMA-*stat*-PPgMa terpolymers (**40**) to create negatively charged materials. The first approach was performed, aiming a molecular weight distribution of 10 kDa and a block ratio of 52:42:6. The reaction was conducted by dissolving all monomers in toluene and using the radical initiator AIBN at 70°C. The first polymer **40a** was obtained with a yield of 66% (Scheme 47).

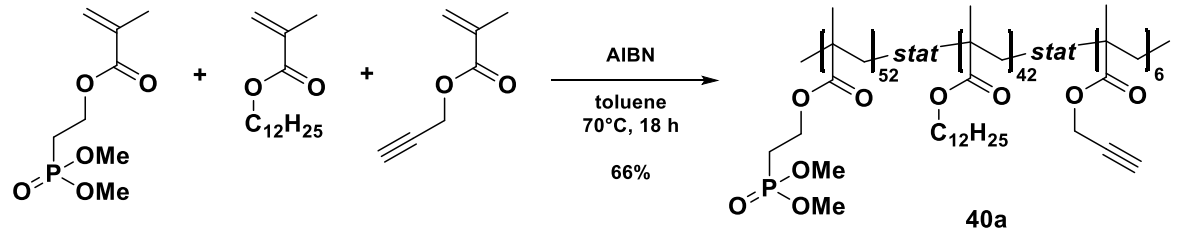

Scheme 47: Synthesis of PMAPHOS(Me)$_2$-stat-PLMA-stat-PPgMA by radical polymerization.

The obtained statistic terpolymer **40a** was characterised by GPC analysis and NMR spectroscopy to determine the block ratio and molecular weight distribution. First, the polymer was analysed by GPC, resulting in a molecular weight distribution of M_w = 6700 g/mol (against PMMA in THF) and a polydispersity of Đ = 1.63 (Table 35, **40a**). The desired molecular weight of around 10 kDa was not reached. The ^{1}H-NMR showed that the polymer was synthesized and purified successfully by displaying all expected proton signals (Figure 91). The calculation of the polymer block ratio was performed from the signal intensity ratio of the CH_2-signals in the proton NMR and resulted in a ratio of 48:44:8 (MAPHOS(Me)$_2$:LMA:PgMA). The block ratio of 52:42:6 was almost reached, but after calculating the molar ratios for the dye-labelling reaction, the ratio of the PgMA-block was considered too high for further modification. A large amount of dye would have been needed for the reaction that was not available in high quantities due to its complex synthesis. Consequently, this polymer was not used for

further modifications and another approach was performed to obtain a polymer with a lower ratio of the propargyl methacrylate block.

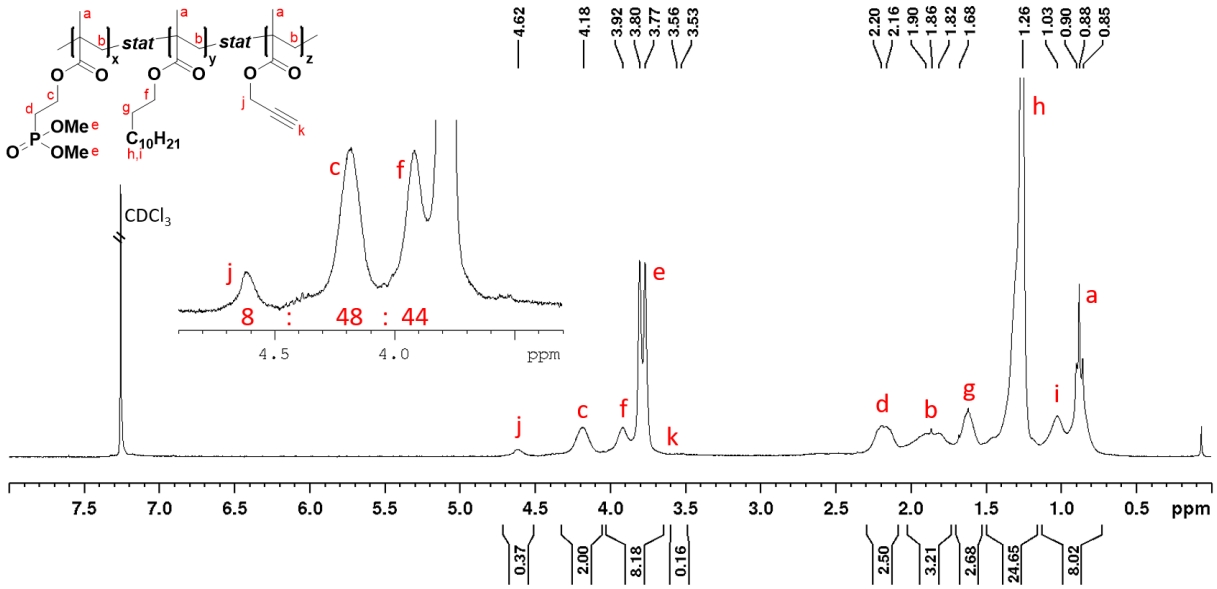

*Figure 91: ^{1}H-NMR spectrum (700 MHz, 300 K, $CDCl_3$) of PMAPHOS(Me)$_2$-stat-PLMA-stat-PPgMA (**40a**) and calculation of the black ratio from signal intensities.*

The second polymer synthesis was conducted under similar conditions. The same radical initiator AIBN was used, but this time the amount was reduced from 0.025 to 0.010 eq. In addition, 0.05 eq of the chain transfer reagent 2-mercaptoethanol was used to reach a higher molecular weight. The final polymer **40b** was obtained with a yield of 86% and was analysed by GPC and NMR spectroscopy (Table 35, **40b**). GPC analysis resulted in a molecular weight distribution of M_w = 16 200 Da, showing that decreasing the initiator and adding a chain transfer agent resulted in higher molecular weight, as expected. The block ratio was calculated from the signal intensities in the proton NMR spectrum and resulted in a ratio of 56:41:3, which was very close to the desired ratio of 52:43:6. Even though the molecular weight was significantly higher than the desired 10 kDa, it was decided that the polymer will be used for further modification, as the block ratio was considered the more important property to meet. Another three polymerizations were conducted to achieve higher and lower weight distributions. In the next approach (Table 35, **40c**) the amount of initiator was increased from 0.01 to 0.02 eq and the chain transfer agent was reduced from 0.05 to 0.02 eq, resulting in a molecular weight of 41 kDa. Further increase of the initiator to 0.03 eq and omitting the chain transfer agent led to slightly decreased molecular weight of 31 kDa (Table 35, **40d**), while addition of 0.05 eq of the chain transfer agent decreased the molecular weight significantly to 11 kDa (Table 35, **40e**). The desired block ratio of **40e** was almost achieved, but the molar ratios of **40c** and **40d** were not reached at all. A high polar moiety was desired, while the obtained polymers had a dominant nonpolar block, according to the proton NMR analysis. Consequently, the last polymer **40e** was used for further modifications,

while the other two with higher weights (**40c**-**d**) were discarded, considering them as unsuitable for the biological experiments after consultation of our collaboration partners. Overall, determining the right molar ratios of the reagents was performed empirically. The desired block ratio was achieved in most cases, according to the calculations from the proton NMR spectra of the polymers.

Table 35: Overview of the synthesized amphiphilic terpolymers with desired and obtained mass average molecular weight (M_w), the block ratio of the monomers and amounts of AIBN and ME used in the polymerization.

No.	Polymer	x:y:z[1]/ x:y:z[2]	AIBN (eq)	ME (eq)	M_w (target) [Da]	M_w (GPC)[3] [Da]
40a	PMAPHOS(Me)$_2$-*stat*-PLMA-*stat*-PPgMA	52:42:6/ 48:44:8	0.025	-	9500	6700 (THF)
40b	PMAPHOS(Me)$_2$-*stat*-PLMA-*stat*-PPgMA	52:42:6/ 57:41:2	0.01	0.05	9500	16200 (DMF)
40c	PMAPHOS(Me)$_2$-*stat*-PLMA-*stat*-PPgMA	54:44:2/ 38:61:1	0.02	0.02	9500	41 000 (DMF)
40d	PMAPHOS(Me)$_2$-*stat*-PLMA-*stat*-PPgMA	54:44:2/ 46:52:2	0.03	-	9500	31 000 (THF)
40e	PMAPHOS(Me)$_2$-*stat*-PLMA-*stat*-PPgMA	53:43:4/ 56:41:3	0.03	0.05	9500	11 000 (THF)

[1] monomer ratio, target block ratio [2] block ratio, calculated from ^{1}H-NMR [3] against PMMA standard

POSTSYNTHETIC DYE-LABELLING VIA CLICK REACTION

One sample of each polymer that was chosen to be tested in biological environment was dye-labelled in the next step. Therefore, a perylene diimide-based fluorescence dye (PDI) was selected that was developed in the Müllen group.[183] It was attached to the polymer via click reaction. To enable the click reaction, perylene diimide was converted to a mono azide (**44**, PDI-N_3) in two synthesis steps (Scheme 48, prepared by [redacted]). The azide was introduced subsequently by stirring the mono imide with 3-azido-1-propanamine at 70 °C. After two days, the final product PDI-N_3 (**45**) was obtained with a yield of 88%.

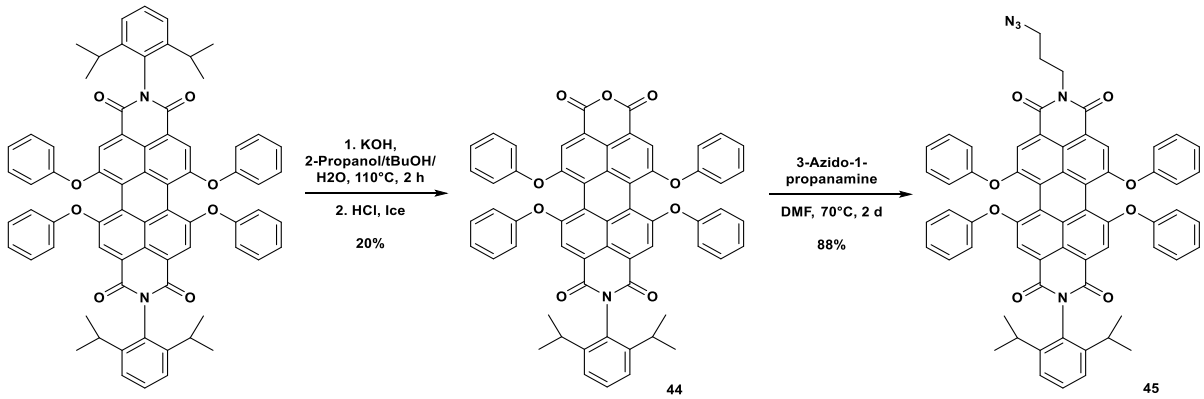

*Scheme 48: Two-step synthesis of the fluorescent dye PDI-N_3 (**45**).*

The final azide-containing dye PDI-N_3 (**45**) was analysed by proton NMR spectroscopy (Figure 92). All protons of the molecule were identified in the spectrum with the expected signal intensities. Remarkable for this dye are the numerous protons in the aromatic region between 7.00-7.50 ppm and at 8.15 ppm. These signals were used as a reference in the following click reaction. The success of the azide-introduction was displayed by the signals at 4.19 ppm (d), 3.38 ppm (f) and 1.96 ppm (e) that were the signals of the propyl chain between the imide and azide.

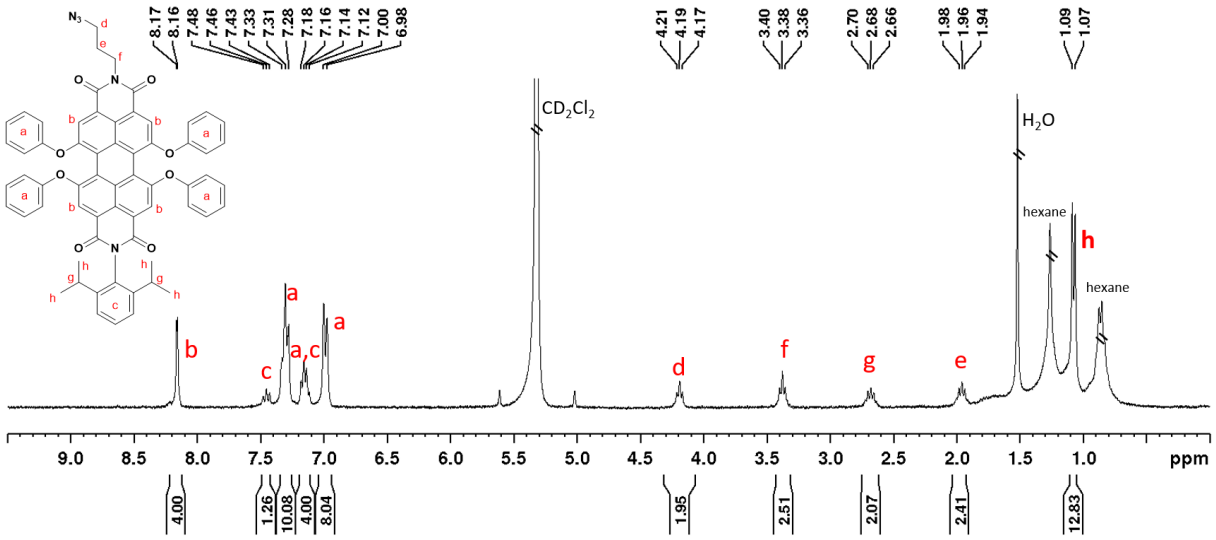

*Figure 92: ^{1}H-NMR spectrum (700 MHz, 300 K, CD_2Cl_2) of azide-modified fluorescent dye PDI-N_3 (**45**).*

The polymer PMAPHOS(Me)$_2$-*stat*-PLMA-*stat*-PPgMa (**40**) was modified with the fluorescent dye PDI-N_3 (**45**) via click reaction by using the catalyst copper(I) bromide and the ligand pentamethyldiethylentriamine (PMDETA).[183] The reaction was taking place between the alkyne in the PgMA side chain and the azide of the dye PDI-N_3, resulting in the formation of a triazole. The product PMAPHOS(Me)$_2$-*stat*-PLMA-*stat*-PDI (**41**) was obtained with a yield of 79% after 2 days of stirring at room temperature (Scheme 49).

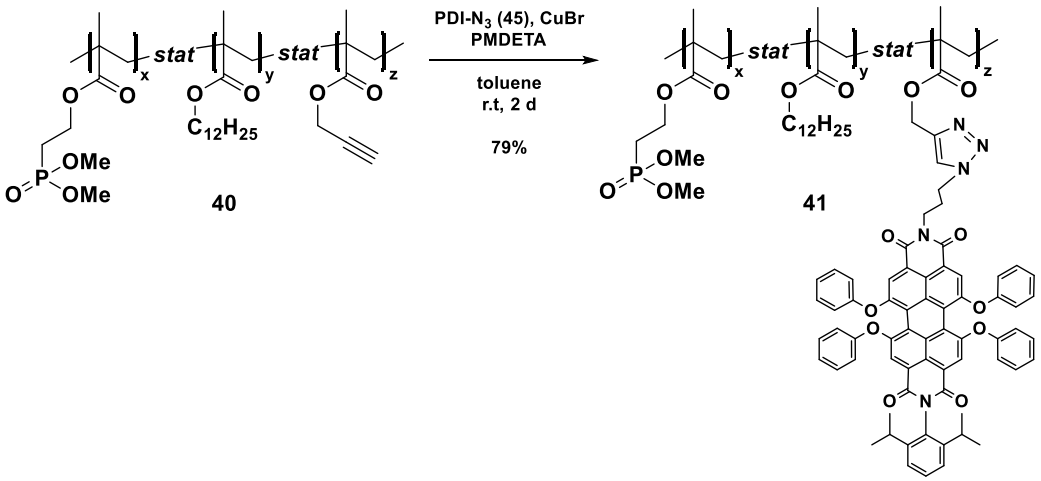

Scheme 49: Dye-labelling of PMAPHOS(Me)$_2$-stat-PLMA-stat-PPgMA by click reaction to PMAPHOS(Me)$_2$-stat-PLMA-stat-PDI.

After the next step, the saponification, the dye-labelled polymer **42** was analysed by DOSY-NMR spectroscopy to confirm the covalent attachment of the fluorescent tag (Figure 93). All signals of the dye (PDI) and polymer (a-j) showed the same diffusion constant, represented by the red line, indicating that the dye-labelling was successful.

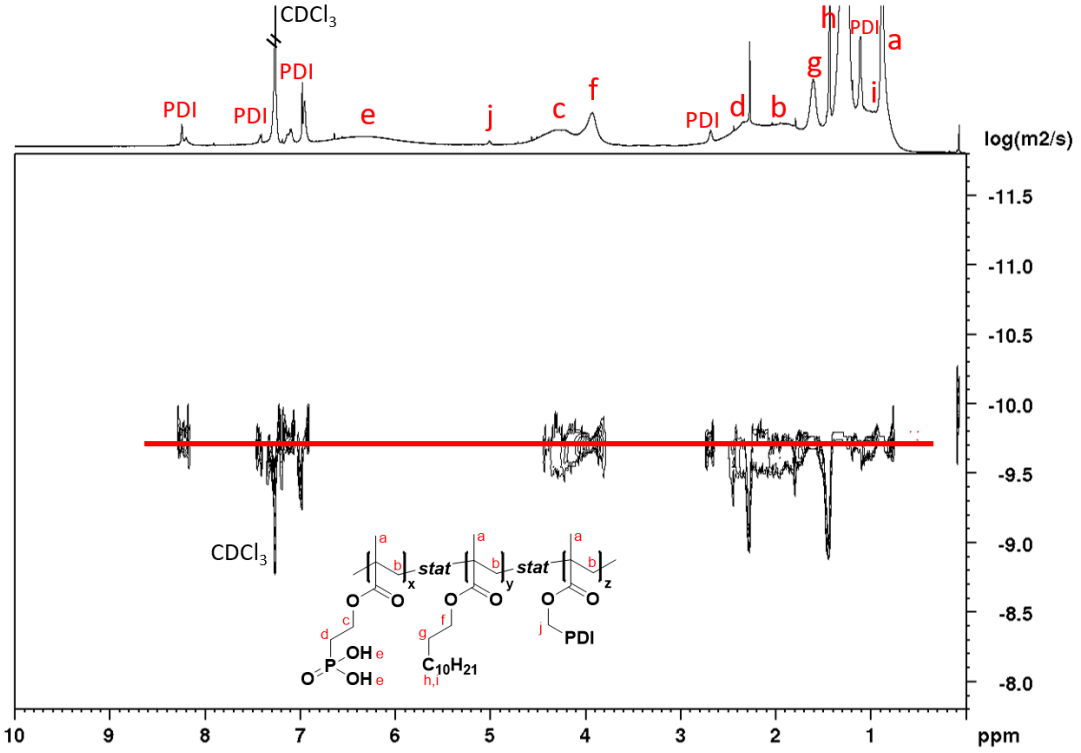

*Figure 93: DOSY spectrums (700 MHz, 300 K, $CDCl_3$) of dye-labelled terpolymer PMAPHOS(Me)$_2$-stat-PLMA-stat-PDI (**42**).*

FORMATION OF THE NEGATIVELY CHARGED TERPOLYMER

The next step after dye-labelling of the terpolymer **41** was the formation of the charge in the polymer side chain.[55] Therefore, the phosphate diester in the MAPHOS side chain was treated with trimethylsilyl bromide to saponify the ester groups, leading to the formation of the negatively charged phosphate salt. The charged polymer **42** was obtained with 74% yield after 24 hours (Scheme 50).

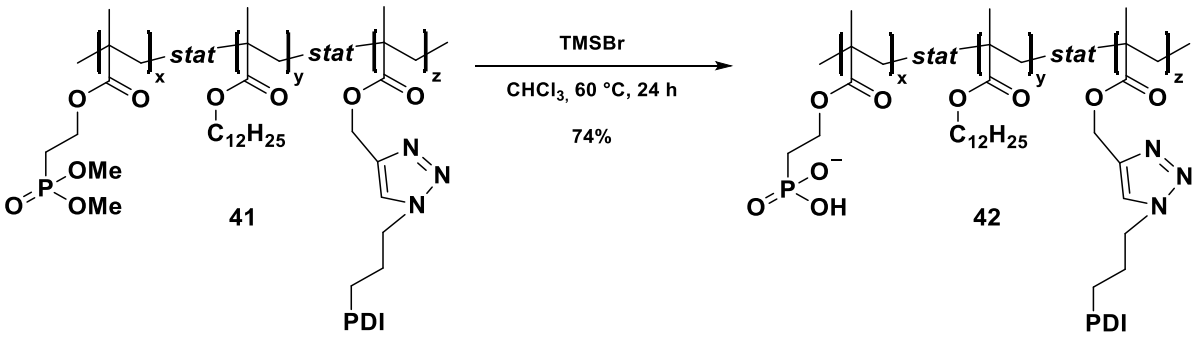

Scheme 50: Formation of the negative charge by saponification of the MAPHOS(Me)$_2$ side chain of the dye-labelled polymer.

At the same time, the unlabelled polymer **40** was treated the same way to saponify the ester groups and form the negative charge in the MAPHOS side chain. The terpolymer **43** with the negatively charged phosphate salt was obtained with quantitative yield after 24 hours at 60 °C (Scheme 51). It was used as a control unit in the subsequent nanoparticle coating and biological studies to ensure that the fluorescent dye has no influence on the protein-interaction of the charged nanoparticle surface.

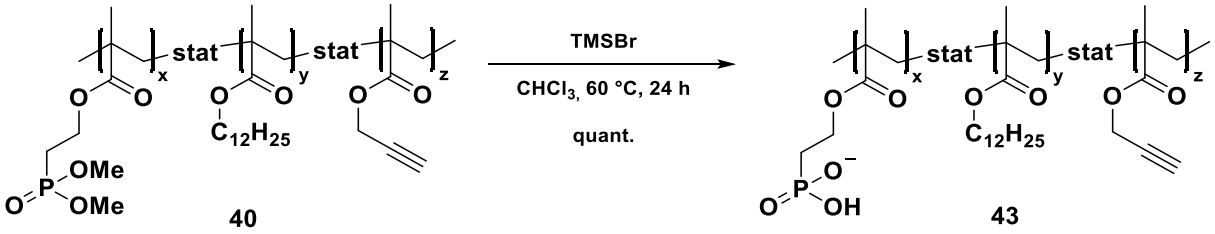

Scheme 51: Formation of the negative charge by saponification of the MAPHOS(Me)$_2$ side chain of the unlabelled polymer.

All negatively charged polymers that were synthesized and sent to the Parak group for further treatment are summarized in Table 36. While the dye-labelling was performed only once for further imaging studies, the unlabelled, negatively charged polymer was synthesized several times to perform and reproduce a set of experiments. All negatively charged polymers had a block ratio of 56:41:3 and a molecular weight distribution of 11 kDa.

*Table 36: Overview of the fabricated negatively charged terpolymers **42-43** with and without the fluorescent tag.*

Sample (pma)	Polymer	x:y:z[1]	Dye-label	M_w[2] [Da]
32	PMAPHOS-*stat*-PLMA-*stat*-PDI (**42**)	56:41:3	Yes	11000
33, 40, 45, 49	PMAPHOS-*stat*-PLMA-*stat*-PPgMA (**43**)	56:41:3	no	11000

[1] block ratio, calculated from ^{1}H-NMR [2] against PMMA standard

All synthesis steps were monitored by proton NMR spectroscopy and compared with each other (Figure 94). The spectrum of the polymer **40** after the polymerization (Figure 94A) showed clearly that all expected signals of the three blocks MAPHOS(Me)$_2$, LMA and PgMA were present, allowing the calculation of the block ratio of 56:41:3 from the signal intensity ratio. After dye-labelling the spectrum of the modified polymer **41** (B) showed the signals of the PDI-dye, especially in the aromatic region between 6.50 and 8.50 ppm, as expected. There were two additional PDI-signals visible at 2.68 and 1.11 ppm, while the remaining signals were overlapping with the polymer signals. Combined with the DOSY spectrum, this indicated the successful dye-labelling of the polymer. The last step was the formation of the negative charge in the MAPHOS side chain of both, unlabelled (**43**) and dye-labelled (**42**) polymers. The saponification of the phosphonate ester groups was confirmed by the disappearance of the methoxy signal at 3.78 ppm (signal e, spectrum C: dye-labelled; spectrum D: unlabelled). The broadening of the methylene signals at 3.70-4.70 ppm was ascribed to the negative

charge in the MAPHOS side chain, resulting in a changing solution behaviour of the polymer. In conclusion, the negatively charged and dye-labelled terpolymers **42-43** were successfully obtained, as confirmed by proton NMR spectroscopy.

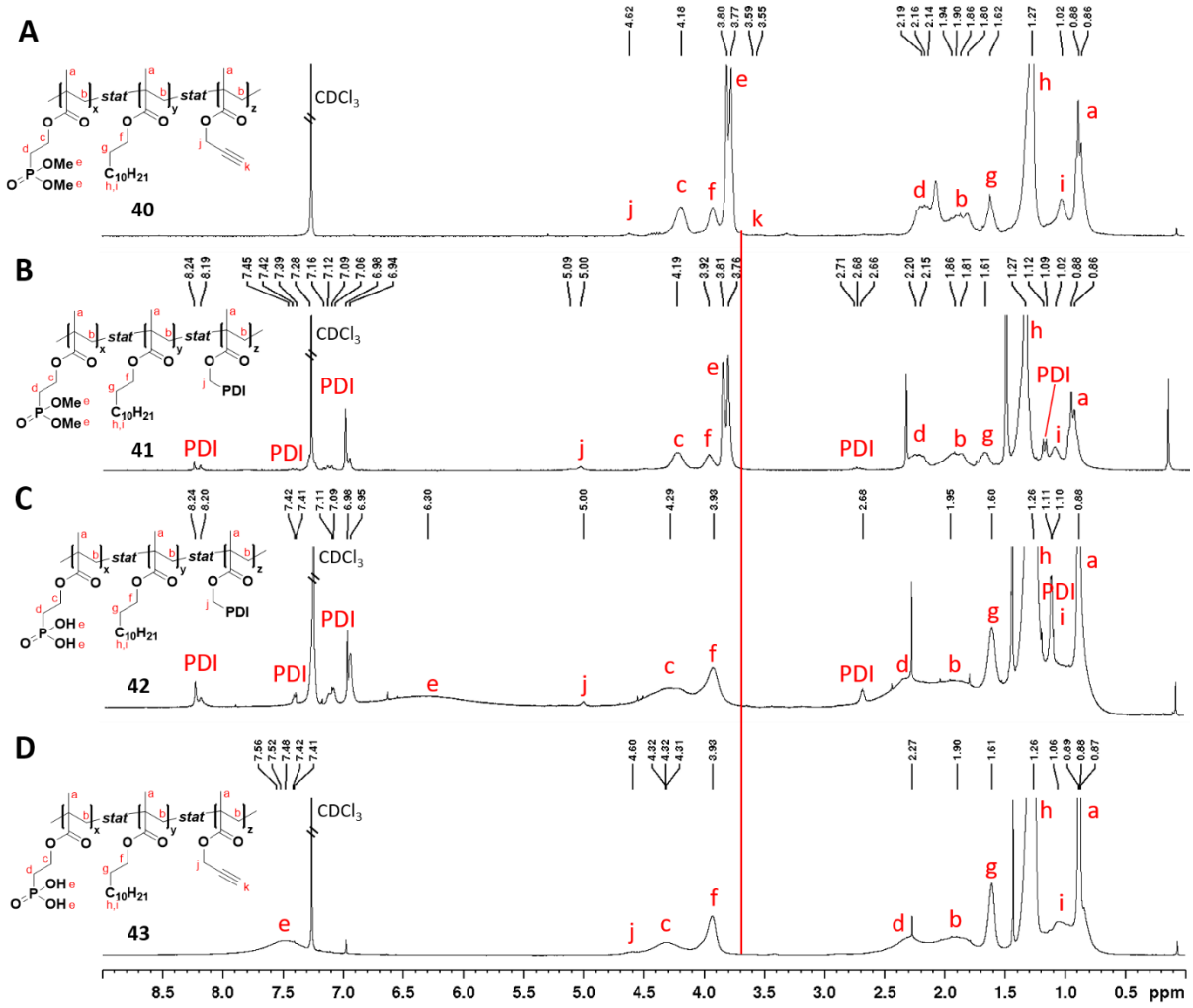

Figure 94: ^{1}H-NMR spectra (700 MHz, 300 K, $CDCl_3$) of the MAPHOS-based terpolymer after synthesis (A), after dye-labelling (B) and after formation of the negative charge (C, dye-labelled; D, without dye).

6.2.2 Positively charged PMA-based terpolymers

SYNTHESIS OF PMA-BASED TERPOLYMERS BY RADICAL POLYMERIZATION

The positively charged polymers were synthesized by free radical polymerization and consisted of three monomers. The first monomer was 2-(dimethylamino)ethyl methacrylate (DMAEMA) and it was used as the polar block by introducing the positive charge by quaternization of the amine in the side chain. The second monomer, LMA, was the nonpolar moiety of the polymer with its alkyl chain and the third block consisted of the alkyne-containing propargyl methacrylate that allowed postsynthetic modification with a dye or targeting unit by click reaction. The positive charge was formed by methylation of the amine in the DMAEMA side chain.[22] The positively charged terpolymers **48-49** were obtained with an overall yield of up to 62% over three steps (Scheme 52).

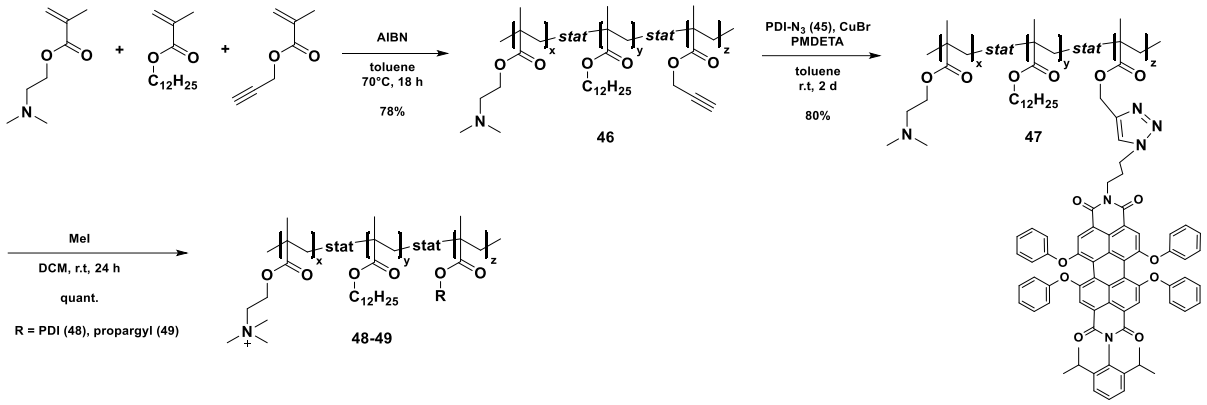

*Scheme 52: Synthesis overview of positively charged (dye-labelled) terpolymers **48-49**.*

In the first step, the polymerization of the terpolymers was conducted. The monomers DMAEMA, LMA and PgMA were used in the presence of the radical initiator AIBN and the chain transfer reagent ME at 70 °C (Scheme 53). After 18 hours, the terpolymer PDMAEMA-*stat*-PLMA-*stat*-PPgMA (**46a**) was obtained with a yield of up to 78%. Several polymers (**46a-e**) were synthesized under these conditions to obtain different block ratios and molecular weights.

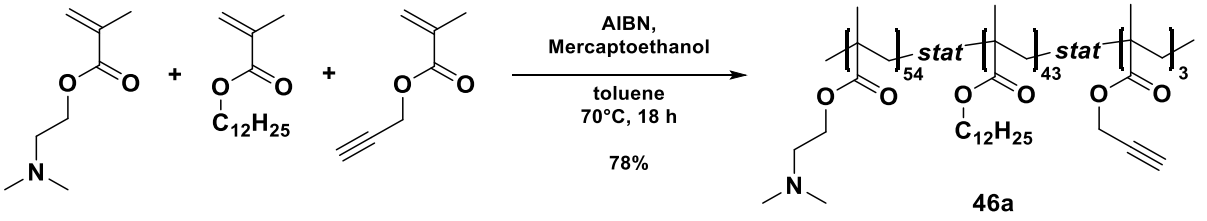

*Scheme 53: Synthesis of PDMAEMA-stat-PLMA-stat-PPgMA (**46a**) by radical polymerization.*

The polymer **46a** was analysed by GPC and NMR spectroscopy. The molecular weight was M_w = 7200 Da in the first approach with a polydispersity of Đ = 1.30. The target weight of 11000 Da was not achieved in this first approach. Then, the polymer was analysed *via* proton NMR spectroscopy.

The block ratio was calculated from the signal intensities of the CH_2-signals in the polymer side chains and resulted in a ratio of 54:42:3 (DMAEMA:LMA:PgMA). It was matching the initial monomer feed ratio of 52:46:4. The polymerization was repeated with different monomer and initiator ratios to achieve different molecular weights and block ratios (Table 37). The ratios of polar and nonpolar blocks were varied to investigate the influence of the charge density in the polymer on the nanoparticle surface in biological environment. The ratio of the PgMA block was supposed to stay below 5 to allow low consumption of the fluorescent dye that could only be synthesized with low yields. In a second approach, the desired molecular weight was 7000 Da at the same monomer ratio of 52:46:4 (**46b**). The polymer was obtained with a molecular weight distribution of 7200 Da and a block ratio of 57:40:3. Both values were matching the theoretical values. The target weight of 11000 Da was not achieved in the first approach and therefore, another reaction was performed with 50% less initiator AIBN and the same amount of chain transfer reagent ME, in order to achieve less chain initiations, but longer chains instead. The GPC analysis resulted in a slightly increased molecular weight of 8100 Da (**46c**) compared to the first approach (**46a**), but the target value of 11 000 Da was not reached. The next approach (**46d**) was performed with more AIBN, 0.03 eq, but no ME and resulted in a M_w of 15600 Da, according to GPC, which was close to the desired value of 17800 Da. The block ratio of 48:48:2 was perfectly met, as calculated by the signal intensities in the proton NMR. In the last approach (**46e**) a polymer with a significantly lower molecular weight and very high polar moiety and a block ratio of 62:36:2 was aimed. The resulting polymer was obtained with a M_w of 3900. The target block ratio was achieved by increasing the amount of initiator (0.05 eq). In conclusion, a handful of different polymers was fabricated with differing molecular weight distributions and block ratios that were further modified in the next steps.

*Table 37: Overview of the synthesized amphiphilic terpolymers **46** with desired and obtained mass average molecular weight (M_w), the block ratio of the monomers and amounts of AIBN and ME used in the polymerization.*

No.	Polymer	x:y:z[1]/ x:y:z[2]	AIBN (eq)	ME (eq)	M_w (target) [Da]	M_w (GPC)[3] [Da]
46a	PDMAEMA-*stat*-PLMA-*stat*-PPgMA	52:46:4/ 54:43:3	0.010	0.05	11000	7200 (DMF)
46b	PDMAEMA-*stat*-PLMA-*stat*-PPgMA	52:46:4/ 57:40:3	0.020	0.05	7000	7100 (THF)
46c	PDMAEMA-*stat*-PLMA-*stat*-PPgMA	48:48:4/ 50:46:4	0.005	0.05	11000	8100 (DMF)
46d	PDMAEMA-*stat*-PLMA-*stat*-PPgMA	48:48:4/ 48:48:4	0.03	-	17800	15600 (THF)
46e	PDMAEMA-*stat*-PLMA-*stat*-PPgMA	62:36:2/ 62:36:2	0.05	0.05	4700	3900 (THF)

[1] monomer ratio, target block ratio [2] block ratio, calculated from ^{1}H-NMR [3] against PMMA standard

POSTSYNTHETIC DYE-LABELLING VIA CLICK REACTION

The next step was the dye-labelling of the polymer (**46a,d**) by click reaction to insert a fluorescent tag.[183] Two polymers with similar block ratios and differing molecular weight distributions of 7200 Da (**47a**) and 15600 Da (**47b**) were dye-labelled before introduction of the positive charge (Table 38). These fluorescent materials were synthesized to visualize the nanoparticles in biological environment.

*Table 38: Overview of the fabricated dye-labelled PDMAEMA-based terpolymers **47**.*

No.	Polymer	x:y:z[1]	M_w[2] [Da]	Yield [%]
47a	PDMAEMA-*stat*-PLMA-*stat*-PDI	54:43:3	7200	80
47b	PDMAEMA-*stat*-PLMA-*stat*-PDI	48:48:4	15600	quant.

[1] block ratio, calculated from ^{1}H-NMR [2] against PMMA standard

The reaction was taking place between the alkyne in the PgMA side chain and the azide of the dye PDI-N_3, resulting in the formation of a triazole (Scheme 54). The reaction was catalysed by copper(I) bromide and after two days the dye-labelled polymer **47** was obtained with a yield of 80-100%.

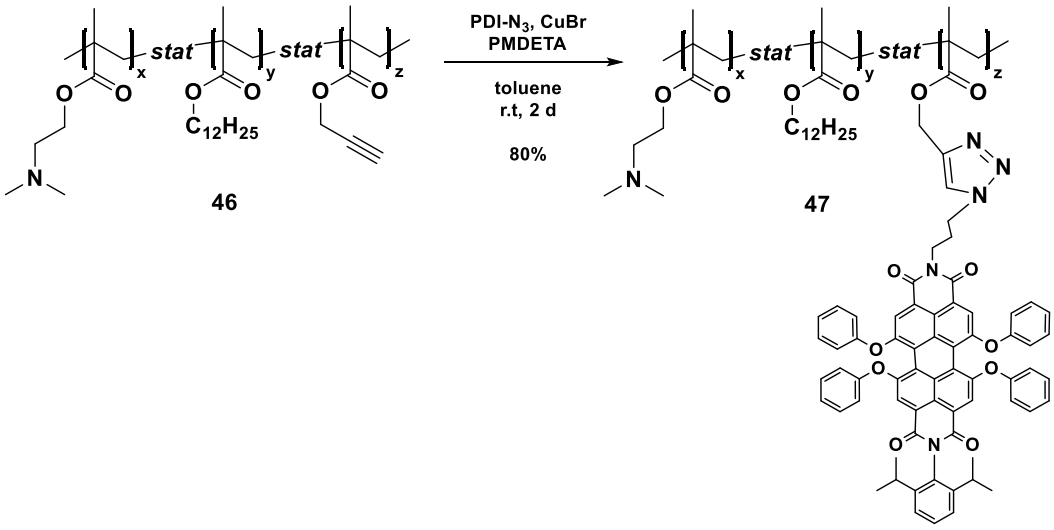

*Scheme 54: Dye-labelling of PDMAEMA-stat-PLMA-stat-PPgMA (**46**) by click reaction to PDMAEMA-stat-PLMA-stat-PDI (**47**).*

The dye-labelled polymer **47** was analysed by DOSY-NMR spectroscopy to confirm the successful binding of the dye in the PgMA side chain. All signals of the dye (PDI) and the polymer (a-j) showed the same diffusion constant, displayed by the red line in Figure 95, confirming the covalent attachment of the dye to the polymer.

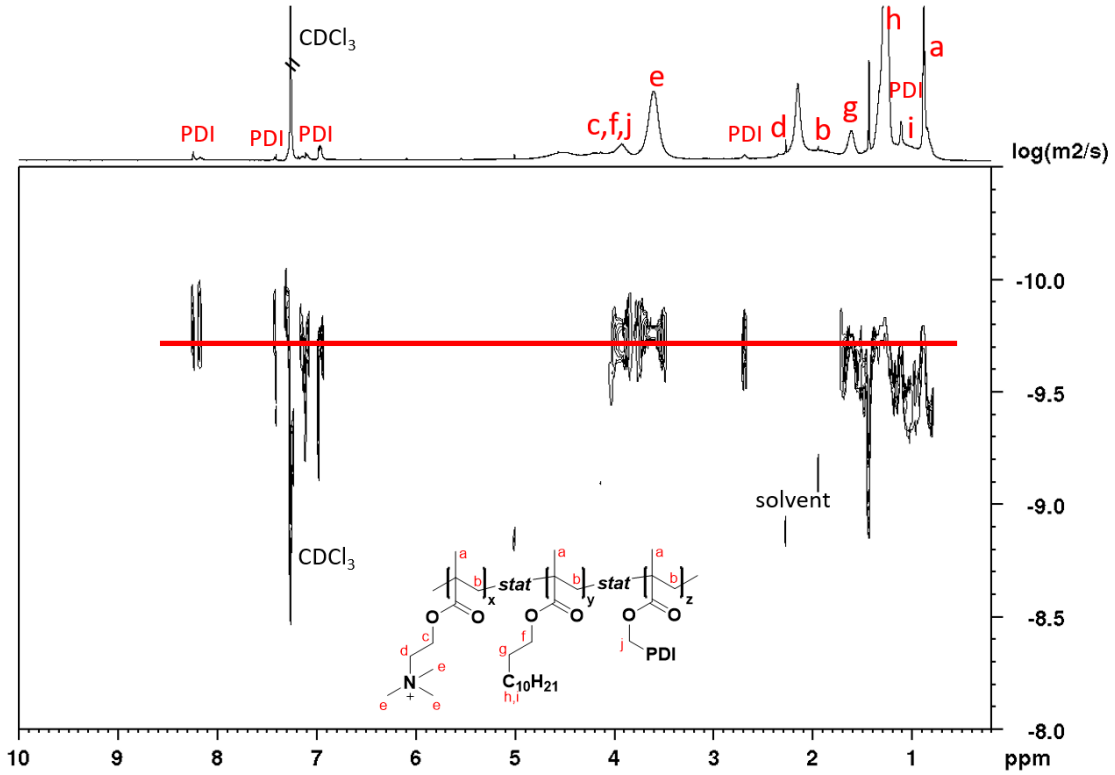

*Figure 95: DOSY spectrum (700 MHz, 300 K, CDCl3) of dye-labelled PTMAEMA-stat-PLMA-stat-PDI (**47**).*

FORMATION OF THE POSITIVELY CHARGED TERPOLYMER

In the last step, the positive charge was formed in the DMAEMA side chain.[22] First, the dye-labelled polymer (**47**) was used to introduce the positive charge by quaternization of the dimethyl amine of DMAEMA with methyl iodide (Scheme 55). After 24 hours reaction time the positively charged terpolymer PTMAEMA-*stat*-PLMA-*stat*-PDI (**48**) was obtained with quantitative yield.

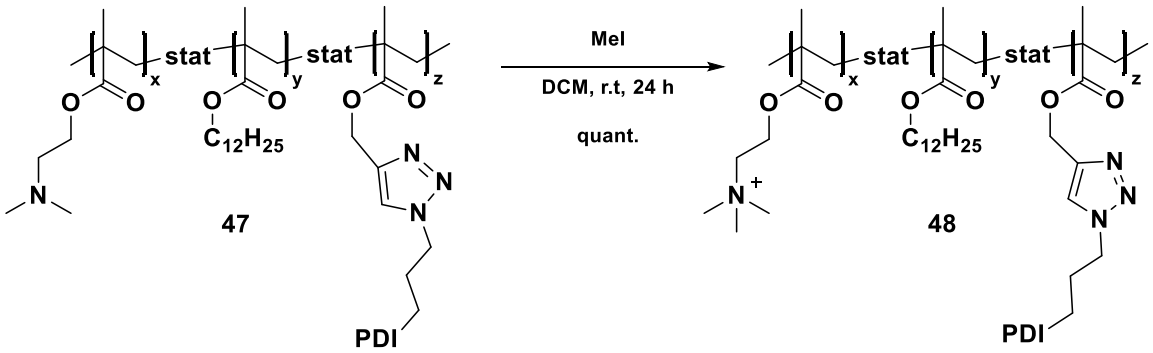

*Scheme 55: Synthesis of the positively charged dye-labelled polymer **48** by quaternization of the amine in the DMAEMA side chain.*

The reaction was then performed under equal conditions with the unlabelled polymer **46**. The positively charged polymer PTMAEMA-*stat*-PLMA-*stat*-PPgMA (**49**) was obtained with quantitative yield (Scheme 56). The unlabelled polymer was used as the control sequence for the nanoparticle

coating and biological studies to ensure that the fluorescent dye has no influence on the protein-interaction and aggregation behaviour of the charged nanoparticles.

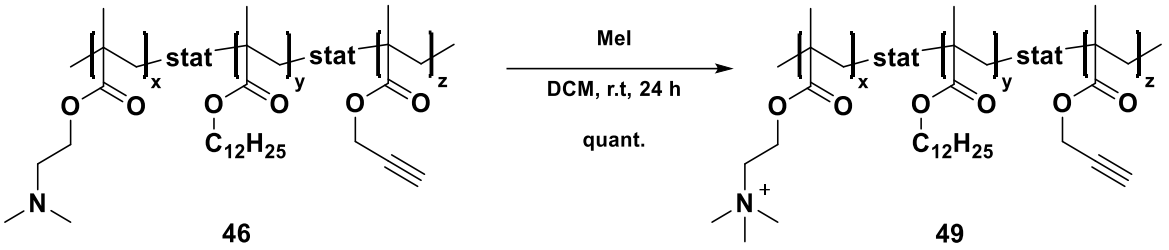

*Scheme 56: Synthesis of the positively charged polymer **49** by quaternization of the amine in the DMAEMA side chain.*

In total, four different positively charged polymers were synthesized (Table 39), differing in the block ratio and molecular weight. The first two were based on the same original polymer with a molecular weight of 7200 Da, and a higher polar moiety with a block ratio of 54:43:3. Both had a positive charge in the DMAEMA side chain and one was dye-labelled (pma07), while the other was unlabelled (pma14). The next two were both based on a polymer with a significantly higher molecular weight of 15600 Da. The polar and nonpolar block ratio was identical (48:48:4) and one was dye-labelled (pma25; pma26,39,44). All these positively charged polymers that were synthesized were sent to the Parak group for further treatment.

*Table 39: Overview of the fabricated positively charged terpolymers **48-49** with and without the fluorescent tag.*

Sample (pma)	Polymer	x:y:z[1]	Dye-label	M_w[2] [Da]
07	PTMAEMA-*stat*-PLMA-*stat*-PDI (**48a**)	54:43:3	yes	7900
14	PTMAEMA-*stat*-PLMA-*stat*-PPgMA (**49a**)	54:43:3	no	7900
25	PTMAEMA-*stat*-PLMA-*stat*-PDI (**48b**)	48:48:4	yes	15600
26, 39, 44	PTMAEMA-*stat*-PLMA-*stat*-PPgMA (**49b**)	48:48:4	no	15600

[1] block ratio, calculated from ^{1}H-NMR [2] against PMMA standard

The polymers were analysed by proton NMR spectroscopy after each step and compared (Figure 97). The spectrum of the basic terpolymer PDMAEMA-*stat*-PLMA-*stat*-PPgMA (**46**) after polymerization showed all expected proton signals (A) and allowed the calculation of the block ratio (54:43:3). Comparing it to the spectrum of the dye-labelled polymer PDMAEMA-*stat*-PLMA-*stat*-PDI (B, **47**) the polymer signals (a-j) showed the same signal intensities and shifts. Additionally, the signals of the dye (PDI) were visible, predominantly in the aromatic region between 8.50-6.50 ppm, and at 2.90 and 1.11 ppm. The remaining signals were overlapping with the polymer signals. Together with the DOSY-spectrum it was confirmed that the dye was successfully incorporated in the polymer. The spectra C and D show the positively charged polymers PTMAEMA-*stat*-PLMA-*stat*-PDI (C, **48**) and PTMAEMA-*stat*-PLMA-*stat*-PPgMA (D, **49**). Introduction of the positive charge by methylation resulted in

broadening of the signals, indicating the success of the reaction. Additionally, a downfield shift of the methyl-signal (e) was observed from 2.30 to 3.60 ppm, as well as an increase in signal intensity from 6 to 9 due to the addition of a methyl group with three protons. In conclusion, the positively charged PTMAEMA-based and dye-labelled terpolymers **48-49** were fabricated successfully.

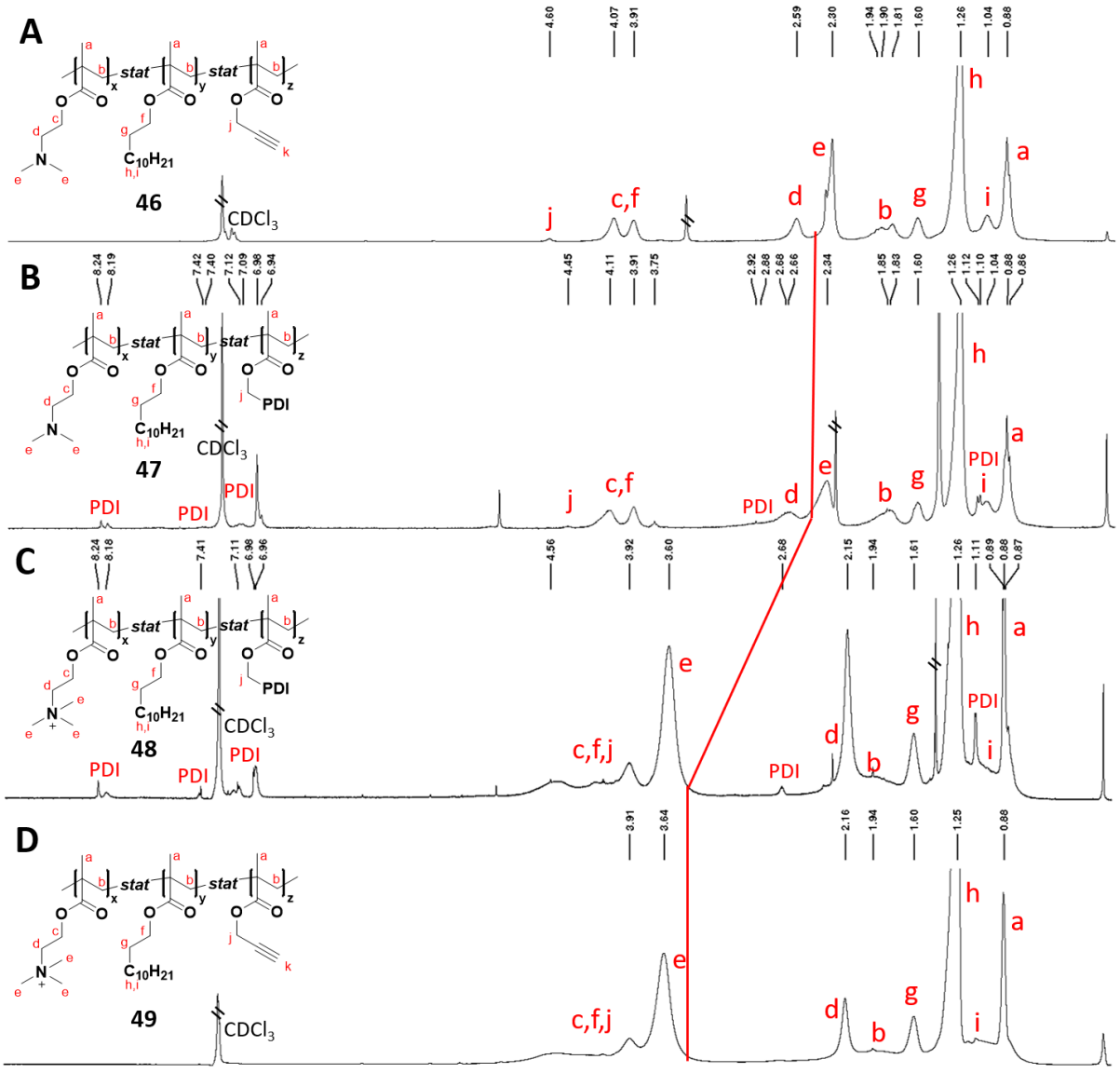

Figure 96: ^{1}H-NMR spectrum (700 MHz, 300 K, $CDCl_3$) of the DMAEMA-based terpolymer after synthesis (A), after dye-labelling (B) and after formation of the positive charge (C, dye-labelled; D, without dye).

6.2.3 Zwitterionic PMA-based terpolymers

The next polymers were synthesized with a zwitterionic group in the side chain of the polar block in order to investigate the anti-fouling properties of such polymers, when used to coat inorganic nanoparticles. Two different zwitterionic monomers were used. The poly(sulfobetaine methacrylate) (PSBMA) block contained a sulfobetaine group with a positively charged quaternary ammonium and a negatively charged sulfonate group (Scheme 57, left). The second zwitterionic block poly(2-methacryloyloxyethyl phosphorcholine) (PMPC) contained a negatively charged phosphate and a positively charged quaternary ammonium at the end of the side chain (Scheme 57, right).

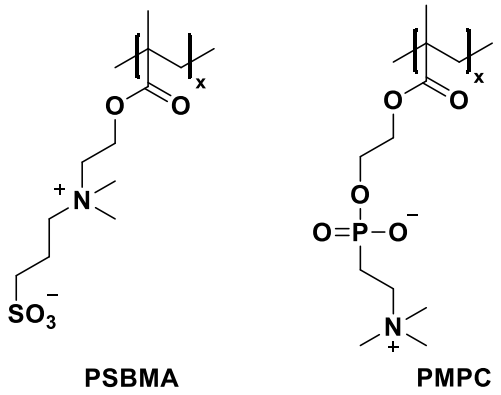

Scheme 57: Chemical structures of zwitterionic polymers PSBMA and PMPC.

ZWITTERIONIC PSBMA-CONTAINING TERPOLYMERS

For the fabrication of the zwitterionic PSBMA-based polymers, no additional polymerizations needed to be conducted.[183] The base polymer was PDMAEMA-*stat*-PLMA-*stat*-PPgMA (**46**) that was synthesized before in numerous variations of block ratio and molecular weight. The next step was the optional dye-labelling with the fluorescent tag PDI-N_3 via click reaction, as discussed before. The reaction was performed with two PDMAEMA-based polymers (**46a,e**) with molecular weights of 7200 Da and 3900 Da and different block ratios (Table 40), where polymer **46e** had a significantly higher polar moiety than **46a** to compare the influence of the charge quantity on the anti-fouling properties of the polymer on the nanoparticle surface.

*Table 40: Overview of the fabricated dye-labelled PDMAEMA-based terpolymers **47**.*

No.	Polymer	x:y:z[1]	M_w[2] [Da]	Yield [%]
47a	PDMAEMA-*stat*-PLMA-*stat*-PDI	54:43:3	7200	quant.
47c	PDMAEMA-*stat*-PLMA-*stat*-PDI	62:36:2	3900	94

[1] block ratio, calculated from ^{1}H-NMR [2] against PMMA standard

In the last step, the zwitterionic charge was introduced into the DMAEMA side chain (Scheme 58). Therefore, the polymer was reacted with 1,3-propane sultone. The tertiary amine was alkylated with propyl sulfonate, resulting in the zwitterionic sulfobetaine group. After 24 hours at 40 °C the zwitterionic, dye-labelled polymer **50** was obtained with quantitative yield.

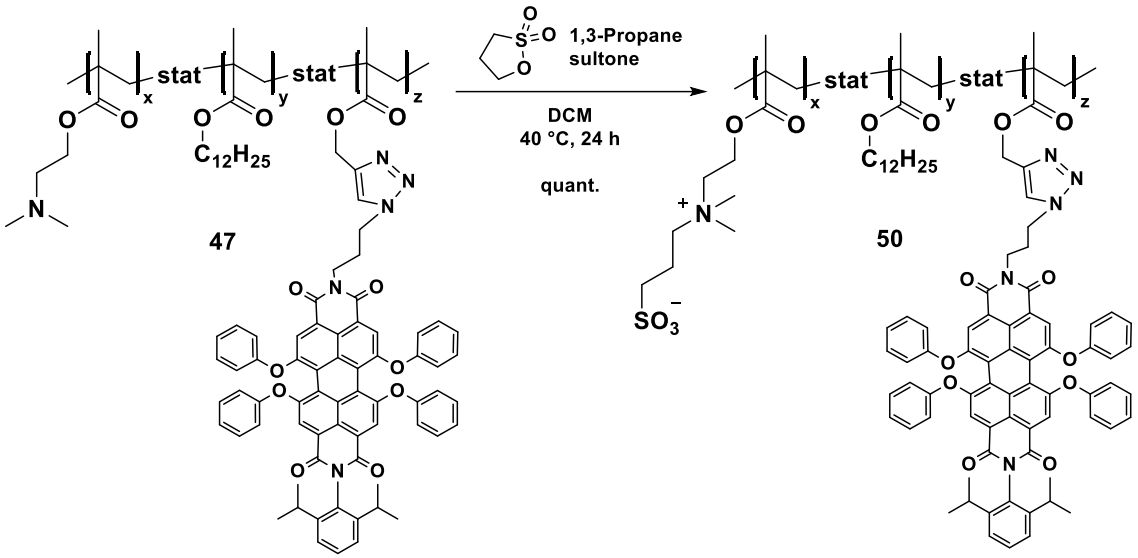

*Scheme 58: Synthesis of dye-labelled zwitterionic terpolymer PDMAEMASB-stat-PLMA-stat-PDI (**50**) by alkylation of the DMAEMA side chain, resulting in a sulfobetaine group.*

The unlabelled terpolymer PDMAEMA-*stat*-PLMA-*stat*-PPgMA (**46**) was alkylated under the same conditions to form the zwitterionic charge in the DMAEMA side chain, using 1,3-propane sultone. After 24 hours the zwitterionic polymer PSBMA-*stat*-PLMA-*stat*-PPgMA (**51**) was obtained with quantitative yield (Scheme 59).

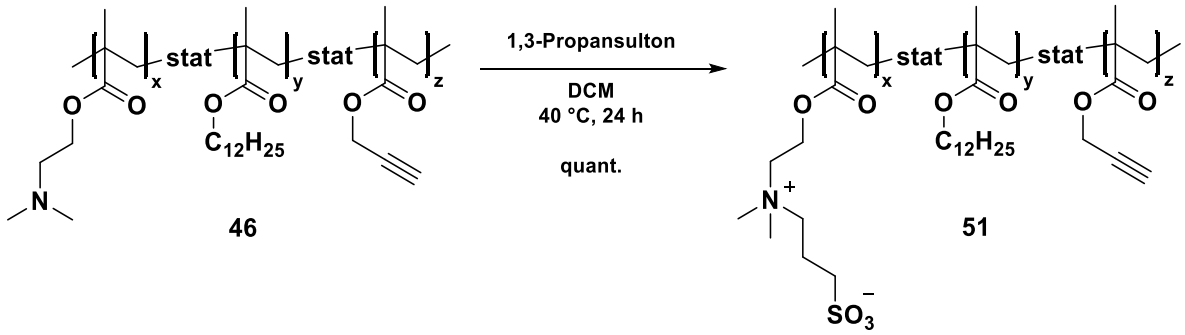

*Scheme 59: Synthesis of zwitterionic terpolymer PDMAEMASB-stat-PLMA-stat-PPgMA (**51**) by alkylation of the DMAEMA side chain, resulting in a sulfobetaine group.*

In total, four different zwitterionic PSBMA-based polymers (**50,51**) were synthesized (Table 41), differing in the block ratio and molecular weight. The first two were based on the same original polymer **46a** with a molecular weight of 7200 Da, and a block ratio of 54:43:3. One was dye-labelled (**50a**), while the other was unlabelled (**51a**). The next two were both based on the polymer **46e** with a significantly lower molecular weight of 3900 Da and a significantly higher polar moiety (62:36:2). Again,

one was dye-labelled (**50b**) and the other was unlabelled (**51b**). All displayed polymers were sent to the Parak group for further investigation.

*Table 41: Overview of the fabricated zwitterionic PSBMA-based terpolymers (**50,51**) with and without the fluorescent tag.*

Sample (pma)	Polymer	x:y:z[1]	Dye-label	M_w[2] [Da]
15	PSBMA-*stat*-PLMA-*stat*-PDI (**50a**)	54:43:3	yes	7200
16, 35, 37, 42, 47	PSBMA-*stat*-PLMA-*stat*-PPgMA (**51a**)	54:43:3	no	7200
27	PSBMA-*stat*-PLMA-*stat*-PDI (**50b**)	62:36:2	yes	3900
28, 36, 41, 43, 48	PSBMA-*stat*-PLMA-*stat*-PPgMA (**51b**)	62:36:2	no	3900

[1] block ratio, calculated from ^{1}H-NMR [2] against PMMA standard

The polymers were analysed by proton NMR spectroscopy after each step and compared (Figure 97). The spectrum of the initial terpolymer PDMAEMA-*stat*-PLMA-*stat*-PPgMA after polymerization displayed all expected proton signals (A, **46**) and allowed the calculation of the block ratio, resulting in a ratio of 54:43:3. Comparing it to the spectrum of the dye-labelled polymer PDMAEMA-*stat*-PLMA-*stat*-PDI (B, **47**) the polymer signals (a-j) showed the same signal intensities and shifts. Additionally, the signals of the dye (PDI) were visible, predominantly in the aromatic region between 8.50-6.50 ppm, and at 2.90 and 1.11 ppm. The remaining signals were overlapping with the polymer signals. Together with the DOSY-spectrum it was confirmed that the dye was successfully incorporated in the polymer. The spectra C and D show the zwitterionic polymers PSBMA-*stat*-PLMA-*stat*-PDI (C, **50**) and PSBM-*stat*-PLMA-*stat*-PPgMA (D, **51**). Extreme broadening of the signals between 5.00-2.50 ppm was observed, caused by the zwitterionic charge in the sulfobetaine chain, indicating the successful introduction of the charge. In addition, an increase in signal intensity due to the attachment of the sulfopropyl-group was observed in the same region. Two additional CH_2-signals were visible and overlapping with the existing signals in this area, resulting in a broad multiplet signal. In conclusion, the zwitterionic PSBMA-based and dye-labelled terpolymers (**50,51**) were successfully fabricated, as confirmed by proton NMR spectroscopy.

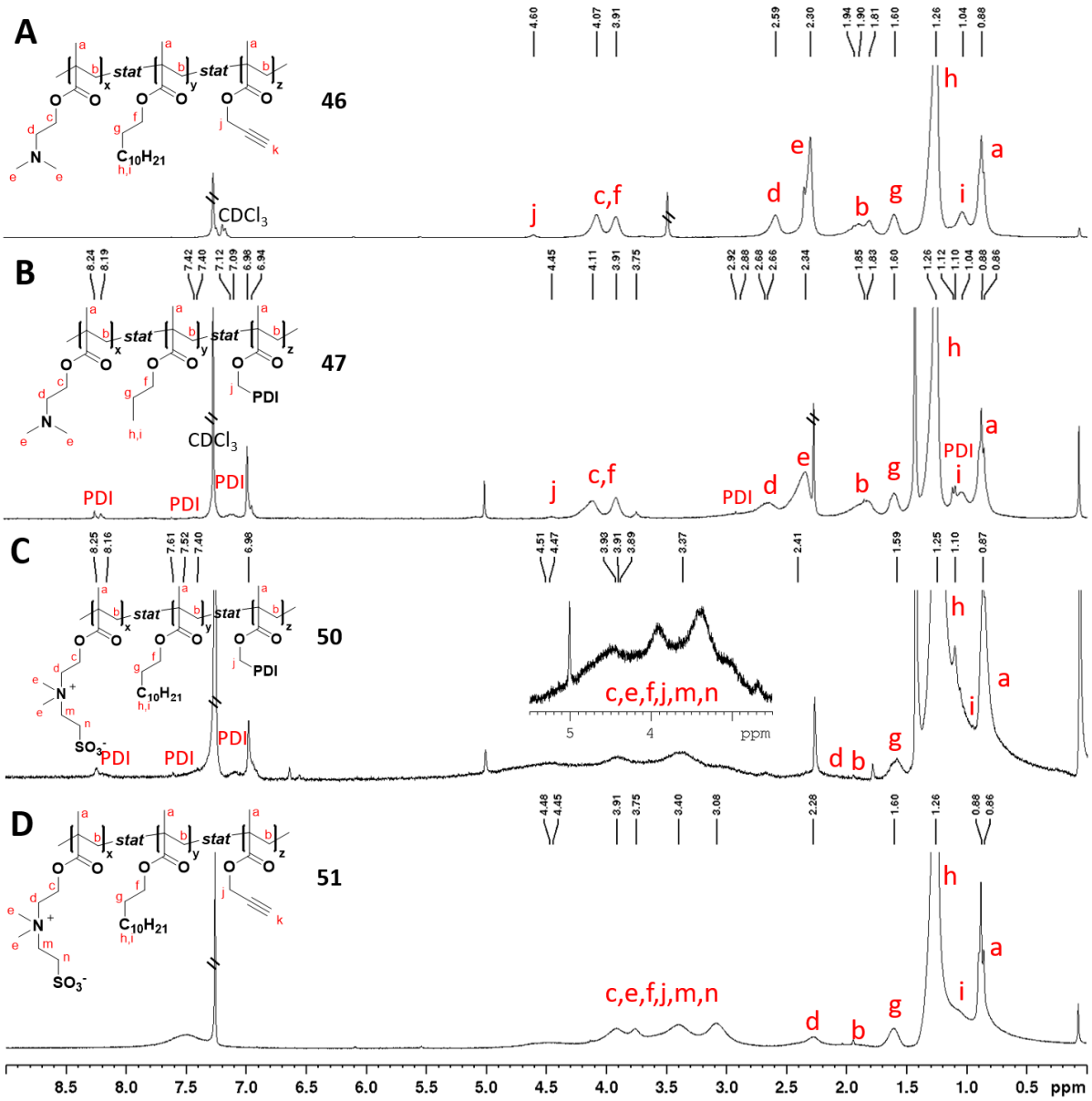

Figure 97: ^{1}H-NMR spectra (700 MHz, 300 K, $CDCl_3$) of the SBMA-based terpolymers after synthesis (A), after dye-labelling (B) and after formation of the negative charge (C, dye-labelled; D, without dye).

ZWITTERIONIC PMPC-CONTAINING TERPOLYMERS

The second zwitterionic polymer that was synthesized contained the zwitterionic MPC block.[183] In contrast to the beforementioned polymers, where the charge was introduced by postsynthetic modification, the MPC monomer already contained the zwitterionic charge. The terpolymer PMPC-*stat*-PLMA-*stat*-PPgMA (**52**) was synthesized by free radical polymerization under slightly modified conditions, compared to the previous approaches. Due to the polarity of the MPC monomer, the solvent was changed from nonpolar toluene to polar ethanol. The initiator AIBN and chain transfer reagent ME remained unchanged. After 18 hours at 70°C the zwitterionic polymer **52** was obtained with a yield of up to 90% (Scheme 60).

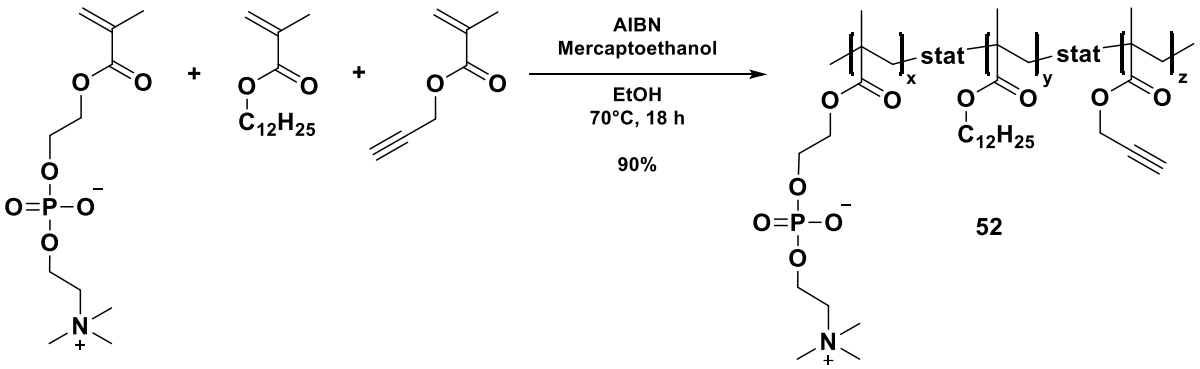

*Scheme 60: Synthesis of the zwitterionic terpolymer PMPC-stat-PLMA-stat-PPgMA (**52**) by radical polymerization.*

In total, four polymerizations were performed to obtain PMPC-containing terpolymers (**52,53**) with different molecular weights and block ratios (Table 42).

*Table 42: Overview of the synthesized amphiphilic terpolymers (**52**) with desired and obtained mass average molecular weight (M_w), the block ratio of the monomers and amounts of AIBN and ME used in the polymerization.*

No.	Polymer	x:y:z[1]/ x:y:z[2]	AIBN (eq)	ME (eq)	M_w (target) [Da]	M_w (GPC)[3] [Da]
52a	PMPC-*stat*-PLMA-*stat*-PPgMA	48:50:2/ 48:50:2	0.010	0.025	22900	21800 (THF)
52b	PMPC-*stat*-PLMA-*stat*-PPgMA	54:44:2/ -	0.009	0.015	30000	2900 (THF)
52c	PMPC-*stat*-PLMA-*stat*-PPgMA	53:43:4/ 50:48:2	0.009	0.015	30000	- (THF)
52d	PMPC-*stat*-PLMA-*stat*-PPgMA	53:44:3/ 46:52:2	0.01	0.025	30000	- (THF)

[1] monomer ratio, target block ratio [2] block ratio, calculated from ^{1}H-NMR [3] against PMMA standard

In the end, the zwitterionic MPC monomer turned out to be challenging in the reaction, leading to incomplete polymerizations (**52b**) or polymers that could not be fully characterized (**52c-d**), as no GPC result was obtained (**52c-d**) or no calculation of the block ratio was possible due to bad resolution of the proton NMR (**52b**). These three polymers were not used for further modification. The polymer **52a**

was successfully synthesized, almost meeting the desired molecular weight of 22900 Da. Achieved was 21800 Da, according to GPC analysis, which was perfectly fitting to the calculated block ratio of 48:50:2. After the synthesis, the polymer **52a** was dye-labelled with the fluorescent tag PDI-N_3 via click reaction. Again, the solvent was changed to the polar ethanol due to the low solubility of the zwitterionic polymer **52** in nonpolar solvents. The reaction was catalyzed by copper(I) bromide and the ligand PMDETA. After two days at room temperature, the zwitterionic and dye-labelled polymer PMPC-*stat*-PLMA-*stat*-PPgMA **53** was obtained with 79% yield (Scheme 61).

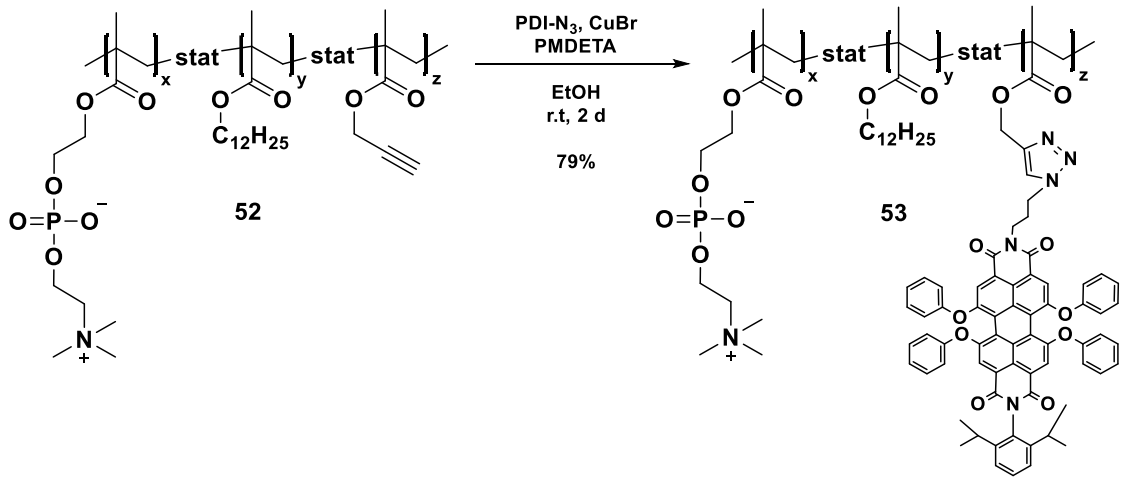

*Scheme 61: Dye-labelling of the zwitterionic terpolymer PMPC-stat-PLMA-stat-PPgMA (**52**) by click reaction with PDI-N_3.*

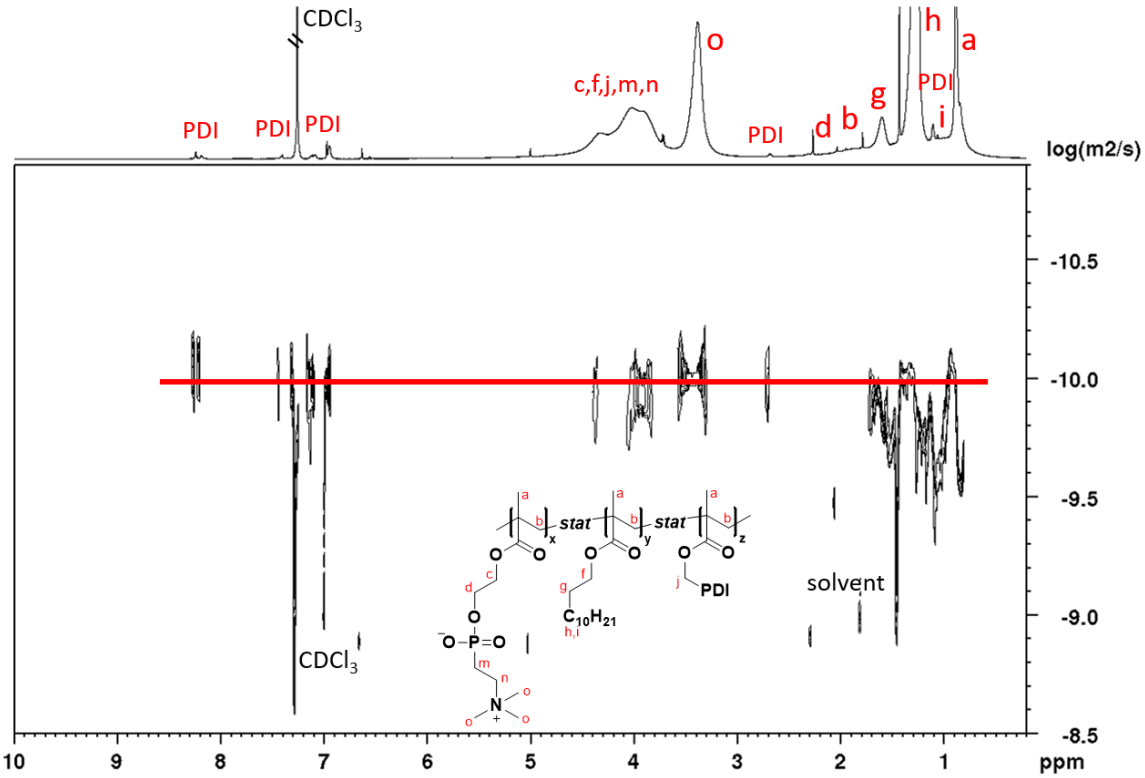

*Figure 98: DOSY spectrum (700 MHz, 300 K, CDCl3) of dye-labelled PMPC-stat-PLMA-stat-PDI (**53**).*

To confirm the covalent attachment of the dye to the polymer **53**, DOSY spectroscopy was performed (Figure 98). The spectrum displayed the diffusion constants of the proton NMR signals. All signals of the terpolymer and the PDI dye showed the same diffusion constant (red line), leading to the conclusion that the click reaction was successful and the polymer was dye-labelled. Then, all polymers **52** and **53** were analysed by proton NMR spectroscopy (Figure 99). All expected signals were visible in the spectrum of the terpolymer PMPC-*stat*-PLMA-*stat*-PPgMA (A, **52a**) after polymerization and allowed the calculation of the block ratio (48:50:2). After dye-labelling of the polymer (B, **53**), the dye signals were clearly visible, predominantly in the aromatic region between 6.5-8.5 ppm, and had the expected signal intensity in relation to the polymer. Together with the DOSY spectrum this indicated the successful covalent attachment of the dye to the polymer.

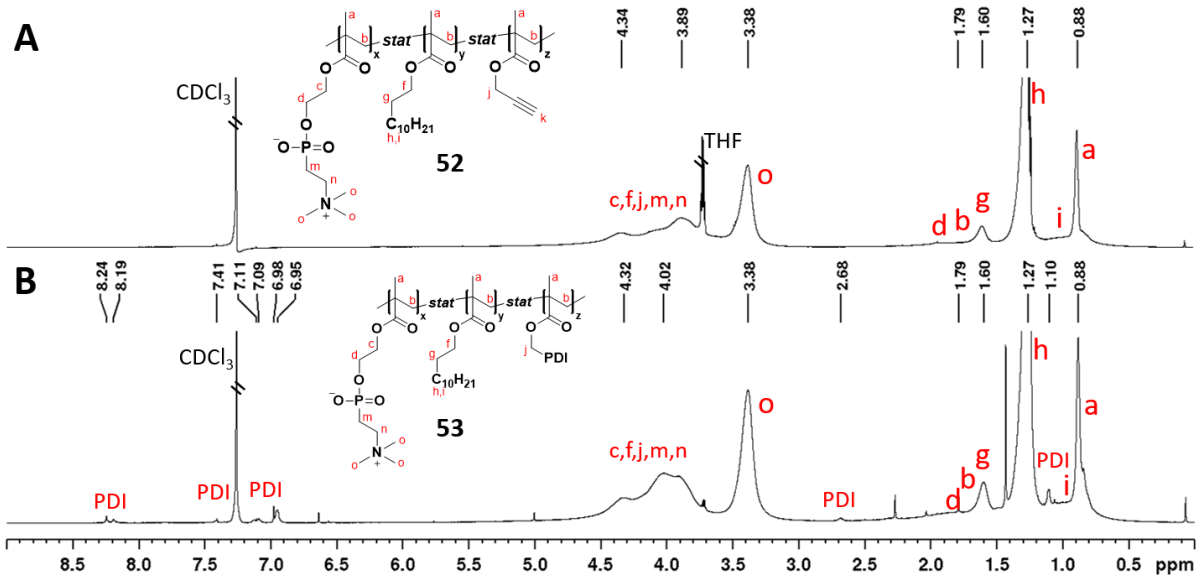

Figure 99: ^{1}H-NMR spectra (700 MHz, 300 K, $CDCl_3$) of the MPC-based terpolymers after synthesis (A) and after dye-labelling (B).

The Parak group extensively studied the stability of the polymer-coated gold nanoparticles in dependence of the surface charge to investigate the anti-fouling properties of the zwitterionic polymers (p. 186, chapter 6.2.4). In addition, the biocompatibility and cell uptake of the particles were tested to evaluate the behaviour of the particles in biological environment as potential drug delivery system. To complete this study, a targeting unit was installed into the zwitterionic MPC-based polymer **52a**. Folic acid (FA) is commonly used as a model ligand for targeting in many cancer cell lines to create site-selectivity in the carrier system.[182,184,185] It was in our study to find out, if active targeting was observed by installing folic acid into the MPC polymer. To synthesize the FA-functionalized polymer **55**, folic acid had to be azide-functionalized first (Scheme 62). Azido-PEG_3-amine was introduced as an amide by NHS coupling with the carboxylic acid side chain of FA and the resulting azido-PEG_3-FA **54** was obtained with 95% yield.

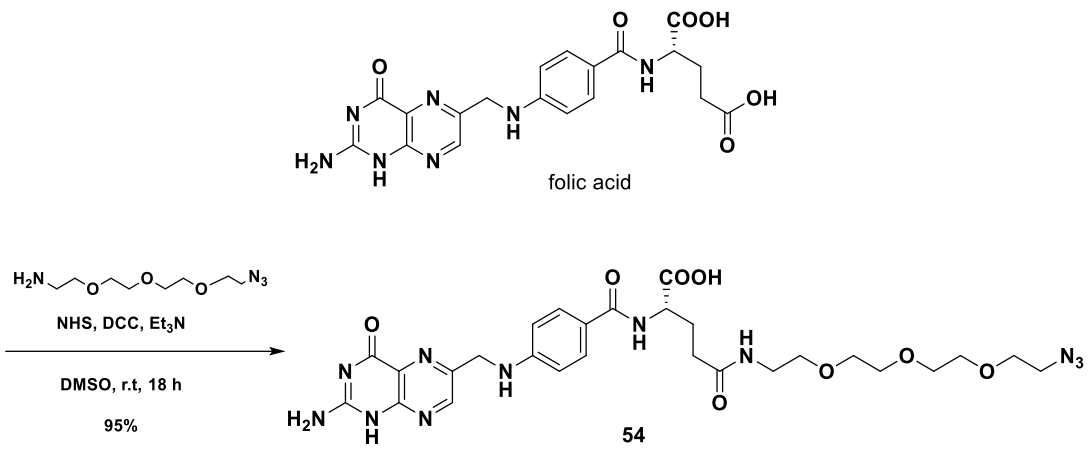

*Scheme 62: Azide functionalization of folic acid by NHS coupling resulting in azid-PEG$_3$-FA **54**.*

Successful functionalization of folic acid with azido-PEG$_3$-amine was confirmed by proton NMR and DOSY spectroscopy (Figure 100). The pure compound **54** was identified by the proton spectrum, where all signals were visible with the expected signal intensities (Appendix, Figure 147). In the DOSY spectrum, all signals of folic acid and PEG showed the same diffusion constant (red line) and had therefore the same diffusion behaviour, compared to the remaining solvent signals. It indicated that the desired compound **54** was obtained by coupling reaction.

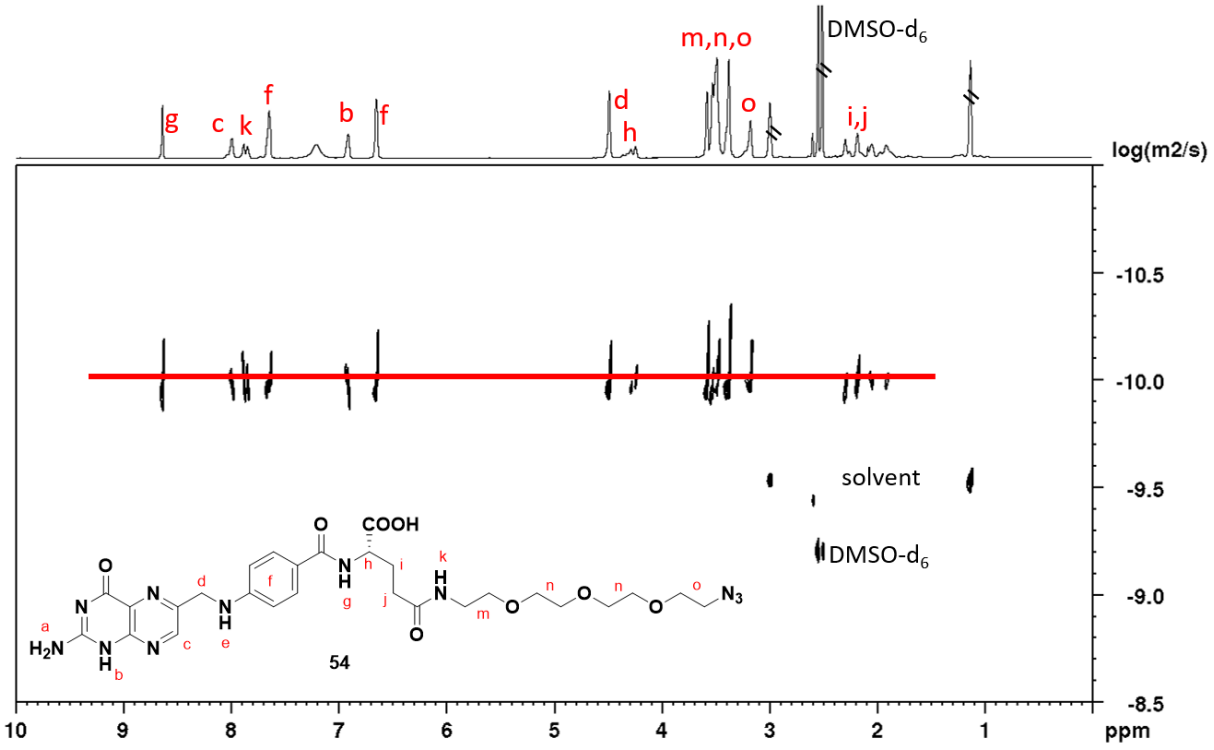

*Figure 100: DOSY spectrum (700 MHz, 300 K, DMSO-d$_6$) of azide-functionalized folic acid (**54**).*

The introduction of FA into the MPC polymer **52a** was performed by click reaction under identical conditions like the beforementioned dye-functionalization (Scheme 63). The alkyne in the propargyl-side chain was used for the reaction with azido-PEG2-FA **54** and after two days, the FA-functionalized, zwitterionic polymer PMPC-*stat*-PLMA-*stat*-FA (**55**) was obtained with 77% yield.

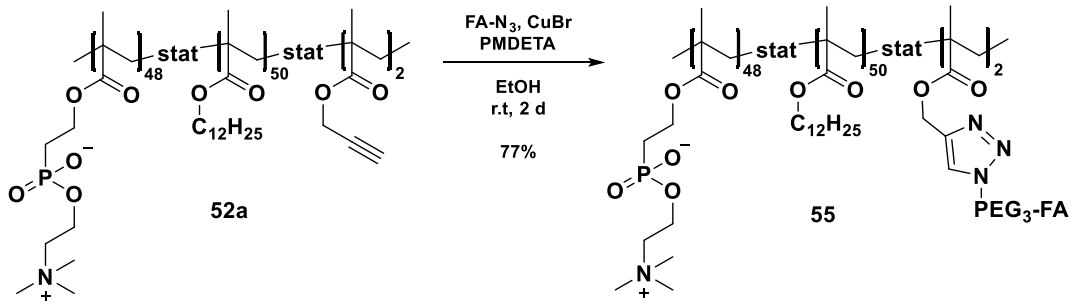

*Scheme 63: Folic acid functionalization of MPC-based polymer **52a** by click reaction, resulting in PMC-stat-PLMA-stat-FA **54**.*

After the click reaction, the resulting polymer PMPC-stat-PLMA-stat-FA (**55**) was analysed by proton NMR and DOSY spectroscopy (Figure 101). In the proton spectrum all expected signals of the polymer **55** were visible (Appendix, Figure 148). The DOSY spectrum showed the same diffusion constant for the polymer signals and folic acid (red line). This proved that folic acid was covalently attached to the propargyl side chain and the targeting unit was successfully incorporated into the polymer side chain.

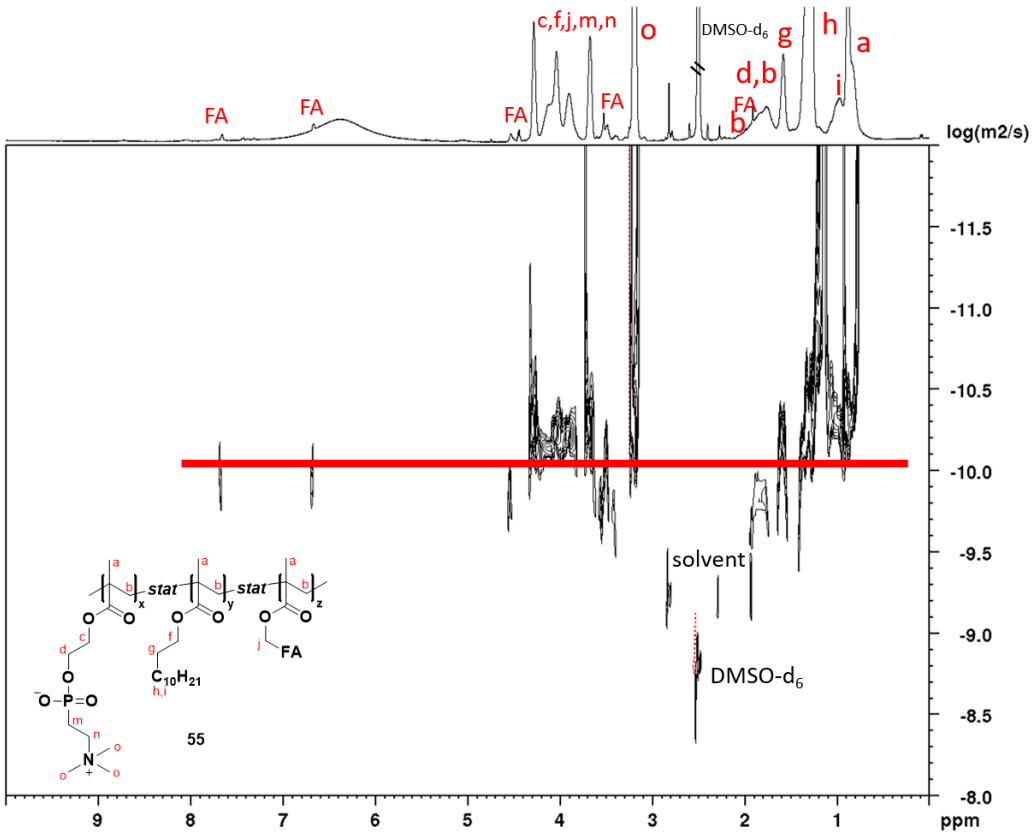

*Figure 101: DOSY spectrum (700 MHz, 300 K, DMSO-d_6) of FA-labelled PMPC-stat-PLMA-stat-FA (**55**).*

In total, three different zwitterionic PMPC-based polymers (**52a, 53, 55**) were synthesized with the same block ratio of 48:50:2 and molecular weight of 21800 Da (Table 43). One was the unlabelled PMPC-*stat*-PLMA-*stat*-PPgMA (**52a**). The other two terpolymers were the dye-functionalized PMPC-*stat*-PLMA-*stat*-PDI (**53**) and the folic acid-functionalized PMPC-*stat*-PLMA-*stat*-FA (**55**). All three polymers were sent to the Parak group for further investigation.

*Table 43: Overview of the fabricated zwitterionic terpolymers **52a** and **53** with and without the fluorescent tag.*

Sample	Polymer	x:y:z[1]	Labelled	M_w[2] [Da]
pma12	PMPC-*stat*-PLMA-*stat*-PPgMA (**52a**)	48:50:2	no	21800
pma20	PMPC-*stat*-PLMA-*stat*-PDI (**53**)	48:50:2	Dye	21800
pma56	PMPC-*stat*-PLMA-*stat*-FA (**55**)	48:50:2	FA	21800

[1] block ratio, calculated from ^{1}H-NMR [2] against PMMA standard

6.2.4 First results from the Parak group on the performance of charged nanoparticles in biological environment

After purification and analysis, the charged terpolymers were sent to our collaboration partners, the Parak group at the University of Hamburg, to execute the nanoparticle coating and stability studies. The experiments presented below were performed by Saad Megahed within his PhD studies.[184] First results of the project were obtained already, starting with stability studies via DLS (Figure 102). Gold nanoparticles (Au-NPs) with a diameter of 17 nm were coated with the charged polymers, dispersed in aqueous sodium chloride solution and analysed by DLS (Figure 102; see Table 44 for details).[184]

Table 44: Hydrodynamic diameter and zeta potentials of polymer-coated nanoparticles.

Sample	Polymer	Charge	$d_{H(N)}$ [nm]	ζ [mV]
pmaNW26	PTMAEMA-*stat*-PLMA-*stat*-PPgMA (**49b**)	+	28 ± 4	48 ± 3
pmaNW14	PTMAEMA-*stat*-PLMA-*stat*-PPgMA (**49a**)	+	25 ± 1	36 ± 1
pmaNW28	PSBMA-*stat*-PLMA-*stat*-PPgMA (**51b**)	+/-	23 ± 1	-32 ± 3
pmaNW16	PSBMA-*stat*-PLMA-*stat*-PPgMA (**51a**)	+/-	23 ± 1	12 ± 3
pmaNW12	PMPC-*stat*-PLMA-*stat*-PPgMa (**52a**)	+/-	21 ± 2	7 ± 2
pmaNW33	PMAPHOS-*stat*-PLMA-*stat*-PPgMA (**43**)	-	20 ± 1	-42 ± 1

The nanoparticle coating was successful with all six polymers, confirmed by the DLS measurements. The graphs show that the charged polymer-coated nanoparticles had good stability and uniform diameters in aqueous sodium chloride solution, resulting in monodispersed particles with diameters between 20-30 nm (summarized in Table 44). While the positively charged nanoparticles had the

highest diameters with 25 and 28 nm, the negatively charged particles were the smallest with 20 nm. The diameters of the zwitterionic particles lied in between with 21 and 23 nm. In addition, the zeta potentials were determined, showing the same trend of decreasing values from positive to zwitterionic to negative charge.[64,184]

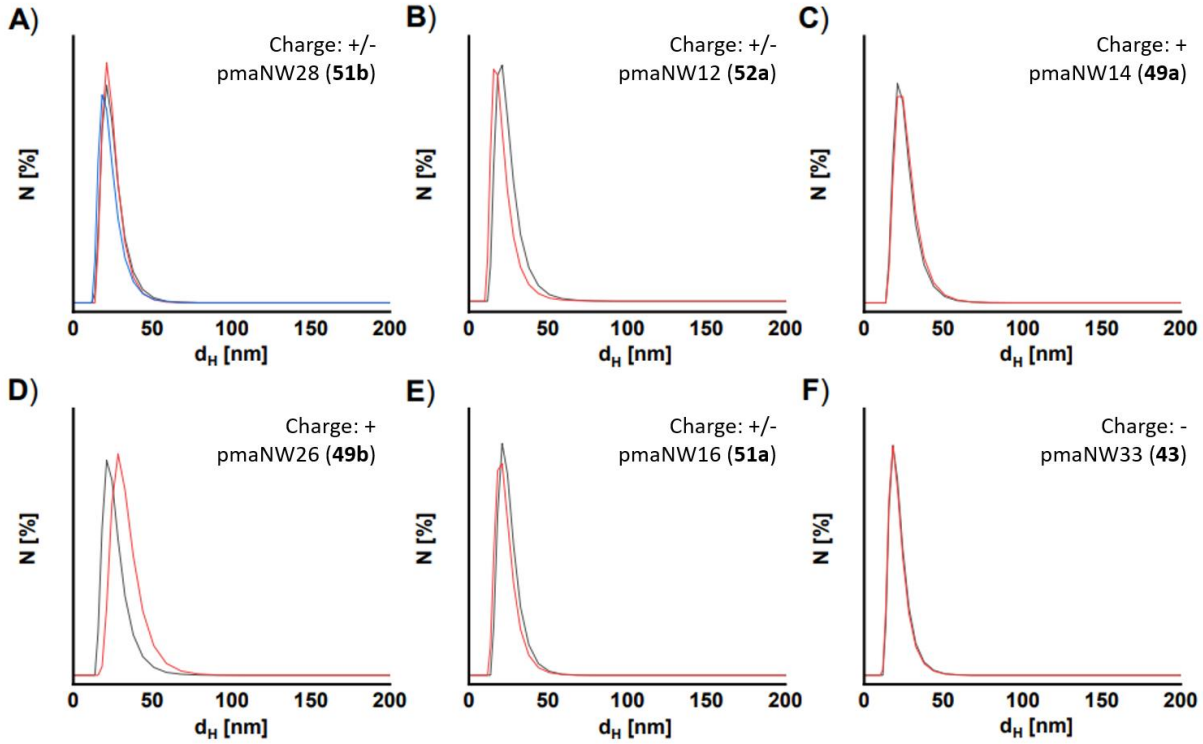

Figure 102: Results of the DLS measurements of 17 nm Au-NPs with A) pmaNW28, B) pmaNW12, C) pmaNW14, D) pmaNW26, E) pmaNW16 and F) pmaNW33, performed by Saad Megahed.[184]

Not only Au-NPs, but also quantum dots (QD) were coated with charged polymer to study the stability of the coated QDs and the influence of the coated QDs surface charge on their anti-fouling properties and behaviour in biological environment. Zwitterionic materials are known to provide good anti-fouling properties by formation of a hydration layer and suppressing the interactions with biomolecules.[32,177,178] The zwitterionic polymer PMPC-*stat*-PLMA-*stat*-PPgMa (**52a**, pmaNW12) was used for the QD coating. The coated QDs were then dispersed in aqueous solution of BSA protein (bovine serum albumin), HSA protein (human serum albumin) or transferrin to study protein corona formation. The hydrodynamic diameter of the charged QDs was determined by DLS at different protein concentrations (Figure 103A). In all three samples, the particle diameter was not changing significantly by increasing the protein concentration. This allowed the conclusion that the interactions with these proteins were suppressed successfully by coating the QDs with the zwitterionic polymer **52a**. The QDs were also coated with the second sulfobetaine-based zwitterionic polymer and tested in HAS and Tf protein solutions. Again, no significant influence on the hydrodynamic diameter of the QDs was

observed, when the protein concertation was increased (Figure 104). Therefore, both polymers **52a** and **51** showed good anti-fouling properties by effective suppression of protein interactions.

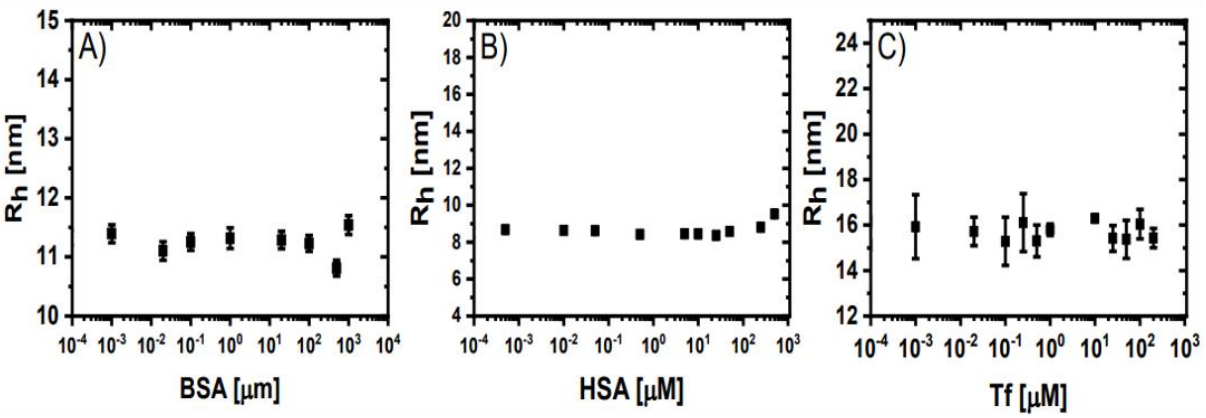

*Figure 103: Hydrodynamic radius of QDs coated with zwitterionic polymer **52a** in A) BSA, B) HSA and C) Tf protein solution.*[184]

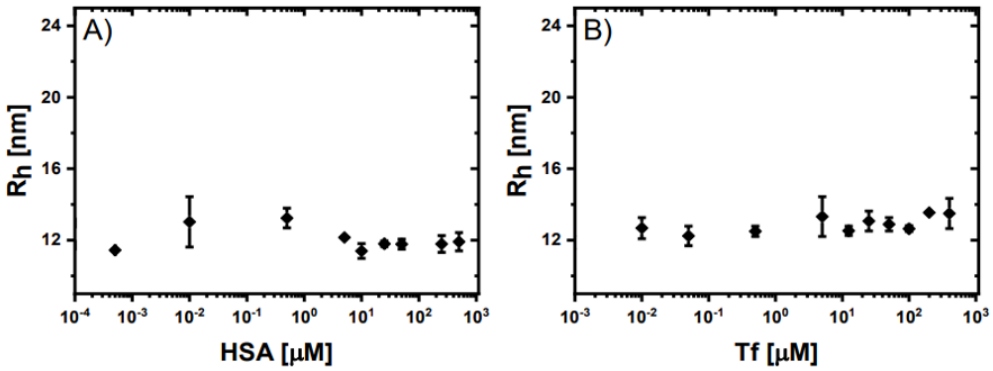

*Figure 104: Hydrodynamic radius of QDs coated with zwitterionic polymer **51** in A) HSA and B) Tf protein solution.*[184]

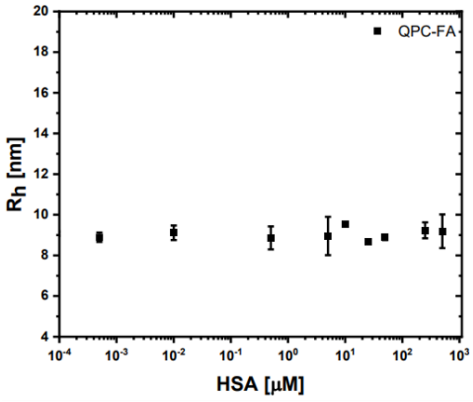

*Figure 105: Hydrodynamic radius of QDs coated with zwitterionic polymer **55** in HSA protein solution.*[184]

Th experiment was then performed with the FA-functionalized polymer PMPC-stat-PLMA-stat-FA (**55**) to ensure that the labelling did not influence the hydrodynamic radius of the coated QDs and with it the anti-fouling properties. It is reported that labelling zwitterionic polymers with either neutral or charged molecules can alter their interaction with surrounding biomolecules in physiological environment.[186,187] The results showed clearly that the folic acid labelling had no influence on the QD

stability and the hydrodynamic radius remained constant (Figure 105). Consequently, the suppression of protein interactions was as effective as with the unlabelled polymer **52a**.

The beforementioned stability studies with BSA, HSA and Tf showed that the zwitterionic QDs did not interact with the proteins to form a protein corona. The hydrodynamic radius was stable over a broad protein concentration range. These proteins are commonly tested, as HSA and Tf are two dominant proteins in the human blood serum, which contains around 50-60% HSA.[188] Consequently, if HSA showed low interactions with our particles, a significant percentage of proteins in the blood serum will not interact with them, if the zwitterionic particles are tested in humans. Before any testing with human tissue, fetal bovine serum (FBS) was used as serum-supplement for cell media in the biological experiments. A main component of FBS is BSA that also showed very low interaction with the zwitterionic QDs.[189] The cell uptake of the coated QDs was tested with different cell lines (HeLa and MCF7) and in a medium with or without FBS. The zwitterionic MPC polymer **52a** was tested in direct comparison to the FA-functionalized polymer **55**. The results showed that in cell medium with FBS, the uptake of both QD samples, with (**55**) and without FA (**52a**) was very low in both cell lines (Figure 106). In the HeLA cell line without FBS, the uptake was higher with and without folic acid at a concentration of 25 nM. Doubling the QD concentration to 50 nM resulted in no improvement for the QDs without FA, while functionalization with FA resulted in a significant increase of cell uptake (Figure 106A). It has to be noted though that the scattering of the values was quite high for the latter, as visualized by the error bar. The results with the MCF7 cell line were comparable at the lower concentration of 25 nM (Figure 106B). Almost no uptake was observed in the presence of FBS, while an increase was noticeable in the medium without FBS. Increasing the QD concentration to 50 nM led to significant increase of the cell uptake of both QD samples, with and without FA. Again, a trend was revealed that the FA-functionalized sample was better uptaken than the non-functionalized.

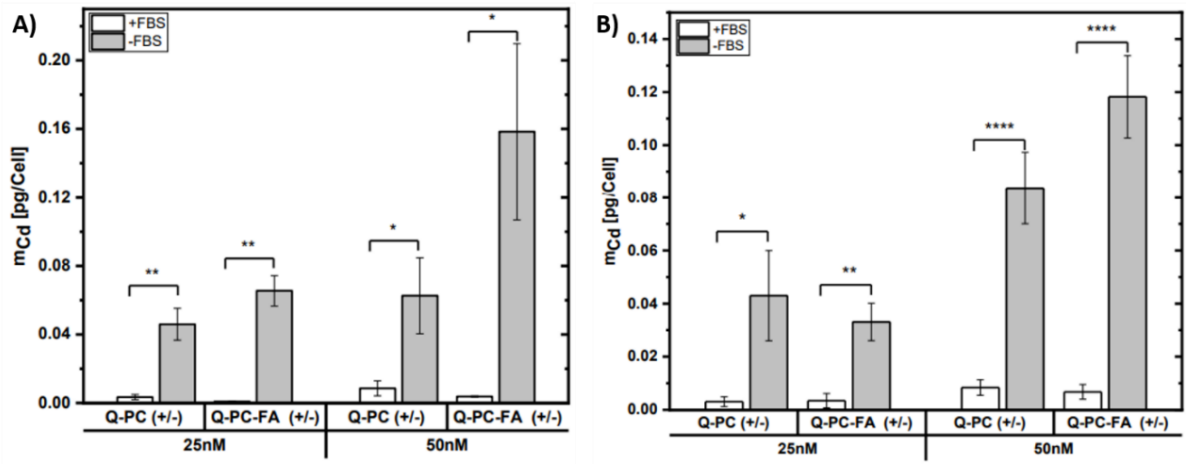

*Figure 106: Cellular uptake of Q-PC and Q-PC-FA by A) Hela cells and B) MCF7 cell line at 6h exposure. The data are shown from at least three different independent measurements ± standard deviation, statistical followed the student's t-test, * represent P<0.001.*[184]

This led to several conclusions. First of all, it was demonstrated that the cell uptake was concentration dependent and folic acid was promoting the cell uptake of the zwitterionic QDs at higher concentrations and in the absence of FBS in the cell medium. At lower concentrations, no advantage of using the FA-functionalized polymer was observed. If the FBS was added to the cell media, almost no cell uptake was happening. This made it clear that there must have been a component in the FBS that was strongly interacting with the zwitterionic polymers, overcoming their anti-fouling properties. BSA is one of the main components in the FBS and it was demonstrated in the stability studies that it did not interact with the zwitterionic polymers. Therefore, another serum was interacting with the QDs. This should be studied in the next step to evaluate, if it is a bovine protein and non-critical or if it was a protein that is present in the human serum as well. In that case, the polymers on the QD surface need to be modified to suppress these interactions, for example by altering the block ratio of charge density.

These first results showed that coating the nanoparticles with charged polymers led to increased stability of the particle dispersions in aqueous salt or protein solution. In addition, coating QDs with zwitterionic polymers provided good anti-fouling properties by prevention of protein corona formation towards BSA, HSA and Tf. Initial cell uptake experiments with the zwitterionic polymer PMPC-stat-PLMA-PPgMA (**52a**) and the FA-functionalized derivative **55** were conducted in FBS with two different cell lines. The experiments showed that in this serum solution, the uptake was drastically reduced compared to the cell medium without the FBS. This led to the conclusion that the QDs were interacting with the serum components, hindering their cell uptake. This was unexpected, as the stability studies showed very positive results and no protein interactions. The next steps would be to find out more about the interactions between the zwitterionic QDs and the serum proteins. It should be evaluated, which proteins caused the inhibition of the cell uptake and if they are present in human blood serum as well. Based on the results, the next steps can be planned to either optimize the zwitterionic polymers to suppress their interactions or to modify the cell medium and use a more suitable serum.

6.3 Summary and Outlook

The scope of this project was the synthesis of statistical methacrylate-based terpolymers with different charges for the coating of gold nanoparticles. The behaviour of the coated nanoparticles in biological environment was investigated, with special interest on aggregation behaviour, protein-interaction and anti-fouling properties. Various polymers with negative, positive or zwitterionic charge were synthesized successfully. They differed not only in their charge, but also in their molecular weight distribution and block ratio to investigate the influence of the charge quantity on the nanoparticle surface on their performance. In addition, every polymer was labelled with the fluorescent dye PDI in order to perform cell uptake experiments. The zwitterionic polymer PMPC-*stat*-PLMA-*stat*-PPgMa (**52a**, pma12) was also functionalized with folic acid to incorporate a targeting unit and investigate, if folic acid would promote cell uptake of the coated particles. After the fabrication and analysis of the polymers they were sent to the Parak group at the University of Hamburg, where the nanoparticle coating and biological experiments were conducted.

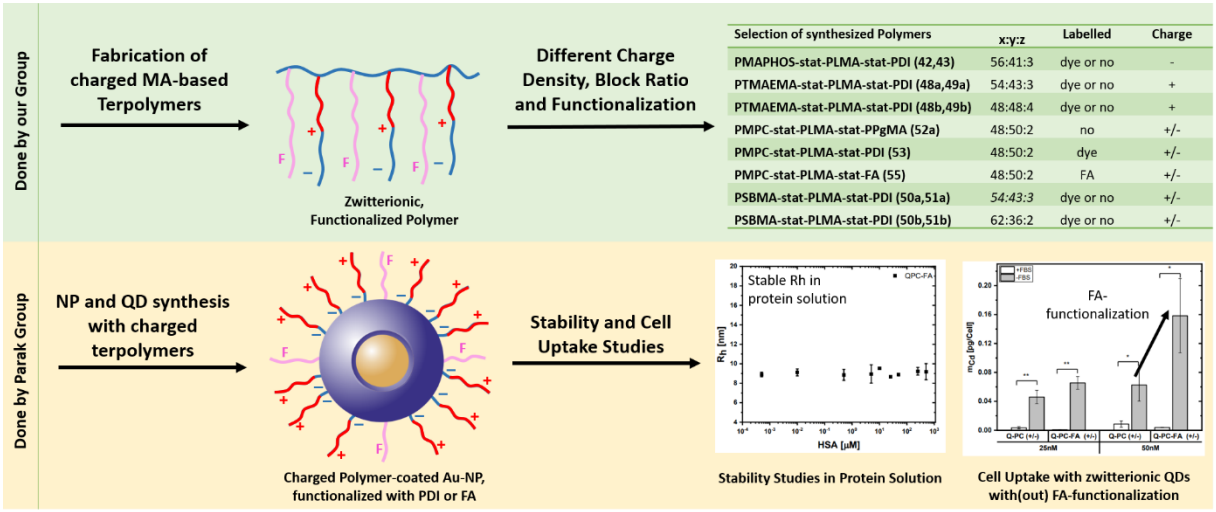

Figure 107: A broad selection of charged MA-based terpolymers was synthesized in our group and functionalized with a fluorescent dye or the targeting unit folic acid to perform biological studies. The polymers were used by the Parak group to coat AuNPs or QDs for stabilization in aqueous media. Protein interaction and cell uptake experiments were performed to investigate the behaviour of the coated particles in dependence of their surface charge.[64,184]

Initially, the polymers were synthesized in collaboration with Lisa Ackermann from our group. Then, the coating process of the gold nanoparticles was established by Daniel Valdeperez from Parak group in regards to charge density and molecular weight of the polymers. The obtained particles were used for stability studies in aqueous sodium chloride and BSA solution where the particles showed stable hydrodynamic radiuses over a broad concentration range of salt or protein. This work was summarized and published, before further experiments were conducted.[64] The subsequent study (discussed in chapter 6.2.4) was performed in collaboration with Saad Megahed from Parak group, beginning with a stability study of the polymer-coated nanoparticles. The particles showed good stability in aqueous

sodium chloride solution with all types of polymers, with positive, negative or zwitterionic charge. Besides the gold nanoparticles, quantum dots (QDs) were coated with the zwitterionic polymer PMPC-*stat*-PLMA-*stat*-PPgMa (**52a**, pma12) or the Fa-functionalized derivative **55** and dispersed in aqueous solution of BSA protein (bovine serum albumin), HSA (human albumin serum) or Tf (transferrin) to study the anti-fouling properties. The hydrodynamic diameter of the coated QDs was determined over a broad protein concentration range and no significant change was observed in any of the three experiments, leading to the conclusion that no protein corona was formed. Therefore, the polymer **52a** (pma12) provided good anti-fouling properties towards these three proteins that are the main components in FBS (fetal bovine serum), used in the following cell uptake studies and human blood serum, respectively. The results of the stability study showed that coating the nanoparticles with charged polymers led to increased stability of the particle dispersions in aqueous salt or protein solution. In addition, coating QDs with zwitterionic polymers provided good anti-fouling properties by prevention of protein corona formation towards BSA, HSA and Tf. Initial cell uptake experiments with the zwitterionic polymer PMPC-stat-PLMA-PPgMA (**52a**) and the FA-functionalized derivative **55** were conducted in FBS with two different cell lines. The experiments showed that in this serum solution, the uptake was drastically reduced compared to the cell medium without the FBS. This led to the conclusion that the QDs were interacting with the serum components, hindering their cell uptake. This was unexpected, as the stability studies showed very positive results and no protein interactions. Nevertheless, a trend was observed that folic acid promoted the cell uptake, at least for high concentrations of QDs and in the absence of FBS. Overall, these results are not optimal and clearly left room for improvement. In order to optimize the performance of the zwitterionic QDs, the next steps would be to find out more about the interactions between the QDs and the serum proteins. It should be evaluated, which proteins caused the inhibition of the cell uptake and if they are present in human blood serum as well. Based on the results, the next steps can be planned to either optimize the zwitterionic polymers to suppress their interactions or to modify the cell medium and use a more suitable serum. The SBMA-based polymers (**51**) are currently under investigation as well. Based on these first results, the study on the performance of the zwitterionic polymers compared to single-charged polymers will be completed to gain more insight into the behaviour of such structures in biological environment. In summary, the biological experiments showed that zwitterionic materials have valuable anti-fouling properties towards certain serum proteins and good stability in biological media and are therefore potential materials for future biological applications.

6.4 Experimental Part

Synthesis of PMAPHOS(Me)$_2$-*stat*-PLMA-*stat*-PPgMA (40)

MAPHOS (0.76 g, 3.42 mmol, 1.00 eq), LMA (0.71 g, 2.78 mmol, 0.81 eq) and PgMA (32.1 mg, 0.26 mmol, 0.08 eq) were evacuated and flushed with argon (3x), then dissolved in toluene (4 mL) and degassed for 30 minutes. AIBN (16.9 mg, 0.10 mmol, 0.03 eq) was dissolved in toluene (1 mL) and added to the monomer solution, followed by addition of 2-mercaptoethanol (12 µL, 0.17 mmol, 0.05 eq). The mixture was heated to 70 °C under inert conditions for 18 h. The crude terpolymer was precipitated twice from cold methanol, centrifuged (7000 rpm, 8 min.) and dried under reduced pressure. The polymer (**40e**, 1.50 g) was obtained as white solid with 86% yield. ^{1}H-NMR (300 MHz, $CDCl_3$, 300 K): δ = 4.62 (s, $CO_2\underline{CH_2}CCH$), 4.18 (s, $CO_2\underline{CH_2}CH_2PO(OCH_3)_2$), 3.92 (s, $CO_2\underline{CH_2}C_{11}H_{23}$), 3.78 (d, $PO(O\underline{CH_3})_2$), 3.54 (m, $C\underline{CH}$), 2.18 (m, $\underline{CH_2}PO(CH_3)_2$), 1.86 ($C\underline{CH_2}$), 1.68 (m, $CH_2\underline{CH_2}(CH_2)_9$), 1.26 (s, $(\underline{CH_2})_9$), 1.03 (s, $CH_2\underline{CH_3}$), 0.88 (t, $C\underline{CH_3}$) ppm.

Table 45: Overview of the synthesized amphiphilic terpolymers with desired and obtained mass average molecular weight (M_w), the block ratio of the monomers and amounts of AIBN and ME used in the polymerization.

Sample	***Polymer***	***x:y:z[1]/ x:y:z[2]***	***AIBN (eq)***	***ME (eq)***	***M_w (target) [Da]***	***M_w (GPC)[3] [Da]***
pma01/ 40a	PMAPHOS(Me)$_2$-*stat*-PLMA-*stat*-PPgMA	52:42:6/ 44:48:8	0.025	-	9500	6700 (THF)
pma03/ 40b	PMAPHOS(Me)$_2$-*stat*-PLMA-*stat*-PPgMA	52:42:6/ 57:41:2	0.01	0.05	9500	16200 (DMF)
pma08/ 40c	PMAPHOS(Me)$_2$-*stat*-PLMA-*stat*-PPgMA	54:44:2/ 38:61:1	0.02	0.02	9500	41 000 (DMF)
pma23/ 40d	PMAPHOS(Me)$_2$-*stat*-PLMA-*stat*-PPgMA	54:44:2/ 46:52:2	0.03	-	9500	31 000 (THF)
pma29/ 40e	PMAPHOS(Me)$_2$-*stat*-PLMA-*stat*-PPgMA	53:43:4/ 56:41:3	0.03	0.05	9500	11 000 (THF)

[1] monomer ratio, target block ratio [2] block ratio, calculated from ^{1}H-NMR [3] against PMMA standard

Synthesis of PDI-monoimide and PDI-N$_3$ (44)

PDI (3.78 g, 3.50 mmol, 1.00 eq) was dissolved in 250 mL 2-propanol/*tert*-butanol (1:1) and KOH (100 g, 1.78 mol, 510 eq) was dissolved in 25 mL H_2O under inert atmosphere. The solutions were combined and refluxed at 110 °C for 2 h. The reaction was monitored by TLC to avoid double saponification of the imides. After the reaction the mixture was cooled to r.t. and poured into 500 mL H_2O and 150 mL HCl (conc.). The product precipitated upon addition of crushed ice. The precipitate was filtered and dried under reduced pressure at 60 °C. The crude product was recrystalized from 100 mL acetic acid at 80 °C and precipitated in H_2O. Further purification was achieved by silica column

chromatography (DCM, pure) and the product PDI-monoimide (**44**, **pmaED04**) was obtained with a yield of 28% as dark red solid.

PDI-monoimide (**44**, 94.0 mg, 102 µmol, 1.00 eq) was evacuated, flushed with argon and dissolved in DMF (3 mL). 3-Azido-1-propanamine (11 µL, 107 µmol, 1.05 eq) was added and the mixture was stirred for 24 h at 70°C. The reaction was not completed, according to TLC, so 5 µL of 3-azido-1-propanamine were added to the solution and stirred again for 16 h at 70°C. The mixture was cooled to r.t. and the solvent was coevaporated with *n*-heptane and the resulting product (**45**, **pma17**, 90 mg, 90 µmol) was dried under reduced pressure and obtained as dark red solid with 88% yield. ^{1}H-NMR (300 MHz, CD_2Cl_2, 300 K): δ = 8.17 (s, C_6H_1), 8.16 (s, C_6H_1), 7.46 (t, *p*-NPh), 7.31 (m, *o*-OPh, *p*-NPh), 7.15 (m, *o*-OPh), 6.99 (m, *o*-OPh), 4.19 (t, ^{3}J = 6.9 Hz, $CH_2CH_2\underline{CH_2}N_3$), 3.38 (t, ^{3}J = 6.7 Hz, $\underline{CH_2}CH_2CH_2N_3$), 2.68 (hept, ^{3}J = 6.8 Hz, $(CH_3)_2\underline{CH}$Ph), 1.96 (q, ^{3}J = 6.8 Hz, $CH_2\underline{CH_2}CH_2N_3$), 1.08 (d, ^{3}J = 6.8 Hz, $(\underline{CH_3})_2$CHPh) ppm.

Synthesis of PMAPHOS(Me)$_2$-*stat*-PLMA-*stat*-PDI (41)

P(MAPHOS(Me)$_2$)$_{56}$-*stat*-PLMA$_{41}$-*stat*-PgMA$_3$ (**40**, 0.20 g, 18 µmol) was evacuated, flushed with argon and dissolved in toluene (8 mL). PDI-N_3 (25.8 mg, 26 µmol, 1.00 eq) and PMDETA (11 µL, 52 µmol, 2.00 eq) were added to the polymer solution. The mixture was degassed with argon für 30 min, copper(I)bromide (3.7 mg, 26 µmol, 1.00 eq) was added and the mixture was stirred at r.t. for 3 days. The reaction mixture was diluted and filtered over a bed of neutral Al_2O_3 to remove the copper complex. The dye-labelled polymer was purified by dialysis in THF to remove the remaining reagents. The product (**41**, **pma31**, 0.21 mg, quant.) was obtained as dark red resin. ^{1}H-NMR (250 MHz, $CDCl_3$, 300 K): δ = 8.24 (s, C_6H_1), 8.19 (s, C_6H_1), 7.42 (t, *p*-NPh), 7.28 (m, *o*-OPh, *p*-NPh), 7.11 (m, *o*-OPh), 6.96 (m, *o*-OPh), 5.05 (s, $CO_2\underline{CH_2}$CC-PDI), 4.19 (s, $CO_2\underline{CH_2}CH_2PO(OCH_3)_2$), 3.92 (s, $CO_2\underline{CH_2}C_{11}H_{23}$), 3.79 (d, $PO(O\underline{CH_3})_2$), 2.68 (hept, ^{3}J = 6.8 Hz, $(CH_3)_2\underline{CH}$Ph), 2.20 (m, $\underline{CH_2}PO(CH_3)_2$), 1.86 ($C\underline{CH_2}$), 1.61 (m, $CH_2\underline{CH_2}(CH_2)_9$), 1.27 (s, $(\underline{CH_2})_9$), 1.11 (d, ^{3}J = 6.8 Hz, $(\underline{CH_3})_2$CHPh), 1.02 (s, $CH_2\underline{CH_3}$), 0.87 (t, $C\underline{CH_3}$) ppm .

Synthesis of PMAPHOS-*stat*-PLMA-*stat*-PDI (42) and PMAPHOS-*stat*-PLMA-*stat*-PPgMA (43)

The polymer (0.20 g, 18 µmol) was evacuated, flushed with argon and dissolved in chloroform (4 mL; 20 mL/g). Bromotrimethylsilane (0.38 mL, 2.89 mmol; 6 eq regarding MAPHOS(Me)$_2$) was added to the polymer solution. The mixture was stirred at 60 °C for 24 h. The solvent was evaporated and the residue was dissolved in THF, followed by precipitation in cold *n*-hexane. The polymer (0.15 g, 73%) was dried under reduced pressure and obtained as colourless or dark red glassy solid.

PMAPHOS$_{56}$-*stat*-PLMA$_{41}$-*stat*-PDI$_3$ (42, pma32): ^{1}H-NMR (700 MHz, $CDCl_3$, 300 K): δ = 8.24 (s, C_6H_1), 8.20 (s, C_6H_1), 7.42 (t, *p*-NPh), 7.28 (m, *o*-OPh, *p*-NPh), 7.10 (m, *o*-OPh), 6.97 (m, *o*-OPh), 6.30 (s (broad), PO(OH)$_2$), 5.00 (s, CO_2CH_2CC-PDI), 4.29 (s, $CO_2CH_2CH_2PO(OCH_3)_2$), 3.92 (s, $CO_2CH_2C_{11}H_{23}$), 2.68 (hept, $(CH_3)_2CH$Ph), 2.32 (m, $CH_2PO(CH_3)_2$), 1.95 (CCH_2), 1.60 (m, $CH_2CH_2(CH_2)_9$), 1.26 (s, $(CH_2)_9$), 1.11 (d, ^3J = 6.8 Hz, $(CH_3)_2$CHPh), 0.88 (t, CCH_3) ppm.

PMAPHOS$_{56}$-*stat*-PLMA$_{41}$-*stat*-PPgMA$_3$ (43, pma33): ^{1}H-NMR (700 MHz, $CDCl_3$, 300 K): δ = 7.48 (s (broad), PO(OH)$_2$), 4.60 (s, CO_2CH_2CC-PDI), 4.32 (s, $CO_2CH_2CH_2PO(OCH_3)_2$), 3.93 (s, $CO_2CH_2C_{11}H_{23}$), 2.27 (m, $CH_2PO(CH_3)_2$), 1.90 (CCH_2), 1.61 (m, $CH_2CH_2(CH_2)_9$), 1.26 (s, $(CH_2)_9$), 1.06 (d, ^3J = 6.8 Hz, $(CH_3)_2$CHPh), 0.88 (t, CCH_3) ppm.

Synthesis of PDMAEMA-*stat*-PLMA-*stat*-PPgMA (46)

DMAEMA (1.12 g, 7.11 mmol, 1.00 eq), LMA (1.81 g, 7.11 mmol, 1.00 eq) and PgMA (83.3 mg, 0.59 mmol, 0.08 eq) were evacuated and flushed with argon (3x), then dissolved in toluene (6 mL) and degassed for 30 minutes. AIBN (11.7 mg, 0.07 mmol, 0.01 eq) was dissolved in toluene (1 mL) and added to the monomer solution, followed by addition of 2-mercaptoethanol (25 µL, 0.36 mmol, 0.05 eq). The mixture was heated to 70 °C under inert conditions for 18 h. The crude terpolymer was precipitated twice from cold methanol, centrifuged (7000 rpm, 8 min.) and dried under reduced pressure. The polymer (**46**, **pma02**, 2.33 g) was obtained as white solid with 78% yield. ^{1}H-NMR (300 MHz, $CDCl_3$, 300 K): δ = 4.60 (s, CO_2CH_2CCH), 4.07 (s, $CO_2CH_2CH_2N(CH_3)_2$), 3.91 (s, $CO_2CH_2C_{11}H_{23}$), 2.59 (s, $CH_2N(CH_3)_2$), 2.30 (d, $N(CH_3)_2$), 1.90 (m, $CH_2CH_2(CH_2)_9$), 1.60 (m, CH_2CH_2, $CH_2(CH_2)_8$), 1.26 (s, $(CH_2)_8$), 1.03 (s, CH_2CH_3), 0.88 (t, CCH_3) ppm.

Table 46: Overview of the synthesized amphiphilic terpolymers with desired and obtained mass average molecular weight (M_w), the block ratio of the monomers and amounts of AIBN and ME used in the polymerization.

Sample	***Polymer***	***x:y:z[1]/ x:y:z[2]***	***AIBN (eq)***	***ME (eq)***	***M_w (target) [Da]***	***M_w (GPC)[3] [Da]***
pma02/ ***46a***	PDMAEMA-*stat*-PLMA-*stat*-PPgMA	52:46:4/ 54:43:3	0.010	0.05	11000	7200 (DMF)
pma04/ ***46b***	PDMAEMA-*stat*-PLMA-*stat*-PPgMA	51:45:4/ 57:40:3	0.020	0.05	7000	7100 (THF)
pma06/ ***46c***	PDMAEMA-*stat*-PLMA-*stat*-PPgMA	48:48:4/ 50:46:4	0.005	0.05	11000	8100 (DMF)
pma13/ ***46d***	PDMAEMA-*stat*-PLMA-*stat*-PPgMA	48:48:4/ 48:48:4	0.03	-	17800	15600 (THF)
pma19/ ***46e***	PDMAEMA-*stat*-PLMA-*stat*-PPgMA	62:36:2/ 62:36:2	0.05	0.05	4700	3900 (THF)

[1] monomer ratio, target block ratio [2] block ratio, calculated from ^{1}H-NMR [3] against PMMA standard

Synthesis of PDMAEMA-*stat*-PLMA-*stat*-PDI (47)

$PDMAEMA_{54}$-*stat*-$PLMA_{43}$-*stat*-$PgMA_3$ (**46**, 0,20 g, 28 µmol) was evacuated, flushed with argon and dissolved in toluene (8 mL). PDI-N_3 (30.8 mg, 31 µmol, 1.00 eq) and PMDETA (13 µL, 61 µmol, 2.00 eq) were added to the polymer solution. The mixture was degassed with argon für 30 min, copper(I)bromide (4.4mg, 31 µmol, 1.00 eq) was added and the mixture was stirred at r.t. for 3 days. The reaction mixture was diluted and filtered over a bed of neutral Al_2O_3 to remove the copper complex. The dye-labelled polymer was purified by dialysis in THF to remove the remaining reagents. The product (**47**, **pma09**, 0.20 mg, quant.) was obtained as dark red resin. ^{1}H-NMR (700 MHz, $CDCl_3$, 300 K): δ = 8.24 (s, C_6H_1), 8.19 (s, C_6H_1), 7.41 (t, *p*-NPh), 7.11 (m, *o*-OPh), 6.96 (m, *o*-OPh), 4.45 (s, $CO_2\underline{CH_2}CCH$), 4.11 (s, $CO_2\underline{CH_2}CH_2N(CH_3)_2$), 3.91 (s, $CO_2\underline{CH_2}C_{11}H_{23}$), 3.75 (t, $\underline{CH_2}CH_2CH_2N_3$), 2.68 (m, $(CH_3)_2\underline{CH}Ph$), 2.67 (s, $\underline{CH_2}N(CH_3)_2$), 2.34 (s, $N(\underline{CH_3})_2$), 1.84 (m, $CH_2\underline{CH_2}(CH_2)_9$), 1.60 (m, CH_2CH_2, $\underline{CH_2}(CH_2)_8$), 1.26 (s, $(\underline{CH_2})_8$), 1.11 (d, ^3J = 6.4 Hz, $(\underline{CH_3})_2$CHPh), 1.04 (m, $CH_2\underline{CH_3}$), 0.87 (t, $C\underline{CH_3}$) ppm.

Synthesis of PTMAEMA-*stat*-PLMA-*stat*-PDI (48) and PTMAEMA-*stat*-PLMA-*stat*-PPgMA (49)

The polymer (0.15 g, 21 µmol) was evacuated, flushed with argon and dissolved in DCM (3 mL; 20 mL/1 g polymer). Methyl iodide (26 µL; 1 eq regarding DMAEMA) was added dropwise to the polymer solution. The mixture was stirred at r.t. for 24 h. The solvent was evaporated, the residue was dissolved in THF and precipitated in cold *n*-hexane (2x). The polymer (0.16 g, quant.) was dried under reduced pressure and obtained as colourless or dark red glassy solid.

$PTMAEMA_{54}$-*stat*-$PLMA_{43}$-*stat*-PDI_3 (48, pma07): ^{1}H-NMR (700 MHz, $CDCl_3$, 300 K): δ = 8.24 (s, C_6H_1), 8.18 (s, C_6H_1), 7.41 (t, *p*-NPh), 7.11 (m, *o*-OPh), 6.97 (m, *o*-OPh), 4.80-3.80 (m, $CO_2\underline{CH_2}CCH$, $CO_2\underline{CH_2}CH_2N(CH_3)_2$, $CO_2\underline{CH_2}C_{11}H_{23}$), 3.60 (s, $N(\underline{CH_3})_2$), 2.90 (m, $(CH_3)_2\underline{CH}Ph$), 2.15 (s, $\underline{CH_2}N(CH_3)_2$), 1.94 (m, $CH_2\underline{CH_2}(CH_2)_9$), 1.61 (m, $CH_2CH_2\underline{CH_2}(CH_2)_8$), 1.26 (s, $(\underline{CH_2})_8$), 1.11 (d, ^3J = 6.1 Hz, $(\underline{CH_3})_2$CHPh), 1.04 (s, $CH_2\underline{CH_3}$), 0.88 (t, $C\underline{CH_3}$) ppm.

$PTMAEMA_{54}$-*stat*-$PLMA_{43}$-*stat*-$PPgMA_3$ (49, pma14): ^{1}H-NMR (700 MHz, $CDCl_3$, 300 K): δ = 4.85-3.81 (m, $CO_2\underline{CH_2}CCH$, $CO_2\underline{CH_2}CH_2N(CH_3)_2$, $CO_2\underline{CH_2}C_{11}H_{23}$), 3.64 (s, $N(\underline{CH_3})_2$), 2.16 (s, $\underline{CH_2}N(CH_3)_2$), 1.94 (m, $CH_2\underline{CH_2}(CH_2)_9$), 1.60 (m, $CH_2CH_2\underline{CH_2}(CH_2)_8$), 1.25 (s, $(\underline{CH_2})_8$), 1.10 (m, $CH_2\underline{CH_3}$), 0.88 (s, $C\underline{CH_3}$) ppm.

Synthesis of PSBMA-*stat*-PLMA-*stat*-PDI (50) and PSBMA-*stat*-PLMA-*stat*-PPgMA (51)

The polymer (0.20 g, 26 µmol) was evacuated, flushed with argon and dissolved in chloroform (4 mL; 40 mL/1 g polymer). 1,3-Propansultone (54.8 mg, 0.47 eq; 1.1 eq regarding DMAEMA) was dissolved in 2 mL chloroform and added dropwise to the polymer solution. The mixture was stirred for 24 h at 40 °C. Then, 2 mL water was added and stirred for 6 hours at 40 °C to hydrolyse unreacted 1,3-propansultone. The reaction mixture was extracted with 1% NaCl solution twice. The polymer (0.15 g, quant.) was dried under reduced pressure and obtained as colourless or dark red solid.

$PSBMA_{54}$-*stat*-$PLMA_{43}$-*stat*-PDI_3 (50, pma15): ^{1}H-NMR (300 MHz, $CDCl_3$, 300 K): δ = 8.24 (s, C_6H_1), 8.18 (s, C_6H_1), 7.41 (t, *p*-NPh), 7.46 (m, *o*-OPh, *p*-NPh), 7.11 (m, *o*-OPh), 6.97 (m, *o*-OPh), 5.10-2.79 (m, $CO_2\underline{CH_2}CCH$, $CO_2\underline{CH_2}CH_2N(CH_3)_2$, $CO_2\underline{CH_2}C_{11}H_{23}$, $\underline{CH_2CH_2}SO_3^-$, $N(\underline{CH_3})_2$), 2.28 (m, $\underline{CH_2}N(CH_3)_2$, $CH_2\underline{CH_2}(CH_2)_9$), 1.60 (m, $CH_2CH_2\underline{CH_2}(CH_2)_8$), 1.26 (s, $(\underline{CH_2})_8$), 1.10 (m, $CH_2\underline{CH_3}$), 0.87 (s, $C\underline{CH_3}$) ppm. (Due to the zwitterionic charge of the polymer, the solubility in deuterated solvents was low and the signals very broad and overlapping, making proper signal integration inaccurate).

$PSBMA_{54}$-*stat*-$PLMA_{43}$-*stat*-$PPgMA_3$ (51, pma42): ^{1}H-NMR (300 MHz, $CDCl_3$, 300 K): δ = 4.48-3.22 (m, $CO_2\underline{CH_2}CCH$, $CO_2\underline{CH_2}CH_2N(CH_3)_2$, $CO_2\underline{CH_2}C_{11}H_{23}$, $\underline{CH_2CH_2}SO_3^-$), 3.08 (s, $N(\underline{CH_3})_2$), 2.28 (s, $\underline{CH_2}N(CH_3)_2$), 1.94 (m, $CH_2\underline{CH_2}(CH_2)_9$), 1.60 (m, $CH_2CH_2\underline{CH_2}(CH_2)_8$), 1.26 (s, $(\underline{CH_2})_8$), 1.10 (m, $CH_2\underline{CH_3}$), 0.87 (s, $C\underline{CH_3}$) ppm. (Due to the zwitterionic charge of the polymer, the solubility in deuterated solvents was low and the signals very broad and overlapping, making proper signal integration inaccurate).

Synthesis of PMPC-*stat*-PLMA-*stat*-PPgMA (52)

MPC (1.04 g, 3.54 mmol, 1.00 eq), LMA (0.94 g, 3.68 mmol, 1.04 eq) and PgMA (18.3 mg, 0.15 mmol, 0.04 eq) were evacuated and flushed with argon (3x), then dissolved in ethanol (6 mL) and degassed for 30 minutes. AIBN (5.81 mg, 0.04 mmol, 0.01 eq) was dissolved in ethanol (1 mL) and added to the monomer solution, followed by addition of 2-mercaptoethanol (6 µL, 0.09 mmol, 0.03 eq). The mixture was heated to 70 °C under inert conditions for 18 h. The crude terpolymer was precipitated twice from cold diethylether, centrifuged (7000 rpm, 8 min.) and dried under reduced pressure. The polymer (**52a**, **pma12**, 1.72 g) was obtained as white solid with 90% yield. ^{1}H-NMR (700 MHz, $CDCl_3$, 300 K): δ = 4.52-3.57 (m, $CO_2\underline{CH_2}CCH$, $CO_2\underline{CH_2}CH_2N(CH_3)_2$, $CO_2\underline{CH_2}C_{11}H_{23}$, $CH_2\underline{CH_2}O$, $\underline{CH_2CH_2}N(CH_3)_2$), 3.38 (s, $N(\underline{CH_3})_3$), 1.79 (m, $CH_2\underline{CH_2}(CH_2)_9$), 1.60 (m, $CH_2CH_2\underline{CH_2}(CH_2)_8$), 1.27 (s, $(\underline{CH_2})_8$), 1.02 (m, $CH_2\underline{CH_3}$), 0.87 (s, $C\underline{CH_3}$) ppm.

Table 47: Overview of the synthesized amphiphilic terpolymers with desired and obtained mass average molecular weight (M_w), the block ratio of the monomers and amounts of AIBN and ME used in the polymerization.

Sample	***Polymer***	***x:y:z[1]/ x:y:z[2]***	***AIBN (eq)***	***ME (eq)***	***M_w (target) [Da]***	***M_w (GPC)[3] [Da]***
pma12/ ***52a***	PMPC-*stat*-PLMA-*stat*-PPgMA	48:50:2/ 48:50:2	0.010	0.025	22900	21800 (THF)
pma24/ ***52b***	PMPC-*stat*-PLMA-*stat*-PPgMA	54:44:2/ -	0.009	0.015	30000	2900 (THF)
pma30/ ***52c***	PMPC-*stat*-PLMA-*stat*-PPgMA	53:43:4/ 50:48:2	0.009	0.015	30000	- (THF)
pma34/ ***52d***	PMPC-*stat*-PLMA-*stat*-PPgMA	53:44:3/ 46:52:2	0.01	0.025	30000	- (THF)

[1] monomer ratio, target block ratio [2] block ratio, calculated from ^{1}H-NMR [3] against PMMA standard

Synthesis of PMPC-*stat*-PLMA-*stat*-PDI (53)

$PMPC_{48}$-*stat*-$PLMA_{50}$-*stat*-$PgMA_2$ (0,20 g, 9 µmol) was evacuated, flushed with argon and dissolved in toluene (8 mL). PDI-N_3 (14.8 mg, 15 µmol, 1.00 eq) and PMDETA (6 µL, 29 µmol, 2.00 eq) were added to the polymer solution. The mixture was degassed with argon für 30 min, copper(I)bromide (2.1 mg, 15 µmol, 1.00 eq) was added and the mixture was stirred at r.t. for 3 days. The reaction mixture was diluted and filtered over a bed of neutral Al_2O_3 to remove the copper complex. The dye-labelled polymer was purified by dialysis in ethanol to remove the remaining reagents. The product (**53**, **pma20**, 0.16 mg, 79%) was obtained as dark red resin. ^{1}H-NMR (700 MHz, $CDCl_3$, 300 K): δ = 8.24 (s, C_6H_1), 8.19 (s, C_6H_1), 7.41 (t, *p*-NPh), 7.28 (m, *o*-OPh, *p*-NPh), 7.10 (m, *o*-OPh), 6.97 (m, *o*-OPh), 4.56-3.63 (m, $CO_2\underline{CH_2}CCH$, $CO_2\underline{CH_2}CH_2N(CH_3)_2$, $CO_2\underline{CH_2}C_{11}H_{23}$, $CH_2\underline{CH_2}O$, $\underline{CH_2CH_2}N(CH_3)_2$), 3.38 (s, $N(\underline{CH_3})_3$), 2.68 (m, $(CH_3)_2\underline{CH}Ph$), 1.79 (m, $CH_2\underline{CH_2}(CH_2)_9$), 1.60 (m, $CH_2CH_2\underline{CH_2}(CH_2)_8$), 1.27 (s, $(\underline{CH_2})_8$), 1.10 (d, $(\underline{CH_3})_2CHPh$) 1.02 (m, $CH_2\underline{CH_3}$), 0.88 (s, $C\underline{CH_3}$) ppm.

Synthesis of Azido-PEG$_3$-FA (54)

Folic acid (100 mg, 0.227 mmol, 1.00 eq) was dissolved in 2 mL DMSO and 50 µL triethylamine (0.362 mmol, 1.60 eq) was addded. N-hydroxysuccinimide (NHS, 52.1 mg, 0.453 mmol, 2.00 eq) and dicyclohexylcarbodiimide (DCC, 93.5 mg, 0.453 mmol, 2.00 eq) were added and stirred overnight at room temperature. The by-product, dicyclohexylurea, was removed by filtration. 2-{2-[2-(2-Azidoethoxy)-ethoxy]-ethoxy}-ethylamin (45 µL, 0.227 mmol, 1.00 eq) was added to the reaction mixture and stirred for 3 h. The product was purified by dropwise addition of the reaction mixture to diethylether/acetone (80:20) and subsequent centrifugation. The filtrate was removed, the solid was washed twice with the solvent mixture and dried *in vacuo*. The resulting azido-PEG$_3$ ester of folic acid (Azido-PEG$_3$-FA, **54**) was obtained as yellow solid with 95% yield. ^{1}H-NMR (700 MHz, DMSO-d$_6$, 300 K): δ = 11.9 (s, 1H, COOH), 8.64 (s, 1H, NH), 8.00 (s, 1H, CH), 7.86 (d, 1H, NH), 7.65 (s, 2H, CH), 6.91 (s, 1H, NH), 6.65 (s, 2H, CH), 4.49 (s, 2H, FA-CH$_2$), 4.29 (m, 1H, FA-CH), 3.58 (s, 2H, PEG-CH$_2$), 3.53 (s, 4H, PEG-CH$_2$), 3.50 (s, 4H, PEG-CH$_2$), 3.37 (s, 2H, PEG-CH$_2$), 3.17 (s, 2H, PEG- CH$_2$), 2.27 (m, 1H, FA-CH$_2$), 2.18 (m, 1H, FA-CH$_2$), 2.05 (t, 1H, FA-CH$_2$), 1.91 (t, 1H, FA-CH$_2$) ppm.

Synthesis of PMPC-*stat*-PLMA-*stat*-FA (55)

PMPC$_{48}$-*stat*-PLMA$_{50}$-*stat*-PgMA$_2$ (0,185 g, 9 µmol) was evacuated, flushed with argon and dissolved in toluene (8 mL). FA-N$_3$ (4.4 mg, 7 µmol, 1.00 eq) and PMDETA (3 µL, 15 µmol, 2.00 eq) were added to the polymer solution. The mixture was degassed with argon für 30 min, copper(I)bromide (1.1 mg, 7 µmol, 1.00 eq) was added and the mixture was stirred at r.t. for 3 days. The reaction mixture was diluted and filtered over a bed of neutral Al_2O_3 to remove the copper complex. The FA-labelled polymer was purified by dialysis in ethanol to remove the remaining reagents. The product (**55**, **pma56**, 0.16 mg, 77%) was obtained as yellow resin. ^{1}H-NMR (700 MHz, DMSO-d$_6$, 300 K): δ = 7.66 (s,2H, FA-CH), 7.43 (s, 1H, FA-NH), 7.31 (s, 1H, FA-NH), 6.66 (s, 2H, FA-CH), 4.53 (s, 2H, FA-CH$_2$), 4.28-3.90 ($CO_2\underline{CH_2}CH_2N(CH_3)_2$, $CO_2\underline{CH_2}C_{11}H_{23}$, $CH_2\underline{CH_2}O$, $\underline{CH_2CH_2}N(CH_3)_2$), 3.67 (s, $N(\underline{CH_3})_3$), 3.48 (m, 16H, FA: PEG-CH$_2$), 2.68 (m, $(CH_3)_2\underline{CH}Ph$), 2.27 (s, 2H, FA-CH$_2$), 1.91 (s, 2H, FA-CH$_2$), 1.91-1.70 (m, $CH_2\underline{CH_2}(CH_2)_9$), 1.58 (m, $CH_2CH_2\underline{CH_2}(CH_2)_8$), 1.29 (s, $(\underline{CH_2})_8$, $(\underline{CH_3})_2CHPh$) 0.97 (m, $CH_2\underline{CH_3}$), 0.88 (s, $C\underline{CH_3}$) ppm.

7 General Summary and Outlook

The overall scope of this thesis was the investigation of nanoparticle behaviour in biological environment in respect of the particle surface composition. Divided into polar-ionic and polar-nonionic surfaces, different materials were synthesized in order to investigate their stability and aggregation behaviour in aqueous solution as well as the interactions with biomolecules like serum proteins or cells (Figure 108). The gained knowledge was used to evaluate different technologies to develop a potent drug carrier system for biomedical applications.

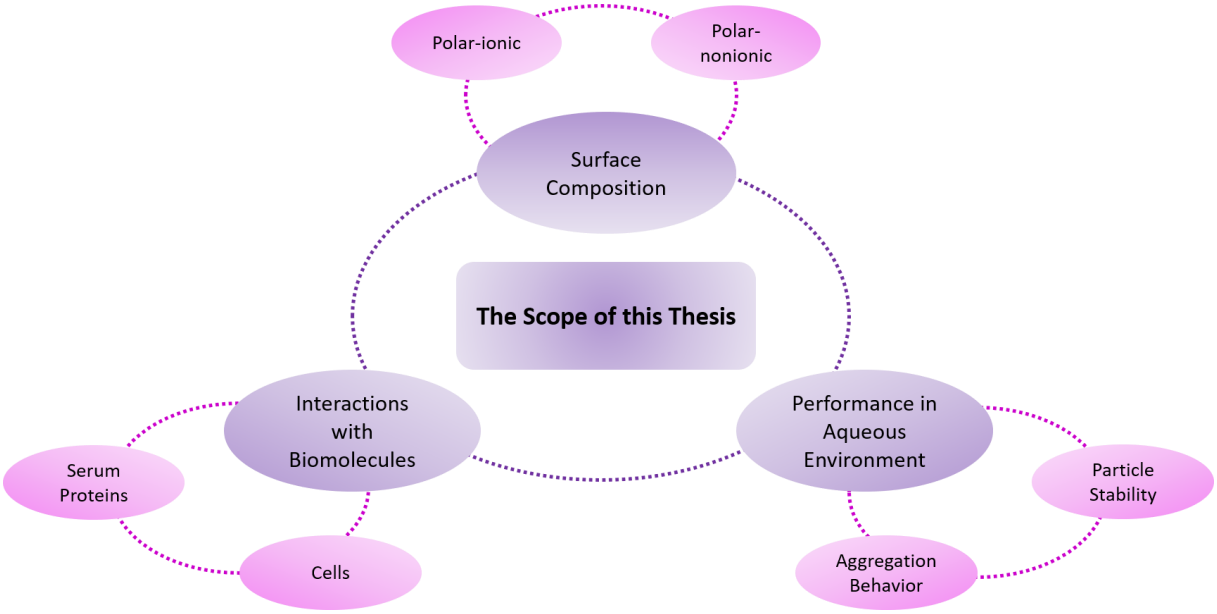

Figure 108: The main scope of this thesis was the investigation of the behaviour of nanoparticles in biological environment depending on the particle surface composition.

The main project focused on the development of a core shell nanoparticle system with a polar nonionic surface for drug delivery applications in cancer therapy. In order to obtain a feasible drug delivery device several requirements had to be fulfilled (Figure 109). Not only an easy and straight forward synthesis strategy was of high interest, but also good aggregation behaviour of the nanoparticles in aqueous environment and minimal interactions with biomolecules. To suppress such interactions, like protein corona formation, the particles were designed with a polar nonionic surface.[90] Polar nonionic materials like PEG are known to barely form a protein corona.[173] In addition, good biocompatibility and biodegradability were crucial factors that had to be met for the use in biomedical applications.[8] To prevent fast clearance and enable long blood circulation times, a particle diameter of around 100 nm was desired.[9] At the same time, the particles had to be fully inert during circulation and release the drug at the target cells only.[10] This should be ensured by the installation of a specific enzyme-cleavable peptide sequence in the particle shell.[6]

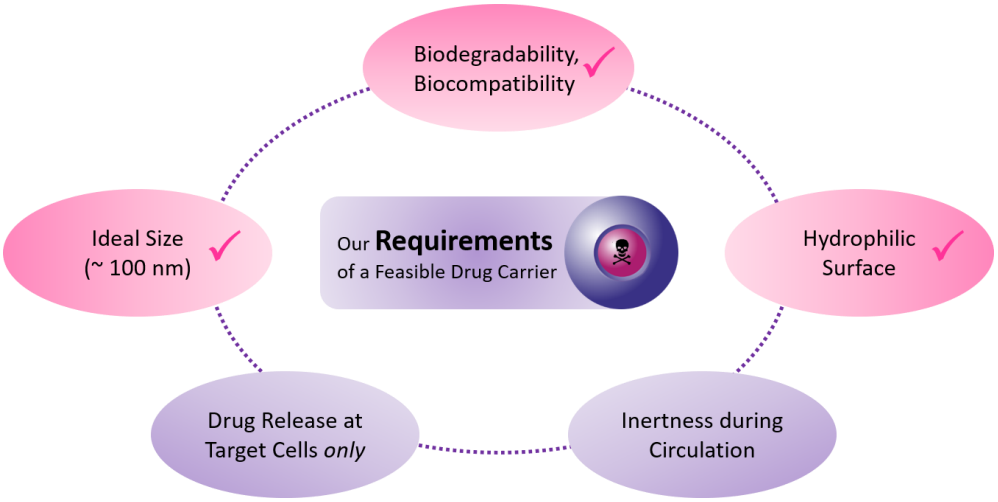

Figure 109: The requirements of our drug carrier system were partially fulfilled within this thesis.

For the nanoparticle synthesis by nonaqueous emulsion polymerization, special effort was put into the synthesis of suitable block copolymers as emulsifiers. These materials had to show good biocompatibility as they shaped the shell of the nanoparticles. They had to be amphiphilic with a high hydrophobic ratio to be dispersible in nonaqueous solution, but at the same time the hydrophobic moiety had to be cleavable to transfer the particles into aqueous solution after the nanoparticle synthesis. Therefore, the synthesis of amino acid-based block copolymers was conducted as they are natural building blocks and easy to functionalize. The natural amino acid serine with its polar nonionic hydroxyl side chain was of special interest. The synthesis of amphiphilic benzyl-serine-based block copolymers was performed successfully and PEG-*b*-PLS(Bn) polymers of different block ratios were obtained. Unfortunately, the quantitative polymerization of the L-serine block could not be achieved due to the amphiphilicity of the block copolymer and strong beta sheet formation of the serine block leading to poor solubility in organic solvents. This issue was fixed by the use of racemic DL-serine in order to suppress the formation of secondary structures. However, both materials were not well dispersible in nonpolar organic solvents and hence not applicable as emulsifiers in nonaqueous emulsion polymerization. Nevertheless, some optimization of the nanoparticle synthesis was achieved by tuning the reaction parameters like solvent system and block ratio of the emulsifier, resulting in spherical nanoparticles of desired size in low yields. It was hypothesized that the hydrophobicity of the benzyl group was too low, even at high block lengths, to stabilize the dispersion. As a result, the solubility in nonpolar solvents was too low to prevent early precipitation of the material. Instead, it led to strong aggregation of the polymers in nonpolar solution and it was decided to change the protecting group from benzyl to the more hydrophobic pyrene. This was also advantageous, as the benzyl group was not cleavable from the polymer side chains, even under harsh conditions, whereas the pyrene group was a photolabile protecting group that can be cleaved under mild conditions by light exposure.

The fabricated Bn-serine based block copolymers did not remain unused (Figure 110). Instead of using them in nonpolar solvents, their performance in aqueous solution was investigated. And indeed, both, L- and DL-polymers, formed stable vesicular structures in aqueous solution with diameters of around 100 nm, confirmed by DLS and Cryo-TEM. The obtained polymersomes had good long-term stability in aqueous solution and excellent cell viability. Drug loading with doxorubicin was performed successfully and the DOX-loaded carriers showed good cell viability. Cell uptake experiments demonstrated that the encapsulation of doxorubicin into the PEG-*b*-PLS(Bn) assemblies resulted in little to no DOX release within 24 hours of incubation, proving that the vesicles were stable in the cell medium during this time period. In addition, the encapsulation changed the distribution of DOX. The DOX-loaded vesicles were uptaken by the cells, but prevented entering the cell nuclei, compared to pure DOX, which was primarily observed in the cell nuclei. Overall, this was a great result, showing that this comparably simple drug delivery system was stable in biological environment, if no trigger mechanism was incorporated into the carrier.

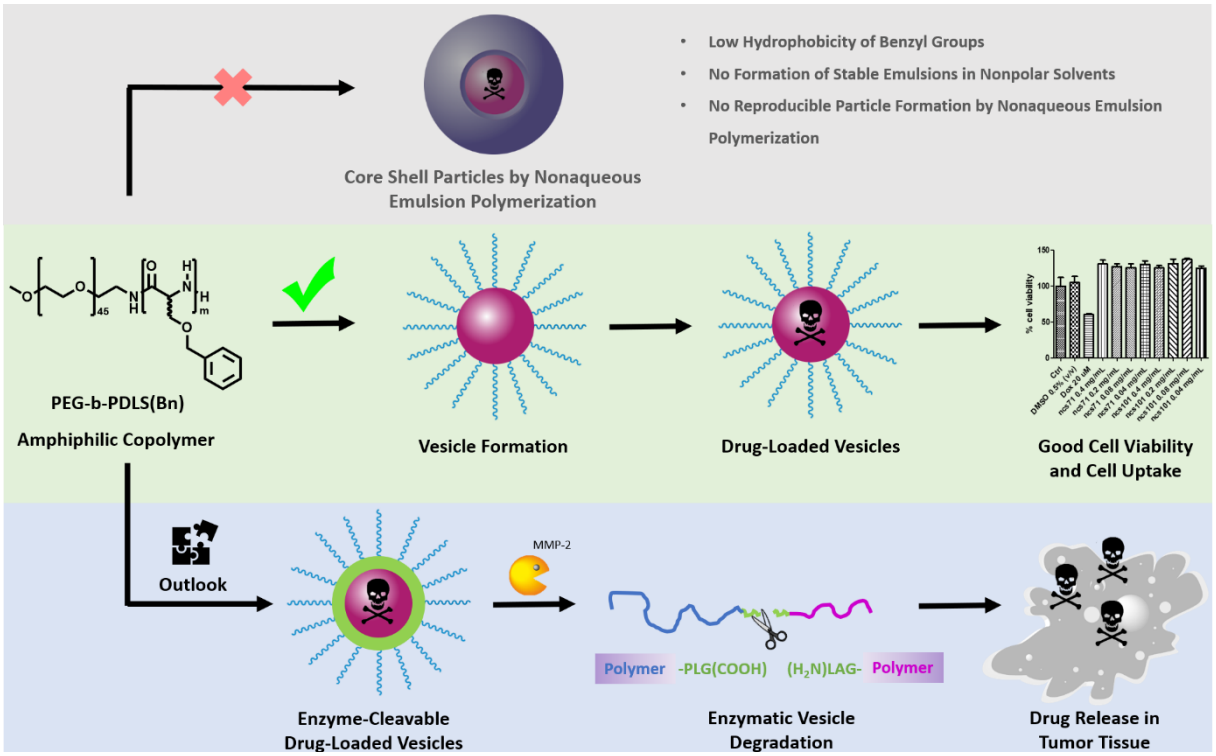

Figure 110: Benzyl-serine based copolymers as promising candidates for vesicular drug delivery systems.

It bears the chance to build a potent carrier to safely deliver a drug into the tumor tissue without drug leakage, followed by a controlled release of the drug at the target tissue. To enable the drug release in the target cells, the installation of an enzyme-cleavable peptide sequence in between the two polymer blocks should be the next step. By enzyme-specific cleavage of the hydrophilic PEG-shell of the micelles within the tumor tissue, the micelles collapse due to precipitation of the hydrophobic poly-benzyl-

serine block, eventually leading to the local release of the drug. Vesicle degradation in the presence of the MMP-2 enzyme should be investigated and drug release studies should be conducted with the carrier system after introduction of the trigger sequence into the block copolymers (Figure 110).

To overcome the dispersity problems of benzyl-serine based polymers in nonpolar organic solvents, a protecting group with higher hydrophobicity was used for the serine side chain. Pyrene was selected as the protecting group, as it is much more hydrophobic than the benzyl group. In addition, the pyrene group is photoactive, enabling the cleavage of the protecting group by light exposure after the emulsion polymerization of the nanoparticles. Different synthetic routes were used to introduce pyrene into the serine side chain as ether, carbonate or ester. Eventually, pyrene carboxylic acid was used to convert the hydroxyl group to an ester group, which was achieved successfully by standard coupling reaction in good yields (Scheme 64). To prevent side reactions with the amine or carboxylic acid of serine, a protected derivative was used, where both functional groups were protected with benzylic protecting groups. To convert the fully protected Cbz-*O*-pyrenyl-serine-benzylester into a cyclic NCA monomer for ROP, a one-pot approach was established, where the deprotection of the N- and C-terminus by catalytic hydrogenation and the cyclization with triphosgene was performed in one single step. The product, *O*-pyrenyl-serine NCA, was obtained in excellent yields. The ROP of this serine derivative with PEG macroinitiators of different block lengths was performed and the corresponding block copolymers PEG-*b*-PDLS(Pyr) were obtained successfully.

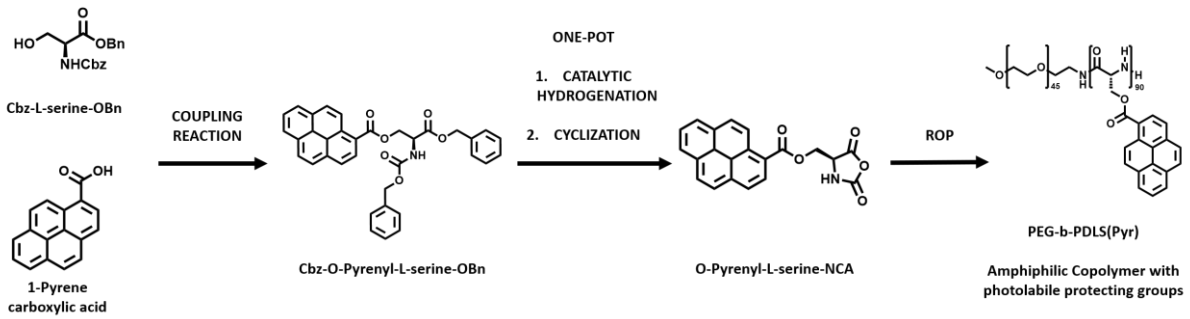

Scheme 64: Synthesis route of photolabile and amphiphilic O-pyrenyl-serine based block copolymers.

Similar to the polymerizations with the Bn-serine derivative, the theoretical DP was not reached during the polymerization, due to the poor solubility of the resulting amphiphilic block copolymers when reaching a certain block length. Changing the solvent and using the racemic monomer slightly increased the DP. Nevertheless, dispersions of the polymers in cyclohexane were studied and showed a clear improvement in comparison to the less hydrophobic benzyl serine polymers in terms of emulsion stability and homogeneity. Nonaqueous emulsion polymerization in the solvent system DMF/DiPE resulted in spherical and dispersed nanoparticles with diameters of 50-100 nm. According to the SEM analysis, they showed a homogenous morphology and significant decrease of aggregated

material, compared to the Bn-serine analogues. With these great results, a solid basis for the development of our nanocarrier system with a polar nonionic shell was built. The next steps would the cleavage of the serine side chain and the optimization of the purification protocol of the nanoparticles to avoid postsynthetic aggregation. Then, the enzyme-cleavable sequence should be incorporated into the nanoparticle shell to allow the selective enzyme-mediated drug-release. Eventually, biological studies should be performed to investigate the cell viability, cell uptake and drug-release mechanism in biological environment.

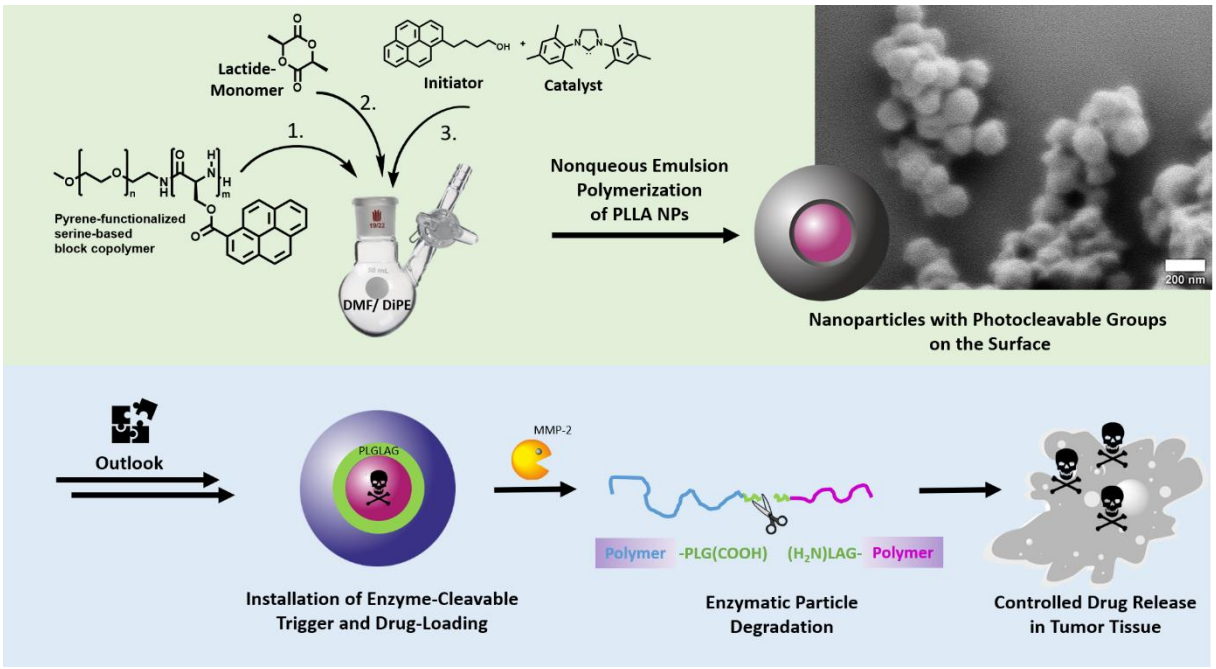

Figure 111: Synthesis of well-defined nanoparticles by using PEG-b-PLS(Pyr) block copolymer as emulsifier in nonaqueous emulsion polymerization of PLLA and outlook on the next steps, the installation of an enzyme-cleavable peptide sequence in the particle shell and the drug loading to allow controlled drug release in the tumor tissue.

The second project was a collaboration with the group of Prof. Dr. Wolfgang Parak from University of Hamburg and focused on investigating the behaviour of charged nanoparticles in biological environment, with special interest on aggregation and protein interactions. The synthesis of amphiphilic PMA-based terpolymers with differing charged side chains for the coating of gold nanoparticles was performed successfully within this thesis. The synthesis of the polymers was conducted by free radical polymerization and statistical terpolymers with negative, positive or zwitterionic charges and varying molecular weights and charge density were obtained. Additionally, the polymers were functionalized by click reaction with the fluorescent dye PDI for imaging of cell uptake experiments or folic acid as a targeting unit to promote cell uptake. (Scheme 65).

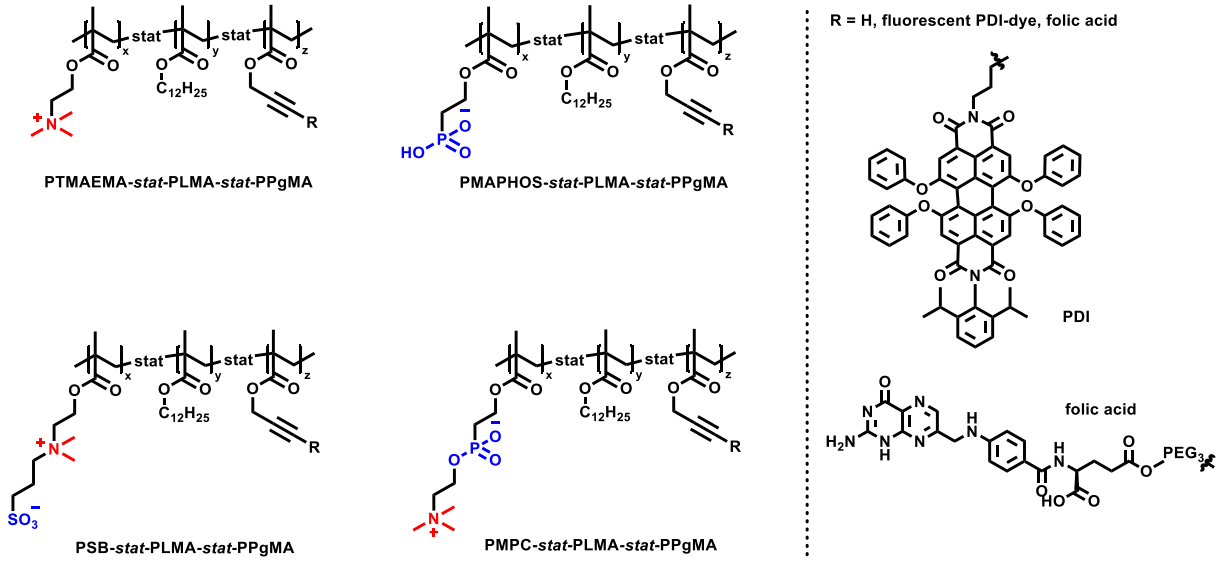

Scheme 65: Synthesized charged PMA-based terpolymers for gold nanoparticle coating.

Nanoparticle coating with these materials and further studies were performed by our collaboration partners. Successful coating and stability of the polymer-coated particles in aqueous sodium chloride media was confirmed by DLS studies. All four systems resulted in equally well dispersed nanoparticles with hydrodynamic diameters of 20-30 nm. FCS measurements of quantum dots that were coated with the zwitterionic MPC-polymer and dispersed in aqueous BSA, HSA or Tf (transferrin) media resulted in constant diffusion properties and particle size. This indicated that the zwitterionic MPC-based polymer indeed had anti-fouling properties against protein corona formation, which was expected for zwitterionic materials. In contrast, HSA proteins showed a high affinity towards the positively charged QDs (quantum dots) due to protein corona formation. Cell viability tests showed good results for all four polymer-coated QDs at concentrations up to 100 nM. Incubation of the QDs with HeLa cells demonstrated that the cell uptake was concentration-dependent and increased with the concentration. The best results were observed at 50 nM. In conclusion, promising results were

obtained with the MPC-based polymer-coated nanoparticles regarding the suppression of protein corona formation. The folic acid-functionalization of the MPC polymer was executed in order to study the effect on the cell uptake of the MPC-polymer coated QDs. Folic acid is reported to promote the cell uptake. The experiments were conducted with cell medium that either contained FBS (fetal bovine serum) or no additional protein serum to study, if protein interactions were observed and had an effect on the cell uptake. Two cancer cell lines, HeLa and MCF7, were used and showed comparable results. If FBS was present in the cell medium, no remarkable uptake of the QDs was observed and folic acid had no positive effect. In the cell medium without FBS, the cell uptake was significantly increased and a trend of higher uptake was shown for the FA-functionalized QDs. These first results indicated that contrary to the stability studies, the FBS contained components that strongly interacted with the QDs and inhibited the cell uptake. On the other side, a positive effect of FA-functionalization was observed. To understand how FBS interfered with the cell uptake of the QDs, further studies are required to understand, which proteins were overcoming the shielding effect of the zwitterionic MPC polymer. We need to understand, if these proteins are critical and present in human serum as well. If these proteins are specific for FBS, another serum needs to be used for further testing. If the corresponding proteins are indeed present in human serum, the anti-fouling properties of our zwitterionic proteins need to be adapted, accordingly. The stability studies proved that the zwitterionic materials have valuable anti-fouling properties towards main components of human blood serum and good stability in biological media. Nevertheless, the MPC-polymers did not provide universal shielding effects towards all components of fetal bovine serum and require further investigation and optimization.

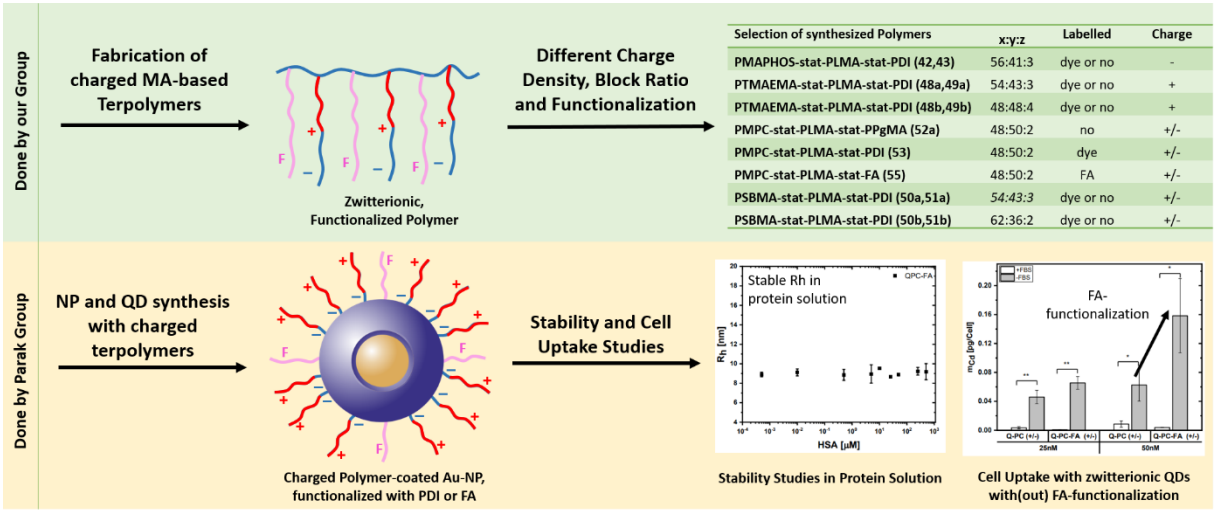

Figure 112: A broad selection of charged MA-based terpolymers was synthesized in our group and functionalized with a fluorescent dye or the targeting unit folic acid to perform biological studies. The polymers were used by the Parak group to coat AuNPs or QDs for stabilization in aqueous media. Protein interaction and cell uptake experiments were performed to investigate the behaviour of the coated particles in dependence of their surface charge.[64,184]

Feasibility and comparison to the literature. In this thesis, different approaches were executed to develop a drug delivery system for cancer therapy. Each concept had clear strengths as well as some drawbacks in comparison to similar systems in the literature. Starting from the organic core-shell nanoparticles, the adaptation of the nonaqueous emulsion polymerization to fabricate biocompatible nanoparticles by using bio-inspired emulsifiers was a challenge itself. While classical polymers disperse well in nonpolar organic solvents,[36,37,47] amino acid-based polymers showed a tendency to strong aggregation. Therefore, the straight-forward synthesis of nanoparticles was not as successful with the serine-based emulsifiers. Even though it is a one-pot synthesis, it is comparably complex, in comparison to the fabrication of other drug delivery systems, like micellar or lipid-based carriers.[134–136,152] The particle surface needed to allow dispersion in nonaqueous solution after the synthesis and good dispersibility in aqueous media after the hydrophilization, requiring a polarity-switchable emulsifier with precise aggregation behaviour. Micellar vesicles or liposome carriers are easily synthesized in aqueous solution without the need of solvent transfers by postsynthetic surface modification.[69,134] Organic solvents that are generally problematic for biomedical applications due to their cytotoxicity are not required for the synthesis of such vesicles.[190,191] Thinking one step further, the commercialization of the system, organic solvents, NHC catalysts or pyrene are comparably expensive reagents that reduce the margin to obtain a profitable business case. All these aspects make it difficult to sell the core-shell nanoparticles as a feasible drug delivery system at the point where we currently are in the project. Nevertheless, core-shell nanoparticles are very stable, preventing common issues in drug delivery like drug leakage during circulation.[6,50] Despite the drawbacks of the nanoparticle synthesis, the concept of an enzyme-responsible drug delivery system is extremely promising and interesting, if further optimized. The specificity of the MMP-2 induced drug release towards tumor tissue was not only proven by our group, but is also well known in literature.[67,167,192] The literature shows that MMP-2 responsive liposome or micelle-based drug delivery systems are working.[27,69] Consequently, keeping the basic concept of enzyme-responsiveness and simplifying the system would be highly beneficial to its feasibility.

Besides the core-shell nanoparticles, vesicular delivery systems based on the PEG-*b*-PSer(Bn) block copolymers were investigated and good results were obtained. The vesicles were fabricated in aqueous solution by standard dialysis method. They consisted of the polymer only without the need of any additional solvents or reagents. To compare it with other systems, DOX as a model drug was encapsulated without any negative effects on the stability of the assemblies. They were reproducible and showed good shelf life without any signs of aggregation. The polymer showed excellent biocompatibility towards A549 cells, even at high concentrations, making them competitive with other vesicles for drug delivery.[27,193] The DOX-loaded vesicles were uptaken by the cells and stayed stable

over a certain time period, without any detectable drug-leakage. This was a great result, proving that polymersome-like aggregates show good stability and low drug leakage.[6,194] Therefore, a potent drug carrier was developed that is not only very simple, but nevertheless very stable in the biological environment. Installing a targeting unit in the carrier system by synthesizing an enzyme-responsive PEG-*b*-PLGLAG-*b*-PSer(Bn) terpolymer might result in a superior material to create a smart drug delivery system that is simple but effective.

Concluding Remarks. Overall, the scope of this thesis, to study the influence of surface chemistry on interactions with biomolecules as well as developing a feasible drug delivery device based on the knowledge about these interactions, was well addressed. Progress was made in the investigation of charged surfaces and protein interactions. In addition, many interesting and positive results were obtained on the functionalization of the serine side chain and its polymerization and aggregation behaviour in aqueous and nonaqueous media. Especially the *O*-pyrenyl-serine derivative is a promising building block for the synthesis of amphiphilic, photo-responsive block copolymers. These performed very well as emulsifiers in the first attempts of nonaqueous emulsion polymerization and allow the design of dual-responsive core-shell nanoparticles. Great results were obtained by using PEG-*b*-PSer(Bn) block copolymers for the synthesis of vesicular assemblies. They showed excellent stability and biocompatibility and promising initial results in cell uptake experiments. This thesis provided a solid basis of results on the development of serine-based drug delivery systems, deserving further investigation to achieve the goal of developing an innovative drug carrier system and overcome the beforementioned drawbacks that were faced during the research.

8 Supporting Information

8.1 Experimental Techniques

Water and oxygen sensitive reactions were performed with standard Schlenk techniques under Argon atmosphere or in a glovebox. 0 °C polymerizations with longer reaction times were cooled with a cryostat from Huber GmbH. The homogenization of emulsions was performed with a Brandelin Sonorex RK255H-W640 Sonifier. Dialysis was executed with membranes purchased from Spectrum Labs.

8.2 Materials

All reagents and solvents were purchased from commercial sources and were used as received, unless stated otherwise. Chemicals and solvents were purchased from Acros Organics, Alfa Aesar, Fisher Scientific, Sigma-Aldrich, TCI Chemicals and VWR. The macro initiators mPEG17-NH2 (750 g/mol) and mPEG45-NH2 (2000 g/mol) were purchased from Rapp Polymere. Lauryl methacrylate (LMA), 2-dimethylethylamino methacrylate (DMAEMA) and 2-(Dimethoxyphosphoryl)ethyl methacrylate (MAPHOS$(OMe)_2$) were dried over calcium hydride and distilled prior to use. Water was deionized by a Merck Millipore Milli-Q system.

8.3 Instrumentation and Methods

Nuclear magnetic resonance spectroscopy (NMR) was conducted on a Bruker DRX250, DRX300, DRX500 or DRX700 spectrometer. ^{13}C-NMR spectra were recorded proton decoupled. Chemical shifts δ are noted as parts per million (ppm) and coupling constants J in Hertz (Hz). Resonance signals of DMSO-d_6 (^{1}H: δ = 2.50 ppm; ^{13}C: δ = 39.52 ppm) , D_2O (^{1}H: δ = 4.79 ppm), $CDCl_3$ (^{1}H: δ = 7.26 ppm) or CD_2Cl_2 (^{1}H: δ = 5.32 ppm) were used as internal standard. Block copolymer formation was investigated via diffusion ordered spectroscopy (DOSY) in DMSO-d_6. The DOSY experiments were done with a 5 mm BBI 1H/X z-gradient probe and a gradient strength of 5.516 [G/mm] on the 700 MHz spectrometer.

Atmospheric pressure chemical ionization mass spectrometry (APCI-MS) was conducted on an ADVION expression compact mass spectrometer (expressionCMS). The ionic masses m/z are expressed in u (units).

Dynamic light scattering (DLS) measurements were performed on a Malvern Zetasizer 3000 HSa with a fixed scattering angle of 90°.

Fluorescence spectroscopy was recorded on an Agilent Carry Eclipse Fluorescence Spectrometer in Milli-Q water in a conventional quartz cell (light pass 10 mm) at an excitation wavelength of 334 nm to determine the critical micelle concentration. Pyrene was used as fluorescence probe.

Fourier Transform IR (FT-IR) spectra were recorded on a Nicolet 730 spectrometer and a Spectrum BX from Perkin Elmer. Systems were equipped with a single-reflection ATR-IR probe head (ATR: Attenuated Total Reflection) from Thermo- Spectra-Tech. Samples were applied to the crystal as a solid or as a KBr pellet and measured using a He/Ne source with an emission wavelength of 633 nm as the laser.

Gel permeation chromatography (GPC) measurements were conducted on a Waters, carried out at 30 °C or 50 °C using MZ-Gel SDplus 10e6, 10e4 and 500 columns in DMF or THF as eluent *vs.* polystyrene (PS) or poly(methyl methacrylate) (PMMA) standards. The detector was an ERC RI-101 differential refractometer and UV detector at 520 nm.

High performance liquid chromatography (HPLC) was performed by an Agilent Technologies Series 1200 instrument with a Rheodyne 7725i injection valve and Varian's ELSD Detector 385-LC. The chiral column was a Daicel Chiralpak IE 250/4/5µm- The eluent was a mixture of THF/n-heptane (24:76). The flow rate was 1 mL/min and the measurement temperature was 20 °C. The peaks were manually integrated to determine the enantiomer ratio.

Scanning electron microscopy (SEM) was performed with a Gemini 1530 microscope from Zeiss at an acceleration voltage of 100 kV. The samples were dropped from dilute dispersion on a Si-wafer.

Transmission electron microscopy (TEM) was performed on a JEM-2000EX (JEOL Tokyo, Japan), operating at an acceleration voltage of 200 kV. For the observation of size and distribution of micellar particles, a drop of sample solution (concentration = 0.1 mg/mL) was placed onto a 200-mesh copper grid coated with carbon. About two minutes after deposition, the grid was tapped with a filter paper to remove surface water, followed by air-drying. Negative staining was performed using a droplet of a 5 wt % uranyl acetate solution.

9 Appendix

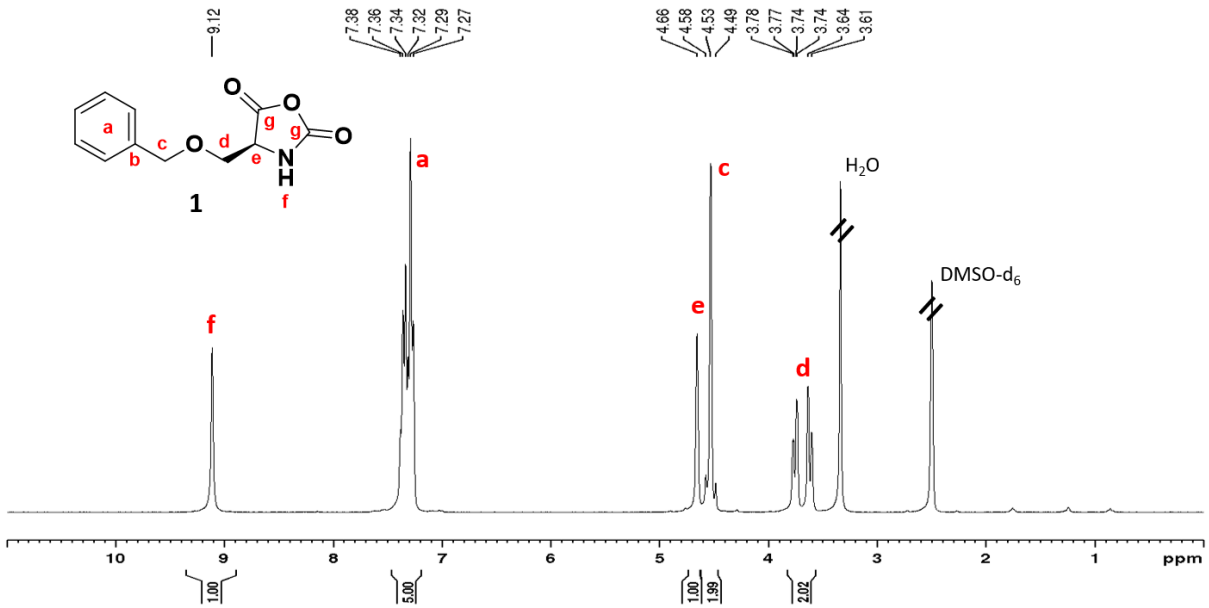

*Figure 113: ^{1}H-NMR spectrum (300 MHz, 298 K, DMSO-d_6) of the O-benzyl-L-serine-NCA (**1**).*

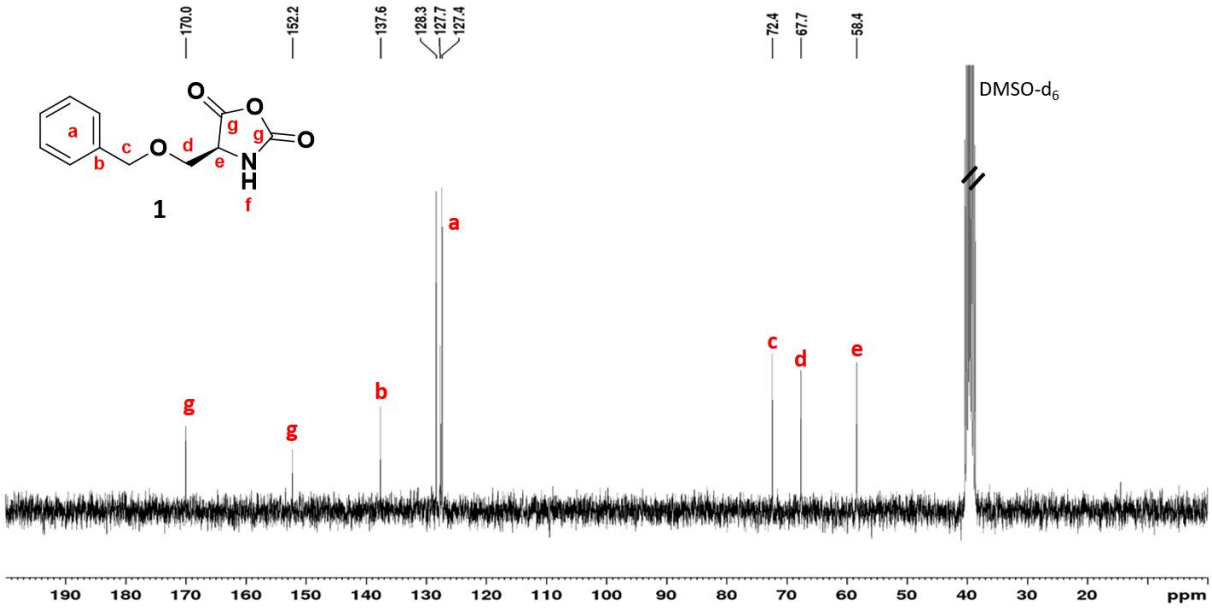

*Figure 114: ^{13}C-NMR spectrum (75 MHz, 298 K, DMSO-d_6) of the O-benzyl-L-serine-NCA (**1**).*

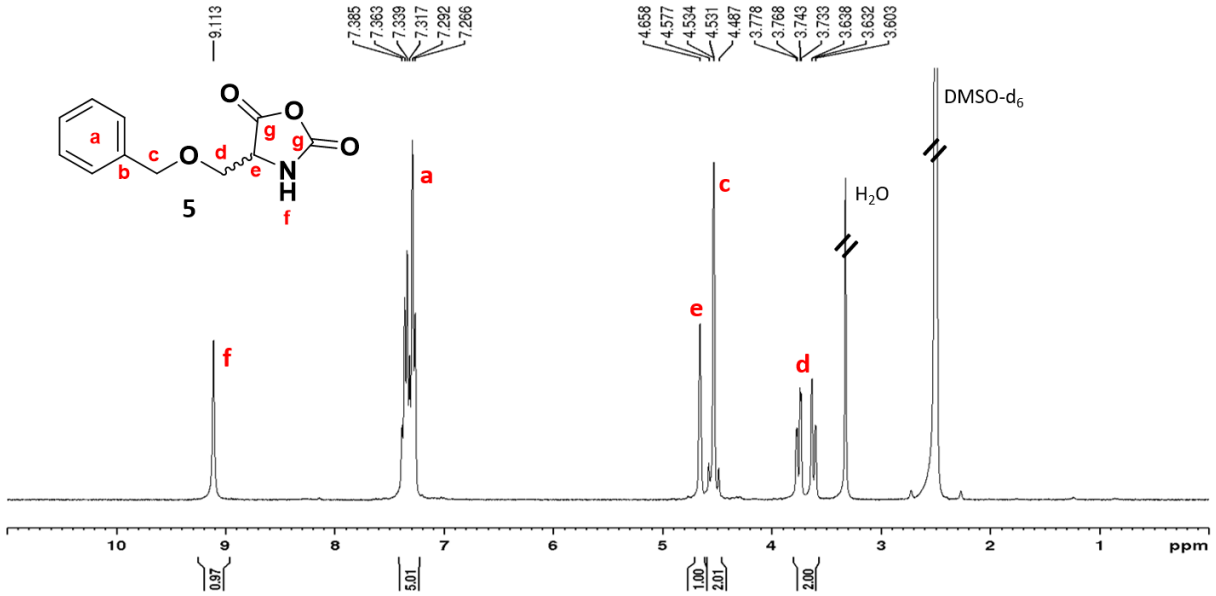

*Figure 115: [1]H-NMR spectrum (300 MHz, 298 K, DMSO-d_6) of the O-benzyl-DL-serine-NCA (**5**).*

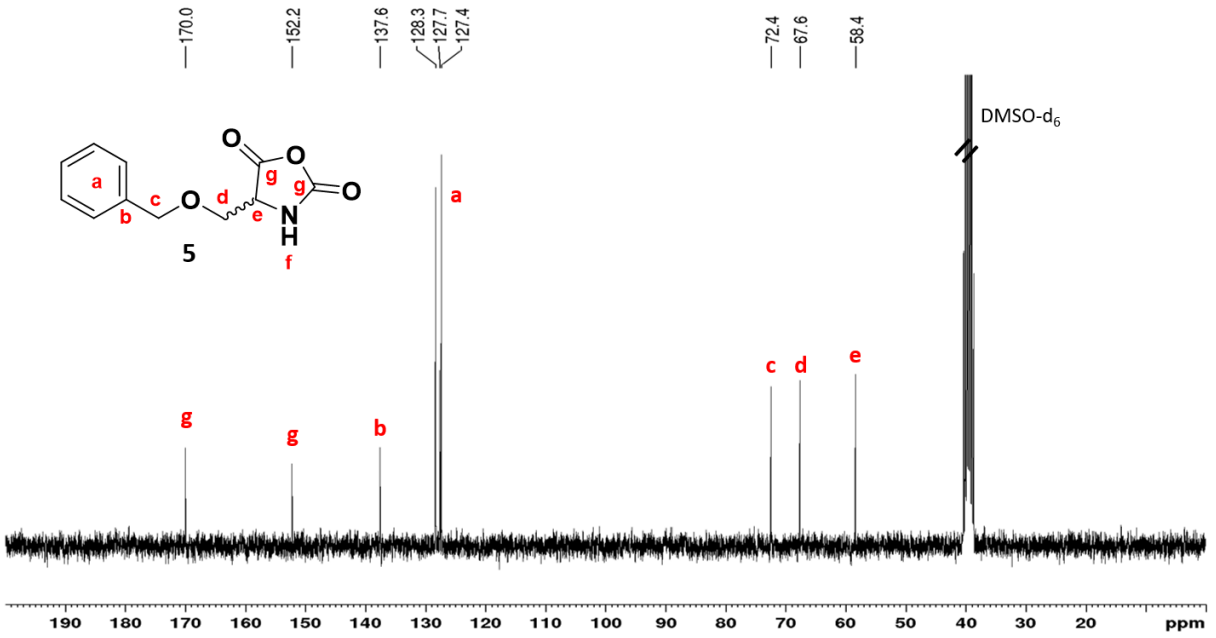

*Figure 116: [13]C-NMR spectrum (75 MHz, 298 K, DMSO-d_6) of the O-benzyl-L-serine-NCA (**5**).*

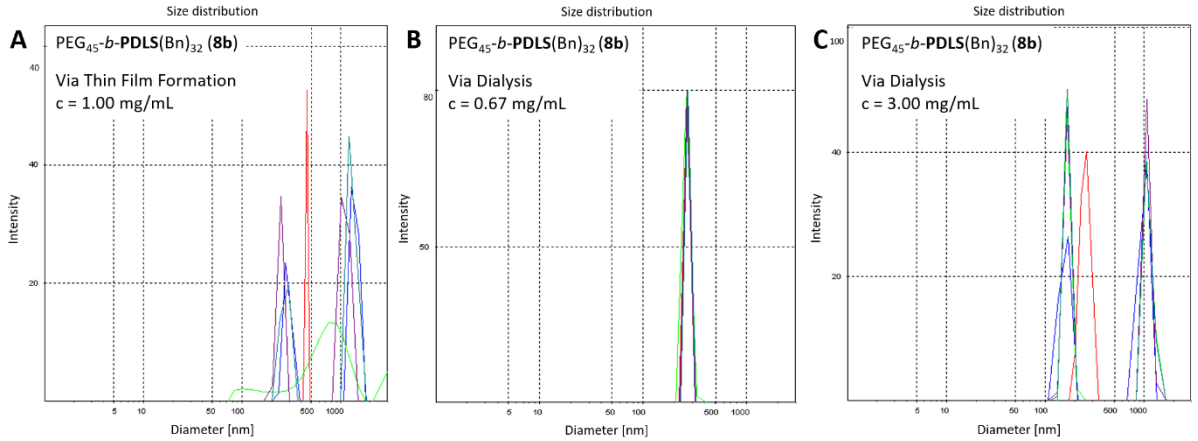

*Figure 117: Size distribution of aqueous micelles of DL-serine polymers (**8b**) after preparation by TFF at c = 1.00 mg/mL vs. dialysis at c = 0.67 mg/mL and 3.00 mg/mL.*

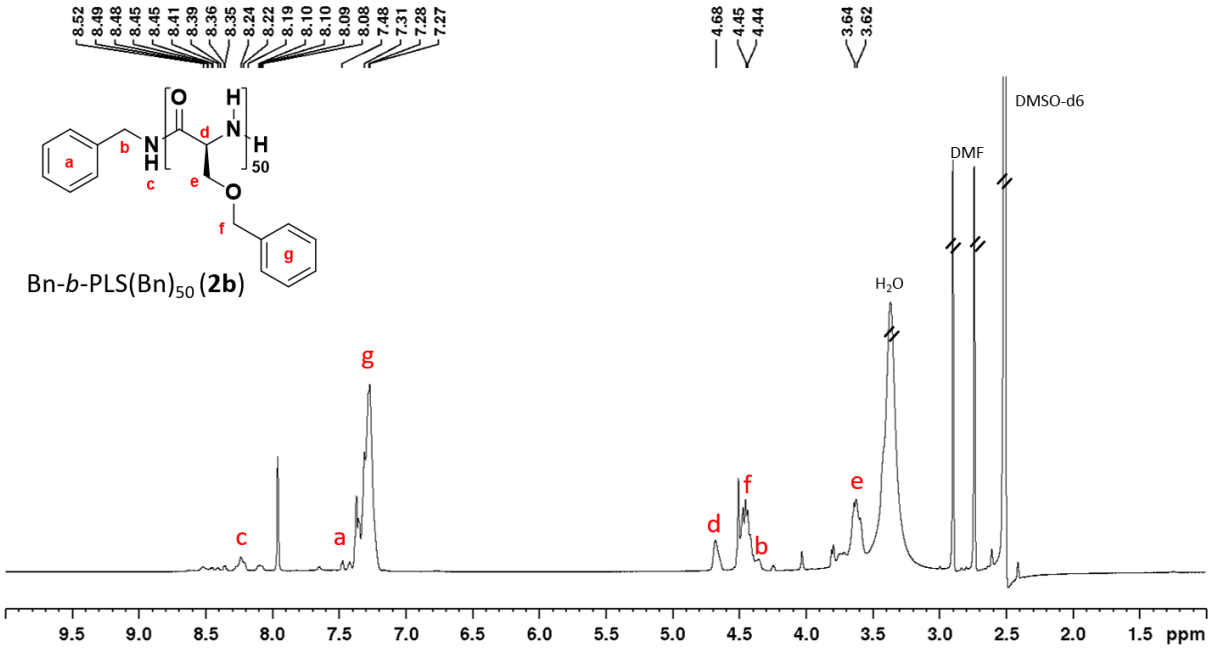

*Figure 118: ^{1}H-NMR spectrum (700 MHz, 333 K, DMSO-d_6) of the homopolymer Bn-b-PLS(Bn)$_{50}$ (**2b**).*

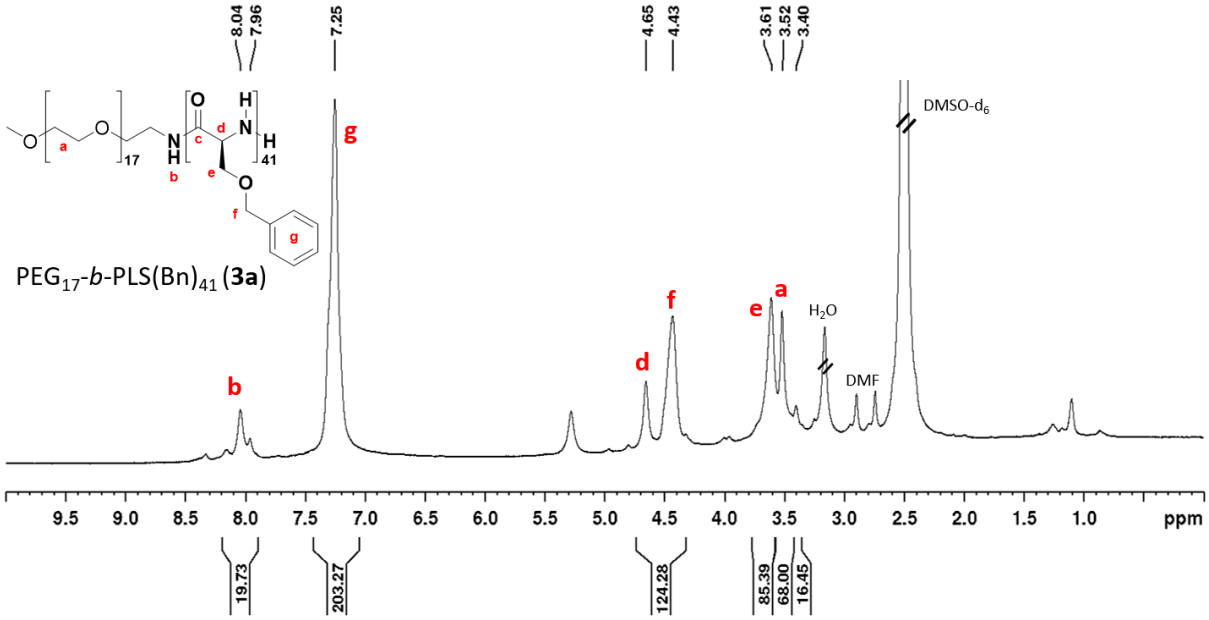

*Figure 119: ^{1}H-NMR spectrum (700 MHz, 298 K, DMSO-d_6) of the block copolymer PEG_{17}-b-$PLS(Bn)_{41}$ (**3a**).*

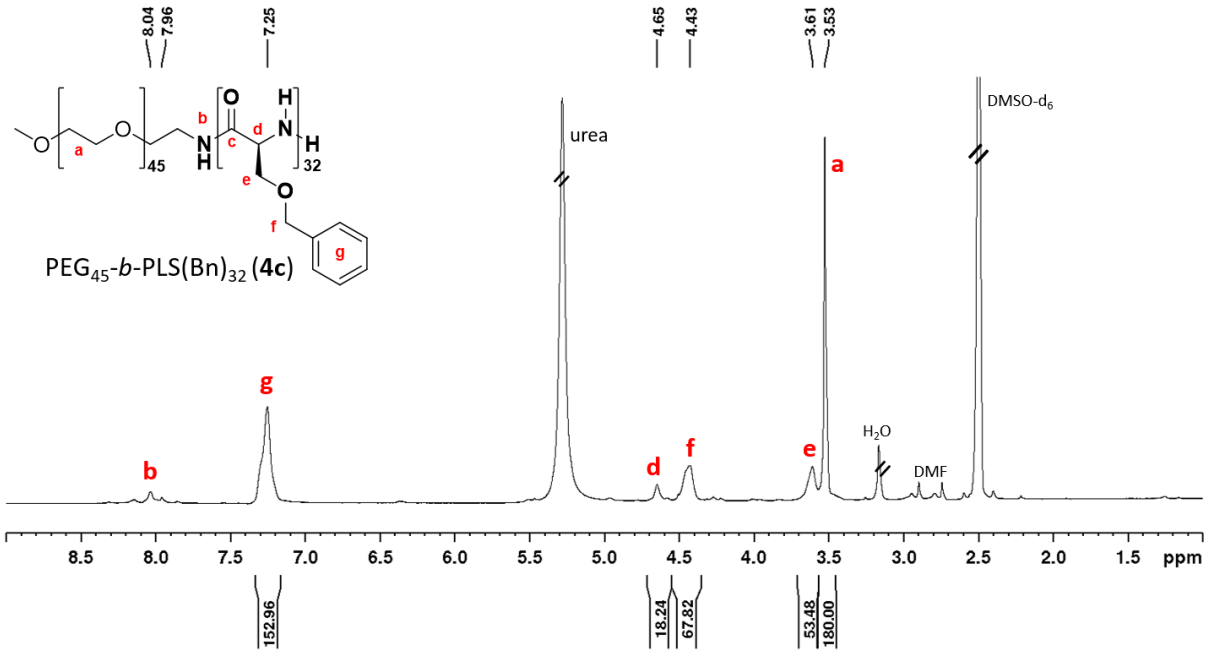

*Figure 120: ^{1}H-NMR spectrum (700 MHz, 333 K, DMSO-d_6) of the block copolymer PEG_{45}-b-$PLS(Bn)_{32}$ (**4c**).*

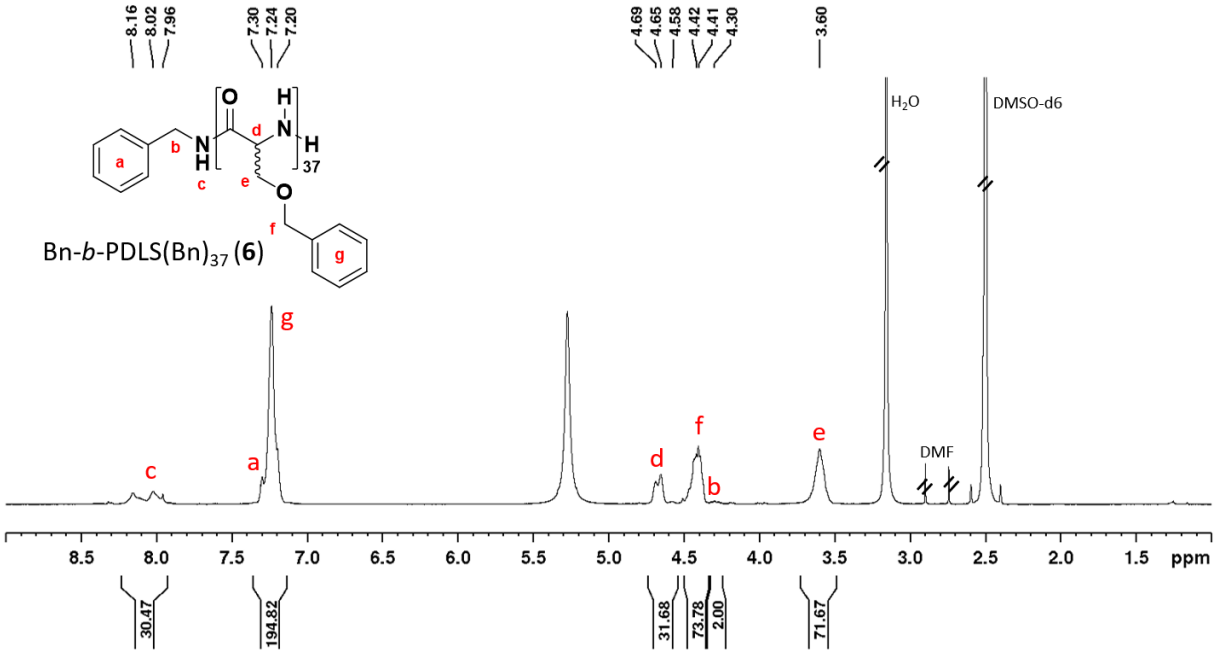

*Figure 121: ^{1}H-NMR spectrum (700 MHz, 333 K, DMSO-d_6) of the homopolymer Bn-b-PDLS(Bn)$_{37}$ (**6**).*

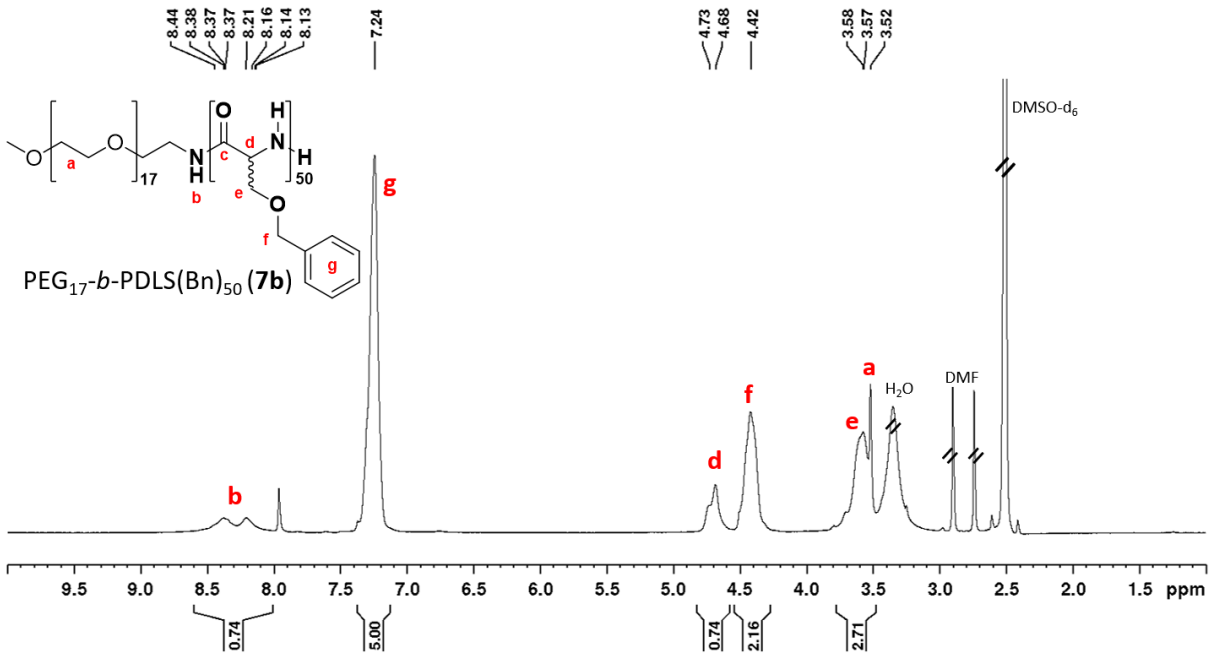

*Figure 122: ^{1}H-NMR spectrum (700 MHz, 333 K, DMSO-d_6) of the block copolymer PEG$_{17}$-b-PDLS(Bn)$_{50}$ (**7b**).*

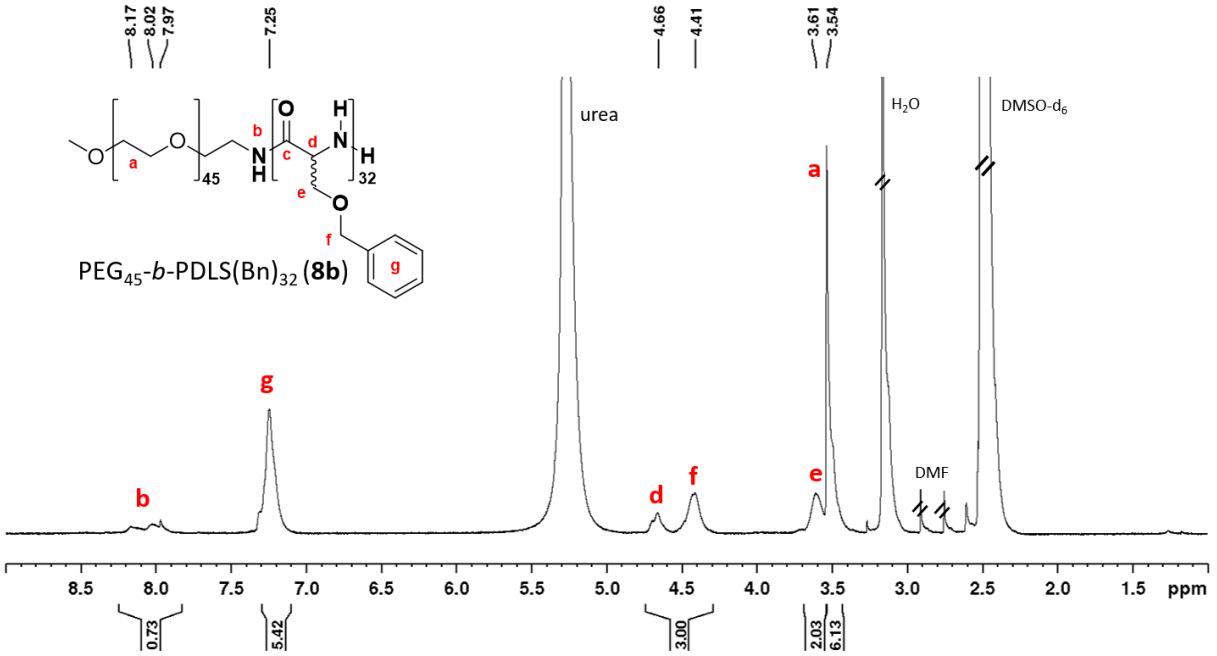

*Figure 123: ^{1}H-NMR spectrum (700 MHz, 333 K, DMSO-d_6) of the block copolymer PEG_{45}-b-PDLS$(Bn)_{32}$ (**8b**).*

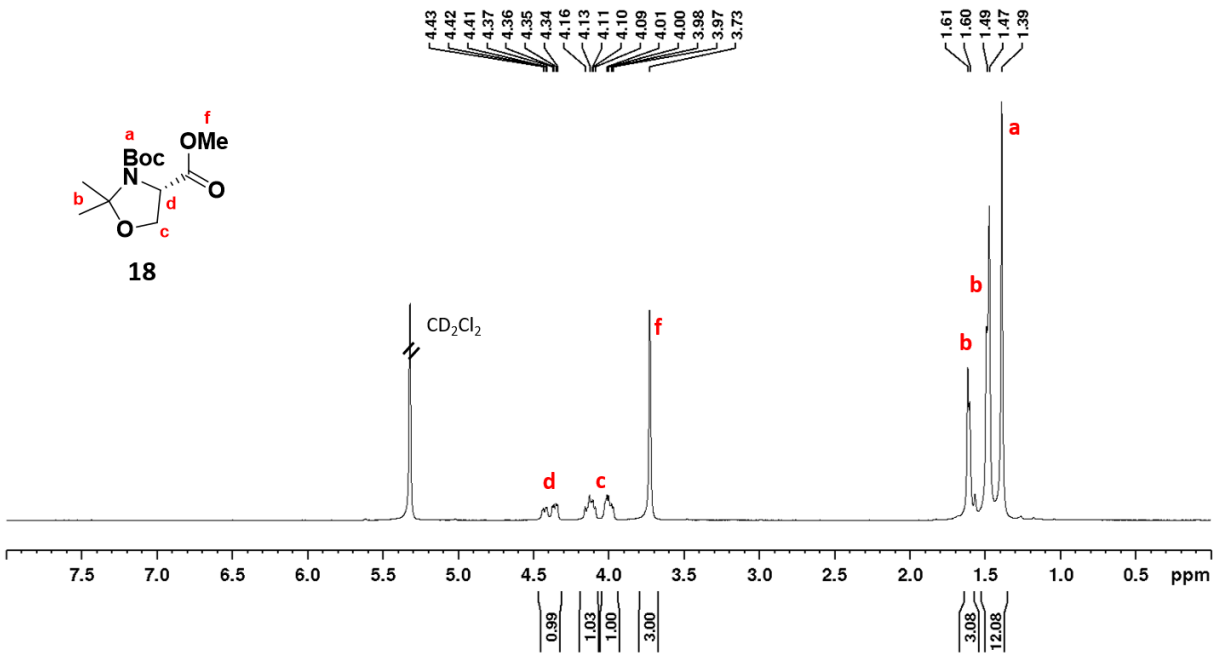

*Figure 124: ^{1}H-NMR spectrum (300 MHz, 300 K, DMSO-d_6) of 3-(tert-butyl)-4-methyl-(S)-2,2-dimethyloxazolidine-3,4-dicarboxylate (**18**).*

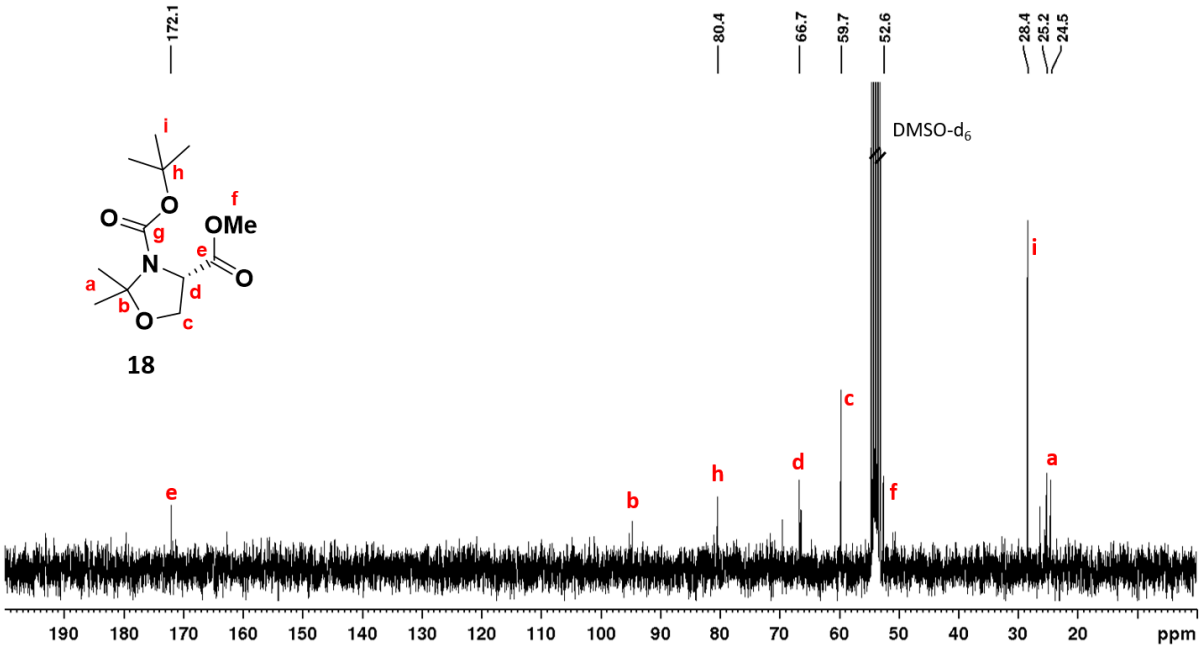

*Figure 125: ^{13}C-NMR spectrum (75 MHz, 300 K, DMSO-d_6) of 3-(tert-butyl)-4-methyl-(S)-2,2-dimethyloxazolidine-3,4-dicarboxylate (**18**).*

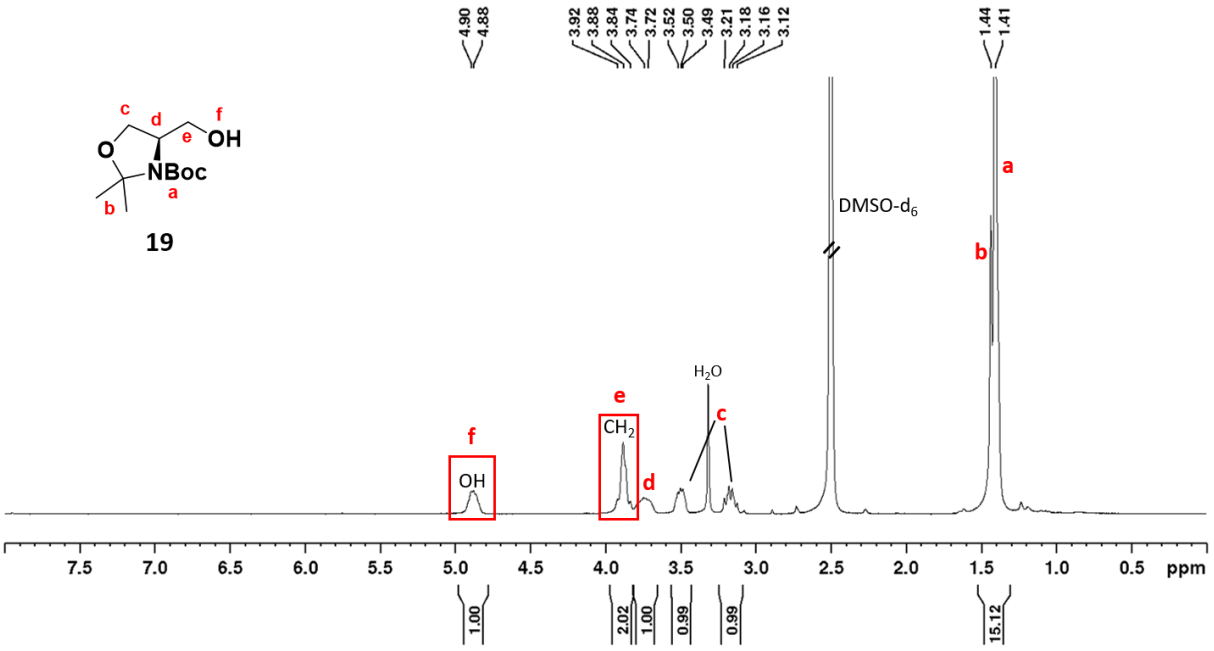

*Figure 126: ^{1}H-NMR spectrum (300 MHz, 300 K, DMSO-d_6) of (R)-N-Boc-4-(hydroxymethyl)-2,2-dimethyloxazolidine (**19**).*

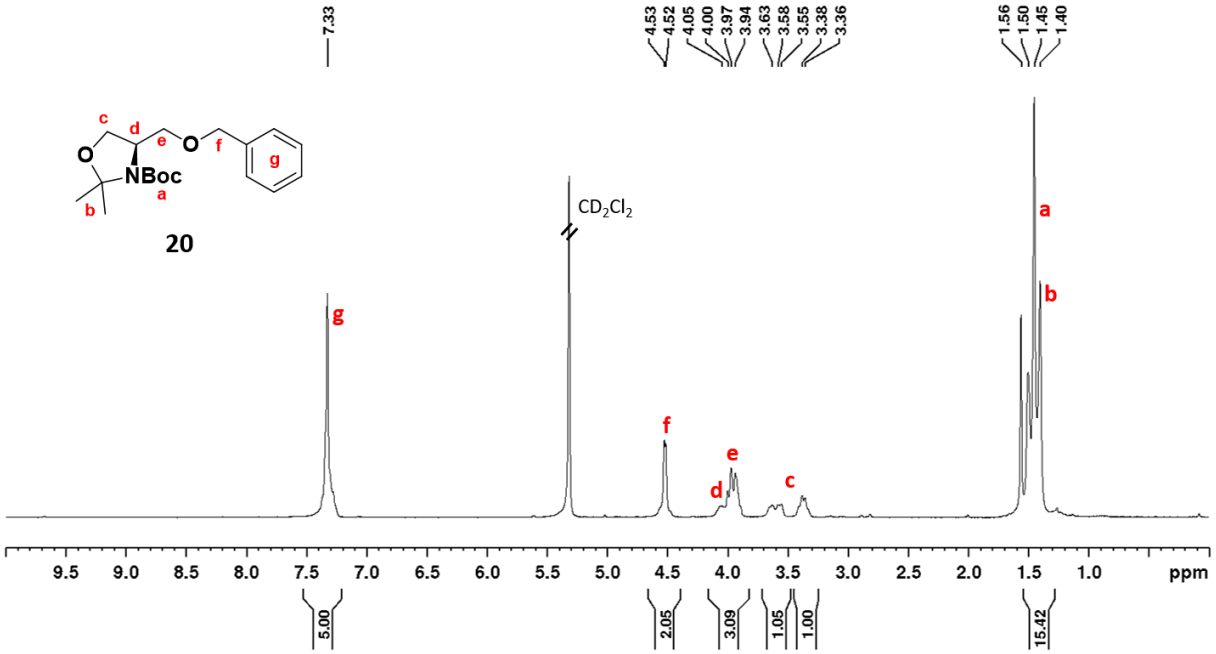

*Figure 127: ^{1}H-NMR spectrum (300 MHz, 300 K, CD_2Cl_2) of (R)-N-Boc-4-((benzyloxy)methyl)-2,2-dimethyloxazolidine (**20**).*

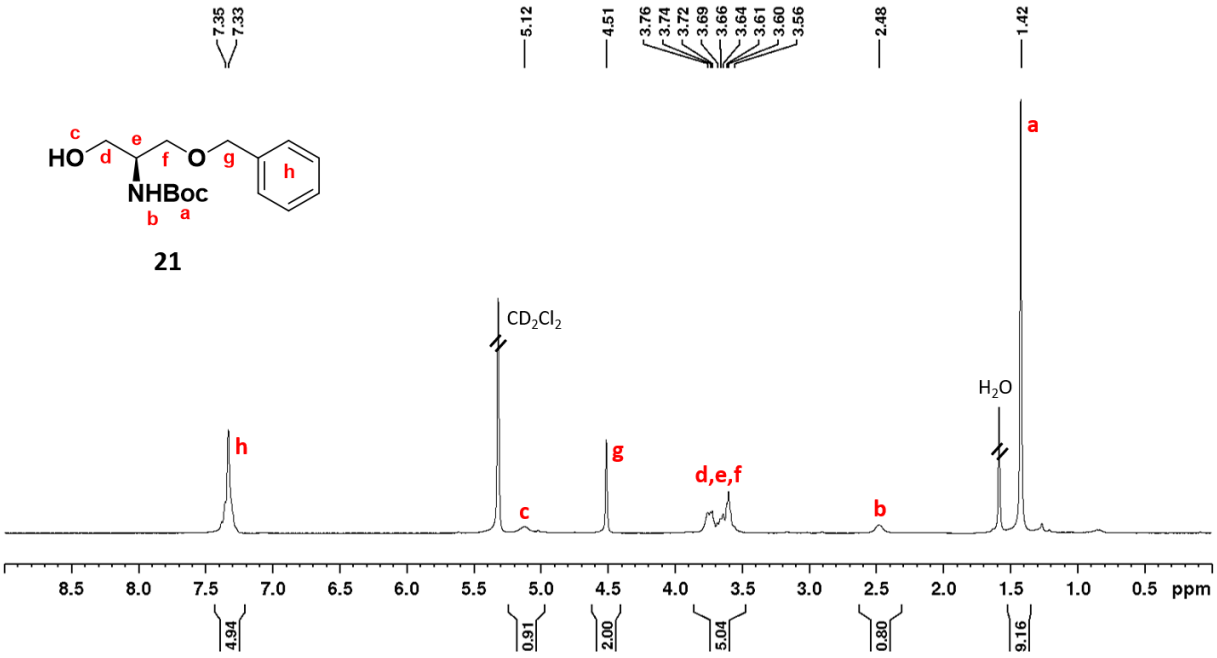

*Figure 128: ^{1}H-NMR spectrum (300 MHz, 300 K, CD_2Cl_2) of (R)-N-Boc-4-((benzyloxy)methyl)-2,2-dimethyloxazolidine (**21**).*

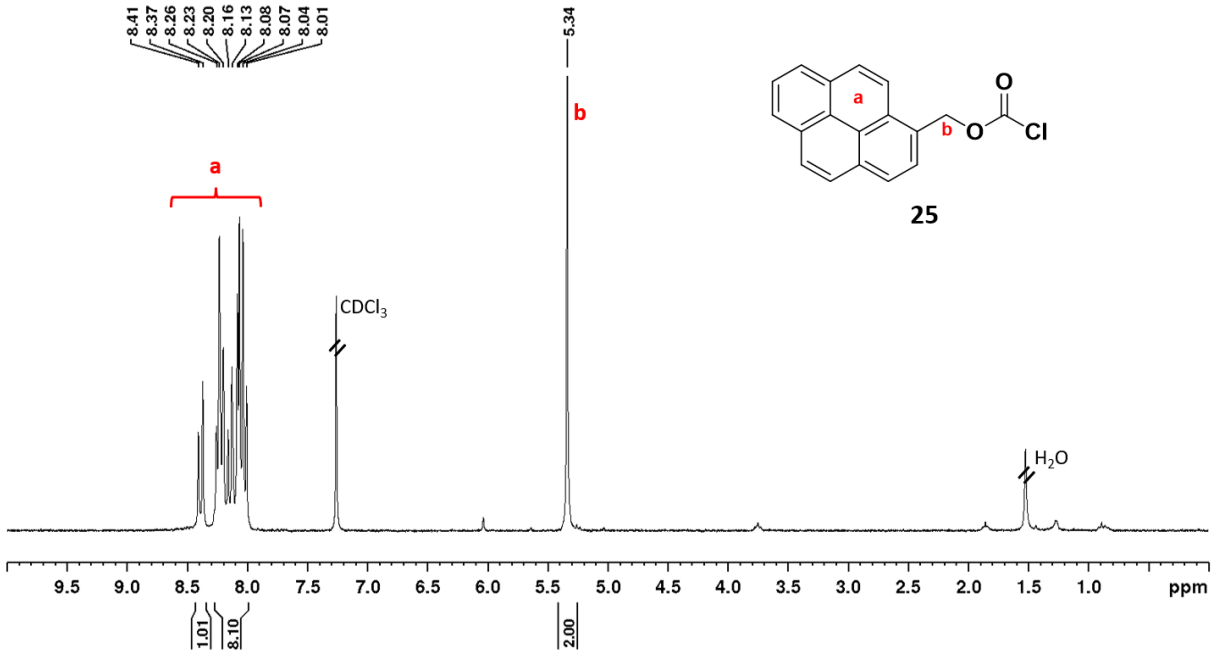

*Figure 129: ^{1}H-NMR spectrum (300 MHz, 300 K, $CDCl_3$) of pyren-1-ylmethyl chloroformate (**25**).*

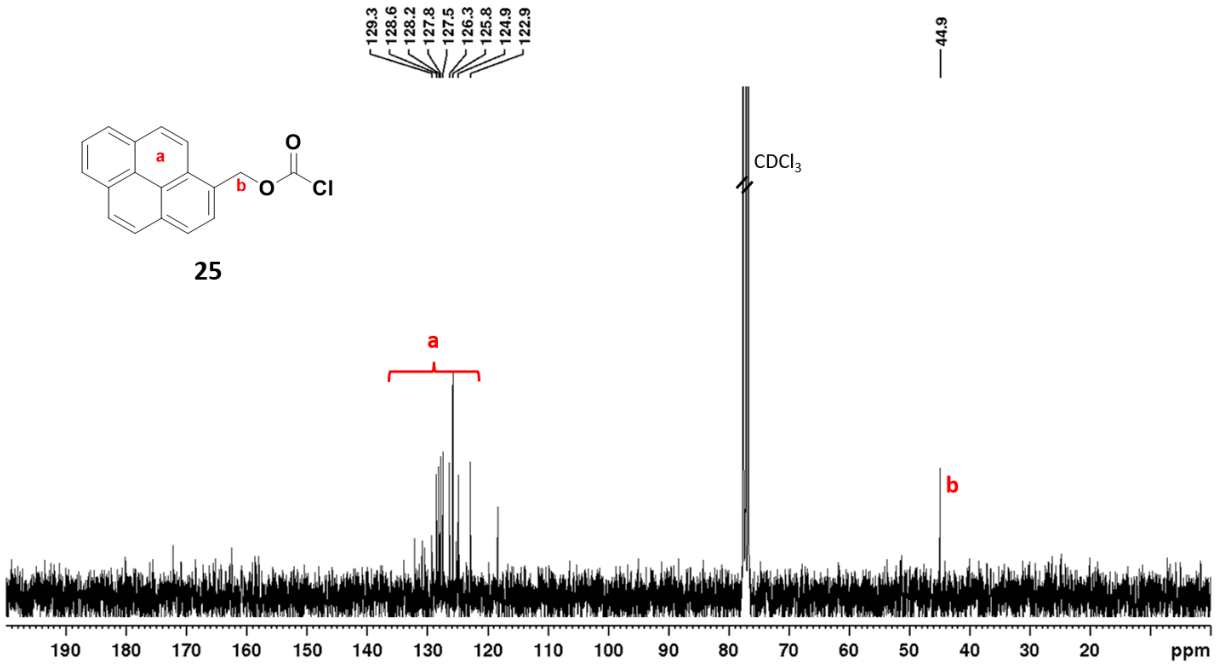

*Figure 130: ^{13}C-NMR spectrum (75 MHz, 300 K, $CDCl_3$) of pyren-1-ylmethyl chloroformate (**25**).*

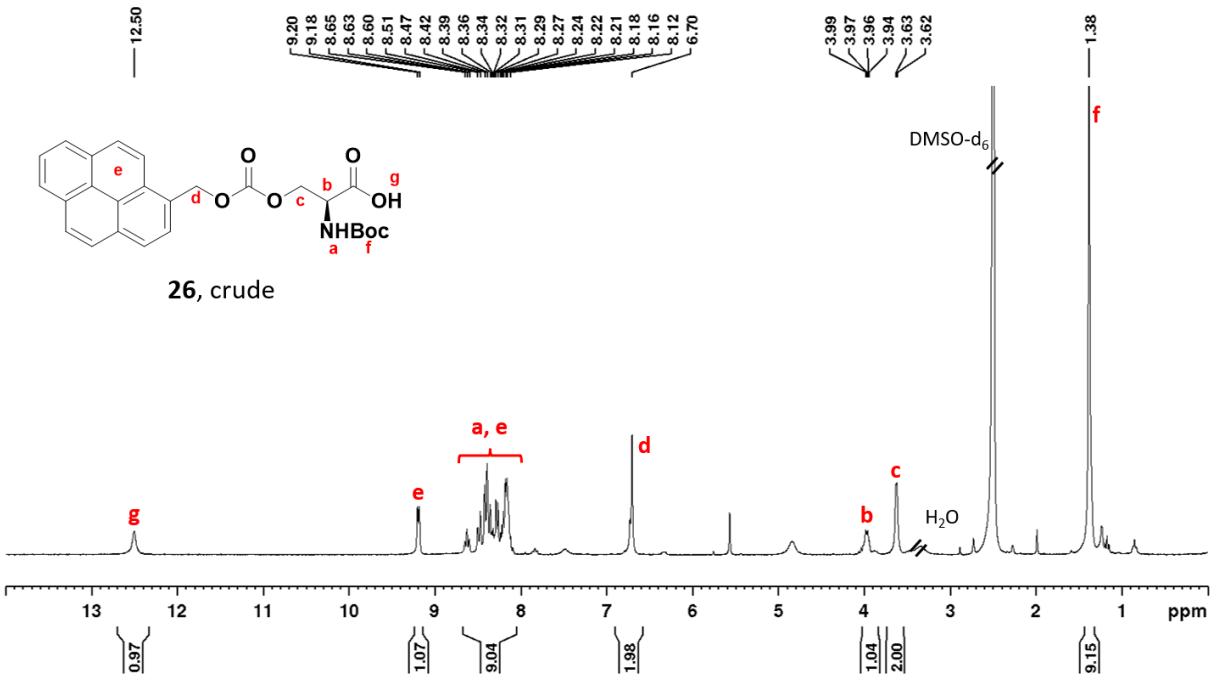

*Figure 131: [1]H-NMR spectrum (300 MHz, 300 K, DMSO-d_6) of N-(tert-butoxycarbonyl)-O-((pyrene-1-methoxy)carbonyl)-L-serine (**26**).*

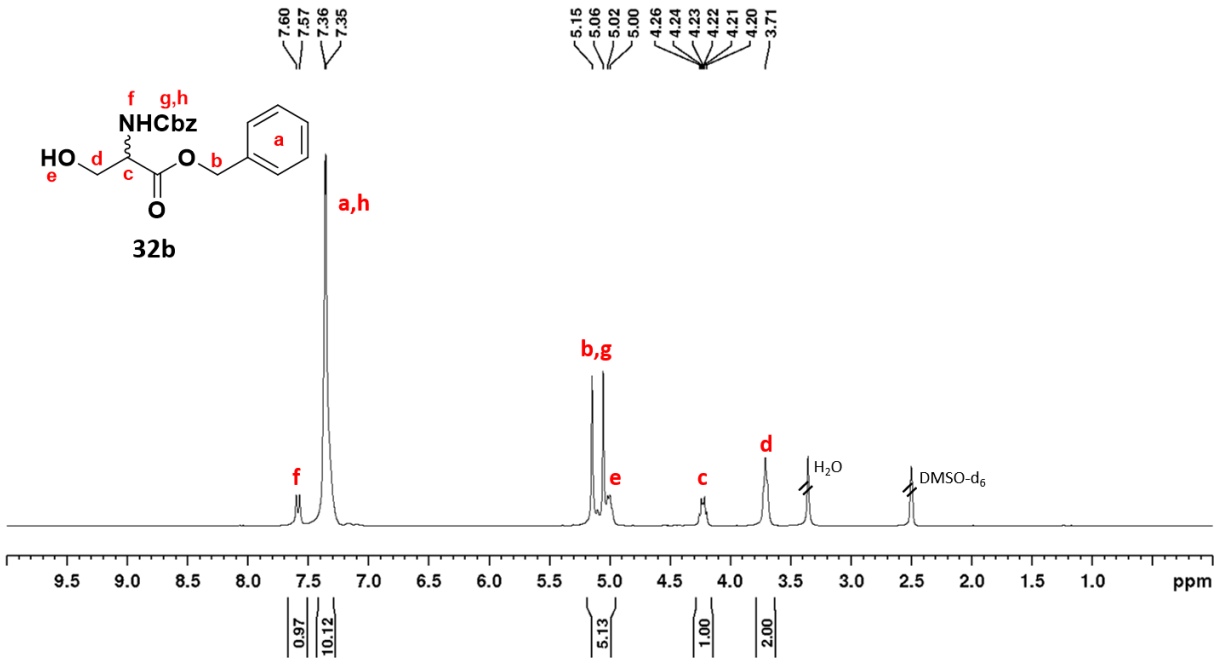

*Figure 132: [1]H-NMR spectrum (75 MHz, 300 K, DMSO-d_6) of N-(benzyloxycarbonyl)-DL-serine benzyl ester (**32b**).*

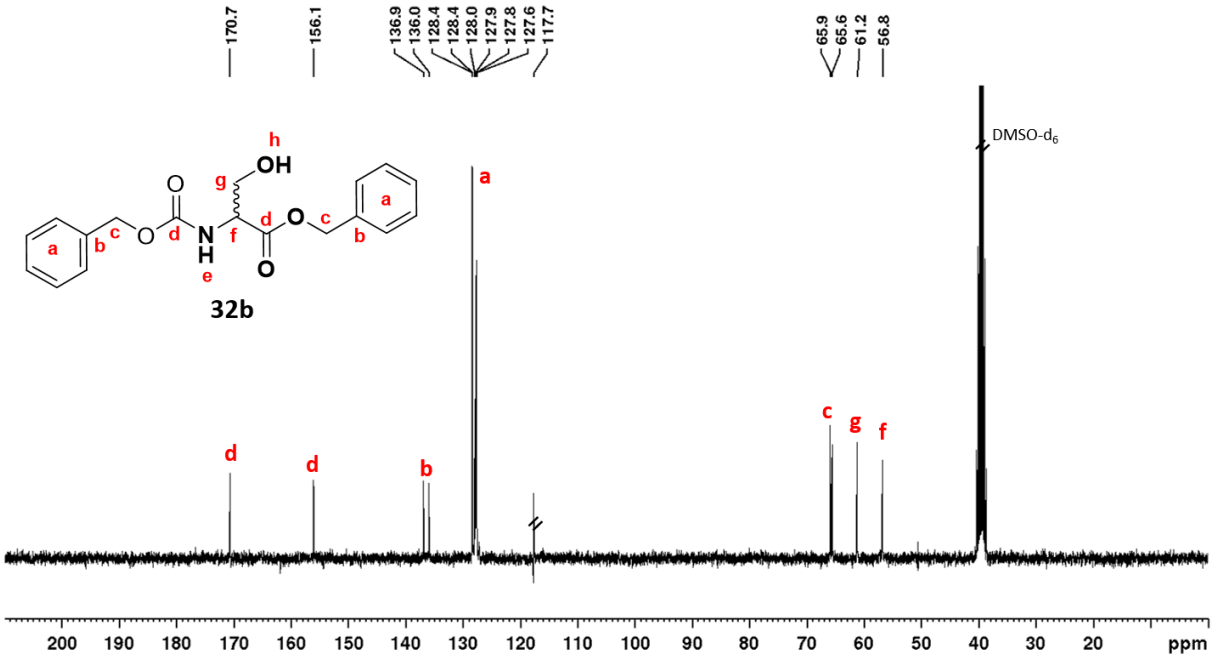

*Figure 133: ^{13}C-NMR spectrum (75 MHz, 300 K, DMSO-d_6) of N-(benzyloxycarbonyl)-DL-serine benzyl ester (**32b**).*

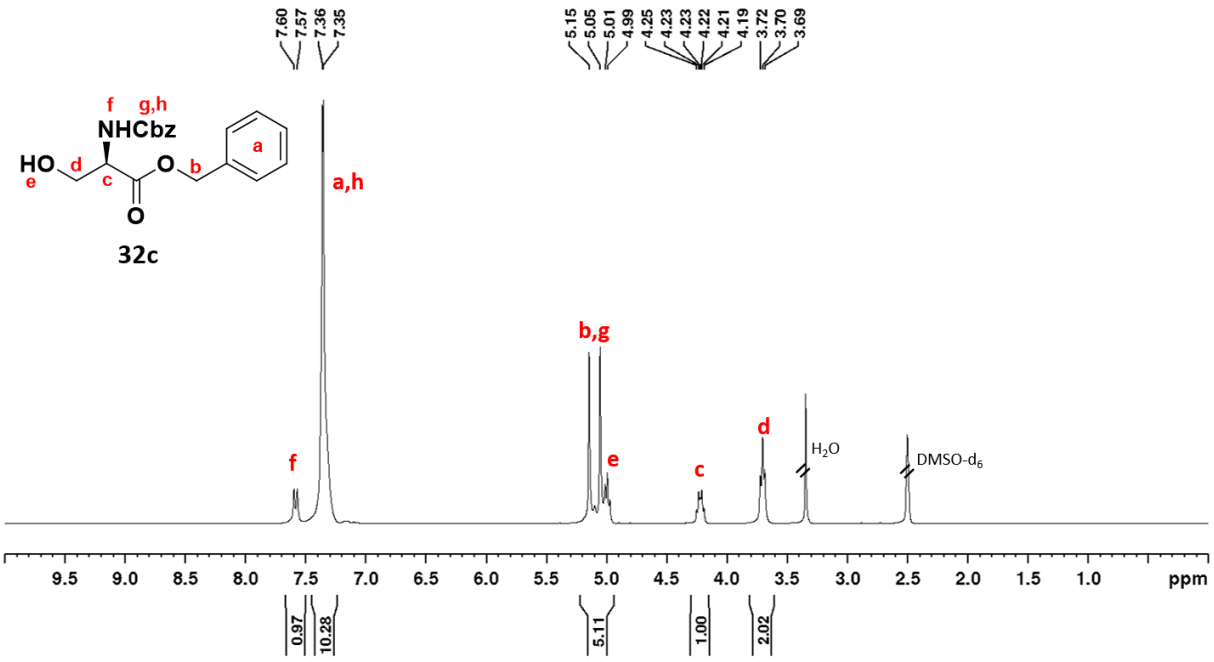

*Figure 134: ^{1}H-NMR spectrum (300 MHz, 300 K, DMSO-d_6) of N-(benzyloxycarbonyl)-D-serine benzyl ester (**32c**).*

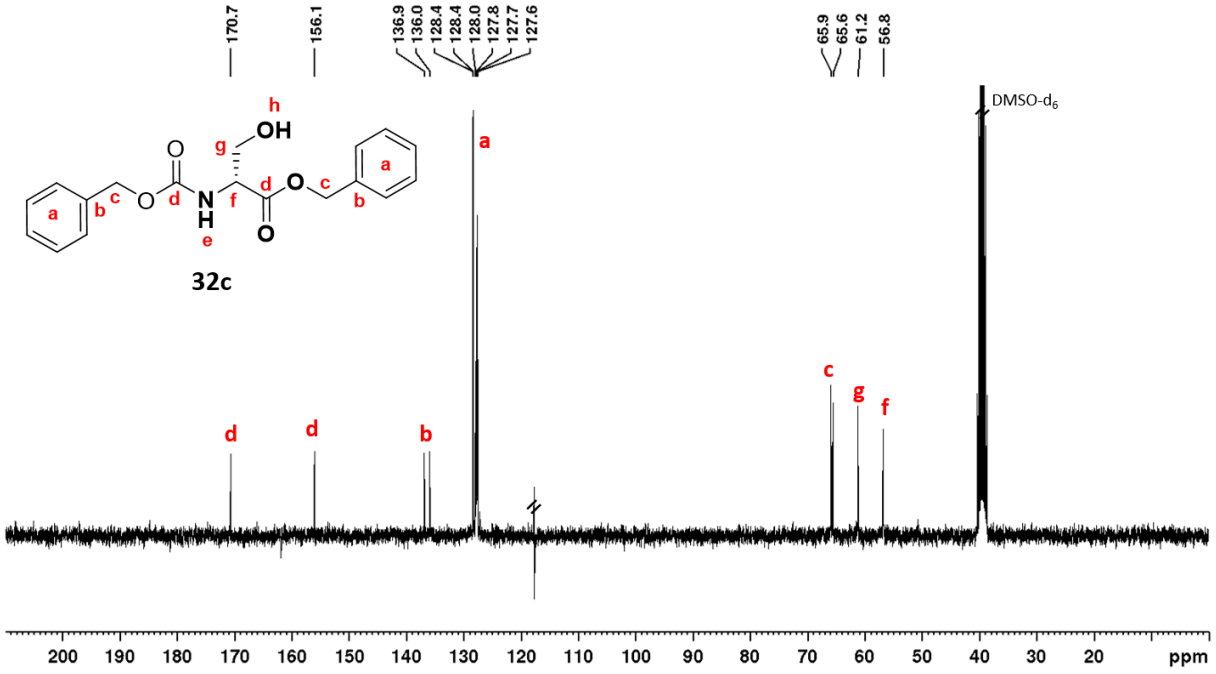

*Figure 135: ^{13}C-NMR spectrum (75 MHz, 300 K, DMSO-d_6) of N-(benzyloxycarbonyl)-D-serine benzyl ester (**32c**).*

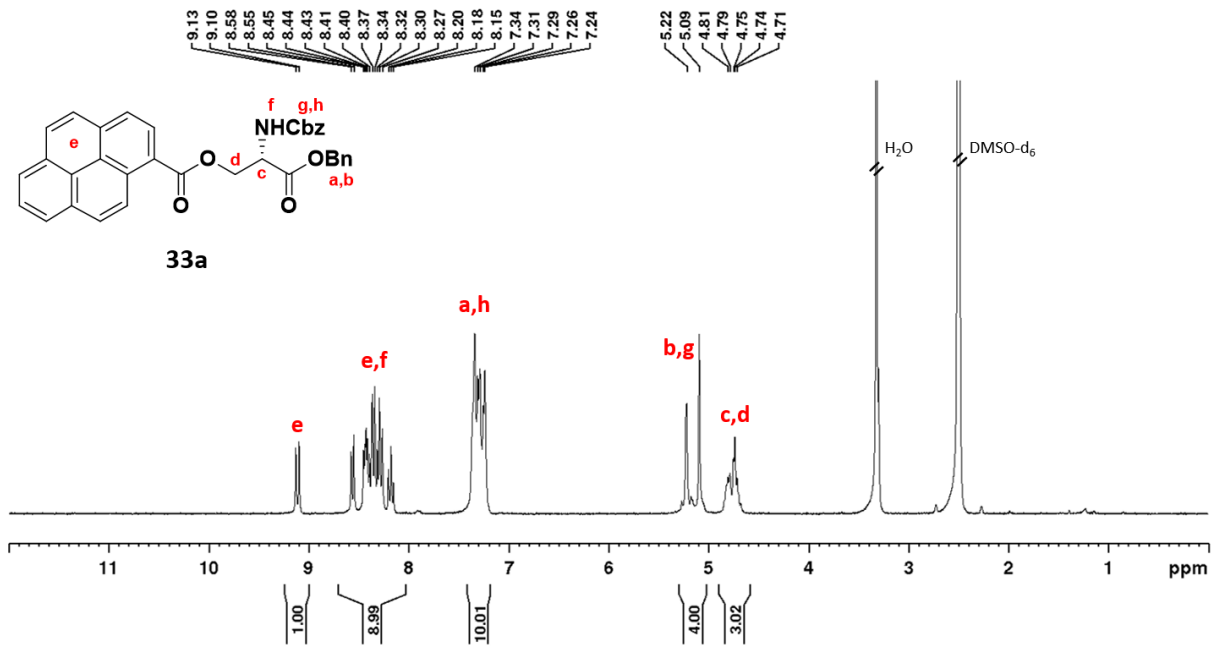

*Figure 136: ^{1}H-NMR spectrum (300 MHz, 300 K, DMSO-d_6) of N-(benzyloxycarbonyl)-O-(pyrene-1-carbonyl)-L-serine benzyl ester (**33a**).*

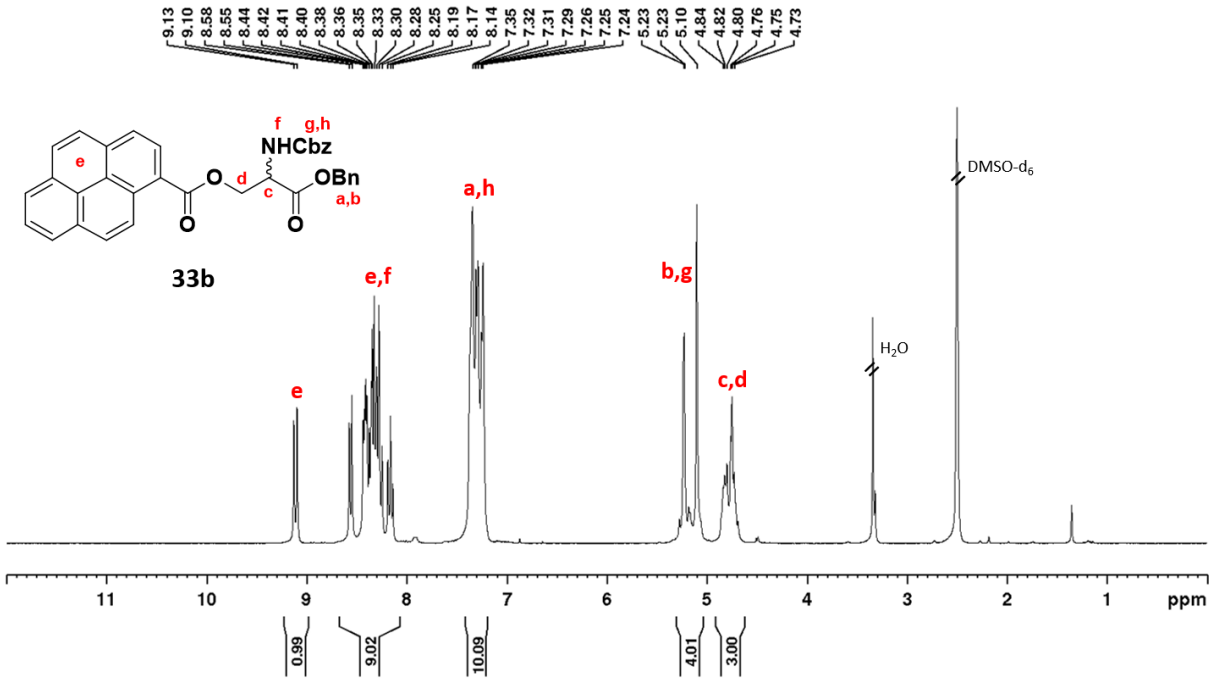

*Figure 137: [1]H-NMR spectrum (300 MHz, 300 K, DMSO-d_6) of N-(benzyloxycarbonyl)-O-(pyrene-1-carbonyl)-DL-serine benzyl ester (**33b**).*

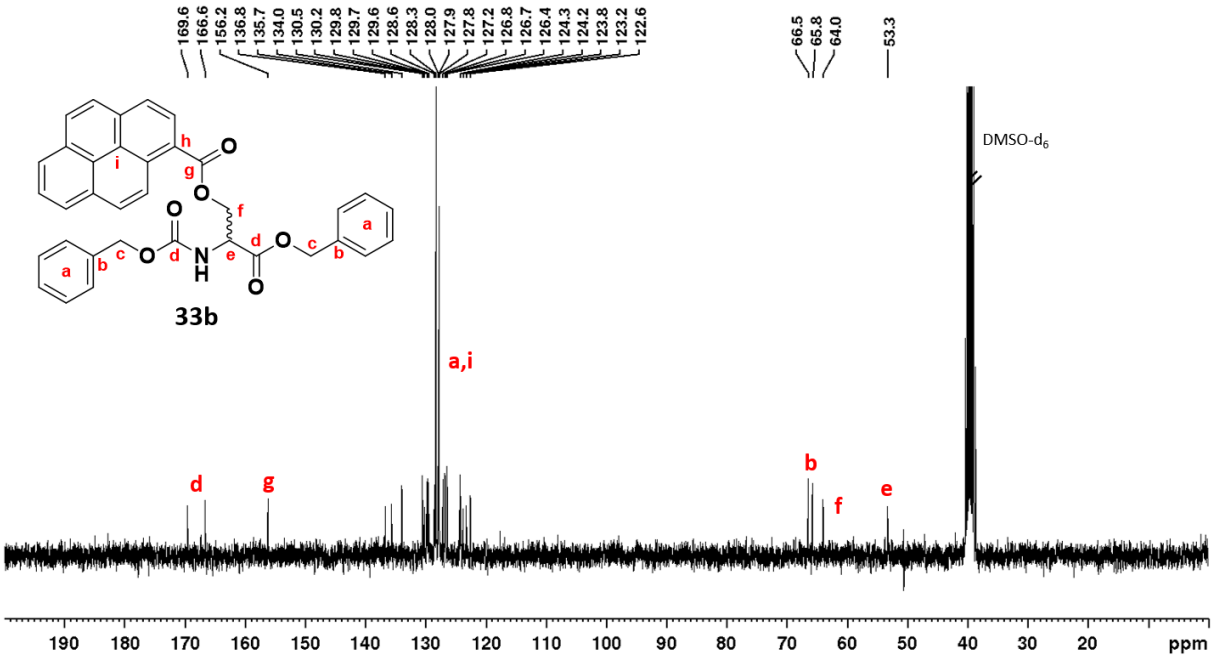

*Figure 138: [13]C-NMR spectrum (75 MHz, 300 K, DMSO-d_6) of N-(benzyloxycarbonyl)-O-(pyrene-1-carbonyl)-DL-serine benzyl ester (**33b**).*

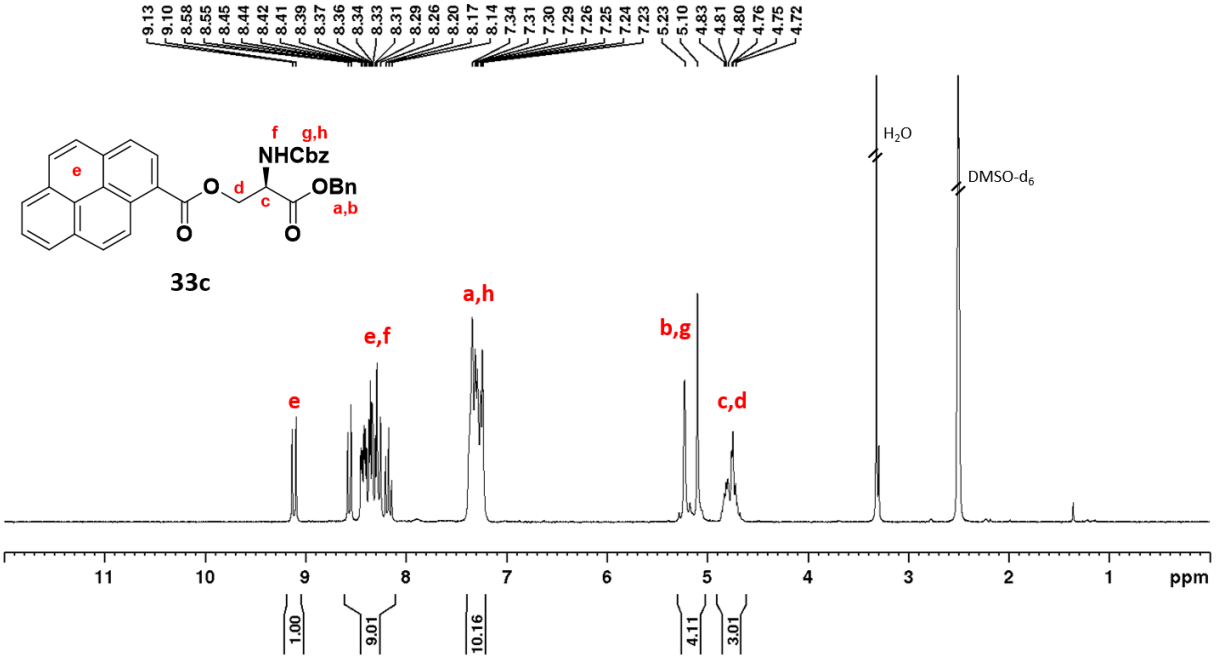

*Figure 139: ^{1}H-NMR spectrum (300 MHz, 300 K, DMSO-d_6) of N-(benzyloxycarbonyl)-O-(pyrene-1-carbonyl)-D-serine benzyl ester (**33c**).*

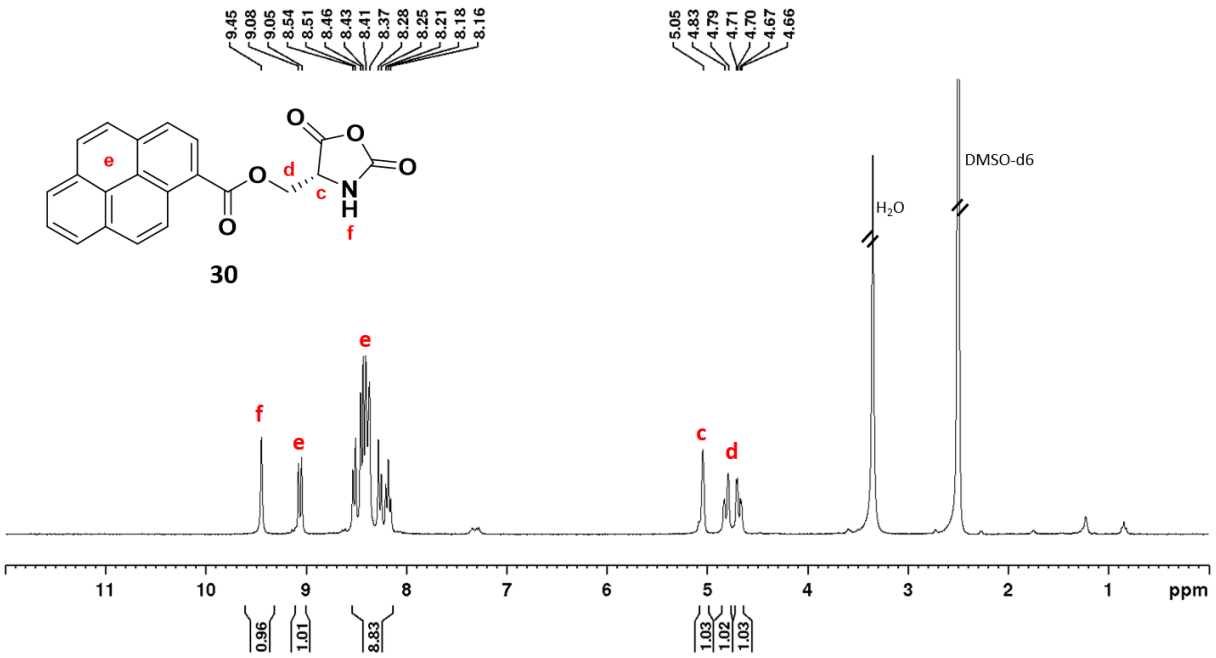

*Figure 140: ^{1}H-NMR spectrum (300 MHz, 300 K, DMSO-d_6) of O-(pyrenyl-1-carbonyl)-L-serine-N-carboxy anhydride (**30**).*

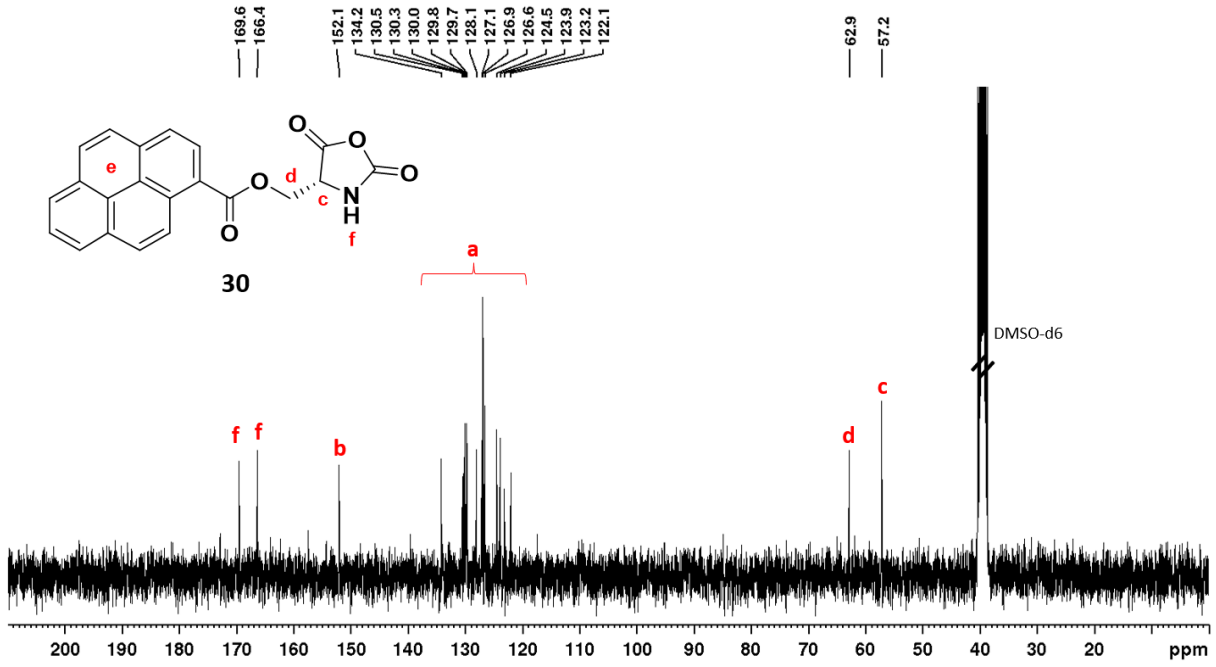

*Figure 141: ^{13}C-NMR spectrum (75 MHz, 300 K, DMSO-d_6) of O-(pyrenyl-1-carbonyl)-L-serine-N-carboxy anhydride (**30**).*

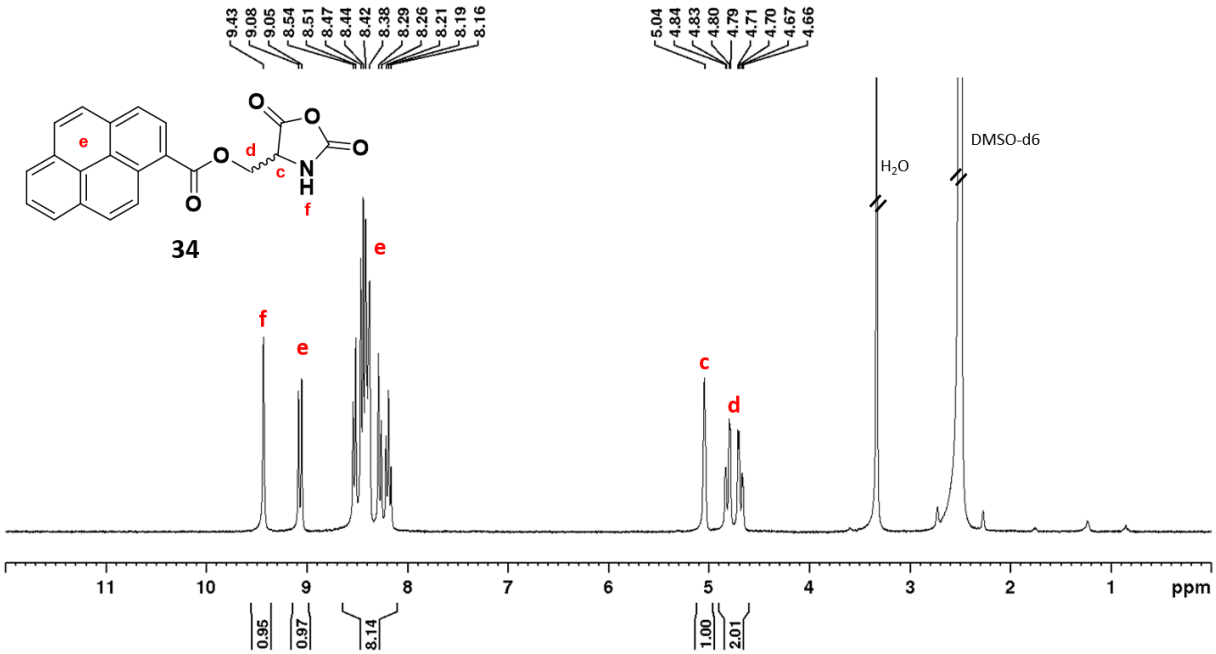

*Figure 142: ^{1}H-NMR spectrum (300 MHz, 300 K, DMSO-d_6) of O-(pyrenyl-1-carbonyl)-DL-serine-N-carboxy anhydride (**34**).*

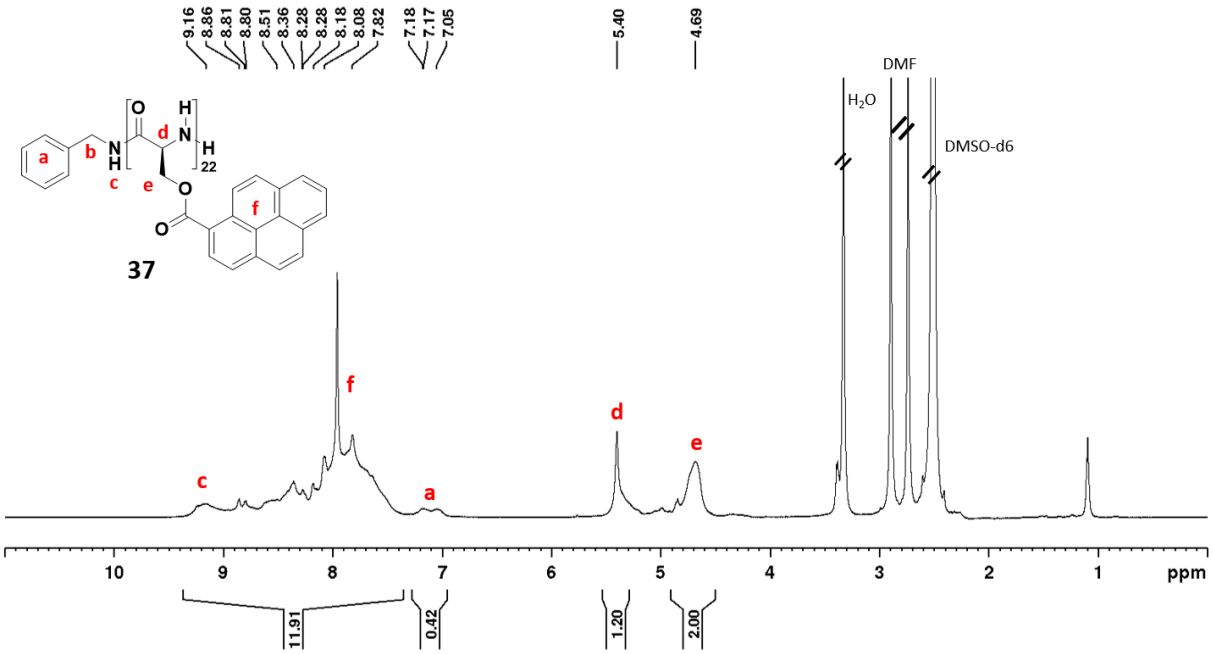

*Figure 143: ^{1}H-NMR spectrum (700 MHz, 333 K, DMSO-d_6) of the homo polymer Bn-b-PDLS(Pyr)$_{22}$ (**37**).*

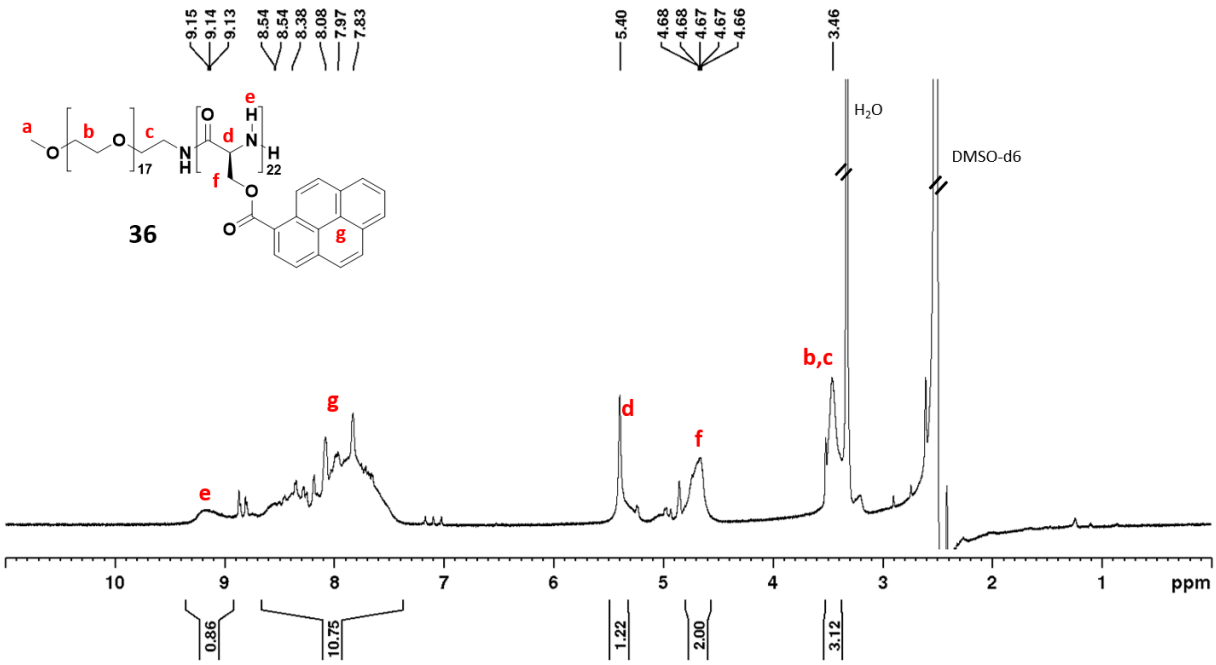

*Figure 144: ^{1}H-NMR spectrum (700 MHz, 333 K, DMSO-d_6) of the block copolymer PEG$_{17}$-b-PDLS(Pyr)$_{22}$ (**36**).*

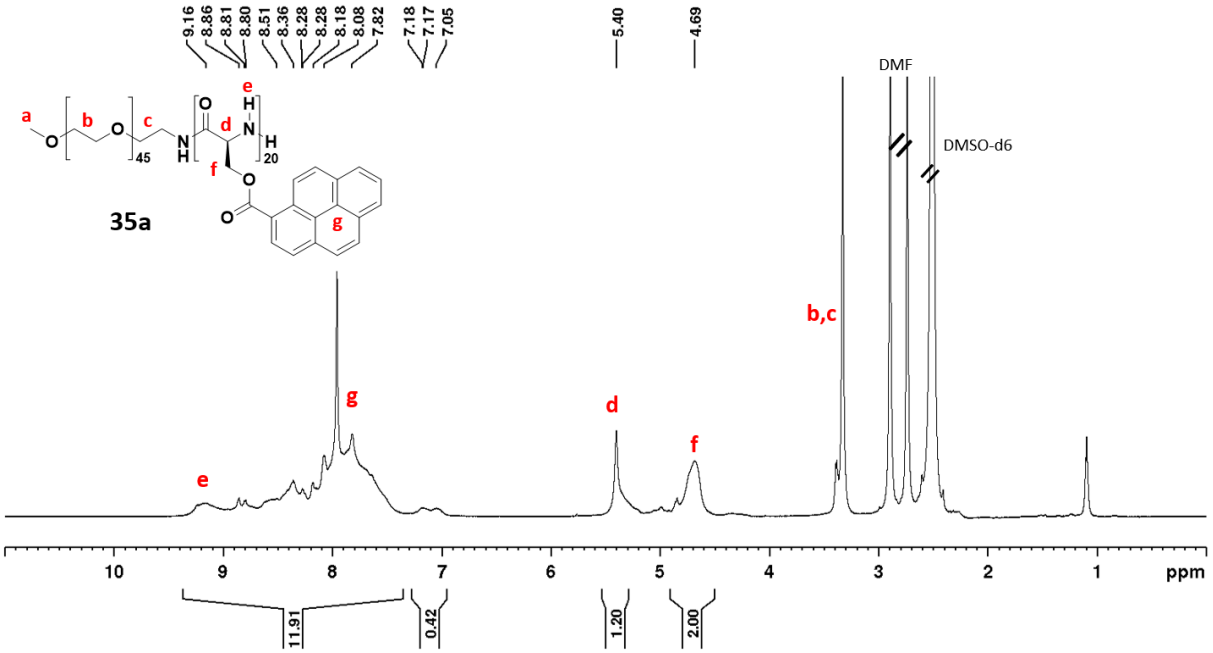

*Figure 145: ^{1}H-NMR spectrum (700 MHz, 333 K, DMSO-d_6) of the block copolymer PEG_{45}-b-$PLS(Pyr)_{20}$ (**35a**).*

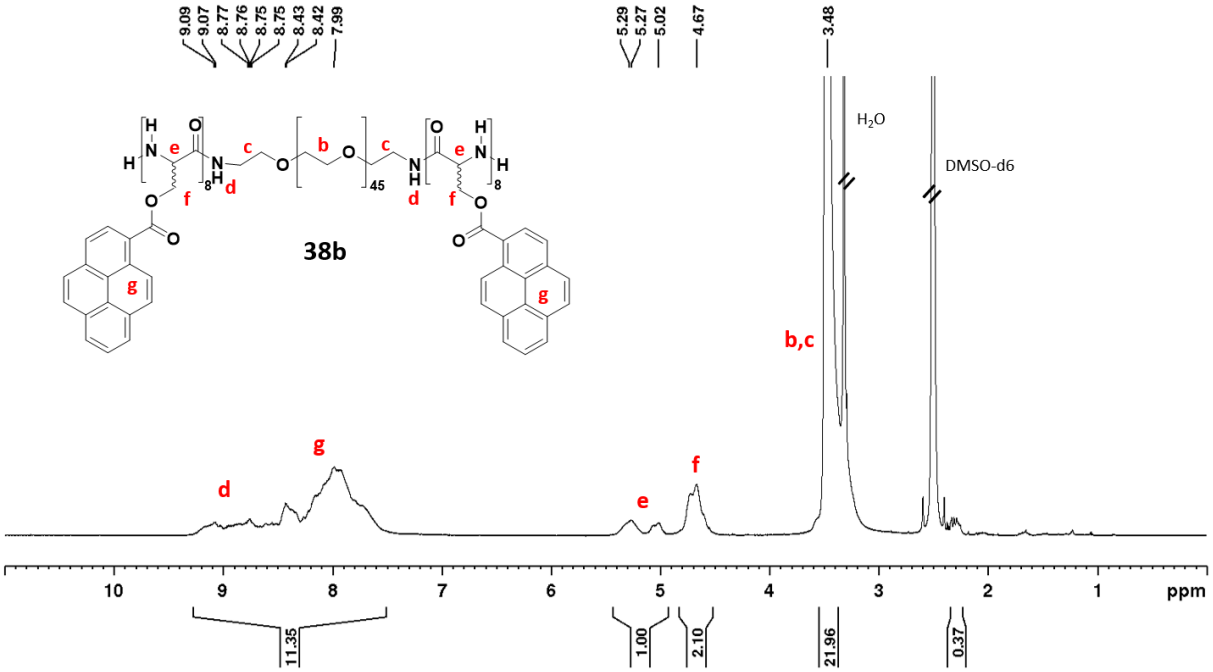

*Figure 146: ^{1}H-NMR spectrum (700 MHz, 333 K, DMSO-d_6) of the triblock copolymer $PDLS(Pyr)_8$-b-PEG_{45}-b-$PDLS(Pyr)_8$ (**38b**).*

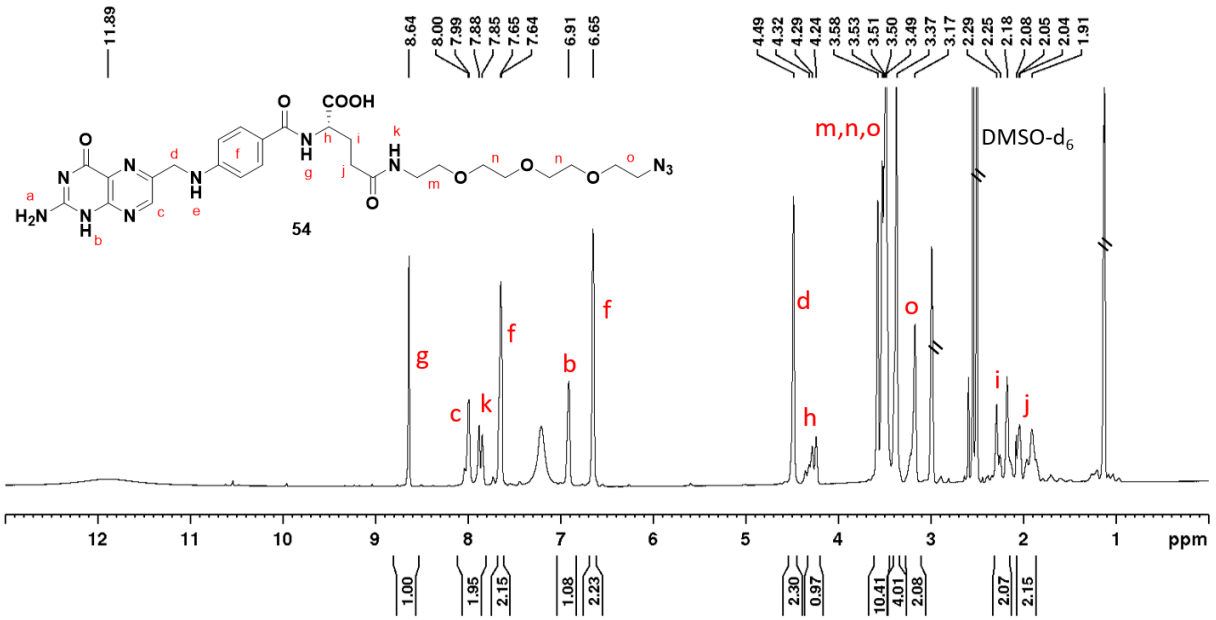

*Figure 147: [1]H-NMR spectrum (700 MHz, 300 K, DMSO-d_6) of azido-PEG_3-FA (**54**).*

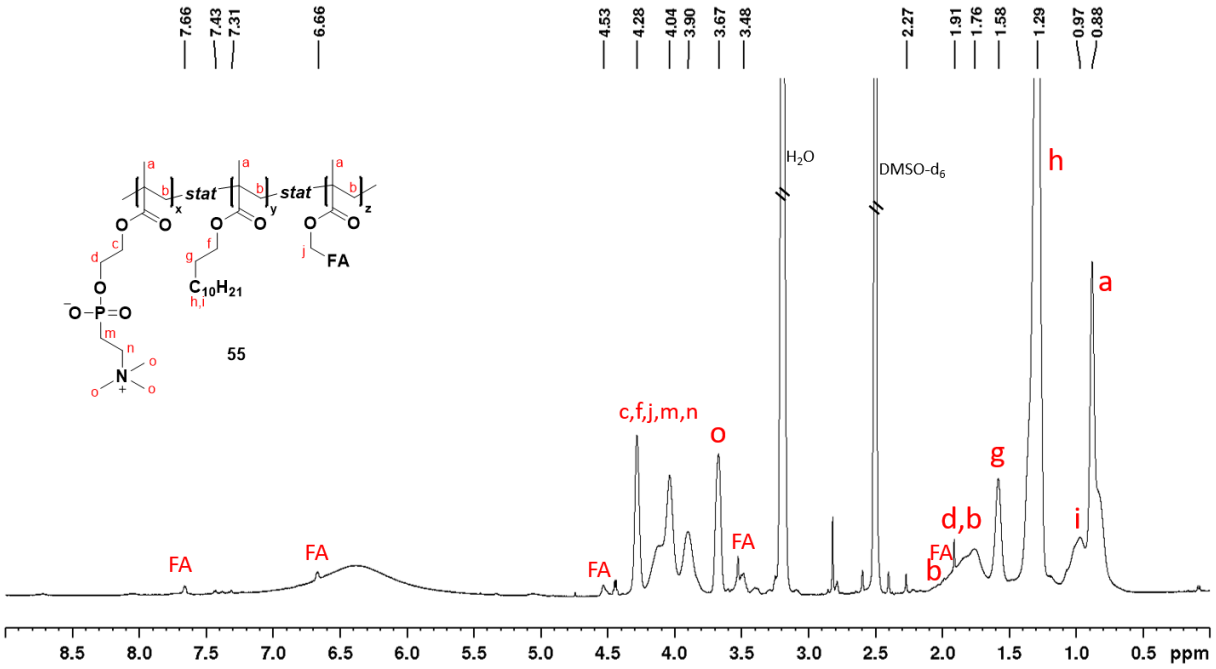

*Figure 148: [1]H-NMR spectrum (700 MHz, 300 K, DMSO-d_6) of the zwitterionic, FA-functionalized PMPC-stat-PLMA-stat-FA (**55**).*

10 References

[1] I. Khan, K. Saeed, I. Khan, *Arab. J. Chem.* **2019**, *12*, 908–931.

[2] A. P. Ramos, M. A. E. Cruz, C. B. Tovani, P. Ciancaglini, *Biophys. Rev.* **2017**, *9*, 79–89.

[3] R. Langer, *Acc. Chem. Res.* **2000**, *33*, 94–101.

[4] J. Shi, P. W. Kantoff, R. Wooster, O. C. Farokhzad, *Nat. Rev. Cancer* **2016**, *17*, 20.

[5] B. Gupta, T. S. Levchenko, V. P. Torchilin, *Adv. Drug Deliv. Rev.* **2005**, *57*, 637–651.

[6] D. Peer, J. M. Karp, S. Hong, O. C. Farokhzad, R. Margalit, R. Langer, *Nat. Nanotechnol.* **2007**, *2*, 751.

[7] F. Alexis, E. Pridgen, L. K. Molnar, O. C. Farokhzad, in *Mol. Pharm.*, American Chemical Society, **2008**, pp. 505–515.

[8] A. Kumari, S. K. Yadav, S. C. Yadav, *Colloids Surf B Biointerfaces* **2010**, *75*, 1–18.

[9] C. Fonseca, S. Simões, R. Gaspar, *J. Control. Release* **2002**, *83*, 273–286.

[10] L. Mu, S. S. Feng, *Pharm. Res.* **2003**, *20*, 1864–1872.

[11] M. Thomas, M. Gajda, C. Amiri Naini, S. Franzka, M. Ulbricht, N. Hartmann, *Langmuir* **2015**, *31*, 13426–13432.

[12] L. J. McCawley, L. M. Matrisian, *Mol. Med. Today* **2000**, *6*, 149–156.

[13] I. D. Goldfine, W. L. McGuire, R. Vigneri, V. Pezzino, *Cancer Res.* **1993**, *53*, 3736–3740.

[14] A. Bernardos, L. Mondragón, E. Aznar, M. D. Marcos, R. Martínez-Máñez, F. Sancenón, J. Soto, J. M. Barat, E. Pérez-Payá, C. Guillem, P. Amorós, *ACS Nano* **2010**, *4*, 6353–6368.

[15] R. Dorresteijn, N. Billecke, M. Schwendy, S. Pütz, M. Bonn, S. H. Parekh, M. Klapper, K. Müllen, *Adv. Funct. Mater.* **2014**, *24*, 4026–4033.

[16] S. E. McNeil, *J. Leukoc. Biol.* **2005**, *78*, 585–594.

[17] S. Logothetidis, *Nanosci. Technol.* **2012**, *61*, 1–26.

[18] C. Fang, B. Shi, Y. Y. Pei, M. H. Hong, J. Wu, H. Z. Chen, *Eur. J. Pharm. Sci.* **2006**, *27*, 27–36.

[19] C. H. Heldin, K. Rubin, K. Pietras, A. Östman, *Nat. Rev. Cancer* **2004**, *4*, 806–813.

[20] W. E. Bawarski, E. Chidlowsky, D. J. Bharali, S. A. Mousa, *Nanomedicine Nanotechnology, Biol. Med.* **2008**, *4*, 273–282.

[21] M. C. Scicluna, L. Vella-Zarb, *ACS Appl. Nano Mater.* **2020**, *3*, 3097–3115.

[22] D. Hühn, K. Kantner, C. Geidel, S. Brandholt, I. De Cock, S. J. H. Soenen, P. Riveragil, J. M. Montenegro, K. Braeckmans, K. Müllen, G. U. Nienhaus, M. Klapper, W. J. Parak, *ACS Nano* **2013**, *7*, 3253–3263.

[23] I. K. Kwon, S. Cheon Lee, B. Han, K. Park, *Analysis on the Current Status of Targeted Drug Delivery to Tumors*, **2012**.

[24] Gregory Russell-Jones, Kirsten McTavish, John McEwan, Bruce Thurmond, *J. Can. Res. Updates* **2012**, *1*, 203–211.

[25] H. S. Yoo, T. G. Park, *J. Control. Release* **2004**, *100*, 247–256.

[26] E. Secret, S. J. Kelly, K. E. Crannell, J. S. Andrew, *ACS Appl. Mater. Interfaces* **2014**, *6*, 10313–10321.

[27] Y. Mi, J. Wolfram, C. Mu, X. Liu, E. Blanco, H. Shen, M. Ferrari, *Pharmacol. Res.* **2016**, *113*, 92–99.

[28] P. A. M. Snoek-van Beurden, J. W. Von Den Hoff, *Biotechniques* **2005**, *38*, 73–83.

[29] T. Jiang, E. S. Olson, Q. T. Nguyen, M. Roy, P. A. Jennings, R. Y. Tsien, *Proc. Natl. Acad. Sci. U. S. A.* **2004**, *101*, 17867–17872.

[30] H. Tang, L. Yin, H. Lu, J. Cheng, *Biomacromolecules* **2012**, *13*, 2609–2615.

[31] T. L. Moore, L. Rodriguez-Lorenzo, V. Hirsch, S. Balog, D. Urban, C. Jud, B. Rothen-Rutishauser, M. Lattuada, A. Petri-Fink, *Chem. Soc. Rev.* **2015**, *44*, 6287–6305.

[32] A. B. Lowe, C. L. McCormick, *Chem. Rev.* **2002**, *102*, 4177–4190.

[33] "Mixture Chemistry Solution, flask | PNGEgg," can be found under https://www.pngegg.com/en/png-zxrkq/download, **n.d.**

[34] "Schwarze Lupe, png | PNGEgg," can be found under https://www.pngegg.com/de/png-bimof/download, **n.d.**

[35] R. Dorresteijn, R. Haschick, M. Klapper, K. Müllen, *Macromol. Chem. Phys.* **2012**, *213*, 1996–2002.

[36] P. A. Lovell, F. J. Schork, *Biomacromolecules* **2020**, DOI 10.1021/acs.biomac.0c00769.

[37] M. Antonietti, K. Landfester, *Prog. Polym. Sci.* **2002**, *27*, 689–757.

[38] B. Brooks, *Chem. Eng. Technol.* **2010**, *33*, 1737–1744.

[39] D. Crespy, K. Landfester, *Beilstein J. Org. Chem.* **2010**, *6*, 1132–1148.

[40] H.-D. Dörfler, *Grenzflächen Und Kolloid-Disperse Systeme*, Springer Berlin, Heidelberg, **2002**.

[41] P. Dagtepe, V. Chikan, *J. Phys. Chem. C* **2010**, *114*, 16263–16269.

[42] J. Periard, A. Banderet, G. Riess, *J. Polym. Sci. Part B Polym. Lett.* **1970**, *8*, 109–114.

[43] R. Dorresteijn, R. Haschick, K. Müller, M. Klapper, K. Müllen, *MRS Online Proc. Libr.* **2013**, *1546*, 632.

[44] A. Imhof, D. J. Pine, *J. Colloid Interface Sci.* **1997**, *192*, 368–374.

[45] R. Dorresteijn, R. Haschick, M. Klapper, K. Müllen, *Macromol. Chem. Phys.* **2012**, *213*, 1996–2002.

[46] M. Klapper, S. Nenov, R. Haschick, K. Müller, K. Müllen, *Acc. Chem. Res.* **2008**, *41*, 1190–1201.

[47] R. Haschick, M. Klapper, K. B. Wagener, K. Müllen, *Macromol. Chem. Phys.* **2010**, *211*, 2547–2554.

[48] K. Müller, M. Klapper, K. Müllen, *J. Polym. Sci. Part A Polym. Chem.* **2007**, *45*, 1101–1108.

[49] R. Dorresteijn, R. Ragg, G. Rago, N. Billecke, M. Bonn, S. H. Parekh, G. Battagliarin, K. Peneva, M. Wagner, M. Klapper, K. Müllen, *Biomacromolecules* **2013**, *14*, 1572–1577.

[50] R. Dorresteijn, *Johannes-gutenb. Univ. Mainz* **2014**.

[51] K. Müller, M. Klapper, K. Müllen, *Colloid Polym. Sci.* **2007**, *285*, 1157–1161.

[52] K. Müller, *Johannes-gutenb. Univ.* **2008**, *Mainz*.

[53] R. Dorresteijn, N. Billecke, S. H. Parekh, M. Klapper, K. Müllen, *J. Polym. Sci. Part A Polym. Chem.* **2015**, *53*, 200–205.

[54] A. Gessner, A. Lieske, B. R. Paulke, R. H. Müller, *Eur. J. Pharm. Biopharm.* **2002**, *54*, 165–170.

[55] C. Geidel, S. Schmachtel, A. Riedinger, C. Pfeiffer, K. Mullen, M. Klapper, W. J. Parak, *Small* **2011**, *7*, 2929–2934.

[56] C. Corbo, R. Molinaro, A. Parodi, N. E. Toledano Furman, F. Salvatore, E. Tasciotti, *Nanomedicine* **2015**, *11*, 81–100.

[57] H. Li, Y. Wang, Q. Tang, D. Yin, C. Tang, E. He, L. Zou, Q. Peng, *Acta Biomater.* **2021**, *129*, 57–72.

[58] B. Pelaz, P. del Pino, P. Maffre, R. Hartmann, M. Gallego, S. Rivera-Fernández, J. M. de la Fuente, G. U. Nienhaus, W. J. Parak, *ACS Nano* **2015**, *9*, 6996–7008.

[59] J. Hühn, C. Carrillo-Carrion, M. G. Soliman, C. Pfeiffer, D. Valdeperez, A. Masood, I. Chakraborty, L. Zhu, M. Gallego, Z. Yue, M. Carril, N. Feliu, A. Escudero, A. M. Alkilany, B. Pelaz, P. del Pino, W. J. Parak, *Chem. Mater.* **2017**, *29*, 399–461.

[60] D. Valdeperez, T. Wang, J. P. Eußner, B. Weinert, J. Hao, W. J. Parak, S. Dehnen, B. Pelaz, *Pharmacol. Res.* **2017**, *117*, 261–266.

[61] D. Valdepérez, P. del Pino, L. Sánchez, W. J. Parak, B. Pelaz, *J. Colloid Interface Sci.* **2016**, *474*, 1–8.

[62] C. Bao, N. Beziere, P. del Pino, B. Pelaz, G. Estrada, F. Tian, V. Ntziachristos, J. M. de la Fuente, D. Cui, *Small* **2013**, *9*, 67.

[63] W. L. Koh, P. H. Tham, H. Yu, H. L. Leo, J. C. Yong Kah, *Nanomedicine* **2016**, *11*, 2275–2287.

[64] D. Valdeperez, N. Wutke, L.-M. Ackermann, W. J. Parak, M. Klapper, B. Pelaz, *Inorganica Chim. Acta* **2022**, *534*, 120820.

[65] N. Feliu, J. Hühn, M. V Zyuzin, S. Ashraf, D. Valdeperez, A. Masood, A. H. Said, A. Escudero, B. Pelaz, E. Gonzalez, M. A. C. Duarte, S. Roy, I. Chakraborty, M. L. Lim, S. Sjöqvist, P. Jungebluth, W. J. Parak, *Sci. Total Environ.* **2016**, *568*, 819–828.

[66] Y. L. Khung, D. Narducci, *Adv. Colloid Interface Sci.* **2015**, *226*, 166–186.

[67] F. Karagöz, R. Dorresteijn, K. Müllen, M. Klapper, in *Control Amphiphile Self-Assembling Mol. Lev. Supra-Molecular Assem. with Tuned Physicochem. Prop. Deliv. Appl.*, American Chemical Society, **2018**, pp. 231–247.

[68] T. A. Aguilera, E. S. Olson, M. M. Timmers, T. Jiang, R. Y. Tsien, *Integr. Biol.* **2009**, *1*, 371–381.

[69] W. Ke, J. Li, K. Zhao, Z. Zha, Y. Han, Y. Wang, W. Yin, P. Zhang, Z. Ge, *Biomacromolecules* **2016**, *17*, 3268–3276.

[70] G. Riess, C. Labbe, *Macromol. Rapid Commun.* **2004**, *25*, 401–435.

[71] K. Müller, M. Klapper, K. Müllen, *Colloid Polym. Sci.* **2007**, *285*, 1157–1161.

[72] Z. Yang, Z. Mao, J. Ling, *Polym. Chem.* **2016**, *7*, 519–522.

[73] Z. Bohak, E. Katchalski, *Biochemistry* **1963**, *2*, 228–237.

[74] W. Stuart, P. Wyatt, *Organic Synthesis: The Disconnection Approach, 2nd EditionTitle*, Wiley-VCH Verlag, **2008**.

[75] Q. X. Zhou, J. Kohn, *Macromolecules* **1990**, *23*, 3399–3406.

[76] N. R. Krogman, A. L. Weikel, N. Q. Nguyen, L. S. Nair, C. T. Laurencin, H. R. Allcock, *Macromolecules* **2008**, *41*, 7824–7828.

[77] M. Frankel, S. Cordova, M. Breuer, *J. Chem. Soc.* **1953**, 1991–1994.

[78] N. M. Tooney, G. D. Fasman, *Biopolymers* **1968**, *6*, 81–96.

[79] P. G. M. Wuts, T. W. Greene, *Greene's Protective Groups in Organic Synthesis*, John Wiley & Sons, Inc., Hoboken, NJ, USA, **2006**.

[80] J. E. Semple, B. Sullivan, K. N. Sill, *Synth. Commun.* **n.d.**, *47*, 53–61.

[81] R. Obeid, C. Scholz, *Biomacromolecules* **2011**, *12*, 3797–3804.

[82] B. Kang, H. Tang, Z. Zhao, S. Song, *ACS Omega* **2020**.

[83] W. Vayaboury, O. Giani, H. Cottet, A. Deratani, F. Schué, *Macromol. Rapid Commun.* **2004**, *25*, 1221–1224.

[84] J. Zou, J. Fan, X. He, S. Zhang, H. Wang, K. L. Wooley, *Macromolecules* **2013**, *46*, 4223–4226.

[85] G. J. M. Habraken, M. Peeters, C. H. J. T. Dietz, C. E. Koning, A. Heise, *Polym. Chem.* **2010**, *1*, 514–524.

[86] I. R. Khalil, V. U. Irorere, I. Radecka, A. T. H. Burns, M. Kowalczuk, J. L. Mason, M. P. Khechara, *Mater.* **2016**, *9*, DOI 10.3390/ma9010028.

[87] S. Manouchehri, P. Zarrintaj, M. R. Saeb, J. D. Ramsey, *Mol. Pharm.* **2021**, *18*, 3652–3670.

[88] H. Lu, J. Wang, Z. Song, L. Yin, Y. Zhang, H. Tang, C. Tu, Y. Lin, J. Cheng, *Chem Commun* **2014**, *50*, 139–155.

[89] O. D. Krishna, K. L. Kiick, *Biopolymers* **2010**, *94*, 32–48.

[90] Q. Mu, T. Hu, J. Yu, *PLoS One* **2013**, *8*, e68559.

[91] A. Barth, *Biochim. Biophys. Acta - Bioenerg.* **2007**, *1767*, 1073–1101.

[92] J. Kong, S. Yu, *Acta Biochim. Biophys. Sin. (Shanghai).* **2007**, *39*, 549–559.

[93] J. D. Robertson, L. Rizzello, M. Avila-Olias, J. Gaitzsch, C. Contini, M. S. Magoń, S. A. Renshaw, G. Battaglia, *Sci. Rep.* **2016**, *6*, 27494.

[94] G. Dvorakova, R. Haschick, M. Klapper, K. Müllen, A. Biffis, *J. Polym. Sci. Part A Polym. Chem.* **2013**, *51*, 267–274.

[95] S. Schultz, G. Wagner, K. Urban, J. Ulrich, *Chem. Eng. Technol.* **2004**, *27*, 361–368.

[96] L. R. Parent, E. Bakalis, A. Ramírez-Hernández, J. K. Kammeyer, C. Park, J. de Pablo, F. Zerbetto, J. P. Patterson, N. C. Gianneschi, *J. Am. Chem. Soc.* **2017**, *139*, 17140–17151.

[97] O. Söderman, P. Stilbs, W. S. Price, *Concepts Magn. Reson. Part A* **2004**, *23A*, 121–135.

[98] Y. Yang, A. Alford, V. Kozlovskaya, S. Zhao, H. Joshi, E. Kim, S. Qian, V. Urban, D. Cropek, A.

Aksimentiev, E. Kharlampieva, *ACS Appl. Polym. Mater.* **2019**, *1*, 722–736.

[99] S. Mantha, S. Qi, M. Barz, F. Schmid, *Phys. Rev. Mater.* **2019**, *3*, 26002.

[100] N. Sato, A. Murata, T. Fujie, S. Takeoka, *Soft Matter* **2016**, *12*, 9202–9209.

[101] P. Sadek, *The HPLC Solvent Guide*, **2002**.

[102] G. Liu, C. M. Dong, *Biomacromolecules* **2012**, *13*, 1573–1583.

[103] T. Vorherr, W. Bannwarth, *Bioorg. Med. Chem. Lett.* **1995**, *5*, 2661–2664.

[104] S. P. Bong, M. L. Hye, *Bull. Korean Chem. Soc.* **2008**, *29*, 2054–2056.

[105] A. Williamson, *London, Edinburgh, Dublin Philos. Mag. J. Sci.* **1850**, *37*, 350–356.

[106] P. O. Adero, D. R. Jarois, D. Crich, *Carbohydr. Res.* **2017**, *449*, 11–16.

[107] T. Iversen, D. R. Bundle, *J. Chem. Soc. Chem. Commun.* **1981**, 1240–1241.

[108] Y.-R. Gao, S.-H. Guo, Z.-X. Zhang, S. Mao, Y.-L. Zhang, Y.-Q. Wang, *Tetrahedron Lett.* **2013**, *54*, 6511–6513.

[109] D. Lelièvre, P. Barta, V. Aucagne, A. F. Delmas, *Tetrahedron Lett.* **2008**, *49*, 4016–4019.

[110] V. K. Chatare, R. B. Andrade, *Angew. Chemie Int. Ed.* **2017**, *56*, 5909–5911.

[111] N. Wutke, Synthese Und Schwefel-Funktionalisierung Grenzflächenaktiver Monomere Und Polymere, Philipps-Universität Marburg, **2017**.

[112] R. F. Nystrom, W. G. Brown, *J. Am. Chem. Soc.* **1948**, *70*, 3738–3740.

[113] D. Y. Ong, J. H. Pang, S. Chiba, *J. Synth. Org. Chem. Japan* **2019**, *77*, 1060–1069.

[114] D. Parker, *Chem. Rev.* **1991**, *91*, 1441–1457.

[115] M. T. Riaz, I. Pohorilets, J. J. Hernandez, J. Rios, N. I. Totah, *Tetrahedron Lett.* **2018**, *59*, 2809–2812.

[116] P. Garner, J. M. Park, *J. Org. Chem.* **1987**, *52*, 2361–2364.

[117] M. Passiniemi, A. M. P. Koskinen, *Beilstein J. Org. Chem.* **2013**, *9*, 2641–2659.

[118] A. Mckillop, R. J. K. Taylor, R. J. Watson, N. Lewis, *Synthesis (Stuttg).* **1994**, *1994*, 31–33.

[119] S. Bhowmik, S. Batra, *European J. Org. Chem.* **2013**, *2013*, 7145–7151.

[120] K. Sankar, H. Rahman, P. P. Das, E. Bhimireddy, B. Sridhar, D. K. Mohapatra, *Org. Lett.* **2012**, *14*, 1082–1085.

[121] A.-K. C. Schmidt, C. B. W. Stark, *Org. Lett.* **2011**, *13*, 4164–4167.

[122] B. Boyer, E.-M. Keramane, J.-P. Roque, A. A. Pavia, *Tetrahedron Lett.* **2000**, *41*, 2891–2894.

[123] K. C. Nicolaou, D. Y. K. Chen, X. Huang, T. Ling, M. Bella, S. A. Snyder, *J. Am. Chem. Soc.* **2004**, *126*, 12888–12896.

[124] L. Van Hijfte, R. D. Little, *J. Org. Chem.* **1985**, *50*, 3940–3942.

[125] S. Loudwig, M. Goeldner, *Tetrahedron Lett.* **2001**, *42*, 7957–7959.

[126] J. Lee, J. Lee, M. Kang, M. Shin, J.-M. Kim, S.-U. Kang, J.-O. Lim, H.-K. Choi, Y.-G. Suh, H.-G. Park, U. Oh, H.-D. Kim, Y.-H. Park, H.-J. Ha, Y.-H. Kim, A. Toth, Y. Wang, R. Tran, L. V. Pearce, D.

J. Lundberg, P. M. Blumberg, *J. Med. Chem.* **2003**, *46*, 3116–3126.

[127] C. Wu, X. Fu, S. Li, *European J. Org. Chem.* **2011**, *2011*, 1291–1299.

[128] R. Adams, L. H. Ulich, *J. Am. Chem. Soc.* **1920**, *42*, 599–611.

[129] T. I. Al-Warhi, H. M. A. Al-Hazimi, A. El-Faham, *J. Saudi Chem. Soc.* **2012**, *16*, 97–116.

[130] B. Neises, W. Steglich, *Angew. Chemie Int. Ed. English* **1978**, *17*, 522–524.

[131] H. Sajiki, *Tetrahedron Lett.* **1995**, *36*, 3465–3468.

[132] A. Bose, S. Jana, A. Saha, T. K. Mandal, *Polymer (Guildf).* **2017**, *110*, 12–24.

[133] A. Bodratti, P. Alexandridis, *J. Funct. Biomater.* **2018**, *9*, 11.

[134] E. Rideau, R. Dimova, P. Schwille, F. R. Wurm, K. Landfester, *Chem. Soc. Rev.* **2018**, *47*, 8572–8610.

[135] A. Blanazs, S. P. Armes, A. J. Ryan, *Macromol. Rapid Commun.* **2009**, *30*, 267–277.

[136] Y. H. A. Hussein, M. Youssry, *Materials (Basel).* **2018**, *11*, DOI 10.3390/ma11050688.

[137] G. Gaucher, M.-H. Dufresne, V. P. Sant, N. Kang, D. Maysinger, J.-C. Leroux, *J. Control. Release* **2005**, *109*, 169–188.

[138] Muhammad Suhail, A. K. Janakiraman, A. Khan, A. Naeem, Syed Faisal Badshah, *J. Pharm. Pharm.* **2019**, *6*, 72–82.

[139] R. P. Brinkhuis, F. P. J. T. Rutjes, J. C. M. van Hest, *Polym. Chem.* **2011**, *2*, 1449–1462.

[140] A. Barth, *Biochim. Biophys. Acta - Bioenerg.* **2007**, *1767*, 1073–1101.

[141] Z. Yang, Z. Mao, J. Ling, *Polym. Chem.* **2016**, *7*, 519–522.

[142] S. Slomkowski, J. V Alemán, R. G. Gilbert, M. Hess, K. Horie, R. G. Jones, P. Kubisa, I. Meisel, W. Mormann, S. Penczek, R. F. T. Stepto, **2011**, *83*, 2229–2259.

[143] P. L. Fuhrmann, G. Sala, M. Stieger, E. Scholten, *Food Res. Int.* **2019**, *122*, 537–547.

[144] A. J. Charlton, N. J. Baxter, M. L. Khan, A. J. G. Moir, E. Haslam, A. P. Davies, M. P. Williamson, *J. Agric. Food Chem.* **2002**, *50*, 1593–1601.

[145] C. D. Kanakis, I. Hasni, P. Bourassa, P. A. Tarantilis, M. G. Polissiou, H.-A. Tajmir-Riahi, *Food Chem.* **2011**, *127*, 1046–1055.

[146] H. Schott, A. E. Royce, *J. Pharm. Sci.* **1983**, *72*, 1427–1436.

[147] S. Matoori, J.-C. Leroux, *Mater. Horizons* **2020**, *7*, 1297–1309.

[148] M. Khimani, H. Patel, V. Patel, P. Parekh, R. L. Vekariya, *Polym. Bull.* **2020**, *77*, 5783–5810.

[149] H. Robson Marsden, A. Kros, *Macromol Biosci* **2009**, *9*, 939–951.

[150] H.-A. Klok, S. Lecommandoux, *Adv. Mater.* **2001**, *13*, 1217–1229.

[151] Y. Zhu, B. Yang, S. Chen, J. Du, *Prog. Polym. Sci.* **2017**, *64*, 1–22.

[152] S. B. La, K. Kataoka, T. Okano, Y. Sakurai, in *Adv. Biomater. Biomed. Eng. Drug Deliv. Syst.* (Eds.: N. Ogata, S.W. Kim, J. Feijen, T. Okano), Springer Japan, Tokyo, **1996**, pp. 321–322.

[153] K. Shinoda, T. Yamaguchi, R. Hori, *Bull. Chem. Soc. Jpn.* **1961**, *34*, 237–241.

[154] A. Patist, S. S. Bhagwat, K. W. Penfield, P. Aikens, D. O. Shah, *J. Surfactants Deterg.* **2000**, *3*, 53–58.

[155] X. Ai, L. Zhong, H. Niu, Z. He, *Asian J. Pharm. Sci.* **2014**, *9*, 244–250.

[156] F. M. Winnik, *Chem. Rev.* **1993**, *93*, 587–614.

[157] A. Mahara, R. Iwase, T. Sakamoto, K. Yamana, T. Yamaoka, A. Murakami, *Angew. Chemie Int. Ed.* **2002**, *41*, 3648–3650.

[158] I. V. Astakhova, V. A. Korshun, J. Wengel, *Chem. – A Eur. J.* **2008**, *14*, 11010–11026.

[159] J. N. Wilson, E. T. Kool, *Org. Biomol. Chem.* **2006**, *4*, 4265–4274.

[160] L. Cai, M. Gochin, K. Liu, *Chem. Commun.* **2011**, *47*, 5527–5529.

[161] E. S. Lee, H. J. Shin, K. Na, Y. H. Bae, *J. Control. Release* **2003**, *90*, 363–374.

[162] S. Pandey, M. Ali, A. Bishnoi, A. Azam, S. Pandey, H. M. Chawla, *J. Fluoresc.* **2008**, *18*, 533–539.

[163] A. E. C. Redpath, Ö. Pekcan, M. A. Winnik, *J. Photochem.* **1983**, *23*, 283–288.

[164] M. R. Eftink, in (Ed.: J.R. Lakowicz), Springer US, Boston, MA, **2002**, pp. 53–126.

[165] S. Perticaroli, J. D. Nickels, G. Ehlers, A. P. Sokolov, *Biophys. J.* **2014**, *106*, 2667–2674.

[166] P. Arenas-Guerrero, Á. V Delgado, K. J. Donovan, K. Scott, T. Bellini, F. Mantegazza, M. L. Jiménez, *Sci. Rep.* **2018**, *8*, 9502.

[167] W. Li, C. Tao, J. Wang, Y. Le, J. Zhang, *RSC Adv.* **2019**, *9*, 31264–31273.

[168] P. Kumar, S. Agnihotri, *Biochem. Physiol. Open Access* **2016**, *01*, 1–6.

[169] X. Gu, M. Qiu, H. Sun, J. Zhang, L. Cheng, C. Deng, Z. Zhong, *Biomater. Sci.* **2018**, *6*, 1526–1534.

[170] D. Valdeperez, N. Wutke, L.-M. Ackermann, W. J. Parak, M. Klapper, B. Pelaz, *Inorganica Chim. Acta* **2022**, *534*, 120820.

[171] S. H. D. P. Lacerda, J. J. Park, C. Meuse, D. Pristinski, M. L. Becker, A. Karim, J. F. Douglas, *ACS Nano* **2010**, *4*, 365–379.

[172] I. Lynch, T. Cedervall, M. Lundqvist, C. Cabaleiro-Lago, S. Linse, K. A. Dawson, *Adv. Colloid Interface Sci.* **2007**, *134–135*, 167–174.

[173] C. Leng, H.-C. Hung, S. Sun, D. Wang, Y. Li, S. Jiang, Z. Chen, *ACS Appl. Mater. Interfaces* **2015**, *7*, 16881–16888.

[174] M. Tonigold, J. Simon, D. Estupiñán, M. Kokkinopoulou, J. Reinholz, U. Kintzel, A. Kaltbeitzel, P. Renz, M. P. Domogalla, K. Steinbrink, I. Lieberwirth, D. Crespy, K. Landfester, V. Mailänder, *Nat. Nanotechnol.* **2018**, DOI 10.1038/s41565-018-0171-6.

[175] P. del Pino, F. Yang, B. Pelaz, Q. Zhang, K. Kantner, R. Hartmann, N. Martinez de Baroja, M. Gallego, M. Möller, B. B. Manshian, S. J. Soenen, R. Riedel, N. Hampp, W. J. Parak, *Angew. Chemie Int. Ed.* **2016**, *55*, 5483–5487.

[176] Z. Cao, N. Brault, H. Xue, A. Keefe, S. Jiang, *Angew. Chemie Int. Ed.* **2011**, *50*, 6102–6104.

[177] S. Jiang, Z. Cao, *Adv. Mater.* **2010**, *22*, 920–932.

[178] J. A. Callow, M. E. Callow, *Nat. Commun.* **2011**, *2*, 244.

[179] X. Liu, H. Li, Y. Chen, Q. Jin, K. Ren, J. Ji, *Adv. Healthc. Mater.* **2014**, *3*, 1439–1447.

[180] X. Jiang, S. Weise, M. Hafner, C. Röcker, F. Zhang, W. J. Parak, G. U. Nienhaus, *J. R. Soc. Interface* **2010**, *7*, S5–S13.

[181] J. B. Schlenoff, *Langmuir* **2014**, *30*, 9625–9636.

[182] B. Stella, S. Arpicco, M. T. Peracchia, D. Desmaële, J. Hoebeke, M. Renoir, J. D'Angelo, L. Cattel, P. Couvreur, *J. Pharm. Sci.* **2000**, *89*, 1452–1464.

[183] L.-M. Ackermann, Oberflächenfunktionalisierung von Anorganischen Materialien, Johannes Gutenberg-Universität Mainz, **2018**.

[184] S. Megahed, Tailoring the Surface Chemistry of the Nanoparticles to Modulate Their Interactions with Proteins and Cells, Universtität Hamburg, **2022**.

[185] C. A. P. Monteiro, A. D. P. R. Oliveira, R. C. Silva, R. R. M. Lima, F. O. Souto, M. O. Baratti, H. F. Carvalho, B. S. Santos, P. E. Cabral Filho, A. Fontes, *J. Photochem. Photobiol. B Biol.* **2020**, *209*, 111918.

[186] M. Debayle, E. Balloul, F. Dembele, X. Xu, M. Hanafi, F. Ribot, C. Monzel, M. Coppey, A. Fragola, M. Dahan, T. Pons, N. Lequeux, *Biomaterials* **2019**, *219*, 119357.

[187] L. M. D. Loiola, M. Batista, L. B. Capeletti, G. B. Mondo, R. S. M. Rosa, R. E. Marques, M. C. Bajgelman, M. B. Cardoso, *J. Colloid Interface Sci.* **2019**, *553*, 540–548.

[188] M. Leeman, J. Choi, S. Hansson, M. U. Storm, L. Nilsson, *Anal. Bioanal. Chem.* **2018**, *410*, 4867–4873.

[189] T. Yao, Y. Asayama, *Reprod. Med. Biol.* **2017**, *16*, 99–117.

[190] L. Zapór, J. Skowroń, M. Gołofit-Szymczak, *Int. J. Occup. Saf. Ergon.* **2002**, *8*, 121–129.

[191] Y. Ilieva, L. Dimitrova, M. M. Zaharieva, M. Kaleva, P. Alov, I. Tsakovska, T. Pencheva, I. Pencheva-El Tibi, H. Najdenski, I. Pajeva, *Toxics* **2021**, *9*, DOI 10.3390/toxics9050092.

[192] T. Ji, S. Li, Y. Zhang, J. Lang, Y. Ding, X. Zhao, R. Zhao, Y. Li, J. Shi, J. Hao, Y. Zhao, G. Nie, *ACS Appl. Mater. Interfaces* **2016**, *8*, 3438–3445.

[193] W. Ke, J. Li, K. Zhao, Z. Zha, Y. Han, Y. Wang, W. Yin, P. Zhang, Z. Ge, *Biomacromolecules* **2016**, *17*, 3268–3276.

[194] T. Anajafi, S. Mallik, *Ther. Deliv.* **2015**, *6*, 521–534.

11 List of Publications

PUBLICATIONS

- M. Klapper, F. Karagoez, N. Wutke. Block copolymer nanocarriers with peptide units for drug delivery. *Abstracts of Papers of the American Chemical Society* **2018**, *256*, 145-COLL.

- D. Valdeperez, N. Wutke, L. Ackermann, W. Parak, M. Klapper, B. Pelaz, Colloidal stability of polymer coated zwitterionic Au nanoparticles in biological media. *Inorganica Chimica Acta* **2022**, *534*, 120820.

- S. Megahed, N. Wutke, M. Klapper, W. Parak, N. Feliu. Role of the surface chemistry on Protein adsorption and cellular uptake. *In progress.*

CONFERENCE CONTRIBUTIONS

- N. Wutke, M. Klapper, A. Beyer, A. Gölzhäuser, A. Schieders, B. Shapira, I. Cohen, E. Avraham, D. Aurbach. “Nanomembranes for cost-effective hybrid desalination-filtration of wastewater (NFCDI).” Status Conference Paper. *BMBF-MOST Cooperation in Water Technology Research* **2017**, Masada, Israel.

- D. Aurbach, E. Avraham, M. Klapper, N. Wutke, A. Gölzhäuser, A. Beyer, A. Schnieders. “Nanomembranes for cost-effective hybrid desalination-filtration of wastewater (NFCDI).” Status Conference Paper. *German-Israeli Cooperation in Water Technology Research* **2019**, Dresden.

- N. Wutke, M. Klapper. “New precursor molecules for the fabrication of carbon nanomaterials for water purification applications (NFCI).” Status Conference Poster. *German-Israeli Cooperation in Water Technology Research* **2019**, Dresden.

12 Acknowledgements

[redacted]